Conference proceedings

Ferro13

Chairmen :

SI LARBI Amir (Professor), Saint-Etienne, France
NASSIF Hani (Professor), New Jersey, USA

Organizing Committee

Co-Chairmen:

- SI LARBI Amir (Professor), Ecole Nationale d'Ingenieurs de Saint Etienne , Ecole Centrale de Lyon (ENISE-ECL), France
- NASSIF Hani (Professor), Rutgers University, New Brunswick, New Jersey, USA

Honorary Chair:

- NAAMAN Antoine E. (Professor Emeritus), University of Michigan, USA

Local Organizing committee

- ALGOURDIN Nonna (Assistant professor), ENISE, ECL, LTDS - France
- DANSOU Anicet (Assistant professor), ENISE, ECL, LTDS - France
- DAOUADJI Ali , (Professor), INSA Lyon, GEOMAS-France
- FERROUKHI Yacine (Assistant professor), ENISE, ECL, LTDS - France
- MESTICOU Zyed (Research engineer), ENISE, ECL, LTDS - France
- PLETTO Isabelle (Assistant support), ENISE, ECL, LTDS - LIRIS - France

Organization support (PHd Students)

- BEREYZIAT Antoine (PHd student), ENISE, ECL, LTDS - France
- KAHN Junaid (PHd student), ENISE, ECL, LTDS - France

Financial support

Centrale Innovation, event's financial management.

Scientific Committee

Chair: Antonio Nanni, USA

Deputy-Chairs: Joseph Hegger, Germany, and Barzin Mobasher, USA

Algourdin Nonna , France
Altoubat Salah , UAE
Aiello M. Antonietta , Italy
Anwar Navid , Thailand
Barros Joaquim, Portugal
Bao Yi, USA
Bonakdar Amir, USA
Bordelon Amanda, USA
Carloni Christian, USA
Casadei Paolo, Italy
Ceravolo R., Italy
Chudoba R. , Germany
Dansou Anicet, France
Djamai Zakaria, France
De Felice Gianmarco, Italy
Di Prisco Marco, Italy
Ekenel Mahmut, USA
El-Debs Mounir, Brazil
Ferroukhi Yacine, France
Gabor Aron, France
Ghannoum Wassim, USA
Hossain Zacaria, Japan
Issam Harik, USA
Jennings Patrick, UK
Kromoser Benjamin, Italy
Lopez De Murphy Maria, USA
Mechtcherine Victor, Germany
Mesticou Zyed, France
Meng Weina, USA
Peled Alva, Israel
Papanicolaou Corina, Greece
Plizzari Giovanni, Italy
Portal Williams Natalie, Sweden
Rodrigues Conrado, Brazil
Sakai Takaschi Japan
Sneed Lesley, USA
Syed Aamer, USA
Wille Kay, USA
Zureick Abdul Hamid, USA

International Committee

Chair : Tine Tysmans, Belgium

Deputy-Chairs: John Bolander USA, and Cai Gaochuang, China

International members :

AUSTRIACO Lilia, Philippines
BANTHIA Nemy , Canada
BEDOYA-Ruiz Daniel, Colombia
BITTENCOURT Tulio, Brazil
DE ANDRADES SILVA Flavio., Brazil
CHIORINOMario, Italy
CURBACH M., Germany
DELVASTO Silvio, Colombia
DIVEKAR Balkrishna, India
FALLIS Garth, Canada
FERRARA Liberato, Italy
GRIES Thomas, Germany
GUERRERO P., Colombia
HAMELIN Patrice, France
KRSTULOVIC-OPARA Neven, USA
LYONS III William, USA
MELO Antonio, Spain
MILINKOVIC Milenko, Serbia
MOSCOSO Mario, Bolivia
MYERS John, USA
NUNES BONIFACIO Savio, Brazil
NEDWELL Paul, UK
OHAMA Y., Japan
PAMA Ricardo, Philippines
PARAMASIVAM P., India
PEKMEZCI Bekir Yilmaz, Turkey
REINHARDT Hans Wolf, Germany
RHYNER Kurt, Switzerland
ROWLAND Larry, USA
SAID Aly, USA
SEMA Pedro, Spain
SHAH Surendra, USA
TAN Kiang Hwee, Singapore
TOLEDO FILHO Romildo, Brazil
TRIANTAFILLOU Thanasis, Greece
UOMOTO Taketo, Japan
VAZQUEZ Jose, Mexico
WALDSHLAGEL Owen, USA
WAINSHTOK Rivas Hugo, Cuba
WANG Kejin, USA
WEHBE Nadim, USA

Monday June 21

All times are in Lyon Time - (6 Hours EST)

8:40-9:00 am (*Lyon time) **Welcoming Message by A. Si Larbi and H. Nassif**

Session 1: Ferrocement: History and Progress		
9:00 - 9:40 **Keynote**	**M. Chiorino and C. Chiorino**	Art and Science of Building in Concrete: The reinvention of Ferrocement by Pier Luigi Nervi
9:40 - 10:00	A.E. Naaman	Ferrocement: a Historical Perspective
10:00 - 10:20	P. Nedwell	Ferrocement: an Appropriate Material for University Project Work
10:20 - 10:30	Questions to speakers	
10:30 - 10:40	Break	
Session 2 : TRC : Mechanical Performance		
10:40 - 11:20 **Keynote**	**B. Mobasher**, C. Pleesudjai & Y. Yao	Hierarchical Modeling of Textile Reinforced Concrete Structural Systems
11:20 - 11:40	N. Douk, X.H. Vu, and A. Si Larbi	Numerical Modeling of Stress and Strain Evolution of RC Beams Reinforced by TRC Subjected to Thermomechanical Loading in Case of Fire
11:40 - 12:00	I. Karakasis, C. Papanicolaou, and T. Triantafillou	Durability of Textile Reinforced Mortars Under Harsh Environments
12:00 - 12:10	Questions to speakers	
12:10 - 13:00	Break	
Session 3 : Ferrocement : Recent Applications		
13:00 - 13:40 **Keynote**	**G. Penelis**, B. Martin, P.Winslow, and K. Paschalidis	The Ferrocement Canopy of the New Athens Opera House
13:40 - 14:00	M. Milinkovic	Sturdy, Durable, Fast-to-Build and Low-Cost Ferrocement Housing
14:00 - 14:20	M. Milinkovic	Sustainable and Flexible System for Construction with Ferrocement
14:20 - 14:30	Questions to speakers	
14:30 - 14:40	Break	
Session 4 : Modeling Ferrocement and TRC		
14:40 - 15:20 **Keynote**	**J.E. Bolander**	Computational Modelling of Ferrocement for Structural Applications
15:20 - 15:40	H. Spartali, R. Chudoba, S. Rastegarian, and N. Will	Moment-Curvature Model for a General Flexural Assessment of Carbon-Concrete Beams
15:40 - 16:00	P. Kapsalis, M. El Kadi, T. Triantafillou, D. Van Hemelrijck, and T. Tysmans	Numerical Modelling of the Flexural Capacity of Heated Textile Reinforced Concrete
16:00 - 16:20	E. Tsangouri, E. Hardy, A. Van Driessche, A. Si Larbi, D. Aggelis	Acoustic emission monitoring of fracture of trc curved structural plates
16:20 - 16:40	C. Signorini, V. Volpini, A. Nobili	Long-Term performance of natural fabrics in inorganic matrix thin composite systems
16:40 - 16:50	Questions to speakers	
16:50	Break for the day	

Tuesday June 22

***All times are in Lyon Time - (6 Hours EST)**

Session 5 : Rehabilitation, Strengthening, Optimization		
9:00 - 9:40 **Keynote**	M.C. Rampini, G. Zani, M. Colombo and **M. Di Prisco**	FRCM-Retrofitting of Steel Fiber-Reinforced Concrete Shallow Beams
9:40 - 10:00	P. Hamelin, Z. Mesticou, N. Algourdin, G. Cai and A. Si Larbi	Design Method for Strengthening Steel-Concrete Beams with Textile Reinforced Cement
10:00 - 10:20	A. de Coster, M. Hennemann, L. De Laet, and T. Tysmans	Modular Shell Structures in Textile Reinforced Concrete (TRC): a Structural Feasibility Study
10:20 - 10:30	Questions to speakers	
10:30 - 10:40	Break	
Session 6 : Ferrocement : Mechanical Behavior and Properties		
10:40 - 11:00	A. Abu-obeidah, W. Nasreddine, H. Nassif, and W. Meng	Early Age Performance of Fiber Reinforced Ferrocement and UHPC in Flexural Repair of Concrete Beams
11:00 - 11:20	A. Abu-obeidah, D. Ortiz and H. Nassif	Early Age Bond Characteristics of Ferrocement-Concrete Interface under Thermal Curing
11:20 - 11:40	S. Rajkumar and D. Gopal	Experimental Investigation on Mechanical Properties of Ferrocement with Nano Silica Synthesized from Zeamays
11:40 - 12:00	B. Leporace Guimil, A. Conforti, G. Plizzari, P.Serna Ros,	Effect of Fiber Orientation on the Behavior of RC Beams in Vibrated and Self-Compacting Concrete
12:00 - 12:10	Questions to speakers	
12:10 - 13:00	Break	
Session 7 : Carbon TRC in Structural Applications		
13:00 - 13:20	R. Mansur De Castro Silva and F. De Andrade Silva	Mechanical Behavior of Carbon Textile Reinforced Concrete Beams
13:20 - 13:40	K. Goliath, D. Cordoso and F. De Andrade Silva	Flexural Creep Behavior of I-Sections Carbon TRC Beams
13:40 - 14:00	D. Schlueter, S. Uhlemann, and M. Curbach	Multifunctional Carbon Concrete Slabs
14:00 - 14:20	M. Kimm, M. Sodagar, V. Overhage & T. Gries	Recycled Carbon Fibers with Improved Surface Characteristics as Reinforcing Material for Fiber Concrete
14:20 - 14:40	M. Tsegaye, M. El Kadi, T. Adugna, D. Van Hemerlrijck, and T. Tysmans	Mechanical Durability and Performance of Cement Composites Reinforced with Aligned Enset Fibers
14:40 - 15:00	Questions to speakers	
15:00 - 15:20	Break	
Session 8 : Examples of Failures and Repair		
15:20 - 15:40 **Keynote**	**S.P. Shah**	Ferrocement: a Personal Perspective
15:40 - 16:00	S.N. Bonifacio	Construction Failure and Repair of Ferrocement Tanks Used in Waste-Water Treatment Plants
16:00 - 16:20	E. Tsangouri, D. Aggelis, and D. Linn Iii	Revealing the Mixed Mode Failure Under Pull-Out of Masonry Retrofitted by Textile Reinforced Mortar (TRM)
16:20 - 16:40	M. Lavi, L. Nahum, A. Peled	Development of non-regular shaped lightweight structural concrete elements (beams) reinforced with carbon fabrics
16:40 - 17:00	P. Saba, T. Honorio, M.O. Ateeq, and F. Bonboudjema	Glass Fiber Reinforced Mortars: Crack Initiation and Propagation Study
17:00 - 17:10	Questions to speakers	
17:10	Break for the day	

Wednesday June 23

**All times are in Lyon Time - (6 Hours EST)*

Session 9 : Studies on TRC		
9:00 - 9:20	M. El Kadi, D. Hemelrijck, H. Rahier, and T. Tysmans	Influence of Discrete Spacers and Anchor Length in Long TRC Elements
9:20 - 9:40	Z. Djamai, A. Si Larbi, and F. Salvatore	A Modified Textile Reinforced Concrete with Phase Change Material
9:40 - 10:00	N. Ospitia, E. Tsangouri, J. Stiens, A. Pourkazemi and D. Aggelis	Elastic and Electromagnetic Wave Monitoring of Early Age TRC
10:00 - 10:20	N. Algourdin, Z. Mesticou and A. Si Larbi	Effect of Surface Treatments on Tensile Strength of Carbon and Basalt Fibers for TRC Applications
10:20 - 10:40	G. Cai, A. Si larbi, A. Ono, K. Ishibashi	An improved TRC: Preliminary study of tensile properties
10:40- 10:50	Questions to speakers	
10:50 - 11:00	Break	
Session 10 : Summary and Closure		
11:00 - 11:40	**Si Larbi and H. Nassif**: Summary, Thanks and Closure by the Chair **A.E. Naaman : Announcement Ferro-14 and IFS New President**	
11:40	Au revoir	

SUMMARY

Session 1
Ferrocement:
History and Progress

ART AND SCIENCE OF BUILDING IN CONCRETE: THE REINVENTION OF FERROCEMENT BY PIER LUIGI NERVI

Mario Alberto Chiorino, Cristiana Chiorino

*****American Concrete Institute and Emeritus Politecnico di Torino ** Pier Luigi Nervi Project Foundation, Brussels

SUMMARY: *Recognized as one of the greatest and most inventive structural engineers of the twentieth century, Pier Luigi Nervi (1891-1979) was part of a glorious period in structural architecture. His masterpieces are scattered the world over. Nikolaus Pevsner, the distinguished historian of architecture, described him as "the most brilliant artist in reinforced concrete of our time." Nervi shared the cultures of architects and engineers, operating at the intersection of art and the science and technology of building. He contributed significantly to create a real "poetry of concrete" reinventing ferricement.. It is not surprising that Nervi was nominated "Professor of Poetry" at Harvard, where he delivered the 1962 Charles Eliot Norton lectures titled "Aesthetics and Technology in Building."His influence is seen in recent works in Italy and worldwide.*

KEY WORDS: *Ferrocemento, Nervi, Italy, prefabrication, experimentatio*

1. INTRODUCTION

The diffusion of reinforced concrete in the early years of the twentieth century opened new horizons in the art of building and architecture. In Europe, the new technique had developed very rapidly thanks to the contribution of a few enlightened pioneers, builders, designers and researchers including Wayss and Koenen in Germany; Ritter and Mörsch in Switzerland; Hennebique, Coignet, de Tedesco and Considère in France; and Guidi and Canevazzi in Italy. Since these early beginnings, scientific and technical progress went hand in hand with a search for a new aesthetics.

Figure 1. *Pier Luigi Nervi (1891-1979): within Palazzo del Lavoro (Courtesy Archivio Storico Fiat, Turin)*

Pier Luigi Nervi (1891-1979) (Fig. 1) was one of the greatest representatives of the subsequent phase of maturation of the technique that lasted well into the second half of the twentieth century. Like many of his predecessors, he was at once designer, builder, researcher and creator of new construction methods. He was also professor and lecturer in universities around the world and author of books debating the conceptual and technological foundations of construction, with particular regard to concrete ([1], [2], [3]).

His use of the most advanced technical solutions was always accompanied both by the pursuit of formal elegance, and by close attention to the technical and economic aspects of the building process. Sharing the cultures of engineers and architects, Nervi operated at the very intersection between structure and architecture, and art and science of building. Architectural historian Nikolaus Pevsner described him in «A Master Builder», The New York Review of Books (3 march 1966) as "the most brilliant artist in reinforced concrete of our time". With his stunning masterworks scattered the world over, Nervi contributed to the creation of a golden age of what has become known as structuralism (Manfredo Tafuri, Francesco Dal Co, Modern architecture, translated from the Italian by Robert Erich Wolf, Publisher: New York : H. N. Abrams; 1st Edition edition, 1979)

In 2009, on the thirtieth anniversary of his death, a broad research and educational program was promoted with the intent of disseminating Nervi's cultural legacy and exploring the complexity of his extraordinary stature as a structural artist. The program culminated in the current international traveling exhibition "Pier Luigi Nervi-Architecture as Challenge" which highlights some of his most celebrated works. This article presents a synthesis of this comprehensive exploration of Nervi's figure and oeuvre (Olmo & Chiorino 2010).

2. EARLY CAREER AND WORKS

Pier Luigi Nervi graduated in civil engineering at the University of Bologna, Italy, in 1913 under the authoritative guidance of Silvio Canevazzi (1852-1918), one of the leading figures in Italy of the new technique of reinforced concrete, during a fertile period for scientific, technical and architectural debate. Like many of the pioneers who had preceded him, after an initial period of training in the technical office of a construction company, Nervi set up his own design and construction business in 1920. Nervi was to maintain this dual role of designer and builder throughout his life.

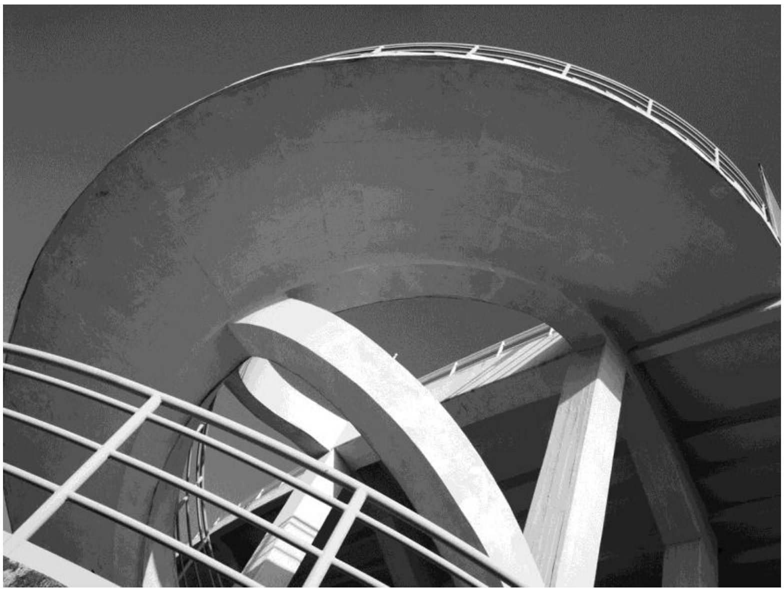

Figure 2. *Nervi's first great work: the Berta Stadium in Florence, 1930. (Photo Mario Carrieri courtesy Pier Luigi Nervi Project Association, Bruxelles)*

The stadium in Florence (1930, Fig. 2) was the first major work that attracted the attention of critics and the public, both in Italy and abroad. Besides its intrinsic beauty, characterized by the elegance and strong visual impact of the curved tapered corbels of the cantilevered roof and the spatial sculptural forms of the helicoidally warped stairs, Nervi won the competition on account of the estimated low cost of construction.

(a)

(b)

Figure 3. *Hangars in Orvieto, 1935 (a) and Orbetello, 1940 (b). (Courtesy Maxxi, Rome, Pier Luigi Nervi Archives)*

From 1935 to 1940, a series of large hangars was built for the Italian air force at Orvieto and Orbetello (Fig. 3). Nervi's designs were probably inspired by hangars and temporary exhibition halls constructed in steel or laminated wood using a network of intersecting geodetic frame elements (primarily in Germany: Junkers and Zollbau systems, respectively). Another likely influence was a new concept in aircraft design, based also on the use of intersecting geodetic aluminum alloy frame elements (e.g. in the Vickers Wellesley and Wellington aircrafts, designed by Barnes Wallis in the early 1930s). Nervi designed a daring geodetic roof with intersecting reinforced concrete arched ribs, which was dramatically simple in structural conception. The first group of hangars was built using traditional scaffolding and wooden forms for the concrete structure. Those that followed were built using prefabricated rib elements connected by cast-in-place reinforced concrete joints.

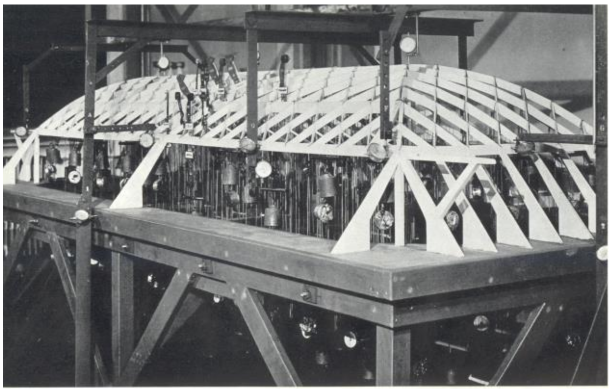

Figure 4. *Celluloid elastic models of the first and second series of hangars tested at the Model and Construction Testing Laboratory at the Politecnico di Milano (Courtesy CESI- ISMES Archives, Seriate, Bergamo)*

The use of prefabricated components would become a constant in Nervi's work as he sought to exploit and maximize the great compositional and structural freedoms offered by this technology. The hangars were also the first structures for which, in addition to static calculations, Nervi had recourse to tests on reduced scale models. The tests were performed by Guido Oberti (1907-2003) at the Politecnico di Milano, Italy, in the Model and Construction Testing Laboratory created by Arturo Danusso (1880-1968), using celluloid elastic models at a 1:30 scale (Fig. 4). Nervi would maintain this procedure for most of his later works.

3. THE REINVENTION OF FERROCEMENT

The technique of ferrocement had been originally developed by Jean Louis Lambot in 1846, at the very dawn of reinforced concrete, to produce a "ferciment" boat hull. The hull comprised a thin layer of concrete reinforced with a thick mesh of small diameter wires, and it exhibited remarkable ductility and resistance to cracking ([4]).

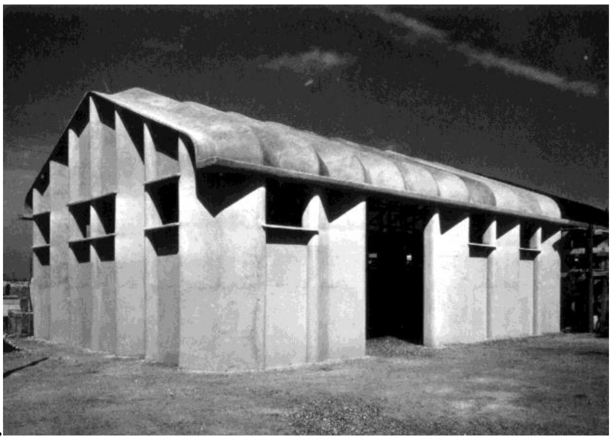

Figure 5. *Nervi reintroduced the use of ferrocement. Experimental warehouse in ferrocement, La Magliana, Rome, 1945 (Courtesy Maxxi, Rome, Pier Luigi Nervi Archives)*

After using it for an experimental warehouse at the site of his construction company at La Magliana, near Rome, Italy, and also for the hulls of small ships (Fig. 5a, b), Nervi made extensive and innovative use of ferrocement in his most daring projects. He is thus credited as the re-inventor of this technique. Nervi used ferrocement to mold prefabricated elements of various shapes. These prefabricated elements were then connected by cast-in-place concrete.

Figure 6. *Central hall (Hall B) of Turin Exhibition Complex, Turin, 1948. (Photo Mario Carrieri courtesy Pier Luigi Nervi Project Association, Bruxelles)*

Figure 7. *Sports Palace in Rome, P.L. Nervi with Marcello Piacentini, 1958-60 (Courtesy Pier Luigi Nervi Project Association, Bruxelles)*

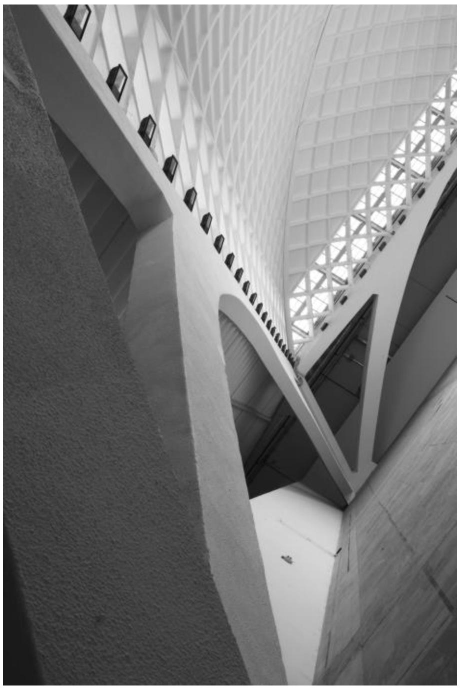

Figure 8. *Hall C of Turin Exhibition Complex, Turin, 1950 (Photo Mario Carrieri courtesy Pier Luigi Nervi Project Association, Bruxelles)*

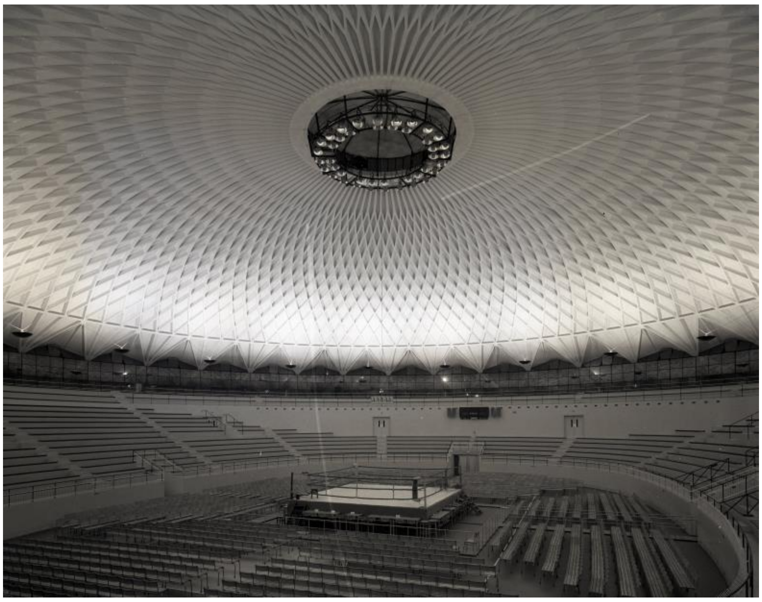

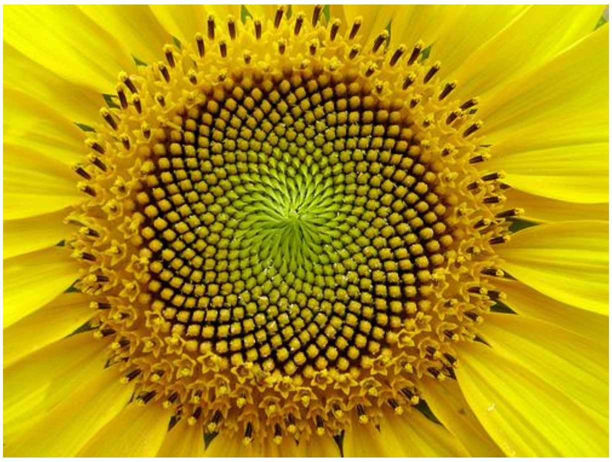

Figure 9. *The small Sports Palace in Rome, Italy, 1957 P.L. Nervi with Antonio Vitellozzi,. The elegant pattern of the concrete ribs seems to be inspired by the geometrical network of a sunflower core. (Photo Mario Carrieri courtesy Pier Luigi Nervi Project Association, Bruxelles)*

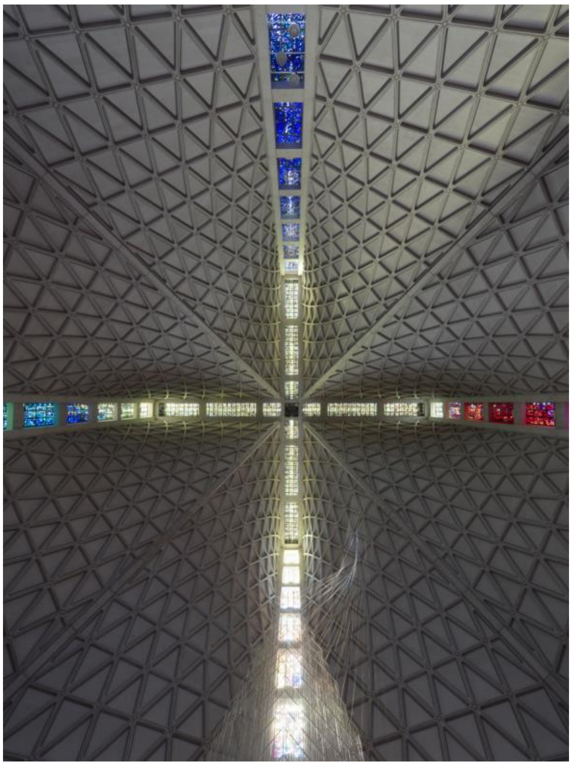

Figure 10. *St. Mary's Cathedral, San Francisco, CA, 1963-71, P.L. Nervi with Pietro Belluschi, McSweeney, Ryan & Leew and Leonard F. Robinson (structural engineer). (Photo Mario Carrieri courtesy Pier Luigi Nervi Project Association, Bruxelles)*

In his first important post-war work—the astonishing central hall (Hall B) of the Turin Exhibition Complex (1948, Fig. 6)—Nervi used ferrocement to make the precast undulating elements for the hall's magnificent, transparent, 94 m span barrel vault. The same type of undulating elements were used for the grandiose ribbed spherical cap dome, with a diameter of almost 100 m, of the large Sports Palace in Rome (1960, Fig. 7). For the 55 x 157 m dome of Hall C of the Turin Exhibition Complex (1950, Fig. 8), the precast ferrocement elements are 20 mm thick, diamond-shaped tiles that were assembled and then served as formwork for cast-in-place concrete on their upper surfaces and within the contact channels formed at the tile edges. The result is a particularly elegant mesh of reinforced intersecting ribs. The same pattern characterizes the structural fabric of the vaults and domes of some of Nervi's most famous later works: the Kursaal at Ostia (1950), the Ballroom at the Chianciano Spa

(1952), the small Sports Palace in Rome (1957, with Antonio Vitellozzi, Fig. 9). In all of these buildings, Nervi was responsible for both the design and construction.

This system came to be known as the “Nervi System” and would be applied by Nervi even in the United States. However, in reality the “Nervi System" was more a trademark than a real building system, since it ran into difficulties in contexts where labor and manufacturing were not as cheap as in postwar Italy: in the Leverone Field House and Thompson Arena at Dartmouth College in Hanover, New Hampshire (1962, with Campbell and Aldrich, 1976); the Norfolk Scope Arena in Norfolk, Virginia at the time, the largest dome in the world with its diameter of 135 m (1965-71, with Williams and Tazewell & Assoc.); and St. Mary’s Cathedral in San Francisco, California (1963-71, with Pietro Belluschi, Fig. 10). In this last work, the ferrocement tiles and the mesh of concrete ribs adapt to the elegant hyperbolic paraboloid surfaces of the dome, a signature feature of the city’s skyline.

In the Gatti Wool Mill (Rome, Italy, 1951), the precast tiles are used to build a flat floor. The design of the rib pattern on the ceiling is derived from the lines of the principal bending moments, again resulting in a particularly refined formal effect that is found in a number of Nervi’s subsequent projects.

4. LATER WORKS AND INTERNATIONAL RECOGNITION

Nervi’s first important work outside Italy was the UNESCO Headquarters in Paris, France (1953-58, in cooperation with Marcel Breuer and Bernard Zehrfuss). The principal architectural element of this building is the exposed concrete folded structure of the walls and roof. A series of other prestigious commissions followed. Besides those already mentioned in the previous section, the list includes: the George Washington Bridge Bus Terminal in New York City (1962); Montreal’s Victoria Square Tower, Canada, at the time the tallest reinforced concrete building (145 m) in the world (1961-66, with Luigi Moretti, Fig. 11); Australia Square and MLC Center Towers in Sydney (1964-72, with Harry Seidler); the hyperbolic paraboloid umbrella roofs for Newark International Airport, New Jersey (1971); the B.I.T. headquarters building in Geneva, Switzerland (1972); and the Italian Embassy in Brasilia, Brazil (1979).

In Italy, the most celebrated works of this later period include: the 135 m tall reinforced concrete Pirelli Tower in Milan (1955-59, with Arturo Danusso and Gio Ponti, Fig. 12); the facilities for the 1960 Rome Olympics, including, besides the two above-mentioned Sports Palaces, the Flaminio Stadium and the Corso Francia Viaduct; the Palazzo del Lavoro in Turin (1959-61, Fig. 13), with its geometrically fascinating columns featuring striped slanting surfaces covered by a steel umbrella-like structure (designed by Gino Covre); the Ponte Risorgimento in Verona (1963-68); and the Papal Audience Hall in the Vatican (with Antonio Nervi, 1963-71, Fig. 14). The latter project recalls themes developed twenty years earlier in the Turin

Exhibition Hall while enhancing them to create an imposing composition also characterized by the sculpturally highly effective shapes of the main supporting columns and of the ribbed ceilings of the proscenium.

Figure 11. *Victoria Square Tower, Montreal, Canada, 1961-66, P.L. Nervi with Luigi Moretti. (photo Mario A. Chiorino)*

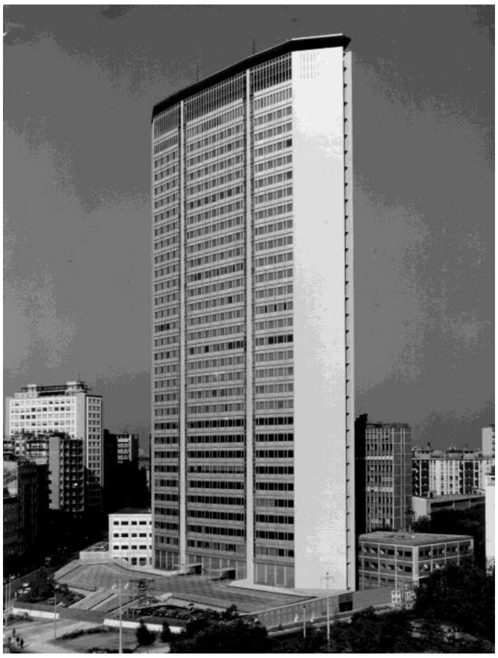

Figure 12. *Pirelli Tower in Milan, Italy, 1955-58, P.L. Nervi with Arturo Danusso and Gio Ponti. (Courtesy Pirelli Archives, Milan)*

Figure 13. *Palazzo del Lavoro in Turin, Italy. 1959-61, P.L. Nervi with Antonio Nervi and Gino Covre (Photo Mario Carrieri courtesy Pier Luigi Nervi Project Association, Bruxelles)*

Figure 14. *Papal Audience Hall, Vatican City, Rome, Italy, 1963-71, P.L. Nervi with Antonio Nervi. (Photo Mario Carrieri courtesy Pier Luigi Nervi Project Association, Bruxelles).*

5. EXPERIMENTATION

Experimentation, including scale models and full-scale prototypes and mock ups, continued to play a major role in Nervi's work. The scientific collaboration between Nervi and Oberti, initiated at the Laboratory of the Politecnico di Milano before the war, continued after 1950 within the new research laboratory of Istituto Sperimentale Modelli E Strutture (ISMES), founded by Danusso in Bergamo with the support of Italcementi, the leading Italian cement corporation.

Nervi and Oberti considered experimentation to be the best strategy to overcome the practical impossibility, at the time, of basing safety checks of complex constructions on adequately accurate and computationally feasible theoretical models ([1], [2]; [5], [6]). This strategy was also followed, not coincidentally, by other leading exponents of structural architecture in the twentieth century, including Eduardo Torroja, Franz Dischinger, Antoine Tedesko, Heinz Hossdorf, and Heinz Isler, to name a few. While the numerical modeling techniques that increasingly appeared in the late 1960s would have gradually opened new frontiers, it is fair to say that experimentation using models became, for Nervi and the above-mentioned protagonists, an extremely refined art form and an essential phase of the design path. Creating physical models, performing the tests and interpreting the results for the benefit of the design and structural assessment was an art form that required, almost in the same way as in real construction, the designer to be able to combine technological expertise and imagination - perhaps justifying Oberti's frequent citation of the adage attributed to Michelangelo by Vasari: "The most blessed monies that are spent by those who would build are on models."

One of the most complex models produced and tested within the ISMES facilities was of the reinforced concrete frame of the Pirelli Tower in Milan, Italy, modeled in 1955/56. The nearly 10 m tall, 1:15 scale model (Fig. 15a, b) was produced in micro-concrete of pumice-stone and Portland cement and tested beyond service conditions up to failure, after a series of tests in the dynamic field to check the effects of wind. Other important testing programs at ISMES included models of the Victoria Tower in Montreal (Fig. 15c) and St. Mary's Cathedral in San Francisco. In the latter case, a small-scale (1:100) model was used for the wind tunnel tests, two medium-scale (1:40 and 1:37) resin models were used for static and dynamic tests in the elastic field (with special attention to seismic response due to the building's location), and a large-scale (1:15) model constructed in micro-concrete was used for tests to failure under gravity loading (Fig. 16). It is of interest to note that the elastic tests for St. Mary's were accompanied by checks using numerical models based on early applications of elastic finite elements analysis, made by the U.S. engineering studio of Leonard Robinson, the firm responsible for the final design. Nervi's concrete towers in Sidney were tested in Australian laboratories and were the only two structures for which model testing was performed outside of ISMES.

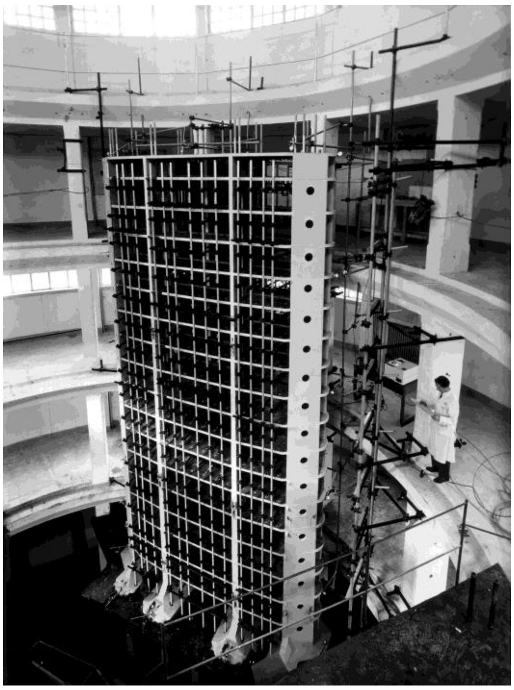

Figure 15. *Test models: micro-concrete large-scale model (1:15) used for tests to failure for the Pirelli Tower, Milan, Italy (Courtesy CESI- ISMES Archives, Seriate, Bergamo)*

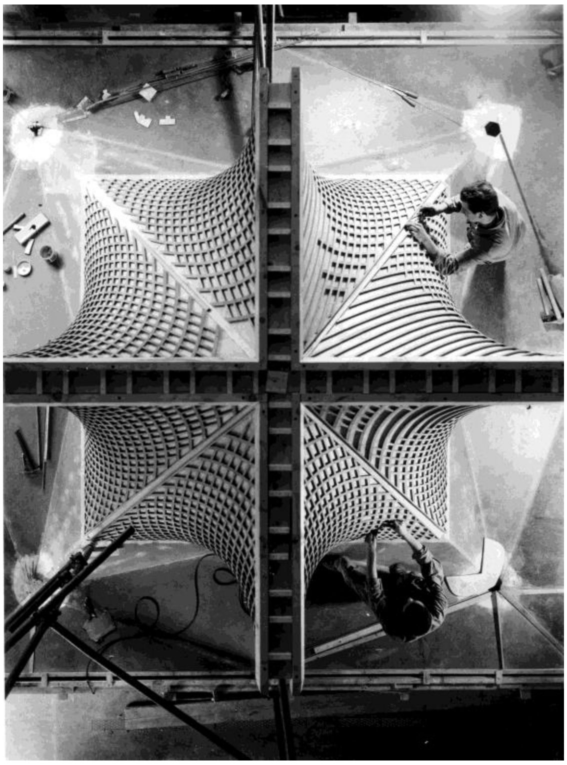

Figure 16. *St. Mary's Cathedral, San Francisco, CA micro-concrete model (1:15) following the ultimate limit state tests under gravity loading. (Courtesy CESI-ISMES Archives, Seriate, Bergamo).*

6. PHILOSOPHY OF STRUCTURES: ART AND SCIENCE OF BUILDING

When Nervi discusses the answer to the fundamental question Scienza o Arte del Costruire (the title of his most famous book Pier Luigi Nervi, Scienza o arte del costruire, Caratteristiche e possibilità del cemento armato, Edizioni della Bussola, Roma 1945) he undoubtedly emphasizes the priority of the intuitive moment in the conception of structural architecture, while acknowledging the importance of the mechanics of structural systems: "The conception of a structural system is a creative action only partly based on scientific data; static sensitivity entering in this process, although deriving from equilibrium and strength considerations, remains, in the same way as aesthetic sensitivity, an essentially personal aptitude." ([1])

This vision that was shared by Torroja, one of the other great masters of structural architecture of the twentieth century, who declared a few years later in Razón y Ser de los Tipos Estructurales, "The birth of a structural complex, the result of a creative process, the fusion of art and science, talent and research, imagination and sensibility, goes beyond the realm of pure logic to cross the arcane frontiers of inspiration.” ([7]).

Both Torroja and Nervi thus prioritize the conceptual phase and artistic inspiration in the design process. They pay homage to the remarkable gifts of intuition and static sensibility of the builders of the past who, without any access to analytical methods, had produced extraordinary works. In this respect Nervi states: “The great built works of the past, and among them the Gothic cathedrals in particular, express in their whole and in their details the superior intelligence, the almost wondrous static sensibility, and the hardly imaginable sum of experience and practical skill that they required from their designers and builders.” [2]. It is interesting, however, that both Nervi and Torroja at the same time are acutely focused on making their projects feasible in terms of construction. In the various phases of the construction process they appear, in fact, to belong entirely to the polytechnic tradition which, developed from the Enlightenment onwards, was responsible, in the nineteenth and twentieth centuries, for a marked division between the system of engineers and the world of architecture. [8].

As the entirety of his work, including his writings and educational message, demonstrates, Nervi is intent on solving the dilemma expressed in the apparent contraposition of the two terms in the title of his book through their interconnection: Art and Science. He resets the two terms in the sequence in which he considers them to be: as the two fundamental poles of his approach to construction. It is this approach that constitutes Nervi's fame. Within this vision, Nervi expressed the fear that the requirement to use analytical models (the main computational tool available at his time) for the reliability assessments of structures might limit a designer’s inventiveness. This struggle for design freedom - already auspicated in the early heroic years of development of reinforced concrete by Félix Cardellach in his Filosofía de las Estructuras Cardellach 1906 - was also the principal justification for Nervi’s keen interest for the experimental research on mechanical scale models discussed above.

At the same time, when, at the end of his career, Nervi was confronted with the new instruments of numerical modeling and computational mechanics in the design of St. Mary’s hypardome in San Francisco, he showed a vivid interest in the new horizons opened by these approaches. It is important to note that in Nervi’s philosophy, the original artistic concept for a structure needed to pass not only the fundamental mechanical and structural requirements,, but needed to make sense from the point of view of its construction: it had to meet technical and economical requirements. Like Félix Candela, who in those years was inspired by Nervi’s approach [10], Nervi is satisfied only when his design -conceived, as Torroja says, in the “arcane frontiers of inspiration”—is correct from both the technical and economical point of view. Costruire correttamente is, in fact, the title of Nervi's second famous book ([2]).

The true art of Nervi, and of the other eminent protagonists of structural architecture of the twentieth century that we have mentioned, is the ability to close the gap between art and technology to create spaces that border on poetry. (It is not by chance both Nervi and Candela were nominated Charles Eliot Norton professors at Harvard in the academic year 1961/62.) They do so without renouncing, in the conversion of the inspiration into a design and of the design into a construction, to the modus operandi of engineers, but rather emphasizing it with original and innovative contributions.

7. PIER LUIGI NERVI: ARCHITECTURE AS CHALLENGE. AN INTERNATIONAL RESEARCH AND EXHIBITION PROGRAM

A broad research-educational program on Nervi's figure and work started in 2009, on the thirtieth anniversary of his death, and it culminated in the international traveling exhibition: Pier Luigi Nervi - Architecture as Challenge. The program, promoted by a foundation, the Pier Luigi Nervi Project Association (PLN), has the scientific and financial support of a broad and international alliance of universities, cultural institutions, and industry sponsors. The exhibition is based on a wide display of drawings, pictures and refined scale models of Nervi's most celebrated works (Fig. 17). It started its successful tour in Brussels, Belgium, in 2010 and continues well into 2014. It is accompanied by a catalog assembling the results of the intense research program [11]; a reprint of Nervi's famous book, Aesthetics and Technology in Buildings, containing the text of his Norton Lectures at Harvard [3], will be available in 2014.This extended program of analysis and critical appraisal of Nervi, and the dissemination of his cultural legacy, are expected to offer a significant contribution to the present intense debate on the role of formal inventiveness in the design of structures and, in a broader perspective, to the dialogue between architecture and engineering. Advanced instruments for the computational analysis of structures and for structural morphogenesis and form-finding processes, seem to offer unlimited freedom to architects and engineers; to use the prophetic words of Cardellach, they promise "new and infinite structural forms which surely exist in that mysterious area from where the beam, the arch, the frame and the cantilever were laboriously extracted by the expert hand of mechanical visionaries." [9].

The sense of almightiness, or, inversely, of bewilderment that may derive from this apparently unconstrained freedom will certainly benefit of the possibilities offered by the deep critical exploration of the art and philosophy of some of the eminent protagonists of modern construction technologies. Pier Luigi Nervi is certainly one of the most outstanding figures in this group, and the recent research and exhibition program centered on his person and work are intended to also contribute to this debate.

Figure 17. *International Exhibition "Pier Luigi Nervi – Architecture as Challenge" in Turin Exhibition Hall, 2011 (Photo Davide Chemise)*

8. REFERENCES

[1] NERVI P.L., SCIENZA O ARTE DEL COSTRUIRE?, EDIZIONI DELLA BUSSOLA, ROME, ITALY, 1945.

[2] NERVI P.L., COSTRUIRE CORRETTAMENTE, ULRICO HOEPLI, MILAN 1955; ENGLISH EDITION: STRUCTURES, TRANSLATED BY GIUSEPPINA AND MARIO SALVADORI, 1956

[3] NERVI P.L., AESTHETICS AND TECHNOLOGY IN BUILDINGS, THE TWENTY-FIRST-CENTURY EDITION. ARCHITECTURAL VISIONS OF CONCRETE AND BEAUTY, CRISTIANA CHIORINO, ELISABETTA MARGIOTTA NERVI AND THOMAS LESLIE (EDS), UNIVERSITY OF ILLINOIS PRESS, CHICAGO, 2018

[4] PEMBERTON J. M., FERRO CEMENT - AN INSIGHT AND REVIEW - SO WHAT IS NEW?, IN A. E.NAAMAN (EDITOR), FERROCEMENT 6: LAMBOT SYMPOSIUM, "PROCEEDINGS OF THE SIXTH INTERNATIONAL SYMPOSIUM ON FERROCEMENT", UNIVERSITY OF MICHIGAN, ANN ARBOR, MI, JUNE, 1998, PP. 75-83.

[5] OBERTI G., THE DEVELOPMENT OF PHYSICAL MODELS IN THE DESIGN OF PLAIN AND REINFORCEDCONCRETE STRUCTURES, L'INDUSTRIA ITALIANA DEL CEMENTO, SPECIAL ISSUE DEVOTED TO "THE PROGRESS OF CONCRETE IN ITALY", 9/1980, PP. 659-689.

[6] Oberti G., "On the "Optimum Design" of Large Structures Using Physical Models," IABSE Periodica, 3/1985, pp.157-166.

[7] Torroja Miret, E., Razón y Ser de los Tipos Estructurales, Instituto Técnico de la Construcción y del Cemento, Madrid, Spain, 1957; English edition: Philosophy of

[8] Picon A., Architectes et ingénieurs au siècle des lumières, Parenthèses, Marseille, 1988; English edition: French Architects and Engineers in the Age of Enlightenment. Cambridge: Cambridge University Press, 1991

[9] Cardellach F., Filosofia de las estructuras: filiacion racional de las formas resistentes empleadas en la ingenieria y en la arquitectura historica y moderna: sintesis de sus procedimientos verificativos: origen, planteo y generalizacion de los principios estructurales: reflexiones conducentes a la obtencion de nuevas estructuras, Libreria de Augustin Bosch, Barcelona, 1910.

[10] Candela F., La obra de Pier Luigi Nervi, Cuadernos de Arquitectura, No. 15, Nov. 1964.

[11] Olmo C., and Chiorino C. (Editors), Pier Luigi Nervi: Architecture as Challenge, SilvanaEditoriale, Cinisello Balsamo, Italy, 2010.

[12] Structures, University of California Press, Los Angeles, 1958.

FERROCEMENT: A HISTORICAL PERSPECTIVE

Antoine E. Naaman[1]

[1]*University of Michigan, Ann Arbor, USA. antoinenaaman@yahoo.com*

SUMMARY: *A brief summary of milestones in the field of ferrocement since its birth is first presented. It identifies two main periods, one dormant period about a century long, and a subsequent slow revival period to date. The initial patent relationship between ferrocement and reinforced concrete is clarified. While progress has definitely been commendable at every level (materials, applications, construction methods, performance, ...), it is nevertheless hindered by the lack of a universally accepted building code dedicated specifically to ferrocement, and supported by a universally accepted authoritative umbrella organization such as ACI, fib, or Rilem. Because this critical need was not being fulfilled, the International Ferrocement Society was founded in 1991by a group of dedicated scholars and charged in priority with the most pressing goal to develop a building code. The Ferrocement Model Code was published in 2000 and while it represents a solid start it is still in need of acceptance by building inspectors worldwide. It is unfortunate that the lack of funding or endowed funding has been very detrimental to the full progress of ferrocement and its potential, and, as a result, has not served the branch of society that could most benefit from it, the public and more particularly its less fortunate component, such as amateur and self-help builders.*

KEY WORDS: *history, bending resistance, concrete, model code, iron wire, mesh, textile, uhpc*

1. INTRODUCTION

Thin reinforced cement-based composites such as ferrocement and TRC (textile reinforced concrete) form a special category within the broader family of reinforced concrete. Such composites can provide slender, light-weight, durable solutions in many structural applications and are often cost competitive with respect to their methods of production and material/structural properties. Their current applications cover both marine (boats, pontoons, docks) and terrestrial structures, as well as repair-rehabilitation for both types. Marine structures also cover floating structures such as floating houses on river banks or in areas prone to flooding. Terrestrial structures include mostly small containment structures (silos, water tanks, waste containment and treatment vessels), and structural and non-structural components for various types of construction (housing, school facilities, agricultural structures, and water channels). A limited number of larger size structures using ferrocement have been built and the trend is increasing but, unfortunately, it is constrained by legal construction issues (mostly because of a lack of a widely accepted building code). Indeed, while there is a building code for ferrocement developed by the International Ferrocement Society [3], its use is limited by the fact that it is not yet adopted and sponsored by large worldwide organizations such as ACI (the American Concrete Institute), fib, or Rilem.

2. BRIEF HISTORY OF FERROCEMENT

In 1824, manufactured Portland cement was invented by *Joseph Apsdin* (England) and became widely available on the market for various applications; at the time, iron wires with some ductility, in the range of 1 mm to 5 mm in diameter, and fencing nets, were also available.

While natural cementitious pozzolanic materials were used in construction in the form of mortar since Roman times, and while iron has been used since the Iron Age, the idea of combining them to develop a self-contained (composite) construction material came only in the mid 19th century. Indeed in 1848-1849 *Joseph Louis Lambot*, a Frenchman, built two small ferrocement row-boats using iron wires arranged into a net like a flexible woven mat to form a skeleton, then added a fencing wire net, and then plastered the resulting structure with a cement mortar. The boats were respectively about 3.6 m and 3 m long, 1.3 m wide and with a shell about 38 mm thick. This makes ferrocement truly the first invention of reinforced concrete, all but on a smaller scale.

The initial definition of ferrocement can be drawn from the French patent application submitted by *Lambot* in 1852. The patent for "fer-ciment," which translates into "iron-cement," contained the following description [5]:

> *My invention shows a new product which helps to replace timber where it is endangered by wetness, as in wood flooring, water containers, plant pots etc... . The new substance consists of a metal net of wire or sticks which are connected or formed like a flexible woven mat. I give this net a form which looks in the best possible way, similar to the articles I want to create. Then I put in hydraulic cement or similar bitumen tar or mix, to fill up the joints.*

Lambot disclosed his patent at the Paris exhibition in 1855 by showing one of his boats. The first boat is now at the Brignoles museum in France. *Lambot* also used ferrocement to build large flower pots and other horticultural objects.

2.1 The Beginning of Ferrocement and Reinforced Concrete

Working independently of *Lambot*, it seems that *Joseph Monier*, a gardener, started as early as 1849 building for the city of Paris, France, large flower pots and garden tubs made out of cement and embedded iron mesh. *Monier* kept improving his technique with time. Much later, starting in 1867, he took a number of patents for iron-reinforced concrete troughs, pipes, basins, applicable to horticulture and, eventually leading to beams, slabs, and bridges. One of *Monier*'s key contributions was his inquiry and understanding that concrete is weak in tension and that the tension region within that concrete is the preferential place where iron rods should be placed.

In 1852, about 3 years after *Lambot* and *Monier*, *Francois Coignet*, a French Industrialist, started experimenting with the idea of using iron rods in bulk concrete. As a publicity stunt he built in 1953 in St. Denis's northern suburb of Paris, a three-story house whose structure was made entirely out of concrete and iron bars. He called his material "beton arme" in French, which means literally "concrete reinforced" ; although the design did not follow the principles of modern "reinforced concrete", compared to *Lambot*'s and *Monier*'s inventions, his can be considered the first application of reinforced concrete in a large structure. In 1998, *Coignet*'s house, still standing, was classed as world patrimony and has become a historical monument. Starting in 1856, *Coignet* took a number of patents and built several large structures using reinforced concrete still standing today, among which the "aqueduct de la Vanne" (1867 to 1874) near Paris, and the lighthouse of Port Said in Egypt. He became famous in the engineering-building profession.

In the history section of many books on reinforced concrete, often the name of either *Lambot*, *Monier* or *Coignet* is mentioned as the first inventor of reinforced concrete. However, based on facts, *Lambot* developed the first application on a small scale (cement mortar with iron wire reinforcement), but both *Coignet* and *Monier* (in that order) scaled the application up to what is reinforced concrete, today the most used construction material in the world.

An excellent review of the history of ferrocement by *J.E. Morgan and R.G. Morgan* can be found in the proceedings of Ferrocement 6, the Sixth International Symposium on Ferrocement, dedicated to *Lambot* [4]. They report in particular that, in 1854, *William Wilkinson*, a builder in New Castle (UK), took a patent for embedding in floors or beams of concrete a network of flat iron bars; this is another possible example of the earliest origins of modern reinforced concrete.

The technology of the second part of the 19th century could not accommodate the efficient and cost effective production of steel wire meshes, and small diameter wires were much more expensive than larger diameter rods. Therefore, larger diameter iron or steel rods were increasingly used, leading to a shift in interest by the engineering profession from ferrocement to standard reinforced concrete construction. Thereafter, reinforced concrete shadowed ferrocement and became the material of choice for construction worldwide.

2.2 First 100 Years in the History of Ferrocement: Dormant Period

Following the realization that the idea of "ferrocement" can be expanded on a much larger scale leading to reinforced concrete, the development of ferrocement slowed down considerably. Some milestones are worth mentioning (Fig. 1).

In 1887 a Dutch man, Mr. *Boon*, built a small craft of ferrocement, the *Zeemeuw* (or seagull) and several barges of reinforced mortar to carry ashes and refuse on water canals. The Zeemeuw was reported to be still floating in a pond at the Amsterdam zoo in 1968. It is currently displayed in the lounge of the Vereniging Nederlands Cement Industries' office in Amsterdam. Similarly in Italy, *Gabellini* (1996) built a ferrocement boat and promoted the use of ferrocement on a wider scale **[4].**

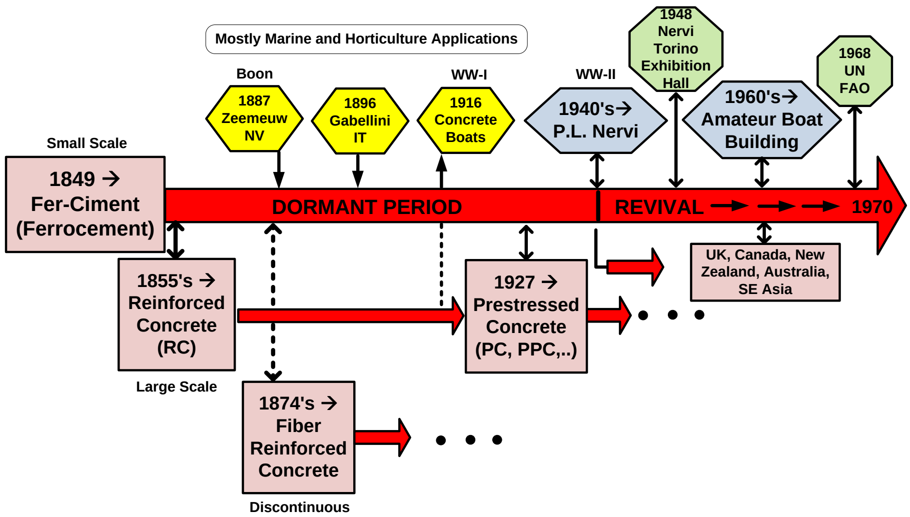

Figure 1. Some milestones during the development of Ferrocement until 1970.

Interest in ferrocement was still slow but steady. During World War I (1914-1918), seemingly inspired by ferrocement applications, relatively large ships and barges were built with reinforced concrete, and this was again attempted during World War II (1939-1945) due to shortages of materials, particularly steel. Such applications were not successful in their function and, by today's standards, can mostly be described as failures. However, because the idea of concrete boats was primarily associated with ferrocement, such failures did not help the cause of ferrocement. In effect, ferrocement was almost forgotten and all activities focused on the full development of reinforced and prestressed concrete with related codes, standards, guidelines, how-to guides, etc... worldwide.

2.3 Revival Period and Modern Developments: 1940's – 2020's

The right section of Fig. 1 illustrates the first part of what could be described as the beginning of the revival of ferrocement. In the early 1940's, *Pier Luigi Nervi*, an Italian engineer-architect, revived the original concept of "ferrocement" by proposing that ferrocement be utilized to build fishing boats **[11].** He pointed out that the distribution of reinforcing meshes in concrete produces a material with approximately homogeneous mechanical properties, capable of resisting high impacts. Following some preliminary tests on slabs, he showed that ferrocement possesses exceptional elasticity, flexibility, strength, and resistance to cracking. In 1943 ferrocement received acceptance by the Italian Navy. *Nervi* demonstrated his pioneering work by using ferrocement in several architectural applications, such as a storage warehouse and the roof of the main exhibition hall in Turin (1948). Most of these structures are still standing today. Shortly after the Second World War, *Nervi* demonstrated further the potential of ferrocement by building a 165 ton motor-sailor *Irene* using a ferrocement hull of thickness 35 mm, which is slightly less than that of a wood hull. The *Irene* proved entirely satisfactory. The boats and structures built by *Nervi* were appreciated only a couple of decades later, time at which the durability and serviceability of ferrocement could be ascertained by the engineering profession. Today the *Pier Luigi Nervi Organization* **[13]** aims to work at preserving most of these structures and providing documentation about their history and construction. Detailed information can be found in several reports and publications such as by *Olmo* and *Chiorino* **[12, 2].** Also, at time of this writing, a group of researchers at Politecnico Torino is involved in a broad research project to evaluate and rehabilitate several of *Nervi*'s still standing large structures with particular attention to mitigating corrosion and improving seismic resistance. [see paper by *R. Ceravolo* in these proceedings].

Figure 2 describes some milestones in the development of ferrocement over about five decades starting in 1970, a period considered part of its modern revival. Likely because of *Nervi*'s contributions (Fig. 1), ferrocement achieved wide acceptance in the early 1960's for boat building of moderate sizes in the United Kingdom, New Zealand, Canada and Australia. In 1968, the Fisheries Department of the Food and Agriculture Organization (FAO) of the United Nations started ferrocement boat building projects in Asia, Africa, and Latin America. Other countries followed, including the Soviet Union, China, and several countries in South-East Asia. In

1972, the US National Academy of Science formed a panel to report on the application of ferrocement in developing countries [**10**]. One of the recommendations of the panel was to establish a worldwide center to collect, process, and disseminate information on ferrocement. Subsequently, in 1976, the International Ferrocement Information Center (IFIC) was established at the Asian Institute of Technology (AIT) in Bangkok, Thailand. In 1975, the American Concrete Institute formed Committee 549, Ferrocement still active today under the name Thin Reinforced Cementitious Products and Ferrocement. In 1991, the International Ferrocement Society (IFS) was established (with headquarters at AIT in Bangkok). It is still active today with a US location (www.Ferrocement-IFS.com).

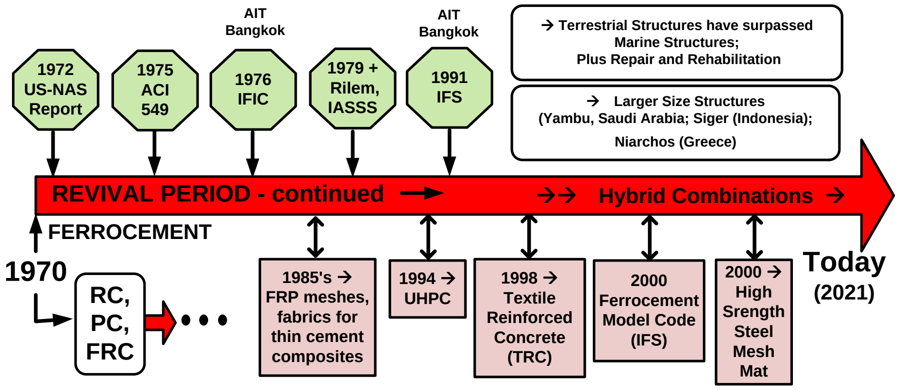

Figure 2. Milestones during the revival period of ferrocement up to date.

Today ferrocement is widely accepted and utilized. Technical information (reports, documents, guides) on ferrocement can be obtained from the American Concrete Institute, RILEM, IASSS, IFS and many ferrocement national centers, such as in India and Brazil. IFS attempts to act as a repository of all information related to ferrocement, including research, applications, guidelines, codes and other. It also organizes symposia, seminars and courses where the science and technology of ferrocement are taught.

3. ACI DEFINITION OF FERROCEMENT

The following definition of ferrocement was given by ACI Committee 549 in a state-of-the-art report on ferrocement (ACI 549R) first published in 1980 and still active (updated) at time of this writing **[1]:**

> *Ferrocement is a type of thin wall reinforced concrete commonly constructed of hydraulic cement mortar reinforced with closely spaced layers of continuous*

and relatively small size wire mesh. The mesh may be made of metallic or other suitable materials.

This definition, while quite general, is surprisingly close to the initial definition of ferrocement described by *Lambot* (see Section 2).

Based on past experience and advances in ferrocement, the author suggested adding the following two short sentences to the ACI definition **[5]**:

The fineness of the mortar matrix and its composition should be compatible with the mesh and armature systems it is meant to encapsulate. The matrix may contain discontinuous fibers.

Note that the ACI definition of ferrocement encompasses the use of non-metallic reinforcements and thus also covers textile reinforced concrete (TRC). However, it is generally believed that the two systems are sufficiently different (such as in their mechanics, bond, modeling, and other compatibility issues) to warrant different approaches **[6, 8]**, but they are also still part of the same family.

4. EVOLUTION AND PROGRESS

In prior publications **[7, 8, 9]** the author had summarized key advancements in the field of ferrocement since its modern development in the1960's. At that time a shift took place whereas ferrocement, which was seen then as a marine material for amateur boat building evolved into a construction material for terrestrial applications as well, particularly starting with small scale agricultural structures. Below is a brief summary of some key issues discussed**.**

1. **Evolution in Cement Matrix**. Here the most notable progress relates to changes in the composition and workability of the cement mortar matrix as modified by various additives or agents; also, its compressive strength which was commonly in the range of 15 to 30 MPa, can today exceed 200 MPa in the case of UHPC (ultra high performance concrete). Furthermore, with UHPC like matrices, the fineness of the matrix and is flow-ability can be ideal in ferrocement mold-cast applications and for excellent surface finish. This could be an expanding application in the future.
2. **Evolution in Reinforcemen**t. Here progress has been quite impressive on several fronts. Initially the reinforcement consisted mostly of chicken wire mesh (also called hexagonal mesh or aviary mesh) made with relatively low tensile strength steel wire (about 300 MPa); it evolved into stronger forms of square woven or welded meshes and more cost-effective ones such as expanded metal mesh. Today the choices are many and include the use of very high strength steel wires or stands (exceeding 2000 MPa) in mat formats, 3D steel meshes (limited commercial availability), 2D or 3D textiles with non-metallic

reinforcements, and hybrid combinations of both steel and polymeric reinforcements with the possible addition of discontinuous fibers.

3. **Evolution in Hybrid Combinations.** These include hybrid combinations of both steel and FRP reinforcements with the possible addition of discontinuous fibers, and the whole spectrum of cementitious matrices including normal strength, lightweight, very-lightweight, and ultra-high performance.
4. **Evolution in Applications.** The most noticeable progress here relates to a significant shift from marine applications to terrestrial applications, particularly at first in small size agricultural structures such as grain silos, water tanks, and housing units. Today we can cite examples of large scale applications such as the roof of the *Siger* monument in Lampung, Indonesia, the roof of the Yambu factory entrance in Saudi Arabia, and the roof of the *Stavros Niarchos* Foundation Cultural Center in Athens, Greece. Moreover, ferrocement boats, barges and tankers of up to 40 meters in length have been built thus significantly expanding the range in marine applications.
5. **Evolution in Mechanical Performance.** Bending resistance in ferrocement plates increased from about 3 MPa per 1% total volume of hexagonal steel wire mesh reinforcement to 24 MPa per 1% total volume of reinforcement consisting of very high strength steel mat. For these numbers the bending resistance is equal for positive or negative moment and for the *X* or *Y* directions. As a result the cost-performance ratio has also improved (decreased) significantly. In conventional ferrocement with conventional square steel wire mesh, a modulus of rupture of about 50 MPa can be achieved with 7% total reinforcement by volume **[5].** A recent investigation has shown that with an ultra-high performance cement matrix and very high strength steel strands in a mat format, a modulus of rupture close to 230 MPa can be achieved; the reinforcement consisted of 6.27% by volume of steel mat and 3.5% by volume of micro steel fibers **[14].** Note that for ferrocement composites with uniformly distributed reinforcement, the direct tensile strength can be assumed equal to about one third the bending resistance.
6. **Evolution in Equipment and Construction Methods.** Here the evolution has been modest and much less noticeable than in other areas. Most applications of ferrocement involve hand trowel-ling over reinforcement armature but the introduction of super-plasticizers and the use of small particles such as fly ash and fine sand allows ferrocement elements to be cast in molds (as in typical reinforced concrete) while guaranteeing penetration of the mesh system by the matrix. This is especially true if a UHPC type matrix is used. However, the most important piece of equipment needed for everyday ferrocement and for both contractors and the amateur builder is a mechanical mesh tying instrument; while rebar tying machines exist for reinforced concrete, they have not been tailored and optimized for use with wire meshes where the opening between wires is relatively very small. It is believed that the development of such instrument can cut the cost of labor in ferrocement structures by half. Since generally labor accounts for more than half of total

cost, such an improvement will have an enormous impact on ferrocement competitiveness.

7. **Evolution in Guidelines and Code - ACI**. Here progress has been slow and the subject is in dire need of a serious effort. Committee 549 of the American Concrete Institute developed two widely used reports, one titled "State-of-the-Art Report on Ferrocement," initially in 1982 and a modified version in 1997 then updated in 2018 [**1**], and the other one titled "Guide for the Design, Construction and Repair of Ferrocement," initially in 1988 and revised versions in 1993 and 2018. The International Ferrocement Society (IFS) published a Ferrocement Model Code in 2000 [3]. When asked, many builders of ferrocement structures mention that they follow some local reinforced concrete code, but adapt it to ferrocement requirements using engineering judgment and past experience; often small structures (such as grain silo, water tank, or small house) are not considered critical and pass local building inspection reviews; however, larger structures are seriously penalized by the lack of a dedicated code approved by a prestigious widely recognized organization such as ACI. The author strongly believes that the development by ACI of a code specifically devoted to ferrocement (or its stamp on an existing code such as the IFS Model Code) would spur not only a large growth in ferrocement use but in new types of applications as well.

Other progress areas related to modeling, technical and professional activities, education, people training, and the like are discussed in [9].

5. CONCLUDING REMARKS

None of the recognized advantages of ferrocement have changed since the onset of its modern development in the 1960's, while both its cost-performance and mechanical effectiveness have improved with the introduction of new materials and systems. It seems that the main deterrent to its progress in practice remains the establishment of a widely accepted and updated building code for its design and construction. Amateur builders and self-help practitioners will continue to use ferrocement in small scale applications, but opportunities for all other applications are hindered by the absence of such a code. Engineers, architects and designer may not necessarily need a code to build a sound ferrocement structure, but building inspectors and licensing authorities need one, representing a major legal challenge. It is unfortunate that the lack of funding or endowed funding has been very detrimental to the full progress of ferrocement and its potential, and, as a result, has not served the branch of society that could most benefit from it, the public and more particularly its less fortunate components including amateur and self-help builders. In order to help, IFS has developed its own Ferrocement Model Code [3]; however, in order to receive wide acceptance, the adoption of such code (or the development of a new one) by a larger umbrella organization such as ACI, fib, or Rilem will be necessary and should bring leap benefits. This seems to be the best route to follow for future progress.

6. REFERENCES

[1] ACI COMMITTEE 549, "State-of-the-Art Report on Ferrocement." *Concrete International*, Vol. 4, No. 8, Aug. 1982, pp. 13-38. Reinstated as ACI 549-R97, in 1997, and 2018 in *Manual of Concrete Practice,* American Concrete Institute, Farmington Hills, Michigan, 26 pages.

[2] CHIORINO, M., "Art and Science of Building Concrete: The Work of Pier Luigi Nervi", *Concrete International*, American Concrete Institute, March 2012, pp. 33-40.

[3] IFS COMMITTEE 10-01, "*Ferrocement Model Code*", International Ferrocement Society, Asian Institute of Technology, Bangkok, Thailand, 2001, 95 pages. (IFS: www.ferrocement-ifs.com).

[4] MORGAN, J.E., & MORGAN, R., "The Armature that Made History: the Boats of Joseph Louis Lambot", in *Ferrocement 6: Lambot Symposium*." Proceedings of the Sixth International Symposium on Ferrocement, Edited by A.E. Naaman, University of Michigan, Ann Arbor, 1998, 699 pages. (available from www.ferrocement-ifs.com).

[5] NAAMAN, A.E., "*Ferrocement and Laminated Cementitious Composites,"* Techno Press 3000, USA, 2000, ISBN0-9674939-0-0, 370 pages. (www.technopress3000.com or on Amazon).

[6] NAAMAN, A.E., "Thin Textile Reinforced Cement Composites: Competitive Status and Research Directions" in Proceedings 2nd *International Conference on Textile Reinforced Concrete*, Aachen, Germany, Sep. 2010, Rilem Pro. 75, Edited by W. Brameshuber, pp. 3-22.

[7] NAAMAN, A.E., "Evolution in ferrocement and Thin Cementitious Composites," in *Arabian Journal of Science and Engineering*, King Saud University of Petroleum and Minerals, Saudi Arabia, 2012, pp. 1-19, Springer No.: DOI 10.1007/s13369-01200187-4; ISSN 1319-8025. See also updated version in the Proceedings of Frrocement 12.

[8] NAAMAN, A.E., "Ferrocement: Progress Review and Most Critical Need for the Near Future", Proceedings of *International Symposium Ferrocement-11 and ICTRC-3*, Aachen, Germany, Rilem PRO 98, Edited by W. Brameshuber, June 2015, pp. 9-14.

[9] NAAMAN, A.E., "Thin TRC Products: Status, Outlook, and Future Directions," Chapter 18 (pp. 413-439) in "*Textile Fiber Composites in Civil Engineering*," Edited by T.C. Triantafillou, Woodhead Publishing Series in Civil and Structural Engineering, No. 60, an imprint of Elsevier, UK, ISBN: 978-1-78242-446-8, 2016, 452 pages.

[10] NATIONAL ACADEMY OF SCIENCES, "*Ferrocement: Applications in Developing Countries."* Report by the Ad Hoc Panel of the Advisory Committee on Technological Innovations, Board of Science and Technology for International Development, Washington, D.C., USA, 1973, 90 pages.

[11] NERVI, P.L., "Ferrocement: Its Characteristics and Potentialities," Library Translation No. 60, Cement and Concrete Association, London, July, 1956, 17 pages.

[12] OLMO, C., & CHIORINO, C., Editors, *"Pier Luigi Nervi: Architecture as Challenge*," Silvana Editoriale, Cinisello Balsamo, Italy, 2010, 240 pp.

[13] PIER LUIGI NERVI ORGANIZATION. www.pierluiginervi.org

[14] WILLE, K., & NAAMAN, A.E., "Preliminary Investigation on Ultra-High Performance Ferrocement," in Proceedings of 10th International Symposium on Ferrocement and Thin Reinforced Cement Composites, La Havana, Cuba, Edited by H. Wainstock Rivas, L. Prada Seoane, and I. Randa Castro, ISBN: 978-959-247-098-9, October 2012, pp. 251-260.

FERROCEMENT: AN APPROPRIATE MATERIAL FOR UNIVERSITY PROJECT WORK

Paul Nedwell[1]

[1]*Paul Nedwell (University of Manchester {retired}, Department of Mechanical, Aerospace and Civil Engineering, The University of Manchester, Oxford Rd, Manchester, M13 9PL, UK, paul.nedwell@manchester.ac.uk, pnedwell@gmail.com)*

SUMMARY: *This paper examines the way in which the various properties of ferrocement may be used to reinforce theory and practice in undergraduate University students when used during project work*

Starting with a background investigation of historical research and then moving forward to experimental planning, specimen fabrication, testing, results processing and presentation Ferrocement is demonstrated to be highly effective in informing and supporting many areas of civil and materials engineering teaching and in acting as a vehicle to enhance study methods and practical skills..

.

KEY WORDS: *Ferrocement, Research, Material Properties, UG Teaching*

1. INTRODUCTION

Although work at undergraduate level is rarely published, it is sometimes used by academic supervisors to provide preliminary investigation in a topic of interest which may lead to deeper study at a higher level.

Ferrocement is well-suited to undergraduate investigation : it provides significant challenges at various levels of complexity including experimental planning, specimen preparation and data analysis all of which enhance the learning experience of students as they progress through the project.

2. SELECTION

The first choice that needs to be made is the topic of research. Ferrocement provides a number of different options from basic material properties of the individual components through to design challenges using the material and its derivatives. If good laboratory facilities are available, then a rigorous experimental programme may be undertaken. If not, then a design project may be more appropriate. Individual supervisors will usually have their own specific areas of expertise and may have individual items of specialist equipment or knowledge bases that may benefit a student. At Manchester there was access to a particularly strong research group who specialised in corrosion. “Durability of Ferrocement” was thus able to become a speciality, - though this was more suited to more in-depth appropriate to Masters and PhD level research.

3. BACKGROUND INFORMATION

At the outset of a project there are challenges with respect to gathering background information. This has been considerably eased in the last 30 years, particularly with the publication of Naaman’s textbook (2000) [1] and the development of multiple on line resources. Despite these however, sources remain relatively sparse and the first choice a student must make is whether a particular piece of information is relevant and then judge whether it is credible and reliable. The recent further development of the International Ferrocement Society (IFS) website [2] also makes, particularly Journal and Proceedings, texts more widely available. However, a good deal of the reporting of early work was anecdotal and much detail was missing, especially in terms of design criteria. There is scope, however, for further reading in areas associated with a particular study, particularly for a design exercise where environmental issues may need to be considered.

3. MATERIALS

At its simplest ferrocement is mesh, sand, cement and water. From a teaching point of view it provides a range of scenarios that a student can investigate to demonstrate the skills required from a competent engineer. Unlike reinforced concrete, ferrocement may be produced on a scale more in keeping with an undergraduate teaching laboratory. This makes it a readily accessible field of study for Undergraduate students.

The welded wire mesh serves as a salutory lesson to young engineers regarding the performance of constituent materials and the thought processes required when considering their use.

From a design point of view it is obviously important to know the characteristics of the material : Young's modulus, yield strength and ultimate strength. However the mesh available and used is not a structural grade and therefore does not come with certification. The student is therefore faced with obtaining this information from tests, but which ones ? The obvious first place to look is in the standards. A University Library usually has access to all British Standards on line so this introduces the student to the concept of database searching. There is, however, no specific standard for Ferrocement reinforcement. By evaluating different standards a student is able to choose the one most closely aligned with the materials they are working with and their intended use. However the student needs to be aware that Standards change with time so they must ensure the correct version is being referred to. In addition there may be other standards, for example ASTM, DIN or BIS, that have been used in work reported from other countries. Another route may be to try to repeat, or extend, work already carried out and reported.

Fig 1 – Individual Wire strand tensile test using Instron servo hydraulic machine

Once a suitable test regime has been established it is then necessary to produce specimens. How many to take and in what form? Usually the standard will dictate this in order to obtain a statistically significant average or range of values. This must be done for each direction of mesh as the production process involves the pulling of transverse wires across the longitudinal ones prior to welding and if the wire has been strain hardened during the manufacturing process then the results, particularly those for modulus, will be different for longitudinal and transverse wires. A further consideration at this stage may be whether the number of individual strands to be tested will make a difference. Is a test on a single strand suitable (Fig 1) or should multiple strands be used ?

So, by taking the example of the decision to use a single particular reinforcing material, the student may learn to consider all possibilities and derive a thinking process which will lead them to select a testing protocol which will meet their needs.

Once the mesh was encapsulated into a tensile specimen novel methods of measuring crack widths in ferrocement were tried and subsequently reported [3].

Once the basic materials have been understood there is scope for more extended work with additives and admixtures. These range from rheology (Fig 2) and strength modifiers through to air entrainment agents and water-proofers. When a new material emerges, a student project can provide the means to carry out initial investigations and to gain a preliminary understanding of potential. One such case in Manchester was the discovery of Graphene which was subsequently incorporated into a number of undergraduate projects to assess its suitability in a ferrocement matrix.. Recent projects (2020/21) include the effect of graphene on compressive, tensile and flexural strengths of portland cement paste as well as its effect on electrical and thermal conductivity and water permeability

Fig 2 – Investigating the difference between sprayed (left) and injected (right) mortar

4. SPECIMEN MANUFACTURE

Many students more recently lack the practical skills of their forebears. Production of risk assessments for practical work introduce the student to thinking about the possible dangers associated with their specimen preparation. Cut mesh handling, particularly, may be a hazardous undertaking and there are also issues involved in using cement based matrices.

Ferrocement also provides opportunity to study basic structural geometries. The similarities and differences in shape between I, T and box sections may be readily created using ferrocement and the resultant performance investigated. See figs 3 & 4

More advanced composites to simulate the use of ferrocement as permanent formwork have also been produced.

Here the student is again challenged to select the information required for analysis from any larger scale test. Standard equipment is available for most measuring situations however the student must select the most appropriate sensor In addition a data acquisition methodology must be selected that is commensurate with the speed of the test and the amount of data being recorded. An impact test obviously requires a different approach to a creep test

Fig 3 Composite slab box section

Fig 4 Ferrocement I Beam

5. SPECIMEN TESTING

A wide variety of testing has been carried out over the years ranging from simple small plate bending, through box and I beams either within a standard test machine or using servo controlled jacks attached to a hydraulic ring main. To investigating the effects of high temperature a loaded ferrocement plate was used as the lid of a kiln and the temperature increased to failure.

Each of these carries its own educational benefit as the student has to plan the experimental programme, provide a full method statement and risk assessment then gather the data and present it, as discussed in the next section.

There is also scope for more novel investigation. One such project, illustrated in Fig 5, involved an investigation of the possibility of using portable X-ray equipment to detect voids. The results of this were reported in Bangkok in 2006 [4]

Fig 5 X-ray testing of ferrocement

6. ANALYSIS AND PRESENTATION OF RESULTS

Once experimental work has been completed the student is required to analyse their results in a coherent and reasoned fashion and assemble them in a form appropriate to the medium of presentation. At Manchester all students have had to present a poster, accompanied by a verbal presentation, as well as providing a written report. At the presentation some small visual aids are permitted. The scale of ferrocement samples readily allows this.

Both analysis and presentation provide opportunities for acquiring communication skills which constitute an important aspect of a students future career.

Manipulation of data to introduce a zero point or to provide a dimensionless figure for comparative purposes needs to be carried out as does the graphical representation of information. The poster poses separate challenges and requires a different approach to the written report, space is limited and it may be necessary to plot more than one graph on the same axes. For the final written submission discussion of the results may be accompanied by selected graphs that illustrate average or typical behaviour. All other results are then provided in appendices.

7. DESIGN

The scope for design incorporates both methods and applications. Methods may be hand- or computer- generated, empirical or following design philosophies and codes together with any combination or comparison between them. These allow the student to evaluate different methods of design and compare their ease of use and apparent accuracy.

Applications may be as diverse as the imagination of the supervisor or student. Solutions to environmental problems using ferrocement are particularly interesting. Examples of past projects at Manchester include design of a flat pack ferrocement emergency shelter capable of being air lifted into a region of need, a flood resistant house which, though fixed in location, could "float", the base for a deep sea wind turbine which would be more corrosion resistant than existing steel ones (Fig 6), a volute casing to a shore based wave power generator and a shaped roof to an external wave tank area of the University (Fig 7).

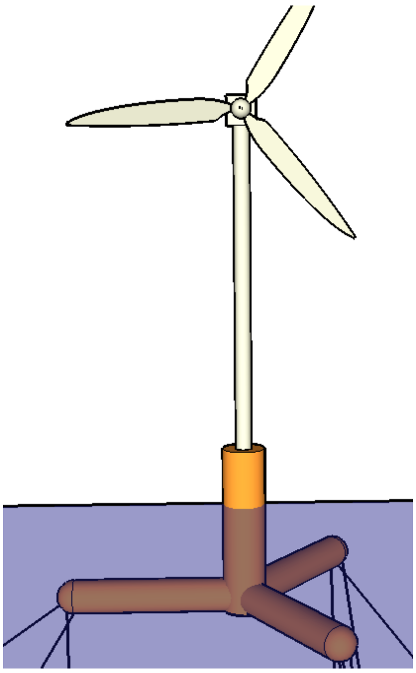

Fig 6 Offshore wind turbine base

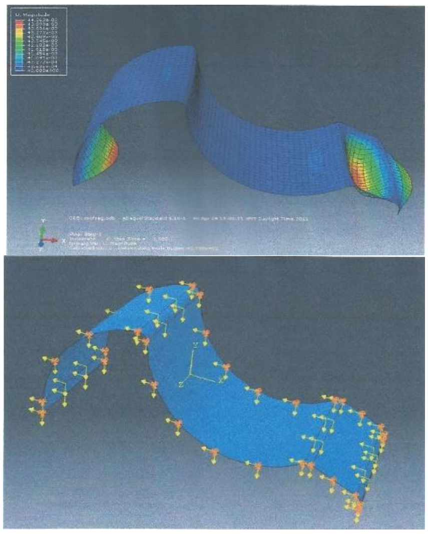

Fig 7 FE modelling of roof

One particular project was designed for a group of four students to undertake over a two year period. A small hotel, whose owner was known to the supervisor, was looking to provide a footbridge over a dam runoff stream to connect the hotel with a proposed car parking area. The project brief was that the students would carry out a feasibility study and provide alternative design proposals for a ferrocement bridge during the first year of the project. For the second year the intention was that a working design and construction method information would be produced and the hotel owner would build the bridge to this specification. Unfortunately the owner failed to engage with the students regarding the information required to design foundations and the actual construction was never completed. Though disappointing in some respects this did introduce the students to the problems of dealing with real clients. [5]

These projects allow students to show "flair" or a novel approach to a problem that would not have been possible in a commercial environment. In some cases it also allows for the introduction of advanced modelling methods, such as finite element analysis, which are not part of the undergraduate curriculum

8. CONCLUSION

This paper has demonstrated the appropriateness and effectiveness of ferrocement as a suitable material for use in University undergraduate student projects. By describing some of the widely varying work carried out over a number years, examples have shown how ferrocement is able to be used effectively in experimental work on a scale appropriate to the facilities available and as a means of investigating novel design solutions to existing scenarios.

9. REFERENCES

[1]. Naaman A., *Ferrocement and Laminated Cementitious Composites*, Techno Press 2000, Michigan, USA, 2000

[2]. https://www.ferrocement-ifs.com/

[3]. Seed J.P., Nedwell P. and Vickridge I., *Accurate Crack Measurement in Ferrocement, Journal of Ferrocement*, Vol 19, No 1, Jan 1989, IFIC, Bangkok,

[4]. Nedwell P. and Nicol R., *The use of X-Rays in the Investigation of Ferrocement,* Proceedings of the Eighth International Symposium on Ferrocement, Bangkok, Feb 2006.

[5]. Worsell A., Williams P., Putman T., Campbell E. and Nedwell P., *Holden Vale: A student Project,* Proceedings BCA 10th Concrete Communication Conference, Birmingham, BCA, 2000

Session 2
TRC :
Mechanical Performance

Hierarchical Modeling of Textile Reinforced Concrete Structural Systems

Barzin Mobasher[a], Chidchanok Pleesudjai[a], Yiming Yao[b]

[a] School of Sustainable Engineering and Built Environment, Arizona State University, Tempe, AZ

[b] School of Civil Engineering, Southeast University, Nanjing 211189, PR China

Abstract

An overview of the modeling work on the structural performance of textile reinforced concrete materials is presented. Key components of the composite response, mechanisms, and modes that contribute to ductility are addressed in terms of crack distribution, strain hardening/softening and tension stiffening. Three different approaches are used for tensile and flexural response of plain and sandwich composites. Crack initiation and propagation lead to a stress-crack-width separation law and the distributed cracking mechanisms evolve as deterministic, or stochastic processes under pure tensile mode loading. A finite difference numerical model relates the stress-crack width to the stiffness implications of the debonded interface and matrix cracking. The closed form solution of internal equilibrium in a flexural mode of loading with a variable neutral axis is used to obtain the characteristic moment-curvature relationship for a homogenized TRC section. This closed form solution is extended into a linearization process to obtain the section rotation and deflection profile and the load-deflection response of a statically determinate loading condition. This process can be used for the serviceability-based design of flexural TRC members. Similar solutions are also extended for sandwich composites made by TRC structural skins and closed form solutions of load-deflection response are presented.

1. INTRODUCTION

Textile Reinforced Concrete (TRC) is made from a cement-based fine-grained matrix that impregnates and is reinforced by multiple layers of a structural fabric. Textiles offer solutions towards the reduction of reliance on rebar reinforcement and cement consumption by significantly reducing the gross weight, corrosion potential, and CO_2 emissions. Tensile response in TRC is primarily governed by stress-strain response of matrix, fabrics, as well as the adhesion and mechanical bond at the interface (Soranakom & Mobasher, 2010). The assemblage of continuous yarns in textiles facilitate the formation of strain-hardening even though the modulus of yarn may be relatively low, however its multifilament structure allows matrix penetration in between filaments and improves the bond (Peled & Mobasher, 2007). Both new structural shapes and repair products can be developed. Repair/strengthening layers of TRC improve the bending moment and shear in structure such as beams (Si Larbi et al., 2012) and slabs (Koutas & Bournas, 2017). Moreover, the favorable properties of TRC contribute to producing thin and light-weight shell structures with high load bearing capacity (Hegger et al., 2018).

In order to facilitate the analysis and design for tensile and flexural loading, stages of response in terms of elastic, inelastic stress distribution, distributed cracking, crack saturation, and widening mechanisms are addressed. The simulation of reduced stiffness due to microcracking is based on experimental data (Mobasher et al., 2006), or analytical models that simulate the gradual debonding of textiles(Sueki et al., 2007). The distributed cracking process is first modeled using a finite difference approach and the resulting composite stress-strain response is used to obtain parametric moment-curvature response which is further applied to structural shapes and sandwich composites. This work also addresses a serviceability-based design procedure for TRC composites.

Figure 1.a shows the nature of the knitted PP based textile used. The modes of damage that accumulate in the TRC section under generalized loading such as microcrack initiation and coalescence leading to transverse cracking as shown in Figure 1.b are addressed first. The transverse cracks distribute throughout the volume of the sample leading to stiffness degradation with significant strain capacity and energy absorption. Models that capture the nonlinearities and transfer the results into a design space are needed.

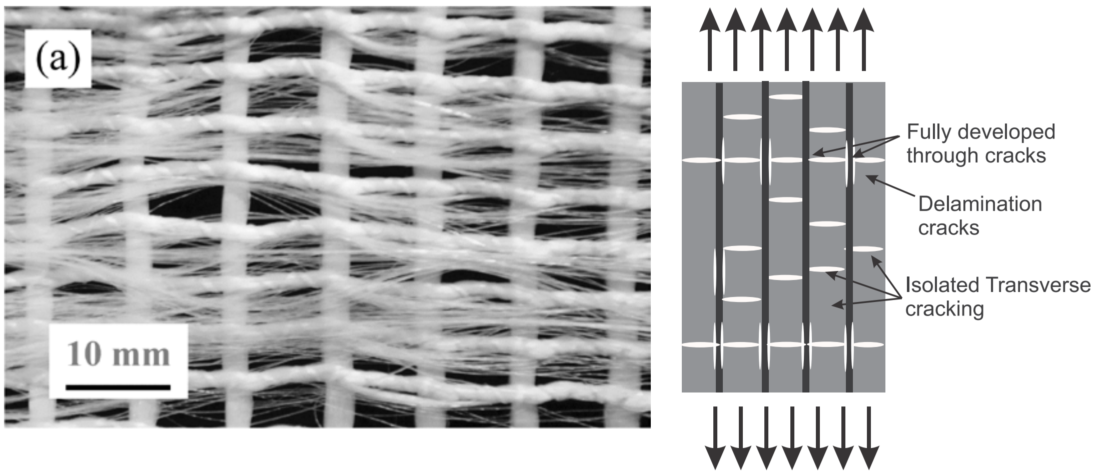

Figure 1. Open weave textiles using microfilament PP yarns. (b) microcracking in tension mode.

1.1. TRC Specimen Preparation

Multifilament polypropylene microfiber yarns were developed by Master Builders Building Solutions, OH, USA. The yarns had 500 thin filaments of 40 microns each and a surface to volume ratio of about 20 as measured from SEM, and denoted as MF40 (Figure 2(a), and (b)). The fibrillated structure of the fabric improved interface bonding between cementitious matrix as the open spaces in the multiple filaments allow for matrix penetration within the fiber structure. TRC specimens were made with a cementitious matrix of Portland cement, flyash, sand, and high range water reducing (HRWR) admixture manufactured by BASF. The water-cement ratio used was 0.45, and relative proportion of the variable constituents were C:FA:S:W 48:8:24:20(Mobasher et al., 2019). Unidirectional fiber composites were manufactured using the filament winding technique and the experimental plan for mechanical tests were conducted on uniaxial tension and flexural tests as discussed in (Mobasher et al., 2019).

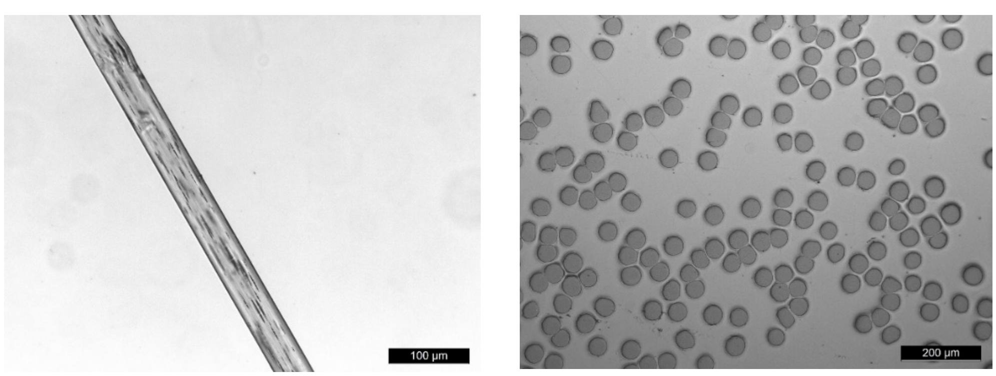

Figure 2. (a) MF40 microfiber filament, (b) multifilament yarn cross section, and (c) textile

Figure 3.a shows the single fiber pullout response of the yarns from a cementitious matrix. The response is initially linear and debonding initiates prior to peak. The fiber pullout region by the sliding friction is also responsible for dissipating a significant energy. This response is used to obtain the constitutive bond-slip response of the sample as shown in Figure 3.b

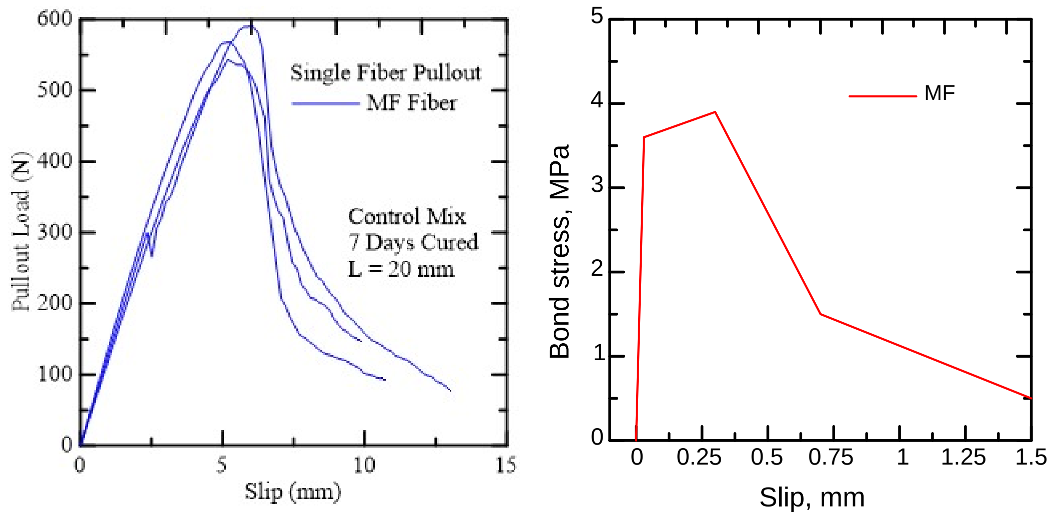

Figure 3. (a) Fiber pullout load vs. slip response and (b) Constitutive bond stress-slip response(Mobasher et al., 2019)

Figure 4 shows the characteristic stress-strain response of a tensile specimen. The stages of response are identified as elastic, distributed cracking, and strain hardening. The contribution of textiles is mostly apparent in the post cracking tensile region, where the stress continues to increase after cracking as shown in Figure 3(a). The post-crack modulus E_{cr} may only be as high as 2-5% compared to the initial stiffness. However, the tensile strain at peak strength ε_{peak} is as high as 100 times compared to the cracking tensile strain ε_{cr}. These unique characteristics cause the flexural strength to increase after cracking. Typical strain-hardening FRC do not have significant post-peak tensile strength, with limited post peak residual strength. The strain softening response is ignored and the maximum stress is used as the limiting value. Therefore, it is sufficient to use ε_{peak} to estimate the maximum moment capacity for design purposes.

Figure 4a shows the state of strain for four different stages of cracking in terms of images A-D. The location of each crack is addressed using the time stamp. Crack spacing is measured by using the difference of the coordinates of two adjacent cracks and shows a random process that leads to an exponential decay curve as shown in Figure 4(a). This functional relationship matches previous derivations by Mobasher et. al. (2019) and (Koerber et al., 2010). Figure 4.b and 4.c show the effect of fiber content on the first crack strength and post crack stiffness. Note that both the results of post crack stiffness and maximum crack width as a function of average crack width increase as the fiber volume content is increased.

2. FINITE DIFFERENCE APPROACH FOR TENSION MODELING

The mechanical properties and damage parameters such as crack spacing and crack width can be integrated into the simulation of the composite tensile stress-strain response (Mobasher, 2011; Mobasher et al., 2014, 2019). A tension stiffening finite-difference method was used(Soranakom & Mobasher, 2009, 2010). The model simulates a tension specimen that is idealized as a series of 1-D segments consisting of textile, matrix, and interface elements, see Figure 5. The matrix is treated as brittle with no strain-softening response, and the differential slip is defined as the cumulation of strain difference between the textile and matrix in Eq (1). One end of the sample is fixed and an increasing load is applied at the other end. As the applied nominal stress reaches the implied tensile strength of the matrix phase, a crack is placed at the section and the load is transferred to the textile phase through the interface elements and the bridging mechanism. Subsequent cracks form as the debonding and pullout segments continue to transfer the load back and forth between the cracked sections and uncracked composite.

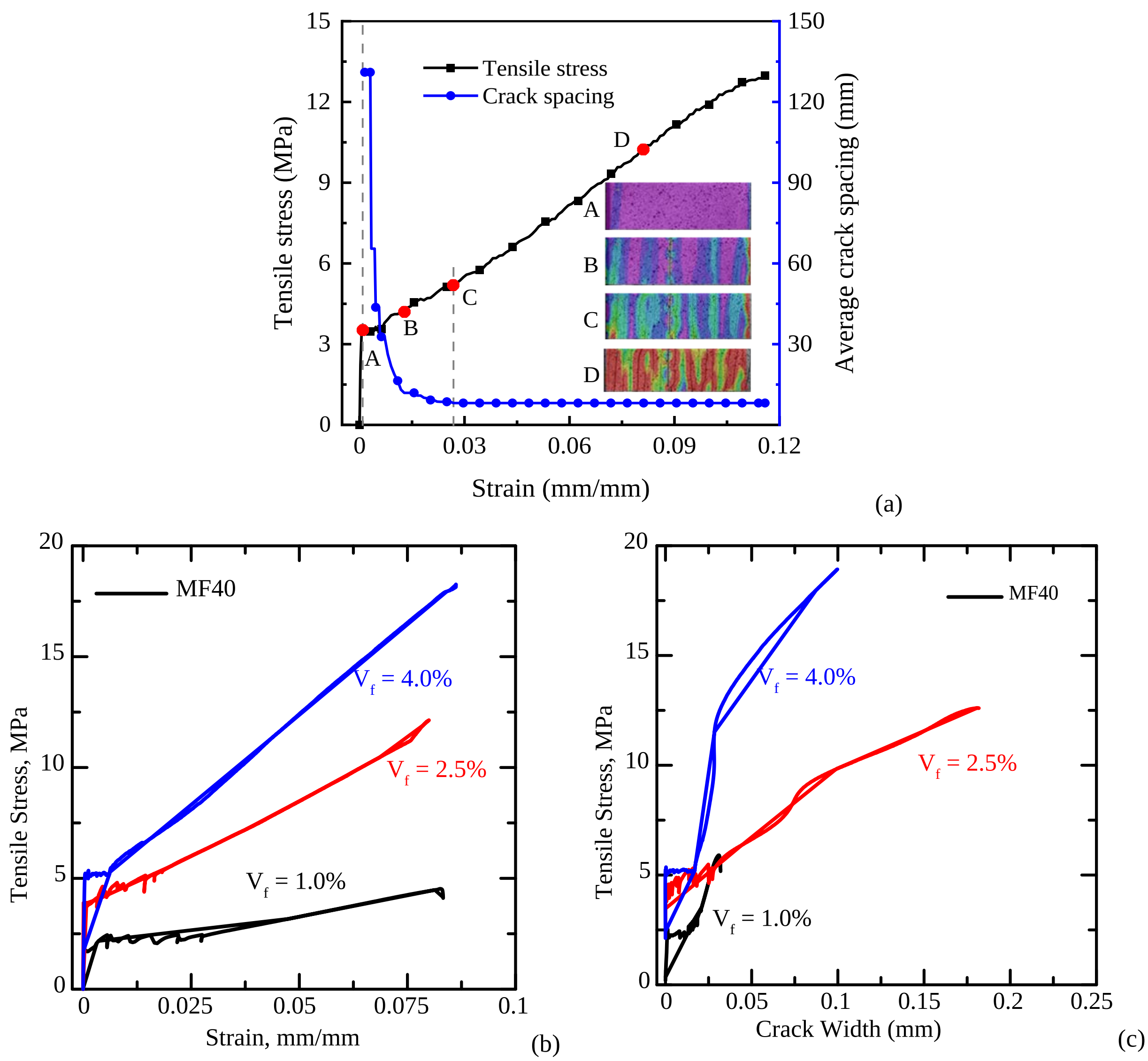

Figure 4. (a) tensile stress strain response and crack spacing in a uniaxial TRC specimen (b) and (c) show the effect of fiber content on the first crack strength and post crack stiffness of the composites.

The total length L is discretized into N nodes of equal spacing, h. Transverse yarns are simulated as springs attached to the nodes at yarn junctions providing resistance to pullout force. Upon cracking, the specimen is divided into smaller segments $L_{s(1)}$, $L_{s(2)}$,... $L_{s(q)}$ each containing n(q) number of local nodes, where q is the segment index. An additional node is inserted so that each cracked segment has its own end node and the problem is solved independently. Free body diagrams of representative nodes are shown in Figure 5b, with the primary variable defined as the nodal slip, s_i , and various operating forces, F_i = nodal fiber force, B_i = nodal bond force, G_i = nodal spring force. The equilibrium equations are derived in terms of the unknown variable slip s, as the relative deformation between the longitudinal yarn and the rigid matrix:

$$s = \int_{x_i}^{x_{i+1}} (\varepsilon_y - \varepsilon_m)dx = \int_{x_i}^{x_{i+1}} \varepsilon_y dx \quad \text{and} \quad \varepsilon_y = s' = \frac{ds}{dx} \tag{1}$$

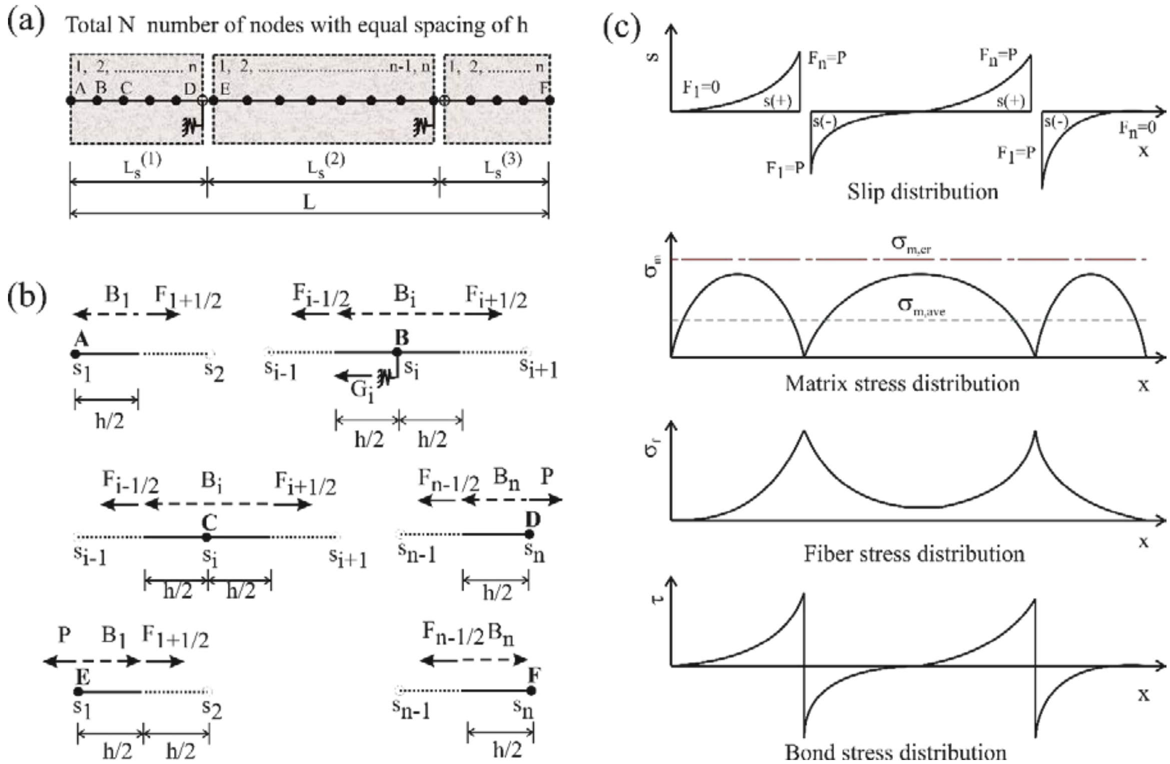

Figure 5. Finite difference model: (a) cracked concrete member, (b) free body diagram of six representative nodes labeled as "A"-"F", (c) distributions of slip, matrix stress, rebar and bond stress.

Where ε_y and ε_m are the textile and matrix strains distributed along the differential length, dx. Figure 5c presents the distribution of slip, matrix stress (σ_m), fiber stress (σ_f) and bond stress (τ) in cracked segments. The stiffness and load carrying capacity of matrix in the uncracked segments does not diminish, hence a portion of the load is always carried by the cracked matrix elements and defined as tension stiffening effect. Equilibrium equations are based on the nodal force as the product of slip and stiffness as the global system of equations use the stiffness matrix [C], nodal slip {S}, and force vector {T}:

$$[C]_{n,n}\{S\}_n = \{T\}_n \tag{2}$$

As the solution of nodal slip values is obtained, the corresponding stress, strain, and crack spacing can be subsequently computed. The load carried by the fiber is transferred back to matrix and σ_m is maximum at the center line of each cracked segment. As the load increases and σ_m reaches matrix cracking strength $\sigma_{m,cr}$, new cracks form. The bond stress varies from its maximum at the crack to zero at bonded region. The simulation of the experimental stress-strain and crack spacing responses was done with the following parameters: E_m = 25 GPa, $\sigma_{m,cr}$ = 4 MPa, E_f = 9 GPa, σ_{ult} = 420 MPa, η = 0.9, τ_{max} = 3.6 MPa. Figure 6 a-d shows the finite difference model accurately predicting the upper bound and lower bound experimental stress-strain and crack spacing-strain responses of the specimens with volume fraction of 1-2.5-4%.

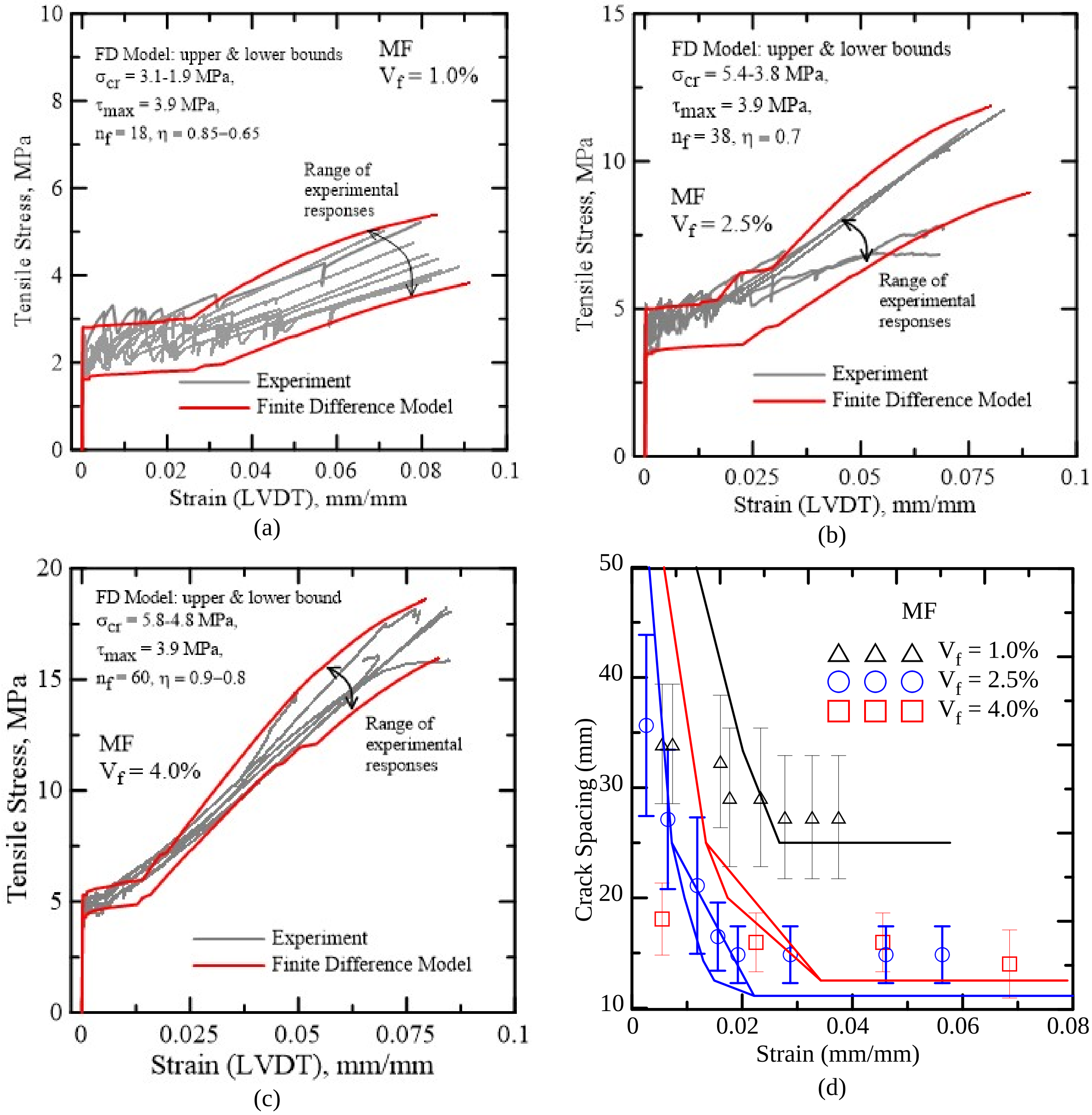

Figure 6. Comparison between experimental data and model simulation for MF fibers.

3. PARAMETRIC FLEXURAL MODEL

3.1. Material Parameters

An elastic-hardening tension and elastic-perfectly plastic compression model is adopted for Textile TRC as shown in Figure 7 as originally derived by (Soranakom & Mobasher, 2008). The tensile response is divided into three stages of: elastic, cracking, and hardening. In the elastic stage, both the fabric and matrix follow the rule of mixtures linearly up to (σ_{cr} , ε_{cr}). In the cracking region, parallel cracks form and subsequently reduce into a complete saturation state (Soranakom & Mobasher, 2010) defined at (σ_{cr} , $\upsilon_1\, \varepsilon_{cr}$). The final stage occurs as the number of cracks remain constant while the load is primarily carried by the textile yarns. The parameters in the tensile response are defined by tensile stiffness, E, first crack tensile strain

ε_{cr}, ultimate tensile capacity, defined at (σ_{ult} , $\beta_{tu}\varepsilon_{cr}$), and post crack modulus $E_1 = \eta_1 E = 0$ and $E_2 = \eta_2 E$. The compressive stress-strain in TRC is assumed to have two stages as in FRC. The elastic stage ends at (σ_{cy} , $\omega\, \varepsilon_{cr}$) and perfectly plastic is terminated at (σ_{cy} , $\lambda_{cu}\, \varepsilon_{cr}$) defined by $E_c = \gamma E$ and σ_{cy} as $\omega\gamma E\varepsilon_{cr}$, where:

$$\varepsilon_{cr} = \frac{\sigma_{cr}}{E}, \quad \beta = \frac{\varepsilon_t}{\varepsilon_{cr}} \tag{3}$$

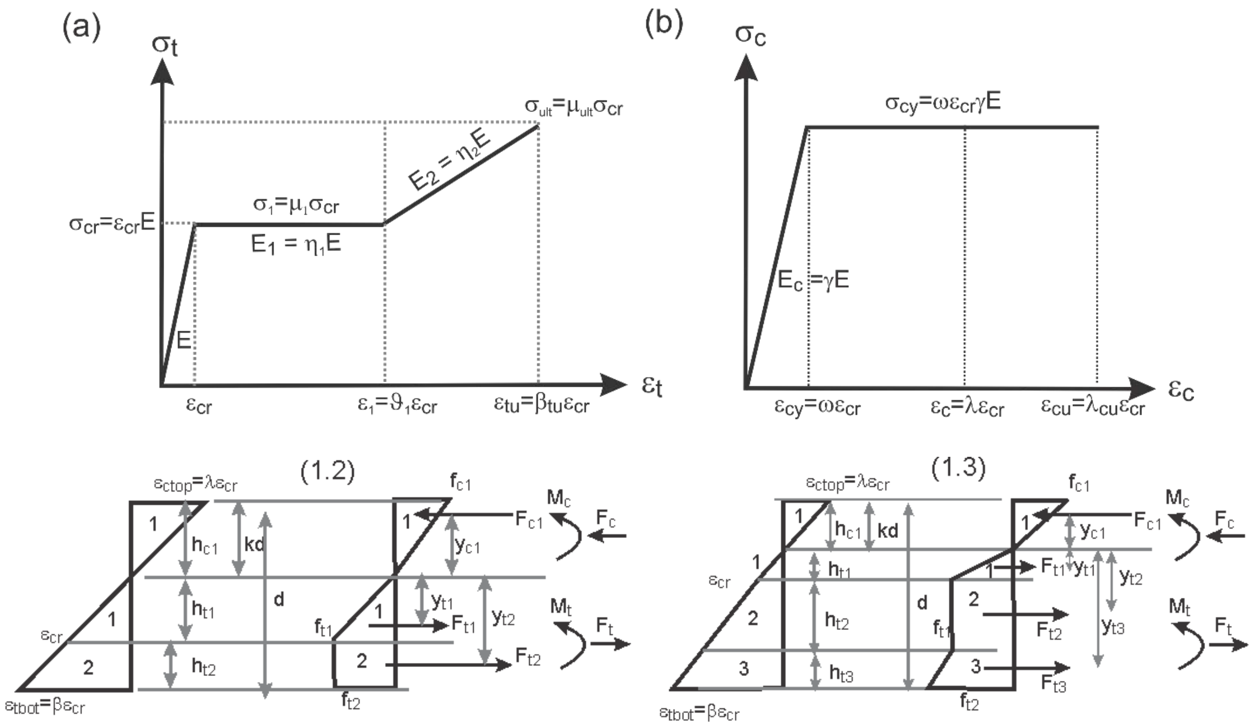

(c)

Figure 7. (a) tension model; (b) compression model, (c) strain and stress distribution on a cross section.

A minimum number of dimensionless parameters are defined for the tensile strain at peak strength, post-crack modulus, tensile and compressive strength as ϑ_1,β_{tu} η_1,η_2, μ and ω, respectively and defined as:

$$\vartheta_1 = \frac{\varepsilon_1}{\varepsilon_{cr}}, \quad \eta_i = \frac{E_{cr}}{E}, \quad \omega = \frac{\sigma_{cy}}{E\varepsilon_{cr}} = \frac{\sigma_{cy}}{\sigma_{cr}}, \; \lambda = \frac{\varepsilon_c}{\varepsilon_{cr}} = \frac{k}{k+1}\beta, \quad \beta_{tu} = \frac{\varepsilon_{tu}}{\varepsilon_{cr}}, \quad \lambda_{cu} = \frac{\varepsilon_{cu}}{\varepsilon_{cr}} \tag{4}$$

Typical strain-hardening TRC shows a higher compressive strength than the tensile strength, thus the flexural capacity is controlled by tension mode. Moment capacity of a beam for an imposed maximum tensile strain ($\varepsilon_t = \beta\varepsilon_{cr}$) is derived based on the linear strain distribution and calculation of the internal forces. Various stages are introduced by the interaction of the tensile and compressive strains magnitudes as shown in Table 1. Using the material and geometrical parameters, the internal equilibrium of each stage is solved for the Neutral axis parameter k, normalized moment m and curvature, ϕ as a function of tensile strain, β for distinct points as shown in Table 1 and plotted in Figure 8. Detailed derivation of this approach and equations are presented by (Vikram Dey et al., 2021; Pleesudjai, 2021). The curvature, moment, and strain for each stage is expressed using the normalization constants ϕ_{cr} , M_{cr} , and ε_{cr} as:

$$M_n = m' M_{cr}\,, \qquad M_{cr} = \frac{\sigma_{cr} b h^2}{6} \qquad \phi = \phi'_i\, \phi_{cr} \qquad \phi'_i = \frac{\beta}{2(1-k_i)} \tag{5}$$

Stage	Tension	Tensile strain	Compression	Compressive strain
1.1	Elastic	$0 \le \beta < 1$	Elastic	$0 \le \lambda < \omega$
1.2	Steady state cracking	$1 \le \beta < \vartheta_1$	Elastic	$0 \le \lambda < \omega$
1.3	Hardening	$\vartheta_1 \le \beta < \beta_{tu}$	Elastic	$0 \le \lambda < \omega$
2.2	Steady state cracking	$1 \le \beta < \vartheta_1$	Plastic	$\omega \le \lambda < \lambda_{cu}$
2.3	hardening	$\vartheta_1 \le \beta < \beta_{tu}$	Plastic	$\omega \le \lambda < \lambda_{cu}$

Table 1. Identification of each stage with the associated tensile and compression parameters

The full response of the moment-curvature is determined by the lower bound envelop curve of all the stages by transition from one point to the other. The limit state is obtained by substituting β_{tu}, or λ_{cu} in the corresponding equation in stage TRC 2.3 or 2.2. The intersection point of any two adjacent stages is the strain magnitude at the transfer point from one mechanism to the other. For example, the coordinates of intersection points (A,B,C,..) of stages 1.2 and 1.3 which intersect at strain $\beta = \vartheta_1$ as shown in Table 1, Figure 8, and Table 2, second row. This methodology facilitates the evaluation of ultimate strength and is applicable for Serviceability Limit Stage (SLS) design as any specific strain can be determined for a given SLS. The values of β, k, m and ϕ at each intersection point are reported in Table 2 for all competing mechanisms in Figure 8. One may define the envelop moment-curvature response using the full equations within the limits specified in Table 1 for perfect accuracy, or use a linear or polynomial fit among the points for ease of use. Thee correct path between two cases is defined by the smaller transitional strain value of β in Table 2. In other words, the path 1.2 may transition to either 2.2 or 1.3, that is determined by the minimum of two limiting strains: $\beta_{1,2-2,2} < \beta_{1,2-1,3}$ by comparing $\frac{1}{2}\left(\omega^2+1\right) < \vartheta_1$

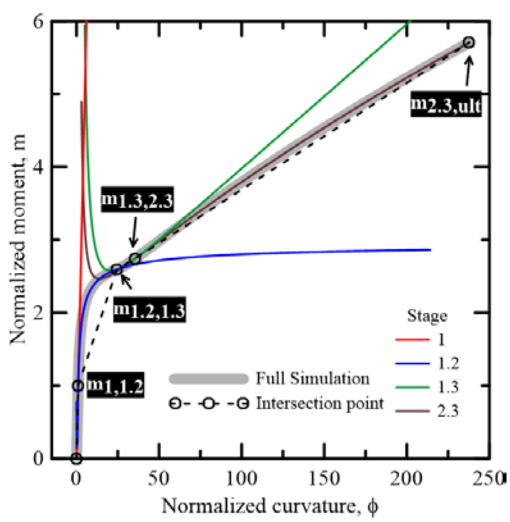

Figure 1. Comparison between full simulation(Table 1) and Intersection point(Table 2)

Intersection	β	k	m	ϕ
A, 1.1 & 1.2	1	0.5	1	1
B, 1.2 & 1.3	ϑ_1	$\frac{1+\vartheta_1 C_1 - 2\vartheta_1}{C_2}$	$\frac{-3\vartheta_1^2+(5\vartheta_1-1)C_1-3\vartheta_1+2}{(\vartheta_1-1)(C_1-\vartheta_1)}$	$-\frac{C_2}{2(C_1-\vartheta_1)}$
C, 1.3 & 2.3	$\frac{C_2+C_4}{\eta_2}$	$\frac{\eta_2\omega}{\eta_2\omega+C_3+C_4}$	$\frac{C_5k^3+C_6k^2+C_7k-2\eta_2\omega^3}{k\omega^2}$	$\frac{\eta_2\omega+C_3+C_4}{2\eta_2}$
D, 1.2 & 2.2	$\frac{1}{2}(\omega^2+1)$	$2\omega(\omega+1)^{-2}$	$\frac{3\omega-1}{\omega+1}$	$\frac{1}{4}(\omega+1)^2$
E, 2.2 & 2.3	ϑ_1	$\frac{\omega^2-1+2\vartheta_1}{\omega^2+2\omega\vartheta_1-1+2\vartheta_1}$	$\frac{C_8k^3+C_9k^2+1+\omega^3-\vartheta_1^2}{\vartheta_1^2}$	$\frac{\omega^2+2\omega\vartheta_1-1+2\vartheta_1}{4\omega}$
F, 2.3 & Ult.	β_{tu}	$\frac{C_{10}}{C_{10}+2\omega\beta_{tu}}$	$\frac{C_{11}k^2+C_{12}k+C_{13}}{\beta_{tu}^2}$	$\frac{1}{2}\frac{\beta_{tu}}{(1-k)}$

$C_1=\sqrt{2\vartheta_1-1}$	$C_7=3\eta_2\vartheta_1\omega^2+6\eta_2\omega^3-3\omega^2$
$C_2=(\vartheta_1-1)^2$	$C_8=1+\omega^3-3\vartheta_1^2-3\omega\vartheta_1^2$
$C_3=\sqrt{1-2\eta_2\vartheta_1+\eta_2+\eta_2\omega^2}$	$C_9=-2-2\omega^3+6\vartheta_1^2$
$C_4=-1+\eta_2\vartheta_1$	$C_{10}=-1+2\beta_{tu}+\eta_2\beta_{tu}^2+\eta_2\vartheta_1^2-2\eta_2\vartheta_1\beta_{tu}+\omega^2$
$C_5=\omega^2(2\eta_2\omega-3-2\omega+3\eta_2\vartheta_1)-\eta_2\vartheta_1^3+1$	$C_{11}=-1-\omega^3+\eta_2\vartheta_1^3+\beta_{tu}^2(3-3\eta_2\vartheta_1+2\eta_2\beta_{tu}+3\omega)$
$C_6=6\omega^2(1-\eta_2\omega-\eta_2\vartheta_1)$	$C_{12}=-2\eta_2\vartheta_1^3+2-4\eta_2\beta_{tu}^3+2\omega^3+6\eta_2\vartheta_1\beta_{tu}^2-6\beta_{tu}^2$
	$C_{13}=-1-\omega^3-3\eta_2\vartheta_1\beta_{tu}^2+\eta_2\vartheta_1^3+3\beta_{tu}^2+2\eta_2\beta_{tu}^3$

Table 2. Normalized tensile strain at bottom fiber (β), neutral axis, *k* at the intersection point, moment, (m), and curvature, (ϕ) with respect to normalization parameters.

3.2. **TRC Flexural Simulation**

Figure 9 (a) shows the experimental flexural response of replicate composite specimens with MF40 fibers at volume fraction of 2.5%. The analytical load-deflection response using the procedure described above is also presented. The simulated responses agree with the experimental trends. Figures 9 (b) shows the experimental tensile stress-strain response with simulated tensile response generated using the simulation parameters. The range of important simulation parameters for MF40 specimens vary from: E = 21 to 38 GPa, η varies from 0.003 to 0.004, and μ varies from 2.0-2.5. The experimental tensile response compares to the analytical parameters with a considerable degree of accuracy. The predicted results closely follow the mechanisms discussed earlier in terms of the individual properties of the fibers and their interaction with cementitious matrix. Thus one can very easily verify the accuracy of the model by developing a predictive tool to determine design parameters for TRC composites in real world construction applications (Vikram Dey et al., 2021; Pleesudjai et al., 2021).

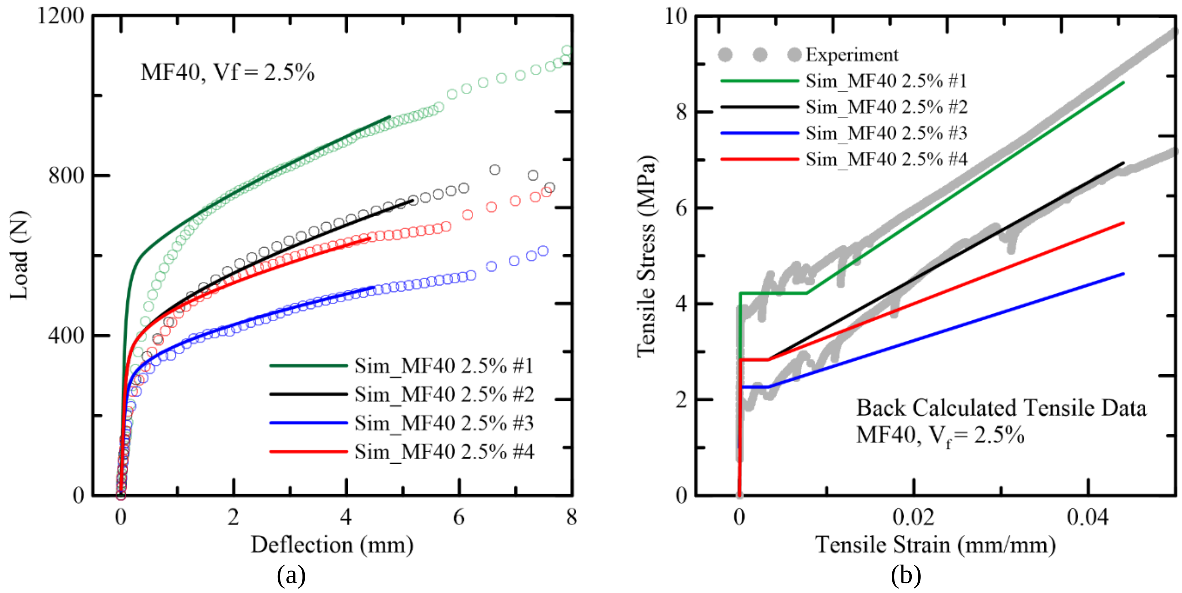

Figure 9. (a) Comparison of the simulation with experimental results of flexural tests and tensile response of MF40 Fibers. (b) Comparison of the model tensile stress strain input and experimental data.

4. FLEXURAL SIMULATION IN STRUCTURAL SHAPES

The aim of this section is to use the simplified approach of moment-curvature representation using the linear interpolation between the control points. This approach can be compared with the performance of the full analysis closed-form solutions currently developed for Sandwich sections, Channels, Angles, and W sections. Figure 10 illustrates the application of TRC in various structural shapes. The geometrical control points are used as the interval in generating stages of flexural response each piecewise function. The geometrical control points are the point that required to determine the strain. The points particularly locate at top, bottom, discontinuity of section and material properties. For example, the sandwich composite(see Figure10(a)) has four geometrical control points in order to calculate the stress resultant. The similar concept, the composite materials with the number of n layers can be analysis by piecewise function by adopting the intervals of geometrical control points and multiple material properties.

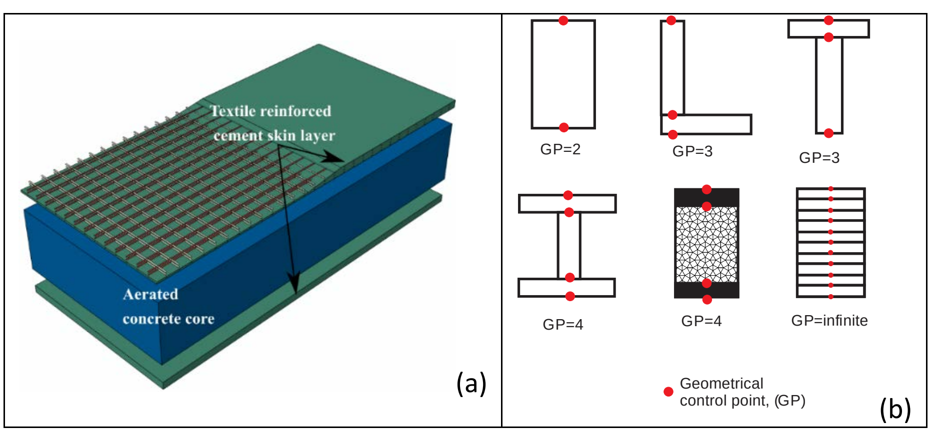

Figure 10. (a) Schematic of the textile reinforced-aerated concrete sandwich composite system, (b)control points used in definition of section geometry

4.1. Sandwich Composite

The typical structure of sandwich includes core material in the middle and skin materials. The core can be a light-weight, low-modulus, fire-resistant or low thermal conductivity material depending on the intended function. TRC skin is adopted for strengthening and ductility in sandwich composites (Colombo et al., 2019; Vervloet et al., 2019) (Cuypers & Wastiels, 2011; Metelli et al., 2011; Shams et al., 2014; Vervloet et al., 2019). A sandwich panel with brittle plain Autoclaved Aerated Concrete(AAC) or Fiber Reinforced Aerated Concrete (FRAC) core is used for potential application in wall and roof elements by allowing larger flexural capacity, and longer span compared to conventional timber materials. Moreover, sandwich panels for walls reduces 40–70% of the embodied energy compared to lightweight or normal weight concrete, wood, or brick construction (ACI 122R-02, 2002). The sandwich section shown in Figure 11 is assumed to have a linearized strain along the section with sufficient strength and stiffness between core and skin layer to ensure a full shear transfer (Salmon et al., 1997). The full derivation and simulation can be found in (Pleesudjai, 2021; Pleesudjai et al., 2021).

The complicated flexural response of sandwich section can be described by piecewise function rather than a single function(see Figure 12(a)). During zone 1.1, tensile and compressive in both core and skin are elastic. Moment-curvature response presents the straight line. After initiation of tensile cracking in core materials, the response moves to zone 2.1 representing cracked core in tension, elastic core in compression and tension in skin also considered elastic. At this stage, the normalized moment of Sandwich composite remains constrained by the cracking when the contribution of residual tensile strength in core is the dominating parameter (V. Dey et al., 2014; Pleesudjai et al., 2021). The end of zone 2.1 has a choice to be governed by perfectly plastic in core compression(zone 3.1 and then zone3.2) or allowing the TRC skin to yield while the core compression is still in elastic (zone2.2 and then zone 2.3 since there are two post-crack stages in the hardening range). In order to consider the multiple cracks, the simulation in Figure 12(b) are assumed the continuity of stress and strain fields to be maintained in the cracked segment and represented by characteristic length, L_p (Yao et al., 2020). The deflection can be evaluated by double-integration method when assuming the Bernoulli-Euler beam Theory. Figure 13 Illustrates the effect of Lp on the multiple cracks captured by DIC in the flexural simulation of sandwich composite. The result show that the increasing of L_p, the simulation curve exhibit more a considerable degree of accuracy.

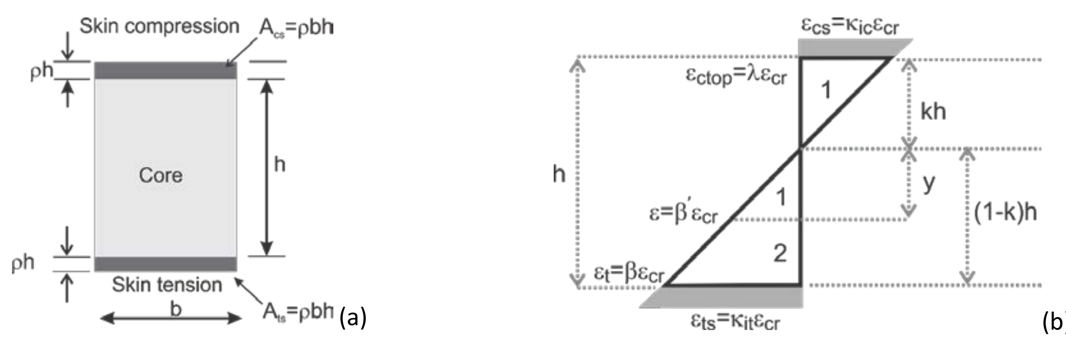

Figure 11. (a) Sandwich section, (b) linear strain distribution along the sandwich section(Pleesudjai, 2021; Pleesudjai et al., 2021).

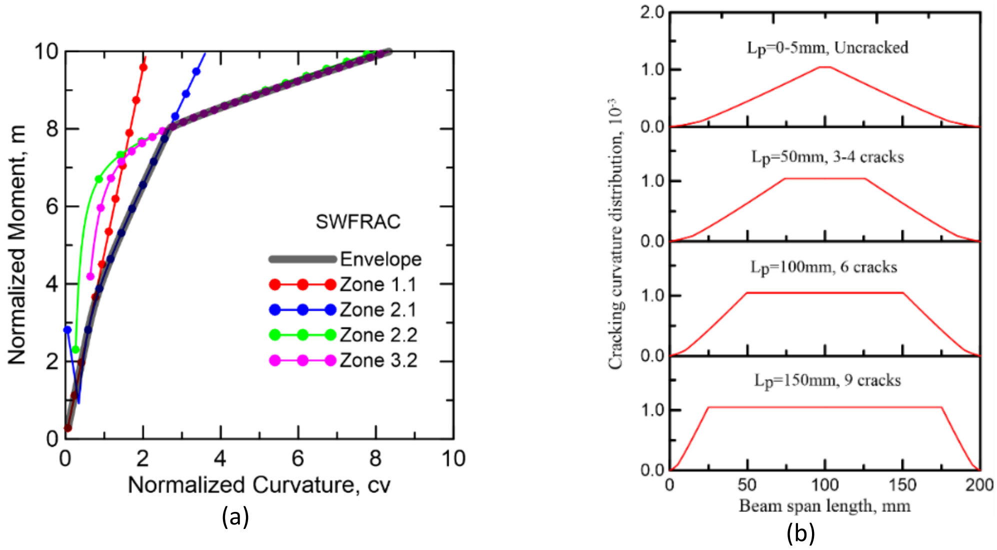

Figure 12. (a)Typical flexural response of sandwich section, (b) The characteristic length, L_p used to describe the multiple cracks.

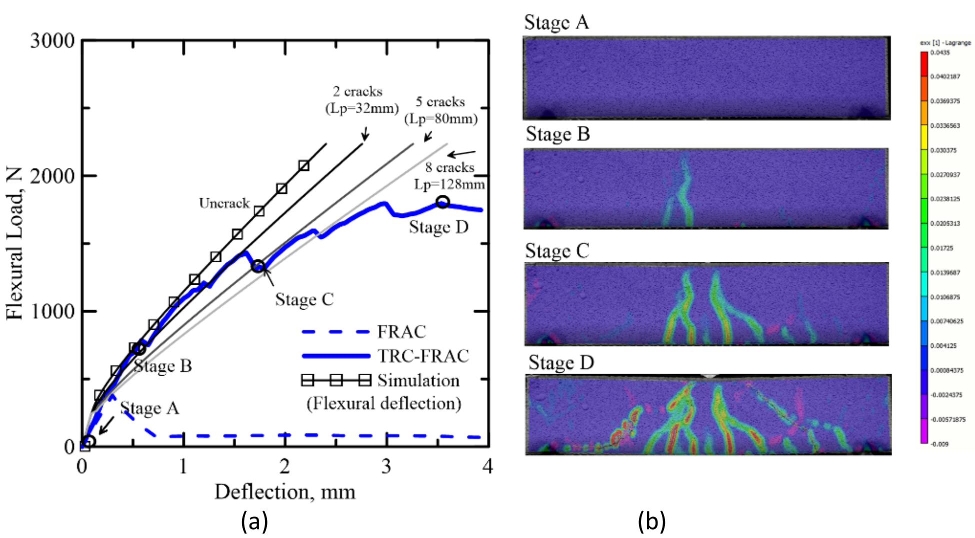

Figure 13. Normalized moment-curvature response at each stage of β sandwich with AAC (a) Effect of number of cracks on the simulation of load-displacement response of TRC-FRAC (50 × 100 × 200 mm), (b) DIC analysis on nominal longitudinal strain at various stages.

References

ACI 122R-02. (2002). Guide to Thermal Properties of Concrete and Masonry Systems. In *American Concrete Institute*.

Colombo, I. G., Colombo, M., & di Prisco, M. (2019). Precast TRC sandwich panels for energy retrofitting of existing residential buildings: full-scale testing and modelling. *Materials and Structures*, *52*(5), 104. https://doi.org/10.1617/s11527-019-1406-1

Cuypers, H., & Wastiels, J. (2011). Analysis and verification of the performance of sandwich panels with textile reinforced concrete faces. *Journal of Sandwich Structures & Materials*, *13*(5), 589–603. https://doi.org/10.1177/1099636211408665

Dey, V., Bonakdar, A., & Mobasher, B. (2014). Low-velocity flexural impact response of fiber-reinforced aerated concrete. *Cement and Concrete Composites*, *49*, 100–110. https://doi.org/10.1016/j.cemconcomp.2013.12.006

Dey, Vikram, Bauchmoyer, J., Pleesudjai, C., Schaef, S., & Mobasher, B. (2021). Correlation of Tensile and Flexural Response of Continuous Polypropylene Fiber Reinforced Cement Composites. *ACI*, *SP-345: Materials*, *Analysis*, *Structural Design and Applications of Textile Reinforced Concrete/Fabric Reinforced Cementitious Matrix Correlation*, 230–242.

Hegger, J., Curbach, M., Stark, A., Wilhelm, S., & Farwig, K. (2018). Innovative design concepts: Application of textile reinforced concrete to shell structures. *Structural Concrete*, *19*(3), 637–646. https://doi.org/10.1002/suco.201700157

Koerber, H., Xavier, J., & Camanho, P. P. (2010). High strain rate characterisation of unidirectional carbon-epoxy IM7-8552 in transverse compression and in-plane shear using digital image correlation. *Mechanics of Materials*, *42*(11), 1004–1019. https://doi.org/10.1016/j.mechmat.2010.09.003

Koutas, L. N., & Bournas, D. A. (2017). Flexural Strengthening of Two-Way RC Slabs with Textile-Reinforced Mortar: Experimental Investigation and Design Equations. *Journal of Composites for Construction*, *21*(1). https://doi.org/10.1061/(ASCE)CC.1943-5614.0000713

Metelli, G., Bettini, N., & Plizzari, G. (2011). Experimental and numerical studies on the behaviour of concrete sandwich panels. *European Journal of Environmental and Civil Engineering*, *15*(10), 1465–1481. https://doi.org/10.1080/19648189.2011.9723354

Mobasher, B. (2011). Single Yarns in Woven Textiles: Characterization of Geometry and Length Effects. In *Mechanics of Fiber and Textile Reinforced Cement Composites* (pp. 83–96). CRC Press. https://doi.org/10.1201/b11181-8

Mobasher, B., Dey, V., Bauchmoyer, J., Mehere, H., & Schaef, S. (2019). Reinforcing Efficiency of Micro and Macro Continuous Polypropylene Fibers in Cementitious Composites. *Applied Sciences*, *9*(11), 2189. https://doi.org/10.3390/app9112189

Mobasher, B., Dey, V., Cohen, Z., & Peled, A. (2014). Correlation of constitutive response of hybrid textile reinforced concrete from tensile and flexural tests. *Cement and Concrete Composites*, *53*, 148–161. https://doi.org/10.1016/j.cemconcomp.2014.06.004

Mobasher, B., Pahilajani, J., & Peled, A. (2006). Analytical simulation of tensile response of fabric reinforced cement based composites. *Cement and Concrete Composites*, *28*(1), 77–89. https://doi.org/10.1016/j.cemconcomp.2005.06.007

Peled, A., & Mobasher, B. (2007). Tensile behavior of fabric cement-based composites: Pultruded and cast. *Journal of Materials in Civil Engineering*, *19*(4), 340–348. https://doi.org/10.1061/(ASCE)0899-1561(2007)19:4(340)

Pleesudjai, C. (2021). *Generalized modeling and Experimental Validation of Flexural Response in Cement Based Composites*. Arizona State University.

Pleesudjai, C., Li, A., Dey, V., & Mobasher, B. (2021). Low-Velocity Impact Experiments and Modeling of TRC Skin-Aerated Concrete Core Sandwich Composites. *Materials*, *14*(2), 390. https://doi.org/10.3390/ma14020390

Salmon, D. C., Einea, A., Tadros, M. K., & Culp, T. D. (1997). Full Scale Testing of Precast Concrete Sandwich Panels. *ACI Structural Journal*, *94*(4), 354–362. https://doi.org/10.14359/486

Shams, A., Hegger, J., & Horstmann, M. (2014). An analytical model for sandwich panels made of textile-reinforced concrete. *Construction and Building Materials*, *64*, 451–459. https://doi.org/10.1016/j.conbuildmat.2014.04.025 M4 - Citavi

Si Larbi, A., Contamine, R., & Hamelin, P. (2012). TRC and hybrid solutions for repairing and/or strengthening reinforced concrete beams. *Engineering Structures*, *45*, 12–20. https://doi.org/10.1016/j.engstruct.2012.06.002

Soranakom, C., & Mobasher, B. (2008). Correlation of tensile and flexural responses of strain softening and strain hardening cement composites. *Cement and Concrete Composites*, *30*(6), 465–477. https://doi.org/10.1016/j.cemconcomp.2008.01.007

Soranakom, C., & Mobasher, B. (2009). Geometrical and mechanical aspects of fabric bonding and pullout in cement composites. *Materials and Structures*, *42*(6), 765–777. https://doi.org/10.1617/s11527-008-9422-6

Soranakom, C., & Mobasher, B. (2010). Modeling of tension stiffening in reinforced cement composites: Part I. Theoretical modeling. *Materials and Structures/Materiaux et Constructions*, *43*(9), 1217–1230. https://doi.org/10.1617/s11527-010-9594-8

Sueki, S., Soranakom, C., Mobasher, B., & Peled, A. (2007). Pullout-Slip Response of Fabrics Embedded in a Cement Paste Matrix. *Journal of Materials in Civil Engineering*, *19*(9), 718–727. https://doi.org/10.1061/(ASCE)0899-1561(2007)19:9(718)

Vervloet, J., Tysmans, T., El Kadi, M., De Munck, M., Kapsalis, P., Van Itterbeeck, P., Wastiels, J., & Van Hemelrijck, D. (2019). Validation of a Numerical Bending Model for Sandwich Beams with Textile-Reinforced Cement Faces by Means of Digital Image Correlation. *Applied Sciences*, *9*(6), 1253. https://doi.org/10.3390/app9061253

Yao, Y., Mobasher, B., Wang, J., & Xu, Q. (2020). Analytical approach for the design of flexural elements made of reinforced ultra-high performance concrete. *Structural Concrete*, *22*(1), 298–317. https://doi.org/10.1002/suco.201900404

Numerical analysis of stress and strain evolution of RC beams reinforced by TRC subjected to thermomechanical loading in case of fire

Najib Douk[1a], Xuan Hong Vu*[2] and Amir Si Larbi[3b]

[1]University of Lyon, Ecole Centrale Lyon, LTDS (UMR 5513 CNRS), 36 Avenue Guy de Collongue, Ecully, France.
[2]University of Lyon, ENISE, LTDS (UMR 5513 CNRS), 58 rue Jean Parot, 42023 Saint-Etienne, France. [3]Université de Lyon, Univérsité Claude Bernard LYON 1; Laboratoire des Matériaux Composites pour la Construction LMC2, Lyon, France.

ABSTRACT

This work was assessed by a multi-scale numerical approach for reinforced concrete (RC) structural elements strengthened by TRC (Textile Reinforced Concrete) composites under thermomechanical loads in case of fire. Initially, this study addressed at a macro-scale the structural behaviour of TRC strengthened reinforced concrete (RC) beams under fire. Then, based on the obtained numerical data (strains, stresses and temperatures), a more substantiated understanding of the thermomechanical phenomenology was established. The results and conclusions drawn from this numerical study showed a close link between the local behaviour at the level of the steel/concrete and TRC/concrete contact zones and the overall structural behaviour of structural elements under thermomechanical loads (case of fire).

KEYWORDS: *Textile reinforced concrete (TRC); structures on fire; ISO 834; numerical modelling; reinforced concrete beams.*

1. INTRODUCTION

In view of the fire vulnerabilities of the composites with a polymer matrix (Fibre Reinforced Polymer – FRP), interest has been focused on FRiB (Fiber Reinforced inorganic Binder) [1] and TRC (Textile Reinforced Concrete) or TRM (Textile Reinforced Mortar) [2]. These materials are new generation composites based on cementitious matrix [3]–[7]. TRCs drew their mechanical advantages from the combination of mortar and continuous textile grids. These materials showed a particularly remarkable fire resistance compared to other composite materials based on polymer matrix. Moreover, the relatively ductile behavior of TRC gave the reinforced concrete structural elements an optimized mechanical load transfer between the heavily loaded structural parts and the least loaded ones. At room temperature, TRC strengthened structural elements were widely studied in the current literature. Some studies [7]–[9] had all highlighted remarkable strengthening capacities of the TRC in bending configurations. In the current state of the art, few studies have addressed the TRC in the context of thermomechanical structural strengthening. As mentioned above, the interest in the TRC strengthening capabilities against fire is in its early stages. Some experimental studies were carried out in this regard; however, they were mainly focused on the material aspects. (Douk et al [10] have numerically studied effects of TRC thickness and thermal loading rate on thermomechanical behaviour of reinforced concrete beams with and without textile reinforced concrete (TRC) strengthening. To the best of authors' knowledge, in literature, no numerical study focusing on the effect of mechanical loading levels on thermomechanical behaviour of reinforced concrete beams with and without textile reinforced concrete (TRC) strengthening has been investigated. For this reason, the authors have focused on the problem mentioned above and showed the numerical results in this paper.

In this study, initially, two numerical models of a reference RC beam (without TRC strengthened) were implemented and then validated through a numerical-experimental confrontation (i.e. temperature fields and the RC beam mid-span deflection evolution). Once the model was validated, a thermo-mechanical model of a TRC strengthened beam was implemented by introducing a TRC layer in the first validated model. It is important to say that the primary objective of this study was exploratory at first, then the findings of the first part were used to investigate the sensitivity of TRC strengthened systems in function of mechanical service load levels. In the following sections, the numerical approach, thermal loadings, thermal and physical properties of the constitutive materials are presented. Thereafter, the results of the numerical models are discussed. Finally, the main conclusions are presented.

*Corresponding author, Associate professor, Ph.D., E-mail: Xuan-Hong.Vu@univ-lyon1.fr
[a] Temporary Lecturer and Research Assistant, Ph.D., E-mail: najib.douk@ec-lyon.com
[b] Professor, Ph.D., E-mail: amir.si-larbi@enise.fr

2. Experimental specimens used for numerical modelling

Two experimental studies ([11] and [12]) were selected to validate numerico-experimentally the thermo-mechanical model. These studies were considered as they provided a complete set of thermo-mechanical properties of the materials used. Also, the application order of the mechanical and thermal loads in these studies recreates the actual loading order during a fire incident (mechanical loading then thermal one). In addition to this, the size of the specimens is of a structural scale as opposed to the majority of the experimental studies where the specimen's dimensions are restricted by the size of the test furnaces.

As mentioned above, the experimental loading tests were carried out in a certain order. First, a mechanical displacement was applied to the test specimen until the desired force was reached. Then the test furnaces were ignited, and their temperatures were monitored so that it followed a real fire temperature evolution (according to the fire curve standard, ISO-834, Fig.1). Accordingly, to maintain realistic test conditions, mechanical loads were kept constant during heating. Table 1 and Fig. 2-3 highlight the information about the geometry, thermo-mechanical loads and properties of the specimens tested in the experimental studies.

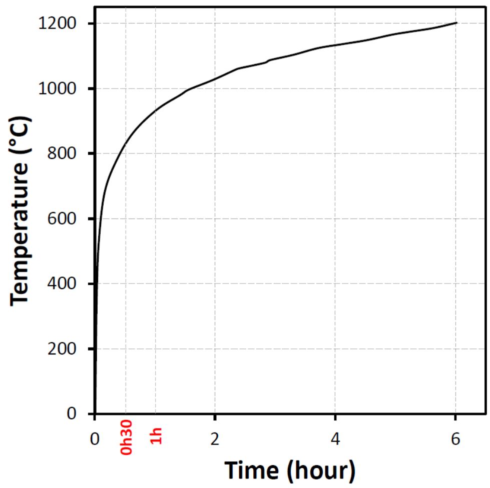

Fig. 1. Temperature evolution with time of the ISO-834 curve

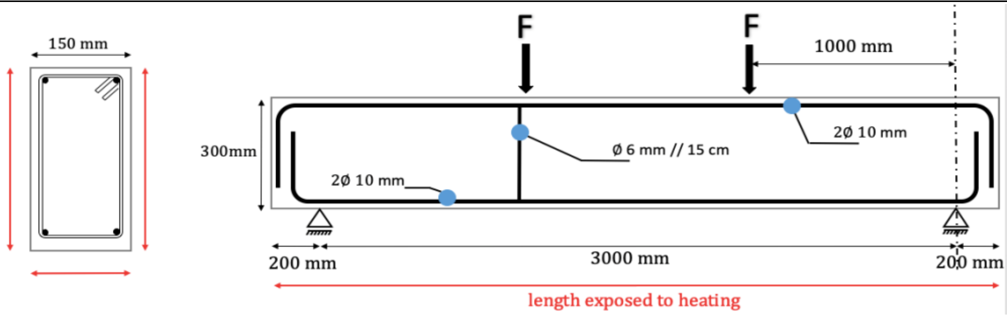

Fig.2. Geometry of "Test Specimen 1" (configuration B1) [11]

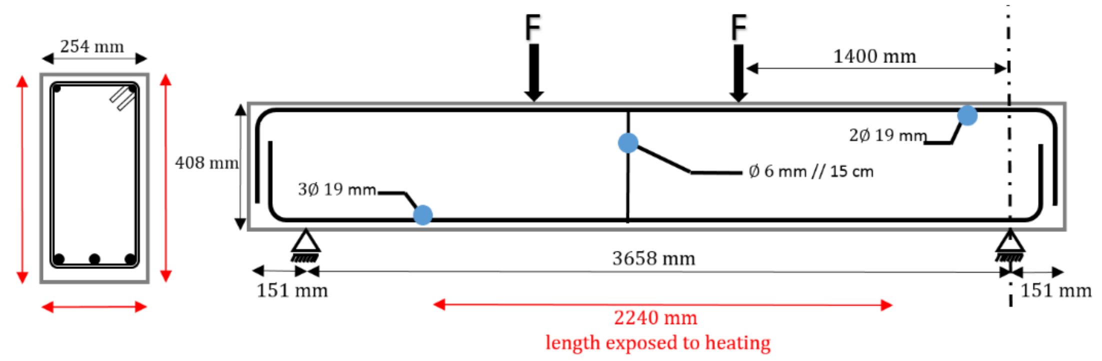

Fig. 3. Geometry of "Test Specimen 2" (configuration B2) [12]

Table 1 Specific information about the experimental test specimens (experimental data sources: [11], [12])

	Test Specimen 1- configuration B1 [11]	Test specimen 2- configuration B2 [12]
Concrete strength (MPa) (mean value)	30,1	32
Steel strength (MPa)	500	542
Thermal load	ISO-834 (lateral and bottom surfaces) see Fig. 2	ISO-834 (lateral and bottom surfaces) see Fig. 3
Mechanical load	24 kN (4-point bending test) see Fig. 2	50 kN each force (4-point bending test) see Fig. 3

3. Numerical methods

3.1. Mechanical loads

3.1.1. Configuration B1 [11](Carlo et al, 2018)

The mechanical load applied on this configuration was replicated similar to one applied in the experimental study [11] from which it is derived. The mechanical loading involves the application of two forces to the upper surfaces of the configuration tested in 4-point bending (Fig. 2). Each force is equal to 11 kN.

3.1.2. Configuration B2 [12](Aqeel et al, 2011)

As the purpose of this study is to establish an assessment of the effects of mechanical loading levels on configurations with and without TRC, it was assumed that both configurations tested experimentally and numerically (B1 and B2) should be in a similar thermomechanical state. Therefore, the mechanical load applied on specimen B2 (shown in Fig. 3) were changed to match the mechanical equilibrium state of the midspan section of specimen B1.

3.1.3. Thermal conditions

Knowing that for the configuration B1 [11] the ISO-834 heat flux was applied on the 3 surfaces all along the tested beam (see Fig. 2 on the left). Therefore, an ISO-834 heat flux was also applied on the 3 surfaces all along the beam B2 (see Fig. 3 on the left) [12].

3.1.4. Mechanical conditions

A new force F1 was applied to the B2 configuration [12]. The purpose of this calculated force is to ensure as similar mechanical state for B1 and B2 at the mid-span section. That is to say, the F1 force was established to ensure a ratio (Steel section recommended by Eurocode 2 (EC2)/Steel section used for this configuration) similar to that of the B1 beam. This force was calculated within Eurocode 2 requirements for RC beams. F1 = 66.5 kN (per force).

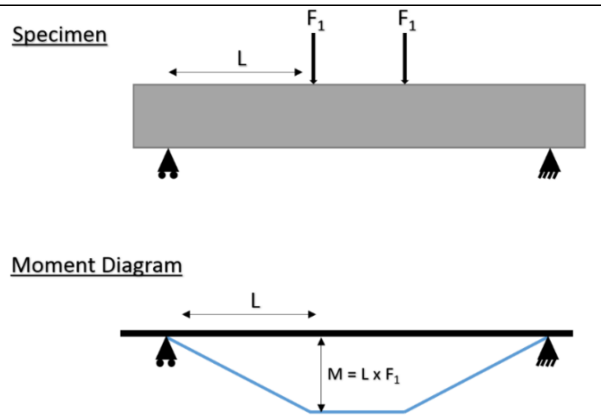

Fig. 4. Mechanical loads and moment diagram for a 4-point bending test

For configuration B1 (Carlo et al, 2018) [11], the mid-span moment is:

$$M = L \times F1$$
$$M = 1\ (m) \times 11000\ (N)$$
$$M = 11000\ (N.m)$$

According to EC2:

$$\mu_u = \frac{M}{b \times d^2 \times f_{bc}}$$

$$\mu_u = \frac{11000\ (N.m)}{0.15\ (m) \times 0.27^2 (m.m) \times 17000000\ (\frac{N}{m.m})}$$

$$\mu_u = \frac{11000\ (N.m)}{0.15\ (m) \times 0.27^2 (m.m) \times 17000000\ (\frac{N}{m.m})}$$

$$\mu_u = 0.0591$$

The steel section recommended by EC2 is: $A_u = 1.09\ cm^2$

The cross-section of tension steels of the B1 configuration (Carlo et al, 2018) [11] is:

$$A_{B1} = 2 \times \pi \times (1/2)^2 (cm^2)\ ; A_{B1} = 1.57\ cm^2$$

The ratio of the steel section recommended by EC2 over the current steel section is: $r_{acier} = \frac{1.57}{1.09} = 1.43$

A reversed calculation was made from a ratio of 1.43 (above) to trace back the force F1 that must be applied on B2. Therefore, F1 is: $F1 = 66.5\ (kN)$

3.2. Thermal loading

A specific loading order was followed to ensure realistic fire conditions. Initially, mechanical loads wereapplied gradually for a duration of 10 minutes as shown on Fig. 5(to allow the model to converge correctly), these mechanical loads included the dead weight of the configurations as well as the 4-point bending loads. Then, after the application of the full mechanical loads, the thermal loading was applied to the surfaces of the assessed configurations.

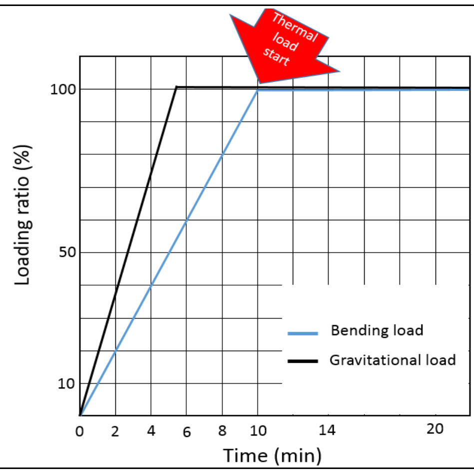

Fig. 5. Mechanical loading distribution with respect to time

Table. 2 shows the values and locations of the loads applied on the beam B1 [11] and the beam B2 [12].

Table. 2.Thermal and mechanical loads

	Test specimen 1 - B1 [11]	Test specimen 2 – B2 [12]
Thermal load	ISO-834 (lateral and bottom surfaces) see Fig. 2	ISO-834 (lateral and bottom surfaces) all along the specimen B2
Mechanical load	12kN each force (4 point bending test) see Fig. 2	66.5kN each force (4 point bending test) see Fig. 3

3.2.1. Numerical models

As shown in Figure 6, the models specified in EN1992-1-2 [13] were adopted to derive the uniaxial properties of concrete at different elevated temperatures [14].

3.3. Concrete and steel

A detailed review of the literature shows that the complexity of the mechanical behavior of concrete manifests in the difference in compressive and tensile behavior, the nonlinearity of the post-elastic behavior, the nonlinear dependence of the multi-dimensional stress state, and the dependence of all these parameters on the temperature of the concrete. Figures 6a, b, c show the evolution of the behavior of concrete as a function of the temperature for the uniaxial mechanical behavior of concrete (compression and tension) (see Figure 6a) [14], for the mechanical behavior of concrete in compression for different temperatures (see Figure 6b) [13](Eurocode 2, 1992) and for the mechanical behavior of concrete in tension for different temperatures (see Figure 6c) [15]. The evolution of the Young's modulus of concrete was extracted from the linear (elastic) part of Fig. 6b. Note that the normalized mechanical property (stress or Young's modulus) of a material is defined as the ratio of the mechanical property at a temperature (T) to that at room temperature.

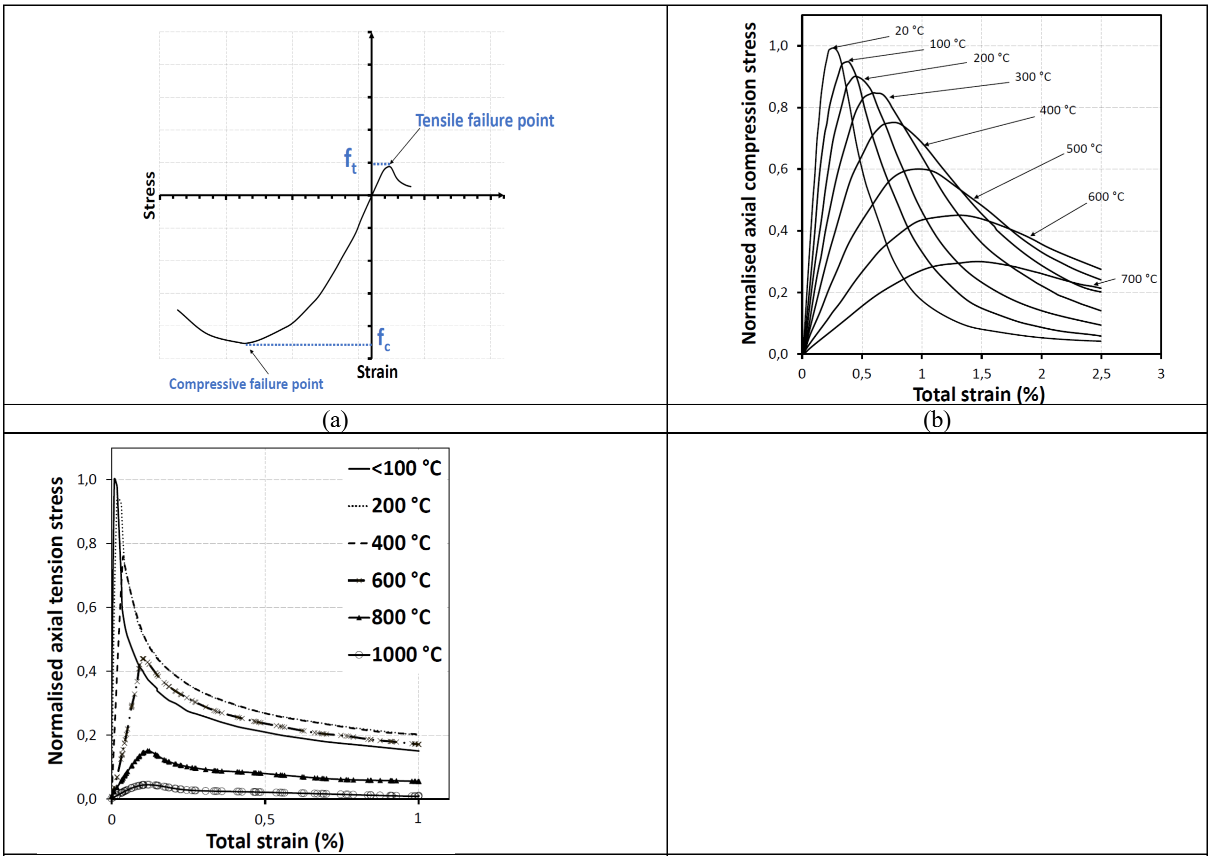

(a) (b) (c)

Fig. 6. Evolution of the thermomechanical properties of concrete as a function of the temperature: (a) Uniaxial mechanical behaviour of concrete (compression and tension) [14]; (b) Mechanical behaviour of concrete in compression at different temperatures [13]; and (c) Mechanical behaviour of concrete in tension at different temperatures [15].

Similarly, as what have done for concrete, the steel's mechanical behaviour in function of the temperature has been extracted from the Eurocode 2 and implemented in the thermo-mechanical model. Fig.7a shows the evolution of stress-strain curves of reinforced concrete's steel for different temperatures. Fig.7b shows the evolution of the normalized steel's Young modulus with temperature. Both of these parameters were extracted from the Eurocode 2.

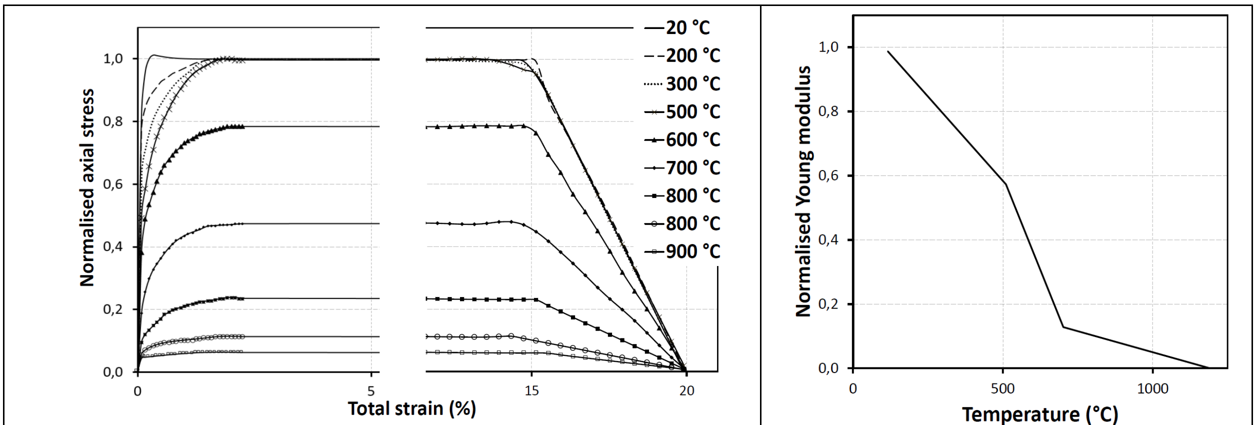

(a) (b)

Fig. 7. Evolution of the normalised mechanical properties of steel as a function of the temperature: (a) Mechanical behaviour of steel (similar in compression and tension) at different temperatures [13]; and (b) Evolution of the normalised Young's modulus of steel as function of the temperature [13]

3.4. Textile reinforced concrete (TRC)

Figure 8a shows the mechanical behavior of a TRC composite for different temperatures (ranging from 25°C to 600°C). These curves were experimentally characterized[16]. Figure 8a shows the thermomechanical behavior (stress-strain relationships) of TRC used as a strengthened material for reinforced concrete beams. This TRC was composed of an aluminous matrix, 2 layers of chopped strand mat glass fibers and 2 layers of carbon grids. The TRC had a total reinforcement ratio of 3.6% ($V_{f1} = V_{carbon\ textile}/V_{TRC}$) and a reinforcement ratio according to the tensile direction of 1.8% ($V_{f2} = V_{carbon\ textile\ in\ the\ tensile\ direction}/V_{TRC}$). The behavior laws, shown in Fig. 8a, were obtained by placing the TRC plates at a constant temperature (25°C, 200°C, 400°C, 600°C) and then tensile forces were applied to the sample until it was failed by the combined effect of temperature and ultimate tensile force. In order to implement the mechanical behavior of TRC, the values of Young's modulus of the studied TRC as a function of the temperature (first slopes of the curves presented in Fig. 8a) were extracted and the evolution of the normalized Young's modulus of the studied TRC is presented in Fig. 8b. Figure 8b shows that the Young's modulus of the TRC composite gradually decreases when the temperature increases from 25°C to 600°C.

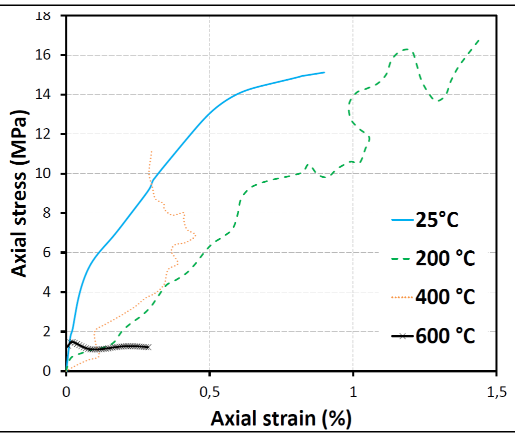

(a)

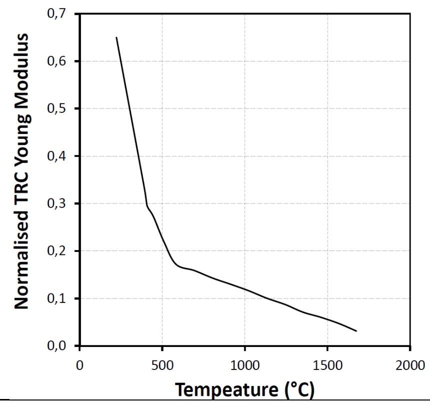

(b)

Fig. 8. Thermomechanical behaviour of TRC for different elevated temperatures: (a) Experimental results obtained by Tlaiji [16]; (b) Evolution of normalised Young modulus of TRC as function of the temperature.

3.5. Numerical implementation

3.5.1. Mechanical implementation

a) Concrete

The plastic law of concrete was implemented using the Buyukuzturk criterion proposed by Buyukuzturk[17]. This is a criterion with a plasticity surface similar to the surface of Drucker-Prager criterion often used in concrete calculations. Once the natural plasticity surface of the concrete was identified, a selection was undertaken to choose the best-fitting plasticity surface available on the MARC MENTAT software (finite element software) [18]. Thus, the Buyukuzturk criterion was chosen. Based on the evolution with temperature of the stress-strain laws of concrete in tension, the softening plasticity law was implemented, this law had two evolving dimensions, the equivalent plastic strain and temperature. One should note that the stress-strain laws of concrete in tension were chosen to implement the behavior of concrete because the authors modeled reinforced concrete beams (loaded in bending) and in this particular case, the failure occurred in the lower part of the structural element that was subjected in tension. This choice was made by the fact that the results of the beam never showed plastic behavior in the compressed part of the beam (upper part of the beam).

b) Steel

Steel in reinforced concrete is less complex than concrete from the point of view of mechanical behavior. Steel can be simply implemented using a Von-Mises plasticity surface. Once the volume of elastic behavior bounded by the plasticity surface is exceeded, plastic behavior is initiated following the plasticity law based on the behavior of steel (Fig.7a).

c) TRC (Textile Reinforced Concrete)

The mechanical behavior of the TRC was assumed to be elastic with irrecoverable strain beyond given stress limit (with respect to temperature). Therefore, and considering that it is stressed only along its axis (in the direction of longitudinal textile and the tensile loading direction), a Von-Mises elastoplastic model was used to implement the damaging behavior of the TRC.

3.5.2. Thermal implementation

Finite element models were developed using the MSC Software MARC Mentat [18]. The structural specimens modelled were firstly subjected to mechanical loads and then subjected to a thermal flux corresponding to the ISO-834 time-temperature curve. The two classical heat transfer modes were taken into account: convection at the surfaces exposed to the thermal flux and conduction within the materials. Once the thermal calculations were done, a map of the temperature fields was extracted from the calculations. Thermal degradation of mechanical properties of the constitutive materials (steel and concrete) was then calculated according to the Eurocode 2 EN1992-1-2 [13].

4. Numerical results

The Figures 9, 10 and other results have shown the following.

- Mechanical contribution
  - Shifting the "failure" time by few minutes (about ten minutes) for the two configurations B1 and B2.
- Mechanical contribution (consolidation and load transfer) and heat shield
  - The deflection at which the specimens failed remained approximately the same before and after the addition of a TRC layer, one could point out that for configuration B2, the final deflections of the curves (Fig. 9) for the 3 load levels (F1, 1.25 F1, 1.5F1) were different, as they did not show the end of the evolution of a classical deflection curve.
  - TRC layer provided a stress bridge for the concrete coat as it transferred the stress from high concentration stress areas to low concentration stress areas.
  - TRC layer preserved the mechanical strength of the concrete coating and helped to relieve its stress throughout the fire incident.
  - Ratios 1 and 2 (their definitions were presented under Fig. 10) showed a peak around 7 minutes and a significant drop immediately afterwards. This amounted to the accumulation of damage of the concrete coat. As a result, there was a momentary acceleration of the deflection, hence the peak of ratios 1 and 2.
  - Ratios 1 and 2 continued to decrease after 5 minutes of thermomechanical loading and then stabilized over the loading time. The decrease and stabilization of ratios 1 and 2 (between minute 7 and minute 20) were driven by the transfer of mechanical loads to the tension steels and TRCs that were not yet damaged. This conclusion was supported by Fig. 10 where ratios 1 and 2 stabilized faster for configurations with a TRC layer.
  - TRC's adhesion to RC elements was more significant than that of the FRP composites in case of fire.

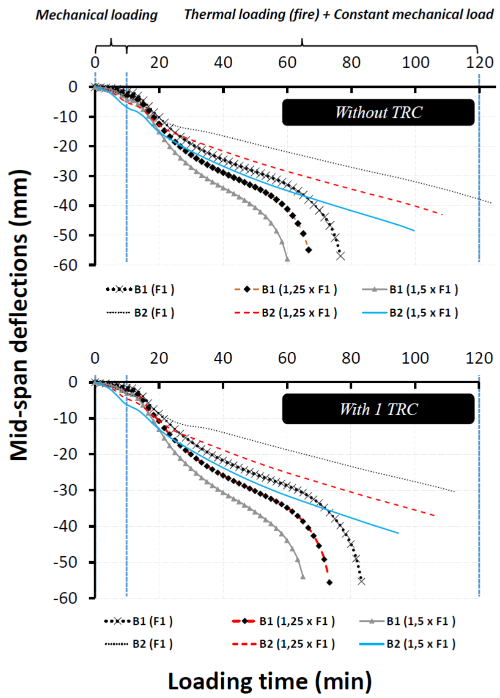

Fig. 9. Numerical deflections of the specimens B1 [11] and B2 [12] (under 3 mechanical loading levels) with and without TRC strengthening with respect to the loading time (mechanical and thermal loads)

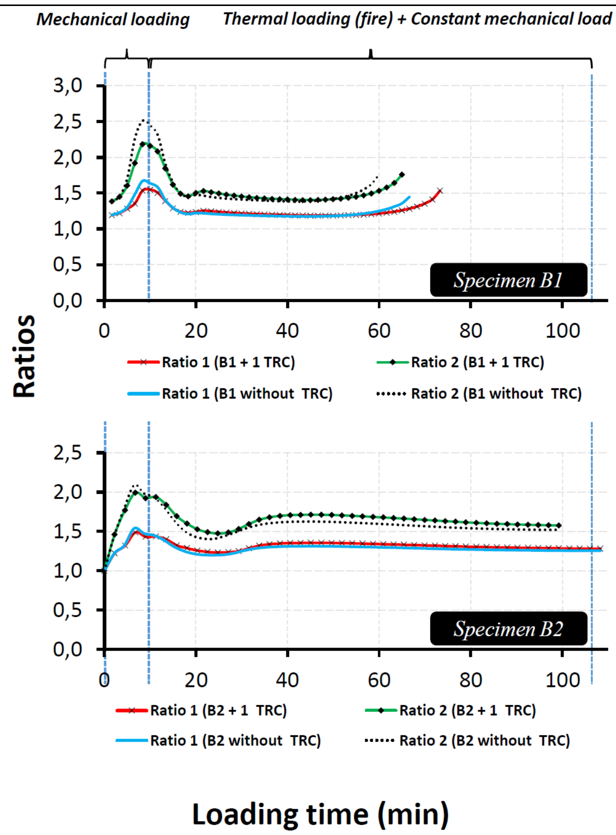

$$\text{Ratio 1} = \frac{\text{Midspan deflection (Mechanical load } \mathbf{1.25xF1}\text{)}}{\text{Midspan deflection (Mechanical load } \mathbf{1xF1}\text{)}}$$

Fig. 10. Evolution of numerical ratios 1 and 2 (between beam’s mi-span deflections) for specimens B1 [11] and B2 [12] with respect to the loading time (mechanical and thermal loads)

5. Conclusion

This study brought forward primary exploratory elements regarding RC element strengthened with TRC composites. It appeared from the results presented herein that TRC strengthening provided a mechanical contribution to the RC beams throughout their fire exposure.

By monitoring the evolution of the deflection over time, as well as the stresses through the specimen's sections (results not included herein), it appeared that the addition of TRC allowed the transfer of stress from higher to lower stressed areas of the concrete coating during a fire. Also, other results have shown that the endurance of the TRC/concrete interface was much more significant than that of the FRP.

6. References

[1] K. T. Q. Nguyen, S. Navaratnam, P. Mendis, K. Zhang, J. Barnett, et H. Wang, « Fire safety of composites in prefabricated buildings: From fibre reinforced polymer to textile reinforced concrete », *Compos. Part B Eng.*, vol. 187, p. 107815, avr. 2020, doi: 10.1016/j.compositesb.2020.107815.

[2] S. M. Raoof et D. A. Bournas, « Bond between TRM versus FRP composites and concrete at high temperatures », *Compos. Part B Eng.*, vol. 127, p. 150‑165, oct. 2017, doi: 10.1016/j.compositesb.2017.05.064.

[3] A. E. Naaman, « Half a century of progress leading to ultra-high performance fiber reinforced concrete : PART I and 2- Overall review », 2011, p. 17‑36.

[4] T. Tlaiji, X. H. Vu, E. Ferrier, et A. Si Larbi, « Thermomechanical behaviour and residual properties of textile reinforced concrete (TRC) subjected to elevated and high temperature loading: Experimental and comparative study », *Compos. Part B Eng.*, vol. 144, p. 99‑110, juill. 2018, doi: 10.1016/j.compositesb.2018.02.022.

[5] T. Ba Tam, A. Si Larbi, et A. Limam, « Numerical modelling of reinforced concrete beams repaired by TRC composites », *Compos. Struct.*, vol. 152, mai 2016, doi: 10.1016/j.compstruct.2016.05.071.

[6] T. Nguyen, X. Vu, A. Si Larbi, et E. Ferrier, « Experimental study of the effect of simultaneous mechanical and high-temperature loadings on the behaviour of textile-reinforced concrete (TRC) », *Constr. Build. Mater.*, vol. 125, p. 253‑270, oct. 2016, doi: 10.1016/j.conbuildmat.2016.08.026.

[7] R. Contamine, A. Si Larbi, et P. Hamelin, « Contribution to direct tensile testing of textile reinforced concrete (TRC) composites », *Mater. Sci. Eng. A*, vol. 528, nº 29, p. 8589‑8598, nov. 2011, doi: 10.1016/j.msea.2011.08.009.

[8] Y. A. Al-Salloum, H. M. Elsanadedy, S. H. Alsayed, et R. A. Iqbal, « Experimental and Numerical Study for the Shear Strengthening of Reinforced Concrete Beams Using Textile-Reinforced Mortar », *J. Compos. Constr.*, vol. 16, nº 1, p. 74‑90, févr. 2012, doi: 10.1061/(ASCE)CC.1943-5614.0000239.

[9] O. Awani, T. El-Maaddawy, et A. El Refai, « Numerical Simulation and Experimental Testing of Concrete Beams Strengthened in Shear with Fabric-Reinforced Cementitious Matrix », *J. Compos. Constr.*, vol. 20, nº 6, p. 04016056, déc. 2016, doi: 10.1061/(ASCE)CC.1943-5614.0000711.

[10] N. Douk, X.H. VU, A. Si Larbi, M. Audebert, R. Chatelin. Numerical study of thermomechanical behaviour of reinforced concrete beams with and without textile reinforced concrete (TRC) strengthening: effects of TRC thickness and thermal loading rate. Engineering Structures, vol. 231, 2021, issue 111737, doi: 10.1016/j.mtcomm.2020.101580

[11] C. Thiago B., R. Joào Paulo C., de L. Rogério C.A., et D. Dhioinis, « Experimental analysis on flexural behviour of RC beams strengthened with CFRP laminates and uder fire conditions », *Compos. Struct.*, vol. 189, p. 516‑528, 2018.

[12] A. Aqeel et K. Venkatesh, « The experimental behavior of FRP-strengthened RC beams subjected to design fire exposure », *Eng. Struct.*, vol. 33, p. 2201‑2211, 2011.

[13] Eurocode 2,EN 1992-1-2, Eurocode 2, design of concrete structures, Part 1.2: General rules – structural fire design. Brussels: Commission of the European Communities; 2004.

[14] Y. Takahashi, « Elastic-plastic constitutive modeling of concrete », *Struct. Mater. Des. Eng.*, 1983.

[15] Z. P. Bazant et M. F. Kaplan, « Concrete at high températures : material properties and mathematical models », *Addison-Wesley*, 1996.

[16] T. Tlaiji, « Développement et caractérisation du comportement thermomécanique des matériaux composites TRC », Université Claude Bernard Lyon 1, 2018 (in French).

[17] O. Buyukuzturk, « Nonminear analysis of reinforced concrete structures », *Comput. Struct.*, vol. 7, nº 149‑156, p. 149‑155, 1975.

[18] « Volume A: Theory and User Information ». MSC Software, 2014.

DURABILITY OF TEXTILE REINFORCED MORTARS UNDER HARSH ENVIRONMENTS

Ioannis Ch. Karakasis[1], Catherine "Corina" G. Papanicolaou[2] and Thanasis C. Triantafillou[3]

[1] Ioannis Ch. Karakasis *(Department of Civil Engineering, University of Patras, Patras, 26504, Greece. ioankarach@upatras.gr)*

[2] Catherine (Corina) G. Papanicolaou *(Department of Civil Engineering, University of Patras, Patras, 26504, Greece. kpapanic@upatras.gr)*

[3] Thanasis C. Triantafillou *(Department of Civil Engineering, University of Patras, Patras, 26504, Greece. ttriant@upatras.gr)*

SUMMARY: *Textile reinforced mortars (TRM) are materials whose mechanical behavior has been extensively investigated during the last years. However, studies on the behavior of these materials after exposure to various aggressive environments are still limited and, hence, their performance during their entire service life remains to be determined. This paper contributes to this grey area of knowledge by investigating: (i) the fibre-matrix bond through pull-out yarn tests and (ii) the TRM-concrete substrate bond through single-lap shear bond tests after exposure of specimens to different aggressive environments, namely accelerated carbonation, freeze/thaw cycles and chloride attack.*

KEY WORDS: *carbonation, chlorides, freeze/thaw, pull-out yarn, shear bond, TRM.*

1. INTRODUCTION

There has been extensive scientific research, during recent years, on Textile Reinforced Mortars (TRM) and their mechanical properties, however, relatively little is known about the durability of these composite materials when used as both stand-alone elements and as parts of reinforced concrete (RC) structures. Nevertheless, relevant research is currently on the rise including topics such as salt crystallization [10], behavior of corroded elements reinforced with TRM [9], influence of alkaline environments [13], use of TRM for cathodic protection [14], exposure to freeze & thaw cycles [3], chloride wet-dry cycle environment [15] and accelerated carbonation [11].

Carbonation, chloride penetration and freeze-thaw cycles (either single-acting or in combination) are the main degradation mechanisms of RC structures. It is known that carbonation and chlorides are the most likely causes of reinforcement corrosion, while freeze-thaw cycles, although do not affect directly the reinforcement, are a common cause of concrete cracking. Taking into account the above, in the context of this research, an effort is made to study the influence of carbonation, chlorides and freeze-thaw cycles on TRM. More specifically, two experimental procedures were selected: (i) pull-out yarn and (ii) TRM-concrete bond. The pull-out yarn test allows the study of the bond between matrix and yarn, while the TRM-concrete bond describes better the behavior of a composite member.

2. EXPERIMENTAL STUDY

2.1. Materials

2.1.1 Mortars

Two types of mortars were used for the production of TRM: a high strength (low water to binder ratio) and a low strength (high water to binder ratio) one (Table 1). In both cases, the proportions of cement: fly ash: silica fume: sand (by weight) are the same. The mix design of the high strength mortar contained superplasticizer, in order to achieve satisfactory flowing capacities.

Table 1. C*omposition of mortars (all in kg/m^3)*

	High strength mortar	Low strength mortar
Cement CEM II/A-M (P-LL) 42.5 N	579	509
Fly Ash	261	229
Silica Fume	58	51
Sand (0-2mm, indoor humidity)	832	731
Water	306	395
Superplasticizer (1.6% binder)	14.38	-

2.1.2 Textiles

Two types of textiles were used: one comprising dry carbon fibers and another made of alkali-resistant coated glass fibers. Their layout and mechanical properties (as provided by the manufacturers), are given in Table 2:

Table 2. *Textile properties*

Technical Data	Carbon textile	Glass textile
Dry fibre density (g/cm³)	1.83	2.60
Dry fibre weight (g/m²)	≥ 170	280
Mesh size (mid-yarn to mid-yarn, mm):	10 x 10	18.2 × 14.2
Tensile strength (kN/m):	>240	~76 kN/m weft, ~77 kN/m warp

2.2. Specimens

2.2.1 Pull-out yarn specimens

In order to investigate the fiber-to-matrix bond following different exposure conditions, prismatic specimens of dimensions 100mm ×600mm ×10mm were produced. In lack of a relevant test standard, previous studies [2, 12] were taken into account during specimens' design. The specimens incorporated a layer of textile placed at mid-thickness. At 200mm from one end a through-thickness notch was created leaving the central part of the composite intact; this configuration aimed at driving the failure to the pull-out of a single yarn. The contact length of the metal end plates with the specimen was 80mm (Figure 1a). The parameters under investigation were the type of textile (bare carbon fibers vs. coated glass fibers), the type of mortar (low strength vs. high strength) and the exposure conditions (ambient, CO_2-rich, chloride contaminated, CO_2/Cl^- combined); the test matrix presented herein is not complete, as the experimental work is still in progress.

2.2.2 Bond specimens

The post-exposure TRM-to-concrete bond was assessed by means of shear bond tests, as per the relevant RILEM recommendation and previous studies [4, 8]. To this purpose, plain concrete blocks measuring 480mm×150mm×150mm were produced and furnished with 400 mm-long carbon fibre TRM strips on three of the four lateral faces (Figure 1b). Each face receiving a 9-yarn TRM strip was first grooved in a lattice grid motif, in order to promote substrate bond with the overlay. The specimens prior to testing were exposed to (or mimicked the effects of) various aggressive environments (carbonation, chlorides, carbonation and chlorides, freeze-thaw cycles). Control specimens were kept under ambient conditions. For the specimens exposed to carbonation and freeze-thaw cycles, special care was given to the protection of all bare concrete surfaces so that damage (if any) would be concentrated on the TRM strips and, consequently, on the TRM/concrete interface.

This protection was achieved by sealing the bare concrete surfaces with an epoxy resin. Both low and high strength mortars (TRM matrices) were investigated.

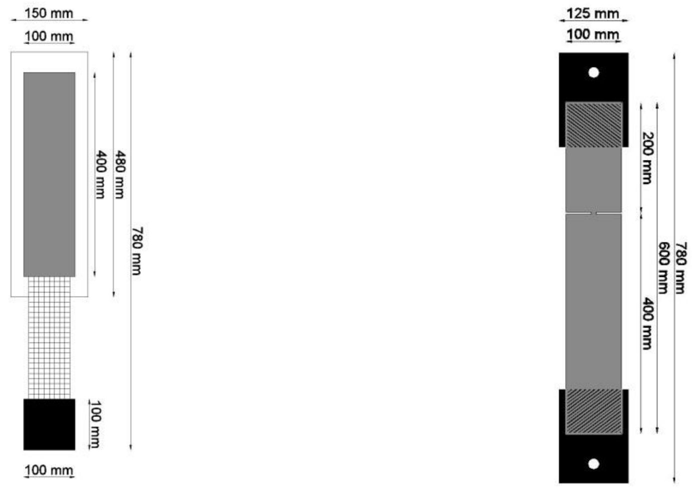

(a) (b)

Figure 1. *Geometry of specimens: (a) bond; (b) pull-out yarn*

2.3. Exposure Conditions

2.3.1 Curing

Specimens not exposed to detrimental environmental conditions were cured in environments with 100% relative humidity (20°±2°C) for 90 days and served as control specimens.

2.3.2 Carbonation

Following a 90-days curing period at ambient conditions (as per 2.3.1), specimens remained for an additional period of 30 days in laboratory conditions and they were subsequently placed in a carbonation chamber at a carbon dioxide (CO_2) concentration of 20% by vol., a relative humidity (RH) of 60% and a temperature equal to T = 40^{o}C, all kept constant throughout the exposure duration.

Regarding the CO_2 concentration, a relatively low value was opted in relation with the values found in the literature (often reaching up to 100%). It should be noted, however, that the CO_2 concentration affects both microstructure and diffusion mechanisms. The role of temperature in carbonation is not easily estimated however, it is considered as having a rather small influence on the phenomenon with the majority of carbonation predictive models ignoring temperature as a parameter. In the present study, the temperature was chosen to be kept at 40^{o}C which is a high but realistic value. The relative humidity level (RH = 60%) was in accordance with relevant standards' ranges [6, 7]. Lastly, the carbonation depth was measured by using a phenolphthalein solution [5].

2.3.3 Chlorides

The marine environment was simulated by introducing sodium chlorides equal to 2.5% of binder weight during the production of specimens (TRM). The latter were then cured as per 2.3.1. The action of chlorides as a function of their origin (admixed or penetrated) is ambiguous for many properties of mortars, such as binding. The same applies to mechanical properties, as many processes (e.g. continuous hydration, leaching) are not reproducible, while cement pastes which are exposed to sodium chlorides instead of seawater do not have identical volumes of phases. However, the introduction of chlorides during mixing is a practice often found in many studies, as it is simple, rapid and straightforward. Finally, the admixed chlorides quantity chosen is thought to be high, yet reasonable.

2.3.4 Combined action of carbonation and chlorides

The simulation of simultaneous exposure to carbonation and chlorides was realized by introducing sodium chlorides equal to 1.4% of binder weight and by exposing specimens to the aforementioned CO_2-rich conditions (in this case, curing was identical to 2.3.2). The introduction of chlorides to the specimens (during mixing) prior to their exposure to carbonation is consistent with the fact that the chlorides penetration is slower than the carbonation, in most cases.

2.3.5 Freeze-Thaw

The specimens – after being cured as per 2.3.1. and an adequate amount of time at standard lab conditions for achieving moisture equilibrium – were subjected to 40 freeze-thaw temperature cycles ranging from +4^{o}C to -18^{o}C and back to +4^{o}C within 4.8h, with freezing taking place in air and thawing into water [1]. The control of the freeze-thaw chamber was based on the temperature measured at the mid-thickness of the TRM strip.

3. RESULTS -DISCUSSION

3.1. Mortar strengths

Table 3 lists the compressive and flexural strengths derived from mortar prisms after subjecting them to different exposure conditions/durations. 90 days' strengths are taken as the basis of comparisons. From Table 3, it can be deduced that in non-carbonated mortars the presence of chlorides does not affect the compressive strength but reduces the flexural one. For the case of low strength chlorides-free mortar, carbonation seems to infer appreciable (> 10%) reduction of the compressive strength for carbonation depths larger than 10 mm. In the presence of chlorides, compressive strength reductions are more pronounced. On the other hand (and, again, for the case of low strength mortar), the flexural strength – although invariably reduced for carbonated and carbonated/chloride-contaminated specimens – varies in a rather erratic manner.

It is known that the presence of chlorides is ambiguous for the strength of concrete. Generally, up to a certain concentration, chlorides act beneficially and then the strength is reduced. This concentration cannot be estimated as it depends on factors such as the concrete age, the water-to-cement ratio, the type of salts formed and the concrete composition. This inconsistency exists as on one hand salts reduce the average pore diameter through hydration products, whereas on the other hand salts are responsible for $Ca(OH)_2$ leaching (in contact with soft water) and genesis of microcracks because of Friedel's salt crystallization pressures (volumetric change due to the formation of the latter is small). Finally, by introducing chlorides the amount of dissolved hydroxyl ions increases thus accelerating the pozzolanic reactions and driving to a refined microstructure

The absence of a trend in the change of flexural strength in carbonated specimens (either with or without chlorides) can be attributed to the fact that the changes in mortar porosity due to carbonation is not an uninterrupted process; fluctuations have been reported during the process while the final porosity of blended cement pastes may be higher than the initial. Also, in the present study, after their exposure to carbonation conditions prisms were cracked. It is reasonable to assume that the presence of random cracks affects strength in an inconsistent way. Since shrinkage microcracking affects less the compressive strength (during compression microckracks close) this inconsistency is reflected more on the flexural strength.

Table 3. *Mortar strengths*

	Low strength mortar		High strength mortar	
Environment	Compression (MPa)	Flexure (MPa)	Compression (MPa)	Flexure (MPa)
Non-aggressive (reference) (28 d.)	45.0(7.9%)	3.69(11.9%)	74.8 (10.1%)	4.31(22.5%)
Non-aggressive (control) (90 d.)	57.4(3.3%)	4.49(11.1%)	89.2(4.8%)	5.56(13.3%)
Chlorides (90 d.)	58.3(2.1%)	3.30(20.1%)	92.4(1.8%)	4.66(6.9%)
Carbonation (≈121 d.) (xc=2.84mm)	58.8(4.7%)	2.48(15.9%)	-	-
Carbonation (≈124 d.) (xc=5.53mm)	57.1(4.5%)	2.33(7.8%)	-	-
Carbonation (≈129 d.) (xc=10.09mm)	50.9(2.0%)	3.45(5.8%)	-	-

Carbonation & Chlorides (≈121 d.)(xc=2.73mm)	55.1(6.8%)	3.21(14.0%)	-	-
Carbonation & Chlorides (≈124 d.)(xc=6.65mm)	50.8(9.2%)	2.74(11.4%)	-	-
Carbonation & Chlorides (≈129 d.)(xc=10.12mm)	47.4(2.9%)	2.98(22.6%)	-	-
Notes:	(…%): coefficient of variation; (...d.): specimens' age at testing (days); xc: measured carbonation depth in prisms; missing values: testing is ongoing			

3.2. Pull-out yarn specimens

For the pull-out carbon yarn specimens manufactured with the high-strength mortar, failure was due to progressive rupture of fibers for both chlorides-free (control) and chlorides-contaminated matrices. However, the presence of chlorides leads to a lower peak stress indicating a change of the fiber-to-matrix bond conditions.

The behavior of the pull-out carbon yarn specimens manufactured with the low-strength mortar is much more complex. The high coefficient of variation associated to each test group (with the exception of the "carbonation and chlorides" and "chlorides" groups) renders any attempt for comparisons risky and unreliable. However, it should be mentioned that increase of mixing water, generally, results in non-uniform and/or bleeding-prone mortar mixes. This may lead to different filament-to-mortar bond conditions between nominally identical specimens. Also, it is known that chlorides accelerate the hydration process and in this way reduce segregation and bleeding risk. This is probably the reason why specimens with admixed chlorides show reduced scattering in comparison with the chlorides-free specimens.

Table 4. *Pull-out carbon yarn results*

	Low strength mortar		High strength mortar	
	Stress (MPa)	Displacement (mm)	Stress (MPa)	Displacement (mm)
Control	1002 (26.7%)	1.457 (56.5%)	1526 (13.3%)	0.548 (19.9%)
Chlorides	766 (21.7%)	1.190 (25.5%)	1378 (12.0%)	1.739 (26.2%)
Carbonation	880 (49.4%)	2.656 (51.2%)	-	-
Carbonation & Chlorides	1206 (10.6%)	4.090 (30.4%)	-	-
Notes:	(…%): coefficient of variation; stress = load / yarn cross-section; missing values: testing is ongoing			

In the case of the pull-out glass yarn specimens, the embedment length and the coating of the yarn dictates the failure mode which is yarn rupture. As seen from the values of Table 5, the type of failure is mortar-related (the larger the mortar strength the larger the ultimate stress).

Table 5. *Pull-out glass yarn results*

	Low strength mortar		High strength mortar	
	Stress (MPa)	Displacement (mm)	Stress (MPa)	Displacement (mm)
Control	434 (7.6%)	1.400 (8.5%)	584 (8.4%)	2.331 (3.6%)
Chlorides	357 (17.4%)	0.631 (21.3%)	476 (14.9%)	1.006 (33.3%)
Notes:	(…%): coefficient of variation; stress = load/ dry yarn cross-section			

3.3. Bond specimens

Table 6 summarizes the results in the form of maximum shear bond stress and respective displacement. For the case of control and chlorides-contaminated specimens, failure was due to fibers rupture. Hence, the maximum shear bond stress is not affected by the properties of the mortar (strength or presence of chlorides). This is in contrast to the relevant finding for the case of pull-out specimens highlighting the difficulties of conclusions extension drawn from one (pull-out yarn specimens) to the other (shear bond specimens).

Carbonated specimens (either with or without chlorides) failed due to fibers' slippage. It should be mentioned that carbonation resulted in cracking of the TRM overlays, leading to the alteration of the textile-to-matrix bond conditions and the shift in failure mode. From Table 6, it becomes clear that carbonation (of either chloride-free or chloride-contaminated specimens) moderately decreases the shear bond strength.

The failure mode and the magnitude of the shear bond strength for specimens undergoing freeze-thaw cycles are similar to those of carbonated specimens. In this case, consecutive freezing and thawing resulted in interlaminar damage manifested by cracks running along the top mortar layer/textile interface; the cracks were visible from the sides of the TRM strips.

Table 6. *Shear bond test results*

	Low strength mortar		High strength mortar	
	Stress (MPa)	Displacement (mm)	Stress (MPa)	Displacement (mm)
Control	1092(16.7%)	0.515(16.5%)	1083(7.9%)	0.391(3.8%)
Chlorides	1135(9.7%)	0.530(15.6%)	1077(13.4%)	0.406(11.5%)
Carbonation	901(9.0%)	0.548(17.1%)	-	-
Carbonation & Chlorides	885(2.8%)	0.446(17.1%)	-	-
Freeze & Thaw	896(7.6%)	0.615(11.8%)	-	-
Notes:	(…%): coefficient of variation; missing values: testing is ongoing			

4. CONCLUSIONS

Although research is in progress some preliminary conclusions are:

- The admixed chlorides reduce the flexural strength of the mortars, but not the compressive strength.
- During carbonation both the compressive and the flexural strength of the low strength mortar are reduced (research is ongoing for high strength mortars).
- Carbonation shrinkage phenomena result in cracking of mortar prisms and TRM strips bonded on concrete substrates (irrespective of chloride presence in the mortar comprising the overlay). This observation is valid for a low strength mortar, whereas research is ongoing for high strength mortars).
- The extension of conclusions drawn from pull-out tests to shear bond tests and vice versa is not feasible in the present study, where the effect of exposure to detrimental environments is considered.
- The type of exposure condition may affect the shear bond failure mode. For the types of TRM/substrate systems investigated herein, admixed chlorides bear no effect on the failure mode and on the shear bond capacity. On the contrary, carbonation of textile-reinforced low strength mortar overlays (through carbonation shrinkage cracking) results in shift of the failure mode from fibers rupture, in control specimens, to fibers' slippage in carbonated ones and in moderate (~18%) shear bond strength reduction. The same applies to composite specimens (concrete blocks furnished with TRM overlays) undergoing consecutive freezing and thawing; in this case, shear bond strength reduction is owed to interlaminar damage of the TRM strip. Research is ongoing for textile-reinforced high strength mortars.

5. REFERENCES

[1] ASTM International, Standard Test Method for Resistance of Concrete to Rapid Freezing and Thawing (ASTM C666 / C666M-15), West Conshohocken, PA, 2015.

[2] BUTLER, M., MECHTCHERINE, V., HEMPEL, S., "Experimental investigations on the durability of fibre–matrix interfaces in textile-reinforced concrete", *Cement and Concrete Composites*, vol. 31, n ° 4, 2009, p. 221-231.

[3] COLOMBO, I. G., COLOMBO, M., DI PRISCO, M., "Tensile behavior of textile reinforced concrete subjected to freezing–thawing cycles in un-cracked and cracked regimes.", *Cement and Concrete Research*, vol. 73, p. 169-183.

[4] DE FELICE, G., AIELLO, M. A., CAGGEGI, C., CERONI, F., DE SANTIS, S., GARBIN, E., GATTESCO, N., HOJDYS, Ł., KRAJEWSKI, P., KWIECIEŃ, A., LEONE, M., LIGNOLA, G. P., MAZZOTI, C., OLIVEIRA, D., PAPANICOLAOU, C., POGGI, C., TRIANTAFILLOU, T., VALLUZI M. R., VISKOVIC A., "Recommendation of RILEM Technical Committee 250-CSM: Test method for Textile Reinforced Mortar to substrate bond characterization", *Materials and Structures*, vol 51, n ° 4, 2018, p. 1-9.

[5] EUROPEAN COMMITTEE FOR STANDARDIZATION, Products and systems for the protection and repair of concrete structures - Test methods - Determination of carbonation depth in hardened concrete by the phenolphthalein method (EN 14630:2006), Brussels, 2006.

[6] EUROPEAN COMMITTEE FOR STANDARDIZATION, Products and systems for the protection and repair of concrete structures - Test methods - Determination of resistance to carbonation (EN 13295:2004), Brussels, 2004.

[7] EUROPEAN COMMITTEE FOR STANDARDIZATION, Testing hardened concrete. Determination of the carbonation resistance of concrete. Accelerated carbonation method (EN 12390-12:2020), Brussels, 2020.

[8] DE SANTIS, S., CAROZZI, F. G., DE FELICE, G., POGGI, C., "Test methods for textile reinforced mortar systems", *Composites Part B: Engineering*, vol. 127, 2017, p. 121-132.

[9] FANG, L., ZHOU, Y., YI, D., YI, W., "Experimental Study on Flexural Capacity of Corroded RC Slabs Reinforced with Basalt Fiber Textile.", *Applied Sciences*, vol. 11, n ° 1, 2021, p.1-22.

[10] FRANZONI, E., SANTANDREA, M., GENTILINI, C., FREGNI, A., CARLONI, C., "The role of mortar matrix in the bond behavior and salt crystallization resistance of FRCM applied to masonry", *Construction and Building Materials*, vol. 209, 2019, p.592-605.

[11] MUMENYA, S. W., TAIT, R. B., ALEXANDER, M. G., "Mechanical behaviour of Textile Concrete under accelerated ageing conditions.", *Cement and Concrete Composites*, vol. 32, n ° 8, 2010, p. 580-588.

[12] PORTAL, N. W., PEREZ, I. F., THRANE, L. N., LUNDGREN, K., "Pull-out of textile reinforcement in concrete", *Construction and Building Materials*, vol. 71, 2014, p. 63-71.

[13] RIZZO, V., BONATI, A., MICELLI, F., LEONE, M., IELLO, M. A., "Influence of Alkaline Environments on the Mechanical Properties of FRCM/CRM and their Materials.", *Key Engineering Materials*, vol. 817, 2019, p. 195-201.

[14] SU, M. N., WEI, L., ZHU, J. H., UEDA, T., GUO, G. P., XING, F., "Combined impressed current cathodic protection and FRCM strengthening for corrosion-prone concrete structures.", *Journal of Composites for Construction*, vol. 23, n ° 4, 2019, p. 1- 11.

[15] YIN, S. P., PENG, C., JIN, Z. Y., "Research on mechanical properties of axial-compressive concrete columns strengthened with TRC under a conventional and chloride wet-dry cycle environment.", *Journal of Composites for Construction*, vol. 21, n ° 1, 2017, p. 1-11.

Session 3
Ferrocement : Recent Applications

DESIGN OF THE FERROCEMENT CANOPY OF THE NEW ATHENS OPERA HOUSE

Gregory Penelis[1], Bruce Martin[2], Pete Winslow[3], Kostas Paschalidis[4]

[1]*MSc, DIC, Phd, CEO of Penelis Consulting Engineers, penelis@penelis.com*

[2] *MA, CEng, MIStructE, Associate Director Expedition Engineering, Bruce.M@expedition.uk.com*

[3] *MEng PhD CEng MIStructE, Associate Director Expedition Engineering, pete.w@expedition.uk.com*

[4]*MSc, Phd, Head of analysis at Penelis Consulting Engineers, kp@penelis.com*

SUMMARY: *The ferrocement canopy over the Athens opera House (SNFCC) is 100mx100m in plan with an aerofoil shape, resting on the opera roof supported by 30 columns -via springs- resulting in a clear span between columns of 75m x 50m, one of the largest ferrocement structures in the world. It is essentially a composite space truss with two ferrocement skins, top and bottom, carrying primary structural loads, connected together by diagonal steel circular hollow tube sections and ferrocement diaphragms. The current paper outlines the analytical approaches utilised, starting from linear elastic dynamic analysis, continuing to nonlinear static (collapse) analysis and nonlinear dynamic analysis combined with dedicated algorithms for section analysis. A companion paper elaborates on the experimental verification of the design approaches presented herein.*

KEY WORDS: *ferrocement, nonlinear, flexure, shear, preconstruction, splice*

1 INTRODUCTION

The Solar Canopy above the Athens Opera House is 100m x 100mx in plan and one of the largest ferrocement structures in the world. The Athens Opera House is a R/C building, part of the Stavros Niarchos Cultural Center (SNFCC), a project designed by Renzo Piano with structural engineers Expedition Engineering, Omete and Penelis Consulting, completed in 2016 with a budget of 550 Million Dollars. Paul Nedwell and Patrick Jennings were involved in several stages of the design and construction of the canopy.

The architectural intent was to create a canopy which was a visually slender as possible, with a finish 'like a yacht' and with no visible joints. The constraint of the opera house below, and general good practice for seismic design required the canopy to be a 'light' structure. The ferrocement skins define the sculpted architectural form and combine structure, waterproofing and finish in a single element. Around the perimeter the ferrocement skins are sculpted to incorporate the rainwater gutter. Ferrocement provided the slimmest and lightest viable design for the canopy. Ferrocement does not require procurement of a special material from a single supplier and has a track record of construction to form complex forms by site teams with limited prior experience of the material. The double curvature shape combined with the thin sections foreseen for the bottom and top skin required to utilise preconstruction of the ferrocement elements using a "standard" panel of 3,50mx7,50m and 60cm splice zones.

The ferrocement canopy is supported on the roof of the base-isolated Opera building through 30 HCS columns and hoisted by spring and damper column heads. It is 100mx100m in plan with an aerofoil shape, and creates an inner column free area with a clear span of 75m x 50m. It is made up of two double curvature monocque ferrocement skins, which are ribbed membranes and carry primary structural loads a well as providing the finished architectural surface, connected together by ferrocement diaphragms and diagonal steel circular hollow tube sections creating a composite space truss. A general view and section of the Ferrocement Canopy and the Opera house is shown in figures 1 and 2.

Figure 1. *Side view of the canopy*

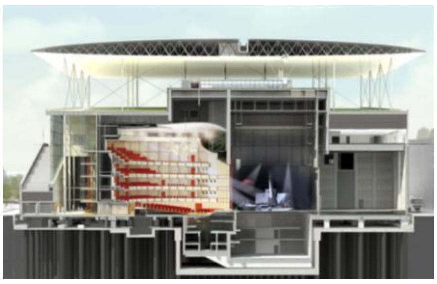

Figure 2. Section of canopy & building

For all sections meshes are arranged in a sandwich pattern in order to create a heavily reinforced ferrocement section (3-6% total volume fraction of reinforcement). The main concept is that the external meshes are thin to provide crack control and durability while the internal are thicker using mesh types of B430A, B500A and B500C steel grade from Ø1.0mm to Ø10mm diameters. Properties of the ferrocement mortar are shown in table 1.

Table1. *Ferocement mortar mechanical properties*

SAMPLES	PROPERTY	MIX DESIGN #1 Superfluid	MIX DESIGN #2 Low Workability
Cubes 100x100x100	Compressive strength (7 days)	64 MPa	64 MPa
	Compressive strength (28 days)	90 MPa	88 MPa
	Shrinkage (28 days)	0.390 mm/m	0.390 mm/m
Cylinders 150x300	Compressive strength (7 days)	56 MPa	56 MPa
	Compressive strength (28 days)	80 MPa	80 MPa
	Elastic modulus	33 GPa	33 GPa
	Density of hardened mortar	< 2290 kg/m^3	< 2290 kg/m^3

2 ANALYSIS

2.1 Elastic Analysis

Several different types of analysis have been utilised in order to accurately simulate the structural behaviour of such a complex structure. The basis of the design was spectral modal dynamic analysis of a complete F.E. model of the opera and the canopy using both Etabs 9.7 and Scia Engineer software code (Figure 3).

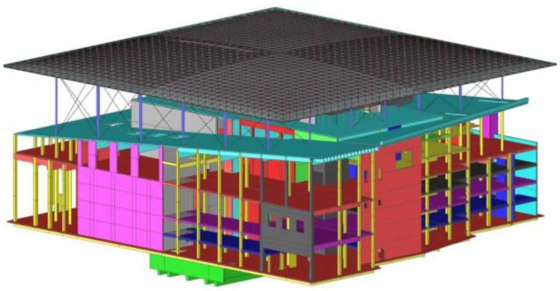

Figure 3. *F.E. model*

The permanent loads of the canopy are shown in table 2.

Table2. *Permanent loads of the canopy*

	Loads
Ferrocement	36700 kN
Steel brackets	2500 kN
Diagonal Tubos	600 kN
Column Heads connection	1500 kN
MEP Area	500 kN
PV Panels	5000 kN
Total weight :	46800 kN

2.2 Nonlinear analysis

Two types of nonlinear analysis were performed static collapse analysis for vertical loads and t-h nonlinear analysis for wind loading and earthquake loading.

Figure 4. Typical *reinforcement cages*

The static nonlinear analysis was executed in order to estimate the nonlinear performance of the canopy (material nonlinearity) under vertical uniformly distributed loads, thus resulting in the available overstrength as well as the available ductility (if any). The analysis required the development of a custom step by step non iterative procedure for the nonlinear application of the loads, which utilised the API of SAP2000 driven by PYTHON scripts. The resulting ultimate capacity of the ferrocement skins of the canopy corresponds to 2.68 x ULS design load which is much more than the most critical element of the whole structure that is the available movement capacity of the canopy 1.35 x ULS (Figure 5).

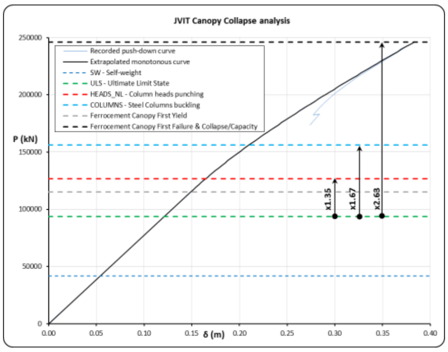

Figure 5. *Push down curve*

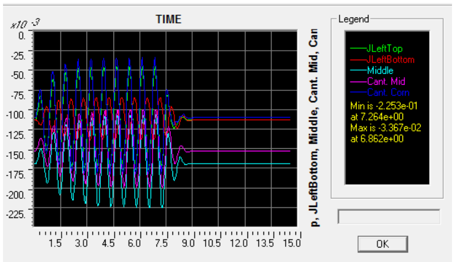

Figure 6. W*ind response with resonance*

The dynamic response of the canopy under wind and earthquake excitation was investigated using t-h nonlinear analysis. The nonlinearity has been lumped in NL elements representing the silicon springs and dampers at each column. The response for the design wind gust as well as the effect of resonance (wind with the same predominant period as the canopy) is shown in **Figure 6**. These verified the maximum deformations predicted using the elastic analysis approach.

3 DESIGN OF SECTIONS

3.1 Design of membrane and rib sections

The design of the ferrocement sections, based on the elastic analysis, was executed using EN1992 as basis, considering that the basic constitutive laws of ferrocement are accurately approximated by those of reinforced concrete (an assumption verified by numerous experimental tests). The following should be noted:

- Considering the slenderness of the sections, section forces were increased due to 2nd order effects (§5.8.8 EN1992-1-1)
- The limited ductility of the section considering ε_{cu2} = 2.6‰-2.9‰ for cement mortar and B430A and B500A for the reinforcement meshes (ε_{uk} = 25‰) led to a limitation of the deformation in the elastic range. So ε_{cu2}= ε_{c2}=2.0+0.085(f_{ck}-50)$^{0.53}$ for cement mortar and $\varepsilon_{uk}=f_{yd}/E_s$ for steel mesh (figure 4).
- All sections of the ferrocement canopy (membranes, T-ribs and beams) were checked against M-N interaction curves using the dedicated software AnySection (Figure 7, Figure 8, Figure 9) [2].

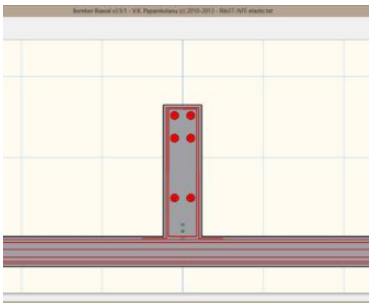

Figure 7. T section analysis

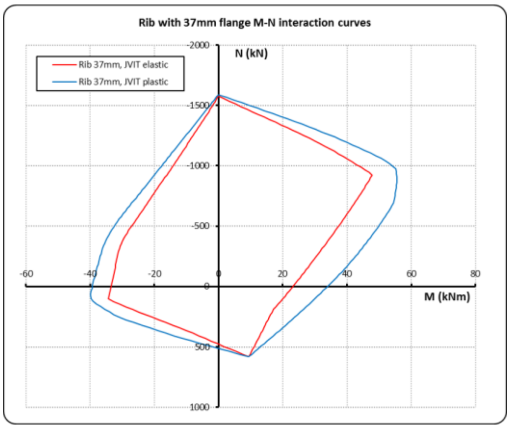

Figure 8. M-N Interaction curves for stages I and II

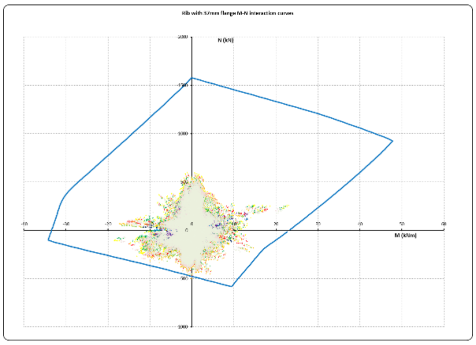

Figure 9. M-N pairs for all design combinations Vs capacity Interaction curves (37mm membrane)

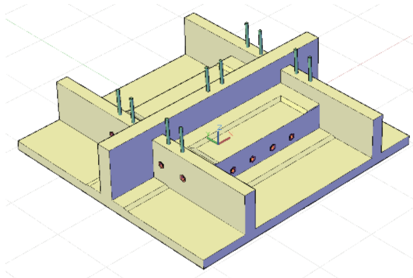

Figure 10. Typical thickening (joint)

- Shear design was executed using the formulae of EN1992-1 and cotθ=2.30-2.50 (VRd,s = VRd, max). It should be noted that all the shear reinforcement consists of external meshes, U bars and ties with diameters of 1.00mm to 1.6mm

3.2 Bracket connections design

The canopy has 893 joints that connect the diagonal steel elements to the top and bottom ferrocement skins. These are realizes with spider brackets that are connecte to the ferrocement skins. These are bolted on ferrocement 140mm thickenings (joints) between the ribs which are considered as corbels to the skin. The initial approach was using a general strut and tie model which being conservative led to the requirement of thick wires which created a problem considering the 3mm cover. The test results also confirmed the considerably high overstrength, so a more detailed 3d approach, using a more accurate strut and tie model, considering all the load paths and each individual wire (tie).

Three individual load directions are defined, X transverse to the ribs, Y parallel to the ribs and Z (**Figure 10**). Fz is transferred directly to the ribs and main beam using anchors hence the calculation is straightforward. Fx is transferred to the membrane through the thickening (corbel) using a strut and tie model shown in Figure 11 in which the actual wires (ties) are modelled at every 50mm and the struts inclinations where selected so that all of them are in compression and all ties are in tension (having cotθ<2,50). The additional vertical eccentricity of Fx is transferred as a force pair to the ribs.

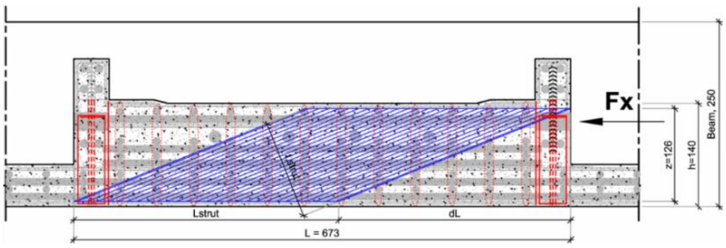

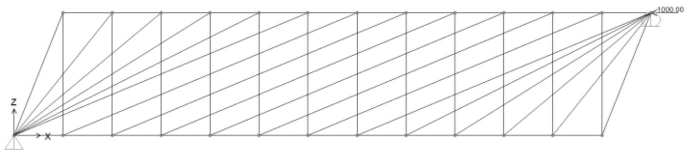

Figure 11. Fx transfer to the ribs and corresponding bow-chord model

For Fy (parallel to the ribs) a 3d F.E. model was created where the joint was modelled using struts and ties (**Figure 12**) having the actual grid of the wires (50mmx50mm) for the ties. As previously the struts inclinations where selected so that all of them are in compression and all ties are in tension (having cotθ<2,50), using an iterative procedure to remove the ties in compression and the struts in tension.

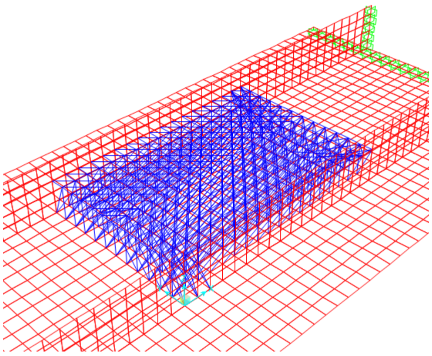

Figure 12. Strut-tie model

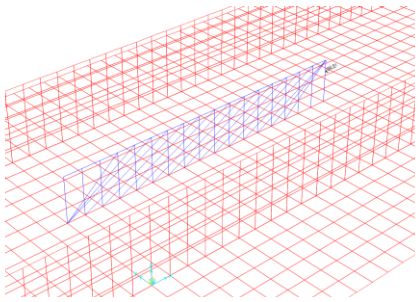

Figure 13. Typical longitudinal truss

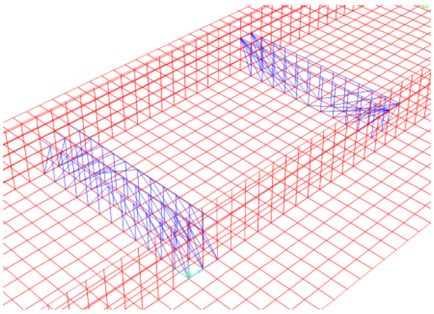

Figure 14. End trusses

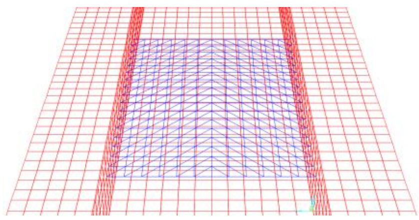

Figure 15. Top surface horizontal truss

Two additional load paths were identified for the transfer of force to the ribs, one is shown in **Figure 16** using a strut and tie approach and in **Figure 17** in deformed shape from the model and the corresponding test (EN1992-1 §6.5).

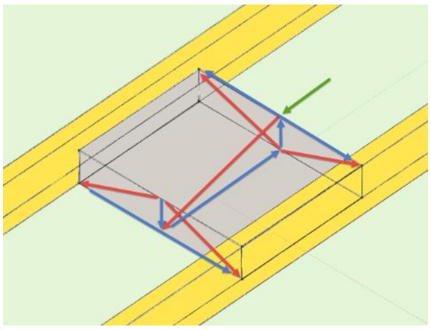

Figure 16. Bow string model

Figure 17. Longitudinal failure mode

The second mechanism includes a load path of horizontal transfer of the shear force to the ribs and then, through the ribs to the membrane. This was modelled with a horizontal truss on the top of the thickening as shown in **Figure 15** which was found to transfer ¾ of the total shear. Additional rebars to connect the joint to the ribs at this surface as well as additional ties between the ribs and the membrane for the safe transfer of this force were added.

3.3 Splicing design

Given the choice for preconstruction the splicing of the rebar meshes of the membranes as well as rebars of the ribs and beams was critical. 600mm cast insitu zones were foreseen. The main rebars of the ribs Ø10-Ø16 were spliced using embedded tie rods 8.8-10.9 and couplersς (Figure 18). The meshes were spliced using lapping lengths by removing the transverse wires of the meshes in the lapping length in order to avoid a thickness increase (Figure 18) and arranging a positive negative orientation in the edges, a constraint that affected the erection sequence. All calculations were based on EN1992-1 §8.7 and verified experimentally.

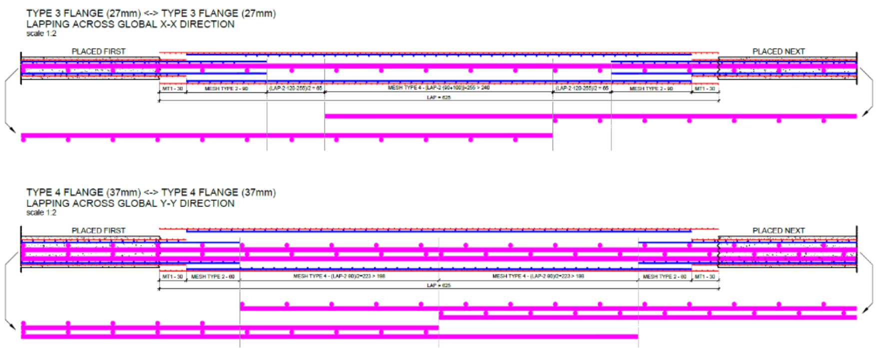

Figure 18. Meshes splicing for 27mm panels in X-X and 37mm panels in Y-Y

4 CONCLUSIONS

This paper demonstrates the global analysis model used by the design team for the SNFCC ferrocement canopy. The elastic dynamic analysis section forces were used for the flexural and shear design of the individual structural members that comprise the top and bottom skins, which include T-beams, membranes and corbels, using the provisions of EN1992-1. All these calculations were also checked using nonlinear static and dynamic analyses. The companion paper includes the experimental verification of these elements.

Figure 19. Ribs splicing using couplers and tie rods

5 REFERENCES

[1] G & G Penelis Consulting Engineers SA (2013), SNFCC Solar Collector Redesign Technical Reports, Calculation Reports & Drawings

[2] Papanikolaou, VK. (2012), “Analysis of arbitrary composite sections in biaxial bending and axial load”, Computers & Structures 2012; 98-99:33-54

[3] EN 1992-1-1:2004Eurocode 2: Design of concrete structures – Part 1-1: General rules and rules for buildings

[4] Expedition Engineering, “Solar Collector Code Compliance” Ref. EXPE-C-S7 EX40 - Rev A, 28th Septemeber 2011

[5] Expedition Engineering, “Ferrocement Analyses – local analyses Theory (RSAP)” Ref. EXPE-C-S7-EY52

[6] American Concrete Institute, ACI 549.1R-93 Guide for the Design, Construction and Repair of Ferrocement. (1999, Reapproved 2009)

[7] Antoine E. Naaman, Ferrocement And Laminated Cementitious Composites, TechnoPress3000, (2000)

[8] International Ferrocement Society, “Ferrocement Model Code”, January 2001

EXPERIMENTAL VERIFICATION FOR THE FERROCEMENT CANOPY OF THE NEW ATHENS OPERA HOUSE

Gregory Penelis[1], Bruce Martin[2], Pete Winslow[3], Kostas Paschalidis[4]

[1]*MSc, DIC, Phd, CEO of Penelis Consulting Engineers, penelis@penelis.com*

[2] *MA, CEng, MIStructE, Associate Director Expedition Engineering, Bruce.M@expedition.uk.com*

[3] *MEng PhD CEng MIStructE, Associate Director Expedition Engineering, pete.w@expedition.uk.com*

[4]*MSc, Phd, Head of analysis at Penelis Consulting Engineers, kp@penelis.com*

SUMMARY: *The Athens Opera House is a R/C building, part of the Stavros Niarchos Cultural Center (SNFCC), a project designed by Renzo Piano with structural engineers Expedition Engineering, Omete and Penelis Consulting, The ferrocement canopy is 100mx100m in plan with an aerofoil shape, resting on the opera roof via 30 columns resulting in a clear span between columns of 75m x 50m. It is essentially a composite space truss with two ferrocement skins, top and bottom, connected together by diagonal steel circular hollow tube sections and ferrocement diaphragms; the ferrocement skins were precast in pieces 3.50mx7.00m and connected insitu with cast zones. The current paper outlines the full scale ferrocement section tests that took place in the NTUA for biaxial compression of characteristic top and bottom skin membranes, 4-point flexural tests for ribs and beams, shear tests and pull-out tests for the joint connections of the diagonals to the ferrocement skins, biaxial testing of ferrocement joints, lapping length tests for the reinforcement meshes between the precast panels, casting joint tests between the ribs and the membrane. A companion paper elaborates on the design approaches used that were verified by the experimental program presented herein.*

KEY WORDS: *ferrocement, testing, shear, flexure, lapping, precast, biaxial, pull-out*

1. INTRODUCTION

The ferrocement canopy of the Athens Opera House (SNFCC) is based on the roof of the Opera building through 30 HCS columns and hoisted by spring and damper column heads. It is 100mx100m in plan with an aerofoil shape, and creates underneath an inner column-free area with a clear span of 75m x 50m. It is made up of two double curvature ferrocement skins, top and bottom skin which are ribbed membranes, connected together by ferrocement diaphragms and diagonal steel circular hollow tube sections creating a composite space truss. The ferrocement skins are composed by 717 preconstructed ferrocement panels with 3.50mx7.00m dimensions connected insitu via casting joints of 60cm. A general view of the ferrocement canopy is shown in figure 1 and a characteristic phase of the assembly of the preconstructed panels is shown in figure 2.

Figure 1. V*iew of the canopy*

Figure 2. V*iew of the canopy assembly*

The ferrocement skins are actually ribbed membranes with ribs at every 60cm and transverse beams every 200cm. The connection of the steel diagonals is realised by ferrocement thickenings (Figure 3). The connection of the precast elements is realised for the ribs and beams with couplers and tie rods while the reinforcement meshes have the required lapping length. All these ferrocement sections and special connections were calculated using dedicated algorithms based on EN1992 and were experimentally verified using unscaled testing in NTUA [2] managed by professor Kourkoulis.

2. TESTING

2.1. Testing Program

The design of the ferrocement canopy was based on the requirements of EN1992 and EN1998 under the assumption that ferrocement can be designed by applying the reinforced concrete guidelines, despite the deviations regarding minimum diameter, rebar cover and dimensions. In order to validate the assumptions and the design procedure elaborated in the companion paper, a set of full scale tests on ferrocement elements were foreseen by the design team and undertaken at the Strength of Materials lab of NTUA. Those tests are the following:

- Biaxial compression of top and bottom ribbed membranes
- 4-point tests for beams and ribs
- Tie rods pull-out and shear tests for joints
- Biaxial compression of joints
- Lapping length tension test
- Cold casting joints

2.2. Biaxial compression of top and bottom ribbed membranes

Six full scale ferrocement membrane elements with 2.00mx2.50m were tested for biaxial compression (Figure 3 and Figure 4). The tests were executed statically by gradually increasing the load in both directions until the calculated compression capacity was reached, and then unidirectionally the load was increased to failure. The test also controlled the out-of-plane deformation of the panels to assess any 2nd order effects. All samples resulted in an increased bearing capacity and did not demonstrate 2nd order effects (Figure 5 and Figure 6).

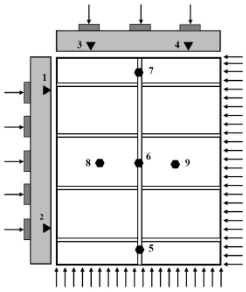

Figure 3. *Biaxial compression test photo* **Figure 4.** Biaxial compression test

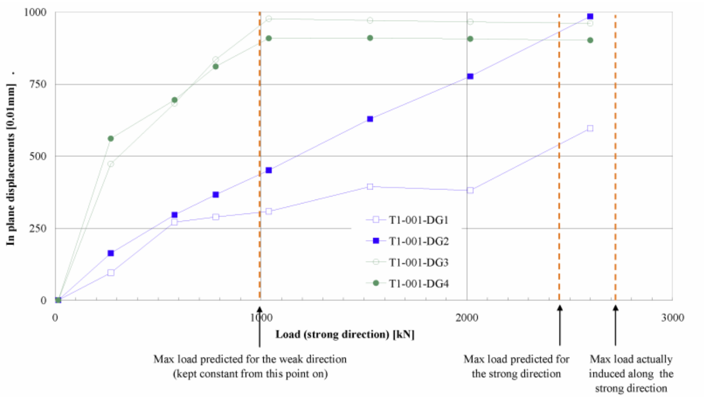

Figure 5. Extensiometer readings 1-4 Vs load (A001)

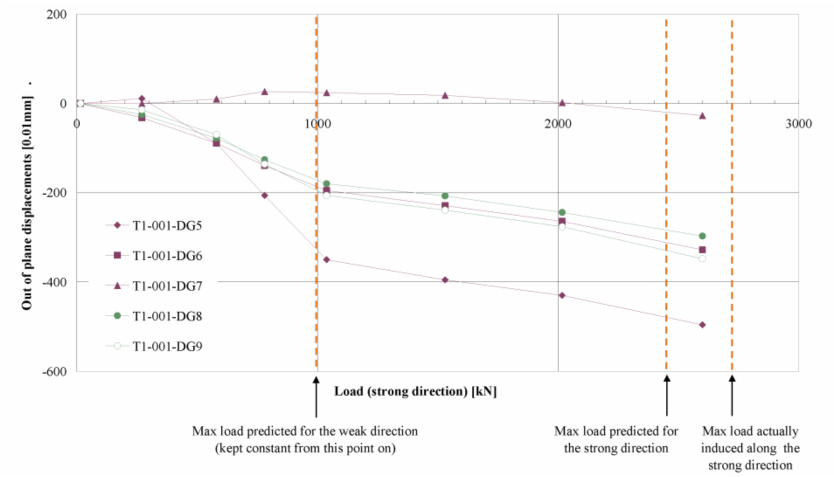

Figure 6. Extensiometer readings 5-9 Vs load (A001)

2.3. 4-point tests for beams and ribs

Full scale tests of the T shaped rib and beam ferrocement elements were executed for flexure and shear using 4 point load setup (Figure 7). The dimensioning of the test elements was selected so that shear failure would supersede the flexural failure having a shear aspect ratio of 600/200=3.0 for the ribs and 600/250=2.4 for the beams. The corresponding flexural and shear ultimate capacity was calculated using EN1992-1 with f_{cm} = 90MPa, f_y = 500MPa, cotθ=2.50 and material SF=1.0.

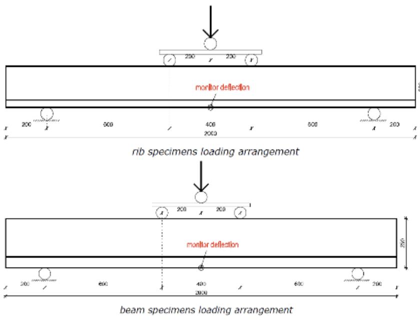

Figure 7. 4-point loading test

Figure 8. Shear failure of T beam

The calculated failure load was verified with accuracy of 1-3% while the design shear capacity was exceeded by 58%.

Table1. *4 point tests for ribs and beams: failure mode and ultimate capacity*

Specimen	Failure Type	Shear at failure	Moment at failure
Rib 49/200/37	Flexural	$1.35xV_{Ru}$	$1.03xM_{Ru}$
Rib 49/200/57	Flexural	$1.54xV_{Ru}$	$1.01xM_{Ru}$
Beam 61/250/57	Shear	$1.58xV_{Ru}$	$0.93xM_{Ru}$

2.4. Tie rods pull-out and shear tests for joints

As has been mentioned, the joints where the diagonals connect to the ferrocement skins are constructed using ferrocement thickenings (**Erreur ! Source du renvoi introuvable.**) with embedded tie rods M10 (10.9). Those were tested both in shear as well as pull-out loading till failure.

In all cases of shear loading the tie rods failed as designed (Figure 9 and Figure 10), while in the pull-out tests the ferrocement only demonstrated hairline cracks (Figure 11 and Figure 12).

Figure 9. Shear loading of tie rods

Figure 10. Failure after shear load

Figure 11. Pullout of tie rods

Figure 12. Failure after pullout

2.5. Biaxial compression of joints

The ferrocement thickenings are actually corbels protruding from the ferrocement membrane. Those were tested full scale with specimens 1.25m x1.25m under biaxial compression. Two different sets of specimens were prepared, (a) with the ribs being on the opposite sides of the beams and thickening (Figure 13) and (b) with ribs and beams on the same side (Figure 14).

Figure 13. Specimen with ribs on same side of beam and thickening

Figure 14. Specimen with ribs on opposite side of beam and thickening

Very detailed strut and tie calculations (Figure 15) as well as the tests (Figure 16) demonstrated that the solution with the ribs and beams on the same side of the membrane were superior by a factor of 2.0, to the solution with the beams and ribs being on the opposite sides of the membrane, thus modifying the original design of the top skin, which originally had the ribs outwards.

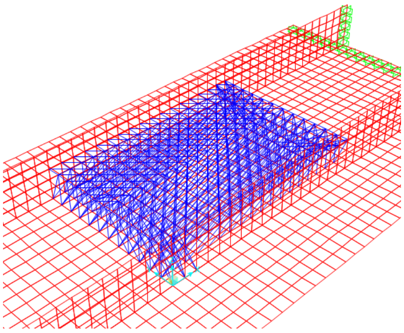

Figure 15. 3d Strut and tie calculation model

Figure 16. Typical failure of original arrangement (a)

2.6. Lapping length tension test

The precast panels are connected in 60cm cast insitu zones using lapping of the meshes. In this length the 6 layers of the meshes are lapped using complete meshes from one side (female) and only the longitudinal wires of the meshes of the other side (male) so that the thickness in the lapping zone would not be increased (Figure 17).

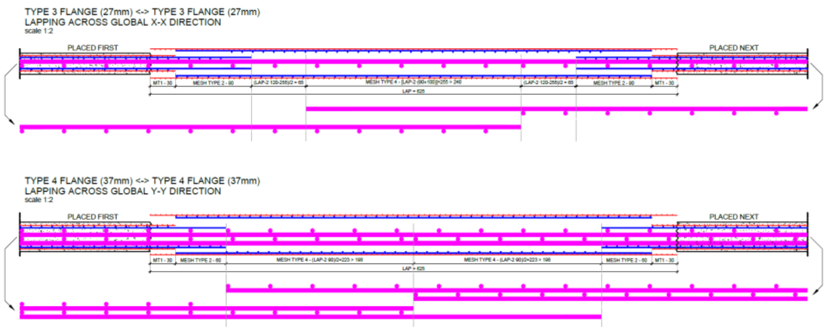

Figure 17. Lapping arrangement for 27mm panels and 37mm panels

For the ribs the solution of using couplers and rods to connect adjacent panels was selected (Figure 18)

Figure 18. Lapping arrangement for ribs using couplers and rods

Dog-bone specimens (Figure 19) were used to assess the calculation formulas used (based on EN1992-1). In all cases the failure was due to mesh cracking and not lapping slippage (Figure 20 and Figure 21).

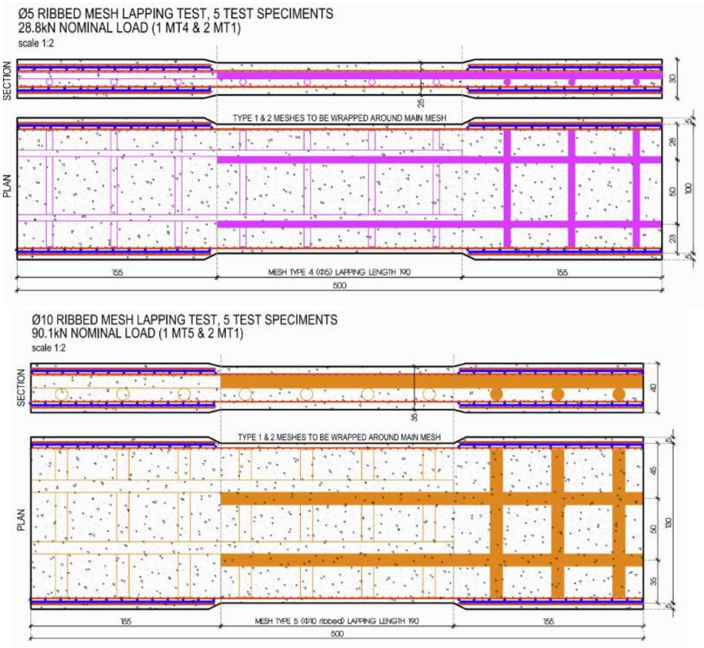

Figure 19. Dog-bone specimen for D5 and D10

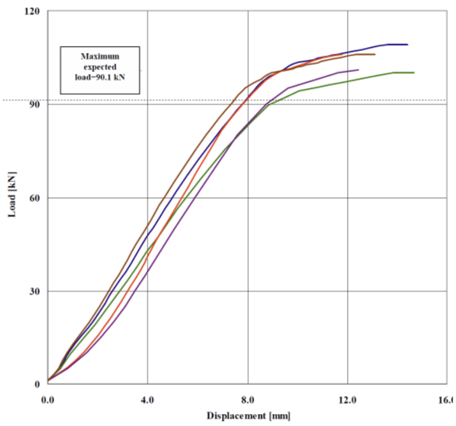

Figure 20. D10mm tests developed Vs Calculated capacity

Figure 21. Cracking of specimen outside the lapping section

2.7. Cold casting joints

The methodology for the preconstruction foresaw two casts, the membrane and the ribs, thus it was necessary to assess the effect of the cold joint. Two sets of specimens were tested (Figure 22 and Figure 23), with and without cold joint, which resulted into identifying a problematic connection for both cases, due to the shear reinforcement arrangement (Figure 24).

Figure 22. Rib-membrane cold joint specimen

Figure 23. Cracking prior to failure

A new reinforcement arrangement was adopted (Figure 25\0 was adopted and the final specimens were tested in the aforementioned 4-point tests.

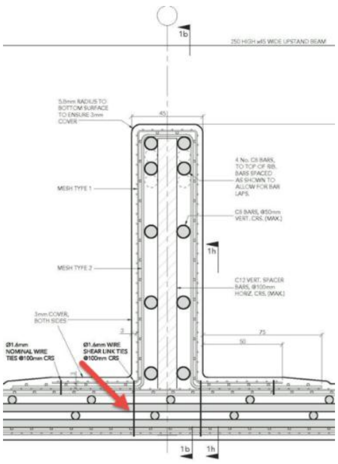

Figure 24. Initial shear reinforcement to rib-membrane joint

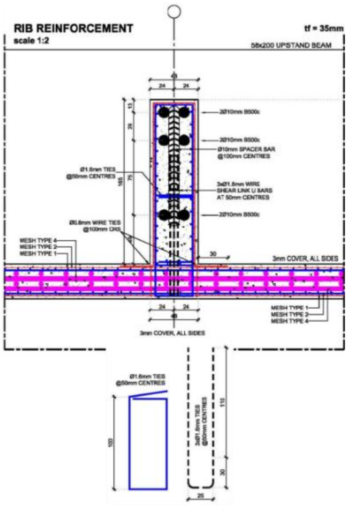

Figure 25. Revised shear reinforcement to rib-membrane joint

3. CONCLUSIONS

This paper outlines the significant modifications that were caused to the initial design assumptions by the extended experimental program that was designed and executed for the design and construction of the SNFCC Ferrocement canopy. The basic result of these tests is that the assumptions and formulas of EN1992 can be adopted for the design of ferrocement although the difference in scale and high "concrete" grade usually result in a slight underestimation of the actual capacity. Additionally the tests demonstrated a required modification in the original shear reinforcement of all the rib elements as well as superiority of the ribs and beams (transverse directions) being on the same side of the membrane instead of them being on opposite sides as originally intended.

4. REFERENCES

[1] G & G Penelis Consulting Engineers SA (2013), SNFCC Solar Collector Redesign Technical Reports, Calculation Reports & Drawings

[2] Kourkoulis, S. (2013), Series of Technical Reports regarding the laboratory testing of the SNFCC Ferrocement Canopy

[3] EN 1992-1-1:2004Eurocode 2: Design of concrete structures – Part 1-1: General rules and rules for buildings

[4] Expedition Engineering, "Solar Collector Code Compliance" Ref. EXPE-C-S7 EX40 - Rev A, 28th Septemeber 2011

[5] Expedition Engineering, "Ferrocement Analyses – local analyses Theory (RSAP)" Ref. EXPE-C-S7-EY52

[6] American Concrete Institute, ACI 549.1R-93 Guide for the Design, Construction and Repair of Ferrocement. (1999, Reapproved 2009)

[7] Antoine E. Naaman, Ferrocement And Laminated Cementitious Composites,

TechnoPress3000, (2000)

[8] International Ferrocement Society, "Ferrocement Model Code", January 2001

STURDY, DURABLE, FAST-TO-BUILD, AND LOW-COST FERROCEMENT HOUSES

Milenko Milinković

Milenko Milinković (M.Sc. in El. Eng. Member of SAIN, MC Systeme Congo s.a.r.l., mcsystemecongo@gmail.com, Kinshasa, DR Congo)

SUMMARY: *This paper presents the experience in building low cost houses in ferrocement technology, arched cross-section with on-site construction, using skeletal method combined with steel hollow structural sections. The author wanted to develop a simpler, faster and more cost-effective system of the construction smaller buildings, retaining their stability and durability, energy-efficiency and resistance to earthquakes and storm winds at the same time. The goal was to enable non-porfessionals to build houses on quick and simple way using standard, easy accessible materials and tools. Houses such as described in this paper were built in DR Congo and have proven to be, fast to build, safe, durable and serviceable with practically no maintenance required. In 2016, 10 such houses have been built in less than four months. The author has promoted the solution for construction such houses in continent climate conditions too, using stronger frame and much better thermal insulation, without thermal bridges.*

KEY WORDS: *Ferrocement, low cost houses, energy-efficiency, resistance to earthquakes.*

1. INTRODUCTION

The author's first experience in ferrocement construction, dates back to 1981. when he constructed his first ferrocement dome using the Skeletal Armature Method described in [1]

Later, the author developed the MC System of sustainable construction which includes the use of prefabricated, flat, thermo-insulated, three-layer ferrocement elements for the rapid construction of permanent semi-cylindrical polygonal structures, with a range of up to 33 m in width (so far), lengths as needed, as intended for different purposes.

One leading application of the MC system with significant cost benefits was found in the construction of sport's halls and covered swimming pools.

However, using the MC System in the construction of individual small residential buildings or housing units, issues with cost-effectiveness become clear, namely: investments in the production and transport of prefabricated ferrocement elements, and on site scaffolding and erection crane for their installation are necessary.

For this reason, the author decided to develop a simpler, faster and more cost-effective system of construction for smaller buildings, retaining their stability and durability, energy-efficiency and, at the same time, resistance to earthquakes and storm winds loading.

Figure 1.1

The goal was to enable non-professionals to build houses on quick and simple way using standard, easy accessible materials and tools.

Simplified procedures for the serial construction of row of low cost, durable, thermally insulated houses are explained. The paper gives a description of construction of open space housing and its folding up from light, arched steel hollow structural sections, light reinforcing mesh and welded wire mesh (Figs. 1.1 and 1. 2)

By fixing the polystyrene boards from the inside of the structure, the exposed shutter for mortar applying is made, at the same time thermal insulation layer of the house is formed.

The procedure of forming a ferrocement shell which provides stabile static system with the steel skeleton of the object is described. In such way, a unique internal space of the object is formed, and it can be partitioned by a dry walling or any other method according to habitants requires. Complete interior space can be easy redesign because the partition walls are not load bearing walls.

Figure 1.2

The shape and dimensions of the house have been carefully chosen, all high-priced materials, steel profiles, reinforcing meshes, polystyrene boards, plaster boards are embedded in standard factory dimensions. In such way the quantities of waste construction material are reduced to minimum.

Paper contains detailed review of construction procedure, material consumption and price analyses. During the year 2016, 10 such objects have been constructed in less than four months.

Houses, especially quick built by described technology are sturdy, durable, energy efficient, resistant to earthquakes and strong winds. Fire cannot make structural damage and objects are hand gun bulletproof, on site testing proved.

These houses are built in DR Congo, Africa, so the thermal insulation of houses is adapting to tropics climate conditions there. The author has promoted the solution for construction such houses in continent climate conditions too, using stronger frame and much better thermal insulation, without thermal bridges. Ferrocement construction is strengthen by ferrocement ribs from outside, dimensions calculated to allow covering with soil in aim to realize an effective green roof. On such way, houses obtained a particular high energy efficiency, up to passive house level.

2. STRUCTURAL DESIGN

Based on an extensive preliminary evaluation and a number of design iterations, the author selected a modified half-cylindrical form as the optimal shape (Fig. 2.1).

Dimensions of such structures are also carefully chosen to match standard factory dimensions of materials used in construction, so as to minimize building waste.

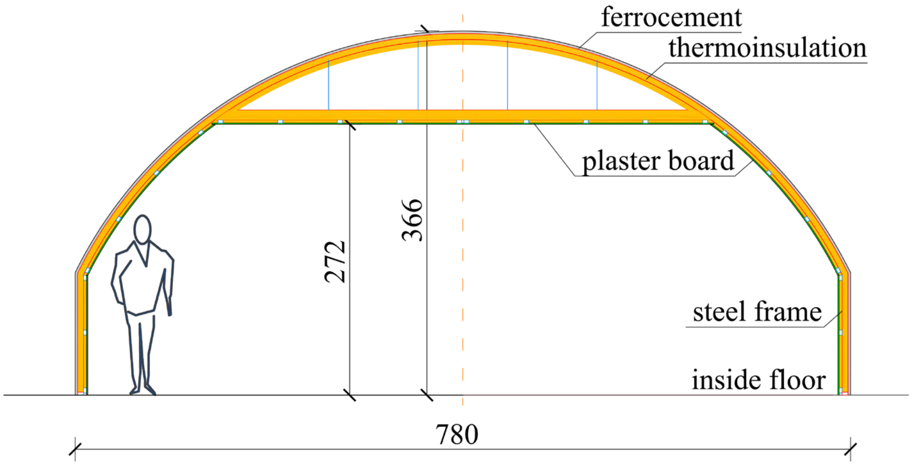

Figure 2.1

3. CONSTRUCTION PROCEDURE

The following steps describe the construction process:

3.1. On the leveled and compact ground, a 7cm thin reinforced concrete slab strengthen by ribs along its edges is poured (Fig. 3.1).

3.2. Arched rib elements from already welded light steel rectangular profiles 60x30x2mm are placed vertically on the concrete foundation edges with 100 cm spacing in between (Fig. 3.2).

Figure 3.1

Figure 3.2

Figure 3.3

3.3. To obtain a firm structure, horizontal steel armature rods are welded to the metal arches (Fig.3.3).

Figure 3.4

Figure 3.5

3.4. Welded wire fabric is then attached and welded to the so formed steel skeleton (Fig. 3.4).

3.5. After that, two layers square welded galvanized wire meshes are placed on the outside of the welded wire fabric (Fig. 3.5).

3.6. Standardized polystyrene boards (100 x 50cm) are placed on the interior side of the structure between the arched profiles and tightened to the structure (bound with thin wires). The polystyrene boards have two roles: during the construction phase they act as support for placing the mortar, and during usage, they form a thermo-insulating layer (Fig. 3.6).

3.7. Next is the cement mortar is plastered from the external sides of structural shell and front walls (Fig. 3.7).

Figure 3.6

Figure 3.7

Figure 3.8

3.8. From outside a hydro-insulation layer is applied (Fig. 3.8).

3.9. From inside of the structure, standard galvanized profiles are mounted to later support plaster boards and ceilings (Fig. 3.9).

Figure 3.9

3.10. Plaster boards are placed and thus the interior space is formed (Fig. 3.10).

3.11. The interior space can be organized without any restriction since the partition walls are not load bearing (Fig.3.11).

Figure 3.10 **Figure 3.11**

3.12. Some examples of possible interior details and lay-out are shown in (Fig.3.12).

Figure 3.12

4. COSTS ANALYSIS

A detailed cost analysis has been carried out for a house of 8 x 12m (Fig. 4.1) including the finished interior as shown in Fig. 3. 12.

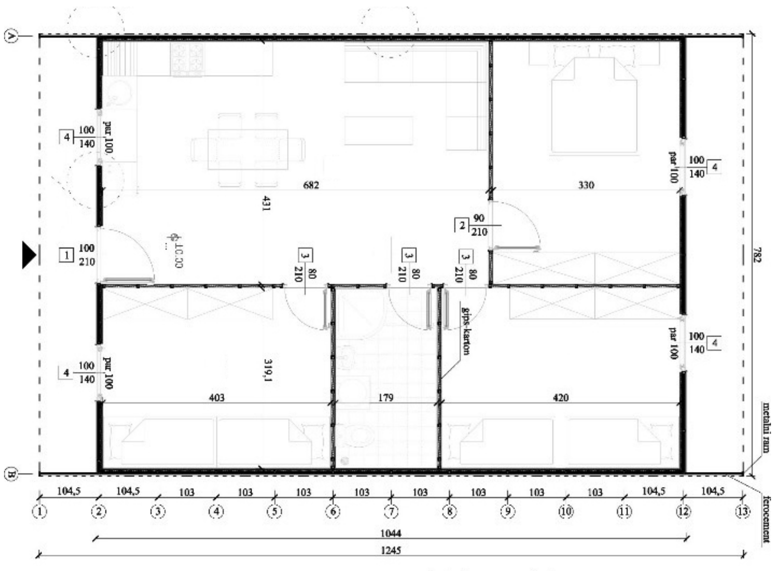

Figure 4.1

Table 4.1

	description	quantity	price per unit	total €
1	Concrete	12m x 8m x 0,08 = 8 m3	65	520
2	Metal profiles	630 kg	0,7	441
3	Reinforcement bars	480 kg	0,6	288
4	Reinforcement mesh	520 kg	0,7	364
5	Wire mesh	370 m2	1,5	525
6	Polystyrene	10 m2	50	500
7	Mortar	6 m3	80	480
8	Gypsum boards with accessories	280 m2	4,5	1.260
9	Windows	4 pieces	90	360
10	Doors	5 pieces	130	650
11	Waterproofing	150 m2	9	1.350
			Total materials	**6.738**
12	Fees for 180 person	180 man/day	20	3600
13	Electrical installations			320
14	Water and sewerage			280
15	Furnishing bathroom			560
			All in total	**11.498**
			per m2	**143**

5. POSSIBILITIES OF APPLICATION

From an architectural design and layout perspective, several possibilities for applications have been considered and are illustrated in Fig 5.1 to 5.5.

Figure 5.1 – Residential

Figure 5.2 – Schools

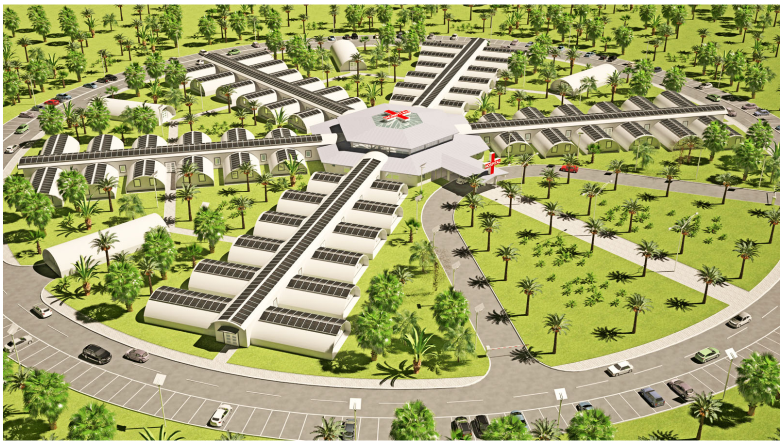

Figure 5.3 – Hospitals

Figure 5.4 – Military ammunition storage

Figure 5.5 – Villa Tanganjika

6. CONCLUDING REMARK

Houses such as described in this paper were built in DR Congo in 2016.

Ten such houses have were built in less than four months, and have proven to be, fast to build, safe, durable and serviceable with practically no maintenance required.

In a similar way the author built his solar house tventy years ago.So far the house has required virtually no maintenance.

The same situation is with the author's first dome built in ferrocement technology forty years ago.A layer of lichen formed on the outside and same color on the inside from the moment of construction.

The ferrocement structure of the shell is completely preserved undamaged.

7. REFERENCES

[1] ANTOINE E. NAAMAN, *'Ferrocement and laminated cementitious composites'*, Techno Press 3000, Michigan, USA, 2000

SUSTAINABLE AND FLEXIBLE SYSTEM FOR CONSTRUCTION WITH FERROCEMENT

Milenko Milinković

Milenko Milinković (M.Sc. in El. Eng. Member of SAIN, Milinkovic Company L.T.D Chairman., milinkovicco@gmail.com., www.milinkovicco.com, Serbia, Belgrade)

SUMMARY:

In this paper the author gives a retrospective of his engagement in ferrocement and explains through numerous examples the advantages of a sustainable system of construction he developed using ferrocement and identified as the MC System. The examples of applications given illustrate the line of thoughts and approaches that led to the final system selected. When about the author learned of the use of ferrocement in yacht construction, he decided to implement that technology in housing application. He built a dome 7m in diameter using ferrocement (1981). He designed and constructed a dome for a solar house, 18,5m in diameter, with semi-cylindrical garage, finally arranged as a green roof, and many other facilities .Compared to other systems for housing, MC System provides cheaper and quicker construction, excellent energy efficiency (min class B), low maintenance cost, durability and resistance to earthquakes, storm winds and fires.

KEY WORDS: *MC System, ferrocement, energy efficiency, green roof, durability, resistance.*

1. INTRODUCTION

From his student's days in the second half of the 20th century, the author analyzed how to build housing structures respecting common user needs and minimum heat losses .It is well known that heat losses are in direct proportion to the amount of external surfaces of houses. On the other hand, it is also well known that of all shapes, a sphere has the smallest surface compared to its volume.

These principles led to exploring semi-spherical forms of building structures which provided, beside minimum heat losses, an elegant solution for statics in terms of structural load resistance. At the time it was not clear which technology allowed the economical construction of such structures.

When about the author learned of the use of ferrocement in yacht construction, he decided to implement that technology in housing applications. In 1981. he built a cupola, 7m diameter dome (Fig 1.1 and 1. 2) using ferrocement.

Figure 1.1

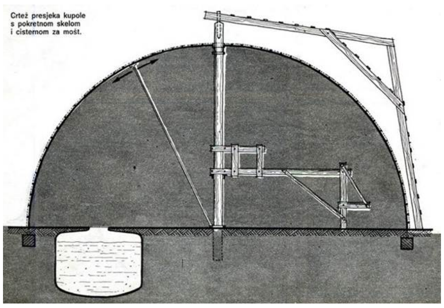

Figure 1.2

2. BACKGROUND

Following this first experience, the author designed and built next structures:

- Two tanks for fruit fermentation (2200 dm3 and 1500 dm3) in 1982.
- Round table (2m) and two elliptic table (3m) in 1983. and 1995.(Figs.2.1 and 2.2)
- Two garden pools (Fig. 2.3)
- Dog house, 1999. (Fig. 2.4)
- An artistic studio, total area of 100 m2, 1999. (Figs. 2.5 and 2.6)

Figure 2.1

Figure 2.2

Figure 2.3

Figure 2.4

Figure 2.5

Figure 2.6

Seeking for the optimal form of building, considered together statics and energy efficiency point of view, the author undertook the project to semi-cylindrical workshop using the Skeletal Armature Method described in [1] (total area 1070 m2, width 15 m, length 65 m, height 7,5m) 1999. (Figs. 2.7 and 2.8). The skeletal method start by building out of steel rods a skeletal structure or frame resembling the final structure.

Figure 2.7

Figure 2.8

Soon after that, he constructed a dome for a solar house, 18,5 m in diameter, with semi-cylindrical garage, all covered with 500 m3 of soil and stone, finally arranged as a green roof (Fig 2.11). Both buildings are fully constructed using two ferrocement shells, 20-30 mm thick, interconnected by ferrocement ribs (40 cm) of the same thickness.

Figure 2.9

Figure 2.10

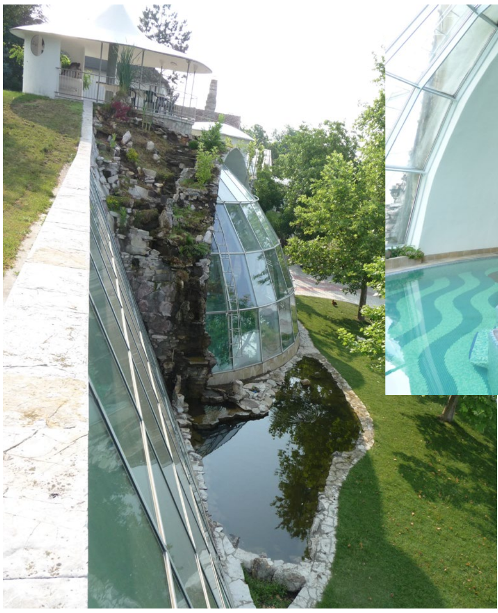

Figure 2.11

3. DECISIONS

To avoid some of the known disadvantages of the skeletal method of construction, the author searched for examples of prefabricated ferrocement elements in semi-cylindrical structures.

As the best fitting form, the optimal structural design of building, the semi-cylindrical (semi-elliptical) cross-section of object has been chosen. A row of prefabricated ferrocement elements in half-ring shape order, constitute the building.
Based on all these experience and acquired knowledge, the author set a goal for himself to achieve maximum level of optimization in process of construction, transport and installation of elements all together. The final achievement was establishment an unique total MC SYSTEM of sustainable ferrocement construction of high-quality, secure, durable, eco-friendly, multifunctional buildings on easy, quick and worthwhile way using one and only one type of prefabricated ferrocement elements.

4. MC SYSTEM

The first experience in using Open and Closed Mold Method, the author acquired by construction ferrocement spiral-shaped stairs in 2000 year.

Trying to develop a system of construction by using the prefabricated ferrocment elements, the author`s first attempt was curved (arched) ferrocement. He first realised that tools for prefabricated curved (arched) ferrocement elements are too complicated to be produced.

He gave up from that solution for two reasons: first - the tools for produce arched elements are too complicated and expansive and second – the author did not succeed in way how to avoid thermal bridges.

He found out that the best solution is to produce flat, three-layer thermal-insulation prefabricated ferrocement elements for construction polygonal arch-form buildings. Dimensions of prefabricated ferrocement elements are chosen to fit best the transport abilities of trucks and containers.
Soon, he built two halls 17 m in diameter and 56 m long in that technology to his own company purpose (Fig.4.3).

Following this breakthrough, what became known as the MC System of sustainable ferrocement construction started and has been improved during years of additional experience.

Figure 4.3

The MC System allows the construction of a house or a structure by using only one type of prefabricated ferrocement element.
All necessary advanced tools for structural elements production are developed. The core of tools are same for all spans of elements. All necessary scaffolds together with appropriate tools are approved in advance for simple and fast assembly of elements.
The MC System allows the construction of large closed spaces designed for very different purposes, having a semi-elliptical shape in cross-section, and of variable length as requested by the customer. It is possible to build structures of different diameters, the largest being 33,8m so far. Desired internal organization of built space is realized as an absolutely independent static system.
Within the capability of the MC System, a solution for high energy efficient covered swimming pools is also available. The pool`s shell is also made of prefabricated ferrocement elements and its assembly is done on the floor of the building.
All certifications for prefabricated elements, tools, scaffolds and final construction has been obtained.
Thermal solar panels that satisfy the daily supplies of hot sanitary water are installed on the roof of each hall. Additional photovoltaic panels with 22 kW of power were also installed on one hall providing the hall with more than necessary electrical energy for its annual consumption. It was the first example energy sustainable construction in Serbia (Fig 5.1).
With just one truck, 12 prefabricated ferrocement elements, enough for 70 m2 floor surface of object constructed can be transported. Low transport costs per m2 give the opportunity that, with elements produced for example in Serbia, houses throughout Europe can be constructed. Transport costs for example between Serbia and Holland are less than 35 euro/m2.
There are three types of elements, and depending on the total number of elements there are nine types of objects (Table 4.1).

Table 4.1

Type	Angle α	No. elements	Net wide (m)	Total wide (m)	Net height (m)	Total height (m)
A	82.5	12	16.8	17.9	8.4	8.9
		13	19.3	20.4	8.4	8.9
		14	21.8	22.9	8.6	9.1
B	84.4	16	22.3	23.4	11.0	11.8
		17	24.7	25.8	11.0	11.8
		18	27.2	28.3	11.2	12.0
C	85.5	20	27.8	28.9	14.0	14.6
		21	30.2	31.3	14.0	14.6
		22	32.7	33.8	14.2	14.8

By time, work experience allowed to obtain new knowledge and improve former solutions in production, transport and assembly of elements.

4.1. Tool design

Tools for production ferrocement elements are designed to be make from prefabricated steel profiles and sheets. Each tool is constructed as a vibrating table.

Figure 4.4

Figure 4.5

4.2. Elements design

Elements are constituted from three layers.
The first layer is ribbed reinforced ferrocement board, 2-3 cm thickness. It contains reinforcement welded wire fabric, steel rods and two-four layers square welded galvanized wire mesh.

Figure 4.6

Figure 4.7

The second layer is thermo-insulating layer. It is made from polystyrene boards and grains joined by cement with special additives supplement. Wishing that constructed objects can be certificate as “A” class of energy efficiency, thickness of 25 cm thermo-insulating layer has been adopted. Thermo-insulating layer made on that way, allowed that prefabricated ferrocement elements got the 60 minutes fire resistant certificate.
The third layer is protection ferrocement layer 2 cm thickness (Figs. 4.6 to 4.8).
During the production of elements, the layers are deposited fresh on each other, so the produced elements are compact.

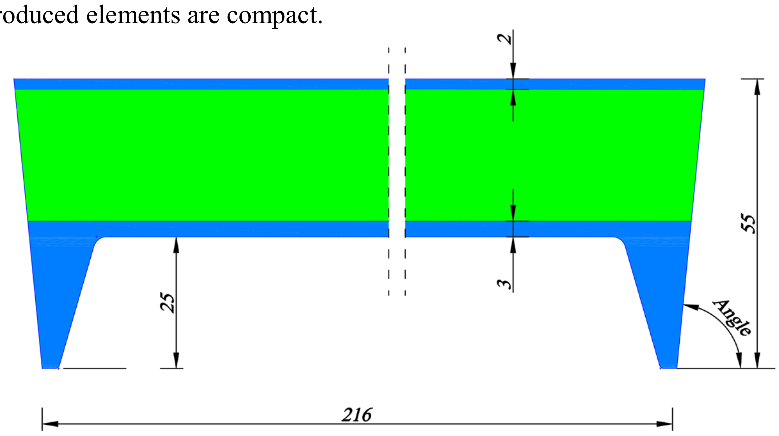

Figure 4.8

4.3. Transport of elements

Dimensions of elements are chosen to take adventure of standard overall dimensions of containers and tracks. Only by one ordinary track tour, it is possible to transport to the construction site 12 elements-three package of four (Fig.4.6), which is enough for cca 70 m2 floor surface of building. Their total weight is approximately 20 t.

4.4. Scaffolding

To make transport of supporting scaffold to construction site more effective, special, separable structures were developed (three type). They may be put together on construction site easy and fast (Fig. 4.9).

For assembly ferrocement elements, not more than seven arched structures are needed because they can be easy transfer over the construction site.

For transporting these scaffold structures as for transporting attached plating to the construction site, four track tours are necessary.

Figure 4.9

Figure 4.10

Figure 4.11

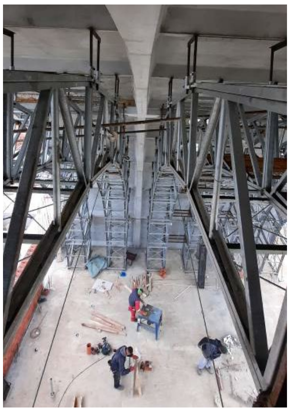

Figure 4.12

4.5. Assembly of elements

On the mounted scaffold on construction site, the prefabricated ferrocement elements are arranged one above the other, like a huge bricks. On such way, the arched rows of elements are formed. Between the rows of elements some space intervals are left. The endings of armature rods from ferrocement elements are going into that space and armature from arches, according to statics calculation, too.
When the plating from inside and outside is set, the space for forming reinforced concrete arches is closed (figs. 4.10 to 4.12).
MC system allows to build object 1000 m2 surface for less than a month.

5. CONSTRUCTED FACILITIES

From 2010. the core company business is to project and construct different buildings by prefabricated ferrocement elements. Up to 2020., ten sports halls was built.

Figure 5.1

Figure 5.2

6. CONSLUCIONS

The advanced MC System of sustainable ferrocement construction enables quick, simple, and cost-effective construction of sustainable buildings which provide savings in the energy and materials for a life time and have low maintenance costs.
Constructed structures (houses, sport`s halls, covered swimming pools) are secure, durable,high level energy efficiency and resistant to earthquakes, storms and fire.
Low transport cost per m2 allows for prefabricated elements produced for example in Serbia, to be used in housing construction throughout Europe. By simply installing photovoltaic panels on the buildings, become SUSTAINABLE, that is, they provide all the necessary energy for their own functioning.

7. REFERENCES

[1] ANTOINE E. NAAMAN, *'ferrocement and laminated cementitious composites'*, Techno Press 3000, Michigan, USA, 2000

Session 4
Modelling Ferrocement
and
TRC

COMPUTATIONAL MODELLING OF FERROCEMENT FOR STRUCTURAL APPLICATIONS

John E. Bolander[1]

[1]*J.E. Bolander, University of California, Davis, California 95616, USA. jebolander@ucdavis.edu*

SUMMARY: *Ferrocement and other laminated cementitious composites offer performance attributes for a variety of applications. This paper summarizes selected developments on the computational modeling of these materials. Near one end of the modeling spectrum, the effects of the reinforcing mesh are smeared out within a simplified representation the cement-based matrix. Toward the other end of the spectrum, the mesh and its interactions with the matrix are explicitly modeled within a volumetric representation of the composite material. The choice of computational model should reflect the design objectives. This paper also briefly reviews the modeling of short-fiber reinforcement, which can be used in conjunction with wire/fabric grids in laminated cementitious composites.*

KEY WORDS: *computational analysis, continuum models, discrete models, fracture, grid reinforcement, short-fiber reinforcement.*

1. INTRODUCTION

Ferrocement is a proven construction material for a variety of marine and terrestrial applications [17]. Ferrocement, along with other thin laminated cementitious composites (TLCCs), can be used for new construction or for the repair/retrofit of existing structures [15]. Whereas the technological bases for structural design have been established, ferrocement can be made from a multitude of different reinforcing grid materials, matrix materials, and processing techniques [16,17]. This multitude of options, along with a wide array of potential load and exposure conditions, suggests opportunities for innovation and design optimization [6]. Along with physical testing and monitoring of field performance, computational modeling is an effective means for material and structural design optimization.

This paper reviews selected developments in the computational modeling of ferrocement and other thin laminated cementitious composites. The modeling of structural concrete is first summarized, since many of the fundamental concepts are relevant to the modeling of ferrocement. The emphasis of this review, however, is on the additional, unique challenges associated with modeling ferrocement and its applications. The review scope includes the modeling of short-fiber reinforcement, which can be used in conjunction with the grid reinforcement [4,22]. The discussions center on cases where the thin laminated composite is spatially discretized in a structural setting, rather than on the modeling of sectional behavior. As part of the conclusions, needs and opportunities for research are mentioned.

2. MODELING CONCEPTS

Ferrocement and reinforced concrete are similar in their material compositions: both are composed of a quasi-brittle cementitious binder with internal reinforcement to accommodate tensile cracking. The reinforcement is commonly in the form of steel wires or bars, but non-ferrous forms of reinforcement are also being used. Models of these composite materials or structures should account for the actions of the cementitious binder and reinforcement, as well as their interactions in the post-cracking state. Whereas laminate theory can be useful for some design purposes, computational modeling can provide fuller understandings of behavior for a broader range of loading conditions.

2.1 Motivations for computational modeling

There are myriad motivations for developing computational models of thin laminated cementitious composites and, in general, concrete materials and structures. The motivations stem from several factors, including:

- practical limitations of physical testing, especially considering the large ranges of length and time scales relevant to many applications. The production of statistically significant and representative test results is generally cost-prohibitive;
- potentially large variations in the properties of the constituent materials. Furthermore, the methods of processing often produce unintended variations in the distributions of constituents, including variations in the positioning of reinforcing components;
- sensitivity of the cementitious binder to early-age thermal, chemical, and physical processes and the dependence of these processes on curing practice;
- aging and degradation of material components under the influences of multiple, potentially aggressive, environmental phenomena;
- three-dimensionality of material structure, transport mechanisms, load paths, and damage processes; and
- lack of quantitative links between these phenomena occurring at different length and time scales.

2.2 Modeling approaches

Most of the advances in the modeling of concrete materials and structures have been accomplished within the framework of finite element methods. The basic techniques for structural analysis under mechanical loading have been developed decades ago, as summarized in an American Society of Civil Engineers (ASCE) committee report [26]. The ASCE document reviews key concepts such as constitutive modeling of concrete under multi-axial stress conditions, representation of cracking (including coverage of smeared versus discrete crack models), inclusion of reinforcement and its associated bond with the concrete, time-dependent effects including shrinkage and creep under sustained loading, and structural response to dynamic loading. The ensuing literature contains an additional wealth of information on the continued development of finite element and alternative modeling strategies. Notable among these publications are those produced by the FraMCoS and EURO-C conference series.

One broad categorization scheme places models into one of two categories, depending on whether the material is represented as a homogeneous continuum or as a collection of discrete entities.

2.2.1 Continuum models

Continuum models provide an average description of material behavior for a representative volume element. Whereas microstructure can be considered within the continuum description (e.g., through the use of homogenization and constitutive modeling techniques), this is done in a mean field sense. The simulation of complex behaviors requires a large number of parameters, which are typically calibrated through comparisons with experimental results. Nonetheless, continuum approaches are attractive for engineering analysis, since sizable domains can be analyzed in a computationally efficient manner. In cases where damage is finely distributed over a region of a structural component, its modeling via a continuum approach is attractive. The influence of reinforcing components can be represented by either embedding their actions within the continuum description or by explicitly representing them as structural elements (e.g., as beam or frame elements). Bond-link elements allow for slippage along the concrete-reinforcement interface.

2.2.2 Discrete models

Discrete models are based on discontinuous approximations of the field variable within the computational domain. This category includes lattice models, in which the system configuration (including disorder) and behavior are represented by a collection of primitive two-node elements. Dense nodal arrays are typically needed to resolve the relevant material features. The idea of discrete structural modeling is not novel, but only through advances in computing technology have these approaches become viable for 3D analyses. These models can be subcategorized, depending on whether contact modeling is an essential part of the solution process (as for the Discrete Element Method, DEM) or elemental connectivity between nodes remains constant throughout the analysis (as for classical lattice models). The former case is applicable to handling particle flows, whereas the lattice is typically better for stress and fracture analyses. As described later, discrete approaches offer various ways to model reinforcement and its bond to the host medium.

2.3 Modeling of TLCCs : unique factors

As previously noted, although the computational modeling of reinforced concrete structures is firmly established in the literature, lesser attention has been devoted to TLCCs (including ferrocement) and structures made of TLCC components. Both construction technologies share common points of interest, but the modeling of TLCCs involves several particular considerations, including

- The thin laminate nature of structural elements;
- The use of small-gauge wire mesh rather than larger, more widely spaced steel bars;
- Multi-dimensionality of the reinforcing mesh and its influences on post-cracking behavior;
- The role of nodal connections between wire mesh (or fabric) line components;
- The outer and inner bond properties of reinforcement composed of multi-filament strands [3,9,11]; and
- Enhanced sensitivities to variations in cross-section depth and reinforcing mesh positioning within the cross-section.

Past modeling efforts have addressed many of these considerations [2,10,19,21]. Soranakom and Mobasher [24,25] employed a finite difference method to analyze fabric reinforced concrete loaded in uniaxial tension. The model explicitly represented the bond properties, anchoring actions of transverse yarns, and slack in the longitudinal yarns. The importance of anchorage effects was clearly demonstrated. An attractive feature of some modeling approaches is their ability to account for multiscale effects, along with the spatial positioning of reinforcement (i.e., the wire mesh and/or short discontinuous fibers) within the material volume [12,13].

3. DISCRETE MODELS OF TLCC AND FIBER COMPOSITES

A distinction can be made between models that average the effects of the reinforcing grid within a representation of the matrix, and those that provide an explicit, spatial representation of the grid within the material volume. This section highlights a class of discrete, particle-based models (i.e., rigid-body-spring models) that are adept at representing fracture and the influences of continuous and short-fiber reinforcement.

3.1 Model components

3.1.1 Matrix phase

The matrix phase is modeled as a rigid-body-spring network, based on the rigid-body-spring concept of Kawai [14]. The rigid-body-spring elements (or lattice elements) interconnect on a set of randomly placed nodal points (Fig. 1). Each element is composed of a zero-size spring set connected to its nodes via rigid-arm constraints. The elasticity and fracture properties of the element are lumped within the spring set. By virtue of the Delaunay/Voronoi definition of the network connectivities and element geometries, the model is elastically homogeneous under uniform modes of straining and energy-conserving with respect to mode-I dominant fracture [7].

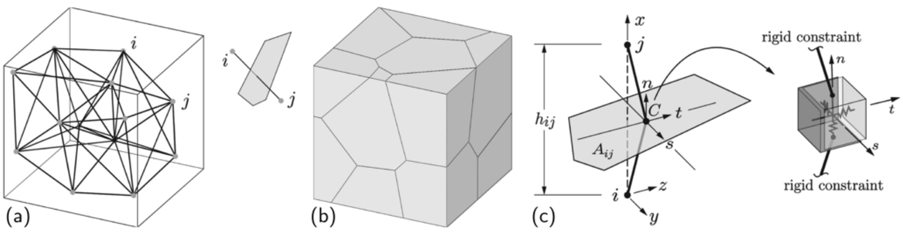

Figure 1 - Domain discretization: (a) lattice topology defined by the Delaunay tessellation of the nodal point set; (b) volume rendering based on the dual Voronoi tessellation of the point set; (c) view of lattice element *ij*

3.1.2 Reinforcement and bond

Reinforcing components can be modeled as a series of frame elements (i.e., line elements that possess both axial and flexural stiffness). These components can be positioned in the material volume regardless of the discretization of the matrix phase, which greatly facilitates model construction. Nodes of the reinforcing component connect to the matrix nodes via a bond link element and a rigid-arm constraint, which is shown in Fig. 2. The bond link accounts for the nonlinear shear stress-slip relationship of the interface along the length of the reinforcing component and the bearing pressures that arise in the orthogonal directions.

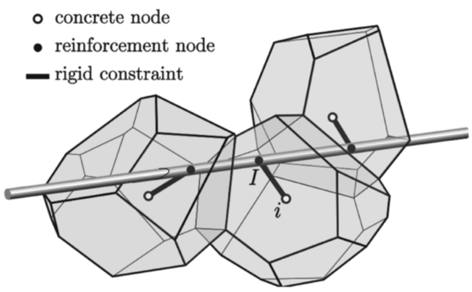

Figure 2 – Modeling of concrete-reinforcement interface: reinforcement node *I* connects to matrix node *i* via a bond link (located at node *I*) and a rigid-arm constraint

3.2 Illustrative examples

Several modeling exercises are presented herein to provide an overview of the capabilities of the modeling approach. Details regarding each exercise can be found in the source documents.

3.2.1 Shrinkage cracking controlled by carbon fiber nets

This discrete modeling approach was used to estimate the time-dependent behavior of concrete reinforced with carbon fiber nets (CFNs) [23], as tested by Yang and Makizumi [29]. Figure 3 shows the layout of the test specimens and one of the corresponding models. The reinforcement grid was made of PAN-type continuous carbon fiber strands, each consisting of filaments bound by epoxy resin. The test program investigated the effectiveness of four configurations of CFN, which differed in the spacing of transverse reinforcement: 5cm, 7cm, 10cm and no transverse reinforcement. Control specimens without reinforcement were also tested. Following a 3-day curing period, specimens were exposed to a controlled drying environment (50±3% RH).

With respect to the models, each carbon fiber strand is explicitly represented by a series of frame elements. Where transverse strands are present, they are rigidly connected to the longitudinal strands at the grid nodes. The shrinkage and creep response of the concrete were estimated using well-known prediction models [5].

When the concrete specimen is subjected to drying shrinkage, tensile stresses develop in the concrete while compression occurs in the restraining steel channels. All specimens (physical and numerical) cracked at mid-length, due to prenotches introduced at that location. As shown in Fig. 4, the simulated and measured crack widths agree well. As expected, the largest crack openings appear for the control specimen without reinforcement. It is also evident that the presence and spacing of transverse strands affect crack opening, due to their role as mechanical anchorages. Smaller spacing leads to smaller crack openings over time.

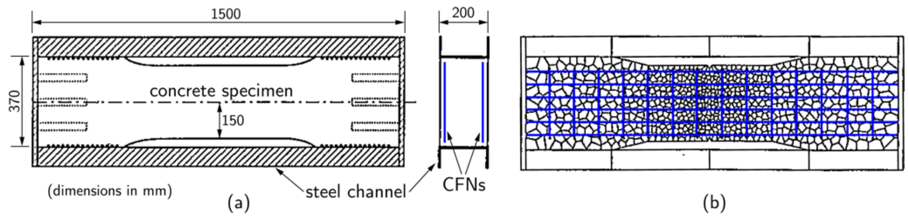

Figure 3 – CFN reinforced concrete: a) specimen; b) numerical model

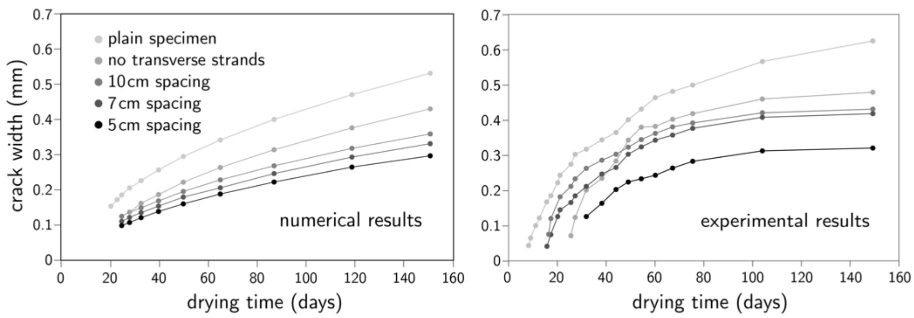

Figure 4 – Effect of transverse strand spacing on crack width

3.2.2 Panel elements subjected to cyclic loading

Yamamoto et al. [28] use a similar approach, also based on the rigid-body-spring concept, to simulate the behavior of structural concrete under reversed cyclic loadings. In particular, they simulated the behavior of reinforced concrete panels subjected to in-plane shear and low-rise walls, also under shear-type loading. A key feature of their approach is the consideration of cyclic load behavior within the constitutive models of the matrix phase and within the bond link elements representing the interface between the concrete and reinforcing bars. The cyclic bond model is shown in Fig. 5, where s and τ represent slip and shear stress, respectively.

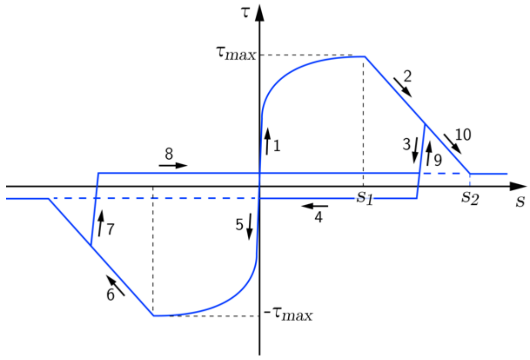

Figure 5 – Bond stress-slip relationship under cycle loading (adapted from Yamamoto et al. [28])

In the experiments [20], in-plane shear force was applied to 2.5m square panels through shear keys attached to the panel edges. The concrete panels had a thickness of 140mm. The principal test parameter was reinforcement ratio ρ which, for each principal direction, ranged from 0.51% to 2.04%.

Results of the panel test simulation for the case $\rho_x = \rho_y = 0.0051$ are presented herein. The average shear stress-strain response to cyclic loading is presented in Fig. 5, along with simulated crack patterns at two different stages of the loading history. The model captures both the shear strength levels and the pinched character of the cyclic load response. The simulated damage patterns feature discrete-like cracks that agree well with the experimental observations. As the reinforcing ratio is increased (within both the experimental and modeling campaigns), shear resistance increases and the extent of loop pinching decreases. Furthermore, the spacing of diagonal cracks becomes smaller as the amount of reinforcing steel is increased. The simulation approach reproduces the experimental results with remarkable accuracy over the whole range of reinforcing ratios. These RC panel test simulations are relevant to applications where ferrocement, or other thin laminate cement composites, are used for structural retrofit or for seismic resistance, in general.

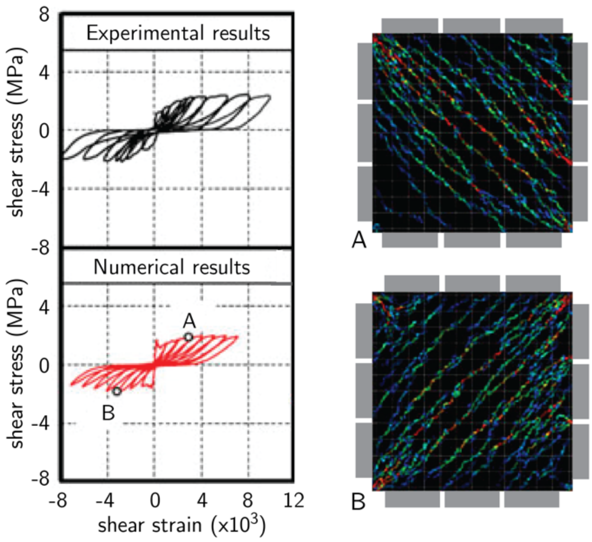

Figure 6 – Average shear stress-strain relationships and simulated crack patterns within the panel specimens at selected load stages (adapted from Yamamoto et al. [28])

3.2.3 Tensile behavior of strain-hardening cement composites

The reinforcement model briefly described in Section 3.1.2, and used in the preceding examples, can be used to model individual fibers within fiber reinforced concrete. Since the definition of the fibers requires nodal degrees of freedom, however, that approach becomes computationally expensive even for small amounts of fibers.

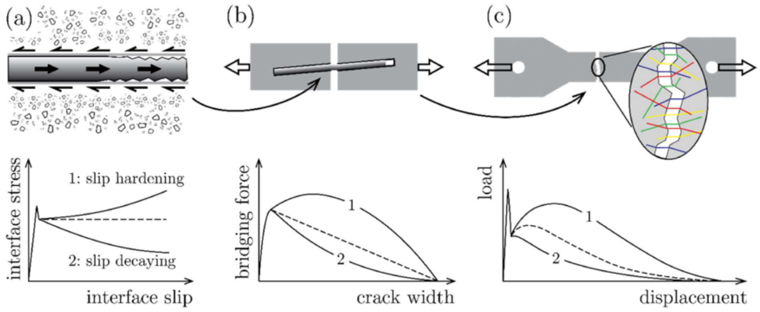

Figure 7 - Multiscale modeling of FRC in tension: (a) slip and stress transfer along matrix-fiber interface; (b) fiber pullout and crack-bridging; and (c) composite behavior of FRC

Alternatively, the pre- and post-cracking actions of fibers can be made dependent on the motion of the particle structure representing the matrix phase [7]. The addition of fibers does not inflate the number of computational degrees of freedom and therefore realistic volumes of FRC can be simulated. The model explicitly represents the debonding and pullout of individual fibers, based on the micromechanics of interfacial slip between fiber and matrix [18]. The simulated macroscopic behavior of these composite materials depends on the collective actions of the numerous individual fibers represented in the multiscale model (Fig. 7). With respect to recent developments of this approach, two are noteworthy [13]: 1) fibers transfer load along their embeded lengths, rather than simply lumping their effect at the crack surfaces (like a cohesive crack law); and 2) handling of cases where multiple cracks cross a single fiber.

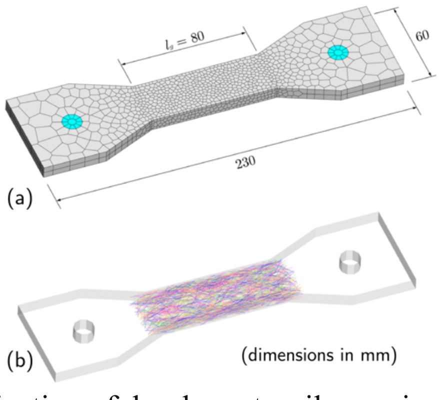

Figure 8 - Discretization of dog-bone tensile specimen: (a) specimen dimensions; (b) placement of fibers within the specimen gauge length

This approach has been used to simulate the behavior of strain-hardening cement composites under tensile loading. In particular, we model the tensile specimens of Adendorff et al. [1,8], who quantified cracking using digital image correlation. The dog-bone type specimens of the experimental campaign are discretized as shown in Fig. 8. The model captured salient features of the load-displacement diagram (Fig. 9), including the ultimate strain at which fracture localization occurs.

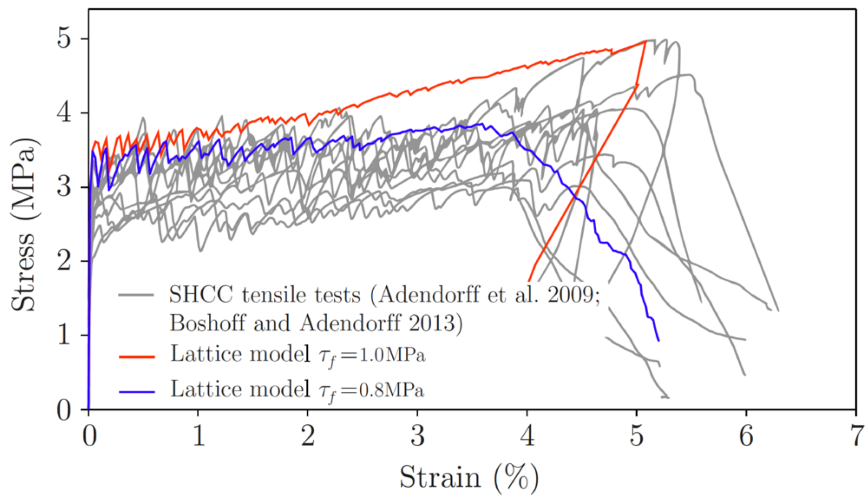

Figure 9 – Comparison of stress-strain response curves

As for the panel specimen simulations described in Section 3.2.2, this type of model is adept at representing distributed discrete-like cracks, as shown in Fig. 10. This capability enables accurate estimations of crack width openings at various stages of the loading history. As shown in Fig. 11, for example, the model can trace the development of the measured crack opening histograms with increasing levels of tensile strain. These results were obtained using a planar model for which a finer mesh was used. The fine mesh was necessary to accommodate the denser arrays of cracks that develop at higher strain levels. From analysis of the model results, it is clear that crack opening is correlated to the distribution of fibers within the region of interest. Larger openings occur where relatively fewer fibers are present.

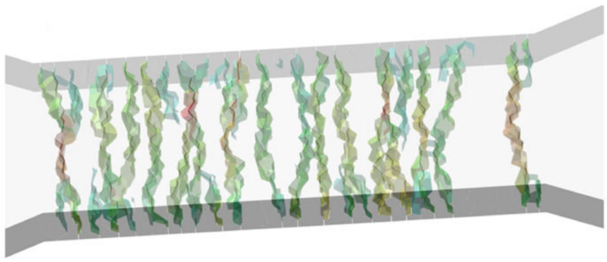

Figure 10 – Simulated multiple cracking pattern at 2% strain level

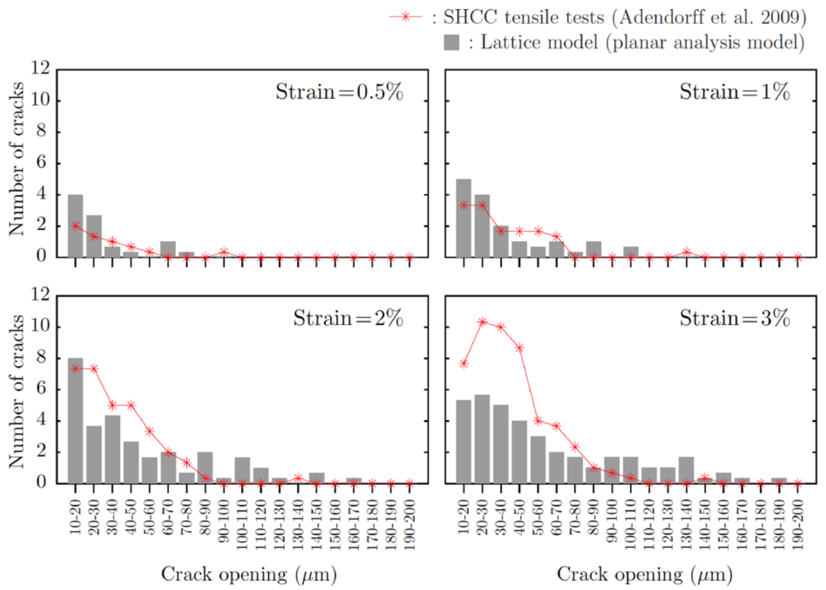

Figure 11 - Comparison of crack count-crack opening histograms for increasing levels of axial strain of the composite material

4. CONCLUSIONS

Ferrocement and other thin laminated cementititous composites can be used for a variety of applications, ranging from new construction to the repair/retrofit of existing structures. Numerous possibilities exist with respect to the choices of the binding phase, grid reinforcement, and production technologies. The choices are governed by many factors, including structural safety, serviceability, economy, and environmental impact over the life-cycle of the application. In addition to laboratory testing and monitoring of field performance, validated computer models offer a means to study cause-and-effect relationships and explore of range of design possibilities.

Models based on laminate theory or sectional analysis have made key contributions to understanding the behavior of TLCCs and basic design issues. For many current research needs, however, it is essential to explicitly represent the binding phase and grid reinforcement within a spatial representation of the TLCC. This enables study of the roles of each material component, and their interactions, for differing production technologies and loading conditions.

Herein, one form of particle-based lattice model was used to provide illustrative examples. Such models provide realistic simulations of distributed, discrete-like damage within the composite materials. The role of the reinforcement, in the form of a grid structure or dispersed short fibers, is captured by the modeling approach.

Moving forward, there is a need for model validation and verification at relevant scales of interest. Such efforts are essential for confidence in a model's predictive capabilities, which in turn are needed for material and structural design optimization. Validated models can simulate nominally identical specimens that differ only in the probabilistic assignment of the position and properties of material phases, which corresponds to the testing of replicate specimens in the physical laboratory. Model validation at multiple length and time scales requires the use of modern sensing technologies and close collaboration with experimentalists.

5. REFERENCES

[1] ADENDORFF C.J., BOSHOFF W.P., VAN ZIJL G.P.A.G., "Characterisation of crack distribution of strain-hardening cement composites (SHCC) under imposed strain", Advances in Cement-based Materials, CRC Press, 2009, p. 215-221.
[2] BALAGURU P., NAAMAN A.E., SHAH S.P., "Analysis and behavior of ferrocement in flexure", *J. Structural Division, ASCE*, vol. 103, n° 10, 1977, p. 1937-1951.
[3] BANHOLZER B., BROCKMANN T., BRAMESHUBER W., "Material and bonding characteristics for dimensioning and modelling of textile reinforced concrete (TRC) elements", *Materials & Structures*, vol. 39, 2006, p. 749-763.
[4] BARHUM R., MECHTCHERINE V., "Influence of short dispersed and short integral glass fibres on the mechanical behaviour of textile-reinforced concrete", *Materials & Structures*, vol. 46, 2013, p. 557-572.
[5] BAZANT Z.P., KIM J.-K., PANULA L., "Improved prediction model for time-dependent deformations of concrete: Parts 1-3", *Materials and Structures*, vol. 24, 1991, p. 327-345, 409-421, and vol. 25, 1992, p. 21-28.

[6] BOLANDER J.E., "US-Thai International Workshop: Advances in the Science and Engineering of Thin Reinforced Cement Composites (TRCC)", Workshop Report, *Cement & Concrete Composites*, vol. 29, 2007, p. 582-584.
[7] BOLANDER J.E., SAITO S., "Discrete modeling of short-fiber reinforcement in cement composites", *Advanced Cement Based Materials*, vol. 6, 1997, 76-86.
[8] BOSHOFF W.P., ADENDORFF C.J., "Effect of sustained tensile loading on SHCC crack widths", *Cement and Concrete Composites*, vol. 37, 2013, p. 119-125.
[9] DVORKIN D., POURSAEE A., PELED A., WEISS W.J., "Influence of bundle coating on the tensile behavior, bonding, cracking and fluid transport of fabric cement-based composites", *Cement and Concrete Composites*, vol. 42, 2013, p. 9-19.
[10] EL DEBS M.K., NAAMAN A.E., "Bending behavior of ferrocement reinforced with steel meshes and polymeric fibers", *Cement & Concrete Composites*, vol. 17, 1995, p. 327-338.
[11] HEGGER J., WILL N., BRUCKERMANN O., VOSS S., "Load-bearing behaviour and simulation of textile reinforced concrete", *Materials & Structures*, vol. 39, 2006, p. 765-776.
[12] JUN P., MECHTCHERINE V., "Behaviour of strain-hardening cement-based composites (SHCC) under monotonic and cyclic tensile loading, Part 2 - Modeling", *Cement and Concrete Composites*, vol. 32, 2010, p. 810-818.
[13] KANG J., BOLANDER J.E., "Event-based lattice modeling of strain-hardening cementitious composites", *International Journal of Fracture*, vol. 206, 2017, p. 245-261.
[14] KAWAI T., "New discrete models and their application to seismic response analysis of structures", *Nuclear Engineering and Design*, vol. 48, no. 1, 1978, p. 207-229.
[15] MECHTCHERINE V., "Novel cement-based composites for the strengthening and repair of concrete structures", *Construction and Building Materials*, vol. 41, 2013, p. 365-373.
[16] MOBASHER B., *Mechanics of fiber and textile reinforced cement composites,* CRC Press, Boca Raton, FL, 2012.
[17] NAAMAN A.E., *Ferrocement and laminated cementitious composites*, Techno Press 3000, Ann Arbor, Michigan, 2000.
[18] NAAMAN A.E., NAMUR G.G., ALWAN J.M., NAJM H.S., "Fiber pullout and bond slip. I: analytical study", *Journal Structural Engineering*, vol. 117, no. 9, 1991, p. 2769-2790.
[19] NASSIF H.H., NAJM H., "Experimental and analytical investigation of ferrocement – concrete composite beams", *Cement & Concrete Composites*, vol. 26, 2004, p. 787-796.
[20] OMORI N., TAKAHASHI T., TSUBOTA H., INOUE N., KURIHARA K., WATANABE S., "Experimental studies on nonlinear behaviours of reinforced concrete panels subjected to cyclic in-plane shear", *Journal of Structural and Construction Engineering, AIJ*, vol. 403, 1989, p. 105-118 [in Japanese].
[21] PANKAJ, ARIF M., KAUSHIK S.K., "Mechanical behavior of ferrocement composites: Numerical simulation", *J. Materials in Civil Engineering*, vol. 14, 2002, p. 156-163.
[22] PEREZ-PENA M., MOBASHER B., "Mechanical properties of fiber reinforced lightweight concrete composites", *Cement and Concrete Research*, vol. 24, no. 6, 1994, p. 1121-1132.
[23] SAITO S., BOLANDER J.E., "Numerical analysis of shrinkage cracking controlled by carbon fiber nets." Proceedings of 3rd International Symposium on Non-Metallic (FRP) Reinforcement for Concrete Structures, Sapporo, Japan, vol. 2, 1997, p. 275-282.
[24] SORANAKOM C., MOBASHER B., "Geometrical and mechanical aspects of fabric bonding and pullout in cement composites", *Materials & Structures*, vol. 42, 2009, p. 765-777.
[25] SORANAKOM C., MOBASHER B., "Modeling of tension stiffening in reinforced cement composites: Part I. Theoretical modeling", *Materials & Structures*, vol. 43, 2010, p. 1217-1230.

[26] Task Committee on Finite Element Analysis of Reinforced Concrete Structures, State of the Art Report on Finite Element Analysis of Reinforced Concrete*,* *American Society of Civil Engineers*, New York, NY, 1982, 545 pp.
[27] WILLIAMS PORTAL N., THRANE L.N., LUNDGREN K., "Flexural behavior of textile reinforced concrete composites: experimental and numerical evaluation", *Materials & Structures*, vol. 50, n° 4, 2017, p. 1-14.
[28] YAMAMOTO Y., NAKAMURA H., KURODA I., FURUYA N., "Crack propagation analysis of reinforced concrete wall under cyclic loading using RBSM", *European Journal of Environmental and Civil Engineering*, vol. 18, no. 7, 2014, 780-792.
[29] YANG S., MAKIZUMI T., "Control of cracking in concrete due to drying shrinkage by using grid-type continuous fiber reinforcement", *Memoirs of the Faculty of Engineering, Kyushu University*, vol. 55, no. 4, 1995, p. 421-441.

MOMENT-CURVATURE MODEL FOR FLEXURAL ASSESSMENT OF TEXTILE-REINFORCED CONCRETE BEAMS

H. Spartali[1], S. Rastegarian[2], N. Will[3], R. Chudoba[4]

[1] H. Spartali, Institute of Structural Concrete, RWTH Aachen University, Aachen, Germany, hspartali@imb.rwth-aachen.de

[2] S. Rastegarian, Institute of Structural Concrete, RWTH Aachen University, Aachen, Germany, saeed.rastegarian@rwth-aachen.de

[3] N. Will, Institute of Structural Concrete, RWTH Aachen University, Aachen, Germany, nwill@imb.rwth-aachen.de

[4] R. Chudoba, Institute of Structural Concrete, RWTH Aachen University, Aachen, Germany, rostislav.chudoba@rwth-aachen.de

SUMMARY: *Several numerical models reflecting the flexural response of steel-reinforced concrete beams have been developed in the past. However, their adaption to carbon-reinforced concrete needs to consider a different type of material behaviour. In addition, they must be able to reflect numerous reinforcement layouts with more flexible configurations of textile fabrics within the cross-section. In this paper, a general cross-section model for the derivation of the moment-curvature and load-deflection curves for concrete beams reinforced with short fibers, bar reinforcement and textile fabrics is introduced, which incorporates materials non-linearities and is easily applicable to cross-sections with arbitrary shapes and reinforcement layouts. The validation shows the ability of the model to reliably reproduce the experimental results.*

KEY WORDS: *textile fabrics, carbon concrete, moment-curvature, SLS, flexural model, nonlinear behaviour, general cross-sections.*

1. INTRODUCTION

A wide range of numerical and analytical models and approaches for the evaluation of the moment-curvature response of steel reinforced concrete elements subjected to bending loading have been presented in the literature [1], [2], [3], [4], [5], [6], [7]. However, most of these models have been established based on specific assumptions for the material models, cross-sectional shape and the layout of the reinforcement layers. Moreover, only few research contributions have handled the case of carbon-reinforced bending elements [8], [9].

Adding to this the fact that, while several concepts for the assessment of the ultimate limit state (ULS) design of carbon-reinforced concrete beams exist, an efficient and flexible approach to the deflection assessment in the serviceability limit state (SLS) is still missing.

In this paper, a generic flexural model for RC bending elements is presented which enables a flexible integration of different material models and an easy selection of any cross-sectional shape and reinforcement layout. This is possible due to the modular implementation of the model code in hierarchal structure of model components using Python programming language in combination with a rapidly evolving ecosystem of scientific computing libraries.

The model can be utilized for different types of concrete composites reinforced with short fibers, bar reinforcement and textile fabrics. It can support the development of hybrid cross-sectional layouts to optimally exploit the properties of high-performance reinforcement materials [10].

The applicability of the model to bending elements is introduced and validated using experimental data on concrete beams reinforced with carbon fabrics, carbon bars and steel bars available in the literature. Using the model, it is possible to generate the moment-curvature curve for a specific configuration of the cross-section for the studied element. Depending on this, the load-deflection response can then be calculated for arbitrary beam support and loading configurations.

The goal of this development is to provide a general, transparent, and efficient assessment procedure for reinforced concrete beam deflection that serves as the basis for applications in engineering practice.

2. MOMENT-CURVATURE MODEL

2.1. General implementation aspects

The computational procedure follows the usual arrangement of the equilibrium and kinematic conditions at a representative cross-section of a beam in combination with non-linear constitutive relations and is similar to the approach described in [10]. For convenience, the kinematic assumption of linear strain profile is directly related to the cross-sectional curvature κ. In this way, the M-κ relation needed for the deflection evaluation can be efficiently obtained using a set of non-linear equilibrium equations. To achieve maximum flexibility, these equilibrium conditions are formulated and implemented as a general integral function that can incorporate any material law for the reinforcement layers and for the concrete in form of multi-linear or continuous functions. Moreover, arbitrary number of reinforcement layers can be included.

The moment-curvature relationship is obtained by solving the equilibrium of the cross section for a pre-defined relevant range of curvature values. By assuming that the cross-section remains flat after deformation, a linear distribution of normal strains along the cross-sectional height is obtained, which yields

$$\varepsilon(z) = \varepsilon_{\mathrm{bot}} + z \cdot \frac{\varepsilon_{top} - \varepsilon_{\mathrm{bot}}}{h} \quad , \ 0 \leq z \leq h, \tag{1}$$

where $\varepsilon_{\mathrm{bot}}$ and $\varepsilon_{\mathrm{top}}$ are the strain values in the bottom and the top of the cross-section, respectively, h is the height of the cross-section and z is the height of the evaluated strain assuming $z = 0$ corresponds to the bottom of the cross-section. The curvature is given as

$$\kappa = -\frac{\mathrm{d}\varepsilon(z)}{\mathrm{d}z} = -\frac{\varepsilon_{\mathrm{top}} - \varepsilon_{\mathrm{bot}}}{h} \Rightarrow \varepsilon_{\mathrm{top}} = -\kappa \cdot h + \varepsilon_{\mathrm{bot}} \tag{2}$$

By combining (1) and (2) we obtain the strain profile over the cross-sectional height

$$\varepsilon(z) = \varepsilon_{\mathrm{bot}} - \kappa \cdot z, \tag{3}$$

where $\varepsilon_{\mathrm{bot}}$ is unknown. This strain profile is used as an input into the constitutive relations defined for concrete and reinforcement in the next section to obtain the cross-sectional stress profile as a function of $\kappa, z, \varepsilon_{\mathrm{bot}}$.

2.2. Constitutive laws

2.2.1 Constitutive laws for the concrete

Figure 1 shows two types of applicable material laws: type (a) shows a material law, that is used in this paper for model validation and is composed of a piecewise linear function for both the compression and tension regions according to Yao et al. [7].

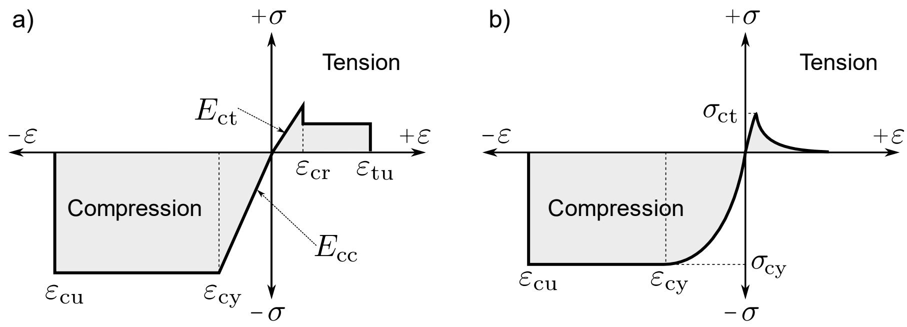

Figure 1. *Two possible variants for the constitutive law for concrete*

The diagram in Figure 1 (b) represents another type of the constitutive law for concrete with a compression curve based on the Eurocode 2 [11] and a continuous curve with nonlinear softening in the tensile regime.

2.2.2 Constitutive laws for the reinforcement

A linear-elastic, brittle model was assumed for the carbon reinforcement as depicted in Figure 2 (a).

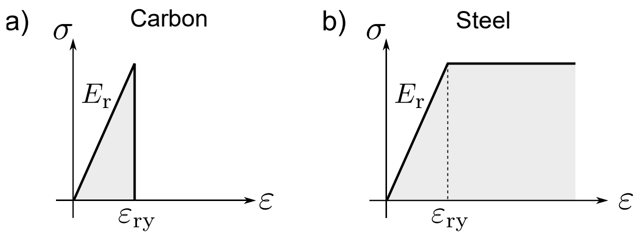

Figure 2. *Constitutive laws used for the reinforcement; a) carbon material law; b) steel material law*

For validation with experimental data with steel reinforcement, the elastic, ideally plastic constitutive law was used for steel , see Figure 2 (b).

The material laws presented above are pre-configured in the model setup. However, the implemented solution algorithm can handle any non-linear material law for both concrete and the reinforcement because the stress values are evaluated for each point along cross-section height.

2.3. Derivation of the moment-curvature relationship

The computational scheme depicted in Figure 3 exemplifies the strain and stress states of a cross-section using the multi-linear concrete constitutive law shown in Figure 1(a). The residual tensile stress in the bottom part of the cross-section represents the effect of short fibers. The calculation procedure illustrated in Figure 3 is caried out in four steps:

1- The curvature values are assumed in a relevant range of the material behavior with the aim of calculating the corresponding moment values for each given curvature using the equilibrium conditions for normal force and moment in the cross section.

2- By substituting equation (3) into the stress relations of concrete and reinforcement $\sigma_c(\varepsilon)$, $\sigma_r(\varepsilon)$, we obtain the stress distribution over the height z as a function of the given curvature κ and the unknown strain on the cross-section bottom $\varepsilon_{\mathrm{bot}}$. In other words, for each curvature value, we get the stresses in the concrete $\sigma_c(\varepsilon(\kappa, z, \varepsilon_{\mathrm{bot}}))$ and in the reinforcement $\sigma_r(\varepsilon(\kappa, z, \varepsilon_{\mathrm{bot}}))$, according to the used material laws.

3- The stress distribution in the concrete is linearly approximated in a piecewise way along the cross-section height. To determine the concrete contribution of the normal force F_c, the stress at height z is multiplied by the corresponding width $b(z)$ and numerically integrated.

$$F_{\mathrm{c}} = \int_0^h \sigma_c(z) \cdot b(z)\,\mathrm{d}z \tag{4}$$

The normal force from the reinforcement F_r is obtained as the sum of all force contributions in all reinforcement layers, i.e.

$$F_{\mathrm{r}} = \sum_i \sigma_{r_i} \cdot A_{r_i} \tag{5}$$

Assuming that the applied normal force is zero, the equilibrium of normal forces in the cross section is simply given as

$$F_{\mathrm{c}}(\kappa, \varepsilon_{\mathrm{bot}}) + F_{\mathrm{r}}(\kappa, \varepsilon_{\mathrm{bot}}) = 0 \tag{6}$$

4- The cross-section equilibrium is then solved numerically for $\varepsilon_{\mathrm{bot}}$ for each given curvature κ in the relevant range $\kappa \in (0, \kappa_{\mathrm{max}})$. The corresponding bending momentvalue can then be evaluated using the following equation

$$M = \sum F_{\mathrm{ri}} \cdot z_i + \int_z \sigma_{\mathrm{c}} \cdot b \cdot z\,\mathrm{d}z \tag{7}$$

κ_{max} is defined such that the associated moment $M(\kappa_{\mathrm{max}})$ is smaller than that of the maximum reached moment, i.e. beyond the peak of M-κ curve.

The calculation exploits the open-source scientific computing library SciPy allowing an efficient solution of the nonlinear set of equations in parallel on a standard computer.

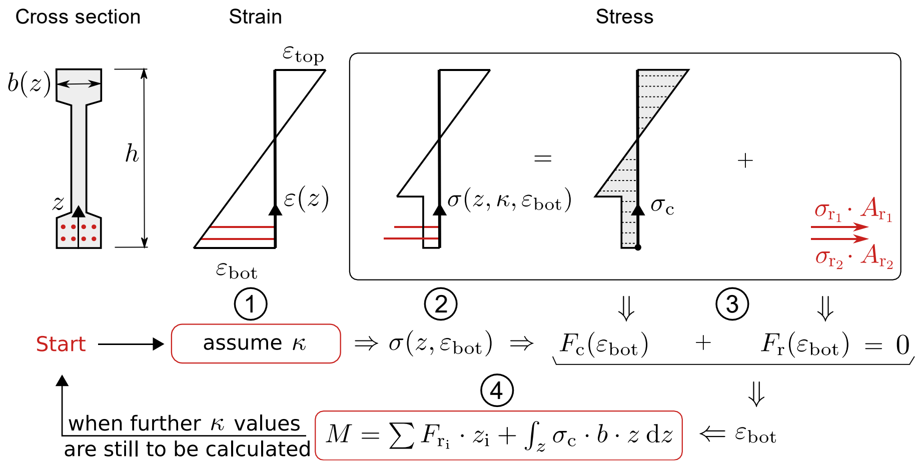

Figure 3. *Summary of the approach used to calculate the moment M corresponding to a given curvature κ*

3. CALCULATION OF THE DEFLECTION

To obtain the beam deflection for an arbitrary configuration of supports and loading, the M-κ curve is inverted into a κ-M curve, as in Figure 4. The moment diagram along the beam is determined for the given loading configuration and discretized as a piecewise linear function along the length of the flexural beam, see Figure 5. At each integration point, the curvature corresponding to the moment is assigned using the M-κ relationship. Finally, the deflection is obtained using a double integration of the curvature curve along the beam over the longitudinal coordinate x, see Figure 5.

The ultimate load for the beam under given boundary conditions $F_{\max}$ is calculated using the maximum moment value $M_{\max}$ in the M-κ curve, see Figure 4. The relation between the moment and the corresponding force can be obtained from the moment diagram of the beam in its peak value, e.g. for the case of simply supported beam with 4-point bending setup, this can be calculated as $F_{\max} = M_{\max}/x_F$, see Figure 5.

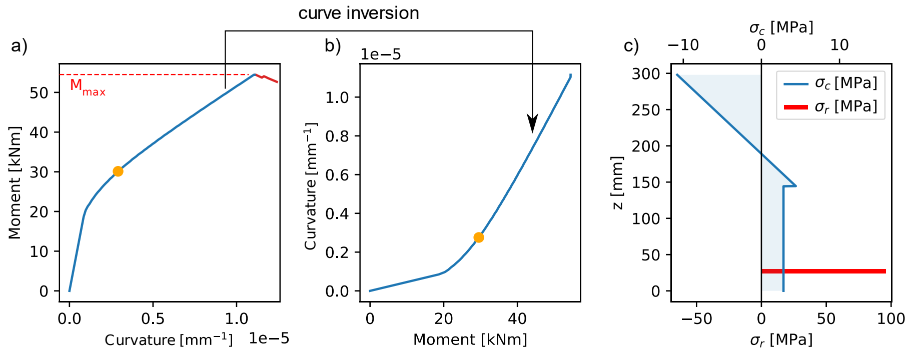

Figure 4. *The calculated M-κ curve with its inversion: a) M-κ curve; b) inverted M-κ curve; c) stress state of the cross-section that corresponds to a loading level indicated by the yellow circle*

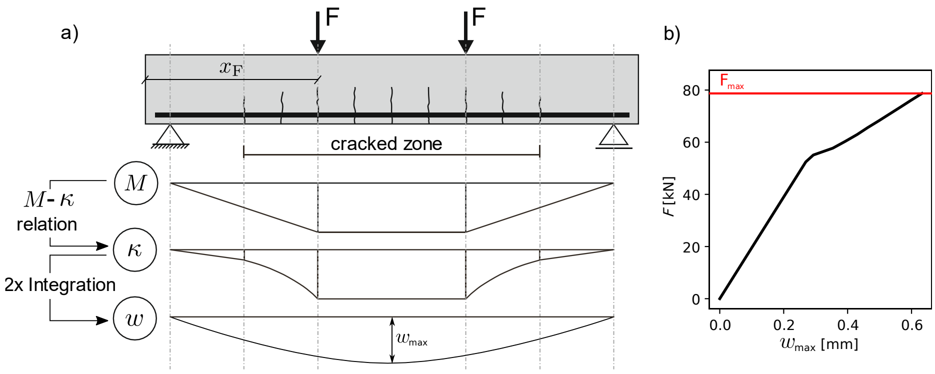

Figure 5. *The calculation of beam deflection based on the obtained M-κ relation.*

4. MODEL VALIDATION WITH EXPERIMENTAL DATA

The moment-curvature and load-deflection curves obtained using the introduced model have been compared with experimental data. To show the feasibility of the model in a broad range of applications, both carbon and steel reinforced concrete sections have been included in the validation. Table 1 summarizes all the used experiments.

Table 1. *List of experiments used for the validation of the model*

	Test ID	ρ [%]	b [mm]	h [mm]	a1 [mm]	a2 [mm]	As1 [mm²]	As2 [mm²]	fs [MPa]	Es [GPa]	fcm [MPa]	Ec [MPa]
Gribniak 2012 (steel)	S3-1-F05	0.3	278	302	24	29	235	56	560	203	56	35000
	S3-1-F15	0.3	279	300	28	26	235	56	560	203	52	34000
Yang 2010 (steel)	R12-1	0.6	180	270	35	-	253	-	600	200	191	46418
	R13-2	0.9	180	270	35	-	380	-	600	200	192	46680
von der Heid 2020* (carbon)	HB-SU-0	0.4	90	30	8	8	7	7	2712	240	72	39500
El Ghadioui 2020 (carbon)	B-M-S-K1	0.6	400	200	19	-	452	-	550	200	64	33525
	B-M-C-K1	0.2	400	200	35	-	140	-	1891	135	64	33525
	B-M-C-K2	0.3	400	200	66	-	140	-	1891	135	64	33525

* Mean values for multiple tests.

4.1. Steel

The first two diagrams in Figure 6 compare the prediction of the M-κ with the experimental results. Figure 6 (a) shows a comparison between M-κ curves for two beams with different short fiber contents conducted by Gribniak et al. [12] and the simulated M-κ response. Two UHPC beams with different reinforcement ratio and a concrete compressive strength $f_{cm} \approx 191$ MPa were conducted by Yang et al. [13]. The experimental M-κ curves are illustrated in Figure 6 (b) with the corresponding curves obtained using the model.

A validation for the load-deflection response for steel reinforcement was provided using experimental results delivered by El Ghadioui et al. [14] for a simply supported beam tested with 4-point bending setup. The load-deflection curves obtained by the model and by the experiment is compared in Figure 6 (c).

The comparison in all three cases shows the ability of the model to correctly reproduce the behavior of the beams including the post-cracking and steel yielding phases of the response.

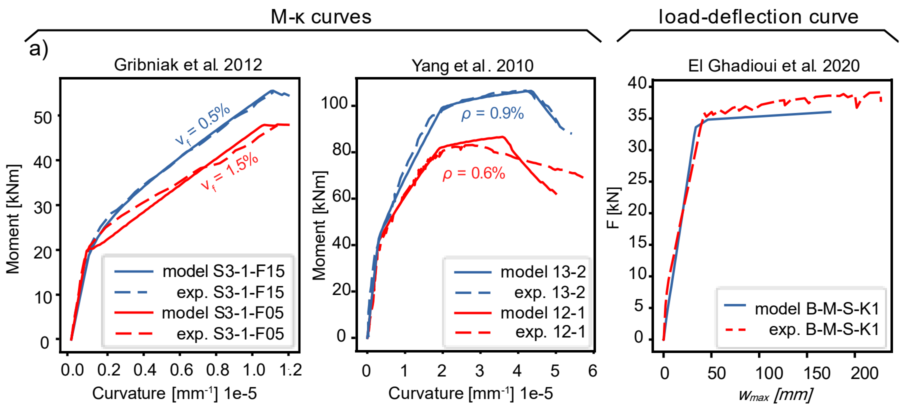

Figure 6: *Comparison between simulated and experimental results for steel-reinforced beams; a),b) M-**κ** curves [12], [13]; c) load-deflection curve [14]*

4.2. Carbon

The load-deflection curves predicted for carbon-reinforced beams by the model are compared with the experimental results in Figure 7.

The experimental results of [14] for two identical beams reinforced with CFRP bars with different static effective heights d are shown in Figure 7 (a). The behavior predicted by the model shows a very good agreement for the initial phase before and after cracking (up to about 10 kN), but after that a slight overestimation of the beam stiffness is observed. This can be attributed to the loss of stiffness due to the multiple cracks, which is evident from the experimental curves and which was not predicted by the current implementation of the model.

The comparison of the test results including two test series by von der Heid et al. [15] with the simulation in terms of the load-deflection curves for the tested plates are shown in Figure 7 (b). The underlying M-κ relation is exemplified in Figure 7 (b*) both for the model and the experiment.

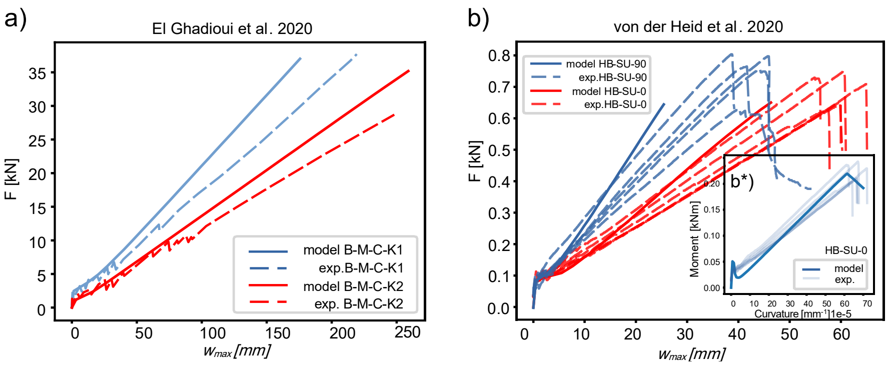

Figure 7: *Comparison between simulated and experimental results for carbon-reinforced elements; a) load-deflection curves by El Ghadioui et al. [14]; b) load-deflection and M-**κ** curves by von der Heid et al. [15]*

5. BASIS FOR SERVICEABILITY DESIGN RULE

The implemented model can serve as a basis of a simple engineering design rule for carbon-reinforced concrete elements in the serviceability limit state (SLS). To comply with the simplified SLS design concept used in the Eurocode 2 [11] and the fib Model Code [16] the relation between the span/depth (L/d) and reinforcement ρ ratios has been evaluated in a parametric study covering the relevant range both for steel and for carbon-reinforced specimens. The results of the study are summarized in Figure 8 showing a qualitatively different shape of the admissible design region. In agreement with the results presented recently by El Ghadioui [17], the carbon reinforced elements exhibit a pronounced transition point between the tensile failure of the reinforcement (left branch) and the compressive failure of concrete (right branch). Two different values of E-moduli and of the carbon tensile strength have been considered in the presented study.

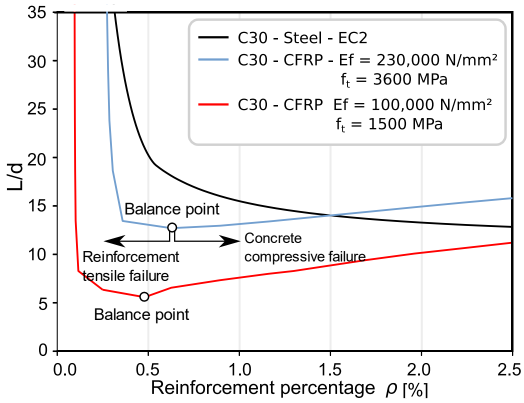

Figure 8: *Comparison between (L/d – ρ) curves for steel and carbon reinforcement*

6. SUMMARY AND CONCLUSION

The described model for the calculation of the moment-curvature relation and the load-deflection response of RC elements exposed to bending load provides a basis for the derivation of general SLS rules as exemplified for beams reinforced with carbon fabrics. The object-oriented model implementation is based on Python programming language and is available on the version control platform GitHub at https://github.com/bmcs-group as part of the brittle-matrix composite structures suite maintained by the authors. This model offers flexibility in several ways. For example, it makes it easy to insert and configure arbitrary types of material models for both concrete and reinforcement, or to use any cross-section shape and reinforcement layout in terms of the number and location of reinforcement layers. The model is based on a numerical piecewise evaluation of the stress and forces along the cross-section and a non-linear solution of the equilibrium of the cross-section that makes use of the SciPy scientific library for Python. The model was validated with experimental data which demonstrated its ability to correctly predict the experimental results for both steel and carbon reinforcement.

In this paper, a multi-linear material law for concrete was used for the validations. In the following refinement steps, more sophisticated constitutive laws will be integrated, exploiting the modular design of the framework. Moreover, an extension of the model to take the effect of the bond behaviour and tension-stiffening in the cracked region along the beam into account is planned. Finally, a comprehensive web application with a wide range of design options will be provided for public access.

7. ACKNOWLEDGMENT

This work was funded by the Deutsche Forschungsgemeinschaft (DFG, German Research Foundation) - SFB/TRR280, Project-ID 417002380.

8. REFERENCES

[1] Pfrang E. O., Siess C. P., and Sozen M., 1964, "Load-Moment-Curvature Characteristics of Reinforced Concrete Cross Sections.", *Journal Proceedings*, 61(7), pp. 763-778.
[2] Domingo J. Carreira, and Kuang-Han Chu, 1986, "The Moment-Curvature Relationship of Reinforced Concrete Members.", *Journal Proceedings*, 83(2), pp. 191-198.
[3] Espion B., and Halleux P., 1988, "Moment curvature relationship of reinforced concrete sections under combined bending and normal force.", *Materials and Structures*, 21(5), pp. 341–351.
[4] W. A. M. Alwis, 1990, "Trilinear Moment-Curvature Relationship for Reinforced Concrete Beams.", *Structural Journal*, 87(3), pp.276-283.
[5] Monti G., and Petrone F., 2015. "Yield and ultimate moment and curvature closed-form equations for reinforced concrete sections.", *ACI Structural Journal* 112(4), p. 463.

[6] Ćurić I., Jure Radic, and Marin Franetovic, 2016. "Determination of the bending moment-curvature relationship for reinforced concrete hollow section bridge columns.", *Tehnicki Vjesnik-Technical Gazette*, 23(3), pp.907-916.
[7] Yao Y., Mobasher B., Wang J., and Xu Q., 2021, "Analytical approach for the design of flexural elements made of reinforced ultra-high performance concrete. ", *Structural Concrete*, 22(1), pp. 298–317.
[8] Barros J. A. O., and Gláucia Dalfré, 2013. "A model for the prediction of the behaviour of continuous RC slabs flexurally strengthened with CFRP systems.", *Proceedings of the 11th International Symposium on Fiber Reinforced Polymers for Reinforced Concrete Structures*, UM, Guimarães.
[9] Rezazadeh M., Barros J., and Costa I., 2015, "Analytical approach for the flexural analysis of RC beams strengthened with prestressed CFRP.", *Composites Part B: Engineering*, 73, pp. 16–34.
[10] Parra-Montesinos, G., and A.E. Naaman, Ed., 2001. "Parametric Evaluation of the Bending Response of Ferrocement and Hybrid Composites with FRP Reinforcements.", *Proceedings of Seventh International Symposium on Ferrocement and Thin Reinforced Cement Composites*, Singapore.
[11] Standardisation E. C. f., 2010, “Eurocode 2: Design of concrete structures - Part 1-1: General rules and rules for buildings. Incl. Corrigendum 1: EN 1992-1-1:2004/AC:2008, incl. Corrigendum 2: EN 1992-1-1:2004/AC:2010,”(EN 1992-1-1:2004).
[12] Gribniak V., Kaklauskas G., Hung Kwan A. K., Bacinskas D., and Ulbinas D., 2012, "Deriving stress–strain relationships for steel fibre concrete in tension from tests of beams with ordinary reinforcement.", *Engineering Structures*, 42, pp. 387–395.
[13] Yang I. H., Joh C., and Kim B.-S., 2010, "Structural behavior of ultra high performance concrete beams subjected to bending.", *Engineering Structures*, 32(11), pp. 3478–3487.
[14] El Ghadioui R., Proske T., Tran N. L., and Graubner C.-A., 2020, "Structural behaviour of CFRP reinforced concrete members under bending and shear loads.", *Materials and Structures*, 53(3), pp.1-16.
[15] Heid A.-C. von der, and Grebe R., 2020, "Perforierte und vollflächige Fassadenplatten aus carbonbewehrtem Beton/Perforated and full-surface façade panels made of carbon-reinforced concrete.", Bauingenieur, 95(06), pp. 210–219.
[16] Beverly P., Ed., 2013. fib model code for concrete structures 2010, Ernst & Sohn, Berlin.
[17] El Ghadioui R., 2020. Bemessung carbonbewehrter Betonbauteile unter besonderer Betrachtung des Gebrauchszustandes: Entwicklung eines Modells zur wirklichkeitsnahen Verformungsberechnung [PhD dissertation], 1st ed., Technische Universität Darmstadt, Institut für Massivbau, Darmstadt.

NUMERICAL MODELLING OF THE FLEXURAL CAPACITY OF HEATED TEXTILE REINFORCED CONCRETE

Panagiotis Kapsalis[1,*], Michael El Kadi[2], Thanasis Triantafillou[3], Danny Van Hemelrijck[4], Tine Tysmans[5]

[1] *Dept. of Mechanics of Materials and Constructions, Vrije Universiteit Brussel, 1050 Ixelles, Belgium, and Dept. of Civil Engineering, Univ. of Patras, Patras GR-26504, Greece. Panagiotis.Kapsalis@vub.be*

[2] *Dept. of Mechanics of Materials and Constructions, Vrije Universiteit Brussel, Pleinlaan 2, 1050 Brussels, Belgium. Michael.El.Kadi@vub.be*

[3] *Dept. of Civil Engineering, Univ. of Patras, Patras GR-26504, Greece. ttriant@upatras.gr*

[4] *Dept. of Mechanics of Materials and Constructions, Vrije Universiteit Brussel, Pleinlaan 2, 1050 Brussels, Belgium. Danny.Van.Hemelrijck@vub.ac.be*

[5] *Dept. of Mechanics of Materials and Constructions, Vrije Universiteit Brussel, Pleinlaan 2, 1050 Brussels, Belgium. Tine.Tysmans@vub.be*

SUMMARY: *This study discusses a modelling technique of the thermomechanical behaviour of textile reinforced concrete (TRC) members, with finite elements. TRC specimens that were subjected to fire tests and subsequently to flexure tests are numerically simulated in a two-step procedure. The first step is a heat transfer analysis, where the temperature profile of the fire exposed specimens is determined. The second step is the implementation of a numerical model that simulates the response of TRC elements subjected to flexure, adopting a semi-smeared (layered) approach. The models are calibrated and verified by existing experimental results. It is concluded that this technique can be used to obtain numerical results that are in reasonable agreement with the experimental data.*

KEYWORDS: *fire, heat transfer modelling, high temperatures, Textile Reinforced Concrete, Textile Reinforced Mortars, thermomechanical modelling.*

1. INTRODUCTION

The use of inorganic matrix composites gains increasing popularity in the last decades, for many types of applications, such as precast, lightweight and insulating structural members, façade panels, retrofitting of existing structural elements, shell structures, etc. However, the mechanical performance of such members after fire exposure is poorly understood [1]. The main reasons are the practical difficulties in conducting tests on such members in fire conditions, as well as the difficulties in extracting general results from studies that have been conducted with different testing conditions and methods. The knowledge gap becomes more evident when it comes to the modelling of the thermomechanical behaviour of these materials. So far, very limited research has been conducted on this topic. Modelling techniques for the behaviour of textile reinforced cement composites (TRC) exposed to increased temperatures have been proposed by [2] for the compressive, tensile and flexural behaviour, [3] for the textile-to-matrix bond, as well as by [4]-[6] for the tensile behaviour. This study presents a methodology to model the flexural behaviour of fire exposed textile reinforced concrete (TRC) specimens, using the finite element software ABAQUS.

2. METHODOLOGY

This study is based on layer-wise numerical modelling approaches of TRC in bending (in ambient conditions), such as the ones presented by [7] and [8]. The goal is to simulate the flexural performance of fire exposed TRC specimens, utilizing the results of an experimental campaign that was previously conducted and presented in [9].

In this campaign, TRC specimens of various compositions were tested in uniaxial tension. They were previously exposed to fire, reaching temperatures in the range of 20 - 700 ^{o}C. Hence, a temperature-dependent constitutive law was determined for each composition. Additional specimens of the same compositions but in thicker layups were manufactured. The thicker specimens were also exposed to fire (only from one side) and then tested in flexure. The specimens designed for tension had dimensions of 10×120×600 mm, while the specimens designed for flexure had dimensions of 32×70×500 mm.

This paper aims to present this modelling technique by explaining the basic ideas and assumptions. Therefore, the current manuscript presents, indicatively, the results of the simulation of only one composition. The considered composition consisted of a cementitious matrix reinforced with two layers of an uncoated carbon fibre textile. The constitutive behaviour of this composition was determined by tensile tests on specimens with the cross-section shown in Fig. 1a. The simulated flexural specimens were exposed to a 28-minute fire test, and after cooling down they were subjected to four-point bending. The cross-section of these specimens is shown in Fig. 1b.

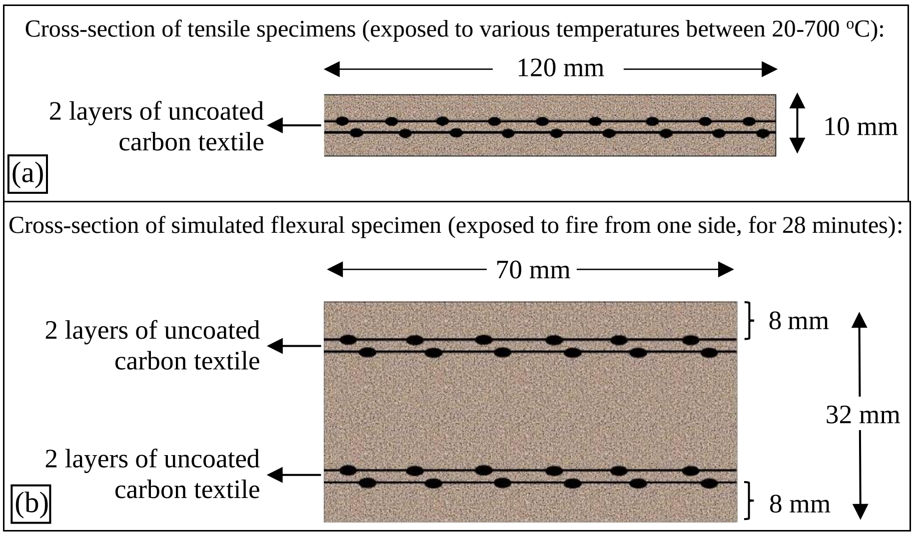

Fig. 1 Cross-sections of tested and simulated specimens

The temperature of the fire exposed flexural specimens was not uniform, but the temperature gradient during the fire test was monitored with thermocouples. Hence, the first step of the modelling is the simulation of the heat transfer in the exposed specimens. The time history of the temperature at the exposed surface of the specimens during the fire tests is given as input. The surface temperature is assumed to be uniform, thus, a simple one-dimensional model is adopted to calculate the heat propagation through the thickness. The output of this step is the maximum temperature reached at every point of the cross-section of the specimens.

The second step is the simulation of the flexure tests. A layer-wise approach is adopted in this study. The material properties are assigned in separate layers of the cross-section (the cross-section is partitioned into layers of *plain mortar* or *textile reinforcement*). This way, the material properties at every point of the cross-section are determined by the material assigned to that point and by the assigned temperature (which was determined in the previous step).

3. RESULTS

3.1 Heat transfer simulation

The flexural specimens were exposed only from one side; the other sides were insulated with mineral wool. The exposed surface was subjected to the tensile zone during the flexural test. Therefore, the layer of reinforcement that was close to the exposed surface defines the “effective depth” during bending. The temperature was monitored at the exposed surface, the effective depth, and the unexposed surface. Fig.

2 shows the temperature measurements at these positions, on the considered specimens.

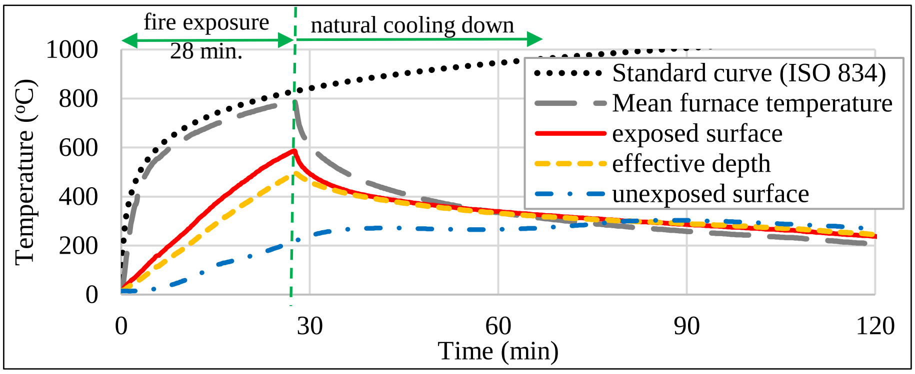

Fig. 2 Temperature recordings to a flexural specimen during the 28-min. long fire test.

The heat transfer analysis was conducted with a simple model. The reinforcement was neglected in this model, thus, only the properties of the matrix were considered. The specimens' cross-section was assumed to be perfectly insulated at the sides that were protected by the mineral wool, as shown in Fig. 3a, hence, the heat flow was allowed only at the through-thickness dimension. The recorded temperature at the exposed surface of the specimen (see Fig. 2) was assigned as a boundary condition at the top border of the simulated cross-section and it served as the input of the analysis. It was given as a time-history (time vs. temperature). The output was the temperature at points deeper in the cross-section. The finite element meshing was done by orthogonal heat transfer elements (DC2D4 in ABAQUS 6.14-1) vertically stacked in the thickness direction. The elements had a thickness of 2 mm and the temperature was exported at the nodes. Thus, the results were obtained every 2 mm through the cross-section depth. Fig. 3b shows indicative results of the temperature gradient in the cross-section.

The basic material properties that affect the heat transfer analysis are the density of the specimens, the specific heat capacity and the thermal conductivity. The density was determined by measuring the specimens' dimensions and weighing them. The specific heat capacity was taken equal to the value proposed by [10], who conducted relevant investigations for cementitious composites. The thermal conductivity (λ) of the material was measured at room temperature. The values ranged approximately between 0.9 and 1.4 W/mK, depending on the presence of reinforcement and the water saturation. Measurements of λ at high temperatures could not be obtained. The relevant European Standards for normal concrete (EN1992-1-2) propose a range for the law describing λ as a function of temperature. The lower limit of the proposed range in ambient conditions is in the order of 1.4 W/mK. Despite the lower measured values for the matrix of this study, the lower limit proposed by EN1992-1-2 was considered here as the closest available approximation. Fig. 3c shows the results obtained by the numerical simulation at the effective depth and the unexposed surface (bottom insulated border) of the considered specimens. The results of the model are compared to the experimental measurements. The agreement between the measurements and the numerical results is very good at the effective depth (where the sensors were cast into the specimen), but the experimental results underestimated the temperature at the insulated bottom due to improper fixing of the sensor and a slight curvature of the specimens (thus, loss of contact between the specimen and the sensor). Since the results of the simulation were obtained every 2 mm through the thickness of the cross-section, the maximum temperature reached to each position was used to assemble the maximum temperature profile (i.e. the exposure temperature envelope) for the specimens. This envelope (shown in Fig. 3d) was given as input to the next step of the modelling procedure (the mechanical modelling).

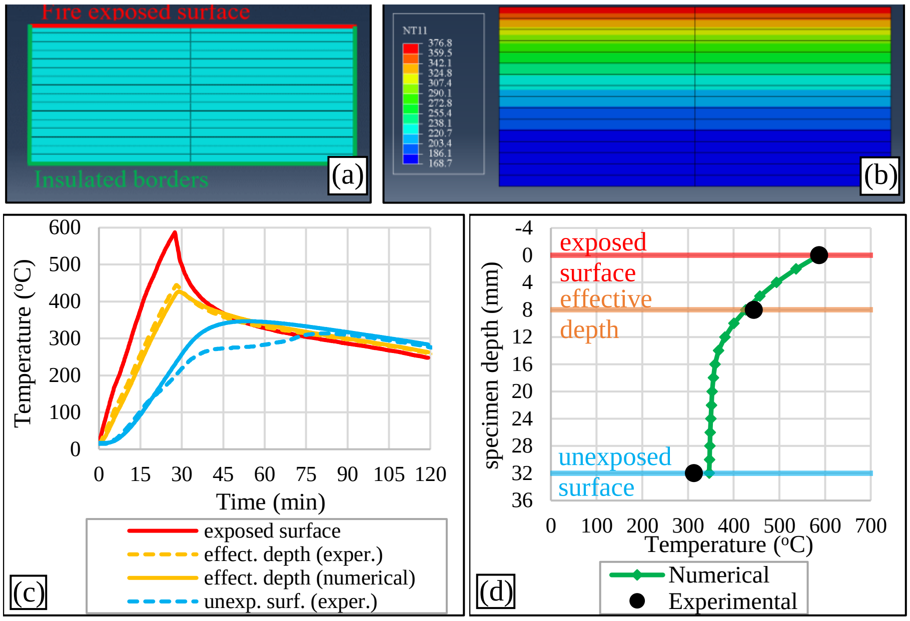

Fig. 3 Heat transfer modelling details: (a) modelled cross-section: mesh and boundary conditions; (b) indicative temperature profile at a specific time; (c) temperature evolution at the monitored positions during the fire exposure: experimental vs. numerical results; (d) envelope of maximum temperatures during the fire exposure: experimental vs. numerical.

3.2 Flexural behaviour modelling

For this step, the specimens subjected to flexure were fully simulated. Fig. 4a presents the geometrical details of the four-point bending test set-up, and Fig. 4b shows the corresponding finite element (FE) model. The load was applied as a displacement on the reference point (RP-1) shown in Fig. 4b. The RP was connected to the loading pins with a "rigid body" constraint. The loading pins were in contact with the top surface of the specimen. The properties of the interaction were assigned as "hard contact" in the normal direction and "frictionless" in the tangential direction. The supports were simulated as boundary conditions where the vertical movement (*V*) is restrained. These choices are explained in detail in [7]. The mesh is built with 3D stress elements (C3D8 in ABAQUS 6.14-1) measuring 1-2 mm in the thickness direction and 10-15 mm in the other two directions (46 elements along the specimen's length). Thus, the model is «layered» in the thickness direction, in layers of 1 or 2 mm (see Fig. 4c).

The temperature profile that was determined in the previous step was assigned as a predefined field. A temperature field was assigned to every layer of 2 mm. The material properties were assigned to the respective layers of the cross-section, as indicated in Fig. 4c.

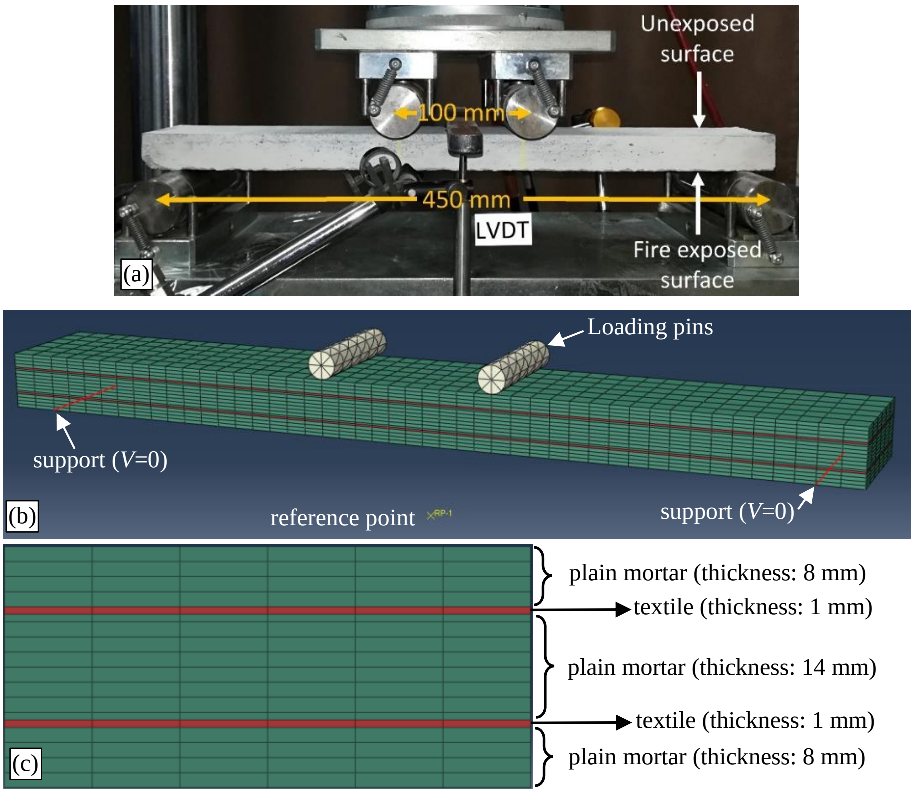

Fig. 4 (a) Flexure tests set-up; (b) basic details of the model of the flexure test; (c) cross-sectional layers of the model, assigned with different materials.

The mechanical properties of the reinforcement were determined based on the results of the tensile tests presented in [9]. The tensile specimens had been exposed to several temperatures, varying between 20 - 700 °C. The resulting stress-strain curves were idealized into tri-linear, according to the following three stages: uncracked stage, multiple cracking stage, post-cracking stage. The tri-linear stress-strain laws are shown in Fig. 5a for all exposure temperatures. The constitutive tensile behaviour of the textile and the matrix were determined by a stress decoupling of the composite, for all exposure temperatures. This is shown indicatively for 20 °C in Fig. 5b. The effective stress-strain law of the textile was considered as the line starting from zero, going up to the maximum strain of the composite, in parallel to the third stage of the composite stress-strain law. By obtaining the effective textile properties based on tests on TRC specimens and not in textile specimens, the effect of the imperfect bond between the textile and the matrix is taken into account (as in [8]). The difference between the stress-strain curve of the composite and the textile is considered as the contribution of the matrix. The compressive strength and the elastic modulus of the mortar were determined, as functions of temperature, by simple compressive tests on mortar prisms that had been exposed to the same fire tests.

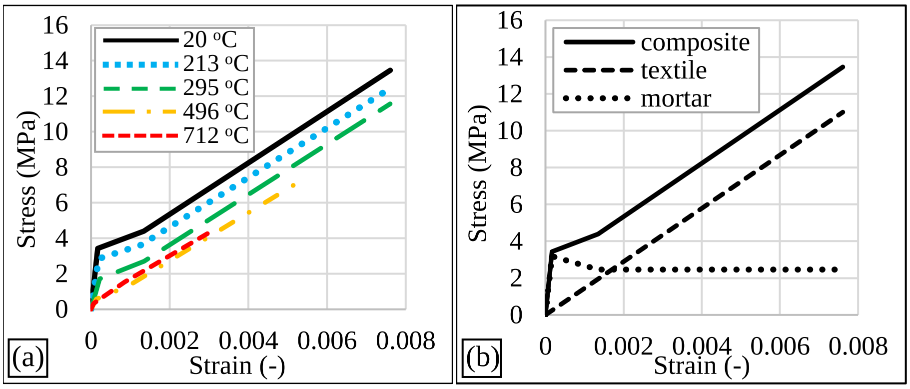

Fig. 5 (a) Idealized experimental results; (b) derivation of the effective stress-strain laws of the textile and the mortar in tension by stress decoupling of the composite behaviour.

The resulting material properties were assigned to the corresponding layers of the model (*plain mortar* or *textile*). The textile properties were previously rescaled (as in [7]) to correspond to the modelled thickness of 1 mm. The stress-strain law of the mortar was assigned as temperature-dependent, via the concrete damaged plasticity model (CDP). More details on the rescaling of the material properties and the utilization of CDP for TRC modelled in ABAQUS are found in [7].

The experimental results from the flexure tests (load-deflection curves) are presented in Fig. 6a, where they are directly compared to the results of the model. The laboratory tests and the simulations were not conducted only for the fire exposed specimens, but also for identical replicants that were kept constantly in ambient conditions. Therefore, the performance of the "heated" (i.e. fire exposed) specimens is discussed with reference to the respective behaviour of the "ambient" (i.e. not exposed) specimens.

First, it is observed that the flexural performance of the specimens shows a three-stage behaviour, like the one witnessed in the tensile tests of the same composition. Hence, as expected, it is concluded that the tensile response of the TRC dominates its flexural response too. This is also verified by the fact that the biggest part of the cross-section is in the tensile zone. This is shown in Fig. 6b, which presents the normal stress distribution in the modelled heated specimen, at the deflection of 10 mm. It is observed that the top reinforcement is bearing tensile stresses too. The compressive zone is approximately 7 mm deep.

The model gives a good approximation of the experimental results in ambient conditions. The uncracked stage is accurately modelled, and the post-cracking stiffness is slightly underestimated. The average post-cracking stiffness of the experimental results is 0.28 kN/mm (with a standard deviation of 0.05 kN/mm), while the post-cracking stiffness of the simulated curve is equal to 0.23 kN/mm. The maximum load is underestimated in ambient and heated conditions. This is attributed to the improved anchorage conditions (larger anchorage length, specimen's curvature) of the reinforcement in the flexural specimens than in the tensile specimens which were tested to obtain the stress-strain curve. Due to the improved anchorage in flexure, the reinforcement is better activated and, thus, its capacity is extended. This has also been explained in [7].

The post cracking stiffness of the heated specimens is underestimated by a larger difference than in ambient conditions. This is attributed to additional uncertainties and errors that are introduced in the model. Apart from the errors associated with the idealized material behaviour, one additional error is associated with the temperature profile that is given as input. The assumptions and simplifications of the heat transfer modelling might lead to errors of the calculated temperature profile; hence, the accuracy of the temperature-dependent material properties is also hindered. For instance, a more accurate assumption for the thermal conductivity of the mortar might lead to improved results. Furthermore, the material properties have been given as input for a small number of temperatures (for instance, the tensile properties of the textile and the mortar were calculated only for the five temperatures, shown in Fig. 5a). The properties for intermediate temperatures are calculated by the software by linear interpolation, which induces additional errors. Therefore, increased discretization of the mesh and the input data would also be advised for higher accuracy. Finally, the possible errors of the experimental data are more in the case of the fire exposed specimens. For instance: (i) the non-uniform heating of the fire exposed tension specimens hinders the accuracy of the stress-strain laws that were obtained, while (ii) the heating rates achieved in the thin tension specimens were not the same as the heating rates achieved in the thicker specimens designed for the flexure tests. Therefore, additional uncertainties are induced; hence, it is reasonable to obtain results with increased errors from the simulation of the heated specimens. Nevertheless, the results are still in reasonable margins. The average post-cracking stiffness of the tested specimens was 0.20 kN/mm (±0.01 kN/mm) while the modelled post-cracking stiffness was equal to 0.16 kN/mm.

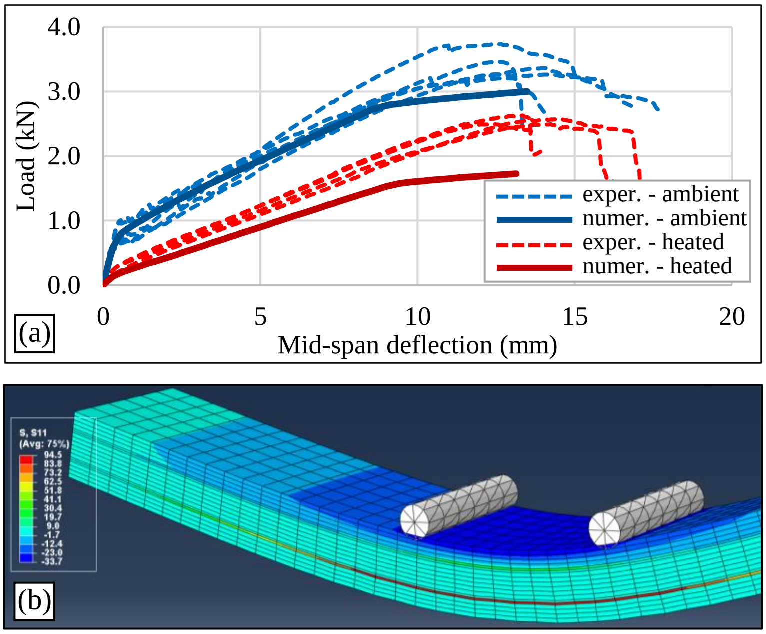

Fig. 5 (a) Load-deflection curves (experimental vs. numerical); (b) normal stresses of the simulated specimen in flexure (at 10 mm deflection).

4. SUMMARY AND CONCLUSIONS

This study presented a two-step numerical, layer-wise modelling technique of the flexural capacity of fire exposed TRC specimens. The first step, which is a heat transfer analysis used to determine the exposure temperature envelope of the fire exposed specimens, gave reasonable results. The second step uses the calculated temperatures as input; hence, the temperature-dependent material properties are assigned separately to each layer of the cross-section. The results indicate that this technique can be used to simulate the load-deflection performance of the specimens in ambient conditions and after heat treatment. In both cases, the model underestimates the maximum load and the post-cracking stiffness (especially at the heated specimens) meaning that utilization of this model for design purposes would lead to conservative solutions.

4. REFERENCES

[1] TLAIJI, T., VU, X. H., FERRIER, E., SI LARBI, A., “Thermomechanical behaviour and residual properties of textile reinforced concrete (TRC) subjected to elevated and high temperature loading: Experimental and comparative study.” *Composites Part B: Engineering*, 144, 2018, p. 99–110.

[2] BLOM, J., & J. WASTIELS. "Modeling textile reinforced cementitious composites-Effect of elevated temperatures." *The 19th International Conference on Composite Materials*. July 2013, Montreal, Canada.

[3] DONNINI, J., Y BASALO, F. D. C., CORINALDESI, V., LANCIONI, G., & NANNI, A. "Fabric-reinforced cementitious matrix behavior at high-temperature: Experimental and numerical results." *Composites Part B: Engineering,* 108, 2017, p. 108-121.

[4] RAMBO, D. A. S., YAO, Y., DE ANDRADE SILVA, F., TOLEDO FILHO, R. D., & MOBASHER, B. "Experimental investigation and modelling of the temperature effects on the tensile behavior of textile reinforced refractory concretes." *Cement and Concrete Composites,* 75, 2017, p. 51-61.

[5] TRAN, M. T., VU, X. H., & FERRIER, E. "Mesoscale numerical modeling and characterization of the effect of reinforcement textile on the elevated temperature and tensile behaviour of carbon textile-reinforced concrete composite." *Fire Safety Journal,* 116, 2020, 103186.

[6] TRAN, M. T., VU, X. H., & FERRIER, E. "Mesoscale modeling of the elevated temperature behavior of the basalt textile reinforced concrete." *Proceedings 9th International Conference on Fibre-Reinforced Polymer (FRP) Composites in Civil Engineering (CICE 2018),* July 17-19, 2018, Paris, France.

[7] EL KADI, M., TYSMANS, T., VERBRUGGEN, S., VERVLOET, J., DE MUNCK, M., WASTIELS, J., & VAN HEMELRIJCK, D. "A layered-wise, composite modelling approach for fibre textile reinforced cementitious composites." *Cement and Concrete Composites,* 94, 2018, p. 107-115.

[8] CHUDOBA, R., SHAREI, E., SENCKPIEL-PETERS, T., & SCHLADITZ, F. "Numerical modeling of non-uniformly reinforced carbon concrete lightweight ceiling elements." *Applied Sciences,* 9(11), 2019, 2348.

[9] KAPSALIS, P. TRIANTAFILLOU, T., TYSMANS, T., “Carbon Textile Reinforced Concrete at ambient and high temperatures” *Proceedings 12th Carbon and Textile Reinforced Concrete Conference,* p. 82-89, September 22-23, 2020, Dresden, Germany.

[10] PODEBRADSKA, J., PAVLIK, J., TOMAN, J., & ČERNÝ, R. “Specific heat capacity of cementitious composites in high-temperature range”. *Working Group of the Slovak Physical Society*, 2003, 18-23.

ACOUSTIC EMISSION MONITORING OF FRACTURE OF TRC CURVED STRUCTURAL PLATES

Eleni Tsangouri[1], Aymeric Hardy[2], Aron Van Driessche[1], Amir Si Larbi[2], Dimitrios G. Aggelis[1]

[1]Dept. Mechanics of Materials & Constructions (MeMC), Vrije Universiteit Brussel (VUB), Pleinlaan 2, 1050 Brussels, Belgium, eleni.tsangouri@vub.be, dimitrios.aggelis@vub.be

[2]Univ Lyon, Ecole Nationale d'Ingénieurs de Saint Etienne (ENISE), Laboratoire de Tribologie et de Dynamique des Systèmes (LTDS), UMR 5513, 58 Rue Jean Parot, 42023 Saint Etienne Cedex 2, France, amir.si-larbi@enise.fr

SUMMARY: *Acoustic emission (AE) is commonly applied for structural evaluation of materials. It uses piezoelectric sensors to detect elastic waves coming from failure processes within the material. Concerning textile reinforced cementitious (TRC) plates, AE parameters have proven their potential to characterize not only the location and the fracture mode of defects but also the developing strain field before visible damage evolves. Matrix cracking events create short elastic signals with high frequencies whereas debonding between layers or fiber pull-out results in longer signals of lower frequency. However, the wave propagation path, plate wave dispersion and heterogeneity result in attenuation and distortion of the signal. These factors change the received AE parameters and therefore, complicate the evaluation especially for large sample dimensions. In this study, curved textile reinforced cement plates with different widths are loaded in bending with concurrent AE monitoring. The aim is to evaluate if damage characterization based on small laboratory specimens can be upgraded to larger scales and different geometries.*

KEY WORDS: *Acoustic emission, textile reinforced cement, frequency, duration, cracking, delamination.*

1. INTRODUCTION

Acoustic emission (AE) has been used for structural health monitoring of cementitious components and structures since decades. The main advantages of AE concern the non-destructive passive application, the detection of active cracking, the potential of three-dimensional localization of damage sources as well as characterization of the dominant fracture mode [1].

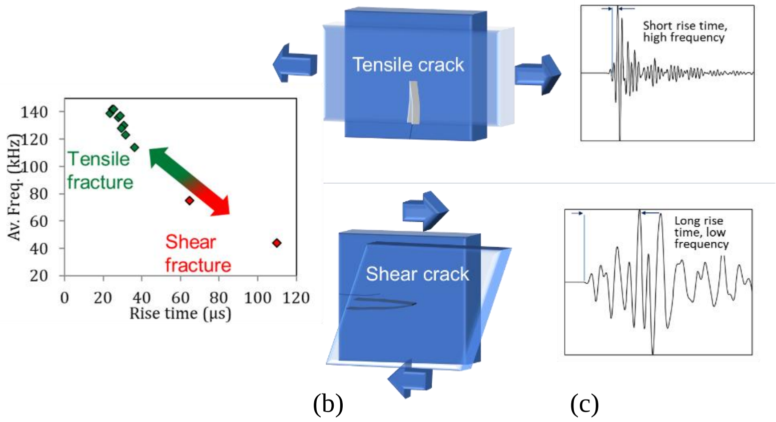

(a) (b) (c)

Figure 1. (a) *Characterization between tensile and shear fracture by AE parameters, (b) basic fracture events with (c) corresponding representative signals AE (right).*

Fig. 1 shows an indicative graph of characterization of AE signals based on their frequency content and rise time. This separation is possible because the different fracture modes include distinct crack tip motions, resulting in excitation of different wave modes. In bulk media these are longitudinal, which are faster, and shear, which are slower. In the case of plates these transform to symmetric and antisymmetric modes resulting in different acoustic signatures (Fig.1c). Even though this separation works in a reliable way in small beam specimens, it has not been tested in larger realistic scale. The influence of dimensions was examined recently on straight plates highlighting the role of lateral dimension on the AE readings [2].

2. RESULTS

In the current work, curved beams of 4 mm thickness with different widths, namely 25, 50, and 300 mm and height 15 mm are mechanically tested in three-point bending with concurrent monitoring of their AE activity (see Fig. 2a) with sensors resonant at 150 kHz. Due to loading and material type the fracture mechanisms are identical in all different specimens, especially at the start of the loading, when matrix cracking occurs. In addition, the placement of the sensors is the same in all specimens. However, the AE parameters differ systematically based on the width of the plates, as seen in Fig. 2b and c. The AE frequency collected by narrow beams is consistently higher reaching approximately 250 kHz, while the plate showed the lowest value being below 200 kHz. Inversely, the large plate exhibited the longest rise time while the narrow beam the lowest. This evidently shows the effect of geometry on the received AE signals. In narrow beams the propagation is essentially one dimensional, as the wave does not spread contributing to high frequency and higher amplitude. On the other hand, in plates, the wave spreads in two dimensions, is attenuated and is reflected only after propagating further when it impinges on the specimen sides. This contributes to longer signals (hence longer rise time) and lower frequencies.

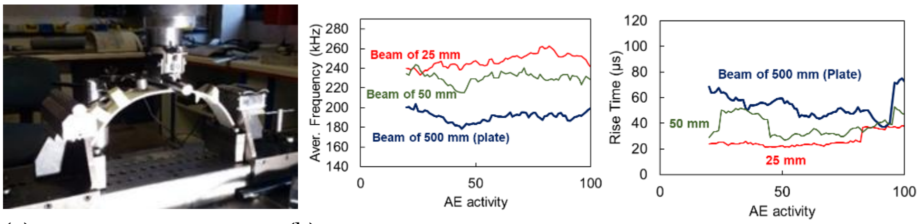

(a) (b) (c)

Figure 2. (a) Experimental setup of three-point bending with AE sensors (stabilized by tape) on the TRC plate, (b) average frequency and (c) rise time of the first 100 AE signals, attributed to matrix cracking.

3. CONCLUSIONS

The results demonstrate that caution should be exercised when results from laboratory scale beams are projected to large dimensions. Alternatively, the experiments should be conducted directly in realistic size plates. A frequency downshift of 20 kHz or a rise time increase of 20 μs, would normally be interpreted as shift from tensile matrix cracking to shear. However, these changes may be induced only by differences in geometry and thus, AE characteristics associated with matrix crack in beams could be easily mistaken for shear in plates even though the actual mechanism is the same. Future work should involve a methodology to correct for the differences or at least establish a distance within which the characterization is reliable.

REFERENCES

[1] GROSSE C.U., OHTSU M. (2008) "*Acoustic emission testing*", GROSSE C.U., OHTSU M. ed. Springer, Berlin, Heidelberg Berlin Heidelberg. doi:10.1007/978-3-540-69972-9.
[2] OSPITIA N., AGGELIS D.G., TSANGOURI E. (2020) Dimension effects on the acoustic behavior of TRC plates. Materials 13:955. doi:10.3390/ma13040955.

LONG-TERM PERFORMANCE OF NATURAL FABRICS IN INORGANIC MATRIX THIN COMPOSITE SYSTEMS

Cesare Signorini[1], Valentina Volpini[2], Andrea Nobili[1,2]

[1] Research Centre CRICT, Department of Engineering "Enzo Ferrari", University of Modena and Reggio Emilia, via P. Vivarelli 10 – 41125 Modena (Italy)

[2] Research Centre En&Tech, Department of Sciences and Methods for Engineering, University of Modena and Reggio Emilia, via G. Amendola 2 – 42122 Reggio Emilia (Italy)

SUMMARY: Natural fibres represent the new frontier towards a sustainable conceptualisation of building materials, with particular emphasis on thin composite systems adopted as high strength reinforcing techniques for valuable masonry structures. In this paper, we analyse the efficiency of several strengthening solutions based on a lime-based inorganic matrix acting as embedding medium for basalt (B) and flax (F) textiles. Spotlight is set on the tensile behaviour of textile-reinforced mortar (TRM) sandwich composites after accelerated ageing cycles. The bearing capacity and the ductility of B-TRM and F-TRM are evaluated by uni-axial tensile tests on 1-ply laminates, manufactured and tested according to the most recent guidelines. The acceptance criteria for design purposes are also addressed, with particular focus on alkaline environment exposure, typical of inorganic embedding matrices.

KEY WORDS: Basalt, Flax, Natural fibres, Textile-reinforced mortar, Mechanical response, Long-term performance.

1. INTRODUCTION

Textile-reinforced mortar (TRM) represents a category of versatile thin composite materials generally adopted as an effective and competitive externally bonded (EB) strengthening strategy for existing buildings [1]. Essentially, TRM are designed to exploit the outstanding mechanical performance of high tenacity multifilament fabrics or steel grids through an inorganic embedding matrix, the last acting as a linking medium able to transfer the external loads applied to the existing structure to the bearing textiles. The use of natural constituents is currently undertaking an increasing development, in order to pursue a more sustainable conceptualisation of TRM. In particular, the use of natural fibres is now object of interest of the research community. Several pioneering contributions can be found in the literature [2,3], in which basalt, flax, jute, sisal, and other kind of fibres are adopted as the reinforcing phase. The most critical issue regarding natural fibres is due to their durability within aggressive environments (namely strongly alkaline), which deeply affects the long-term performance of the composite system. Surprisingly, only a few studies are devoted to durability. The current Italian guidelines for the design of TRM [4] present a very simplified way to take into account the long-term performance losses as a consequence of ageing. Indeed, the so-called environmental conversion factors to be adopted at the design stage are gathered in Tab.3.1 of the CNR DT 215/2018 document, regardless of the fabric type. However, it is well-known that diverse textiles behave in deeply different manners [5,6]. To this aim, a comprehensive study has been recently published, considering several fabrics in a wide scenario of steel reinforced grout (SRG) and textile reinforced mortar (TRM) strengthening systems, among which basalt is considered [7]. In the present contribution, we present the assessment of basalt and flax TRM through uni-axial tensile tests. We find that natural fibres represent a feasible and sustainable reinforcing strategy in TRM, but some design limitations may occur in the presence of strengthening interventions.

2. EXPERIMENTAL ACTIVITY

2.1. Materials and methods

Mechanical tests are conducted on TRM coupons made of a commercially available pre-mixed mortar. Basalt fabrics are embedded in a cementitious fine-grained mortar, whereas flax textiles are accommodated in a hybrid (lime + cement) mortar. The reinforcing phases at hand consist in multifilament balanced biaxial or uniaxial woven textiles, made of different kinds of fibres. In particular, we consider a basalt multifilament textile and a flax biaxial woven fabric.

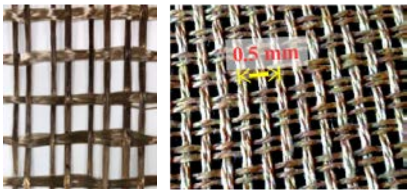

(a) (b)

Figure 1. *Basalt (a) and flax (b) biaxial fabrics*

1-ply coupons are manufactured on an individual basis and then subjected to uni-axial tensile tests according to the prescription given in the most recent guidelines [8]. The main operational steps are displayed in Fig.2.

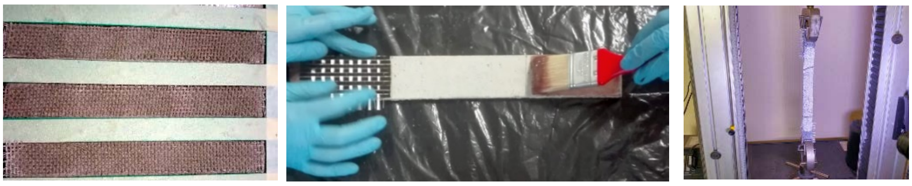

(a) (b) (c)

Figure 2. *Flax TRM specimens manufacturing (a-b) and testing (c).*

The gripping system consists in a rigid clamping on the coupons edges, duly equipped with a G-FRP tab. Uni-axial tensile tests are performed at a controlled displacement rate of 0.5 mm/min [9]. Durability against accelerated ageing within an alkaline aggressive environment is also investigated, by immersing tensile coupons in an alkaline solution (NaOH, pH 10) for 1000 hours, before testing. For the sake of comparison, unexposed specimens are considered as the reference condition, and are left in air for 1000 hrs, after curing.

3. RESULTS

Figure 3 shows the mean strength curves obtained for basalt (a) and flax (b) TRM, alongside the respective peak values with the relevant standard deviation bands for comparative purposes.

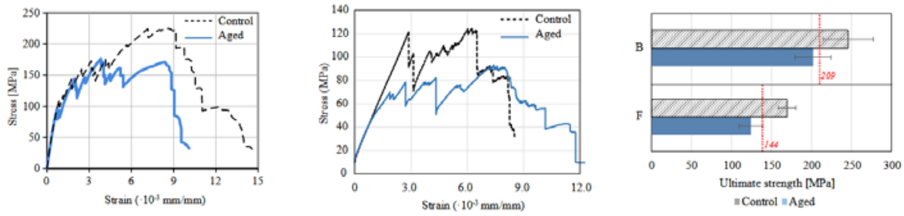

(a) basalt (b) flax (c) comparison

Figure 3. *Mean strength curves for basalt (a) and flax (b) TRM, alongside their mean strength values comparison (c)*

Experimental tests evidence that the mechanical performance of natural fibres in TRM is susceptible to aggressive environments, as far as alkaline exposure is concerned. Alkaline ageing is proven to impair the mechanical performance of basalt TRM composites, inducing a reduction of 18% and 28% in the ultimate strength and strain, respectively [7]. An even more significant detrimental effect is observed for flax TRM, which experienced a 26% loss in the bearing capacity for aged samples. Data scattering evaluated out of 5 specimens for each group is well aligned with other similar experimental activities, standing in all the cases at hand under 15-20% for the ultimate strength values [5]. The reliability of the experimental campaign is therefore validated. As far as the failure modes are considered, the poor interphase adhesion induces the formation of a coarse crack pattern (see Fig.4), which promotes the diffusion of aggressive compounds within the composite system. Failure is hence attained at low stress values (with respect to the theoretical bearing capacity of the dry fabrics) by fabric pull-out. This failure mode is observed regardless of the exposure to aggressive environments, since it is triggered by the poor interphase bond established between the matrix and the fabric, which is usual and well-documented for TRM and other inorganic composite materials [10–13].

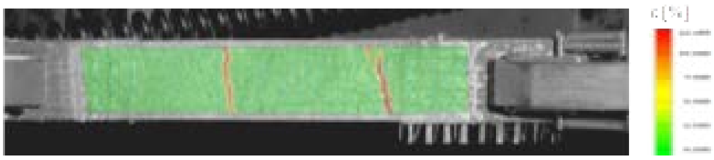

Figure 4. *Crack pattern highlighted by Digital Image Correlation (DIC) technique*

In this sense, the use of an appropriate surface coating, which enhances the affinity at the matrix-to-fabric interphase, may have the twofold advantage of protecting the fibres and improving the crack diffusion throughout the coupon during loading.

4. CONCLUSIONS

In this study, the long-term mechanical behaviour of flax biaxial fabrics embedded in a lime-based mortar is assessed through a series of comparative tensile tests on prismatic TRM coupons. A reduction higher than 15% is regarded as unacceptable for the recent prescriptions, and this threshold is overcome for both basalt and flax. For this reason, further investigations regarding the chemical and thermal stability are required to classify natural fibres as reliable reinforcing strategy for historic buildings, especially for those located in coastal areas or in conditions of high environmental pollution. In addition, adequate preparatory treatments (such as coatings with polymeric films) are advocated to protect the fibres against the attack of aggressive environmental agents.

5. REFERENCES

[1] L.N. Koutas, Z. Tetta, D.A. Bournas, T.C. Triantafillou, Strengthening of Concrete Structures with Textile Reinforced Mortars: State-of-the-Art Review, J. Compos. Constr. 23 (2019) 3118001. https://doi.org/10.1061/(ASCE)CC.1943-5614.0000882.

[2] N. Trochoutsou, M. Di Benedetti, K. Pilakoutas, M. Guadagnini, Mechanical Characterisation of Flax and Jute Textile-Reinforced Mortars, Constr. Build. Mater. 271 (2020) 121564. https://doi.org/10.1016/j.conbuildmat.2020.121564.

[3] D.A.S. Rambo, F. de Andrade Silva, R.D. Toledo Filho, O. da F.M. Gomes, Effect of elevated temperatures on the mechanical behavior of basalt textile reinforced refractory concrete, Mater Des. 65 (2015) 24–33.

[4] CNR DT215, Guide for the Design and Construction of Externally Bonded Fibre Reinforced Inorganic Matrix Systems for Strengthening Existing Structures, 2018.

[5] F. Micelli, M.A. Aiello, Residual tensile strength of dry and impregnated reinforcement fibres after exposure to alkaline environments, Compos. Part B Eng. 159 (2017) 490–501. https://doi.org/10.1016/j.compositesb.2017.03.005.

[6] J. Donnini, Durability of glass FRCM systems: Effects of different environments on mechanical properties, Compos. Part B Eng. (2019) 107047.

[7] C. Signorini, A. Nobili, Comparing durability of steel reinforced grout (SRG) and textile reinforced mortar (TRM) for structural retrofitting, Mater. Struct. 54 (2021) 1–15. https://doi.org/10.1617/s11527-021-01729-3.

[8] ICC AC434, Acceptance criteria for masonry and concrete strengthening using fiber-reinforced cementitious matrix (FRCM) composite systems, 2013.

[9] A. Nobili, C. Signorini, On the effect of curing time and environmental exposure on impregnated Carbon Fabric Reinforced Cementitious Matrix (CFRCM) composite with design considerations, Compos. Part B Eng. 112 (2017) 300–313. https://doi.org/10.1016/j.compositesb.2016.12.022.

[10] Z. Cohen, A. Peled, Effect of nanofillers and production methods to control the interfacial characteristics of glass bundles in textile fabric cement-based composites, Compos. Part A Appl. Sci. Manuf. 43 (2012) 962–972. https://doi.org/10.1016/j.compositesa.2012.01.022.

[11] M. Messori, A. Nobili, C. Signorini, A. Sola, Mechanical performance of epoxy coated AR-Glass fabric Textile Reinforced Mortar: Influence of coating thickness and formulation, Compos. Part B Eng. 149 (2018) 135–143.

[12] C. Signorini, A. Nobili, Targeting functionalised carbon nanotubes at the interphase of Textile Reinforced Mortar (TRM) composites, Compos. Part A Appl. Sci. Manuf. 144 (2021) 106330. https://doi.org/10.1016/j.compositesa.2021.106330.

[13] C. Signorini, V. Volpini, Mechanical performance of fiber reinforced cement composites including fully-recycled plastic fibers, Fibers. 9 (2021) 1–15. https://doi.org/10.3390/fib9030016.

Session 5
Rehabilitation, Strengthening, Optimization

FRCM-RETROFITTING OF STEEL FIBER-REINFORCED CONCRETE SHALLOW BEAMS

Marco C. Rampini[1], Giulio Zani[2], Matteo Colombo[3], Marco di Prisco[4]

[1] *DICA Department, Politecnico di Milano, Piazza Leonardo da Vinci 32, Milano, marcocarlo.rampini@polimi.it*

[2,3,4] *DICA Department, Politecnico di Milano, Piazza Leonardo da Vinci 32, Milano.*

SUMMARY

In the last decades, there has been an increase of the use of the Steel Fiber-Reinforced Concrete (SFRC) material to realize floor slabs and shallow beams. The cast procedure plays a significant role in the effectiveness of the execution and due to the limited experience of the workmanship, it is important to clarify how to intervene in case of bearing capacity limitations due to a bad design or a bad execution. Fabric-Reinforced Cementitious Matrix (FRCM) composites represent an efficient solution to restore and to upgrade the load carrying capacity of these structural elements, thanks to their strain-hardening behavior and to the good compatibility with concrete substrates. In this paper, the effect of the FRCM retrofitting on a series of SFRC shallow beams previously damaged at the ultimate limit state was investigated. The experimental campaign also involved the characterization of the composite materials and of the bond properties at the mortar-to-substrate interface. The results and the comparison with a simplified theoretical prediction are presented and discussed.

KEY WORDS

Fabric-Reinforced Cementitious Matrix composites (FRCM)

Steel Fiber-Reinforced Concrete (SFRC)

Flexural retrofitting

Shallow beams

1. INTRODUCTION

In Italy, the recently promulgated Italian Standard allows the designer to use the Fabric-Reinforced Cementitious Matrix (FRCM) composites in the retrofitting and strengthening applications, providing a qualification procedure of the system formed by mortar and fabric.

FRCM composites seem to be a promising solution also for the retrofitting of damaged reinforced concrete structures, as they exploit a better compatibility with irregular surfaces and concrete substrates with respect to other reinforcing techniques (i.e. Fabric-Reinforced Polymers, FRP) [1]. Moreover, the FRCM solution, thanks to the possibility to be applied on quite extensive surfaces, seems to be suitable for application on shallow beam and 2D slabs.

In this paper, to assess the potential of this reinforcing solution, full-scale tests were performed on shallow beams previously damage under severe condition and then retrofitted with the application of a FRCM composite layer at the intrados. Two type of beams were investigated: the BF beams, realized in Steel Fiber-Reinforced Concrete (SFRC), and the BR ones, with a hybrid reinforcement consisting of both steel fibers and longitudinal bars (2Φ12mm). The FRCM system was composed by a cementitious thixotropic mortar and an Alkali-Resistant glass fabric.

It the end, a preliminary simplified approach to estimate the ultimate capacity of the FRCM-retrofitted beams is presented, underlining advantages and critical issues.

2. MATERIALS CHARACTERIZATION

2.1 Steel Fiber-Reinforced Concrete (SFRC)

The cast material of all the shallow beams is a self-compacting SFRC, realized with an amount of 35 kg/m^3 of double hooked-end steel fibers (length 60 mm, diameter 0.9 mm, aspect ratio of 65) and characterized by mean cylindrical compressive strength of 58.0 MPa, and 3c class evaluated on 12 beams according to EN 14651, tested at 34 days. The identified multilinear constitutive laws in tension (average ‘’m’’ and characteristic ‘’k’’) are defined according to the MC2010 provisions [2] in the range 167-220 days from the casting (in parallel to the full-scale pre-damage tests). The pre-peak stress-strain and the post-peak stress-crack opening curves are reported in Figure 1a, and the complete stress-strain law, computed choosing the depth of the beams section as characteristic length, is depicted in Figure 1b. The mix design and the characterization are shown in [3].

2.2 Longitudinal steel bars

Four identical B450C grade Φ12mm steel bars were tested under direct tension. The average yield and ultimate strength are respectively 527 MPa and 647 MPa and the recorded mean ultimate strain is equal to 16%. The nominal stress-strain curves of each test are reported in Figure 2.

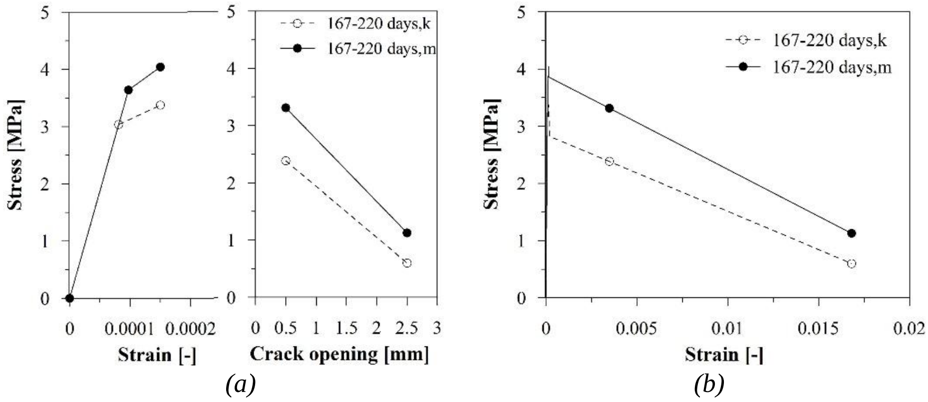

Figure 1. *SFRC constitutive law: experimental identification at different ages (a) and stress-strain curves computed considering l_{cs}=150 mm (b).*

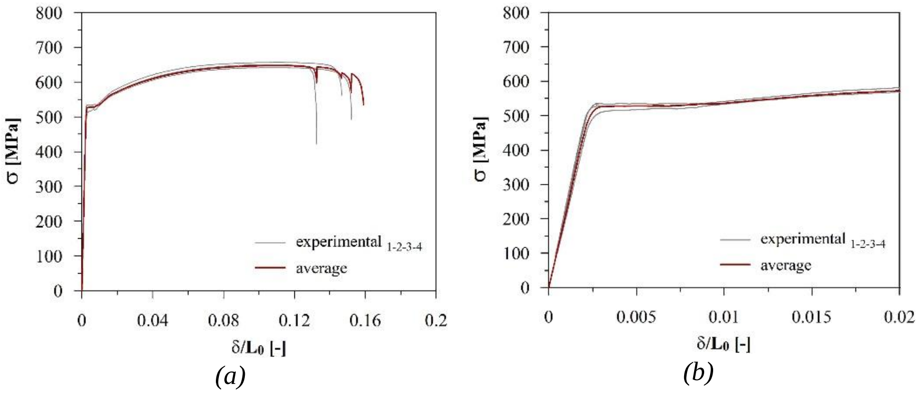

Figure 2. Experimentall*y obtained tensile constitutive law of the longitudinal steel bars (a) and detail of the elastic branch (b).*

2.3 Fabric-Reinforced Cementitious Matrix (FRCM) composite

The chosen FRCM system is made by a shrinkage-compensated thixotropic cementitious mortar characterized by an average cubic compressive strength of 58.9 MPa and a flexural tensile strength of 7.0 MPa and an AR-glass double leno weave fabric, the characteristics of which are reported in Table 1.

The maximum average load of the AR-glass fabric was evaluated on five uniaxial tests for each direction, according with the ISO 4606 procedure [4]. The efficiency parameter, EF_f, evaluated as proposed by Rampini et al. in [5] provides an information on the rate of utilization of the material.

Table 1. *Alkali-Resistant glass fabric characteristics. (*average on 4 specimens)*

Characteristic		Warp	Weft
Wire spacing	mm	38	38
Roving fineness	Tex	2 x 2400	4 x 2400
Filament diameter	μm	27	27
Equivalent thickness	mm	0.093	0.093
Maximum load	kN	12.50*	11.70
Fabric Efficiency (EF_f)	-	0.87	0.82

The FRCM composite was characterized in tension, testing three nominally identical specimens for each direction (70 × 400 × 9 mm^3 in size), imposing a constant stroke rate of 0.02 mm/s. In Figure 3, the experimental composite stress-normalized displacement curves are reported. Please note that, when one of the specimen curves is lost, the average is still evaluated among the remaining specimens.

The composite efficiency parameters, EF_{FRCM}, were computed dividing the average maximum load reached by the composites, 9.13 kN and 7.00 kN respectively for the warp and the weft direction, by the ones of the plain fabrics and they result 0.73 and 0.60. A higher value of efficiency can be generally reached testing composite with a larger anchorage length and with more than two wires within the section, allowing the stress redistribution and reducing the effect of possible misalignments.

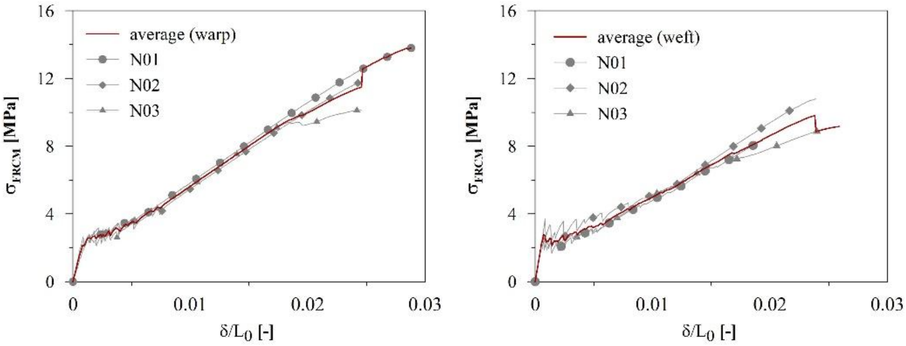

(a) *(b)*

Figure 3. *Average tensile response of the FRCM composite system in the warp (a) and the weft direction (b) in terms of composite stress vs. normalized displacement.*

3. INTERFACE PROPERTIES CHARACTERIZATION BY MEANS OF SINGLE LAP SHEAR TESTS

With the aim to characterize the bond-slip behavior at the composite-to-mortar interface, three Single-Lap (SL) shear tests were performed. The test specimens (70 × 200 × 9 mm^3) and the setup apparatus are depicted in Figure 4a. The composite strips, with the fabric in the warp direction, were cast on blocks produced with the same SFRC material of the beams, after the hydro-scarification of the substrate with a water pressure of 1800 atm. Tests were conducted under displacement control at a stroke rate of 0.01 mm/s and two Linear Variable Displacement Transducers (LVDT) were placed to measure the slippage, δ_{slip}, between the mortar and the concrete substrate.

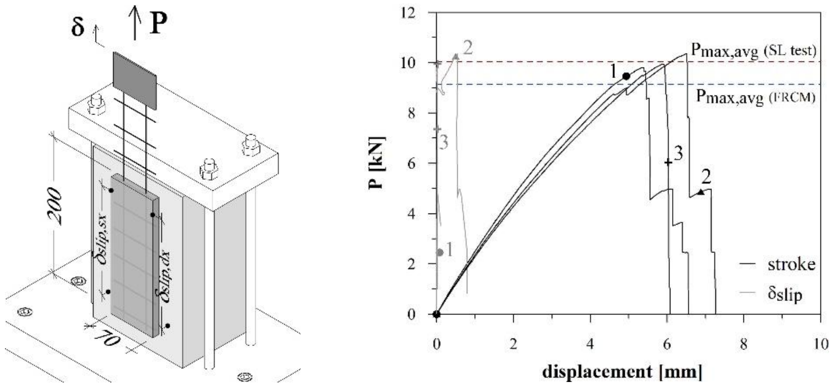

Figure 4. Setup of the Single-Lap shear tests (a) and results of the three experiments in terms of load vs stroke and load vs slip curves (b).

In Figure 4b, both the load-stroke and the load-slip curves are reported. It is possible to note that the fabric rupture occurred at the end of each test and the slippage between the mortar and the substrate are negligible. Thanks to the adequate machining option, which provides a sufficient substrate roughness improving the mechanical adhesion at the interface level, the average maximum load reached in the shear tests, 10.04 kN, results higher than the FRCM tensile capacity, 9.13 kN in the investigated warp direction.

In the design of the retrofitting intervention the full tensile capacity of the FRCM composite can be used, in according with the qualification procedure proposed by the Italian Guidelines [6]. A more detailed study on the effect of the substrate roughness on the FRCM performance efficiency is reported in [7].

4. FULL-SCALE TEST ON RETROFITTED SHALLOW BEAMS

4.1 Test setup and application of the reinforcing FRCM layers

All the shallow beams (350 × 1450 × 150 mm^3) were preliminary damaged in four-point bending over a shear span of 1350 mm and a loading knife distance of 450 mm. The tests were displacement controlled at a stroke rate of 3 μm/s and six (3+3) LVDTs were placed at the intrados and at the extrados to measure the crack opening and the compression shortening, respectively. Two Potentiometer Displacement Transducer (PDT) were used to measure the mid-span deflection. The same setup (Figure 5) and procedure were used in the tests on the retrofitted beams.

The reinforcing layer at the intrados was 200 mm thick, 350 mm wide and 1200 mm long (Figure 5). The fabric was oriented with the warp parallel to the longitudinal direction (9 warp yarns). The preparation of the substrate was the same of the SL tests and the FRCM composite was applied following the typical hand lay-up technique.

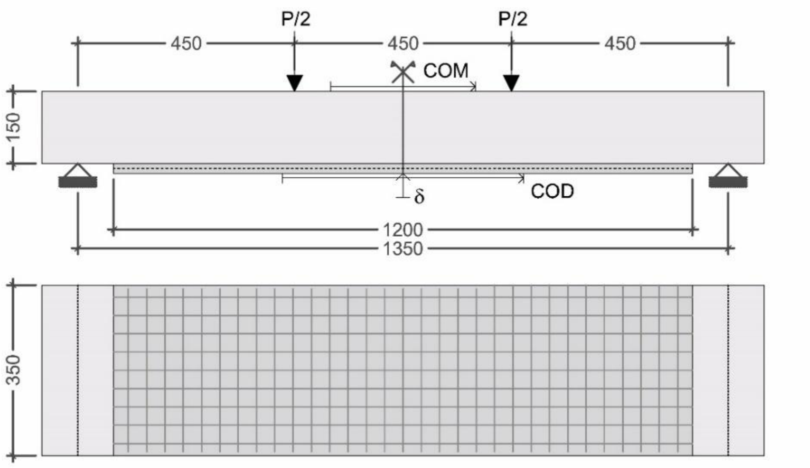

Figure 5. *Four-point bending test setup and representation of the FRCM application at the beam intrados.*

4.2 Retrofitted SFRC beams test responses

In Figure 6, the comparison between the pre-damaged and the retrofitted BF beams responses is reported. The maximum capacity of the retrofitted beams corresponds to 39.69 kN, with an increase of around 28% with respect to the previous maximum, 31.05 kN, and equal to three times the residual load, 11.53 kN. At the end of all the tests the fabric rupture occurred and no mortar detachment was visible, as confirmed by the direct ultrasonic wave velocity measurement reported in Figure 7 (time of flight from intrados to extrados) with the crack patterns.

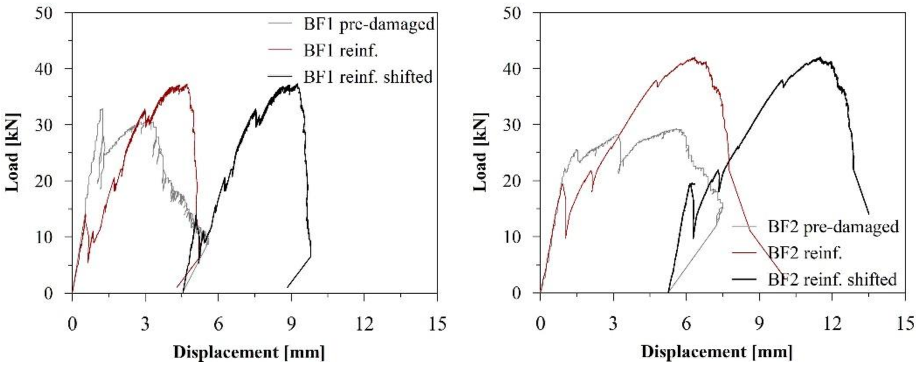

(a) *(b)*

Figure 6. Load vs. mid-deflection curves of the BF1 (a) and BF2 (b) beams.

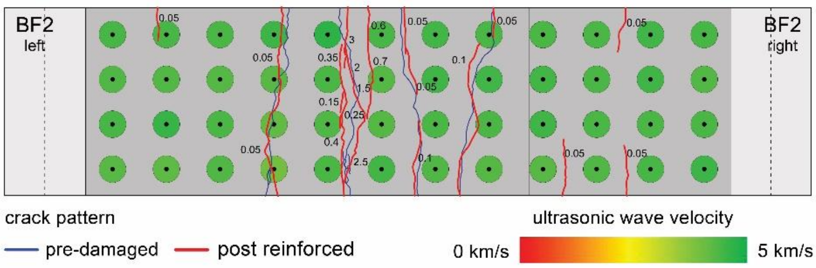

Figure 7. *Crack patterns at the end of the pre-damage and post-reinforced tests and ultrasonic wave velocity contour plot of the BF2 beam.*

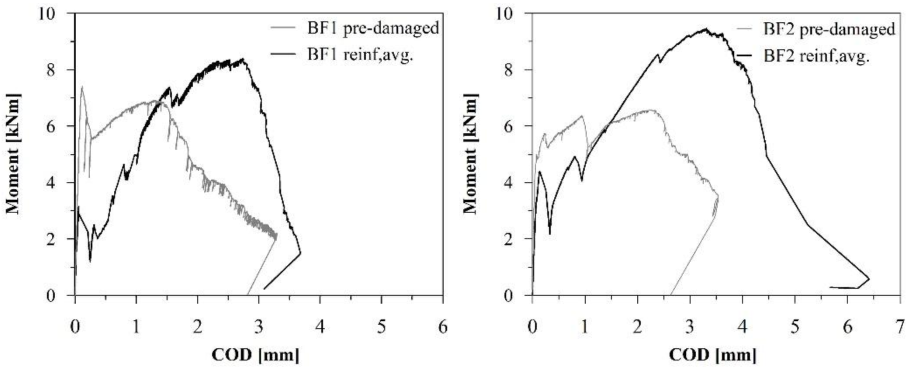

(a) *(b)*

Figure 8. Moment vs. COD curves of the BF1 (a) and BF2 (b) beams.

Moreover, the FRCM addition provided a recovery of the initial stiffness (see shifted curves) and it offered a control of the crack openings, as visible in Figure 8. The COD values recorded at the retrofitted beams intrados at a load corresponding to the maximum capacity of the integer SFRC beams were lower than the ones at the end of the pre-damage tests (around 1.5 mm compared to more than 3 mm in both the beams).

4.3 Retrofitted hybrid beams test responses

The average ultimate load reached by the retrofitted BR beams was equal to 108.97 kN, corresponding to an increase of 14% and 35% with respect to the average maximum and residual loads recorded in the pre-damage tests (95.19 kN and 80.99 kN respectively). It is possible to appreciate the recovery of the initial stiffness in the first part of the BR1 response curve (shifted curve in Figure 9a). In BR2 case, the beginning of the response was influenced by a compression damage under one of the loading knives, which causes the initial and well visible non-linearity (Figure 9b). Please note that pre-damage tests were arbitrarily stopped.

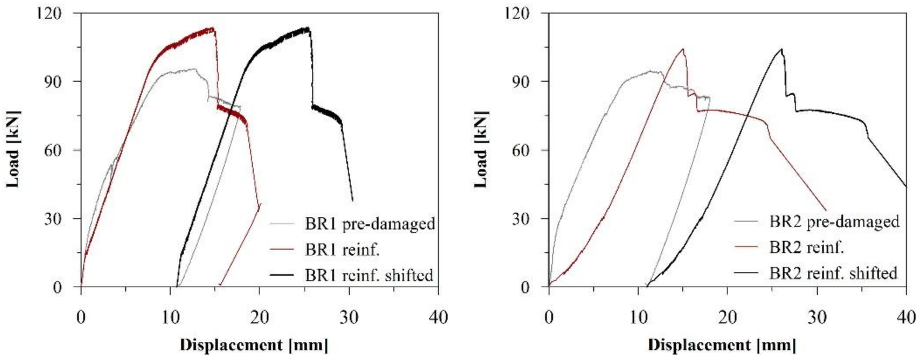

Figure 9. *Load vs. mid-deflection curves of the BR1 (a) and BR2 (b) beams.*

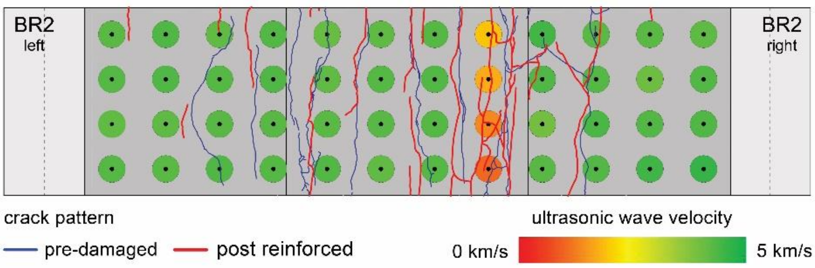

Figure 10. *Crack patterns at the end of the pre-damage and post-reinforced tests and ultrasonic wave velocity contour plot of the BR2 beam.*

At the reaching of the peak, the failure was caused by both the fabric and the steel bar rupture. In correspondence of the failure position a reduction of the ultrasonic wave velocity was recorded (Figure 10), representing a concentration of the local damage. Moreover, focusing on the crack pattern, it is possible to notice that the crack pattern on the FRCM layer was strongly influenced by the previous crack distribution.

5. SIMPLIFIED ESTIMATION OF RETROFITTED BEAMS CAPACITIES

To obtain a prediction of the ultimate capacity of the investigated retrofitted shallow beams and to provide a simple tool to design the reinforcing intervention, the simplified procedure described in the following is performed. The computation aims to evaluate the amount of the sustained bending moment, *ΔM*, related to the addition of the FRCM layer at the intrados. The basic assumptions are: i) the FRCM composite fully exploits its maximum capacity; ii) the internal lever arm is considered equal to 0.9 times the distance of the fabric from the compressed extrados; and iii) the additional moment is added to the residual one, $M_{residual}$, to obtain the retrofitting ultimate capacity.

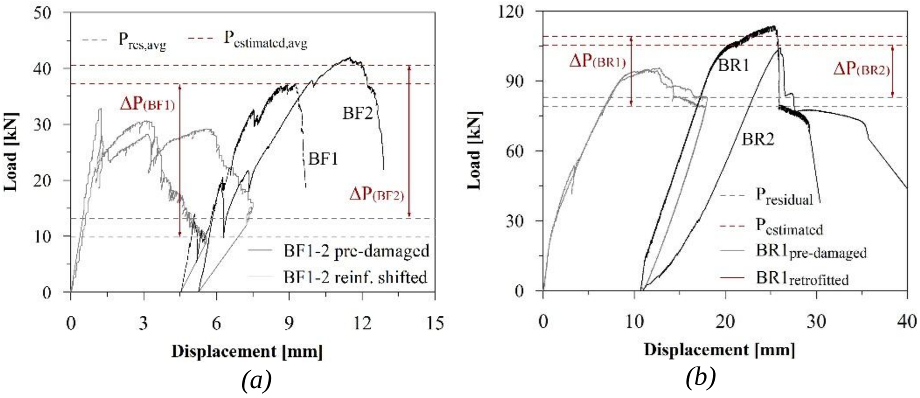

Figure 2. *Simplified analytical estimation of the maximum capacity after the application of the FRCM reinforcing layer for the BF (a) and the BR (b) beams.*

In Figure 11, the results of this simplified procedure are reported. The estimated loads are 36.11 kN and 41.93 kN for the BF1 and BF2 beam, and 105.42 kN and 109.15 kN for the BR1 and BR2 beams. The committed errors result in the 1%-5% range for both the shallow beam types, confirming the good level of approximation of this simplified approach.

6. CONCLUSIONS

Based on the experimental and analytical results already presented, it is possible to draw some conclusions: 1) an adequate substrate machining guarantees the fully exploitation of the FRCM capacity in the retrofitting intervention; 2) the FRCM reinforcing technique seems to provide a recovery of both the ultimate capacity and the initial stiffness of the integer beams up to the cracking of the FRCM layer; 3) the composite layer acts stabilizing the residual behavior of the damaged beams and controlling the crack evolution; and 4) the simplified approach presented could be an effective preliminary tool in the design of the retrofitting intervention on shallow beams.

The authors would like to acknowledge Gavazzi Tessuti Spa and MBS Italia Spa. The research is financially supported by RELUIS WP14 – 2019/2021.

7. REFERENCES

[1] De Santis S. and De Felice G., "Tensile behaviour of mortar-based composites for externally bonded reinforcement systems" *Compos. Part B Eng.*, vol. 68, pp. 401–413, 2015.

[2] CEB-FIP, *Model Code 2010 - Volume 1*. 2010.

[3] di Prisco M., Colombo M., and Pourzarabi A., "Biaxial bending of SFRC slabs: Is conventional reinforcement necessary?" *Mater. Struct. Constr.*, vol. 52, no. 1, pp. 1–15, 2019.

[4] I. 4606, "Textile Glass—Woven Fabric—Determination of Tensile Breaking Force and Elongation at Break by the Strip Method" Geneva, Switzerland, 1995.

[5] Rampini M. C., Zani G., Colombo M., and di Prisco M., "Mechanical Behaviour of TRC Composites: Experimental and Analytical Approaches" *Appl. Sci.*, vol. 9, no. 7, p. 1492, 2019.

[6] Consiglio Superiore dei LL. PP., "Linea Guida per la identificazione, la qualificazione ed il controllo di accettazione di compositi fibrorinforzati a matrice inorganica (FRCM) da utilizzarsi per il consolidamento strutturale di costruzioni esistenti.", 2018.

[7] Rampini M. C., Zani G., Colombo M., and di Prisco M., "The role of concrete substrate roughness on externally bonded Fabric-Reinforced Cementitious Matrix (FRCM) layers," *First Fib Italy YMG Symp. Concr. Concr. Struct.*, pp. 56–63, 2020.

STRENGTHENING STEEL CONCRETE BEAM WITH TEXTILE REINFORCED CEMENT: DESIGN METHOD AND APPLICATION TO UNIDIRECTIONAL HYBRID CARBON-BASALT GEOPOLYMER COMPOSITE

P. Hamelin[1], Z. Mesticou[2], N. Algourdin[2], G. Cai[2], A. Si Larbi[2],

[1]*I2C Ingénierie Composite Construction consultant, 188 Chemin de la Maby, 69250 Poleymieux au Mont d'or*

[2] *Univ. Lyon, Ecole Nationale d'Ingénieurs de Saint-Etienne (ENISE), Laboratoire de Tribologie et de Dynamique des Systèmes (LTDS), UMR 5513, 58 rue Jean Parot, 42023 Saint-Etienne Cedex 2, France*

SUMMARY:

The aim of the current study is the substitution of FRP fiber reinforcement polymer by TRC textile reinforced cement for strengthening existing steel concrete structure. The choice is justified by the fact to minimize the carbon footprint of the process and improve the thermo-mechanical behaviour (fire stability) of the composite.

First, mechanical data based on experimental tests, especially for geopolymer unidirectional carbon-basalt composite, is presented. Second, different calculation steps, necessary for checking resistance and durability at ultimate limit state and serviceability state, for steel concrete beam reinforcement is explained.

KEY WORDS*: Rehabilitation, repairing, composite, geopolymer, structure design.*

1. INTRODUCTION

Rehabilitation, maintenance of existing infrastructures is a real and important stake for civil engineers. Particularly in the case of steel concrete structures, it is necessary to reinforce, to repair structural elements such as beam or column which present specific pathologies induced by corrosion and aging or by modification of loading conditions (serviceability and accidental). During these last thirty years, many building and infrastructures (bridges, tunnels…) have been strengthened using FRP (fiber reinforced polymer). Nowadays, recommendations such as ACI 44 [1], JCI [2], EUROCODE [3] and f.i.b. model code [4] clearly explain the conditions of application and the design methods for these composite reinforcements. The analysis of the technical limits for these construction process [5] corresponds to different critical points:

– Considering sustainable development criteria, the use of polymer produced form petroleum industry increases the carbon foot-print level. On another hand, considering hygiene and safety of workers or end users, the European recommendations REACH [6] is not favorable to the use of epoxy resin in construction.
– On a technical and performancial point of view, the thermo-mechanical behavior of FRP is not satisfying. The maximum temperature for construction is limited to 60°C – 80°C [7]. It can also be highlighted the low efficiency ratio for the use of high-performance composite limited by shear resistance of interface substrate (concrete). Finally, even if the ultimate resistance of FRP is significantly important for ULS checking, the serviceability conditions which consider "crack opening verification" is not clearly justified with FRP reinforcement.

Consequently, considering recent research works developed by HEGGER [8], NAAMAN [9], MOBASCHER and al [10], the FRP is replaced by TRC (textile reinforced cement and concrete) for strengthening steel concrete beams [11]. Specifically, the current study will consider geopolymer binder combined with unidirectional carbon basalt fibers for reinforcements at high temperature (fire conditions).

2. TEXTILE REINFORCED CEMENT CHARACTERIZATION

2.1. TRC formulations studied

2.1.1 Mineral matrix

The geopolymer formulation is defined by Table 1. Experimental tests are performed following the standard methods proposed for mortars, which allow to evaluate (Table 2) the main mechanical characteristics of the mineral matrix.

Table 1. *GPHS formulations and physical properties*

Metakaolin	69 % SiO_2 21 % Al_2O_3
Alkaline solution	45 % (SiO_2/K_2O) "mixture" 55 % H_2O
Density	1.87
Grain size d_{50}	75 µm

Table 2. *Mechanical performances of GPHS*

GPHS	7 days	28 days
Compressive strength	55-60 MPa	70-80 MPa
Tensile strength	1.2-1.5 MPa	5-6 MPa
Ultimate strain in tension	0.06-0.08 %	0.1-0.15 %
Young modulus	9500 MPa	12000 MPa

2.1.2 *Textile reinforcement*

A hybrid unidirectional textile is considered combining approximately the same quantity of carbon fibers and basalt fibers, as defined in Table 3 and 4.

Table 3. *Carbon and basalt fibers characteristics*

Textile fibers	Carbon TORAY T700S	BCF Basaltex 19 - 1200
Density (g/cm3)	1.8	2.67
Sizing type	Epoxy	Silane
Filament diameter (µm)	7	19
Yarn count of roving (Tex)	12000	1500
Tensile strength (MPa)	4900	2900
Young's modulus (GPa)	230	87-90
Tensile strain (%)	2.1	3
Temperature stability (°C)	300	550-1200

Table 4. *Unidirectional textile reinforcement (UDCB200)*

Reference		UDCB200
Weight of strip (g/m^2)		200
Width of strip (mm)		100
Thickness of yarn (mm)		0.5
Number of yarn per 100 mm	Carbone	10
	Basalt	10
Theoretical yarn area (m^2)	Carbone	4.616 10^{-7}
	Basalt	4.251 10^{-7}
Spacing between yarn (mm)		2
Predicted equivalent young modulus (MPa)		150 000
Predicted average tensile stress (MPa)		2 700

The mix of two fibre types is justified by an optimization between tensile resistance, tensile stiffness, adhesion with mineral matrix and economic conditions, specific to construction

2.2. Working method for TRC

Composites TRC plates (Table 5) are molded with two different and complementary methods: The first working process considers usual hand lay-up approach (Figure 1). In the second case, after impregnation, the composite is submitted to additional external pressure (vacuum bag) (Figure 2) which minimize porosity and favor matrix penetration inside the yarns.

Table 5. *Main characteristics of TRC*

Working process	Stacking Sequence	Thickness	Density (Kg/m^3)	Volume percentage of textile
Hand lay-up technic	1 mat/1 UD/1mat	3.5 -3.9 mm	1.38	2.1 - 2.5 %
Vacuum pressure	1 mat/1 UD/1mat	1.8 - 2 mm	1.5	4.5 - 4.7 %

To try to increase the shear resistance of the mineral matrix, a low percentage of chopped alkali-resistant glass fiber is introduced with a ratio of (1.5 % in volume) as proposed by Shgeyuki Akhihama and al [12]. To increase the interface adhesion between textile yarns and geopolymer, a specific sizing product (ZP1) is developed in the current experimental work. It combines aqueous organic binder and micro silica powder [13].

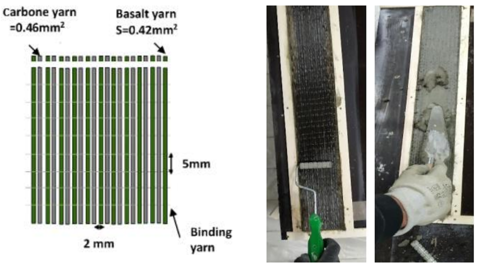

Figure 1. *Textile hybrid and hand lay-up process*

Figure 2. *Vacuum bagging process for TRC and composite plate for test*

2.3. *Behavior law and experimental data for design*

2.3.1 Tensile behavior law

As for FRP, it is necessary to identify the behavior law in tension of the TRC. The considered experimental method is clearly defined by the technical committee TC 232 [14].

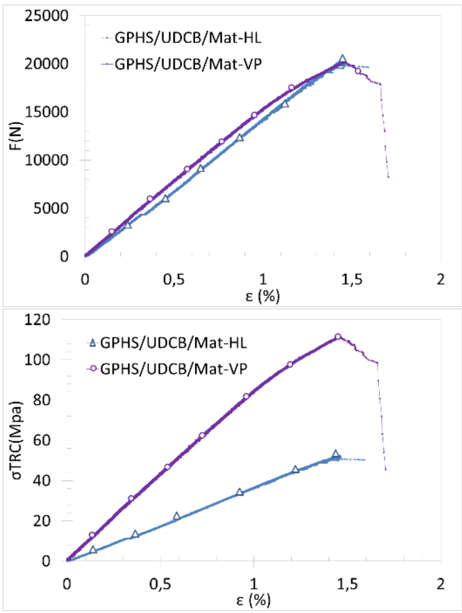

Figure 3. *Tensile behavior law of TRC*

Table 6. *Mechanical data for design*

	Vacuum pressure process	hand lay up process
Ultimate stress $f_{f_{TRC,uk}}$(MPa)	~110	~ 51
$f_{f,u,k}$ average ultimate stress in textile (MPa)	~2400	~ 2400
Ultimate strain % $\varepsilon_{f_{TRC,u}} = \varepsilon_{f,u,k}$	~1.5	~1.5
E_{TRC} Young modulus (MPa)	~ 25000	~ 3300
E_f Young modulus equivalent textile (GPa)	~150	~150

The Figure 3 and Table 6 give the main data which are necessary to consider for strengthening design. As the failure mode is essentially controlled by anchorage conditions and internal delamination or telescopic slipping effect of textile fibers in mineral matrix [15], it is considered, in this study, a notion of average stress in tension $f_{f,TRC}$ for the whole TRC cross section and a specific stress value f_f where the maximum force F_{TRC} is divided by the effective cross section of textile fibers A_f.

Indeed, ZP1's surface treatment leads to modify and improve the adhesion between geopolymer and textile reinforcement. The ultimate behavior between the two manufacturing process is quite the same. The main difference concerns the thickness of the composite which modifies the evaluation of tensile stress and young modulus.

2.3.2 Additional tests: image correlation analysis

Particularly for service ability conditions design, it is necessary to check crack initiation and crack opening size in function of tensile stress level of TRC. Experimentally, optical measurement method (image correlation technique) is applied developed by A. SILARBI and al. [17] which gives the variation of average crack opening size as the function of stress level (Figure 4).

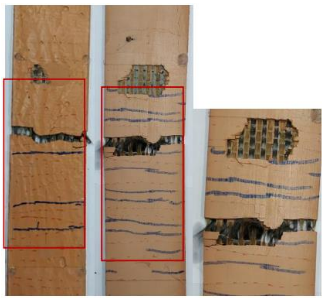

Figure 4. *Crack opening size as the function of tensile stress*

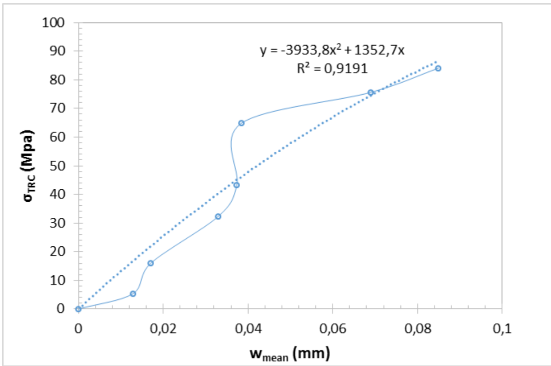

Figure 5. *Crack opening size as the function of tensile stress*

The last characteristics, which are important for design, concern the critical stress of geopolymer adhesion on concrete substrate (τ_{adh} or ν_{adh}) and the inter-laminar shear stress (τ_{inter} or ν_{inter}). These data can be obtained by pull off adhesion test as defined by standards [18] or by specific tensile-shear test as proposed by AFGC recommendation [19] (Figures 5 and 6).

The Table 7 summarizes the main results obtained for geopolymer TRC.

Table 7. *Critical shear resistance for design (28 days)*

	$\nu_{adh,k}$	$\nu_{inter,k}$	$f_{f,u,t,k}$ for $l = 200$ mm	$f_{f,u,t,k}$ for $l = 500$ mm
TRC (hand lay up)	≥ 3.5MPa	∼0,9 MPa	≥ 51 MPa	~ 70 MPa
TRC (vacuum process)	≥ 3.8MPa	∼1.5 MPa	≥ 110 MPa	~ 150 MPa

Figure 5. *Experimental set up for tensile shear test on TRC [19]*

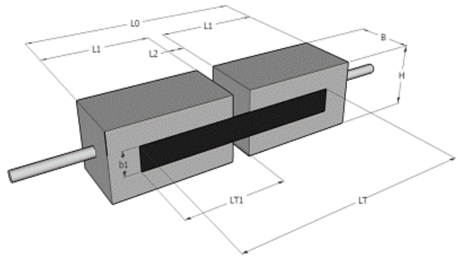

	L0	L2	L1	H	B	LT	LT1	b1
[mm]	560	40	260	140	140	440	200	50

Figure 6. *Standardized size of specimen (AFGC method) [19]*

2.4. *Synthesis of TRC characterization*

The tensile behavior law could be linear or nonlinear. The ultimate behavior is essentially controlled by fiber resistance. The load supported by textile is significantly affected by fiber-matrix inter-action which depends on workability conditions and impregnation factors. Experimental analysis allows also to underline that the load supported by fibers depend on experimental conditions (anchorage length in the clamp). In the Table 8, it is suggested to take into account the following specific ponderation factors:

Table 8. *Partial safety factors for design*

ULS	SLS
$f_{f,TRC,u,d} = \frac{F_{f,TRC,u,k}}{\gamma_{f\,TRC}}$ (1) $f_{f,t,u,d} = \frac{f_{f,t,u,k}}{\gamma_f}$ (2) with $\gamma_f = 1$	$f_{f,TRC,u,d} = \frac{F_{f,TRC,u,k}}{\gamma_{f\,TRC}}$ (3) $f_{f,t,u,d} = \frac{f_{f,t,u,k}}{\gamma_f}$ (4) with $\gamma_f = 2$

3. DESIGN METHOD FOR REINFORCEMENT OF STEEL CONCRETE BEAM BY TRC

3.1. General context and main assumptions

As for FRP, this study will consider existing design rules and durability criteria proposed by EUROCODE 2 recommendations. The additional experimental data which concern "material TRC" have been clearly established previously. For "structural behavior" the basic assumption of Navier-Bernouilli principle, the notion of perfect adherence between each material and displacement field continuity is retained for flexural behavior of beam. As shown by the Figure 7, the equilibrium of a steel concrete cross section reinforced by a TRC (A_f) is determined by two basic equations.

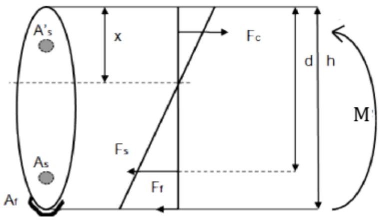

Internal equilibrium of forces:

$$F_{f_d} + F_{s,d} = F_{c,d} \quad (5)$$

External (M_E) and internal (M_R) equilibrium of moments:

$$M_{R_d} = \min\{M_{Rd,c};\ M_{Rd,s} + M_{Rd,s}\} \leq M_{E,d} \quad (6)$$

Figure 7. *Cross section of a beam, reinforced by TRC*

Where A_f is the real cross section of textile fiber at ultimate limit state and $A_{f\,TRC}$ is the global cross section of the TRC composite for serviceability limit state consideration.

3.2. Ultimate limit state approach

3.2.1 A_f cross section of textile fibers satisfying anchorage conditions

The condition of anchorage (L) on concrete for a TRC with a width b_f:

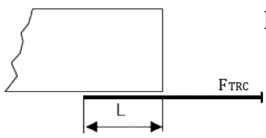

$$F_{max\,TRC,u} \leq L\,.\,b_f\,.\,\bar{\tau}_u = A_{f_{TRC}}\,.\,f_{f_{TRC,d}} = A_f\,.\,f_{f,u,d} \quad (7)$$

$$\text{with } \bar{\tau}_u = \min\{\nu_{adh,d};\ \tau_{i,inter}\} \quad (8)$$

$$\text{and } \nu_{adh,d} = \min(2{,}0\text{ MPa};\ \frac{f_{tk}}{2}) \quad (9)$$

Figure 8. *Anchorage zone*

Where f_{tk} is determined by pull off adhesion test and $\bar{\tau}_u$ is defined for each application. The value of $f_{f,u,d}$ is determined experimentally (Table 6) for the same conditions of anchorage applied on site (L = 200 mm or L = 500 mm).

Consequently, the cross section of textile fiber is determined by the following expression:

$$A_{f_1} \leq L\,.\,b_f\,.\,\bar{\tau}_u/f_{f,u,d} \quad (10)$$

3.2.2 A_f cross section of fibers satisfying U.L.S. resistance conditions

The internal bending moment M_{Rd} is equal to:

$$M_{Rd} = \min\{M_{Rd,c};\ M_{Rd,s} + M_{Rd,f}\} \quad (11)$$

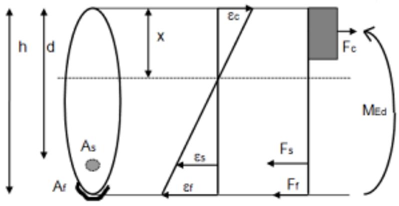

Figure 9. *Internal forces distribution*

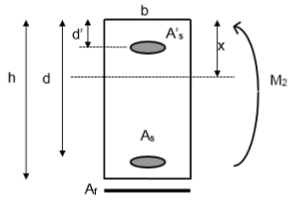

Figure 10. *Rectangular cross section*

The maximum bending moment for concrete is equal to:

$$\mathrm{M_{Rd,c}} = 0{,}8\mathrm{x} \,.\, \mathrm{f_{cd}} \,.\, \mathrm{b}(\mathrm{d} - 0{,}4\mathrm{x}) \qquad (12)$$

Case study 1: When steel rebars are over their yield point:

$\varepsilon_{\mathrm{s,u,d}}$ = ultimate strain of steel; $\varepsilon_{\mathrm{s_1}}$=steel rebar strain during TRC application

$\varepsilon_{\mathrm{f,u,d}}$ = ultimate strain of fiber in TRC

TRC deformation will be equal to:

$$\varepsilon_{\mathrm{f,d}} = \varepsilon_{\mathrm{TRC,d}} = \min\left\{1{,}1\left(\varepsilon_{\mathrm{s,u,d}} - \varepsilon_{\mathrm{s_1}}\right); \varepsilon_{\mathrm{f,u,d}}\right\} \qquad (13)$$

Bending moment is supported by steel rebars:

$$\mathrm{M_{Rd,s}} = \mathrm{A_s} \,.\, \mathrm{f_{y,d}} \,.\, \mathrm{z_s} \text{ with } \mathrm{z_s} \simeq 0{,}9 \qquad (14)$$

Bending moment is supported by textile fibers:

$$\mathrm{M_{Rd,f}} = \mathrm{A_f} \,.\, \mathrm{f_{f,d}} \,.\, \mathrm{z_f} \text{ with } \mathrm{z_f} \simeq \mathrm{d} \qquad (15)$$

$$\mathrm{f_{f,d}} = \min\left\{\mathrm{E}_f \,.\, \varepsilon_{\mathrm{f,d}}; \frac{\mathrm{F_{TRC,u,d}}}{\mathrm{A_f}}\right\} \qquad (16)$$

Case study 2: When the strain of steel rebars is at the yield point limit:

$$\varepsilon_{\mathrm{s,e,d}} = \varepsilon_{\mathrm{s,y,d}} \quad \text{and} \quad \varepsilon_{\mathrm{f,d}} \leq 1{,}1\left(\varepsilon_{\mathrm{s,y,d}} - \varepsilon_{\mathrm{s_1}}\right) \qquad (17)$$

$$\mathrm{M_{Rd,s}} = \mathrm{A_s} \,.\, \mathrm{f_{yd}} \,.\, \mathrm{z_s} \text{ with } \mathrm{z_s} \simeq 0{,}9\mathrm{d} \qquad (18)$$

$$\mathrm{M_{Rd,f}} = \mathrm{A_f} \,.\, \mathrm{f_{f,d}} \,.\, \mathrm{z_f} \text{ with } \mathrm{z_f} \simeq \mathrm{d} \qquad (19)$$

Case study 3: Steel rebars strain $< \varepsilon_{\mathrm{s,y,d}}$ and $\varepsilon_{\mathrm{s}} = \min\left\{\varepsilon_{\mathrm{s_0}} + 0{,}91\,\varepsilon_{\mathrm{fu,d}}; \frac{\mathrm{f_{yd}}}{\mathrm{E_s}}\right\}$

$$\mathrm{M_{Rd,s}} = \mathrm{A_s} \,.\, \mathrm{E_s} \,.\, \varepsilon_{\mathrm{s}} \,.\, \mathrm{z_s} \text{ with } \mathrm{z_s} = 0{,}91 \qquad (20)$$

$$\mathrm{M_{Rd,f}} = \mathrm{A_f} \,.\, \mathrm{f_{f,d}} . \mathrm{z_f} \text{ with } \mathrm{z_f} = \mathrm{d} \qquad (21)$$

Consequently, for a beam submitted to an external bending moment $\mathrm{M_{E,d}}$, the critical cross section of textile fibers $\mathrm{A_f}$ for ultimate resistance will be determined by the following equation:

$$\mathrm{A}_{f_2} = \frac{\left(\mathrm{M_{E,d}} - \mathrm{M_{Rds}}\right)}{\mathrm{f_{f,d}} \,.\, \mathrm{z_f}} \qquad (22)$$

Finally:

$$\mathrm{A_f} = \min\left\{\mathrm{A_{f_1}}, \mathrm{A}_{f_2}\right\} \qquad (23)$$

3.2.3 Serviceability limit state

Two cases of applications are distinguished as described by Figure 11 and 12.

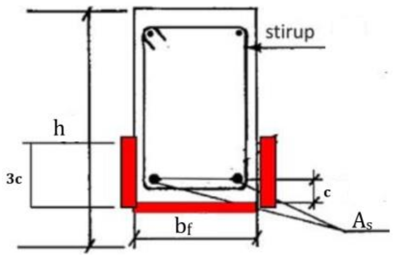

Figure 11. *Case a*

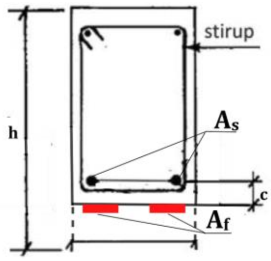

Figure 12. *Case b*

Case a: If the TRC composite is applied on the whole part of concrete in tension (case recommended by the authors), it could be considered that the protection of steel rebars is insured completely by TRC if the final crack opening size satisfied the conditions of EUROCODE 2. As the serviceability young modulus of TRC is smaller than concrete one and the tensile strain of TRC is more important than steel rebars, the steel rebars stress can reach the following level:

$$.\varepsilon_{s_{max}} = 0{,}8\, f_{yk}/E_s \tag{24}$$

The service stress $f_{f,d}$ for TRC for SLS will be determined from experimental curve (Figure 4) and finally:

$$f_{f,TRC,d} = \frac{f_{f,TRC,k}}{\gamma_s} \tag{25}$$

With $\gamma_s = 2$ for SLS conditions with $\varepsilon_{f,TRC,d} \leq 1{,}1 \, . \frac{0{,}8\, f_{yk}}{E_s}$

Finally, the maximum bending moment at serviceability state which can be carried by the strengthened steel concrete beam is equal to:

$$M_{e,d\,(SLS)} \leq A_s \, . \frac{0{,}8\, f_{yk}}{\gamma_s \, . E_s} \,(d - 0{,}3x) + A_f \, . f_{f,d} \, . (h - 0{,}3x) \tag{26}$$

Remark: As the TRC cross section is not especially important in comparison with steel concrete beam and the TRC young modulus is extremely low, the neutral position axis x at SLS is not really modified with or without reinforcement.

Case b: If we consider TRC composite plate bounded on the bottom face of the beam (Figure 12), the crack opening size is not perfectly controlled. For a first approach we will consider the steel strain ε_s under initial external bending moment supported by TRC application. If ε_{fTRC} is equal to ε_S, the moment supported by TRC will be defined as,

$$M_{TRC} \geq A_{TRC} \, . E_{TRC} \, . \varepsilon_S \, . (h - 0{,}3x) \tag{27}$$

4. CONCLUSION

The potentialities of textile reinforced cement are confirmed. Indeed, the mineral matrix prevents any composite ignition. Then, the thermal stability of geopolymer (> 600°C) combined with thermo-mechanical resistance of carbon fibers (> 300°C) and basalt fibers (> 500°C) is a real progress for high temperature reinforcements in comparison with FRP. The design method for strengthening steel concrete beam is governed at ULS by anchorage condition of TRC on concrete surface. The ultimate bending moment increasing is essentially controlled by fibers resistance which reaches a level of 2000 MPa. In the current study, it was confirmed that, for serviceability state, the best results for increasing the external bending moment are obtained when the whole part in tension of the beam is covered by TRC. In this case, repairing durability is controlled by composite crack opening which is for proposed formulations lower than the most unfavorable condition imposed by EUROCODE 2 recommendations. Further research developments will concern experimental tests on steel concrete beams reinforced by TRC and submitted to standard fire conditions.

5. REFERENCES

[1] American concrete institute: guide for the design and construction of externally bonded FRP systems for strengthening concrete structures. ACI Committee 440-2R; 2008

[2] Guidelines for structural design of FRP reinforced concrete building structures Japanese ministry of construction, July 1995

[3] EN 1992-1-1, 2004/AC, 2010-11, Eurocode 2, Design of concrete structures, European committee for standardization, 2011

[4] fib model code for concrete structures, "non metallic reinforcement", chap. 5.5, p.139-150, 2010

[5] HAMELIN P., MESTICOU Z., SI-LARBI A., "Design methods for strengthening underground steel concrete structures with high performance textile reinforced cement", *proceeding of ACCUS conference*, Hong Kong, China, November 2018

[6] REACH recommendations, European rule n° 1907/2006, 2014

[7] MAROUANI S., CURTIL L., HAMELIN P., "Composite realized by hand lay up process: initial properties and durability", Materials and structures, RILEM, vol. 41, issue 5, June 2008

[8] HEGGER J., "Textile reinforced concrete", *proceeding of the 1st international RILEM symposium PRO50*, RILEM publication, 2006

[9] NAAMAN A., "Ferrocement and thin reinforced cement composites: five decades of progress", *proceeding of 12th international symposium on ferrocement and thin composites*, Brazil, July 2018

[10] MOBASCHER B., "Modeling of cement based composite laminates", *proceeding ACI special publications*, SP-224, 2005

[11] HAMELIN P., MESTICOU Z., SI-LARBI A., « Thermo-mechanical characterization of textile reinforced concrete. Application to short concrete column strengthening submitted to fire conditions", *proceedings international conference SHCC4*, Dresden, Germany, September 2017

[12] SHIGEYUKI AKIHAMA and al, "Mechanical properties of carbon fiber reinforced cement composite and the application to buildings", KICT report n°65, October 1986

[13] HOJCZYK M. and al, "Cement in polymer dispersions as coating for roving and textiles", *proceeding RILEM PRO75*, p. 78-89, Aachen 2010

[14] Recommendations of RILEM TC 232-6TDT, "Test methods and design of textile reinforced concrete", *materials and structures*, May 2016

[15] LEPENIES L., RICHTER M., ZASTRAU B., "On the hierarchical materiel modelling of textile reinforced concrete", *proceeding of 1st international RILEM symposium PRO50*, Aachen, 2006

[16] SI-LARBI A., CONTAMINE R., HAMELIN P., « TRC and hybrid solution for repairing and for strengthening reinforced concrete beams", *engineering structures 45*, p. 12-20, 2012

[17] CONTAMINE R., SI-LARBI A., HAMELIN P., »Contribution to direct tensile textile of textile reinforced concrete", *materials science and engineering A528*, 2011

[18] ASTM C 1583 standard, "Test method for tensile strength of concrete"

[19] AFGC : association française de génie civil, « Réparation et renforcement des structures en béton au moyen des matériaux composites »

6. ACKNOWLEDGMENTS

This study has been founded by AUVERGNE-RHONE ALPES region within the frame work research program BOOSTER 2015 "AC2M2" in cooperation with ATG composites and ALCAM concept companies.

MODULAR SHELL STRUCTURES IN TEXTILE REINFORCED CONCRETE (TRC): A STRUCTURAL FEASIBILITY STUDY

Arnaud De Coster[1], Marie Hennemann[2], Lars De Laet[3], Tine Tysmans[4]

[1] A. De Coster (Department of Mechanics of Materials and Constructions (MeMC), Vrije Universiteit Brussel (VUB), Pleinlaan 2, 1050 Brussels, Belgium, arnaud.de.coster@vub.be)

[2] M. Henneman (Department of Mechanics of Materials and Constructions (MeMC), Vrije Universiteit Brussel (VUB), marie.hennemann@ulb.ac.be)

[3] L. De Laet (Department of Architectural Engineering (ARCH), Vrije Universiteit Brussel (VUB), lars.de.laet@vub.be)

[4] T. Tysmans (Department of Mechanics of Materials and Constructions (MeMC), Vrije Universiteit Brussel (VUB), tine.tysmans@vub.be)

SUMMARY:

Shell structures suffer from labor intensive fabrication techniques, characterized by extensive in situ formwork and falsework. Labelled by a prominent economic impact, combined with an environmental impact (e.g. single-use formworks made from EPS), these structures lost their initial value in industry. This research proposes a modular design method for the facilitated manufacturing of shell structures, using textile reinforced concrete (TRC) composites. The investigation is two-fold. The first part is a geometrical study, defining formwork modules with which several different shell configurations can be achieved. The form-finding process for the design of such configurations, will be briefly discussed. The second part is a structural study, in which the structural behavior of the modular shells is evaluated. Finite element simulations were performed on a study case, under its most determining load case, in order to evaluate the design result. The results demonstrate the structural feasibility of the modular shell design strategy.

KEY WORDS: *finite element, form finding, membrane stresses, Textile Reinforced Concrete (TRC), thin shell structures.*

1. INTRODUCTION

The structural efficiency of shell structures has always been of prime importance for architects and engineers. The optimal force flow within their structural layout, enables them to achieve impressive spans over single uninterrupted spaces. With a dominant membrane stress state as result, the building material is most efficiently used [1].

Unfortunately, concrete shell structures are frequently associated with two drawbacks. First, the existing fabrication techniques like timber molds are labor intensive and time consuming. Single-use formwork (e.g. EPS foam blocks) moreover goes hand in hand with an important environmental footprint, being not aligned with the current approach for circular construction. Secondly, steel reinforcement causes a non-structural additional thickness in the construction of concrete shells, due to the indispensable minimal cover against corrosion. Due to these practical reasons, freeform structures today have a considerable economic and environmental impact, which leads to a decrease in their application during the last decades [2].

Based on the previous issues, this research proposes a modular design method for the facilitated manufacturing of freeform structures in Textile Reinforced Concrete (TRC). The manufacturing process has been considered from the design stage on, by developing a range of different 'freeform' shapes from a limited number of curved shell geometries and thus from a limited set of formworks (see section 2.). Furthermore, TRC with non-corroding textile reinforcement, enhances its implementation in the efficient realization of shells, characterized by a small cross-sectional thickness [3].

Figure 1. *Example of timber formwork combined with extensive falsework (left) (https://architecturetoday.co.uk/bosjes-chapel/) and the robotic assembly carving of EPS foam blocks (right) (https://www.researchgate.net/profile/Brandon-Clifford), as fabrication techniques in concrete shell construction*

To assess the structural behavior of the modular shell designs, one modular configuration has been selected in this paper and structurally investigated under its most determining load case which combines self-weight, wind and snow, based on the Eurocode EN 1991-1-(3 and 4). Using finite element calculations (see section 3), the internal force patterns and corresponding in-plane principal stresses were predicted, by which the structural behavior of the shell was evaluated (see section 4).

Firstly, the analysis focused on the general behavior of the structure and secondly, further attention is spent on the structural design.

2. DESIGN METHOD

The form-finding and parametric modelling of the formwork modules took place in Grasshopper, a visual programming language and environment that operates within the Rhinoceros 6 3D computer-aided design (CAD) application. Kangaroo 1,2 plugins have been used for the form-finding of a synclastic triangular element, while Lunchbox and Weaverbird contain the geometrical tools to create the modular segments. Both Kangaroo 1 and 2 plugins are based on particle-spring systems. These systems have been used to find a shape composing axial forces under self-weight load, which could be tessellated along a plane [4].

The methodology is established on the form-finding of an equilateral triangular shape with three identical arched sides. The form-finding of this equilateral triangle started with the parametrization of a flat surface in the XY plane. This surface, with a side length of 8 m, has been converted to a mesh being discretized into triangular finite elements using the “Weaverbird’s split triangles subdivision” function. All vertices are defined as particles of the system, characterized by equal masses, being connected by massless springs to ensure the cohesion during the process. The last and most important parameter here, before performing the form finding, was the definition of the boundaries. Three identical arches having the same curvature, the same length, and the same height, were defined. During form-finding all side particles are attracted to these fixed arches, all acting as supports of the resulting synclastic shape, ensuring three identical module edges that could be linked to one another in different configurations afterwards. The mesh obtained in grasshopper will be the same as for the finite element model with a sizing control set to 1.00 [5].

To broaden the possible configurations, this form found triangle was subdivided into smaller synclastic modules, which can be assembled in more various ways. Based on an intersection with the planes of symmetry, a pair of modules is recognized and used as repeating set for other configurations. The synclastic triangular shape accompanied by three additional configurations are visualized in figure 2. These have been obtained after tessellation of the modules in the XY-plane with respectively three, ten, sixteen and eighteen pairs of modules from left to right.

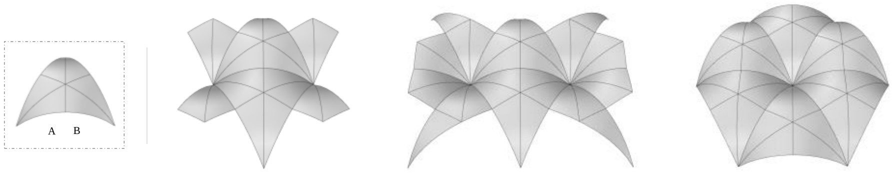

Figure 2. *Perspectives of the form found shape (left) and three other configurations, all assembled with one pair of repeating modules (A and B, left)*

3. FINITE ELEMENT MODEL

For this research, the synclastic triangular shape was selected and considered as study case for the structural feasibility study. To avoid some unrepresentative stress concentrations at the supports, one triangular element was removed at each ground connection to achieve a larger base of 0,46 m. These boundary conditions were assumed to be hinged, to limit the bending produced under loading in the shell and to promote the membranal actions. To provide sufficient free height, the shape has been rescaled to have a side span of 8 meters, as it was initially designed for. This led to a free height under the apex of 2.10 m. All dimensions are summarized in figure 3.

After identifying the surface as a monolithic conventional shell in the finite element software ABAQUS, additional parameters were implemented for the analysis such as the material properties and the load. A fictitious, linear, and homogeneous TRC material is assumed for this preliminary analysis. The experiments concerning this TRC material are led at the Department of 'Mechanics of Materials and Constructions' in Brussels (VUB), being in line with the recommendation stated by the RILEM TC 232-TDT [6] [7]. A self-compacting Ordinary Portland Cement (OPC) is used as concrete matrix which is reinforced with AR-glass fiber textiles usually shaped into a grid structure. The three main values as well as the assumed thickness of the shell used in this work, are summarized in table 1 [7] [8]. In this case, the E-modules was assumed equal to the compressive stiffness of 26 GPa, for the main reason that shells mainly work in compression [9].

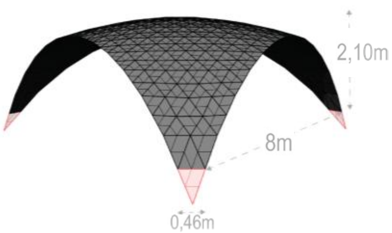

E-modulus	**26**	**GPa**
Poisson ratio	**0,21**	**-**
Density	**2000**	**kg/m^3**
Shell thickness	**0,1**	**m**

Figure 3. *Ground connection enlargement (0.46m) of the synclastic basic triangle for structural analysis, having a maximal height of 2.10 meters and side span of 8 m.* **Table 1.** *Implemented material properties (approximated TRC) in the finite element model for the structural analysis.*

Concerning the permanent load, the self-weight of the shell will be inspected in the first part of the structural analysis by means of a 'Gravity load'. Concerning the wind and snow loads, it is important to recognize that, concerning the computation of these load cases, this specific shell shape is not fully covered by the Eurocodes. This leaves the field free to some interpretations and assumptions, depending on the situation and the fundamentals provided by the standards. The first step is to expose the most relevant wind and snow load values obtained to perform the analysis under load combination in Abaqus. Then, the criteria that need to be fulfilled for Ultimate Limit State and Serviceability Limit State with the corresponding safety and combination factors will be exposed. Finally, the result of the most unfavorable load combination meaning the most critical loading patterns for the structure and thus assumed to generate the worst effects on the structure and the largest stresses and displacements, on the basic equilateral triangle with synclastic curvature will be figured out.

Ten load combinations have been investigated, but only the determining load case (LC3) will be specified in this section. In this case, the applied downward wind pressure is asymmetrical which would lead to increased bending in the structure. The snow load moreover is asymmetrical as well, where the right part displays higher downward forces than the left one due to the drifted snow assumption.

The load pattern with corresponding wind pressure values is based on the canopy roof of 'Eurocode 1: Actions on structures – Part 1.4' (table 2) [10]. For the snow load, the drifted conditions are considered for a domed roof of Part 1-3 [11]. The snow consists of a triangular load, with the maximum characterized by the arrows in between the values going from 0 to 600 N/m^2 for the left part and 0 to 1200 N/m^2 for the right part. Both load patterns are asymmetric for LC3 and are visualized on figure 4.

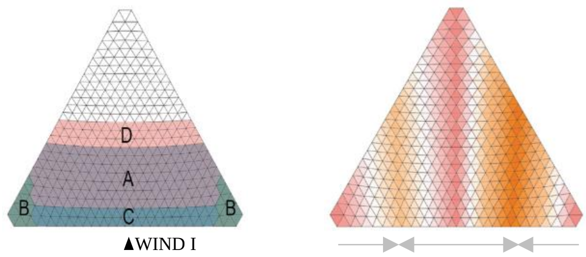

Figure 4. *Load pattern of the most determining wind and snow case on the structure*

		A	B	C	D
WIND I 1,2,3	$C_{p,\,net}$	1,3	1,9	1,6	0,7
	W_e	**592,15**	**865,45**	**728,8**	**318,85**
WIND I 4,5,6	$C_{p,\,net}$	-1,4	-1,81	-1,4	-2
	W_e	**-637,7**	**-824,45**	**-637,7**	**-911**

Table 2. *Wind pressure values [N/m²] of zones with upwards or downward pressure*

$$1{,}35 * \mathrm{SW} + 1{,}5 * \mathrm{Wind(asymm)} + 1{,}5 * 0{,}5 * \mathrm{Snow(asymm)} \qquad (1)$$

Formula 1. *Formula of the most determining load case for the structure, based on approximations referring to the Eurocode EN 1991-1-(1, 3 and 4)*

4. STRUCTURAL ANALYSIS OF A CASE STUDY

4.1 Behavior under self-weight

The numerical analysis of the triangular shell shape under self-weight constitutes a way to verify the efficiency of the form finding procedure in terms of material use, stresses, and displacement. A comparison will be made with the analysis on a flat triangular plate covering the same ground surface as the synclastic triangular shell, i.e. equilateral with a 8m-long side under the same loading (SW) and with the same boundary conditions (hinged to the ground). Their structural behavior is visualized in figure 5, with the summarized zones of stresses and maximal displacements.

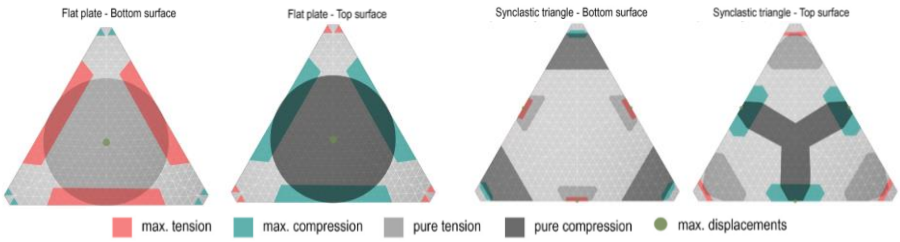

Figure 5. *Summarized zones of stresses and maximal displacements under SW - Flat plate analysis (left) – synclastic triangular configuration analysis (right)*

	Max. in-plane principal stresses [MPa]		Min. in-plane principal stresses [MPa]		Displacement [mm]
	Bottom	Top	Bottom	Top	Maximum
Flat plate	**7,5**	**2,3**	**-2,3**	**-7,5**	**-37,0**
Synclastic triangle	**1,0**	**1,6**	**-2,3**	**-0,7**	**-0,9**
Location	**Middle boundary**	**Middle pillar**	**Middle pillar**	**Middle boundary**	**Central point**

Table 3. *Summarized maximal values of stress and maximal displacements under SW-Flat plate analysis (above) – synclastic triangular configuration analysis (under)*

As shown in the scheme, the middle part of the boundaries and the area close to the supports are the weakest zones due to the occurrence of bending. The boundaries are weaker zones, showing a maximum tension of 1.0 MPa on the bottom surface and a maximum compression of 0.7 MPa on the top surface. This can be explained with the flow of forces, which can only be transferred in a single direction along these boundaries, creating a concentration of the force. This boundary, located far from its support, experiences a lower stiffness with bending as result. At these specific locations, the bending is coupled with additional tension, due to the side boundaries being pulled towards the center of the shell. In addition, the shape has been form found in between fixed boundaries, deviating from its most natural path in case only the corner points were selected as supports. This could explain why larger bending occurs at these edges compared to the center of the structure. Like in the case of an arch, the axial forces increase while reaching the supports. In addition to that, all the forces experienced in the shell are redirected to the ground by means of three pillars functioning as a reduced cross section leading to higher stresses/compression.

In comparison with the plate, the curvature of the shell allows to reduce the bending moments in the central part of the structure. Indeed, the top surface is subjected to pure compression (max in plane figure) while the bottom one has a lower level of tension (closed to zero on min in plane figure). Net reduction of the bottom tension and of the top compression are displayed (>85%) and the displacements of the synclastic shell are almost insignificant as the maximum value has been reduced by 95% reaching less than 1 mm.

4.2 Behavior under load combinations

In this second part, the thin-walled element will be submitted to additional loads such as wind and snow, according to the load combination defined in section 3.

The weakest areas of the shell under this load combination are similar to the ones under pure self-weight. The bottom boundary (in plan) is being pushed inside due to the large and uneven wind pressure applied at this location. This movement downward and towards the center generates a kind of uplift effect (bumping) of the top part (outermost left pillar). Therefore, as the supports were already weaker zones in the pure SW analysis, this top support undergoes the largest hogging moment coupled with the largest displacements (top maximum tension and large bottom compression) as it must re-equilibrate the deformation. While looking at the two other support areas, the ones which are directly subjected to the wind pressure, it can be noticed that the tension is lower on the top surface while the zone of larger compression is still visible at the bottom surface meaning that the bending moment is relatively low and coupled with compression, at the opposite of the top one which is coupled with tension.

The other weaker zones highlighted by the SW analysis and noticed once more, are the arched boundaries which are displaying differences in their stresses and displacements. Indeed, the two side ones (left and right) are undergoing larger bending. This can be explained by the fact that it is at this specific location that the wind upward and downward zones are meeting. Moreover, these two boundaries are influenced by the support areas being pushed inwards (left and right) and upwards at the support at the top, accentuating the stress in them. The right one is also slightly more bent than the left one as it is subjected to higher snow. In the same idea, no large differences are visible in between the left and right side even if the snow load applied is different and asymmetrical. It can be deduced that this load is not determining for the structure and the dimensioning as it affects the structure less than the wind.

Although these maximum values are increased compared to the pure SW analysis, the ULS and SLS criteria are still fulfilled as neither the tensile and compressive strengths of the material nor the displacements are exceeded (see Table 4). The maximum compression of 4.2 MPa is only a fraction of the allowed 38.7 MPa. Although it is safe, the 3.1 MPa tensile stress is closer to the maximum limit set at 4 MPa. A note can be added here to explain why TRC, even if it provides low tensile resistance, is chosen for such a structure. Indeed, the tensile strength is way lower than the compressive one but in general shell behavior, the stresses are really limited as demonstrated before. Therefore, this material allowing slender cross-sections is performant for these kinds of structures. Finally, the maximum displacement of 2mm, occurring where the hogging moment is the largest, is still largely acceptable compared to the 32 mm allowed even if they are computed under an ULS, more severe, combination.

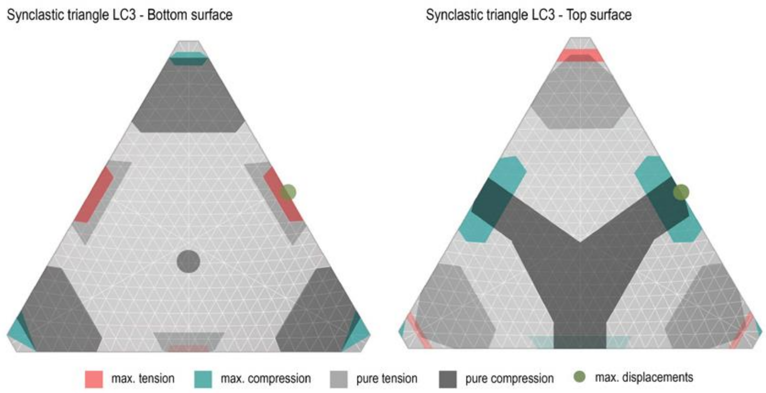

Figure 6. *Summarized zones of stresses and maximal displacements under its most determining load case LC3 – synclastic triangular configuration analysis*

	Max. in-plane principal stresses [MPa]		Min. in-plane principal stresses [MPa]		Displacement [mm]
	Bottom	Top	Bottom	Top	Maximum
Only SW	**1,0**	**1,6**	**-2,3**	**-0,7**	**0,9**
Load case	**2,1**	**3,1**	**-4,2**	**-2,0**	**2,0**
	Design tensile strength ($\sigma_{t,d}$)		Design compressive strength ($\sigma_{c,d}$)		Span/250
CRITERIA	**4,0**		**-38,7**		**32,0**

Table 4. *Summarized values of the max and min in-plane principal stresses and maximum displacements of the structure, under its most determining load case LC3*

5. CONCLUSIONS

As the results show, the form found shell experiences mainly membrane action under self-weight. The bending moments and stresses remain limited. This demonstrates the necessity of form-finding processes allowing to have efficient structural shapes. The stress levels, especially the bending (in term of value but also zone extension), and the displacements are appreciably low.

Moreover, the preliminary design simulations show that a thin TRC section of only a few centimeters would suffice to withstand all load combinations. It has been shown by the load combination that the asymmetrical wind loading generally produces the worst effect on the structure, leading to large bending and hogging moments coupled with displacements due to the differential behavior between different zones. The case leading to the largest values of the stresses and displacement is LC3, with downward wind I (bottom of the shape) and downward drifted snow almost reaching the assumed tensile strength. As explained in previous section it can be explained by the fact that the wind acts on a larger zone, pressing the three free edges with the largest intensity on the bottom of the shape, fully covered by it. In conclusion, the modular design approach shows to be not only resource-effective on the level of the repetitive use of formwork, but also on the structural efficiency of the TRC modular shell itself.

Concerning further research in this field: for the geometrical part, one can extend the scope by experiencing other shell configurations. This research only covers the module combination in the XY-plane, whereas more freedom could maybe be reached by also manipulating the modules in the third dimension. Concerning the early stage structural part, several improvements are still needed to be implemented. As previously stated, this research consists in a preliminary design and neither the non-linear tensile behavior of the TRC with the layering of the material, nor the buckling occurring in slender elements under compressive loads have been considered here. Moreover, in this case only the basic synclastic triangle has been explored under the load combinations. To finally close the loop and entirely handle the subject, the connections between two modules or between the module and the ground could be mastered. Besides that, the manufacturing techniques and on-site installations are also significant aspects that could not be neglected.

6. REFERENCES

[1]KROMOSER B., KOLLEGER J., "Pneumatic forming of hardened concrete – building shells in the 21st century", *Structural Concrete*, vol. 16, n ° 2, 2015, p. 161-171.

[2]SCHOLZEN A., CHUDOBA R., HEGGER J., "Thin-walled shell structures made of textile-reinforced concrete", *Structural Concrete*, vol. 16, n ° 1, 2015, p. 106-114.

[3]VERWIMP E., TYSMANS T., MOLLAERT M., BERG S., "Experimental and numerical buckling analysis of a thin TRC dome", *Thin-Walled Structures*, vol. 94, 2015, p. 89-97.

[4]PIKER D., "Kangaroo: Form Finding with Computational Physics", *Architectural Design*, vol. 83, n ° 2, 2013, p. 136-137.

[5]KILIAN A., OCHSENDORF J., "Particle-spring systems for structural form finding", *Journal of the International Association for Shell and Spatial Structures*, vol. 46, 2005, p. 77-84.

[6]DE SANTIS S., CAROZZI F. G., DE FELICE G., POGGI C., "Test methods for Textile Reinforced Mortar systems", *Composites Part B: Engineering*, vol. 127, 2017, p. 121-132.

[7]VERVLOET J., TYSMANS T., EL KADI M., DE MUNCK M., KAPSALIS P., VAN ITTERBEECK P., WASTIELS J., VAN HEMELRIJCK D., "Experimental and numerical evaluation of textile reinforced cement (TRC) sandwich walls in compression: A geometrical study", *Construction and Building Materials*, vol. 240, 2020.

[8]VERVLOET J., " Design of textile reinforced cement sandwich panels as load-bearing walls: modelling, testing and analysis", *in PhD diss.*, Brussels, 2019.

[9]EL KADI M., TYSMANS T., VERBRUGGEN S., VERVLOET J., DE MUNCK M., WASTIELS J., VAN HEMELRIJCK D., "A layered-wise, composite modelling approach for fiber textile reinforced cementitious composites", *Cement and Concrete Composites*, vol. 94, 2018, p. 107-115.

[10] Belgian Standardization Institute, EN 1991-1-4 Eurocode 1: Actions on the structures - Part 1-4: General actions - Wind actions, Brussels: Belgian Standards, 2005.

[11] Belgian Standardization Institute, EN 1991-1-3 Eurocode 1: Actions on the structures - Part 1-3: General actions - Snow loads, Brussels: Belgian Standards, 2003.

Session 6
Ferrocement : Mechanical Behavior and Properties

EARLY AGE BOND CHARACTERISTICS OF FERROCEMENT-CONCRETE INTERFACE UNDER THERMAL CURING

Adi Abu-Obeidah[1], Daniel Ortiz[2] and Hani Nassif[3]

[1] Rutgers Infrastructure Monitoring and Evaluation (RIME) Group, Department of Civil and Environmental Engineering, Rutgers, the state University of New Jersey, Piscataway, NJ, 08854, asa119@scarletmail.rutgers.edu

[2] Rutgers Infrastructure Monitoring and Evaluation (RIME) Group, Department of Civil and Environmental Engineering, Rutgers, the state University of New Jersey, Piscataway, NJ, 08854, dfo13@scarletmail.rutgers.edu

[3]Rutgers Infrastructure Monitoring and Evaluation (RIME) Group, Department of Civil and Environmental Engineering, Rutgers, the state University of New Jersey, Piscataway, NJ, 08854, nassif@soe.rutgers.edu

SUMMARY: *The efficiency of ferrocement laminates applied for strengthening of concrete substrates and subjected to shear or bending, is dependent on the characteristics of the interfacial bond especially at early age. Early age bond strength and performance of fiber-reinforced ferrocement-concrete composite sections under different thermal curing conditions is investigated in this study. The experimental program takes into consideration three variables: (1) fibres utilized in the mortar mix (steel and polypropylene), and (2) thermal curing temperature. The bond testing is evaluated through 1) pull-off strength applied on slabs (305 mm x 305 mm), 2) Compatibility test, 2) splitting tensile as well as 4) slanted shear tests (76 mm x 152 mm). Mechanical properties under the same condition for all mixes are presented and discussed.*

KEY WORDS: *bond, strengthening, heating, pull-off, fibers.*

1. INTRODUCTION

To extend the service life of reinforced concrete deteriorated members, innovative materials and composites are necessary. Various strengthening materials and systems have been implemented such as fiber reinforced polymers (FRP), self-consolidating concrete (SCC), and ferrocement. Ferrocement has been utilized extensively in Australia, New Zeeland and the United Kingdom since early 1960's for different repair applications especially for historic structures repairs [1]. Many reasons contributed to their popularity such as ease of mouldability, lightweight and low cost [2]. Although, strengthening using ferrocement has been extensively proven by many scholars to be effective in increasing reinforced concrete member's capacity under bending, shear, and torsion [5-8,17], the ferrocement-concrete interface remains a critical parameter that needs further understanding [4] and clarification especially at early age within the first 3 days. Significant research has been conducted to investigate the bond strength of ferrocement/concrete [2,3]. However, studies incorporating the pull-off characterizations are very limited [1, 4, 16] especially at an early age. For repair purposes, early age pull-off strength of ferrocement is crucial as it indicates the bond capacity under direct tension which can be also used to derive bond-slip relationships [15]. Understanding the bond capacity of ferrocement/concrete at early age can assist in saving construction time. Given than, this paper aims at investigating the bond characteristics of ferrocement mixes to class A concrete at ages 8 hours to 3 days through 1) pull-off strength applied on slabs (305 mm x 305 mm), 2) Compatibility test, 2) splitting tensile and 4) slanted shear tests (76 mm x 152 mm). The bond performance is tested under heat blankets, which aims to accelerate the hydration process, and is compared to specimens cured at ambient temperature. In addition, use of cementitious materials, silica fume and slag, combined with polypropylene or steel fibers are tested.

2. MATERIALS AND METHODS

2.1. Material Characteristics

2.1.1. Mix Design

Recently, there has been a growing trend towards the use of supplementary cementitious materials, such as silica fume, fly ash, and blast furnace slag in the production of composite cements due to the economical, technical, and environmental benefits. Research shows that the incorporation of silica fume enhances the bond between concrete and overlay [9,13,14]. In addition, slag is a more environmentally friendly material which reduces energy consumption by 90 % in production and it is able to achieve higher compressive strength compared to cement [11,12,10]. For those reasons, two mixture designs were investigated and prepared in this study utilizing silica fume (5%) and a combination of slag (15%) and silica fume (5%) of the cementitious material. Both mixtures are summarized in Table *1*.

Table 1. *Mixture proportions (kg/m^3)*

*Mix ID**	*Cement*	*Silica fume*	*Slag*	*Total cementitious*	*w/c*	*Sand*
FC-S	617	33 (5%)	-	650	0.4	1300
FC-SSL	520	33 (5%)	97 (15%)	650	0.4	1300

* FC: ferrocement, S: Silica fume, SL: slag

2.1.2. fibers

Figure 1 illustrates the steel and synthetic polypropylene fibres utilized in this study. The steel fibers (S) are 13 mm with a 2850 MPa tensile strength and the macro polypropylene fibres (M) are 19 mm with 600-650 MPa of tensile strength. In addition, combination of micro and macro polypropylene fibers (H) at a ratio of 1:4 has been tested.

(a) (b) (c)

Figure 1. *19 mm Polypropylene fibres (a) Macro, (b) Micro (c) 13 mm Steel fiberes*

3. CURING METHODS

3.1. Heat Blanket

As presented in Figure 2, Two curing methods are applied, which are, 1) ambient curing, and 2) thermal curing. Thermal or heat blanket are applied on the ferrocement for three (3) hours with at temperature ranges between 110-120^{o}F, after which only wet burlap is applied. Similarly, the ambient cured specimens have wet burlap applied once casted. This study will present an insight of the composite under thermal blanket.

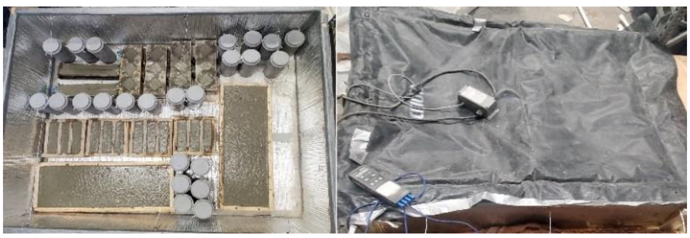

Figure 2. *Curing Method: (a) Ambient, and (b) Thermal Curing*

4. EXPERIMENTAL PROGRAM

An experimental program is conducted to evaluate the bond strength of fiber-reinforced ferrocement when applied on concrete substrates at early age (within 3 days). The bond testing is evaluated through pull-off strength using slabs (305 mm x 305 mm), splitting tensile, and slanted shear testing (76 mm x 152 mm). In addition, the test developed by Czarnecki et al. [9] to examine the compatibility of the repair materials with the substrate is conducted. All testing included in this program are summarized in Table 2 and Figure 3. The substrate surface for all specimens is water-jetted to provide a rough surface interface. Prior to casting the ferrocement layer the surfaces are cleaned from any debris and saturated with water to promote the ferrocement/substrate bonding.

Table 2. Experimental Program Summary for each Curing Method

Test Standards	Test Methods	Age*	Size mm (number)
ASTM C1583	Pull-off	8h, 12h, 1d, 3d	305 x 305 slabs (2)
ASTM C882	Slanted Shear	8h, 12h, 1d, 3d	76 x 152 (8)
ASTM C496	Splitting Tensile	8h, 12h, 1d, 3d	76 x 152 (8)
Czarnecki et al. [9]	Compatibility test	8h, 12h, 1d, 3d	406 x 102 (8)
ASTM C39, ASTM C496	Compressive Strength Tensile Strength	8h, 12h, 1d, 3d	76 x 152 (16)

* h: hours, d:days

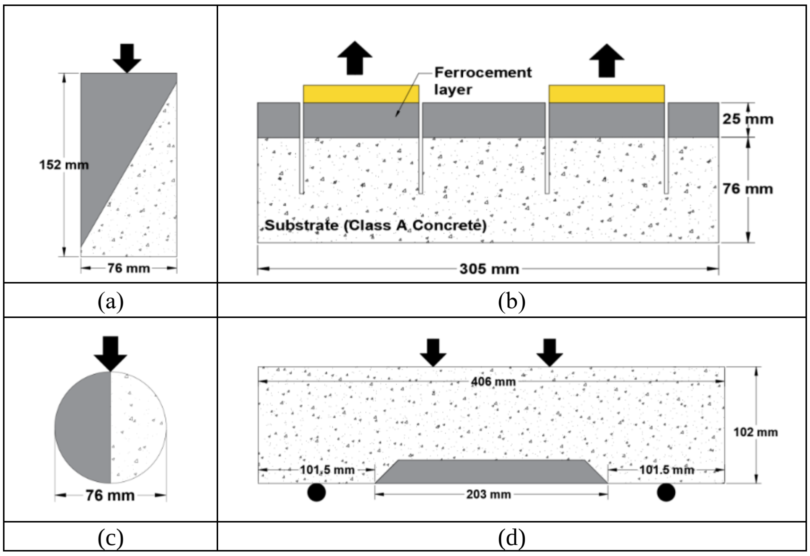

Figure 3. *Interfacial Bond Strength tests: (a) Slanted Shear, (a) Pull-off test setup, (c) Splitting Tensile, and (c) Compatibility test*

5. RESULTS AND DISCUSSION

5.1. Mechanical Properties of the Mixtures

5.1.1. *Control Mixtures*

Figure 4 illustrates the compressive and the tensile strength for the control mixtures FC-S and FC-SSL (defined in Table 1) under both curing methods. As presented, FC-S did not achieve any noticeable compressive strength (< 2 MPa) nor tensile strength at 8 hours with or without thermal heating. At 12 hours, thermal curing improved the compressive and tensile strength of the FC-S mixture by 287% (4.87 MPa → 18.84 MPa) and 190% (0.59 MPa → 1.71 MPa), respectively, compared to the ambient cured specimens. On the other hand, utilizing 15% of slag in FC-SSL mixture produced higher strength at early age (8 and 12 hours) compared to FC-S mixture. As shown in Figure 4, FC-SSL improved compressive strength at 8 and 12 hours by 600% (2 MPa → 15.2 MPa) and 12.6% (18.8 MPa → 21.17 MPa), respectively compared to FC-S under heating conditions. Similarly, tensile strength for FC-SSL improved up to 718% and 162% compared to FC-S mixture under heating and ambient condition, respectively. Beyond 12 hours, the heating effect on both the compressive and tensile strength was minimal with both FC-S and FC-SSL mixtures.

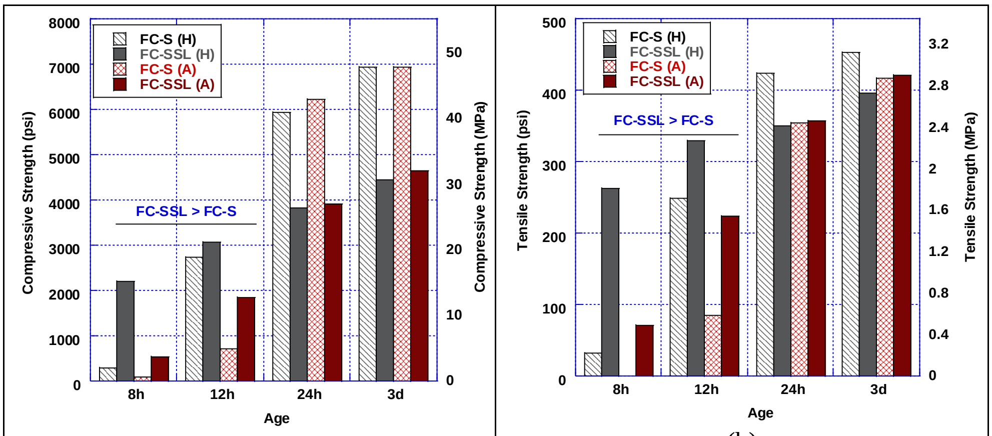

Figure 4. Mechanical Properties of the Control Mixes (FC-SSL and FC-S), (a) Compression Strength and (b) Tensile Strength. (H) for heated – (A) for Ambient

5.1.2. Fibrous Mixtures

Figure 5 and Figure 6 illustrates the compressive and the tensile strength for both mixtures, FC-S and FC-SSL, under both curing methods after fibers is added. As presented, FC-S did not achieve any noticeable compressive strength (< 2 MPa) nor tensile strength at 8 hours with or without polypropylene fibers (FC-S-0.2M, FC-S-0.2H) under heating or ambient conditions. FC-S-0.2M is the designation for the mixture with 0.2% by volume of polypropylene macro fibers and FC-S-0.2H is the designation for the mixture with 0.17% polypropylene macro fibers and 0.03% polypropylene microfibers. To promote the compressive and tensile strength at 8 hours, slag replaced 15% of cement and polypropylene fibers' content was increased to 0.4% (FC-SSL-0.4H). These two changes improved compressive and tensile strength up to 20 MPa and 1.5 MPa, respectively. In addition, those changes improved FC-SSL-0.4H tensile strength up to 907% for all ages tested (Figure 6), which could be an indication of better bond characteristics. Moreover, 0.4% of steel fibers was tested for FC-SSL-0.4S and it shows improvements in the compressive and tensile strength at 8 and 12 hours up to 84% under ambient curing condition.

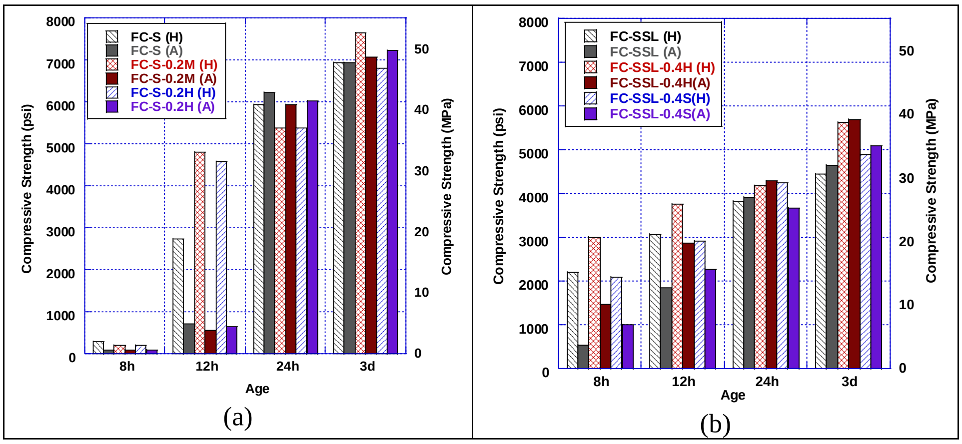

Figure 5. Compressive Strength comparison to fibrous mixtures, (a) FC-S-0.2M, FC-S-0.2H, compared to FC-S, and (b) FC-SSL-0.4H, FC-SLL-0.4S compared to FC-SSL

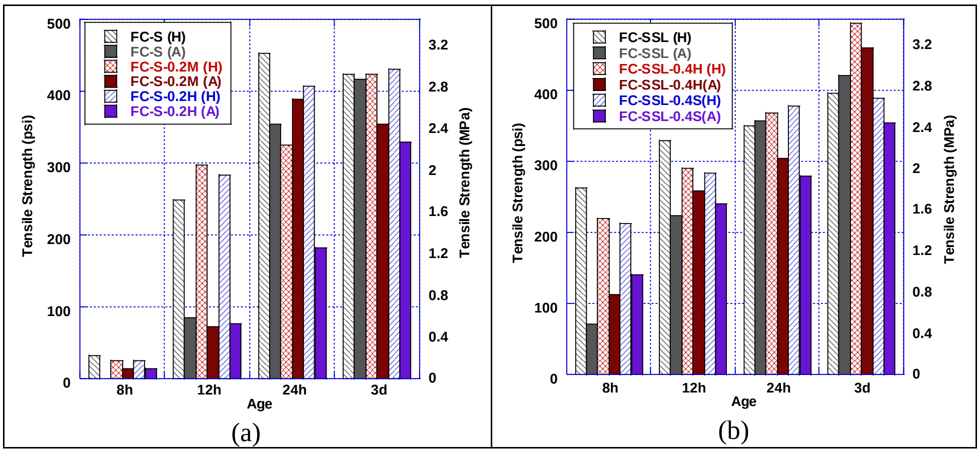

Figure 6. Tensile Strength comparison to fibrous mixtures, (a) FC-S-0.2M, FC-S-0.2H, compared to FC-S, and (b) FC-SSL-0.4H, FC-SLL-0.4S compared to FC-SSL

5.2. Bond Characteristics of the Mixtures

Slag-based mixtures presented better mechanical properties at 8 and 12 hours and for that reason they qualify for early age bond testing compared to silica-fume-based mixtures. FC-SSL (control mix), FC-SSL-0.4H (0.06% of micro and 0.34% macro polypropylene fibers) and FC-SSL-0.4S (0.4% of steel fibers) are the three mixtures utilized in this study.

5.2.1. *Effect of thermal curing*

Thermal curing under heat blanket at a temperature ranging from 100 – 120^{o}F for three hours had a positive effect on the bond characteristics investigated in this study for all mixtures. As illustrated in Figure 7, slanted shear capacity was improved up to 309%, 96% and 31% for FC-SSL, FC-SSL-0.4S and FC-SSL-0.4H, respectively. as illustrated in **Figure 8** (b) for ambient and heated curing, the failure occurred at the interface for 8 and 12 hours testing and on the repair/substrate materials for 24 hours and 3 days testing, which indicates that full-bond occurred. Similarly, heating conditions improved splitting tensile up to 194% for FC-SSL, 73% for FC-SSL-0.4S and 100% for FC-SSL-0.4H.

Pull-off strength significantly improved with the thermal curing. At 8 hours, all mixtures were not hard enough to perform the testing under ambient conditions. However, after heating for three hours, the pull-off capacity improved to 28 MPa, 51 MPa and 78 MPa, for FC-SSL, FC-SSL-0.4S and FC-SSL-0.4H, respectively. It was also observed that ambient cured specimens' failure occurs at within the ferrocement layer for 12 hours and at the ferrocement/substrate interface for other ages (as illustrated in **Figure 8** (c)). However, for the heated samples, the failure occurred at the ferrocement/substrate interface at 8 and 12 hours and at the substrate beyond there, which confirms the effectiveness of the heating for early age bond strength.

Similarly, the compatibility strength between the ferrocement and substrate was improved under heating conditions up to 13%, 34% and 10% for FC-SSL, FC-SLL-0.4H, FC-SSL-0.4S, respectively. It was observed that most ambient cured specimens suffered failure at the bond interface (debonding), however, many of the heated specimens failed at the substrate, as presented in **Figure 8** (a).

5.2.2. *Effect of fibers*

Bond characteristics were affected by the addition of polypropylene and steel fibers. The use of fibers adversely affected the slanted shear and splitting tensile capacity up to 4% and 27% when compared to the control mix under heated conditions. This occurs because the bond between the mortar and fibers were not achieved yet especially that both test results was improved at later ages up to 74% for polypropylene fibers and 86% for steel fibers. On the other hand, pull off testing results indicated an improvement for 8 and 12 hours up to 342% for FC-SSL-0.4H and 104% for FC-SSL-0.4S, but not for 24 hours and 3 days. In addition, pull-off capacity was reduced up to 50% when steel fibers are utilized under ambient temperature compared to the control mix. However, when polypropylene fibers are utilized the pull-off capacity was improved up to 70% at all ages under the same conditions. The results shows that FS-SSL-0.4H achieved higher slanted shear, splitting tensile and pull-off strength compared to FS-SSL-0.4S, at most ages under ambient and heated conditions. Nevertheless, the compatibility test shows that steel fibers are more effective in improving flexural capacity of the substrate when compared to polypropylene fibers with the same dosage.

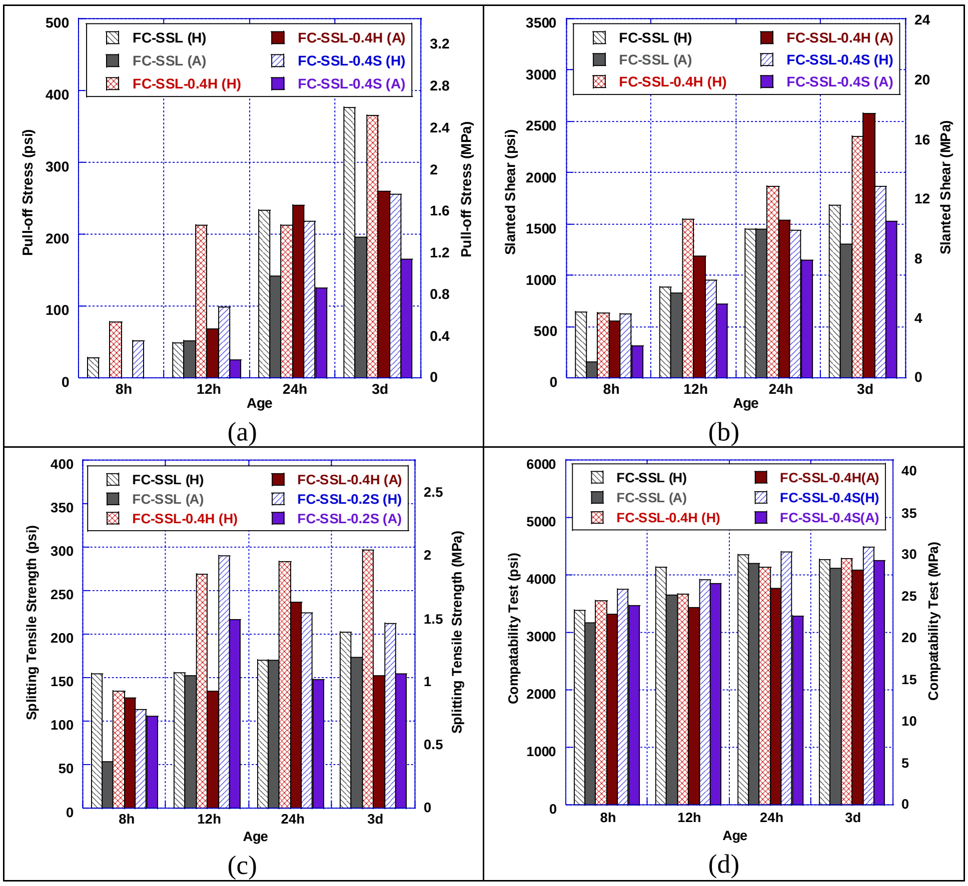

Figure 7. Bond Characteristics, (a) Pull-off Strength, (b) Slanted Shear, (c) splitting tensile, (d) Compatibility test

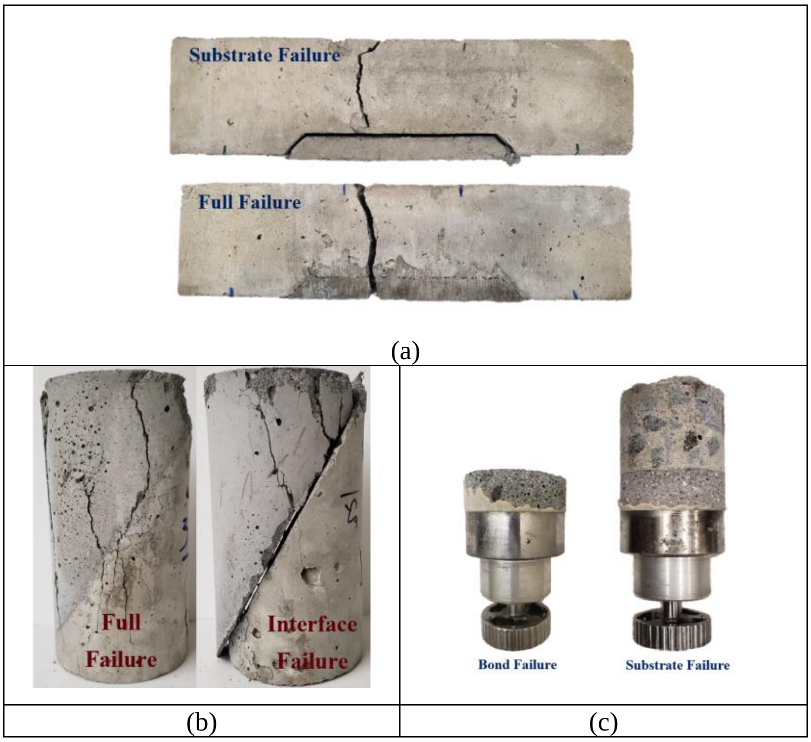

(a) (b) (c)

Figure 8. Failure Criteria, (a) Compatibility test, (b) Slanted Shear, (c) Pull-off

6. CONCLUSIONS

This paper presented the results for the bond characteristics of mortar mixture utilizing silica fume and slag and the following conclusions are drawn:

- Heating method under thermal blankets with a temperature ranging from 100-120ºF for three hours can assist in improving the bond strength between overlay and substrate surface which could accelerate the construction and repair process.
- polypropylene fibers achieve higher slanted shear, splitting tensile and pull-off strength compared to steel ones, at most ages under ambient and heated conditions.
- The compatibility test shows that steel fibers are more effective in improving flexural capacity of the substrate when compared to polypropylene fibers at the same dosage.

7. REFERENCES

[1] DONNINI J., CORINALDESI V., NANNI A., Mechanical properties of FRCM using carbon fabrics with different coating treatments, Compos B Eng 2016;88:220–8. https://doi.org/10.1016/j.compositesb.2015.11.012.

[2] D'AMBRISI A., FEO L., FOCACCI F., Experimental analysis on bond between PBO-FRCM strengthening materials and concrete. Compos B Eng 2013;44:524–32. https://doi.org/10.1016/j.compositesb.2012.03.011

[3] SNEED L., D'ANTINO T., CARLONI C., Investigation of bond behavior of polyparaphenylene benzobisoxazole fiber-reinforced cementitious matrix composite concrete interface. ACI Mater J 2014;111:569–80. https://doi.org/10.14359/ 51686604.

[4] EBEAD U., YOUNIS A., “Pull-off characterization of FRCM/Concrete interface”, *Composites Part B: Engineering*. 2019 May 15;165:545-53.

[5] NASSIF H.H, NAJM H., “Experimental and analytical investigation of ferrocement–concrete composite beams”,. *Cement and Concrete Composites*. 2004 Oct 1;26(7):787-96.

[6] NASSIF H., ABU-OBEIDAH A., NA C., OZBAY K., GAO J., KHAYAT KH.,. Flexural Performance of Concrete Beams Strengthened using Different Repair Techniques. United States. Dept. of Transportation. Office of the Assistant Secretary for Research and Technology; 2019 Jun 1.

[7] MIAH MJ, MIAH MS, ALAM WB, MONTE FL, LI Y., “Strengthening of RC beams by ferrocement made with unconventional concrete”, *Magazine of Civil Engineering*. 2019 Sep 1;89(5).

[8] KAZEMI MT, MORSHED R. “Seismic shear strengthening of R/C columns with ferrocement jacket”,. *Cement and Concrete Composites*,. 2005 Aug 1;27(7-8):834-42.

[9] CZARNECKI, L., GARBACZ, A., LUKOWSKI, P., & CLIFTON, J., *Polymer composites for repairing of portland cement concrete*: compatibility project. 1999

[10] FERNÁNDEZ-JIMÉNEZ A., PALOMOB J., PUERTAS F., (1999) Alkali-activated slag mortars: mechanical strength behavior. Cem Concr Res 29(8):1313–1321

[11] BILIM C., ATIS C., (2012) Alkali activation of mortars containing different replacement levels of ground granulated blast furnace slag. Constr Build Mater 28(1):708–712

[12] SHI C., QIAN J., (2000) High performance cementing materials from industrial slags—a review. Resour Conserv Recycl 29(3):195–207

[13] MOMAYEZ, A., RAMEZANIANPOUR, H., RAJAIE, M., Ehsani, Bi-surface shear test for evaluating bond between existing and new concrete, ACI Mater. J. 101 (2) (2004) 99–106.

[14] M. KURODA, T., WATANABE, N. TERASHI., Increase of bond strength at interfacial transition zone by the use of fly ash, Cem. Concr. Res. 30 (2) (2000) 253–258.

[15] LIU K., WU Y., Analytical identification of bond-slip relationship of EB-FRP joints. Compos B Eng 2012;43:1955–63. https://doi.org/10.1016/j.compositesb.2012.01. 048

[16] CAROZZI FG, POGGI C. Mechanical properties and debonding strength of Fabric Reinforced Cementitious Matrix (FRCM) systems for masonry strengthening. Compos B Eng 2015;70:215–30. https://doi.org/10.1016/j.compositesb.2014.10. 056.

[17] KHAN SU, RAFEEQI SF, AYUB T., “Strengthening of RC beams in flexure using ferrocement”. *Iranian Journal of Science and Technology*. Transactions of Civil Engineering. 2013 Dec 1;37(C):353.

EARLY-AGE PERFORMANCE OF FIBER REINFORCED FERROCEMENT AND UHPC IN FLEXURAL REPAIR OF CONCRETE BEAMS

Adi Abu-Obeidah[1], Wassim Nasreddine[2], Hani Nassif[3], and Weina Wang[4]

[1] Rutgers Infrastructure Monitoring and Evaluation (RIME) Group, Department of Civil and Environmental Engineering, Rutgers, the state University of New Jersey, Piscataway, NJ, 08854, asa119@scarletmail.rutgers.edu

[2] Rutgers Infrastructure Monitoring and Evaluation (RIME) Group, Department of Civil and Environmental Engineering, Rutgers, the state University of New Jersey, Piscataway, NJ, 08854, wn67@scarletmail.rutgers.edu

[3]Rutgers Infrastructure Monitoring and Evaluation (RIME) Group, Department of Civil and Environmental Engineering, Rutgers, the state University of New Jersey, Piscataway, NJ, 08854, nassif@soe.rutgers.edu

[4] Department of Civil and Environmental Engineering, Stevens Institute of Technology, Hoboken, NJ, 07030, wmeng3@stevens.edu

SUMMARY: *This paper investigates the performance of fiber reinforced ferro-cement (FRFC) and ultra-high-performance concrete (UHPC) in retrofitting reinforced concrete beams at early age. This program evaluates the ability of these materials in restoring the load carrying capacity and deflection of the reinforced concrete (RC) beams at early ages (up to 3 days). The beams were designed to fail in flexure and during testing, cracking widths were measured at several loads. Two main variables are analyzed in the analysis which are 1) curing regimes and 2) Mesh type. For the curing regimes, two methods will be investigated: (1) Wet-burlap, and (2) Thermal Curing (Heat Blanket) for three hours. In addition, standard steel mesh and basalt mesh will be utilized in this study. In addition to the FRFC and UHPC efficiency in retrofitting concrete beams, the flexural toughness for each material was investigated through the panel testing.*

KEY WORDS: *strengthening, heating, basalt mesh, flexural toughness, repair.*

1. INTRODUCTION

In this paper, the effect of fiber reinforced ferrocement and ultra-high-performance concrete (UHPC) is investigated in the retrofitting of concrete reinforced (RC) beams with loss in concrete cover. The use of ferrocement is renowned for retrofitting capabilities due to simplicity and speed of application to a substrate. On the other hand, there is limited research on the early age (up to 3 days) efficiency of ferrocement and UHPC in restoring load carrying capacity, deflections, and improving cracking performance compared to unrepaired beam (full depth) is investigated. Previous studies have investigated the use of ferrocement or UHPC in the repair of beams in flexural in later ages. Nassif et al. (2004) studied the effect of mesh, mesh layers and shear studs on the behavior of beams repaired with ferrocement [1]. It was concluded that full composite between the ferrocement/concrete layer can not be attained based on rough surfaces without any shear studs [1]. For UHPC, Zhang et al. (2021) utilized UHPC to repair pre-damaged beams and achieved at least 57% improvement in cracking load and 72% in ultimate loads compared to control beams [2]. As stated, many scholars confirmed that UHPC and ferrocement are efficient in restoring load carrying capacity at 28 days and beyond. However, limited studies are investigating the efficiency of those materials in retrofitting RC beams at early age. This study focuses on experimental testing and analysis of specimens at early age (1 and 3 days), which could assist in accelerated construction time if the results are satisfactory.

2. EXPERIMENTAL PROGRAM

2.1. Flexural Panels

An experimental program is conducted to evaluate the flexural toughness of fiber-reinforced ferrocement and UHPC laminates when reinforced with one layer of standard steel mesh or basalt mesh. The fibers utilized in the mortar mix are macro and micro polypropylene fibers as well as steel fibers (**Figure 1**). Two curing methods are applied including, 1) wet burlap, and 2) thermal curing. Thermal or heat blanket is used to heat the repair material for three hours, at a temperature between 100 – 120ºF, combined to wet-burlap, after which only wet-burlap is applied. To investigate the flexural toughness of the fiber-reinforced ferrocement composite, 550 x 150 x 32 mm specimens (Figure 3) are fabricated and tested under four-point bending manner. Cracking and failure behavior for each specimen will be compared to other specimens to determine the effect of mesh, curing and mix on the overall flexural behavior.

(a) *(b)* *(c)*

Figure 1. 19 mm Polypropylene fibers (a) Macro, (b) Micro, (c) Steel fibers

(a) *(b)*

Figure 2. *Curing methods (a) Heated conditions, (b) Ambient conditions*

2.2. Flexural Strengthening

In this study, twelve RC beams were casted with 30 mm loss in the concrete cover at the soffit of the beam. Each beam has a total depth of 150 mm, width of 150 mm, and a clear span length of 914 mm. Figure 4 illustrates the specimens' dimensions for the concrete beams strengthened with ferrocement/UHPC. As presented in Table 1, the beams retrofitted with fiber reinforced ferrocement are designated as FRFC and the ones with UHPC are designated as UHPC. Class A concrete which is common in New Jersey bridges will be used as the substrate for all mixes.

Table 1. *Testing plan*

Curing	*Beam type**	*Mesh type*	*Testing Age*	*Specimens #*
Ambient Curing	*Full Class A-C*	*NA*	*1 and 3 days*	*2*
	FRFC-S	*Steel*		*2*
	FRFC-B	*Basalt*		*2*
Heat Curing	*FRFC-S*	*Steel*		*2*
	FRFC-B	*Basalt*		*2*
	UHPC-C	*NA*		*2*
	UHPC-B	*Basalt*		*2*

** C for control, S for steel mesh, B for basalt mesh*

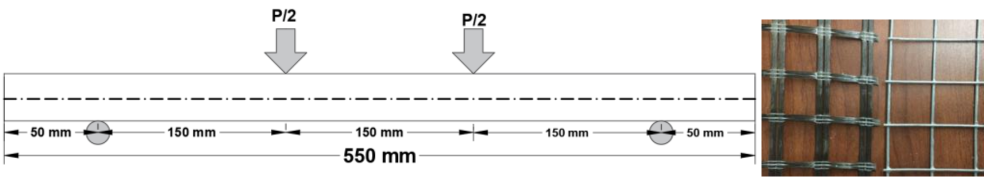

Figure 3. *Flexural Toughness: Specimen dimension, mesh, and Setup*

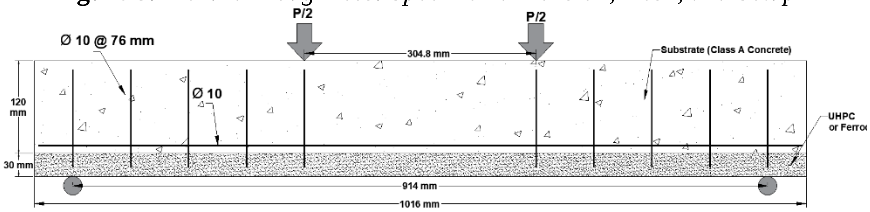

Figure 4. *Retrofitted Beam dimension and reinforcement setup*

3. RESULTS AND DISCUSSION

3.1. FRFC Mechanical Properties

3.1.1 Mix Design

In this study, two mixtures utilizing silica fume (5%) and a combination of slag (15%) and silica fume (5%) were casted with several fibers' content. Proportions of each mix are summarized in Table 1. As shown in Figure 5, curing under heating conditions increased the compressive up to 125% for silica-fume based mixture (FC-S, FC-S-0.4H) and up to 32% for slag-based mixtures (FC-SSL, FC-SSL-0.4H, FC-SSL-0.4S). Moreover, it was observed that combining slag, silica fume with 0.4 of steel fibers (FC-SSL-0.4S) resulted in the highest tensile capacity among all mixtures. For UHPC, a non-proprietary mixture that combines 14% and 21% (by weight) of river sand and light weight sand and utilizes cement, slag and steel fibers is used in this study. This mixture achieved a compressive and tensile strength of 70 and 10.2 MPA in three days, respectively.

Table 2. *Mixture proportions (kg/m^3)*

*Mix ID**	*Cement*	*Silica fume*	*Slag*	*Total cementitious*	*w/c*	*Sand*
FC-S	617	33 (5%)	-	650	0.4	1300
FC-SSL	520	33 (5%)	97 (15%)	650	0.4	1300

* FC: ferrocement, S: Silica fume, SL: slag

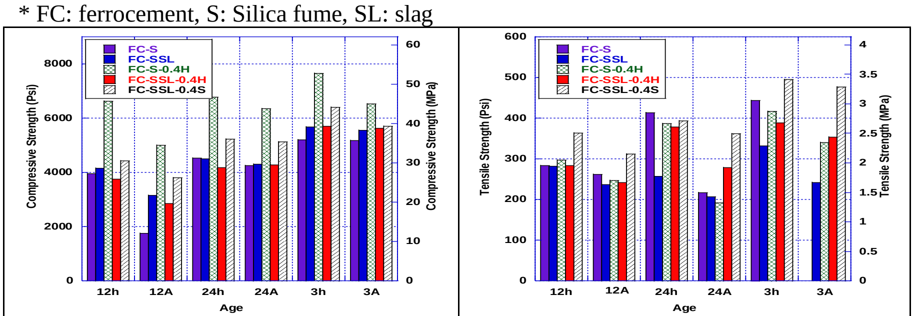

(a) (b)

Figure 5. *(a) Compressive Strength, (b) Tensile Strength (h: heating, A: ambient)*

3.2. Flexural Analysis of the Panels

Panel flexural testing is conducted to evaluate the flexural capacity of fiber-reinforced ferrocement and UHPC laminates when supported with one layer of standard steel mesh or basalt mesh. Figure 6 (a) illustrates the four-point loading setup for the panels with a linear variable differential transformer (LVDT) installed for accurate measurements of the mid-span deflection.

presents the cracking and ultimate load and deflection for tested specimens under heating and ambient conditions. As presented, thermal curing conditions increased cracking load when FC-SLL, FC-SSL-0.4H and FC-SSL-0.4S mixtures are used up to 45%, 48% and 28% for panels reinforced with steel or basalt mesh at 24 hours, respectively. Similarly, the deflection at cracking was also improved for the same mixtures at 24 hours up to 32%, 47% and 42%. On the other hand, the heating did not show similar improvements when applied to FC-S and FC-S-0.4H mixtures at 24 hours and 3 days. The results shows that both FC-S and FC-S-0.4H presented a drastic drop in the cracking and ultimate load at 3 days especially when combined with basalt mesh (-22.4%, -20%). Based on the results, FC-SLL-0.4S presented the best improvements in terms of cracking and ultimate load and deflection under heating conditions and for that, this mixture is proposed for retrofitting in this study. Regarding the UHPC panels, it was observed that the specimen start failing once the crack occurred which makes the cracking and ultimate load identical. UHPC panels exhibited the highest ultimate/cracking capacity compared to all specimens.

(a)

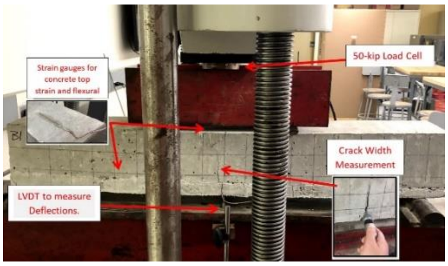

(b)

Figure 6. *Testing Setup, (a) Panels, (b) Retrofitted beams*

Table 3. *Load and Deflection Summary at Cracking and Ultimate (kN, mm)*

Speciemen ID	24-hour				3-day			
	Cracking		Ultimate		Cracking		Ultimate	
	P_{cr}	Δ_{cr}	P_u	Δ_u	P_{cr}	Δ_{cr}	P_u	Δ_u
FCS-S-N-A	1721	0.76	2024	8.8	1828	0.89	2086	4.3
FCS-S-N-H	2033	1.37	2073	4.5	1806	0.99	NA	NA
FCS-B-N-A	1748	0.89	2002	15.5	1508	0.86	2447	17.4
FCS-B-N-H	1561	0.76	1979	7.1	1441	0.81	2402	16.5
FCS-S-H-A	2260	1.14	2260	1.1	2589	0.86	NA	NA

FCS-S-H-H	2157	1.07	2157	1.1	2162	1.19	NA	NA
FCS-B-H-A	1877	0.91	2318	17.8	2269	0.66	2811	10.3
FCS-B-H-H	1935	1.19	2460	12.7	1761	0.86	2242	11.0
FCSSL-S-N-A	1503	1.02	2095	8.0	2002	1.07	2060	3.2
FCSSL-S-N-H	2180	1.27	2180	1.3	1935	1.30	2184	9.9
FCSSL-B-N-A	1432	0.79	2051	12.9	2157	1.02	2295	13
FCSSL-B-N-H	1882	1.04	2402	11.5	2046	1.02	2251	9.0
FCSSL-S-S-A	1383	1.04	2495	8.7	2406	1.30	3216	6.6
FCSSL-S-S-H	2046	1.07	2896	8.2	2989	1.98	3283	7.8
FCSSL-B-S-A	1499	0.81	2691	17.5	2402	1.93	2838	13.9
FCSSL-B-S-H	2135	1.19	3060	16.4	2318	1.55	3323	15.8
FCSSL-S-H-A	1423	0.79	1842	6.2	1868	1.65	2291	5.3
FCSSL-S-H-H	1819	1.12	1984	5.1	2531	2.08	2295	7.2
FCSSL-B-H-A	1521	0.81	2340	20.9	1944	2.03	2571	15.9
FCSSL-B-H-H	1557	0.86	2380	20.8	2082	1.57	2544	25.2
UHPC-N-S-A^	3438	5.7	3438	5.7	5872	5.6	5872	5.6
UHPC-N-S-H^	4586	5.0	4586	5.0	6503	6.8	6503	6.8
UHPC-B-S-A^	3363	4.9	3363	4.9	3839	5.1	3839	5.1
UHPC-B-S-H^	3296	3.9	3296	3.9	NA	NA	NA	NA

*Desgination (A-B-C-D). A for mix design : UHPC/FRS/FRSLL, B for Mesh type : N for no mesh/B for basalt/S for steel, C for fiber type : H for hybrid polyprobelene fibers/S for steel fibers, D for curing method : H for thermal heating/A for ambient conditions.

3.3. Flexural Analysis of the Repaired Beams

In this study, twelve RC beams were strengthened with the proposed laminates and tested until failure (concrete crushing on top). Figure 7 illustrates the casting process for the substrate and the repair layer. In addition, Figure 6 (b) shows the location of the sensors and load-cell utilized in measuring applied load, deflection, and cracks width during the test.

(a) (b)

Figure 7. *Retrofitted Beam Casting, (a) Substrate Casting, (b) Layer casting*

3.3.1 Load and Deflection Analysis of FRFC beams

Figure 8 and Table 4 illustrates the load and deflection FRFC strengthened beams at cracking, yielding and ultimate loads. Compared to the control beam, all strengthened beams had a higher cracking, yielding and ultimate load but not ultimate deflection, which was reduced at least up to 21%. It was also observed that the thermal heating of FRFC beams had a positive effect on the cracking load at 24 hours. For beams reinforced with steel mesh, cracking, yielding and ultimate load was improved by 23%, 15% and 6%, respectively. Similarly, when the basalt fiber mesh is utilized, the improvement achieved was 19%, 3.4% and 11.2% for cracking, yielding and ultimate load, respectively. At 3 days, the improvements for the cracking load were minimal, however ; the ultimate and yielding load increased by 19% and 14% in beams with steel mesh and by 6% and 16.6% in beams with basalt mesh, respectively.

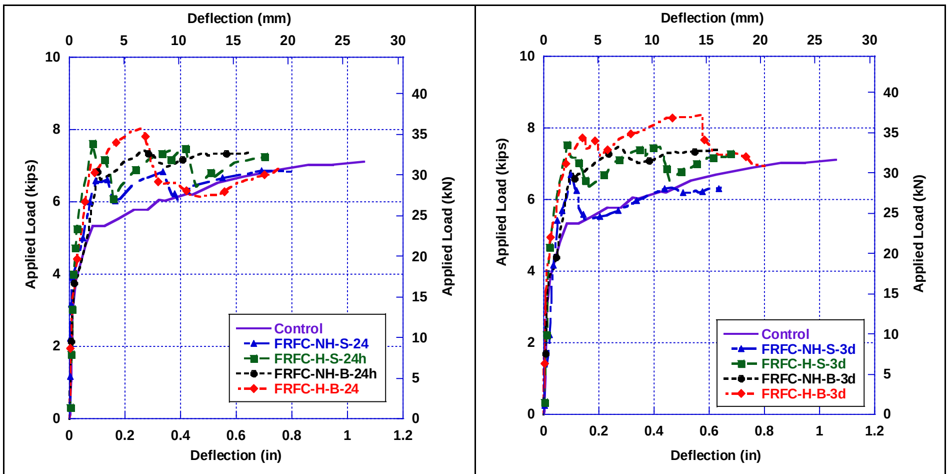

(a) *(b)*

Figure 8. *Load-deflection of beams retrofitted with FR-FC*

Table 4. *Summary of the applied load and deflection at different loading stages (kN, mm)*

Beam Designation*	P_{cr}	Δ_{cr}	P_y	Δ_y	$P_u^{\wedge}$	Δ_u
Control	17	0.58	23.7	2.11	31.5	27.11
FRFC-A-S-24h	16.8 *(-1%)**	0.25 *(-57%)*	29.5 *(+25%)*	2.36 *(+12%)*	30.8 *(-2%)*	20.22 *(-25%)*
FRFC-H-S-24h	20.6 *(+21%)*	0.55 *(-7%)*	33.9 *(+43%)*	2.16 *(+2%)*	32.6 *(+4%)*	17.78 *(-34%)*
FRFC-A-B-24h	15.2 *(-11%)*	0.41 *(-29%)*	30.3 *(+28%)*	2.62 *(+24%)*	32.9 *(+5%)*	16.51 *(-39%)*
FRFC-H-B-24h	18.0	0.51	31.3	2.03	36.6	6.43

	(+6%)	*(-13%)*	*(+32%)*	*(-4%)*	*(+16)*	*(-76%)*
FRFC-A-S-3d	18.4 *(+8%)*	0.89 *(+52%)*	29.8 *(+26%)*	2.59 *(+23%)*	28.7 (-9%)	16.76 *(-38%)*
FRFC-H-S-3d	18.8 *(+11%)*	0.13 *(-78%)*	35.7 *(+50%)*	1.73 *(-18%)*	32.7 *(+4%)*	13.97 *(-48%)*
FRFC-A-B-3d	17.8 *(+5%)*	0.48 *(-17%)*	32.4 *(+37%)*	4.75 *(+125%)*	31.9 *(+1%)*	17.40 *(-36%)*
FRFC-H-B-3d	17.6 *(+4%)*	0.20 *(-67%)*	34.3 *(+44%)*	3.76 *(+78%)*	37.2 *(+18%)*	14.53 *(-46%)*
UHPC-H-N-24h	25.9 *(+53%)*	1.19 *(+104 %)*	36.5 *(+54%)*	2.08 *(-1%)*	33.9 *(+8%)*	8.64 *(-68%)*
UHPC-H-B-24h	25.9 *(+52%)*	0.85 *(+45%)*	37.5 *(+58%)*	2.19 *(+4%)*	37.0 *(+18%)*	5.82 *(-79%)*
UHPC-H-N-3d	22.2 *(+31%)*	0.51 *(-13%)*	32.8 *(+38%)*	1.99 *(-5%)*	34.9 *(+11%)*	16.58 *(-39%)*
UHPC-H-B-3d	31.5 *(+85%)*	1.29 *(+121%)*	46.3 *(+95%)*	4.55 *(+116%)*	41.4 *(+31%)*	14.30 *(-47%)*

* Desgination (A-B-C-D). A for mix design : UHPC/FRFC, D for curing method : H for thermal heating/A for ambient conditions, B for Mesh type : N for no mesh/B for basalt/S for steel, D for Age : 24 hours (24h) and 3 days (3d) . ^ ultimate load after yeilding occured

3.3.2. Load and Deflection Analysis for UHPC

As illustrated in Figure 9, four beams were retrofitted with UHPC under heating conditions for three hours. Like FRFC retrofitted beams, UHPC improved the cracking and yielding load of the retrofitted beams up to 53% and 54% when no mesh was added and up to 85% and 95% when basalt mesh is utilized. When ultimate capacity is analyzed, the improvements achieved in the load reach 31% with basalt mesh and up to 11% with no mesh, compared to the control beams. However, the deflection at ultimate was reduced by 32% and 21%, with no-mesh and with basalt mesh, respectively.

3.3.3. Comparison between FRFC and UHPC Strengthened Beams

The load-deflection curves for beams strengthened with FRFC and UHPC are shown in figure 10. At 24 hours, the cracking capacity of the UHPC retrofitted beams (UHPC-H-N-24h, UHPC-H-B-24h) was higher than FRFC-H-B-24h by ~43%. At 3 days, the basalt mesh presented a higher cracking, yielding and ultimate capacity by 79%, 35% and 11%, respectively, when added to the UHPC layer.

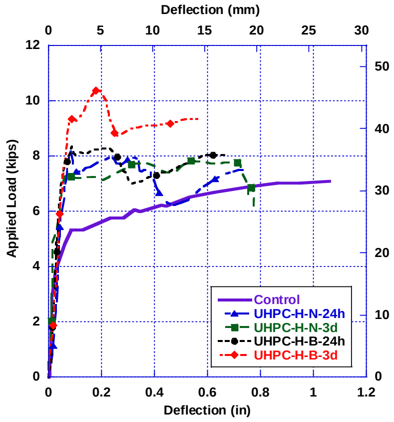

Figure 9. *Load-deflection of beams retrofitted with UHPC*

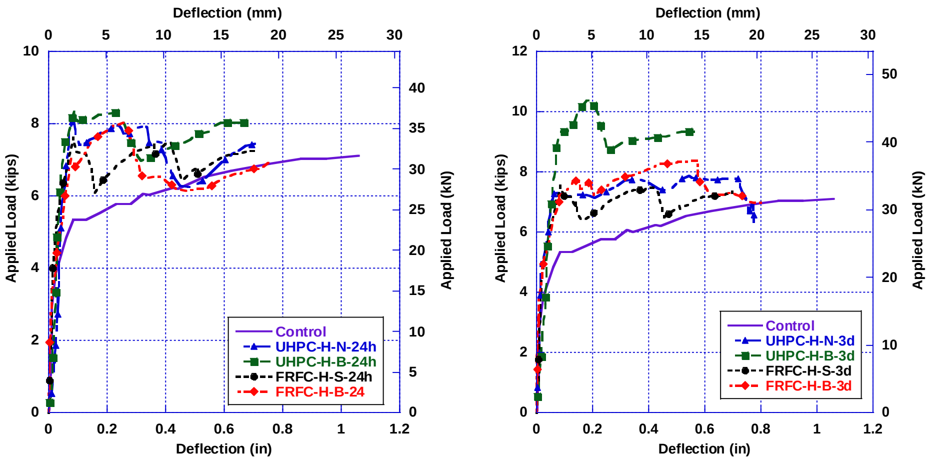

(a) *(b)*

Figure 10. *Load-deflection of beams retrofitted with UHPC vs FR-FC for (a) 24 h, (b) 3d*

3.3.4. Cracking analysis for the strengthened beams

As illustrated in Figure 11, the use of mesh within the repair layer combined with the heat curing presents a better crack control system compared to the ambient cured specimens. At 3 days, the crack width at the yielding of the flexural reinforcement level was reduced up to 43%, 49.5% and 46% for UHPC-H-B-3d, FRFC-H-B-3d, FRFC-H-S-3d. Compared to FRFC-H-B, UHPC repaired beams were effective in reducing the crack width by up to 12 and 57%, with no-mesh and with one layer of basalt fiber mesh. However, at 3 days, FRFC-H-B crack width was 59% and 11% less than UHPC-H-N and UHPC-H-B, respectively.

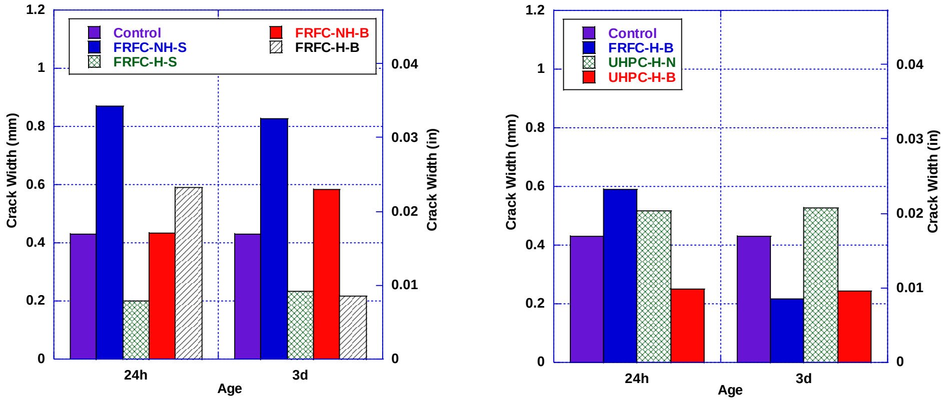

(a) (b)

Figure 11. *Crack Width Analysis at Yielding (a) 24 hours, (b) 3 days*

3.4. Conclusion and Recommendations

This paper presents the results of RC beams strengthened with fiber reinforced ferrocement and UHPC layer. Based on this study:

- The use of thermal blankets at a temperature between 100-120°F assists in accelerating the strength development of the FRFC and UHPC when used as a repair material.
- The use of basalt mesh in UHPC repair materials is crucial to control the crack width.
- Both UHPC and FRFC allow the strengthened member to exceed the ultimate capacity but not necessarily the deflection when measured at the concrete crushing point, compared to the control specimen.

4. REFERENCES

[1] NASSIF, H. H., & NAJM, H. (2004). "Experimental and analytical investigation of ferrocement–concrete composite beams". *Cement and Concrete Composites*, *26*(7), 787-796.
[2] ZHANG, Y., Li, X., ZHU, Y., & SHAO, X. (2020). "Experimental study on flexural behavior of damaged reinforced concrete (RC) beam strengthened by toughness-improved ultra-high performance concrete (UHPC) layer". *Composites Part B: Engineering*, *186*, 107834.

EXPERIMENTAL INVESTIGATION ON MECHANICAL PROPERTIES OF FERROCEMENT WITH NANOSILICA SYNTHESISED FROM ZEAMAYS

G.DEEPANA[1*], Dr.D.SHOBA RAJKUMAR[2*],

[1]. *Research Scholar, Department of Civil Engineering, Government College of Engineering, Salem, Tamilnadu, India*

[2].*Professor and Head, Department of Civil Engineering, Government College of Engineering, Salem, Tamilnadu, India*

SUMMARY: *Amorphous silica has been obtained from some agricultural waste yet with downsides on agglomeration challenges. In this work, the enhancement in the mechanical properties of ferrocement due to addition of nanosilica obtained from zea mays was investigated. Extraction of nanosilica from Zea mays was done by a series of process, which include corrosive pre-treatment by acid wash, calcination, draining, sol-gel adjustment, and post-filtration method. Nanosilica obtained by the process were portrayed by XRD, SEM, TEM and E-DAX for morphology, essential structure, molecular size, and surface size. Results got uncovered that pre-calcination corrosive treatment of the Zea mays improves the silica yield however decreased the Van der Waal's cooperation of the silica particles bringing about silica particles with a little level of agglomeration. Sodium silicate adjusted with ethylene glycol sol-gel treatment preceding titration decreased silica agglomeration. The stem, cob, leaves and husk of Zea mays plant were burnt separately at a temperature of 625^{0}C in a furnace and by XRD analysis it was found that the maximum silica content was present in leaves of Zea mays. NaOH was added to silica powder obtained by burning the leaves in order to get sodium silicate precipitate and then HNO_3 was added to the precipitate drop by drop and the residue was heated in oven at a temperature of 575^{0}C for about 1.5 hrs to obtain nanosilica powder which had a nanosilica content of 96.59% when analyzed by XRD. The size of the particle of the nanosilica obtained was measured to be 10 nanometer determined by TEM and SEM. The obtained nanosilica was added to cement mortar used for ferrocement specimen in various proportions of 1%, 1.5% and 2% and the mechanical properties were investigated. From the results it was concluded that the optimum percentage addition of nanosilica was 1.5% by weight of cement*.

KEYWORDS: *Zea mays, Nanosilica, Ferrocement, Mechanical properties, XRD, TEM, SEM.*

1. INTRODUCTION:

Nano materials are any organic, inorganic and organo metallic material with chemical, physical and electrical properties that also differ as a function of the material shape and size. This is commonly seen in the size ranging from 1 nm to a few ten nanometers in at least one dimension. These materials have very high proportions of surface atoms relative to interior ones. Also, due to quantum confinement effects, they are also subjected to properties variation. For both natural and industrial environment, nano material growth, dissolution and evaporation, surface reactivity and aggregation states play key roles in the lifetime. Several materials have recently been used for the improvement of concrete properties. Nanosilica is a reasonable admixture to cement, which contributes to better engineering properties. Nanosilica is a highly reactive pozzolana and could consume calcium hydroxide (CH) to form secondary C-S-H [15,16]. It reduces thermal cracking, improves durability, and increases strength. Silica is another term for silicon dioxide chemical compound. Each silica unit contains one silicon atom and two oxygen atoms.

2. LITERATURE REVIEW

Abdul Wahab et al (2013) has described the continuous demand of concrete to meet the various requirements and to carry out the research work in the area of concrete technology. Now a days, Nano technology is used in concrete in the form of nano materials like nano silica fume etc. to give superior properties. **PrasadaRao D.V. and Pavan Kumar M. (2014)** conducted experimental research to find the effect of nanosilica and fly ash on the strength properties of concrete with partial replacement for cement. **Lazaro A Quercia and Brouwers H.J.H. (2014)** studied the application of nanosilica in concrete produced by dissolution of olivine which showed high puzzolonic activity. This method is very cheaper than the other commercial methods because of low cost of the raw material and also less energy requirement. **Mikrajuddin Abdullah (2015)** suggested that the application of nanotechnology is an efficient way for reduction in the environmental pollution and to improve the durability of concrete. In his work, nanosilica was used as a filler material for concrete refractories to enhance particle packing**. Goltermann P. et al (1997)** discussed the main principle behind the high packing density concept and the minimization of void content. The result was low cement consumption, porosity, and low shrinkage; thus, concrete can achieve high performance. This concept was used in the mix design of high-performance cementitious mixes.

3. PREPARATION METHOD:

Dried Zea mays plants were collected from the nearby agricultural land after the harvest, rinsed with distilled water to remove soil and other particles, and then dried for 24 hours in open air. The stem, cob, leaves and husk were separated and ground subsequently to fine powder.

Figure 1. *Zea mays plant.*

4. EXPERIMENTAL TEST:

Nanosilica particles synthesized at high temperature was analyzed by various methods of characterization, such as X-ray diffraction (XRD), Scanning Electron microscope (SEM) and Transmission Electron Microscope (TEM)

4.1. Determination of the amount of silica present in various parts of zea mays plant by XRD:

Silica powder was prepared from various parts of the Zea mays such as stem, leaves, husk and cob burnt at a temperature 625ºC in muffle furnace. The XRD pattern of silica powder obtained from various parts analyzed separately showed a sharp peak of $2\theta = 23°$, which indicates that little or no crystalline structure occurs and that a large percentage of the particles are amorphous. The acid treatment of the Zea mays at temperature of 625ºC resulted in the formation of pure silica.

The synthesized silica particles were characterized under X-Ray Diffractometer with the radiation source of wavelength λ = 1.54Å. The XRD patterns of the nanosilica powder obtained from various parts of zea mays are shown in Figure2.

From the results obtained by XRD, it was found that zea mays leaves ash have high percentage of silica. In order to extract pure silica nano particles, 50 g of zea mays leaves ash was first boiled in a solution of 250 ml NaOH in order to form sodium silicate solution. pH of the solution was adjusted to 7.0 by adding HNO_3 drop by drop which thereby forms a precipitate. Thereafter, the sample was calcinated in the furnace for about 1.5hrs at the temperature of 575°C.

The experimental investigation was carried out further using the nanosilica powder obtained from zea mays leaves burnt at 575°C. The mechanical characteristics, i.e. compressive strength, tensile strength and flexural strength of cement mortar and ferrocement specimens due to addition of 1%,1.5% and 2% nanosilica was investigated.

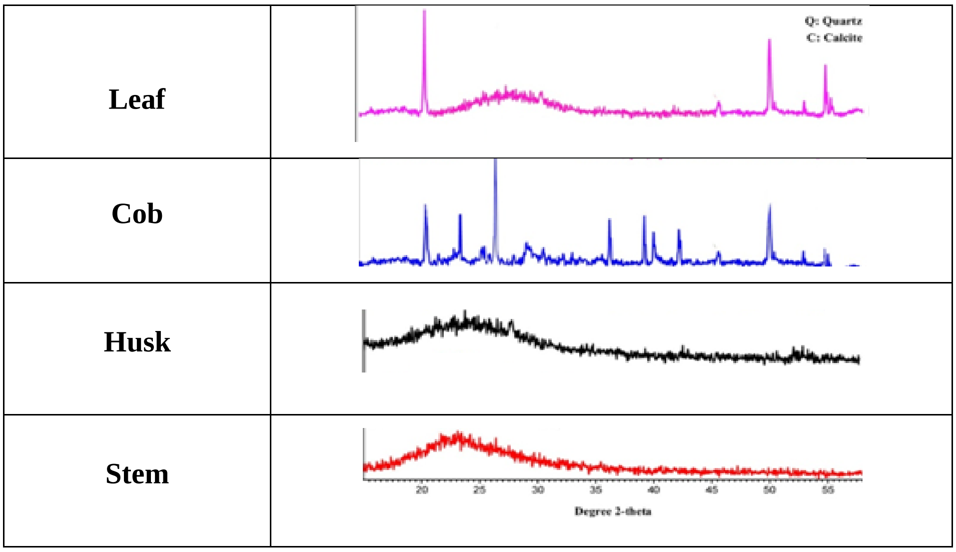

Figure 2. *XRD result of leaf, cob, husk and stem.*

4.2 Mix Proportions

The Cement mortar cubes were cast with cement sand ratio of 1:2, with water cement ratio of 0.4 and inclusion of nanosilica in percentages of 1%, 1.5% and 2% by weight of cement.

4.3 Casting of Specimen

Cement mortar cubes of size 100mmx100mmx100mm, ferrocement prisms of size 500mmx100mmx20mm and ferrocement tensile specimen (I shaped) with rib size of 300mm x 50mm x30mm were cast with various percentage inclusions of nanosilica. The cement mortar cubes and the ferrocement prisms were cured for a period of 3 days, 7 days and 28 days.

4.4 Testing of Specimen

Cement mortar cubes cast with and without nanosilica were tested on compression testing machine to find the compressive strength at 3 days, 7 days and 28 days. Also the flexural strength and tensile strength of ferrocement specimen with and without nanosilica were determined on Universal testing machine.

5. RESULTS AND DISCUSSIONS:

5.1.1. Determination of particle size of nanosilica by SEM:

Figure 3 Shows the SEM image of silica nanoparticles produced from ash obtained from leaves of Zea mays at ×3000 magnification. The particles were observed to be spherical with reduced silica-silica agglomeration. The average particle size of the extracted silica particles size were found to be between 10 to 0.5nm at 575°C.

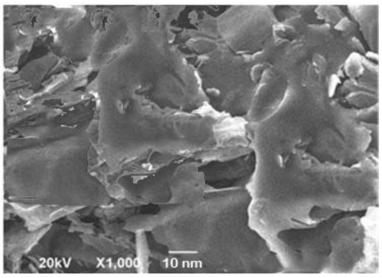

Figure3.*SEM image of nanosilica obtained from Zea mays leaf ash*

5.1.2. Analysis by TEM:

In transmission electron microscope, electron beam is transmitted through the thin sample. In order to get the best images, the best electron source needs to be used. The electrons produced by the gun are accelerated by the applied voltage. This accelerating voltage decides the electron wavelength. The wavelength of the electron (λ) is related to the accelerating potential (V) by an equation:$\lambda = (1.5 / V)^{1/2}$ where, λ is the wavelength in nanometers (nm) and V is the accelerating voltage in volt. Figure 4 exhibits the cross sectional view through TEM of nanosilica obtained from ash of Zea mays leaves.

The stream of the accelerated electrons is converged into a small, coherent beam by using electromagnetic lenses. The collimated beam of electrons falls on the specimen and some part of it is transmitted through the sample. This transmitted electron beam is focalized by the objective lens into an image. The image is then passed towards projector lens.

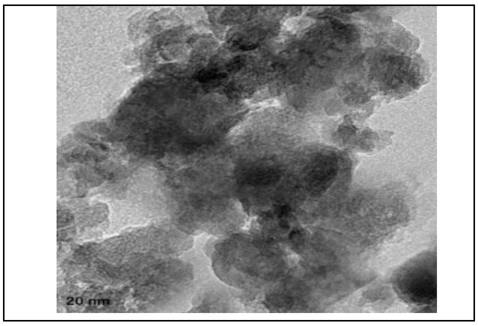

Figure4. *TEM image of nanosilica obtained from ash of Zea mays leaf.*

The image (electron beam) strikes the phosphor image screen and then the image become visible. The greyscale image can be viewed directly on TV screen. The dark area of TEM image, the region which is thick or dense indicates that few electrons were transmitted through the region. The light area of TEM image indicates those area of the specimen through which large number of electrons were transmitted as the region of sample is less dense or thin.

5.1.3. Determination of the amount of Nanosilica present by EDX:

Energy Dispersive X-Ray Analysis (EDX) is an X-ray technique used to identify the elemental composition of materials

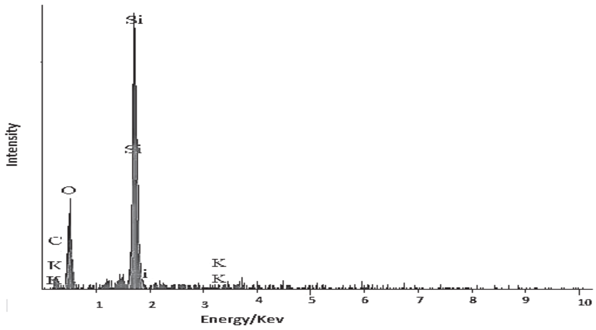

Figure5. *EDX image of nanosilica obtained from Zeamays leaf ash*

The technique can be qualitative, semi-quantitative, quantitative and also provide spatial distribution of elements through mapping. EDX result analysis pattern of nanosilica obtained from treated Zea mays leaves at 575℃ predicts that silica and oxygen have the highest peaks. A strong intensity of Si and O as shown in the EDX spectra in Figure5, confirms that silica (SiO_2) is the predominant element in the sample which is 96.59% of the total composition with negligible impurities.

5.2.1. Determination of Compressive strength of cement mortar:

The average compressive strengths for four configurations are presented in Table 1 and Figure 6. The average compressive strengths for the cement mortar with and without nanosilica are determined at 3days, 7days and 28 days. For all specimens, as the days elapsed the compressive strengths went on increasing. The increase in rate of compressive strength up to 7 days is fast and beyond 7days the strength gain is in slow phase.

Table 1 *Compressive strength of cement mortar with and without nanosilica*

S.No	Percentage addition of Nanosilica	Average Compressive strength (MPa)		
		3days	7 days	28 days
1	Control mix	25.46	31.065	34.335
2	1.0%	27.94	34.335	36.624
3	1.5%	30.55	36.297	42.837
4	2.0%	27.47	34.008	36.297

From the above result it was found that the optimum percentage addition of nanosilica is 1.5% as a decrease in strength was observed with increase in percentage of nanosilica. The 3days, 7days and 28 days compressive strength values for 1.5% addition of nanosilica were found to be 30.55MPa, 36.297MPa and 42.837MPa respectively. This shows that the increase in compressive strength due to addition of 1.5% nanosilica is 24.761%

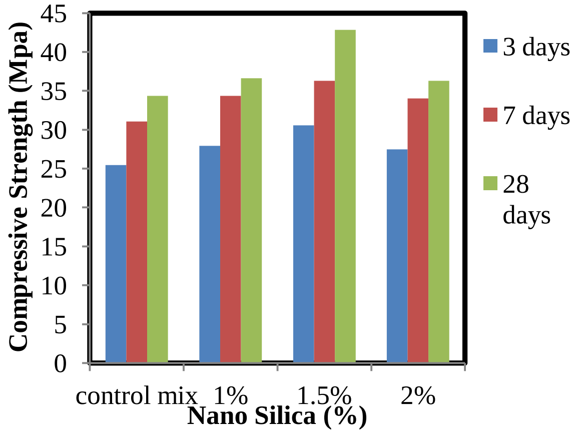

Figure 6.*Compressive strength of cement mortar with various percentage inclusion of nanosilica*

The cement mortar comprises of cement and fine aggregate. When cement mortar is made by mixing cement with fine aggregate and compaction is done, the cement particles fill the voids between the fine aggregate. Cement acts as a binding material. When nanosilica is added to cement mortar, the particles fill the voids at nano level between the cement particles. Till an addition of 1.5% nanosilica there is strength gain as the particles completely fill the voids and make the mortar component dense and impermeable. On further addition of nanosilica which is filler material, it doesn't contribute to any further increase in density or reduction in void ratio, porosity, impermeability, etc. but leads to reduction in binding of matrix by cement and therefore a decrease in strength is observed.

5.2.2. Determination of Flexural strength:

The average flexural strengths for four configurations are presented in Table 2 and Figure 7. The average flexural strength for the ferrocement specimens with and without nanosilica were determined at 3days, 7days and 28 days.

Table2 *Flexural Strength of ferrocement with and without nanosilica*

S.No	Percentage addition of nanosilica	Average Flexural strength MPa		
		3 days	7 days	28 days
1	Control mix	2.07	3.82	4.89
2	1%	2.58	3.97	5.06
3	1.5%	2.71	4.19	5.40
4	2%	2.46	4.03	5.20

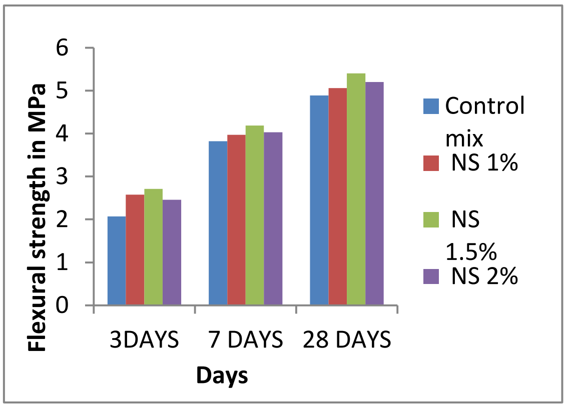

Figure7. *Flexural strength of ferrocement specimens with various percentage inclusion of nanosilica*

From the above results it was found that the optimum percentage addition of nanosilica is 1.5% as a decrease in strength was observed on increase in addition of nanosilica. The 3days, 7days and 28 days flexural strength values for 1.5% addition of nanosilica were found to be 2.71MPa, 4.19MPa and 5.40 MPa respectively. This shows that the increase in percentage of flexural strength due to addition of 1.5% nanosilica is 10.43%.

5.2.3. Determination of Tensile strength:

The average Tensile strengths for the four configurations are presented in Table 3 and Figure 8. The average tensile strength of cement mortar with and without nanosilica were determined at 3days, 7days and 28 days. .

Table 3 *Tensile Strength of Ferro cement specimen with and without nanosilica*

S.No	Percentage addition of nanosilica	Average Tensile strength (MPa)		
		3days	7 days	28 days
1	Control mix	1.91	3.53	4.52
2	1%	2.38	3.66	4.67
3	1.5%	2.51	3.87	4.98
4	2%	2.27	3.72	4.80

From the above results it was found that the optimum percentage addition of nanosilica is 1.5% as a decrease in strength was observed beyond this percentage addition of nanosilica. The 3days, 7days and 28 days tensile strength values for 1.5% addition of nanosilica were found to be 2.51MPa, 3.87MPa and 4.98 MPa respectively. This shows that the increase in percentage of tensile strength due to addition of 1.5% nanosilica is 10.18 %.

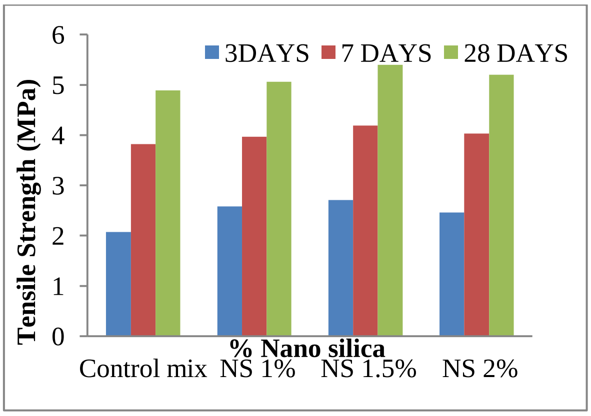

Figure8. *Tensile strength of ferrocement specimens with various percentage inclusion of nanosilica*

6. CONCLUSION:

In this work, the enhancement in mechanical properties of ferrocement due to addition of 1%, 1.5% and 2% of nanosilica was investigated. The compressive strength, tensile strength and flexural strength of ferrocement with the above percentage additions of nanosilica were found at 3 days,7 days and 28 days and the following conclusions are drawn. The addition of 1.5% nanosilica by weight of cement was found to be the optimum dosage for improvement in the mechanical properties. As the percentage of nanosilica was increased above 1.5%, its effect on strength gain decreased. The increase in compressive strength due to addition of 1.5% of nanosilica was found to be 24.76%. The increase in flexural strength was 10.43% and tensile strength increase by 10.18% due to addition of 1.5% of nanosilica. Hence, the mechanical properties are highly influenced by the inclusion of nanosilica in cement mortar.

7. REFERENCES:

[1]. Alberto Lazaro Garcia, George Quercia, Prof.Dr. H.J.H. Brouwers. (2010) “Production and application of a new type of Nanosilica in concrete”

[2]. Dr.D.V.PrasadaRao, M. Pavan Kumar IJARET (2014) vol.5 pp. 94-102. “A study on influence of fly ash and Nanosilica on strength properties of concrete”

[3]. Forood Torabian Isfahani et.al. Hindawi (2016), “Effects of Nanosilica on Compressive Strength and Durability Properties of Concrete with Different Water to Binder Ratios”

[4].G.Quercia&H.J.H.Brouwers(2010)"Application of Nanosilica (ns) in concrete mixture”

[5]. G.Quercia "8th fib PhD symposium in kgs.lyngby, Denmark (2010). “Application of Nanosilica in concrete mixtures”

[6]. HasanBiricik, NihalSarier (2014). "Comparative studies of the characteristics of Nanosilica, silica fumes and flyashincorporated cement mortars."

[7]. Hongxia Yang EMEIT (2012) "Strength and shrinkage property of Nanosilica power concrete"

[8]. Maheswaran S, Bhuvaneshwari B., Palani G.S, Nagesh R Iyer1 and Kalaiselvam S. (2012). "An overview on the influence of Nanosilica in concrete and research initiative"

[9]. Mohammad Reza ZamaniAbyaneh, Seyed Mahdi Mousavi, AlirezaMehran, Seyed Mohammad Mahdi Hoseini, Soroosh Naderi,3Farhad MesbahIrandoos Australian Journal of Basic and applied sciences,(2013) "Effects of Nanosilica on permeability of concrete and steel bars reinforcement corrosion."

[10]. Supit, S. W. M., &Shaikh, F. U. A. (2015). Durability properties of high volume fly ash concrete containing nano-silica. Materials and structures, 48(8), 2431-2445

[11]. Goltermann, P., Johansen, V., &Palbøl, L. (1997). Packing of aggregates: an alternative tool to determine the optimal aggregate mix Materials Journal, 94(5), 435-443

[12]. Haruehansapong, S., Pulngern, T., &Chucheepsakul, S. (2014). Effect of the particle size of nanosilica on the compressive strength and the optimum replacement content of cement mortar containing nano-SiO_2 Construction and Building Materials, 50, 471-477.

[13]. Berra, M., Carassiti, F., Mangialardi, T., Paolini, A. E., &Sebastiani, M. (2012). Effects of nanosilica addition on workability and compressive strength of Portland cement pastes, Construction and Building Materials, 35, 666-675

[14]P. Hou, S. Kawashima, D. Kong, D. J. Corr, J. Qian, and S. P. Shah, "Modification effects of colloidal nanoSiO_2 on cement hydration and its gel property," *Composites Part B: Engineering*, vol. 45, no. 1, pp. 440–448, 2013.

[15] S. Haruehansapong, T. Pulngern, and S. Chucheepsakul, "Effect of the particle size of nanosilica on the compressive strength and the optimum replacement content of cement mortar containing nano-SiO_2," *Construction and Building Materials*, vol. 50, pp. 471–477, 2014.

[16] Abdul waheb,B.Dean Kumar "Concrete Composites With Nanosilica , Condensed Silica Fume and Fyash-Study of Strength Properties",*International journal of scientific and Technology & Engineering Research,Volume 4, Issue5*,May 2013

[17] MikrajuddinAbdullah ," Improvement of concrete durability by nanomaterials",*the 5th international conference of Euro Asia Forum*125(2015)608-612.

EFFECTS OF FIBRE ORIENTATION ON THE BEHAVIOUR OF RC BEAMS IN VIBRATED AND SELF-COMPACTING CONCRETE

Bruno Leporace-Guimil[1], Antonio Conforti[2], Giovanni Plizzari[3], Pedro Serna[4], Francesco Sonzogni[5] and Claudio Failla[6]

[1]*University of Brescia, Brescia, Italy, b.leporaceguimil@unibs.it*

[2] *University of Brescia, Brescia, Italy, antonio.conforti@unibs.it*

[3] *University of Brescia, Brescia, Italy, giovanni.plizzari@unibs.it*

[4] *Universitat Politècnica de València, Valencia, Spain., pserna@cst.upv.es*

[5] *Magnetti Building S.p.A., Carvico, Italy, f.sonzogni@magnetti.it*

[6] *Civil Engineer, Milan, Italy, cla.failla@gmail.com*

SUMMARY: *Structural design of fibre-reinforced members should take into consideration fibre orientation since the residual properties of the material can be different as a function of the cracking plane position and inclination. Designers must be aware of the possible negative influence of fibre orientation and they may take advantages from its positive effect. Some international standards (i.e., fib Model Code 2010 and German standard DafStb) define a factor that should take into account the orientation effects. In this context, the present paper presents the results of an experimental program aimed at evaluating steel fibre orientation in RC beams. Three beams (0.15 m x 0.70 m x 4.10 m) were cast at Magnetti Building (Carvico, Italy) factory following the most common casting process adopted in practice by using vibrated and self-compacting concrete.*

KEY WORDS: *Steel fibres, fibre orientation, RC beams, fibre reinforced concrete, vibrated concrete, self-compacting concrete.*

1. INTRODUCTION

The *fib* Model Code 2010 (2012) [1] (hereafter MC2010) takes into consideration the fibres orientation in the design of Fibre Reinforced Concrete (FRC) elements since this factor can significantly affect the material residual properties. In a similar way, German standard DadStb (2012) [2] underlines the importance to consider this influence by a specific factor, which varies from 0.5 to 1. This factor represents the different post-cracking performances present in a real structure due to a different fibre orientation, as compared to the ones obtained from standard tests (i.e., small beams according to EN 14651). Therefore, designers must be aware of the negative influence of fibre orientation but they may also take advantages from its positive effect. Many studies demonstrate that fibres are oriented in concrete and different factors can affect their orientation [3-5]. However, the value of this factor is not clearly defined by standards due to the lack of experiments on real elements. Its values also depend on several factors: wall effect, casting and compaction process, fibre stiffness, among others. In addition, in self-compacting fibre reinforced concrete (SCFRC) a significant flow effect was observed; consequently, the casting procedures can modify the orientation of fibres along the elements. Other important factors are the geometry of the elements, as the depth or the width, and its relationship with the fibre length; the type of fibres (steel, polymer, glass) can also affect their orientation [6-7]. This paper presents the results of an experimental study performed with the aim of defining orientation factors for the design of RC beams reinforced by steel fibres. In fact, it is still questionable the value of the orientation factor that should be adopted in the design of structural elements. The orientation of fibres in Vibrated (VFRC) and Self-Compacting FRC was studied in RC beams 15 cm thick, 70 cm depth and 410 cm long. Based on this study, suitable orientation factors both for Serviceability Limit State (SLS) and Ultimate Limit State (ULS) verifications were provided.

2. EXPERIMENTAL PROGRAM

2.1. Materials

Three RC beams (Figure 1), one in VFRC and two in SCFRC (varying the casting procedure), were cast incorporating the same volume fraction (0.64%) of steel fibres. A base-concrete mixture was adopted for batches of VFRC and SCFRC. This base-concrete mixture was characterised by 400 kg/m^3 of Portland Cement 52.5 R, 130 kg/m^3 of filler, 670 kg/m^3 of sand, 440 kg/m^3 of washed sand, 610 kg/m^3 of gravel and a water/cement ratio of 0.43. Moreover, the same type and steel fibre content (50 kg/m^3) were employed for both materials (i.e., VFRC and SCFRC). The characteristics of the fibres are the following: hooked-end shape, length (l_f) of 50 mm, diameter (ϕ) of 1.05 mm, aspect ratio (l_f/ϕ) of 48 and tensile strength of 1000 MPa. Additionally, the amount of superplasticiser was varied in each concrete to obtain a good workability. VFRC showed a slump of 170 mm while SCFRC had a slump flow of 700 mm ± 20 mm. It should be noted that, aside from superplasticiser amount, all the other mix variables were kept constant.

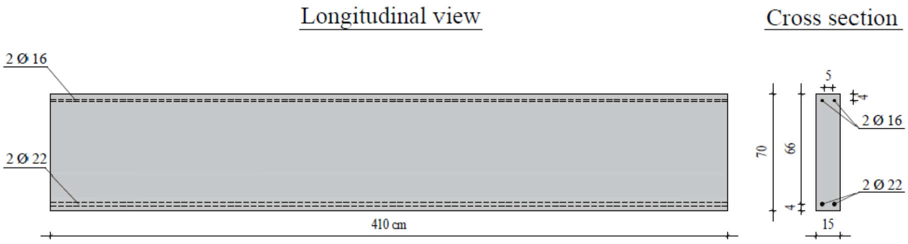

Figure 1. *Reinforcement details and geometry of RC beams (measures in cm).*

2.2. Test details

Three beams (15 x 70 x 410 cm), reinforced at the top with two rebars of diameter 16 mm and at the bottom with two rebar of diameter 22 mm (Figure 1), were cast employing two different casting procedures. In addition, beams (i.e., 150 x 150 x 600 mm), according to EN 14651 [8], were cast for FRC mechanical characterization and they are considered as Reference Specimens (RS) for VFRC, SCFRC and SCFRC-side, respectively. As already underlined, VFRC beam was compacted by external vibration, while SCFRC beams were made without any type of vibration.

As previously mentioned, two casting procedures were adopted. The left and right casting procedure was carried out placing the bucket above the left edge of the formwork and moving the bucket from the left to right. Using this procedure, the beam in VFRC and one in SCFRC were cast (Figure 2). The remaining RC beam in SCFRC was cast with the bucket fixed above the left edge allowing the mix flowing freely up to a height of 65 cm approximately, then the beam was completed shifting the bucket from the left to right edge, as shown in Figure 3. The latter was named SCFRC-side. Once again, it should be underlined that VFRC beam was externally vibrated while no vibration was adopted in the case of SCFRC and SCFRC-side beams.

After 28 days of ageing, the RC beams were sawn in order to evaluate their material mechanical characterisation in different directions, namely the vertical and horizontal ones. The RC beams was divided in several elements, as shown in Figure 4: top elements 15 x 7 x 104 cm (TOP 1,2,3,4); bottom elements 15 x 7 x 104 cm (BOTTOM 1,2,3,4); twelve vertical and horizontal small beams of about 15 x 15 x 55 cm. Consequently, the dimensions of the vertical and horizontal small beams, cut off from the RC beams, were chosen perfectly in accordance with EN 14651 [8].

The cut of top and bottom elements was instead carried out for the purpose of understanding how the rebars could influence the fibre orientation. All small beams were notched prior to testing.

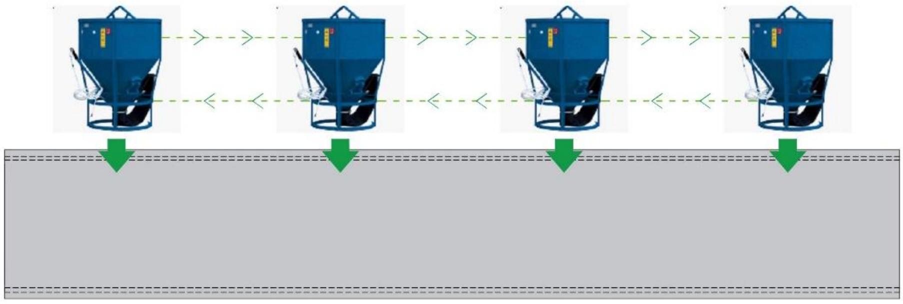

Figure 2. *Casting procedure adopted for VFRC and SCFRC beams.*

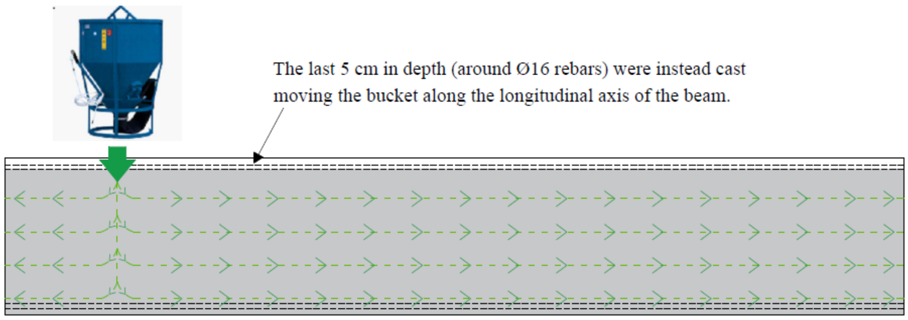

Figure 3. *Casting procedure adopted for SCFRC-side beam.*

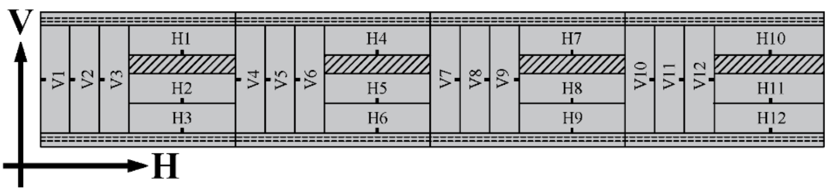

Figure 4. *Schema of vertical and horizontal small beams with specimen identification.*

Three-Point Bending Tests (3PBT) were carried out (according to EN 14651) to analyse the post-cracking behaviour of the vertical and horizontal small beams previously described. Since each full RC beam was characterised by twenty-four small beams, the whole experimental program dealt with ninety small beams among vertical, horizontal and reference specimens. The limit of proportionality (f_L), as well as the residual flexural tensile strength f_{R1}, f_{R2}, f_{R3} and f_{R4}, corresponding to a Crack Mouth Opening Displacement (CMOD) value of 0.5, 1.5, 2.5 and 3.5 mm, respectively, were measured. At the end of bending tests, the number of fibres on the fracture surface was also counted to determine the fibre density.

3. EXPERIMENTAL RESULTS AND DISCUSSION

Table 1 shows the mechanical properties of each FRC material in terms of mean values of cube compressive strength and post-cracking flexural tensile strength (measured on Reference Specimens (RS) according to EN 14651). The latter concern the limit of proportionality (f_L) and the residual strengths f_{R1} and f_{R3} (the coefficients of variation (CV) are provided in brackets). As expected, vibrated concrete and self-compacting concretes have the same compressive strength (around 60-65 MPa), respectively. Besides, the post-cracking response is almost similar in vibrated and self-compacting FRC even if VFRC and SCFRC/SCFRC-side are characterised by very different workability properties.

Table 1. *Mechanical properties of vibrated and self-compacting concretes.*

FRC	$f_{c,\,cube}$ [MPa]	f_c [MPa]	$f_{L,\,RS}$ [MPa]	$f_{R1,\,RS}$ [MPa]	$f_{R3,\,RS}$ [MPa]
VFRC	77.1 (0.07)	64.0	5.05 (0.08)	6.09 (0.12)	6.29 (0.15)
SCFRC	72.0 (0.02)	60.0	6.76 (0.06)	6.96 (0.08)	6.39 (0.08)
SCFRC-side	78.5 (0.04)	65.2	4.95 (0.09)	6.38 (0.17)	6.10 (0.17)

Figure 5 compares the stress–CMOD curves obtained from vertical and horizontal small beams sawn from VFRC, SCFRC and SCFRC-side full-beams. It is worth noting the variability on the post-cracking response of FRC, which is remarkably higher than that of the standard specimens (EN 14651). Analysing the results from VFRC beam, it can be appreciated that neither vertical nor horizontal small beams were able to reach the mean curve of Mean RS-VFRC (in red continuous line). In fact, the mean curve for vertical small beams (i.e., Mean-V) is around 74% lower than Mean RS- VFRC while the reduction of the horizontal small beams (i.e., Mean-H) is around 45%. A similar behaviour was found for SCFRC beam where the mean curves of the vertical and horizontal small beams are still under the Mean RS-SCFRC, showing a reduction of 64% and 25% (as compared to the reference specimens) for Mean-V and Mean-H, respectively. When referring to the SCFRC-side beam, the mean curve of the vertical small beams is still under the mean curve of the reference specimens (66% reduction compared to Mean RS- SCFRC-side) but in the horizontal small beams the situation is much better since the mean curve differs roughly ±10% from that of the reference specimens. Furthermore, for SCFRC-side beam, the performance in the post-cracking phase is better than in the reference specimens for 50% of the horizontal small beams. Therefore, for a given casting procedure, the fibre orientation in RC beams made of VC and SCC is not significantly different, while the fibre orientation becomes more evident when the casting position is mostly kept in one side of the beam and a significant concrete flow can be observed.

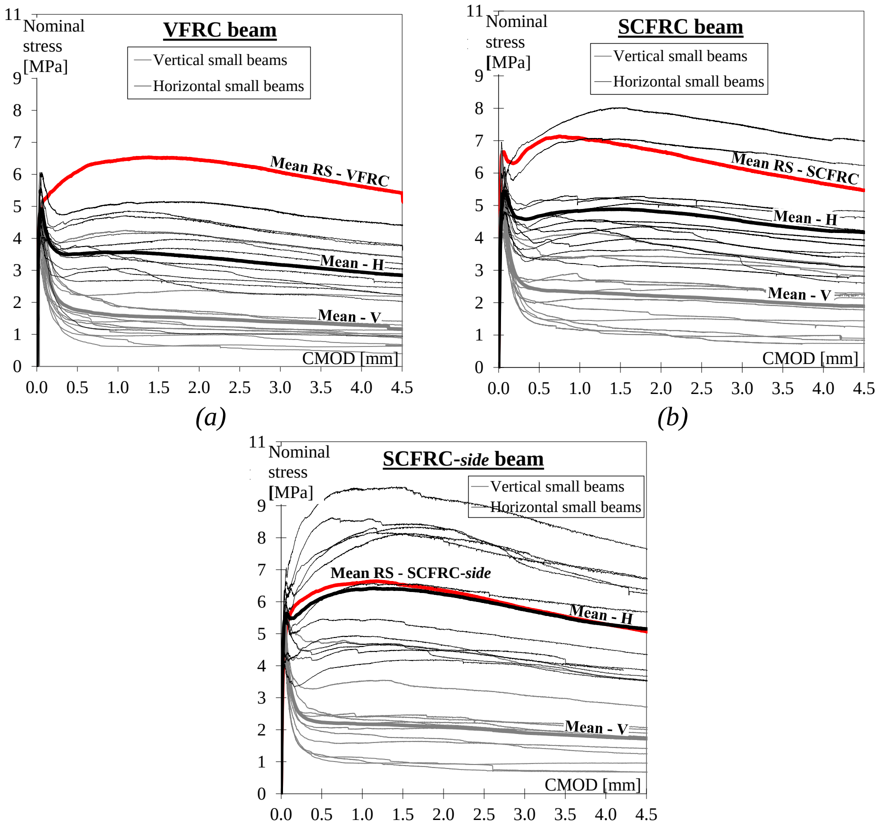

Figure 5. *RC beam in VFRC (a), SCFRC (b) and SCFRC*-side *(c).*

The ratio between residual flexural strength of VFRC, SCFRC and SCFRC-side small beams (i.e., vertical and horizontal ones) and the residual strength of Mean RS, at 3.5 mm (f_{R3}) of CMOD, are compared in Figure 6. The ratios are represented with cold colours for low ratios from 0.09 to 0.79, and warm colours for ratios between 0.80 and 1.47. Besides, the grey colour concern the parts that were not tested under 3 PBT. The contrast between cold and warm colours represents how fibres are oriented into the beams at different points. As already underlined, horizontal small beams have a better post-peak behaviour than vertical small ones, showing that fibres tend to be oriented in a horizontal plane instead of a vertical one. Figure 6 shows also the different fibre orientation observed in SCFRC-side beam, as compared to the other ones, evidencing the positive influence of both flow and wall effect.

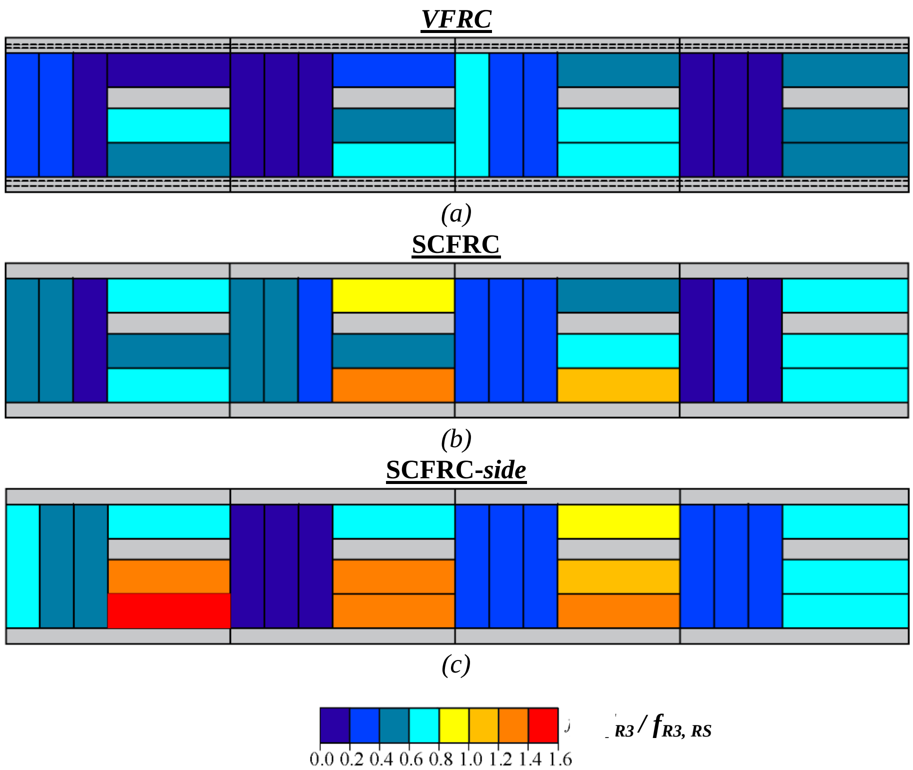

Figure 6. *$f_{R3}/f_{R3,\,RS}$ ratios in RC beams in VFRC (a), SCFRC (b) and SCFRC*-side *(c).*

In MC2010 (2012) [1] an orientation factor "*K*" is introduced to take into account the possible anisotropy of fibre distribution. This *K* is smaller than one for favourable effects or bigger than one for unfavourable effects. In this work, a step forward is made to include in *K* the effect of the manufacturing process and concrete rheology since this effect can change the post-cracking behaviour of FRC structural members. Based on the previous results, orientation factors to better evaluate the crack control at Serviceability Limit State (SLS) and the bearing capacity at the Ultimate Limit State (ULS) were evaluated and the values are listed in Table 2. The proposed factors were calculated in different sections considering the depth of the neutral axis at both SLS and ULS. Figure 7 shows the case of SLS where the effective tension area of concrete ($A_{c,ef}$) was adopted in order to quantify the contribution of the fibres, according to MC2010 (2012) [1]. At ULS, the part of the cross section in tension (thus cracked) was considered to take into account fibre contribution. Based on diagrams of the flexural residual strength versus fibre density, obtained in this research and reported in [9], f_{R1} and f_{R3} were found for VFRC, SCFRC and SCFRC-side members at the zones where f_{R1} and f_{R3} were not available.

Table 2: *Orientation factors for crack control (SLS) and flexural (ULS) design of RC beams in VFRC, SCFRC and SCFRC-side.*

Beam	SLS K_{SLS} Positive moment	ULS K_{ULS} Positive moment
VFRC	1.1	1.6
SCFRC	0.8	1.4
SCFRC-side	0.7	0.8

Positive bending moments were considered since this beam represents a web of a precast element simply supported at its ends. It can be observed in Table 2 that orientation factors are different between VFRC, SCFRC and SCFRC-side beams, due to the positive influence of flow and wall effects in SCFRC (especially at beam bottom) and SCFRC-side beams.

However, future works should be carried out to analyse these factors also in the case of shear strength predictions.

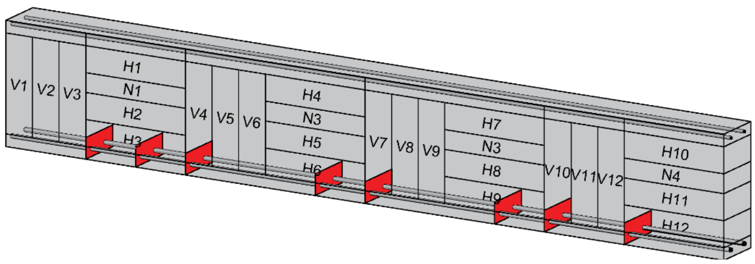

Figure 7. Areas ($A_{c,ef}$) considered to evaluate the orientation factor for crack control at SLS.

4. CONCLUDING REMARKS

Orientation factors in RC beams made with vibrated (VFRC) and self-compacting (SCFRC/SCFRC-side) fibre reinforced concretes were experimentally studied. The following conclusions might be drawn:

- For a given fibre amount, the post-cracking mechanical properties evaluated by three-point bending tests on notched beams (according to EN 14651) are similar between vibrated and self-compacting fibre reinforced concrete.

- For a casting procedure characterized by the bucket in movement along the beam axis, the fibre orientation in RC beams made in VC and SCC is not significantly different (excluding the zones close to beam bottom), while the fibre orientation becomes pointedly different when the casting position is mostly kept in one side of the beams. This is due to wall and flow effects.

- Orientation factors for the design at SLS (crack control) and ULS (flexural bearing capacity) of RC beams made of either vibrated or self-compacting concrete with 50 kg/m^3 of steel fibres were provided. These factors are summarized in Table 2.

Further studies will be carried out on the influence of fibre orientation on the shear behaviour of RC beams.

ACKNOWLEDGEMENTS

The Authors are indebted to the technicians Luca Martinelli and Andrea Delbarba of the Laboratory for Testing Materials and Structures “P. Pisa” of the University of Brescia, for the assistance provided during the entire experimental program.

4. REFERENCES

[1] Fédération Internationale du Béton (2012). fib Model Code for Concrete Structures 2010. (MC2010); [Volume 1, ISBN 978-2-88394-105-2; Volume 2, ISBN 978-2-88394-106-9].

[2] Deutscher Ausschuss für Stahlbeton (DAfStb) (2012). Guideline. German Committee for Reinforced Concrete, Steel fibre reinforced concrete; design and construction, specification, performance, production and conformity, execution of structures – draft.

[3] EDGINGTON J. and HANNANT D.J. (1972). “Steel fibre reinforced concrete. The effect on fibre orientation of compaction by vibration”. *Material and Structures*; 5(1):41-44.

[4] KOOIMAN A.G. (2000). Modelling steel fibre reinforced concrete for structural design. Ph.D. Thesis, Dept. of Structural and Building Eng., Delft University of Technology, 184 p.

[5] TORRIJOS M.C., BARRÁGAN B., and ZERBINO R. (2010) “Placing conditions, mesostructural characteristics and post-cracking response of fibre reinforced self-compacting concretes”. *Construction and Building Materials*; 24:1078-1085.

[6] Conforti A, Cuenca E, Zerbino R, Plizzari G. 2021. Influence of fibre orientation on the behavior of fibre reinforced concrete slabs, *Structural Concrete*, DOI: 10.1002/suco.202000612.

[7] ZERBINO R., TOBES J.M., BOSSIO M.E., and GIACCIO G. (2012). “On the orientation of fibres in structural members fabricated with self-compacting fibre reinforced concrete”. *Cement and Concrete Composites*; 34:191-200.

[8] EN 14651 (2005). European Committee for Standardization (2005). Test method for metallic fibre concrete; pp. 18.

[9] Leporace-Guimil B. (2021). “Design aspects and chloride-induced corrosion behaviour of fibre reinforced concrete structures”. Università degli Studi di Brescia, 2020.

Session 7
Carbon TRC
in
Structural Applications

MECHANICAL BEHAVIOUR OF CARBON TEXTILE REINFORCED CONCRETE BEAMS

Rebecca Mansur de Castro Silva[1], Flávio de Andrade Silva[2]

[1]*R.M.C. Silva, Department of Civil and Environmental Engineering, Pontifícia Universidade Católica do Rio de Janeiro, Rio de Janeiro, Brazil, beccamansur@hotmail.com*

[2] *F.A. Silva, Department of Civil and Environmental Engineering, Pontifícia Universidade Católica do Rio de Janeiro, Rio de Janeiro, Brazil, fsilva@puc-rio.br*

SUMMARY: *Textile reinforced concrete (TRC) is a cementitious composite reinforced with multiple layers of fabrics. It presents elevated mechanical properties, thus showing a good potential to be employed as external strengthening for existing structures and for the construction of new elements. Due to the non-corrosive characteristic of the textiles, the TRC is an interesting alternative for steel reinforced concrete in elements that are more prone to suffer from corrosion. This work aims to study the mechanical behaviour of small beams made of carbon TRC. Two different textile reinforcement layouts were analysed. The results obtained from four-point bending tests showed that the beams presented the typical deflection hardening characteristic of the TRC. Furthermore, the experimental maximum bending moments were compared to theoretical ones.*

KEY WORDS: *Textile reinforced concrete, carbon fabric, mechanical behaviour, structural elements.*

1. INTRODUCTION

Textile reinforced concrete (TRC) is a cementitious matrix composite reinforced with one or more layers of two- or three-dimensional fabrics [1]. These materials present elevated mechanical properties and load-bearing capacity, being suitable for external strengthening applications [2–4] and construction of new elements [5–7].

The mechanical behaviour of the TRC is influenced by the properties of the cementitious matrix and the textile reinforcement, and also by the bond between these two phases. A way to improve the bond between the fabrics and the cementitious matrix is impregnating the textile yarns [8–11]. Usually polymeric coatings are used. However, some delamination between the matrix and the textile layers may occur [11]. The addition of a sand layer over the fresh polymer can avoid this, and further increase the bond between the reinforcement and the matrix by creating a friction mechanism [10].

Due to the non-corrosive nature of the textile reinforcements [12,13], the TRC appears as a suitable alternative for the conventional steel reinforced concrete in the cases where the structural elements are more prone to suffer from corrosion, such as in marine environments. However, due to the lack of design recommendations and codes, the TRC is still not used regularly in the civil construction practice.

This work aims to present a study on the mechanical behaviour of a short beam made of carbon textile reinforced concrete. Four-point bending tests with a span of 1100 mm were performed. Two reinforcement configurations were analysed: one with textile reinforcement only in the longitudinal direction of the beam (B1) and the other with textile reinforcement in both longitudinal and transversal directions (B2). A self-compacting concrete with 2% (by volume) of dispersed steel fibres was used as matrix, and a carbon fabric with a coating of styrene-butadiene resin, developed by V.Fraas GmbH, was used as reinforcement. To improve the bond between the carbon fabric and the cementitious matrix, an additional coating made with epoxy resin and sand was applied to the fabrics. Additionally, the theoretical maximum bending moment was obtained through two different methods and compared to the experimental one.

2. EXPERIMENTAL PROGRAM

2.1. Materials

A self-compacting concrete (SCC) with 2% (by volume) of dispersed steel fibers (SF) was used as cementitious matrix, with composition as presented in Table 1. The SCC had a water/cementitious materials ratio of 0.25. The hooked end steel fibers were supplied by Dramix® and presented 30 mm length, aspect ratio of 45 and tensile strength of 1270 MPa. The average compressive strength and elastic modulus at 28 days of the SCC-SF was 81 MPa and 35 GPa, respectively.

A carbon fabric developed by V.Fraas GmbH with a styrene butadiene resin as polymeric coating was used as primary reinforcement. With an opening mesh of 10 x 8.5 mm (Figure 1.a), the fabric presents tensile strength of 1700 MPa and elastic modulus of 250 GPa. An additional coating made with epoxy resin Sikadur®-32 and sand was applied over the fabric (Figure 1.b) to enhance its bond with the concrete [14].

Table 1. *Cementitious matrix composition.*

	kg/m³
Cement Type CP-V ARI	360
Gravel (9.5 mm)	438
River sand (0.850 mm)	100
River sand (0.150 mm)	827
Fly ash	168
Silica fume	45
Silica 325	70
Water	166
Superplasticizer	19.8
Steel fiber	157

(a) (b)

Figure 1. *Carbon fabric* **a)** *plain;* **b)** *with epoxy resin and sand coating.*

2.2. Composite manufacturing

Two carbon textile reinforced concrete beams with 1200 x 150 x 150 mm (length x width x height) and a 25 mm notch in the mid-span were produced. The beam B1 presented only longitudinal textile reinforcement, while the beam B2 presented both longitudinal and transversal textile reinforcement. The longitudinal and transversal directions are related to the beam axis. The textile longitudinal reinforcement consisted of 2 layers of the carbon fabric with the additional epoxy resin and sand coating for both beams, resulting in a longitudinal textile reinforcement level of 0.356%.

The beam B1 was casted with a hand lay-up technique: (i) a thin layer of 30 mm of concrete was placed in the bottom of a wood mold; (ii) the first layer of the textile reinforcement was placed over it; (iii) a second layer of 30 mm of concrete was placed over the fabric; (iv) the second and final layer of the textile reinforcement was placed; (v) the mold was filled up with the concrete; (vi) the concrete was consolidated. Figure 2.a shows the process of the beam B1 casting.

The beam B2 was casted similar to a conventional steel reinforced concrete beam, due to the presence of the transversal textile reinforcement. First, the reinforcement was assembled, as shown in Figure 2.b, and then it was positioned inside the wood mold. The concrete was poured over it and then consolidated.

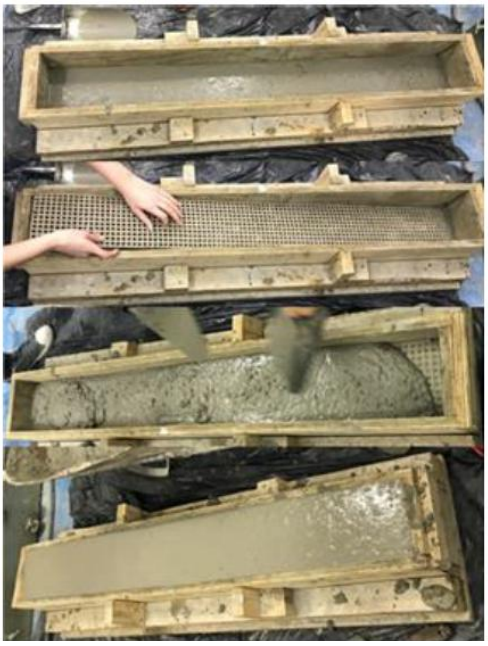

(a)

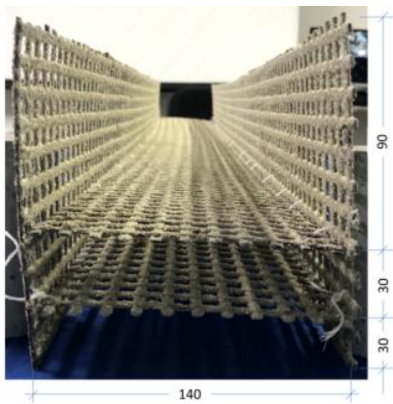

(b)

Figure 2.a) *Hand lay-up technique for the casting of the beam B1.* **b)** *Cross section of the textile layout of the beam B2.*

2.3. Bending tests

Four-point bending tests were performed to obtain the flexural behavior of the carbon textile reinforced concrete beams. The tests were conducted in an MTS servo-controlled hydraulic system with 500 kN capacity by a displacement control of 1mm/min. Two LVDTs were used to obtain the deflection at the mid-span of the beams. Figure 3 shows the setup used for the bending tests. Both support and load application rollers had free horizontal displacement.

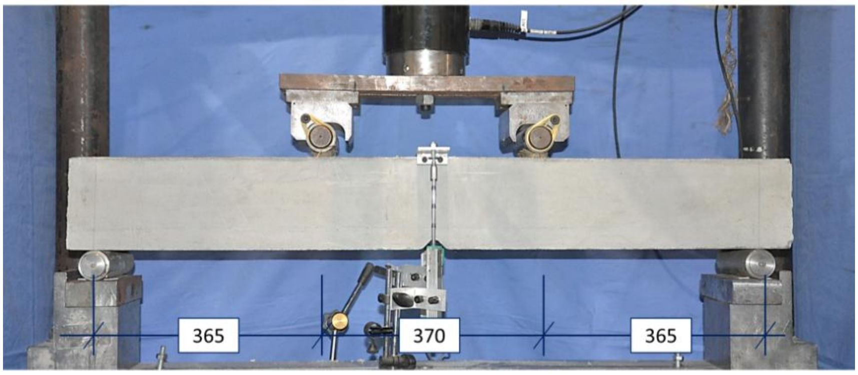

Figure 3.*Setup for the 4-point bending tests. (Dimensions in mm)*

3. RESULTS AND DISCUSSION

The load *vs.* displacement curves obtained from the bending tests are shown in Figure 4. Both beams presented multiple flexure cracks and a deflection hardening behaviour, which is consistent with the typical mechanical behaviour of TRC [15]. The beam B1 presented a shear and flexure failure. The crack that led to the element rupture was formed at one of the load application points, where both shear and bending stresses are maximum. The dispersed steel fibres contribute to the support of the tensile forces through diagonal cracks, enhancing the shear strength of concrete elements under flexure loadings. In beams without stirrups, they can lead to multiple diagonal cracking, enhancing the element ductility [16,17]. The beam B2 presented a pure flexure failure. The difference in the failure mode indicates that the transversal textile reinforcement was able to support the shear stress that could not be withstood by the short dispersed steel fibres.

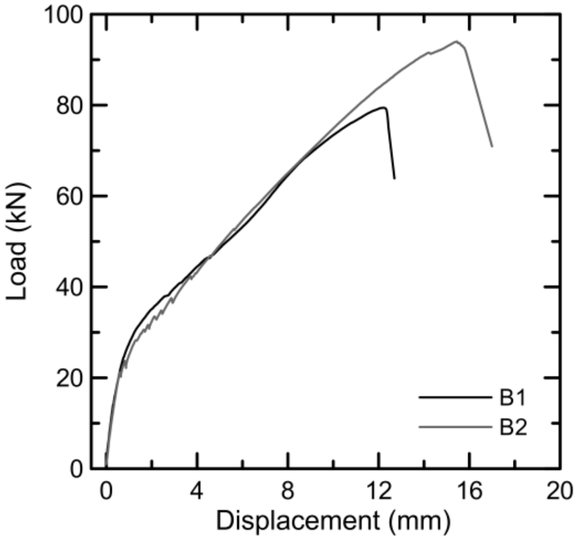

Figure 4. *Load vs. displacement curves obtained from the bending tests.*

The maximum bending moments were theoretically obtained by using the Rilem Report 36 method ($M_{max,Rilem}$) [15] and the simplified Henager and Doherty's model ($M_{max,H-D}$) [18]. The main difference between the models is that the first one does not consider the tensile strength of the concrete, which is enhanced by the addition of the short fibres.

In the Rilem Report 36 method, the bending moment is obtained through Eq. 1.

$$M_{\max} = k_{fl,\rho} \cdot F_{ctu} \cdot z \tag{1}$$

$$F_{ctu} = k_1 \cdot k_2 \cdot k_{0,\alpha} \cdot A_t \cdot f_t \tag{2}$$

$$k_1 = \frac{\sigma_{\max}}{f_t} \tag{3}$$

Where $k_{fl,\rho}$ is a factor that considers the effect of the beam curvature on the fabric; F_{ctu} is the design tensile strength of the textile reinforcement; z is the inner level; k_1 is the factor for the textile efficiency; k_2 is the factor for biaxial loading; $k_{0,\alpha}$ is the factor for orientation of the reinforcement; A_t is the cross-sectional area of reinforcement in the beam; f_t is the tensile strength of the reinforcement; and σ_{max} is the tensile strength of the reinforcement in the composite. Usually, $z \sim 0.9d$ and d ~ $0.9h$, where d and h are the effective and full height of the element, respectively. In this work, k_1 was calculated as 0.79 (see below), and k_2 and $k_{0,\alpha}$ was considered 1.

The factor $k_{fl,\rho}$ is obtained correlating the tensile strength of the textile reinforcement of specimens submitted to tensile and flexural loadings. For carbon fabrics, [15] recommends:

$$k_{fl,\rho} = 0.9 + 0.55 \cdot \rho \tag{4}$$

Where ρ is the beam longitudinal reinforcement ratio (0.356%).

To obtain the tensile strength of the reinforcement in the composite (σ_{max}) the ultimate load obtained in the direct tensile test performed by [14] was divided by the cross-sectional area of reinforcement. For a composite with two layers of the SBR with the additional epoxy and sand coating carbon fabric, the maximum strength obtained was 32.8 MPa. The cross-sectional area of the reinforcement corresponds to the area of the longitudinal yarns inside the composite (9 longitudinalyarns/layer). According to the supplier, the yarns are made of 48k carbon filaments. The diameter of a carbon filament is considered approximately 7 μm.

In the simplified Henager and Doherty's model, the non-dimensional parameters k_x and μ are obtained from equilibrium conditions.

$$k_x = \frac{x}{h} = \frac{\rho_t \, {f_t}/{f_c} + {f_{ctr}}/{f_c}}{{f_{ctr}}/{f_c} + \eta\lambda} \tag{5}$$

$$\mu = \frac{M}{A_c \cdot h \cdot f_c} = \rho_t \frac{f_t}{f_c}\left(0.9 - \lambda \frac{k_x}{2}\right) + \frac{f_{ctr}}{f_c}\frac{(1-k_x)}{2}\left[1-(1-\lambda)k_x\right] \tag{6}$$

Where M is the bending moment; f_c and f_{ctr} are the compressive and the residual tensile strength of the concrete, respectively; f_t is the tensile strength of the textile reinforcement (1700 MPa); ρ_t is the longitudinal textile reinforcement ratio (0.356%); η and λ are coefficients for the parabola-rectangle diagram of the concrete compression zone. It was assumed $\eta = 1$ and $\lambda = 0.8$. The residual tensile strength of concrete (f_{ctr}) corresponds to the strength obtained for a crack opening of 2.5 mm in a 3-point bending test [19]. In this work, $f_{ctr}=0.88$ *MPa*, as described in [20].

Table 2 presents the results of the maximum bending moments of the TRC beams obtained experimentally ($M_{max,exp}$) and theoretically, using the Rilem Report 36 method ($M_{max,Rilem}$) [15] and the simplified Henager and Doherty's model ($M_{max,H\text{-}D}$) [18]. The small difference in the experimental and Rilem theoretical results for the beam B1 could indicate that this method is suitable for the maximum bending prediction. However, it is important to note that the beam B1 did not reach its maximum bending capacity since its failure was not a pure flexure rupture. Furthermore, the theoretical maximum bending capacity could be under-designed once that the concrete tensile strength is not considered. The beam B2 presented a pure flexure failure, thus reaching its maximum bending capacity. For the beam B2, the difference between the experimental and the Rilem Report 36 model and the Henager and Doherty's model results is 1.20 and 0.91, respectively. The lower difference of the second method indicates that this method seems to be more adequate for the prediction of TRC beams with the addition of short fibres.

Table 2.*Maximum bending moments for the TRC beams.*

Beam	$\rho_{longitudinal}$ (%)	$M_{max,exp}$ (kNm)	$M_{max,Rilem}$ (kNm)	$M_{max,H\text{-}D}$ (kNm)
B1	0.356	14.6	14.3	18.8
B2	0.356	17.2	14.3	18.8

4. CONCLUSIONS

The following conclusions can be draw from the present work:

- The carbon TRC beams presented multiple flexure cracks and a deflection hardening behaviour.
- The short dispersed steel fibres contributed to support part of the tensile stress through diagonal cracks.
- The beam B1 presented a combined shear and flexure failure, indicating that in the volume fraction that they were added, the steel fibres were not able to fully support the shear stresses.
- The beam B2 presented a pure flexure failure. The transversal textile reinforcement combined with the steel fibres was able to support the shear stresses.
- The simplified Henager and Doherty's model seems to be more adequate than the Rilem Report 36 method to design the flexural capacity of TRC beams with short dispersed fibres. This model considers the tensile strength of the concrete, which is not negligible due to the presence of the short fibres.

5. REFERENCES

[1] NAAMAN A.E. Textile reinforced cement composites: competitive status and research directions. *International RILEM Conference on Material Science*., Aachen: 2010, p. 3–22.

[2] TRIANTAFILLOU T.C., PAPANICOLAOU C.G. Shear strengthening of reinforced concrete members with textile reinforced mortar (TRM) jackets. *Materials and Structures*, vol.39, 2006, p. 93–103.

[3] NANNI A. A New Tool for Concrete and Masonry Repair. *Concrete International*, vol. 34, n° 4, 2012, p. 43-49.

[4] BABAEIDARABAD S., LORETO G., NANNI A. Flexural strengthening of RC beams with an externally bonded fabric-reinforced cementitious matrix. *Journal of Composites for Construction*, vol. 18, n° 5, 2014, p. 04014009-12.

[5] HEGGER J., VOSS S. Investigations on the bearing behaviour and application potential of textile reinforced concrete. *Engineering Structures*, vol. 30, n° 7, 2008, p. 2050-2056.

[6] HEGGER J., KULAS C., SCHNEIDER H.N., BRAMESHUBER W., HINZEN M., RAUPACH M., BÜTTNER T. TRC Pedestrian Bridge - Design, Load-bearing Behavior and Production Processes of a Slender and Light-weight Construction. *International RILEM Conference on Material Science*, vol. 1, 2010, RILEM Publications SARL, p. 353-364.

[7] SCHUMANN A., MICHLER H., SCHLADITZ F., CURBACH M. Parking slabs made of carbon reinforced concrete. *Structural Concrete*, vol. 19, n° 3, 2018, p. 647-655.

[8] RAUPACH M., ORLOWSKY J., BÜTTNER T., DILTHEY U., SCHLESSER M., HEGGER J. Epoxy-impregnated textiles in concrete-Load bearing capacity and durability. *1st International RILEM Conference on Textile Reinforced Concrete*, 2006, Aachen, RILEM Publications SARL, p. 77-88.

[9] BÜTTNER T., KEIL A., RAUPACH M. Improvement of the load-bearing capacity and durability of textile-reinforced concrete due to the use of polymers. *15th Congress of the Glassfibre Reinforced Concrete Association International*, 2008, Prague, p. 20-23.

[10] DONNINI J., CORINALDESI V., NANNI A. Mechanical properties of FRCM using carbon fabrics with different coating treatments. *Composites Part B: Engineering*, vol. 88, 2016, p. 220-228.

[11] DVORKIN D., PELED A. Effect of reinforcement with carbon fabrics impregnated with nanoparticles on the tensile behavior of cement-based composites. *Cement and Concrete Research*, vol. 85, 2016, p. 28-38.

[12] MECHTCHERINE V. Towards a durability framework for structural elements and structures made of or strengthened with high-performance fibre-reinforced composites. *Construction and Building Materials*, vol. 31, 2012, p. 94-104.

[13] ARBOLEDA D., BABAEIDARABAD S., NANNI A. Durability of fabric reinforced cementitious matrix (FRCM) composites. *7th International Conference on FRP composites in civil engineering*, 2014.

[14] SILVA R.M.C, SILVA F.A. Carbon textile reinforced concrete: materials and structural analysis. *Materials and Structures*, vol. 53, n° 1, 2020, p. 17.

[15] BRAMESHUBER W. *Report 36: textile reinforced concrete-state-of-the-art report of RILEM TC 201-TRC*. Rilem Publications, 2006.

[16] CUCCHIARA C., LA MENDOLA L., PAPIA M. Effectiveness of stirrups and steel fibres as shear reinforcement. *Cement and Concrete Composites*, vol. 26, n° 7, 2004, p. 777-786.

[17] DINH H., PARRA-MONTESINOS G.J., WIGHT J.K. Shear strength model for steel fiber

reinforced concrete beams without stirrup reinforcement. *Journal of Structural Engineering*, vol. 137, n° 10, 2011, p. 1039-1051.

[18] HENAGER C.H., DOHERTY T.J. Analysis of Reinforced Fibrous Concrete Beams. *Journal of Structural Division*, vol. 102, n° 1, 1976, p. 177-188.

[19] International Federation for structural concrete. *fib Model Code - Bulletin 66*, 2012.

[20] CARDOSO D.C.T., PEREIRA G.B.S., SILVA F.A., SILVA FILHO J.J.H., PEREIRA E.V. Influence of steel fibers on the flexural behavior of RC beams with low reinforcing ratios: Analytical and experimental investigation. *Composite Structures*, vol. 222, 2019, p. 110926.

FLEXURAL CREEP BEHAVIOR OF I-SECTIONS CARBON-TRC BEAMS

Kissila Botelho Goliath[1], Daniel Carlos Taissum Cardoso[2], Flavio de Andrade Silva[3]

[1] *Pontifical Catholic University of Rio de Janeiro, Brazil, kissilagoliath@aluno.puc-rio.br*

[2] *Pontifical Catholic University of Rio de Janeiro, Brazil, dctc@puc-rio.br*

[3] *Pontifical Catholic University of Rio de Janeiro, Brazil, fsilva@puc-rio.br*

SUMMARY: *TRC structures have been largely investigated and used in many applications. However, there is insufficient data to provide an adequate framework for long-term assessment of TRC elements subject to sustained loads. The main objective of the current research is to study the long-term behaviour of I-sections beams reinforced with carbon fabrics under sustained loading. Short- and long-term four-point bending tests were performed in two carbon-TRC beams. The influence of the fabric coatings, i. e. styrene butadiene resin (SBR) and an extra impregnation with sand-epoxy was explored in order to define their influence on flexural creep. All beams were subjected to sustained load for three months and their crack opening and mid span deflections were measured.*

KEY WORDS: *Textile Reinforced Concrete (TRC), long-term behavior, Carbon textile, flexural creep.*

1. INTRODUCTION

Research on Textile Reinforced Concrete (TRC) has been extensively studied [1-4]. To investigate the long-term behavior in TRC, both durability and fatigue were analyzed [5] but little effort has been devoted to assessing the creep behavior in structural members.

The flexural creep behavior comprehension is essential to the design of load-bearing structural members such as concrete beams. This property can affect the serviceability of these components and their lifespan. When subjected to sustained loading, increases in deflections and crack width are likely to occur in TRC members. In addition, creep rupture may occur for higher stresses at constituent materials.

Creep performance in beams is dependent on concrete, textile and interface properties, where the latter two have a stronger influence on the long-term displacements/strains at the tension zone. For the textile, the behavior is a function of its constituents, i.e., fiber and coating material [6]. For the interface, the performance is dependent on the compatibility between yarn and concrete, as well as on the presence of transverse yarns. This study aims to report the results of creep tests performed on structural TRC beams, contributing to the knowledge about the topic.

2. EXPERIMENTAL PROGRAM

Four carbon-TRC 2000 mm long beams were produced with I-sections measuring 80 mm of flange width, 180 mm of depth and 12.5 mm of thickness for both web and flange (Figure 1). The mix design and casting process is described in [7]. A carbon fabric impregnated with SBR was used in two conditions: plain textile (SBR) and the manually impregnation of the textile with epoxy resin and sand (SND). Two beams for each condition were produced, one for short-term test and another for the long-term test.

Figure 1 – Overview of the four-point bending setup and cross-section beam.

Short-term tests were conducted using a servo-controlled hydraulic actuator with load capacity of 500 kN under displacement control at a rate of 1 mm/min. The deflection was measured with a displacement transducer placed at the mid-span. In addition, a DIC technique was used to measure the crack width. Figure 1 shows an overview of the setup test.

To perform long-term test, three steps were carried out: pre-cracking, sustained loading and residual strength. In the first step, the specimens were pre-cracked at the 28 days at 4 kN with the same setup showed in Figure 1. Subsequently, these beams were reloaded and subjected to a sustained load for the three months. The test configuration was based in a four-point bending configuration, with a constant moment region of 300 mm, as shown in Figure 2. The beams were kept in a room with controlled temperature (24 ± 1.5° C) and humidity (55 ± 5 %). The same service load of 4 kN was chosen for all specimens. The main objective was to analyze the behavior of the beams in the same serviceability load level.

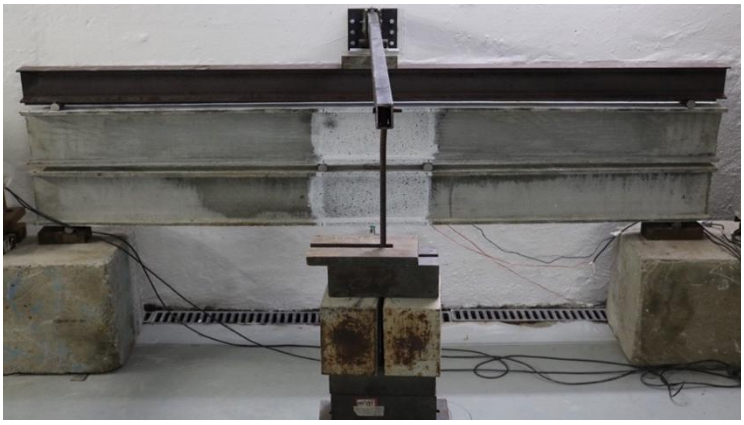

Figure 2 – Long-term test setup.

The midspan deflection, compressive strain on the top of the beam and the crack opening were continuously monitored during test. It is important to note that only the maximum crack width obtained in pre-cracking process was monitored along the long-term test. All comparisons made throughout this article refer to the widest crack (w_{max}) in both tests. The test lasted 90 days. DIC technique was used during unloading to analyze the crack closure and capture the new cracks formation. After unloading, the beams were kept in the test setup for another 10 days and the deflection recovery was monitored during this time. Finally, the specimens were subjected to a complete four-point bending test at the same configuration described for the short-term test until failure. The residual strength was later analyzed.

3. RESULTS AND DISCUSSIONS

Table 1 summarizes the main properties obtained in the tests and the Figure 3 shows the load-deflection curve of the short and long-term test for SBR (Figure 3a) and SND (Figure 3b). For the long-term test, the results obtained throughout the three steps adopted in process (pre-cracking, sustained loading and residual strength) are plotted. The sustained load of the 4 kN subjected the SBR and SND beams to 30% and 25% of the ultimate load (F_u) obtained in quasi-static test, respectively.

Table 1 – Parameters of interest for short- and long-term test.

Test		Parameter	SBR	SND
Quasi-static		First crack load - F_{cr} (kN)	1.17	1.76
		Ultimate load - Fu (kN)	13.45	16.06
		Ultimate deflection - δ_{Fu} (mm)	26.89	25.48
		Crack width at 4 kN - w_{4kN} (mm)	0.249	0.030
		Ultimate crack width - w_{Fu} (mm)	1.100	0.223
		Number of the cracks at 4kN - n_{4kN}	3	3
		Number of the cracks at F_u - n_{Fu}	3	14
Long-term	Pre-cracking	First crack load - F_{cr} (kN)	2.20	3.66
		Deflection at 4 kN- δ_{4kN} (mm)	5.76	1.38
		Crack width at 4 kN - w_{4kN} (mm)	0.880	0.090
		Number of the cracks at 4kN - n_{4kN}	1	1
	Sustained Loading	$F_{service}$ / F_u	1.30	1.25
		Immediate deflection - δ_i (mm)	3.77	3.58
		Deflection at 90 days - δ_{90} (mm)	8.67	5.72
		Creep coefficient at 30 days - φ_{30}	2.07	1.48
		Creep coefficient at 60 days - φ_{60}	2.17	1.55
		Creep coefficient at 90 days - φ_{90}	2.30	1.61
		Immediate recovery - r_i (mm)	0.40	0.51
		Crack width at 90 days - w_{90} (mm)	2.120	0.120
		Number of the cracks at 90 days - n_{90}	1	12
	Residual Strength	Residual load - F_{res} (kN)	13.85	21.15
		F_{res} / F_u	1.03	1.32
		Deflection at F_{res} - δ_{Fres} (mm)	25.63	29.13

Crack width at F_{res} - w_{Fres} (mm)	2.562	0.190
Number of cracks at F_{res} - n_{Fres}	2	24

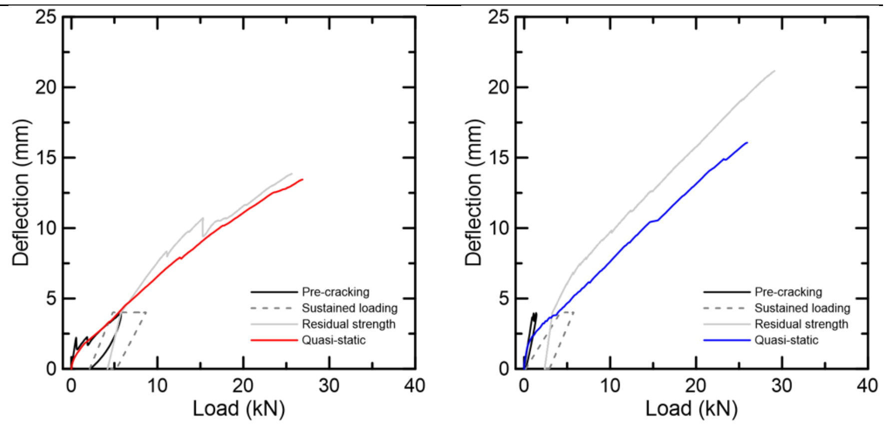

Figure 3. Quasi-static and Long-term results for (a) SBR and (b) SND.

Comparing both beams, slight differences were observed during the uncracked stage for short-term tests. However, the cracked stage was significantly different. The effectiveness of the sand-epoxy treatment was observed and SND specimen exhibited a higher capacity. On the other hand, as expected, SBR-impregnated carbon fiber composites presented lower bending capacity and higher crack width, as previously reported by [7].

Comparing the short-term test and the pre-cracking for the long-term test, there was an increase in the first crack load (F_{cr}) of 74% and 108% for SBR and SND beams, respectively, despite their good agreement on the elastic stage. Observing the DIC analysis (Figure 4) for the same loading stage (4 kN) in the tests, it is possible to notice that SBR beam opened three cracks in quasi-static test (Figure 4a) while a single crack formed for the pre-cracking process (Figure 4c) at this load level. SND beam showed a similar behavior, yet with two cracks in the pre-cracking stage (Figure 4c). For the SND beam there was a quick crack after the appearance of the first crack. This behavior also explains the difference between the maximum crack opening in the tests for the same loading level (Table 1).

Over the sustained loading period (90 days), the number of cracks of the SBR beam remained the same (Figure 4d) and only crack growth was observed. The crack width in this period for SBR beam was 2.12 mm having an increase of 98% regarding the maximum crack width obtained in pre-cracking process. This opening is 92.7% greater than the maximum crack width obtained in quasi-static test for the same specimen at ultimate load. For the beam with sand-impregnation, only one crack formed in pre-cracking process as well (Figure 4c). However, the number of cracks increased to twelve under sustained loading (Figure 4d). Over the sustained loading period, the crack width of the SND beam increased 20% in comparison to the crack in pre-cracking where the maximum crack due to creep was of the 0.12 mm. This also confirms the treatment efficiency in terms of crack opening.

SBR SND

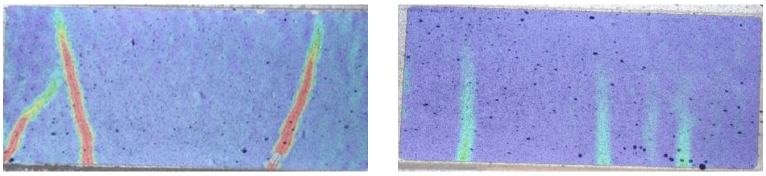

(a) F = 4 kN

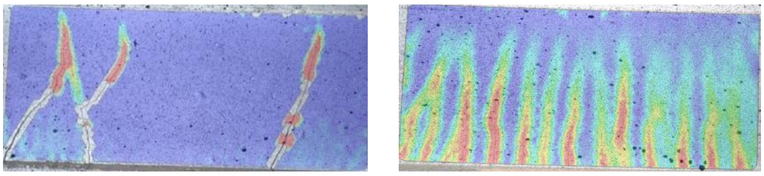

(b) F_u

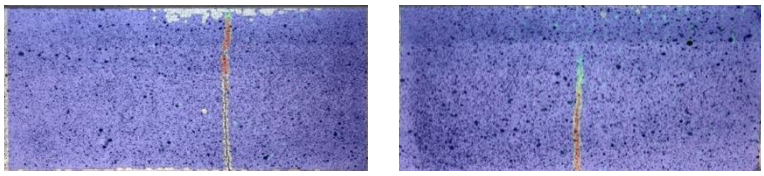

(c) Pre-cracking (F_{4kN})

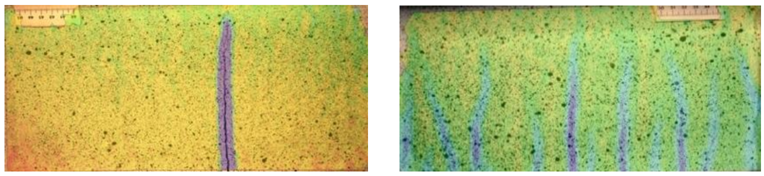

(d) Unloading

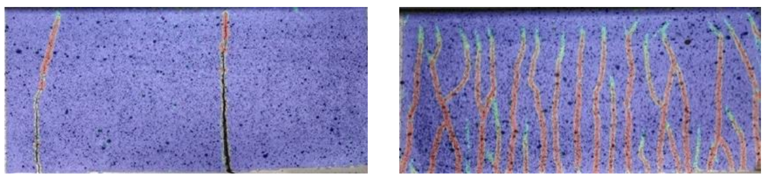

(e) Residual strength (F_{res})

Figure 4 – DIC analysis for short-term test - (a) at 4 kN; (b) ultimate load; and long-term test - (c) pre-cracking; (d) unloading; (e) ultimate load.

As expected, there was no loss in the load capacity of the carbon-TRC beams after the sustained loading period. A slight increase on the stiffness of the SBR beam was observed (Figure 3b) with a 3% increment in the ultimate load. On the other hand, there was a more pronounced difference for the SND beam with an increase of 32% in the load capacity and a relevant stiffness gain before the sustained loading period. In addition, the number of cracks in the residual load (F_{res}) has doubled in comparison to the quasi-static test (Figure 4e). The behavior of this beam in all the tests carried out in the long-term test is consistent, since the beam has already shown signs of improvement in the adhesion between the materials at the pre-cracking stage. The improvement in load capacity may be related to the behavior at the interface of the sand-impregnated textile and the. For a full comprehension of this phenomenon, it is necessary to understand the individual responses of the cementitious matrix, filaments, fiber-matrix interface and filament-filament interaction for sustained load [20].

Figure 5 shows the deflection over the time in the sustained loading period. Table 1 lists the required parameters for a better understanding of the creep behavior: immediate deflection (δ_i) and recovery (r_i), creep coefficient with the time ($\varphi_j = \delta_i/\delta_j$), deflection in different time (δ_j). In terms of immediate deflection, the beams presented the small difference between them (6.2%) of 3.77 mm and 3.55 mm for the SBR and SND, respectively. However, when analyzing the creep coefficient at 90 days (φ_{90}), it is was possible to notice that the deflection of the SBR specimen had an increase of the 1.3 times over the test period. At 30 days, the midspan deflection has doubled (φ_{30}= 2.07). SND beam presented an increase of 0.61 times at 90 days being more efficient for controlling both cracks and deflections under sustained loading. The unloading process occurred after 90 days and the immediate recovery (r_i) was recorded (Figure 5). The creep deflection development over the sustained loading period could not be fully recovered and a little amount was retained. Overall, the immediate recovery is smaller than the immediate deflection. The r_i of the beams was of the 0.40 mm and 0.51 mm for SBR and SND, respectively.

The sand-treatment was able to reduce in 34% the flexural creep deflection (δ_{90}) in comparison to the SBR beam, with δ_{90} of the 5.72 mm and 8.67, respectively. According to the fib Model Code 2010 [8], the deflection for reinforced concrete structural elements must be less than L/250 in the serviceability limit state where L is equal to 1800 mm for I-section beams. Therefore, the maximum displacement allowed by standard at service would be 7.2 mm for the beams investigated. Under sustained service loading analyzed in this study, the beam reinforced with plain SBR textile did not comply with the requirements presented in the standard for the service limit state (SLS). However, as previously mentioned, the impregnation with epoxy and sand was efficient to control the mid-span deflection under sustained service load within in the Model Code 2010 [8].

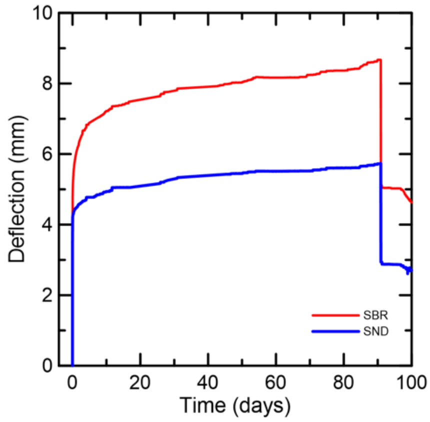

Figure 5. Deflection *vs* Time curves.

3. CONCLUSIONS

To investigate long-term behavior of the carbon-TRC beams, short- and long-term bending tests were performed in two carbon fabric conditions, plain textile and with sand-impregnation. The load level for pre-cracking and long-term tests was determined based on the serviceability limit state (SLS).

Results for plain SBR-impregnated carbon fiber textiles were compared to those additionally treated with sand-coating, to overcome the poor adhesion properties of the former. The effectiveness of the treatment was also confirmed by the smaller displacement and crack width compared to plain textile over time. In addition, the number of the cracks increased considerably for the specimens with extra impregnation, evidencing the improvement in adhesion.

SBR-coating fabrics as reinforcement in structural members subjected to bending may be limited due to the excessive displacement under sustained service load. The use of a sand-impregnation improved this behavior, reducing the displacement and becoming-smaller than the allowed value in standards.

No loss in beam strength occurred for the two beams. In the case of the beam with sand impregnation, there was an increase in load bearing capacity that could be associated to the better positioning of the textile in the formwork and the improvement in the materials interface, confirming preliminary considerations. More studies need to be carried out to better understand the behavior of the textile-matrix interface over time.

4. REFERENCES

[1] S. Rempel, C. Kulas, J. Hegger, Extremely light and slender precast pedestrian bridge made out of textile-reinforced concrete (TRC). High tech concrete: where technology and engineering meet. Switzerland (Cham): Springer Verlag, (2017) 2530–2537. https://doi.org/10.1007/978-3-319-59471-2_288.

[2] A. Scholzen, R. Chudoba, J. Hegger, Thin-walled shell structures made of textile-reinforced concrete: Part I: Structural design and construction, Struct. Concr. 16, (2015) 106–114. https://doi.org/10.1002/suco.201300071.

[3] E. Sharei, A. Scholzen, J. Hegger, R. Chudoba, Structural behavior of a lightweight, textile-reinforced concrete barrel vault shell, Compos. Struc. 171 (2017) 505-514. http://dx.doi.org/10.1016/j.compstruct.2017.03.069.

[4] A. Schumann, H. Michler, F. Schladitz, M. Curbach, Parking slabs made of carbon reinforced concrete, Struct. Conc. 19 (2018) 647–655. https://doi.org/10.1002/suco.201700147.

[5] Spelter, A., Bergmann, S., Bielak, J., & Hegger, J. "Long-term durability of carbon-reinforced concrete: An overview and experimental investigations", Applied Sciences, 9(8), 2019, 1651. https://doi.org/10.3390/app9081651.

[6] Seidel, A., Lepenies, I., Engler, T., Cherif, C., & Zastrau, B. W. Aspects of creep behavior of textile reinforcements for composite materials. The Open Materials Science Journal (2009), 3(1).

[7] Goliath, K. B., Cardoso, D. C. T., de Andrade Silva, F. "Flexural behavior of carbon-textile-reinforced concrete I-section beams". Composite Structures, v. 260, p. 113540, 2021. https://doi.org/10.1016/j.compstruct.2021.113540.

[8] fib Bulletin No. 66. Model Code 2010, Final draft, Volume 2. fib – fédération internationale du béton, International Feder-ation for Structural Concrete. Lausanne, 2012.

MULTIFUNCTIONAL CARBON CONCRETE – OPTIMIZATION IN FOUR STEPS

Dipl.-Ing. Dominik Schlüter[1], Sophie Uhlemann[2], Univ.-Prof. Dr.-Ing. Dr.-Ing. E.h. Manfred Curbach[3]

[1]Institute of Concrete Structures, Technische Universität Dresden, D-01062 Dresden, Germany, Dominik.schlueter@tu-dresden.de

[2] Institute of Concrete Structures, TU Dresden, Sophie.Uhlemann@mailbox.tu-dresden.de

[3] Institute of Concrete Structures, TU, Manfred.Curbach@tu-dresden.de

SUMMARY: *The material and energy costs of building structures can be reduced through an optimized reinforcement design, optimization of the external form in the sense of a shell construction, and through topology optimization - i.e., improvement of the internal component structure. In addition, embedding renewable energy technologies can reduce the environmental impact during the use phase. A new way of embedding renewable technologies into optimized, textile reinforced concrete structures will be presented including the design concept, the production concept and a joint system. Some aspects of the structural behaviour of TRC slabs with cavities like bending behaviour, shear capacity and pull-out behaviour of the anchorage will be outlined.*

KEY WORDS: *Carbon reinforced concrete, energy storage, multifunctionality, optimization, topology*

1. INTRODUCTION

Buildings are primarily erected to protect their users from environmental impacts. In addition, buildings serve to supply their inhabitants with heat and electricity. For an optimized building part design – in terms of material reduction, space saving, and economic viability – all functions must be considered equally. For a new slab design, four optimization approaches were pursued and combined: i) Use of textile reinforced concrete (TRC) allows reduced concrete covers and therewith the production of thin concrete elements. ii) Through the integration of cavities into TRC slabs further material savings can be generated without losing the structural integrity. iii) The structural flexibility of the textile reinforcement allows an optimized positioning of the reinforcement that leads to savings of the reinforcement material. Furthermore the flexibility enables the production of single or double curved, reinforced shell structures which is an efficient way of saving resources. iv) A high degree of prefabrication minimizes the planning risks through a highly automated and weather independent production. By integrating renewable energy technologies – like photovoltaics, electrical energy storage, capillary systems - into the prefabrication process, the advantages of prefabrication (shown in [11]) shall be extended to increase the ecologic benefits of renewable energy technologies and reduce the energy demand of buildings during its use phase. In the following, a concept to combine all these four approaches is presented.

2. DESIGN AND PRODUCTION APPROACH OF AN OPTIMIZED, MULTIFUNCTIONAL SLAB

2.1 Integration of functionalities into TRC slabs

In order to successfully embed functional components e.g. ESDs in TRC slabs, fundamental design criteria must be fulfilled. This includes an easy maintenance and, if necessary, interchangeability of sensitive components. Interchangeability can be realized at building level, building part level or component level. In the case of sensitive functional components, direct interchangeability should be sought, while less sensitive functional components can be permanently integrated into replaceable building parts or permanently integrated into the building structure. This design criteria was fulfilled through a design that enables the interchangeability of single functional units like ESDs and PV, whereas robust infrastructure like cables and capillary systems were fully embedded into the concrete matrix of the slab (Figure 1). The slab was further designed in regard of load-bearing capacity, initial cracking behavior and storage volume as presented in detail in [12].

Cavities on the backside of the slab are provided for functional integration (Figure 1), e.g. can be filled with storage material. Threaded sleeves with an anchor plate are fully embedded in the slab. Newly developed anchoring systems [2] or already existing anchoring systems like the HALFN FPA-5-SL30 can be attached to the sleeves for easy mounting and dismounting of single slab elements if needed.

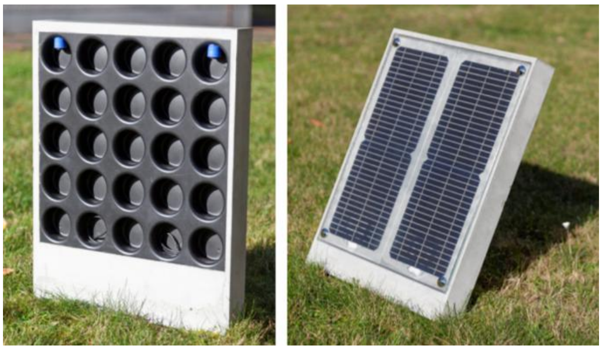

Figure 1 *Slab with cavities for the embedment of functional elements ; left : backside ; right : frontside*

2.2 Structural optimization

The concrete cover of carbon reinforcement – normally needed to protect steel reinforcement against corrosion – can be reduced to several millimeter which leads to thin-walled elements. The thickness of a steal reinforced concrete façade of 8-10 cm can be reduced to 3 cm thickness [6] leading to massive reduction of global warming potential (GHG) [9, 10]. The reduced element thickness however, leads to a decreased effective high respectively increased deflection. The increased deflection and low embedding height further leads to low anchoring forces, why conventional anchorage systems – designed for thick steel reinforced slabs – cannot be used. Through the embedment of cavities a cassette structure is created that leads to a higher section modulus and higher effective height with the same amount of material (Figure 2). E.g. for the investigated geometry a thickness of 4.5 cm is obtained, using the amount of material of a 3 cm solid slab. Anchoring and bending behavior is improved compared to a massive TRC slab. The structure was chosen considering not only structural but also interchangeability and storage volume. Design selection and the investigation of further geometries is shown in [12]. The plastic structure (hereafter referred to as semi-finished-product, SFP) can be filled with electric storage material as shown in [8], acting as structure-forming formwork and battery housing at the same time [12].

Figure 2 *Cross section of the TRC slab with integrated cavities*

By optimizing the reinforcement guidance, the structural-mechanical behavior of the slab can be improved or reinforcement material can be saved. Due to the flexible textile reinforcement and special joints between the SFP and the reinforcement, it is possible to change the direction of the reinforcement at any place within the slab and fixing its position until concreting (Figure 3**,** left). Further material can be saved by adapting the outer shape of the slab. The SFP was designed in such a way, that it follows single or double curved shapes (Figure 3**,** right).

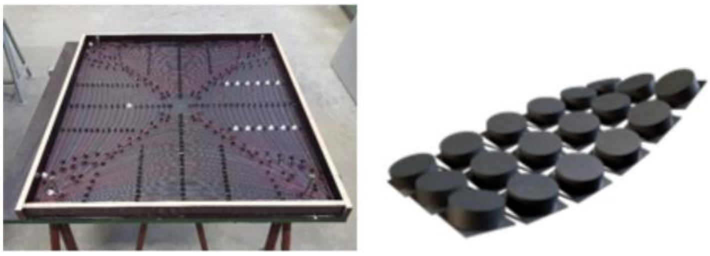

Figure 3 *Plastic structure as semi-finished part; left: used for variable yarn placement (picture : Hildrun Werchan, TU Dresden); right: for double curved slabs (design : Iurii Vakaliuk, TU Dresden)*

2.3 Integration of functionalities into the precast production process

To enable innovative products enter the market successfully, an economically viable and competitive production must be offered. At the same time, initial investment costs needs to be low to empower also small and medium sized precast companies to produce material reduced, functional TRC elements. Through the use of a centrally produced semi-finished part (SFP) (Figure 4) investment costs for the precaster shall be kept low. The semi-finished element was designed in such a way, that it already includes the reinforcement positioning, functional elements like ESDs, anchoring devices and the needed infrastructure like cables and capillary systems. The SFP is placed on the formwork by the precast element manufacturer and concreted out.

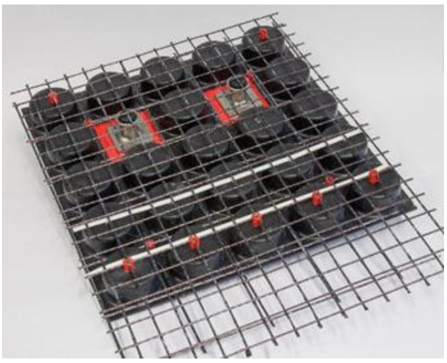

Figure 4 *Semi finished part with embedded cable and anchor plate (picture : Stefan Groeschel, TU Dresden)*

3. STRUCTURAL BEHAVIOUR OF THE DESIGNED SLAB

3.1 Material and Geometry

As most energy-efficiency investments going into envelopes, the developed design will be projected to the application scenario ventilated curtain wall. The investigated slab had two layers of carbon textile reinforcement of the type SIT-grid041KK (producer: Wilhelm Kneitz Solutions in Textile GmbH). One layer had a mesh size of 25.4 mm (70.51 mm²/m). Between the cavities the mesh size was increased to 76.2 mm (23,53 mm²/m) to comply with the cavity order. The slabs cavities had a diameter of 6cm, a depth of 3 cm and distance of 76,2 cm . Both textiles had an average tensile strength of 3011.4 N/mm² [12].

3.2 Bending behavior

Considering the application as façade slab, bending moments are to be expected in both directions. The narrow pressure zone of high-strength concrete and the selected cavity depth leaves the pressure zone undisturbed, avoiding notch tensions, so that the load bearing behavior can be modeled with conventional bending dimensioning (e.g. [5]) taking into account the reduced cross section. Bending tests and values for the initial crack load were already presented in [12] support this thesis.

3.3 Shear crack behavior

The investigation of the shear capacity of TRC slabs without shear reinforcement has already been subject of investigations [3 ,4], whereas there are no models for TRC with cavities. Furthermore there are models for the description of hollow core slabs [1] using reduction factors. For a first estimation of the reduction factor an experiment-based study with low parameter variation was carried out. Figure 5 shows the test setup and dimensions of the investigated specimens, resulting in a shear slenderness of 3.95. The shear slenderness describes the ratio of the distance between support and load introduction to the static effective height. The supports are two roller bearings with a span of 30 cm. The load is applied in the center of the slab from above, also via a roller. The cavities were inserted on the underside. Three plates each with and without cavities were tested.

The concrete had a compressive strength f_{cm} of 76.3 N/mm² – and flexural strength $f_{ct,fl}$ of 9.9 N/mm² (average of 3 specimens). To provoke a shear force failure of the thin TRC slab at reasonable slenderness, even without cavities, the textile between the cavities was doubled, leading to an absolute cross section of 0.148 cm² with a static height of d = 3.97 cm (measured average of 6 slabs).

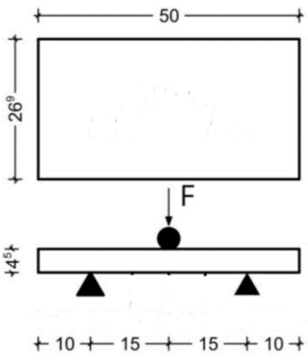

Plate name		Failure mode	Maximum Force [kN]
Without Cavities	D-1	shear	21.1
	D-2	shear	22.0
	D-3	bending	25.5
With Cavities	D-4	shear	17.6
	D-5	shear	15.0
	D-6	shear	13.0

Figure 5: Setup and results of the three-point bending test

Results are presented in Figure 5, the failure pattern can be seen in Figure 6. Two of the three specimen without cavities failed on shear, one specimen had a failure mode showing a fracture of the reinforcement. According to the model from section 3.2, bending failure was expected at 27 kN. By contrast, all the specimen with cavities showed a clear failure on shear compression, with a failure crack crossing the cavities. The reduction of the cross-section (by 45%) due to the arrangement of cavities reduces the load-bearing capacity on average from 22.9 kN to 15.2 kN (33%). Whether this reduction factor can be transferred to other geometries, shear slenderness and non-metallic reinforcements must be verified in an advanced parameter studies.

Figure 6 *Cracks after failure at three-point bending test; left: slab without cavities; right: slab with cavities (pictures : Hildrun Werchan, TU Dresden)*

3.4 Investigation of the anchoring system

With the objective to determine the anchoring capacity of the threaded sleeves, pull-out tests, oblique tensile tests and punching tests were carried out. It was found in preliminary tests, that the arrangement of the sleeves in close vicinity of the cavities significantly reduce the load-bearing capacity. In the presented tests, therefore, an area of 2 x 3 cavities is left free per anchor, in which the anchoring element is installed centrally. The anchor was placed on the side of the cavities. The concrete compressive strength was determined to 79.1 N/mm² (tested on three specimen at 10 × 10 × 10 cm³).

The pull-out test consisted of the specimen with 50 × 31 × 4.3 cm (Figure 7), a support with a span of 30 cm and a central load application. The punching test consisted of the specimen with the dimension 50 × 31 × 4.3 cm³, a support with a span of 30 cm and a central load application (Figure 8). Both tests included three test specimens (A-1, A-2, A-3 and B-1, B-2, B-3) with and three test specimens (A-4, A-5, A-6 and B-4, B-5, B-6) without supplementary reinforcement. The supplementary reinforcement had a size of 22 × 14 cm^2 and mesh size of 25,4 cm, which fits in between the cavities, and was placed around the sleeve directly on the reinforcement (Figure 7). The oblique tensile test consist of specimen with the dimension 64 cm × 41 × 4.3 cm³, a support with a span of 60 cm and load application at an angle of 45 degrees (Figure 8). Three specimen (C-1, C-2, C-3) were with and three (C-4, C-5, C-6) without supplementary reinforcement, whereas C-3 and C-6 had no cavities.

Table 1 *Test results of the anchorage system*

Plate name		Supplementary reinforcement	Maximum Force [kN]	Failure mode
Pull-out	A-1	*Yes*	13.5	Anchor
	A-2	Yes	12.7	Anchor
	A-3	Yes	13.5	Anchor
	A-4	No	11.6	Anchor
	A-5	No	11.2	Anchor
	A-6	No	11.5	Anchor
Punching	B-1	Yes	29.7	Shear
	B-2	Yes	31.2	Shear
	B-3	Yes	32.9	Shear
	B-4	No	30.0	Shear
	B-5	No	29.3	Shear
	B-6	No	36.3	Anchor
Oblique tensile	C-1	No	11.9	Anchor
	C-2	No	9.5	Anchor
	C-3	No (no cavities)	11.0	Anchor
	C-4	Yes	12.3	Anchor
	C-5	Yes	13.4	Anchor

	C-6	Yes (no cavities)	15.4	Anchor

Figure 7 *Formwork of the test specimen; left: oblique tensile test with supplementary reinforcement; right: punching and pull-out test*

Results are presented in Table 1. All anchors at the pull-out test failed due to concrete breakout. After the initial crack (on average at 5 kN), a significant increase of load was still observed. The pull-out conus of the anchor didn't interact with the cavities. The break-out force could be increased through a supplementary reinforcement from 11.42 kN to 13.5 kN (14%).

The failure pattern of the oblique tensile test showing an asymmetric breakout cone. For the specimen with cavities (C-1, C-2, C-4, C-5) an average initial cracking load of 2.6 kN (4.8 kN for C-3 and C-6) was observed with a significantly increase of load until brake out. The break out force of C-3 (without cavities) didn't exceed the break out force of C-1 and C-2 (without cavities), showing that the anchorage doesn't interact with the cavities. Through the supplementary reinforcement the maximum force could be increased from 10.7 kN to 12.85 kN (17%). However this also increased the size of the break out cone, now interacting with the surrounding cavities. The specimen without cavities therefore showed increased maximum load of 16% compared with specimen without cavities.

The push-out force was initially calculated with the model presented in [7] to be at 26.58 kN. This calculated break-out force was exceeded, so that a shear failure of the slab occurred. Only slab C-6 showed a break out cone at 36 kN. Through the experiments it was shown, that the push-out resistance of the anchor exceeds 31.6 kN (average of all 6 specimen).

Figure 8 Test configuration for anchoring testing; left: oblique tensile test; middle: pull-out test; right: punching test

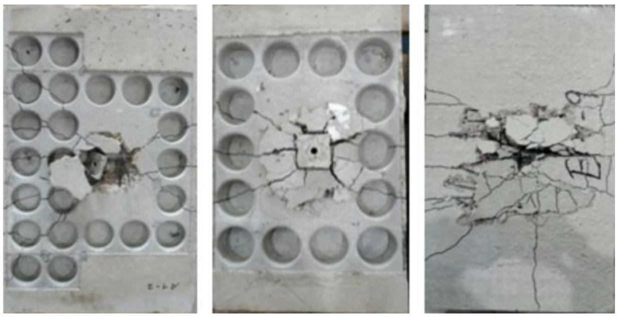

Figure 9 *Anchor failure pattern; left: oblique tensile test; middle: pull-out; right: punching test*

4 CONCLUSION

Within the paper a concept was presented that has the potential to join different strategies of structural optimization in a single building part. For the specific use scenario “façade panel” the structural integrity could be validated.

On the base of the presented concepts and investigations, the economic and ecologic feasibility need to be elaborated. Models for the structural behavior of TRC with cavities need to be outlined to transfer the investigated geometry to other use scenarios and increase the adaption rate of structural optimized TRC building parts.

ACKNOWLEDGEMENT

The developments and investigations were part of the project C3-V4.6 "Energy-storing carbon concrete" (FKZ 03ZZ0346B) was funded by the German Federal Ministry of Education and Research (BMBF), Project Management Agency FZ Jülich, as part of the research project "C³ - Carbon Concrete Composite".

LITERATURE

[1] ALBERT A.; BUSCH D. (2020): *STAHLBETONHOHLKÖRPERDECKEN. BEMESSUNGSHINWEISE UND NEUE ENTWICKLUNGEN*. IN: KONSTRUKTIVER INGENIEURBAU KI (NR.1)

[2] AYOUBI M.; SOBOTTA S.; SCHLUETER D.; MICHLER H.; KROPP T.; THUESING K.; KALLNIK S.; SCHUMANN A.: *Aktive Verbinder für Bauelemente aus Carbonbeton*. Bautechnik 98(6) (2021), DOI: 10.1002/bate.202000088

[3] BIELAK J.; ADAM V.; HEGGER J.; CLASSEN M (2019A): *SHEAR CAPACITY OF TEXTILE-REINFORCED CONCRETE SLABS WITHOUT SHEAR REINFORCEMENT*. IN: APPLIED SCIENCES 9 (7), S. 1382. DOI: 10.3390/APP9071382

[4] BIELAK J.; WILL N; HEGGER J. (2020): *ZWEI PRAXISBEISPIELE ZUR QUERKRAFTTRAGFÄHIGKEIT VON BRÜCKENPLATTEN AUS TEXTILBETON*. IN: BAUTECHNIK 97 (7), S. 499–507. DOI: 10.1002/BATE.202000037.

[5] HÄUßLER- COMBE U.; WESELEK J. (2020).: *ERMITTLUNG VON TEILSICHERHEITSBEIWERTEN BEI CARBONBETON. BETON- UND STAHLBETONBAU*, 115(3), 209–217. HTTPS://DOI.ORG/10.1002/BEST.201900047

[6] HERING BAU GMBH & CO. KG (2017): A*LLGEMEINE BAUAUFSICHTLICHE ZULASSUNG Z-10.3-723:FASSADENPLATTEN "BETOSHELL NEO 30" AUS TEXTILBETON ZUR VERWENDUNG BEI VORGEHÄNGTEN HINTERLÜFTETEN AUßENWANDBEKLEIDUNGEN*.

[7] HORSTMANN K.; HEGGER J.: *SANDWICHFASSADEN AUS TEXTILBETON - EXPERIMENTELLE UNTERSUCHUNGEN*, BAUTECHNIK, JG. 88, NR. 5, S. 281–291, 2011, DOI: 10.1002/BATE.201101461.

[8] KROIS K.; HÜFNER L.; GLÄSEL J.; ETZOLD B. J. M.: *SIMULATIVE APPROACH FOR LINKING ELECTRODE AND ELECTROLYTE PROPERTIES TO SUPERCAPACITOR PERFORMANCE*. CHEMIE INGENIEUR TECHNIK 91 (2019) H. 6, S. 889–899 – DOI: 10.1002/CITE.201800198

[9] KIRMSE S.; KAHNT A.; HUTH S.; TIETZE M.; HÜLSMEIER F.: *VAKUTEX: VAKUUMGEDÄMMTE FASSADENELEMENTE AUS TEXTILBETON*, FORSCHUNGSINITIATIVE ZUKUNFT BAUEN, S. 69–71, 2013.

[10] KULAS C., SCHNEIDER M., WILL N., GREBE R.: *HINTERLÜFTETE VORHANGFASSADEN AUS TEXTILBETON: TRAGVERHALTEN UND AUSFÜHRUNG*, BAUTECHNIK, JG. 88, NR. 5, S. 271–280, 2011, DOI: 10.1002/BATE.201101462.

[11] LI Z.; SHEN, G. Q.; XUE X.: *Critical review of the research on the management of prefabricated construction*. Habitat International Volume 43 (2014), S. 240–249

[12] SCHLUETER D.; RIEGELMANN P.; SCHEERER S.; CURBACH, M.: *Bauteiloptimierung durch Funktionsintegration. Beton- und Stahlbetonbau* 115 (2020) 8, S. 598-606 - DOI: https://doi.org/10.1002/best.202000027

RECYCLED CARBON FIBERS WITH IMPROVED SURFACE CHARACTERISTICS AS REINFORCING MATERIAL FOR FIBER CONCRETE

Magdalena Kimm[1], Maryam Sodagar[1], Vanessa Overhage[1], Thomas Gries[1]

[1]Institut fuer Textiltechnik of RWTH Aachen University, Germany, magdalena.kimm@ita.rwth-aachen.de

SUMMARY: *Carbon fibre reinforced polymers (CFRP) are taking over the aerospace, automotive, construction and wind energy sector. The growing demand for CFRP leads to a growing mass of waste. Land filling and incineration are not effective and environmentally friendly routes for CFRP waste. Therefore, the aim of this research paper is to enhance the usage of recycled carbon fibres (rCF) from CFRP waste as short fibre reinforcement in concrete. rCF were treated with different dispersants and functional coatings to improve the distribution and adhesion in the concrete.*
Recycled carbon fibre reinforced concrete (rCFRC) specimens were prepared. These specimens consist of 0.5 vol.-% rCF with the length of 10-30 mm. 4-point bending test procedure was performed for the characterization of the specimens.

KEY WORDS: *fibre reinforced concrete, carbon fibre reinforced polymer, recycled carbon fibre*

1. INTRODUCTION

Carbon Fiber Reinforced Polymers (CFRPs) have captured attention in numerous industries such as aerospace, automotive, the production of massive wind energy blades with high-efficiency rates, robust and lightweight pressure vessels or material efficient building structures with so-called “carbon concrete”. This demonstrates the potential to replace conventional materials like steel due to carbon fiber’s high strength-to-weight ratio, stiffness and high durability [1, 2].

The global demand for CFRP in 2018 was approximately 75.5 kt. It is predicted that this demand will reach 120.5 kt expected in 2022 [3]. The increasing demand for

CFRP also directly leads to an increase in production and end-of-life waste. Disposal of CFRP products upon completion of the service life is the biggest issue today. The incineration is not a suitable solution for fiber reinforced plastic waste, because 50 to 70 % of the slag from incinerated FRP were minerals and ashes, which still need to be landfilled [4].Considering the disposal of CFRPs, high quality virgin carbon fibers are a precious raw material in the price range of 20 to 30 €/kg. The recovery and recycling of the material makes a lot of sense, as material properties were nearly completely preserved and as the price range of 5 to 10 €/kg for recycled carbon fiber (rCF) is much more affordable. However, when recovering carbon fibers from CFRPs, degradation of fiber length cannot be avoided, which results in an end product form of short carbon fibers.

An attractive approach is the use of rCF from CFRP waste as reinforcement for concrete replacing short steel and glass fibers, see Figure 1 a) [5].

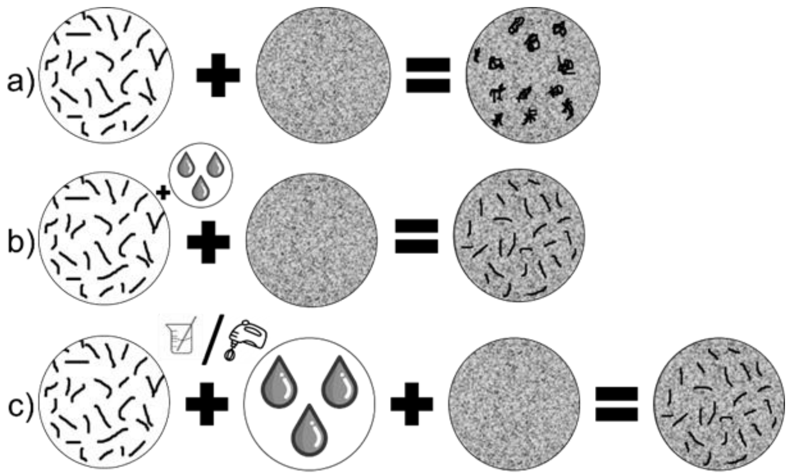

Figure 1. *a) Motivation: Use of rCF in concrete without any treatment; two approaches of this paper: b) adhesive treated rCF; c) dispersant treated rCF using two mixing methods*

The addition of fibers in the concrete improves the strain properties as well as the resistance to crack propagation, ductility, flexural strength and toughness. Mechanical properties of conventional fibres made of steel and alkali resistant glass can be surpassed by rCF by equivalent or even lower costs. Applications under improper environmental conditions often lead to corrosion of the most used steel fibers, which subsequently contributes to the deterioration of reinforced concrete structures. rCFs have inert surface which provides a huge advantage for non-corrosiveness and non-degradability of the concrete component, but also hinders the concrete matrix to bond to the fiber very well [6]. Therefore, dispersibility and bonding or rCF in concrete are two main determining factor to qualify this excellent secondary material as reinforcement. Dispersants shall enhance a homogeneous distribution of the fibers in the concrete matrix and prevent the creation of fibre bulks. This shall lead to improved and uniformly distributed mechanical properties, see Figure 1 b). By applying an adhesive coating, functional groups, e.g. hydroxyl (OH) and carboxyl groups (COOH) shall be formed. These changes lead to surface activation, so that the calcium hydroxides contained in the cement can form ionic compounds with the fiber surface during the pozzolanic reaction in concrete. By this, the flexural strength of the specimens with treated rCF shall be increased, see Figure 1 c).

2. MATERIALS AND METHODS

2.1 Materials

rCF as a short-fibre reinforcement from CFK Valley Stade Recycling GmbH & Co. KG, Wischhafen, Germany, with the length of 10-30 mm were used in this experiment. In order to improve the adhesion of rCF and concrete the rCFs were treated with 3-Glycidyloxypropyl Trimethoxysilane from Sigma-Aldrich Chemie GmbH, Darmstadt, Germany. Moreover, to improve the distribution of short rCF in the concrete, the rCFs were treated with three different dispersants from CHT Germany GmbH, Tuebingen, Germany.

The concrete matrix for silane treatment experiment is composed of the concrete premix “DP-Moertel 04 Weiss” from Durapact 2.0 Kompetenzzentrum Faserbeton GmbH, Haan, Germany, with a water content of 15 mass-% and additional polycarboxylate ether-based plasticizer of 0.3 mass-% to improve the flow properties. The matrix employed in dispersion improvement experiment is composed of cement CEM I 47.5 R (490 kg/m^3), fly ash (175 kg/m^3), micro silica powder (Elkem Microsilica® 940U, 35 kg/m^3), quartz powder (500 kg/m^3), sand 0.2–0.6 mm (713 kg/m^3), water (280 kg/m^3) and Polycarboxylate Ether-based plasticizer (7 kg/m^3). An overview on the series is shown in Table 1.

2.2 Specimen Preparation

The silane treated rCFs were added in small quantities to the dry concrete premix with a fibre volume content of 0.5 vol.-% to avoid fibre agglomeration. Then, the liquid components of concrete were added.

2.2.1 Adhesion improvement of rCF with concrete

In this experiment, the fibres were first coated with silane. Therefore, an aqueous solution were prepared by adjusting the PH value of the distilled water to about 4.5 with acetic acid. Then the silane with the concentrations of 0.1, 0.5 and 1.0 wt.-% (based on water/acetic acid solution content) were added and stirred for 15 minutes. rCFs were added to the solution and stirred using a glass stirring rod and were rested for 30 minutes.

Table1. *Specification of the samples and labeling*

	Con-crete	Sam-ple	rCF	Treatment	Treatment concentration	Mixing Apparatus for fiber dispersion
			[vol.-%]		[wt.-%]	
Adhesive improvement	DP Moertel 04 Weiss	A_S0	0	-	-	-
		A_S1	0.5	-	-	-
		A_S2	0.5	Silane	0.1 **	-
		A_S3	0.5		0.5 **	-
		A_S4	0.5		1	-
Dispersion improvement	ITA Mixture	D_S0	0	-	-	-
		D_S1	0.5	-	-	GR*
		D_S2	0.5	-	-	HM*
		D_S3	0.5	TUBICOAT EMULGATOR HF	1.1 **	GR*
		D_S4	0.5		1.1 **	HM*
		D_S5	0.5	SARABID OPTI	1.1 **	GR*
		D_S6	0.5		1.1 **	HM*
*GR: Glass Rod; HM: Hand Mixer **based on ***based on cement content						

After applying the silane, rCFs were wrapped in metal grid and dried for 30 minutes at 110 ˚C in oven to activate the silane coating by driving the condensation of silanol groups at the surface and to remove traces of methanol from hydrolysis of the methoxy silane. Afterwards, silane treated rCFs were added in small quantities to the dry concrete to avoid fibre agglomeration. Liquid components of concrete including water and Polycarboxylate Ether-based plasticizer were mixed separately. Then the liquid components were gradually added to the mixture of rCF and dry concrete and mixed with the help of a hand mixer, see Figure 2. The concrete mixtures were placed on vibrating table for 30 sec before casting.

2.2.2 Distribution improvement of rCF in concrete

In this experiment, the dispersants were mixed in water for concrete with the concentration of 1.1 wt.-% (based on cement content) for 2 min. Then the rCFs with 0.5 vol.-% (based on concrete volume) were added into the solution and stirred for 2 minutes, either using a hand mixer or a glass rod. The fibres were rested for 5 minutes in the dispersant solution.

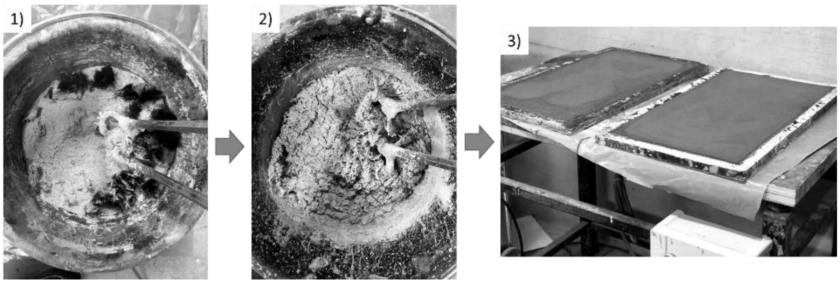

Figure 2: *1) Mixing silane-coated-rCF with cement dry components, 2) Mixture of water with dry components 3) Specimens on vibrating table.*

Besides, the dry components of concrete were mixed together in bucket mixer for 1 minute with the rotational speed of 50 rpm (see Figure 3). Subsequently, the water-dispersant-rCF-solution is added gradually to the dry components. The concrete mixtures were placed on vibrating table for 30 sec before casting.

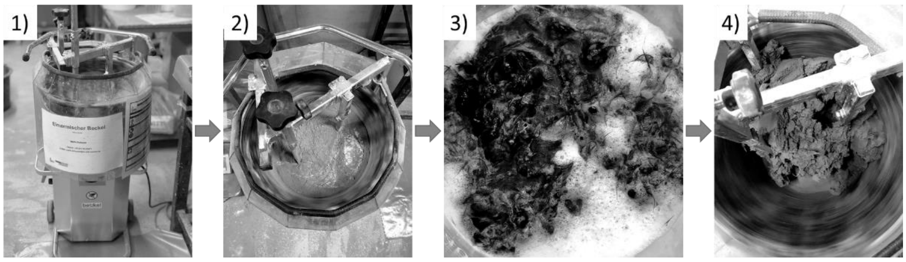

Figure 3. *1) Bucket mixer 2) Dry components 3) rCF/dispersant solution 4) Mixing of dry and wet components.*

2.2.3 Concrete specimen preparation

Molds were filled with the mixture and rCFRC specimens in fresh state were placed on a vibrating table for 20 s. Specimens were covered with plastic sheets and left to dry for 1 day. Then, the specimens were placed in a water bath for 7 more days and 20 more days to dry in a room climate of 22 ± 3 °C. As a reference, a series without fiber reinforcement (0 vol.-%) and a series with uncoated rCF (0.5 vol.-%) were prepared.

2.3 Flexural Tests

In order to determine the flexural strength, four-point bending tests were carried out on ten samples per series of rCF-reinforced concrete (rCFRC) in a standard climate of EN ISO 139 according to EN 1170-55 (see Figure 4).

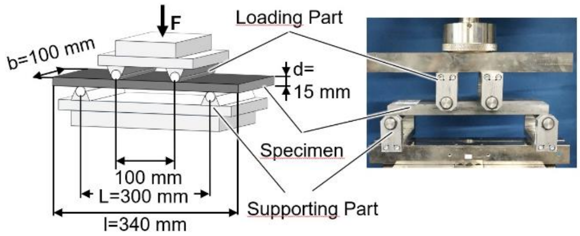

Figure 4. ***Flexural test setting***

Therefore, the specimens with the dimensions of 340 mm×100 mm×15 mm were tested after 28 days of storage. A standard climate according to EN ISO 139 was maintained during the tests. The four-point bending test in this experiment is conducted using a testing speed of 1.8 mm/min. The tests were done with the pre-force of 1 N until the maximum distortion of 6 mm or an upper force limit of 15 kN is reached. In Figure 5 and Figure 7 the averages of ultimate flexural stresses and strains results for all experiments are presented.

3. RESULTS

All the flexural stress values were lying very close together and they were mostly with-in statistical deviation, so it is difficult to make a statement about the effect of the treatment on flexural strength of the specimens.

3.1 Results of treated rCF with adhesive

Analysis of the results displayed in Figure 5 shows that the addition of 0.5 vol.-% rCF to concrete can increase the flexural strength of the DP-Moertel Weiss Premix concrete by 14 %. Furthermore, silane-treatment of 0.1 and 1.0 wt.-% of rCF leads to negligible improvements compared to untreated rCFRC. Maximum flexural strength is achieved by incorporating 0.5 wt.-% silane treated rCF (series A_S03). This value is 20 % higher than the flexural strength of plain concrete and results in an additional 6 % improvement compared to untreated rCFRC. The ultimate strain (elongation at break) is lowered by the silane coating compared to untreated rCFRC.

In adhesive treated rCFRC, rCF cannot be distinctly distinguished in the crack cross-section, see Figure 5. Therefore, the conclusion can be made that the fibres were failed under load simultaneously and some of the fibres were stretched out until failure occurs which was also observed by Naaman. [8]

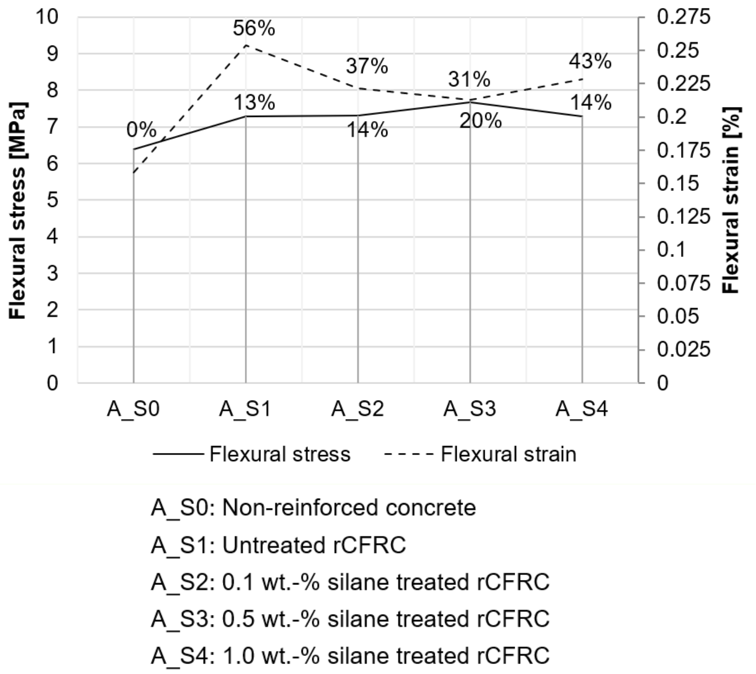

Figure 5. *Variation of the mean of ultimate flexural stresses and strains of adhesive treated rCFRC*

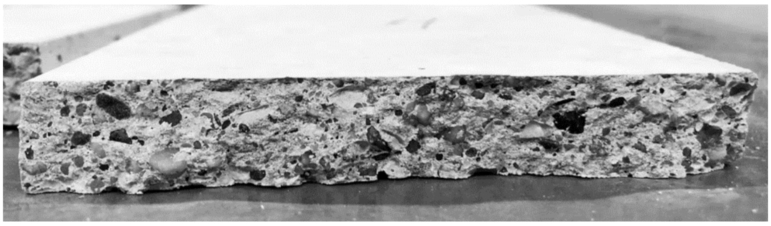

Figure 6. Cracked cross-section of adhesive treated rCFRC specimen

3.2 Results of treated rCF with adhesive

By analysing the results displayed in Figure 7, it can be stated that addition of 0.5 vol.-% rCF to concrete in the case when rCF is first mixed with water using glass rod and hand mixer, can increase the flexural strength of ITA concrete mixture by 23 % and 15 %, respectively (series D_S1 and D_S2).

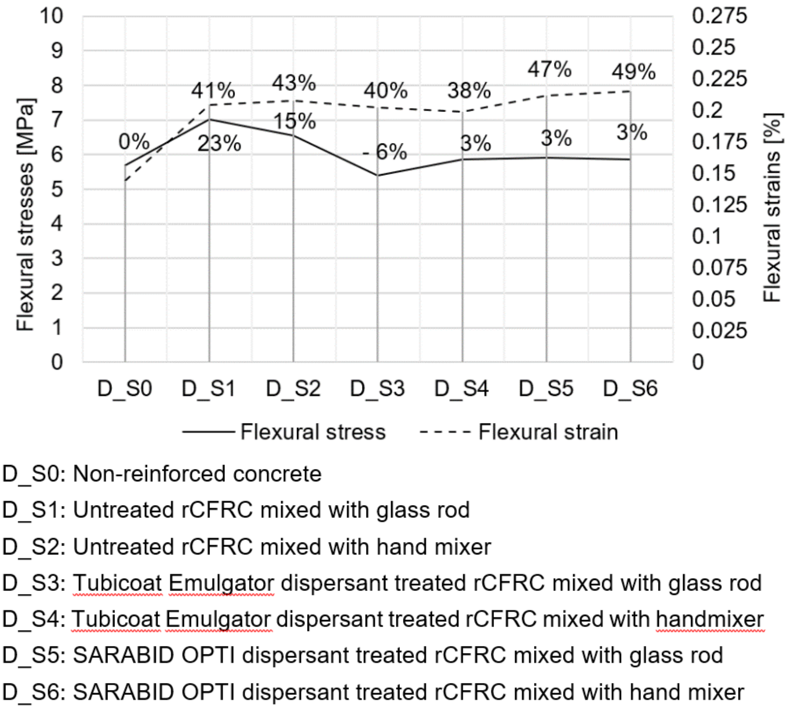

Figure 7. *Variation of the mean of the ultimate flexural stresses and strains of dispersant treated rCFRC*

Furthermore, both dispersants using both mixing methods have a negative or a negligible positive effect on the flexural strength (series D_S3 to D_S6). However, dispersant treatment with SARABID OPTI increases the workability of the concrete and shows an even distribution visually. Usually, the amount of total dispersing materials including plasticizer and dispersant, should be in the range of 0.2 – 1 wt.-% based on cement content. Therefore, one potential reason for improvement of the workability and decrease of the flexural strength, can be that the dispersants and PCE-plasticizer with the total mass of 2.5 wt.-% (based on cement content) were applied in current work, which is above the recommended percentage.

By investigating the results, it can also be stated that mixing of untreated rCF with water using an electric hand mixer decreases the flexural strength of concrete compared to glass rod mixing method. One potential reason can be that the extensive mixing leads to shearing, friction and therefore breakage of rCF which has a brittle structure. Moreover, glass rod mixing of rCF treated with TUBICOAT EMULGATOR decreases the flexural strength by 6 % compared to hand mixer mixing method. The reason to this observation can be traced back to the fact that this dispersant needs more energy to be activated. Analysis of the cracked surface shows that hand glass rod mixing method causes fiber nest building in concrete, see Figure 8, D_S1.

TUBICOAT EMULGATOR dispersant has no recognizable effect on the elongation at break, while SARABID OPTI dispersant slightly increases it.

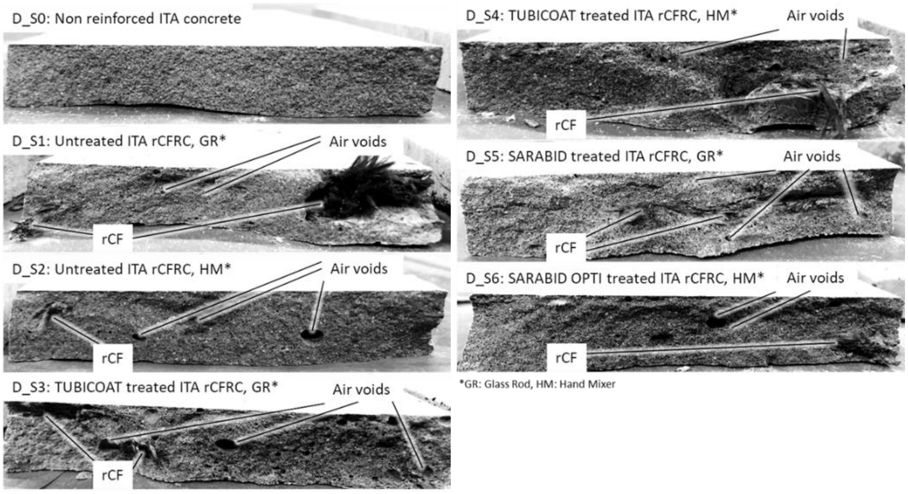

Figure 8. *Cracked cross-section of dispersant treated rCFRC specimen*

4. CONCLUSION AND FUTURE WORKS

This paper is conducted to determine the influence of adhesive and dispersant treatment of rCF on reinforcement of fiber reinforced concrete with 0.5 vol.-% of rCF (based on concrete volume). Adhesive and dispersant treated short rCFs were added into concrete and the results of flexural tests were analysed. Adhesive treatment is carried out to enhance the bonding between rCF and concrete, while dispersant treatment is conducted to improve the distribution of fibres in concrete. Meanwhile, two different methods of mixing rCFs in a water-dispersant solution is employed to investigate the effect of mixing process on the dispersion of rCFs in concrete matrix.

The conclusion based on analyzing the results of flexural tests were:

- Addition of 0.5 vol.-% of untreated rCF has improved the flexural strength of concrete in the range of 13 to 23 % depended on the concrete type.
- Silane adhesive treatment of rCF slightly improves the flexural strength of rCFRC. A maximum is achieved by incorporating 0.5 wt.-% silane treated rCF in premixed concrete which increases the flexural strength only by 5 % as compared to untreated rCF.
- Silane treatment of rCF slightly decreases the elongation at break.

- Dispersants have slight negative effect on flexural strength of concrete although workability of the mixture was improved. A potential reason for this can be that dispersants and plasticizer were used with the total mass of 2.5 wt.-% (based on cement content), which is above the usually recommended percentage.
- TUBICOAT EMULGATOR dispersant has no recognizable effect on the elongation at break, while SARABID OPTI dispersant slightly increases it.

Considering further sustainability aspects, it can be stated that reinforcement fractions used in this work were below the allowable share of 5 mass-% for organic components in construction waste in Germany according to the German waste code number 17 01 07. Also, to the current state of knowledge, carbon fibre fragments and dust have no effect on health [7].

REFERENCES

[1] S. J. PICKERING, “Recycling technologies for thermoset composite materials—current status,” *Composites Part A: Applied Science and Manufacturing*, vol. 37, no. 8, pp. 1206–1215, 2006, doi: 10.1016/j.compositesa.2005.05.030.
[2] S. DAS, J. WARREN, D. WEST, and S. M. SCHEXNAYDER, “Global Carbon Fiber Composites Supply Chain Competitiveness Analysis,” 2016. Clean Energy Manufacturing Analysis Center
[3] E. WITTEN, M. SAUER, and M. KÜHNEL, “Composites-Marktbericht 2018: Marktentwicklungen, Trends, Ausblicke und Herausforderungen,” Carbon Composites e.V., AVK e.V., Augsburg, 2018.
[4] M. MASTALI and A. DALVAND, “The impact resistance and mechanical properties of self-compacting concrete reinforced with recycled CFRP pieces,” *Composites Part B: Engineering*, no. 92, pp. 360–376, 2016, doi: 10.1016/j.compositesb.2016.01.046.
[5] M. KIMM, D. PICO, and T. GRIES, “Investigation of surface modification and volume content of glass and carbon fibres from fibre reinforced polymer waste for reinforcing concrete,” *Journal of hazardous materials*, no. 390, 2020, doi: 10.1016/j.jhazmat.2019.121797.
[6] M. KIMM, “Ressourceneffizientes und recyclinggerechtes Design von Faserverbundwerkstoffen im Bauwesen,” Dissertation, Rheinisch-Westfälische Technische Hochschule, Aachen, 2020.
[7] N. Bienkowski *et al.*, “Bearbeitung von Carbonbeton - eine bauverfahrenstechnische und medizinische Betrachtung,” *Bauingenieur*, 2017/2018, pp. 110–118, 2017.
[8] A. NAAMAN, “Fiber reinforced cement and concrete composites“ Sarasota Florida: Techno Press 3000, 2017

MECHANICAL PERFORMANCE AND DURABILITY OF CEMENT COMPOSITES REINFORCED WITH ALIGNED ENSET FIBERS

Markos Tsegaye[1,2], Michael El Kadi[1], Tamene Adugna[2], Danny Van Hemelrijck[1], Tine Tysmans[1]

[1,2]Markos Tsegaye (Department Mechanics of Materials and Constructions (MeMC), Vrije Universiteit Brussel (VUB), Pleinlaan 2, 1050 Brussels, Belgium, markos.tsegaye.beyene@vub.be)

[1]Michael El Kadi (Department Mechanics of Materials and Constructions (MeMC), Vrije Universiteit Brussel (VUB), Pleinlaan 2, 1050 Brussels, Belgium, michael.el.kadi@vub.be)

[2]Tamene Adugna (Jimma University, Jimma Institute of Technology, Faculty of Civil and Environmental Engineering, Jimma, Ethiopia tamene_adu2002@yahoo.com)

[1]Danny Van Hemelrijck (Department Mechanics of Materials and Constructions (MeMC), Vrije Universiteit Brussel (VUB), Pleinlaan 2, 1050 Brussels, Belgium, danny.van.hemelrijck@vub.be)

[1]Tine Tysmans (Department Mechanics of Materials and Constructions (MeMC), Vrije Universiteit Brussel (VUB), Pleinlaan 2, 1050 Brussels, Belgium, tine.tysmans@vub.be)

SUMMARY: *Driven by the need for alternative construction materials, recent developments have been steered towards the use of natural fiber reinforced cement composites. Ensete Ventricosum (Ev) offers a promising candidate as reinforcement in cement matrices but has not yet been studied in the literature. This research assessed the mechanical performance and durability of Ev fiber reinforced cement composites. Cracking behaviour was studied using the optical Digital Image Correlation (DIC) technique. The Ev fiber reinforced composites achieved a desirable post-cracking behaviour and the stiffness, toughness, and flexural strength increased with increasing fiber dosages. After 6 and 12 wet/dry cycles and 50 heat/rain cycles, all composites showed significant strength losses. This was attributed to the severe degradation of the Ev fibers and their low volume fraction.*

KEYWORDS: *Cement composite, Fiber reinforced, Fibre volume fraction (V_f), Natural fiber, Heat/rain cycle, Wet/dry cycle*

1. INTRODUCTION

Cement-bonded composites are made of a cementitious matrix and reinforcing fibers. The source of the fibers can be both natural and synthetic [1]. Even though natural fibers are promising reinforcement materials, their use until now remains more traditional than technical. Natural fibers exhibit a set of significant benefits, such as high availability at a relatively low price, bio-renewability, can be found in a wide range of morphologies, ability to be reused, biodegradability, non-threatening nature, fascinating physical and mechanical properties (low density and well-balanced stiffness, toughness, and strength) [2]–[5].

Investigations on plant-based natural fiber reinforced cement composites, using flax, jute, hemp, agave family, kenaf, sisal, coir, and bamboo fibers, have shown promising mechanical properties [5]–[7]. Jose Castro and Antoine E. Naaman reported that natural fiber of the agava family can be used as a reinforcement in cement based composites, whereas R.S Olivito et al. [8] and R.D. Toledo Filho et al. [9] developed a durable composite using flax, coconut, and sisal fibers as reinforcement in the cement matrix. The potential application of Ensete Ventricosum (Ev) fibers in cementitious composites has however not been investigated in literature and is the subject of current study.

In the design of cementitious-based composites, consideration of durability of the composite is very important since it has a significant impact on the long-term performance. Studies have shown that natural fiber reinforced cement-based composites are susceptible to degradation in cement matrices due to the alkaline nature of the cement attacking the lignin of these fibers [10]. Plant-based natural fiber reinforced cementitious composites can be considered suitable construction materials if they possess desirable serviceability and strength characteristics [11]. The material is said to be serviceable only when it is found to be durable under various exposure conditions in practical applications. Durability relates to its resistance against degradation due to internal and external causes, the internal causes such as alkali environment in concrete and external causes such as weathering action and exposure conditions [12], [13].

If Ev fiber reinforced cement-based composites are to be used for applications where performance must be guaranteed after undergoing different aging processes, the effects of repeated exposure on natural weathering and cyclical wetting/drying on performance must be known. B.J. Mohr et al. [14] have investigated the durability of pulp fiber reinforced cement composites and found that the composite lost its post cracking peak strength and toughness after 5 wet/dry cycles. On the other hand, B. P. Soroushian et al. [15] have noticed that the flexural strength of kraft pulp fiber reinforced cement composites increased with wet/dry cycling. Additionally, after 12 wet/dry cycles, a significant drop in flexural toughness was observed. Mohr et al. [14] have identified a series of degradation mechanisms that occurred in the natural fiber reinforced cement composites subjected to various wet/dry cycles: (i) fiber to cement debonding after 2 wetting/drying cycles; (ii) continuous reprecipitation hydration compounds within the void space at the former fiber to cement interface during the initial 10 wet/dry cycles; (iii) after 10 wet/dry cycles, fiber mineralization occurred which led to fiber embrittlement, which was indicated by relatively minor increases in strength and no recovered toughness. Similarly, Toledo Filho et al. [16] examined the alkaline attack of the fibers after exposure to different wet/dry cycles. They assessed the durability of sisal and coconut fibers in cementitious composites and alkaline media. They noticed that sisal and coconut fibers immersed in alkaline media of calcium hydroxide for 300 days completely lost their flexibility. This was due to the crystallization of lime in the lumen, walls, and voids in the fiber. The fiber embrittlement was related to the mineralization of fiber due to the migration of hydration products, especially calcium hydroxide, to the fiber lumen, walls, and voids. They also noticed that for composites manufactured using shorter fibers, greater embrittlement was observed than composites reinforced with long fiber. The authors credited this effect to the higher number of endpoints and larger surface area of the short fibers, which permitted a faster penetration of cement hydration products and following mineralization of the fibers.

This study aimed to investigate the influence of the fiber dosage and the effect of wet/dry and heat/rain cycles on the mechanical performance of Ev fiber reinforced cementitious composites. The durability of the natural fiber composite was evaluated based on four-point bending tests that were performed after the accelerated aging of the specimens, in comparison to reference, unaged specimens. The investigation was performed on 28 similar specimens: six specimens for 50 heat/rain cycles, six specimens for 6 cycles of wet/dry, six specimens for 12 cycles of wet/dry, and twelve reference specimens. The specimens were manufactured by reinforcing the thin cementitious matrix section with one layer of aligned Enset fibers with a 0 % (plain mortar) and 3 % volume fraction. To measure strains and displacements and to visualize cracks, Digital Image Correlation (DIC) was used [17]. This full-field optical measurement technique allowed us to have a more complete view of the mechanical performance of the composite, focusing not only on the residual strength and stiffness but also on the influence of aging on the crack distribution.

2. MATERIALS AND METHODS

2.1 Material characteristics

The material properties of both the mortar and the natural fibers are described below.

2.1.1 Ensete Ventricosum (Ev) fibers

The Ensete ventricosum (Ev) fibers (Figure 1) used in this research were obtained from the Jimma in Ethiopia. The fiber was extracted from the stalk part of the Ev

Figure 1: Enset (Ev) fiber bundles

plant by using a hand scrapping method [18] and sun-dried without any prior treatment. The Ev fibers had a rough surface, white color, and an irregular cross-section.

2.1.2 Matrix

For the matrix, SIKAGROUT, which contains an Ordinary Portland Cement-based, fine-grained siliceous sand, admixtures, and self-compacting mortar was selected [19]. The main requirement for the choice of the cementitious matrix was its pourability to impregnate the fibers easily.

2.1.3 Specimen manufacturing

The Ev fiber reinforced cementitious composites were manufactured by integrating one layer of Ev fibers aligned with the loading direction, resulting in a fiber volume fraction of 0 % and 3 %. The specimens had the following dimensions: 450 mm x 60 mm x 15 mm. Before matrix preparation, the fibers were cut at 45 cm length, weighted, and separated. The matrix was produced using a bench-mounted mechanical mixer with a capacity of 20 L. The mortar mix was poured at the bottom of the mold to achieve a 5 mm cover (Figure 2 (a)). Secondly, a layer of fibers was placed on top of this mortar layer and finally, the rest of the mold was filled by matrix (Figure 2 (b)). The exact location and alignment of the fibers were controlled first by manual tensioning and then fixing the fiber at the edge of the mold by screws. A vibrating table was used to allow the mortar to fully penetrate the fiber layer. Once the mold was filled, the excess mortar was removed using a flattening ruler and the mold was covered with a stiff plastic foil and sealed off. All samples were stored at ambient temperature (~20 ℃) and RH between 45 % and 60 % for

28 days before the accelerated aging process was started. Virgin samples (not aged), as well as the samples that were subjected to a lower number of cycles, remained in

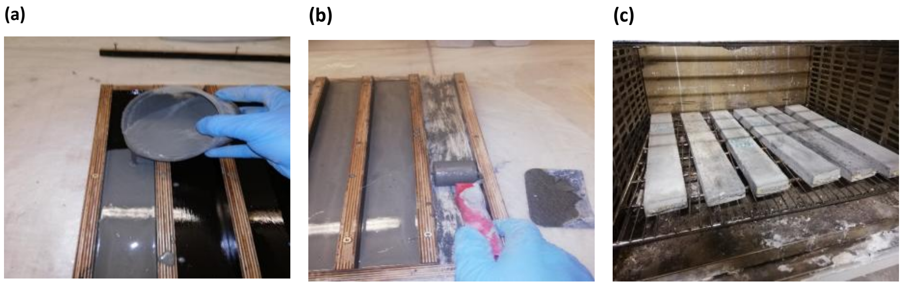

Figure 2: (a) Pouring of the first matrix layer (b) straightened fibers placement and impregnations (c) casted specimens undergoing accelerated aging in the oven.

the curing process for longer periods so that all samples were mechanically tested at the same age.

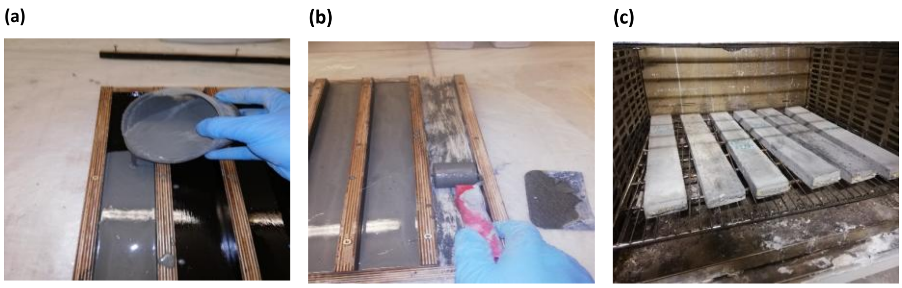

2.2 Experimental test setup

Four-point bending tests on the specimens were conducted using an Instron 5900R test bench under a controlled crosshead speed of 2 mm/min. The distance between the supports was 350 mm and between the loading pins 100 mm. DIC was used to monitor the side view of the specimens to obtain the cracking pattern.

2.3 Durability

The samples were exposed to 6 or 12 wet/dry and 50 heat/rain cycles. A wet/dry cycle was defined as 23 hours and 30 minutes drying in an oven at 60 ± 5 °C and 20 ± 5 % RH, followed by 30 minutes air drying at 22 ± 5 °C and 60 ± 5 % RH, then 23 hours and 30 minutes soaking in the water at 20 ± 2°C and finally 30 minutes of air-drying. Following the standard EN 12467 (2012) [20], the specimens were heated up to 60 °C within 15 min during the heat/rain cycle and kept at that temperature for another 45 min. Instead of subjecting the samples to a water spray, they were cooled by submersion in a 20 °C water bath for 30 min and paused for 10 min.

3. RESULTS AND DISCUSSION

3.1 Mechanical property of unaged Ev fiber composite

Load-deflection curves obtained from the four-point bending tests on specimens are shown in Figure 3. Parameters used to assess the flexural performance of the composites were the strength loss in terms of ultimate load, the post cracking stiffness (slope of the load-deflection curve), post cracking toughness [21]. Post-cracking toughness is defined as the area under the load-deflection curve beyond the first cracking up to the maximum failure load.

Contrarily to the plain mortar specimens (Figure 3 (b)), the unaged Ev fiber reinforced specimens (Figure 3 (a)) exhibited a clear strain hardening behaviour in the post-cracking stage. This is due to fiber bridging of the cracks that ensured a post-cracking behaviour. The use of Ev fibers as a reinforcing component resulted in a significant increase in flexural strength (Figure 3 (a)). In the specimens containing plain mortar, only one major crack was observed whereas the Ev fiber reinforced specimens presented multiple cracks. The unaged reference specimens failed gradually after reaching the failure load. The samples showed pull-out after achieving the average ultimate load of 842 ± 89 N at the maximum deflection of 11 ± 2 mm. The reference specimens show an average first crack load of 507 ± 76 N, post cracking stiffness of 58 ± 5 N/mm, and toughness of 7234 ± 522 N mm. During the mechanical flexural tests, crack patterns were mapped using DIC and there was a formation of multiple cracks (see Figure 3 (a)). A post cracking ductility and multiple cracking behavior were thus observed for the reference specimens.

3.2 Effect of Wet/Dry cycles

The durability issues of Ev fiber reinforced cement-based composites were demonstrated by the drop in flexural properties. A wet/dry cycle at higher temperatures has been adopted to accelerate the degradation of natural fiber in the cement matrix [9], [14], [21]. Samples were tested at 6, and 12 wet/dry cycles to measure the development of degradation. Figure 3 (d) and (e) show typical load-deflection curves after 6 and 12 cycles. The ultimate failure load of specimens after 6 wet/dry cycles was 415 ± 55 N, after 12 wet/dry cycles 347 ± 73 N, while for the reference unaged specimens the ultimate failure load was 842 ± 89 N. In fact, the ultimate failure load of the wet/dry aged specimens approaches the failure load of the plain mortar specimens. There is a 51 % and 59 % loss of peak strength after 6 and 12 wet/dry cycles respectively. These results are consistent with those reported by other researchers on Kraft pulp fibers cement composite at a 4% fiber volume fraction which found a peak strength loss of 51–72 % after 25 wet/dry cycles and the aged specmen failure load was much lower than that of the unaged specimens [14]. Both specimen series undergoing 6 and 12 wet/dry cycles exhibited softening in the post-cracking stage and present lower strength indicators in comparison to reference specimens. The decrease or even disappearance of post-cracking behavior not only demonstrates the increasing brittleness of Ev fiber reinforced composites, but also indicates the degradation of Ev fiber.

The DIC analysis showed only one crack with an abrupt brittle failure. This highlights the loss of composite action due to the wet/dry cycles and proves that the fibers can no longer warrant a post-cracking behaviour. A possible explanation is that the fibers were so severely degraded after the aging process (and their tensile properties so reduced) that with the relatively low fiber volume fraction of 3 %, no composite action could be achieved. The degradation of Ev fibers could happen due to direct attack by the Portland cementitious matrix due to reactions with the highly alkaline pore water or attack by external agents which penetrate through the cementitious matrix into the fiber [22].

3.3 Effect of Heat-Rain Cycles

Samples were tested after 50 heat/rain cycles to measure the progression of damage. Figure 3 (c) illustrates typical load-deflection curves after 50 heat/rain cycles. The curves show a short post cracking toughness behavior with an average failure load of 493 ± 64 N at 1.3 ± 0.4 mm deflection. The specimens undergoing heat/rain cycles still showed multiple cracking behavior. The post cracking stiffness and toughness was 32 ± 4 N/mm and 1254 ± 124 N mm respectively. It can be seen that there is a 75 % loss of first crack strength, a 41 % loss of peak strength, and 86 % loss of post-cracking toughness after 50 heat/rain cycles.

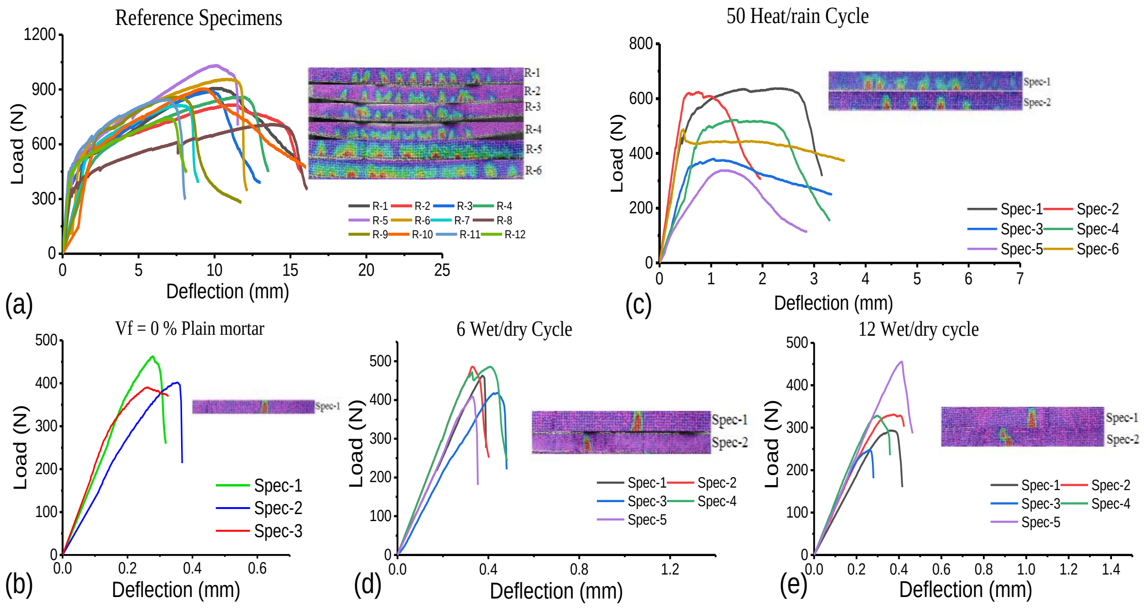

Figure 3 : Load vs Deflection and crack pattern: (a) Reference specimens (Vf = 3 %), (b) Plain mortar (Vf = 0 %), (c) 50 heat/rain cycle, (d) 6 wet/dry cycle, (e) 12 wet/dry cycle.

4. CONCLUSION

This paper investigated the loadbearing performance and durability of aligned Ev fibre reinforced cement composites. Based on the results, the following conclusions can be drawn:

As per the result from DIC measurements, the use of Ev fibers as reinforcement in cement composites resulted in a material with multiple cracking behaviour under four-point loading. The flexural strength, post-cracking stiffness, and post-cracking toughness of the Ev fiber reinforced cement composites increased as compared with plain mortar specimens.

The reference specimens (unaged) presented a clear post-cracking behaviour and composite action whereas the specimens exposed to 6 and 12 wetting/drying cycles did not. This was attributed to the severe damage of the Ev fibers, which were present in the composite section at a relatively low fiber volume fraction. Specimens exposed to 50 heat/rain cycles presented a limited post-cracking behaviour.

According to the authors' knowledge, no study in the literature has investigated the durability of Ev fiber reinforced cementitious composites. Further research should investigate the effect of accelerated aging and natural weathering. The improvement of the cement composite reinforced with Ev fiber needs to be investigated, e.g. by means of matrix composition alteration, in order to use the composite for indoor and outdoor applications.

Acknowledgments

This work is made possible by collaborating with different departments from different universities, the MeMC department from Vrije Universiteit Brussel, JU, JIT faculty of Civil and environmental engineering, Ethiopia, and collaboration between Ghent University and Jimma university under a NASCERE project.

Conflict of interest

The authors declare no conflict of interest.

5. REFERENCES

[1] KARADE S.,"Developments in Cement-Bonded Composite Material Technology," in National Seminar on Modern Trends in Architectural and Civil Engg. Practices, Roorkee, 23-24 Nov., Nov. 2007, pp. 57–64.

[2] SATYANARAYANA K. G., ARIZAGA G. G. C., and WYPYCH F., "Biodegradable composites based on lignocellulosic fibers - An overview," Prog. Polym. Sci., vol. 34, no. 9, pp. 982–1021, Sep. 2009, doi: 10.1016/j.progpolymsci.2008.12.002.

[3] WAMBUA P., IVENS J., and VERPOEST I., "Natural fibres: Can they replace glass in fibre reinforced plastics?," Compos. Sci. Technol., vol. 63, no. 9, pp. 1259–1264, 2003, doi: 10.1016/S0266-3538(03)00096-4.

[4] SILVA F. de A., CHAWLA N., and FILHO R. D. T., "Mechanical Behavior of Natural Sisal Fibers," J. Biobased Mater. Bioenergy, vol. 4, no. 2, pp. 106–113, Jun. 2010, doi: https://doi.org/10.1166/jbmb.2010.1074.

[5] CASTRO J., and NAAMAN A. E., "Cement Nortar Reinforced with Natural Fibers," in Journal of the American Concrete Institute, 1981, vol. 78, no. 1, pp. 69–78.

[6] XIE X., ZHOU Z., JIANG M., XU X., WANG Z., and HUI D., "Cellulosic fi bers from rice straw and bamboo used as reinforcement of cement-based composites for remarkably improving mechanical properties," Compos. Part B, vol. 78, pp. 153–161, Mar. 2015, doi: 10.1016/j.compositesb.2015.03.086.

[7] SEDAN D., PAGNOUX C., SMITH A., and CHOTARD T., "Mechanical properties of hemp fibre reinforced cement: Influence of the fibre/matrix interaction," J. Eur. Ceram. Soc., vol. 28, no. 2008, pp. 183–192, May 2007, doi: 10.1016/j.jeurceramsoc.2007.05.019.

[8] OLIVITO R. S., CEVALLOS O. A., and CARROZZINI A., "Development of durable cementitious composites using sisal and flax fabrics for reinforcement of masonry structures," Mater. Des., vol. 57, pp. 258–268, 2014, doi: 10.1016/j.matdes.2013.11.023.

[9] ROMILDO D T.F., GHAVAMI K., ENGLAND,G. L. and SCRIVENER K., "Development of vegetable fibre-mortar composites of improved durability," Cem. Concr. Compos., vol. 25, no. 2, pp. 185–196, 2003, doi: 10.1016/S0958-9465(02)00018-5.

[10] SUVASH CHANDRA PAUL B. Š., GIDEON P.A.G. van Zijl, "Effect of Fibers on Durability of Concrete : A Practical Review," Materials (Basel)., vol. 13, no. 4562, pp. 1–26, Oct. 2020, doi: 10.3390/ma13204562.

[11] ACI 544.1R-96, "Report on Fiber Reinforced Concrete Reported by ACI Committee 544," 2002.

[12] SWAMY R. N., "Concrete technology and design, vol. 1. New concrete materials," Int. J. Cem. Compos. Light. Concr., vol. 6, no. 2, pp. 130–131, 1984, doi: 10.1016/0262-5075(84)90048-4.

[13] BERHANE Z., “Performance of natural fibre reinforced mortar roofing tiles,” Mater. Struct., vol. 27, no. 6, pp. 347–352, Oct. 1994, doi: 10.1007/BF02473427.

[14] MOHR B. NANKO J., H., and KURTIS K. E., “Durability of kraft pulp fiber-cement composites to wet/dry cycling,” Cem. Concr. Compos., vol. 27, no. 4, pp. 435–448, 2005, doi: 10.1016/j.cemconcomp.2004.07.006.

[15] SOROUSHIAN B. P., MARIKUNTE S., and P. WON J.-, “Wood Fiber Reinforced Cement Composites under Wetting-Drying and Freezing-Thawing Cycles,” J. Mater. Civ. Eng., vol. 6, no. 4, pp. 595–611, 1994, doi: doi:10.1061/(ASCE)0899-1561(1994)6:4(595).

[16] TOL R. D., SCRIVENER K., ENGLAND G. L., and GHAVAMI K., “Durability of alkali-sensitive sisal and coconut fibres in cement mortar composites,” Cem. Concr. Compos., vol. 22, no. 2, pp. 127–143, Oct. 2000, doi:10.1016/s0958-9465(99)00039-6.

[17] SUTTON J. J. O. M. A. and SCHREIER H. W., Image Correlation for Shape, Motion and Deformation Measurements. Boston, MA: Springer US, 2009.

[18] TELI M. D., and TEREGA J. M., “Chemical, Physical and Thermal Characterization of Ensete ventricosum Plant Fibre,” Int. Res. J. Eng. Technol., vol. 04, no. 12, p. 9, Dec. 2017, [Online]. Available: http://www.irjet.net.

[19] SIKA, Sikagrout 217. 2016. Note de produit.” [Online]. Available: https://fra.sika.com/dms/getdocument.../sikagrout_217_nt810.pdf.

[20] BELGISCH INSTITUUT VOOR NORMALISATIE(BIN) NBN EN 12467, “Fibre cement flat sheets – Product specification and test methods Toelating.” 2007.

[21] WEI J., and MEYER C., “Degradation rate of natural fiber in cement composites exposed to various accelerated aging environment conditions,” Corros. Sci., vol. 88, pp. 118–132, Jul. 2014, doi: 10.1016/j.corsci.2014.07.029.

[22] BENTUR A., and MINDESS S., Fibre Reinforced Cementitious Composites, Second. 2 Park Square, Milton Park,Abingdon, Oxon OX14 4RN, 2007.

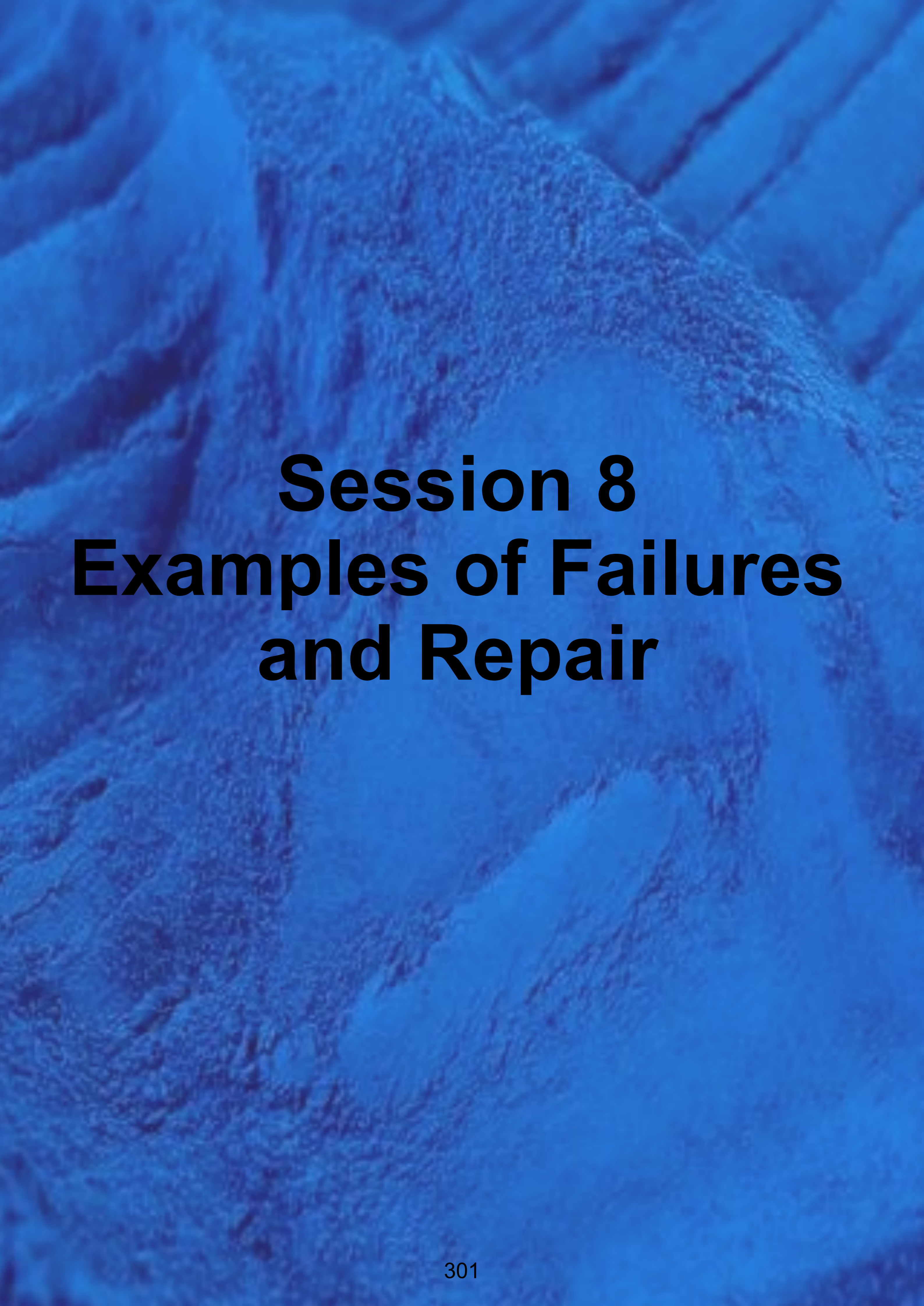

Session 8 Examples of Failures and Repair

CONSTRUCTION, FAILURE AND REPAIR OF FERROCEMENT TANKS USED IN WASTE WATER TREATMENT PLANTS

Sávio Nunes Bonifácio1, Cristiano Martins Quintão2, Frieda Keifer Cardoso3

[1]*Author1 (Civil Engineer, Specialist in Sanitation at CEFET-MG and Master in Sanitation at UFMG. Address 1): Rua Mar de Espanha, 525 – Bairro Santo Antônio – Belo Horizonte – Minas Gerais – CEP: 30270-900 – Brazil – Tel .: +55 (31) 3250-1770 – e-mail: savio.nunes@copasa.com.br)*

[2]*Author2 (Civil Engineer from the Federal University of Viçosa. Specialist in Sanitary Engineering at UFMG. Master in Civil Construction at UFMG.)*

[3]*Author3 (Civil Engineer from the Pontifical Catholic University of Minas Gerais – PUC Minas. Specialist in Water and Waste Management at Hydroaid. Master in Sanitation, Environment and Water Resources at UFMG).*

SUMMARY: In Minas Gerais Brazil, since 1998, a Waste Water Treatment Plant has been built, composed of UASB reactors (Upflow Anaerobic Sludge Blanket Reactors) in modules for flow rates up to 30 L/s and efficiency average 80% removal of organic load.-This article presents a case study of repair and protection of ferrocement structure of a WWTP that after 18 years of operation, presented collapse of your upper slab. The study contemplates the diagnosis to detect anomalies, the reapir project, the choice of protective coating and waterproofing and monitoring with a survey of the real cost of the work. The study aimed to return Waste Water Treatment Plant requirements for strength, safety, durability and operational efficiency.

***KEY WORDS**: Ferrocement, recovery, protection, Waste Water Treatment Plant*

1. INTRODUCTION

Ferrocement, in its literal definition in the Code Model edited by the International Ferrocement Society (IFS, 2001), is defined as follows: “Ferrocement is a type of reinforced concrete, commonly built with hydraulic cement mortar, reinforced with several layers of relatively thin diameter wire mesh. This screen can be metallic or another suitable material. The fineness of the mortar matrix and its composition must be compatible with the braiding and the openings of the structural mesh system, making it possible to involve it with the cement mass. The matrix may contain staple fibers”.

The Ferrocement Waste Water Treatment Plant was developed from research on the state of the art of applying this technology throughout Brazil and worldwide. The hydrosanitary project applied to the treatment of domestic sewage with a UASB reactor follows the parameters of the literature, in particular recommended by Chernicharo (1997, 2007), such as: hydraulic detention time; volumetric organic load; upward flow velocity; reactor dimensions; effluent distribution system; surface application rate in the decanter; hydraulic holding time in the decanter; checking the speed in the passages of the three-phase separator; speed in the openings for the decanter; estimation of treatment efficiency; sludge production, sampling and removal; production and collection of biogas; verification of biogas release rates; and, foam removal system.

The UASB reactor was first developed and applied in the Netherlands. The process consists of an ascending flow of sewage through a dense sludge bed of high activity. In the internal part, there is a device called a three-phase separator, which aims at separating the generated gases (biogas), the sludge, and the liquid effluent. At the top is the decanter with the effluent outlet, and the gas and scum chamber. It is today one of the most used reactors for the treatment of domestic sewage. It stands out for its simplicity and the lack of filling material and sophisticated equipment.

Since 1998, UASB ferrocement reactors have been built in the WWTPs in Minas Gerais, Brazil, with more than 50 units installed, in modules, with a flow rate of up to 30 L/s. This success is attributed to the fact that the construction and operation are simple, with low cost of implantation, in comparison to reinforced concrete structures, and the efficiency of the treatment, an average of 80% of removal of the organic load. However, in UASB reactors, the cover dome and other parts that are in contact with the gases have high corrosion rates.

The technique of UASB reactors in ferrocement expands with dozens of units built according to a survey carried out by Lapa (2014) (FIG. 1).

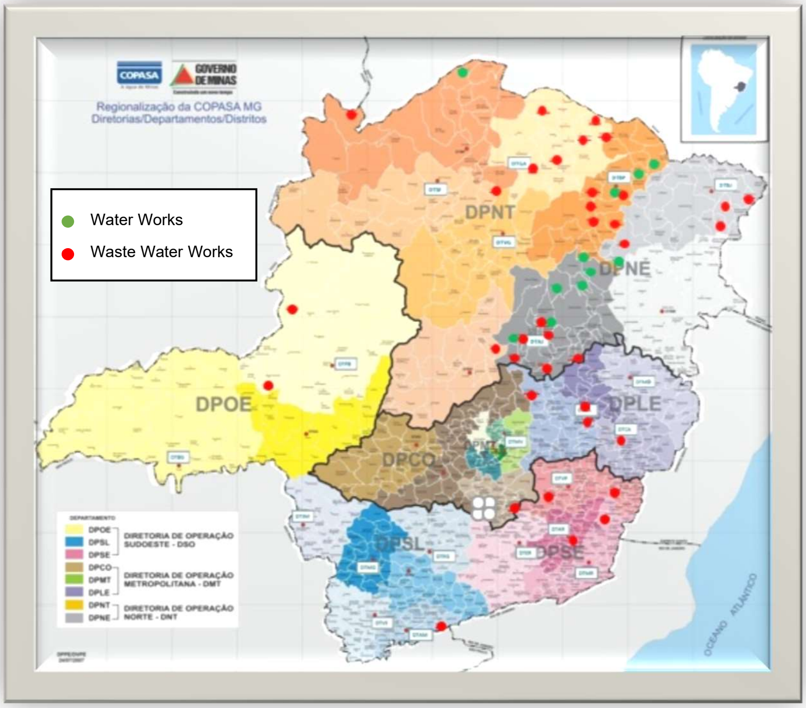

Figure 1 – *Spatial distribution of works in ferrocement in the State of Minas Gerais, Brazil, by COPASA MG regionals, in government programs, from 2003 to 2010.* Source: Lapa. COPASA, 2010.

COPASA MG, seeking to solve the sewage treatment of small towns in the rural area of the State of Minas Gerais, developed the ferrocement projects (FIG. 2 and 3) of UASB reactor, based on the studies by CHERNICHARO (1997, 2007). The technology requires less area for settlement; low cost of implementation and simplified operation.

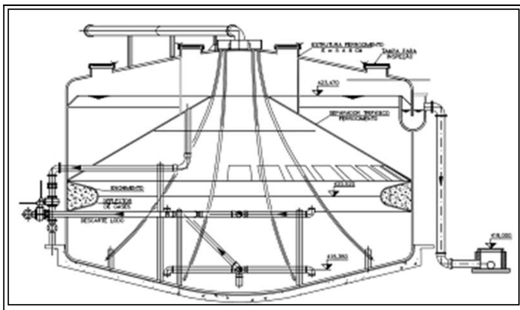

Figure 2. *UASB Reactor – Ferrocement – CUT.*

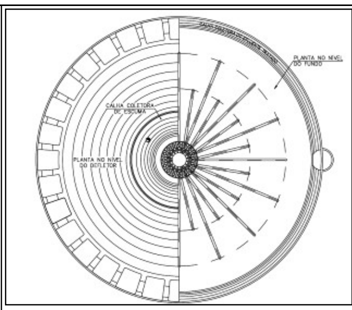

Figure 3. *UASB Reactor – Ferrocement – PARTIAL DETAIL – PLANT.*

This article contextualizes the construction of a Waste Water Treatment Plant using ferrocement by the Companhia de Saneamento de Minas Gerais – COPASA MG and presents a case study of corrosion, where the recovery and protection of the structure in ferrocement was carried out.

2. OBJECTIVE

The purpose of this article is to present a case study of recovery and protection of ferrocement structure used for the treatment of sanitary sewage, composed of two UASB reactors.

3. METHODOLOGY

The methodology used to carry out this work included the following activities: diagnosis, recovery project and monitoring of the work.

3.1 Diagnosis

Evaluation of the structures of the UASB reactors through visual inspection and non – destructive tests (END) to detect existing anomalies and analyze projects.

3.1.1 – Characteristics of Existing Structures

Two anaerobic reactors, built in ferrocement, in circular geometry, semi-buried, with an external diameter of approximately 10.00 meters and 4.60 meters of external height and 7.00 meters of internal height. The walls have a thickness that varies from 3 to 8 cm. Internally, each UASB reactor has divisions used in the sewage treatment process and the roof slab is domed. In the roof slab there are entrance hatches for access to the interior of the reactor and for cleaning. The internal surface, notably the area in contact with the gases, is exposed to an environment with class of aggressiveness IV (very strong) according to NBR 6118: 2014

The studies, at the time, focused on the production of biogas, a flammable gas of energy value. Bonifacio (2005), in his research, checked the components of biogas: 75% methane (CH_4); 25% carbon dioxide (CO_2) and other gases, such as hydrogen sulphide (H_2S) by 0.3%.

Confirming the importance of biogas production has the history of rural biodigesters in ferrocement for animal waste (ANDRADE et al, 1994). For waterproof coating for the internal area of the hood indicate:

- Coating with chlorinated rubber base;
- Polyurethane cover;
- Epoxy paint;
- Asphalt-based coating.

3.1.2 - Corrosion

Corrosion problems on the underside of the roof slab begin to appear in concrete and ferrocement reactors and prompt a bibliographic search to detect the reasons.

Chernicharo (1997, 2007) points to the formation of hydrogen sulphide gas, which in the gaseous atmosphere of the UASB reactor decanter, has the opposite production to the biogas collected from the same reactor. This gas reacts in the environment and forms sulfuric acid that attacks the cement mortar, forming the late etringite, which disintegrates the structure (FIG. 3 and 4).

Figure 3. *Deterioration of mortar subject to gas attack on the underside of the reactor cover slab UASB (*Source: Author).

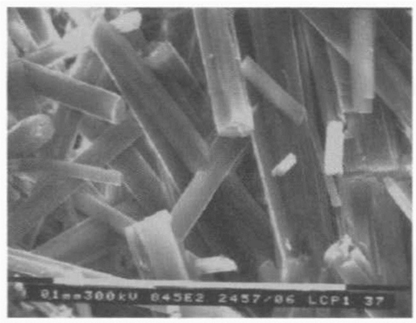

Figure 4. *Etringite needles, the result of a sulfatic attack on concrete (Source: Silva; Pinheiro. IBRACON, 2005)*

The bibliographic research clarified the biodeterioration of the concrete/ferrocement, with the formation of microorganisms, especially thiobassillo concretivorus and thiobacillo thioxidans, are aerobic bacteria that oxidize the sulfuric gas formed in the digestion of the sewage and turns it into biogenic sulfuric acid in its metabolic processes. pH lower than 0.7, causing great deterioration in the structures (FIG. 5 and 6).

Figure 5 – *Structure with severe deterioration and loss of the cement and steel section.*

Source: Author.

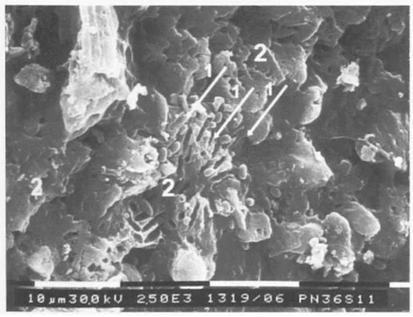

Figure 6 – *Thiobacillus type bacteria, seen in deteriorating structures.*

Source: Silva; Pinheiro. IBRACON, 2005.

3.2 Recovery Project

COPASA, attentive to the problems detected, gathered a group of designers (BONIFÁCIO; QUINTÃO; D'ÁVILA. 2015) and hired consultancy for diagnosis (Rel_Recoveryação_Arquivo_2013). Tests were carried out on the affected tanks and a solution scope was proposed.

3.2.1 – Characteristics of Existing Structures

For analysis and dimensioning of the structure of the UASB reactor in ferro cement, the Finite Element Method (FEM) modeling was performed and the maximum circumferential membrane force (Nθ) of 16,772 kgf/m was found (FIG. 7). The detail of the typical transverse frame of the reactor wall is shown (FIG. 8).

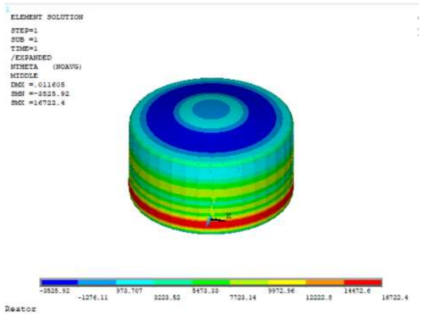

Figure 7 – *Reactor – Circumferential Membrane Force N_θ*

Source: FCO_ Reactor UASB Ferroc, 2018.

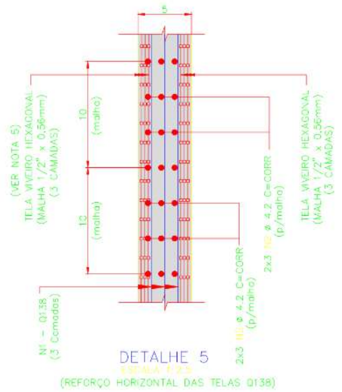

Figure 8 *Horizontal reinforcement of the reactor wall*

Source: FCO_ Reactor UASB Ferroc, 2018.

3.2.2 – Visual inspection

To identify and locate all visible pathological manifestations and register, the intensities and severities.

Figure 9 – *Detail of reinforcement exposed in a general way in the reactor cover slab.*

Source: Rel_Recuperação_Arquivo_2013

Figure 10 – *Some points with disruption of the steels. between the wall and cover slab of the reactor.*

Source: Rel_Recuperação_Arquivo_2013

3.2.3 – Carbonation Depth Measurement

The results showed low advances in the carbonation front, with an average of 2.5 mm in depth, proving that these are structural elements constructed of mortar of good quality and compactness.

Figure 11 – *Detail of sample extraction to perform the carbonation front test.*

Source: Rel_Recuperação_Arquivo_2013

Figure 12 – *Carrying out the carbonation front test.*

Source: Rel_Recuperação_Arquivo_2013

3.2.4 – Surface resistance through sclerometry

The values obtained are above the design specification, with compressive strength greater than 25 MPa, obtaining average results of 41 MPa.

Figure 13 – *Execution of sclerometry on the reactor wall.*

Source: Rel_Recuperação_Arquivo_2013

Figure 14 – *Execution of sclerometry on the reactor wall.*

Source: Rel_Recuperação_Arquivo_2013

3.3 Monitoring of the work

- It started with the emptying and removal of sludge and cleaning with hydrojetting.
- The roof slab was demolished and rebuilt according to the original design.
- Exposed reinforcement and cracks were treated.
- The internal surfaces received a crystallizing cementitious mineral coating and waterproofing to protect surfaces in contact with water.

- The covering slab in contact with gases from anaerobic digestion coatings were researched: with high-thickness polyurea systems; polyurea/polyurethane hybrids; adding an antimicrobial crystalline admixture to the reconstitution mortar followed by an internal layer of anti-acid geopolymer coating. For the Sewage Treatment Station under study, it was opted for the coating in vinyl ester resin reinforced with glass fiber (PRFV) applied to the ferrocement substrate.
- Fiberglass covers were made and installed; external painting with acrylic paint and pultruded fiberglass railing in the outline of the roof slab.

4. RESULTS

4.1 Sequency of the Work

The services follow the one applied by Bonifácio *et. al* (2015), the following sequence:

 **Figure 1 –** *Opening a service window.*	 **Figure 2 –** *Removal of debris and sludge from the bottom*	 **Figure 3 –** *50 cm scarification on the side of the reactor wall*
 **Figure 4 –** *Execution of the reinforcement for ferrocement.*	 **Figure 5 –** *Mortar application with vibrating box (Wainshtok Rivas, 2009)*	 **Figure 6 –** *Application of cementitious waterproofing on the submerged wall.*
		

Figure 7 – *PRFV application in the gas chamber*	**Figure 8 –** *Installation of FRP inspection window covers.*	**Figure 9 –** *Installation of guardrails and access stairs to the UASB reactor.*

Source: Author.

4.2 Real Cost

The construction cost of each UASB reactor in ferrocement for the Waste Water Treatment Plant was US$ 126,765 (BONIFÁCIO; QUINTÃO; COELHO. 2020).

The cost of recovery measured at the site of each UASB reactor was US$ 75,905, approximately 60% of the cost of implementing a new Sewage Treatment Station (BONIFÁCIO; QUINTÃO; COELHO). 2020).

5 CONCLUSIONS AND RECOMMENDATIONS

The UASB reactor in ferrocement is a technology applied in Minas Gerais, Brazil, in cases where the structure needed repairs were carried out following the methodology described above.

With this work, products for internal corrosion protection covered in vinyl ester resin reinforced with glass fiber became known, which will require monitoring of its efficiency as a protective element against ferrocement.

It is of great importance the training of qualified workers in ferrocement and the monitoring and inspection of the work by professionals with the technical competence that guarantee the execution of the work according to the project.

6 REFERENCES

[1] AGUIAR, José E.; SOUZA, Evandro C.; MORAES, Ana C. L. RECUPERAÇÃO S.E. Engenharia. *Betim – Estação de Tratamento de Esgoto – Reator anaeróbio*. [Relatório Técnico]. Belo Horizonte: COPASA. Arquivo: 00727949-ES-EP-01-ETE-RAN01-EO-001-0-REC-2013, 2013.

[2] ANDRADE, Márcio A. *et al. Cartilha do biodigestor rural em ferrocimento artesanal.* Fortaleza: Centro de Tecnologia da UFC, 1994.1994.

[3] ASSOCIAÇÃO BRASILEIRA DE NORMAS TÉCNICAS. NBR 6118: *Projeto de Estruturas de Concreto – Procedimento. Rio de Janeiro, 2014.*

[4] BONIFACIO, S.N. *O que fazer com o biogás? – a casa do fogo sagrado.* 2006. Monografia (Especialização em Engenharia Sanitária e Meio Ambiente). Belo Horizonte: CEFET-MG, 2006.

[5] BONIFÁCIO, Sávio N.; QUINTÃO, Cristiano M.; COELHO, Daniel S. *Diagnóstico, projeto e obra de recuperação e proteção de reator UASB de ETE em ferrocimento.* In: SIMPÓSIO LUSO-BRASILEIRO DE ENGENHARIA SANITÁRIA E AMBIENTAL, 19, 2020, Recife – Pernambuco. Anais... Rio de Janeiro: ABES, 2020.

[6] BONIFÁCIO, Sávio N.; QUINTÃO, Cristiano M.; D'ÁVILA, Carlos A. C. *Vida útil, patologias e terapias de ETE em ferrocimento – Estudo de caso de sucesso em uma companhia de saneamento.* In: CONGRESSO BRASILEIRO DE ENGENHARIA SANITÁRIA E AMBIENTAL, 28, 2015, Rio de Janeiro. Anais... Rio de Janeiro: ABES, 2015.

[7] CHERNICHARO, Carlos A. L. *Reatores anaeróbios – Princípios do tratamento biológico de águas residuárias; 5.* Belo Horizonte: DESA/UFMG, 1997, 2007.

[8] COMPANHIA DE SANEAMENTO DE MINAS GERAIS. *Norma Técnica T.186: Ferrocimento para Obras de Saneamento.* Belo Horizonte: COPASA, 2016.

[9] INTERNATIONAL FERROCEMENT SOCIETY. *Ferrocement Model Code: Building Code Recommendations for Ferrocement.* Klong Luang, Pathumthani, Tailândia: IFS, 2001.

[10] LAPA, Gelson A. *Saneamento para Comunidades de Pequeno Porte – Ferrocimento: Resultado da pesquisa quantitativa e qualitativa na COPASA (ETA, ETE e RESERVATÓRIO)*. Encontro Técnico COPASA, Belo Horizonte, 2010.

[11] RIBEIRO, Gabriel O.; BARROS, Felício B.; PITANGUEIRAS, Roque L. S. Fundação Chrisiano Otoni. *Análise e dimensionamento da estrutura do reator UASB em ferrocimento*. [Relatório de Consultoria Técnica]. DEES-UFMG. Belo Horizonte: COPASA, 2018.

[12] SILVA, Moema R.; PINHEIRO, Sayonara M. M. *Biodeterioração do Concreto*. Concreto, Ensino, Pesquisa e Realizações, Geraldo Cechela Isaia (Editor), IBRACON, São Paulo, Cap. 28, p. 857-878, 2005.

[13] WAINSHTOK RIVAS, Hugo. *Ferrocemento – Diseño y Construccion*. Riobamba, Equador: EcoSur, 2010.

REVEALING THE MIXED MODE FAILURE UNDER PULL-OUT OF MASONRY RETROFITTED BY TEXTILE REINFORCED MORTAR (TRM)

David Martin Linn III[1], Dimitrios G. Aggelis[1], Eleni Tsangouri[1]

[1]Dept. Mechanics of Materials & Constructions (MeMC), Vrije Universiteit Brussel (VUB), Belgium, david.martin.linn.iii@vub.be , eleni.tsangouri@vub.be, dimitrios.aggelis@vub.be

SUMMARY: *The performance of TRM retrofit solutions for damaged masonry structural elements is evaluated in this study using pull-out testing procedure recommended by the RILEM TC 250-CSM. The parametric analysis (textile/interface surface treatment/setup configuration) is designed to trigger different failure modes during testing and the damage progress is continuously and online tracked by an integrated monitoring system that combines the acoustic emission and digital image correlation techniques. Based on inspection outcome and the load-displacement curves obtained, it is evident that different damage modes occur simultaneously while the effect of boundary conditions and interface surface treatment is highlighted.*

KEY WORDS: *Masonry retrofit, textile reinforced mortar, adhesion, detachment, pull-out, failure mode, digital image correlation, acoustic emission*

1. INTRODUCTION

Masonry consists of the building-up construction of individual units, which are often laid and bound together by an assembling material such as mortar. Many decaying historical and modern structures around the world are built up in masonry that are in urgent need of repair. The effective conservation, repair and retrofit of masonry structures is a research topic that has attracted the scientific community since great efforts are focused on the design of TRM external layering [1]. TRM materials should be mechanically and physically compatible to the existing masonry structure but must also be reversible to ensure the structural integrity with respect to the aesthetic and structure's historical identity. The bond between the individual constituent materials of TRM repaired masonry plays a critical role in the quality of the retrofit repair. Special attention should be placed on not just the overall performance of the TRM, but the evolution of debonding progress and ultimate failure mode. Several studies were conducted to understand the bond behavior of TRM-masonry retrofit repairs and the failure mode [2-4]; however, the variety of experimental set-ups highlighted the need for an agreed upon testing protocol. RILEM TC 250-CSM provides guidelines for an accurate shear bond pull-out testing of the TRM-substrate to assess the materials' structural performance and the final failure mode of the TRM on masonry [5]. These guidelines prescribe test set-up details such as boundary conditions, specimen dimensions, and recording methods. Researchers utilizing the RILEM guidelines have attempted to improve the understanding of damage progress of TRM retrofit repairs on masonry substrate through stress-displacement relationships [6-8]. However, the point at which the stress-transfer is fully established and debonding starts is not easily determined with this current approach. This highlights the importance of detecting the point of debonding, and the ability to track the damage progress throughout the experimental tests of TRM-masonry specimens. Due to the limitations of the test outcome and result variability, this study implements acoustic emission (AE) and digital image correlation (DIC) techniques to provide an integrated monitoring methodology that detects the onset and tracks the progress of damage progress of the TRM-masonry bond relation. Recent studies on damage evolution in masonry and concrete retrofit solutions have demonstrated the complimentary nature of AE and DIC results [9-11]. When used together, DIC supplies accurate strain development and damage localization on the surface (i.e. crack patterns), while AE collects acoustic activity from below the TRM surface that specifies the failure onset and characterizes the fracture mechanism.

The aim of this study is to provide further understanding into the debonding behavior and materials' interaction for TRM retrofit on masonry small-scale walls while following the RILEM guidelines. With the addition of continuous monitoring, provided by AE and DIC, it is possible to detect the instance of debonding of TRM-masonry pull-out tests which is otherwise not possible. With this novel approach it is now possible to track damage progress as early as the failure onset.

2. MATERIALS AND METHODS

Traditional red-clay bricks and cement-based mortar were chosen to construct masonry wall samples, while cement-based mortar with glass and carbon fibers were selected for the TRM layer. The experimental testing guideline and specimen preparation prescribed by RILEM were followed to evaluate the shear bond performance of retrofitted masonry. The AE experimental setup consisted of six narrow band 150 kHz resonant piezoelectric R15α Mistras AE sensors placed on the surface of the masonry and TRM retrofit layer. DIC utilized two high resolution cameras to provide a 3D stereoscopic vision. For the application of the technique, a randomized black-white speckled pattern was applied on the surface.

3. RESULTS

A parametric study is designed to trigger a diversity of failure modes. This way the non-destructive monitoring methodology will be calibrated and tuned to provide an insightful view of the damage progress.

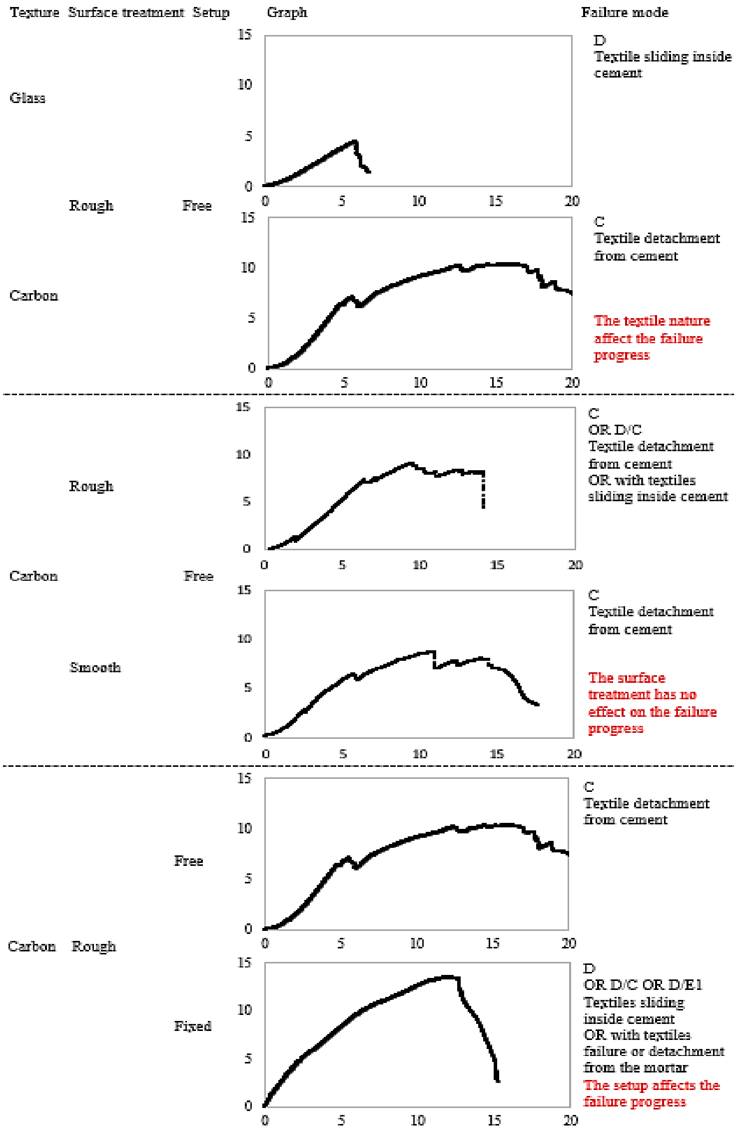

Figure 1 : Overview of the cases under study

In Figure 1, the cases under study are enlisted, and the respective load-displacement curves are plotted. The x-axis shows the displacement evolution (mm), whereas the y-axis provides the load progress (kN). Additionally, the final failure mode is also given according to the RILEM guidelines. Under pull-out loading, the textiles slide and finally break with similar ultimate load for the TRM retrofit layers when glass textiles are used. In contrast, the carbon TRM retrofit layers fail due to textile detachment from the mortar with varying ultimate load. It is evident that the textile stiffness and strength control the failure of the retrofit layer, however, this does not affect the interfacial adhesion with the masonry. The interface surface treatment was proven to have no impact on the damage progress. As shown in Table 1, the samples of masonry that are smoothened to ensure good interfacial adhesion lead to TRM-substrate failure at higher loads and at greater extension. In both rough and smooth interfacial surface treatment though, the final failure mode is the same, i.e. textiles sliding and failure at the TRM failure. The confinement of the substrate under loading ensures that misalignments do not occur, and that only the TRM is axially pulled out. Only in this configuration, the textiles slide, and cracks are developed along the TRM layer. Inversely, the freely moving samples break due to textiles detachment from the mortar.

This analysis provides little information into the onset and evolution of debonding in the TRM and final failure mechanism. This is especially true if there are multiple failure mechanisms involved throughout the pull-out test. As previously stated, the combination of AE and DIC has demonstrated effectiveness at revealing the debonding phenomenon throughout the pull-out tests. For example, interfacial debonding between the constituent materials is detected on the surface of the TRM layer by measuring out of plane displacement and strain changes throughout the pull-out tests. Furthermore, DIC is also able to track damage progress globally from textile sliding and rupture outside of the bonded TRM layer. Figure 2 below highlights the evidence of crack formation and evolution of a representative sample from the first instance of a crack to the ultimate failure of the sample. The change in vertical strain is tracked from the first instance of a crack forming, to the successive cracks, until ultimate failure. The ability to detect the formation of cracks is important in detecting evidence of debonding. Debonding evidence is found by evaluating the change in W-displacement (out-of-plane displacement) along the TRM surface. The final failure mode is then confirmed with visual confirmation.

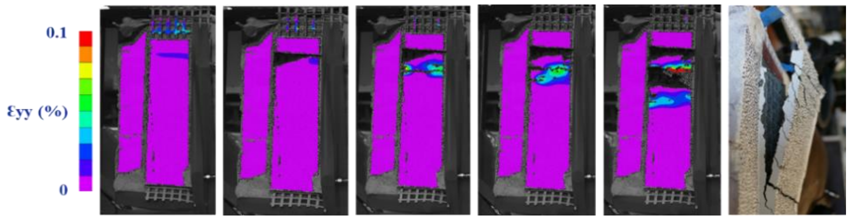

Figure 2. DIC strain map and crack evolution for progressive debonding of TRM layer

Simple AE information such as AE energy released and hits throughout the pull-out tests provides information that is confirmed with DIC. Ultimately, the key difference observed comparing AE information is more AE activity was recorded for the freely moving samples, which corresponds to failure by interfacial debonding. An example of a free moving sample, that experiences textile detachment from cement, is shown in Figure 3 with respective AE information. AE energy and hits released during load drops caused by debonding illustrates the ability to continuously track the debonding progress throughout the pull-out test. In addition, AE damage source localization was able to consider the complex nature of the TRM-masonry samples. The first AE localization approach considers information from all AE sensors placed on the masonry and TRM layer. The second approach considers only AE sensors placed along the TRM surface. This information provides 3D visualization of damage occurred in the TRM layer. Ultimately, the combination of both AE localization approaches, and DIC, allows for more accurate damage source tracking and localization compared to traditional approaches.

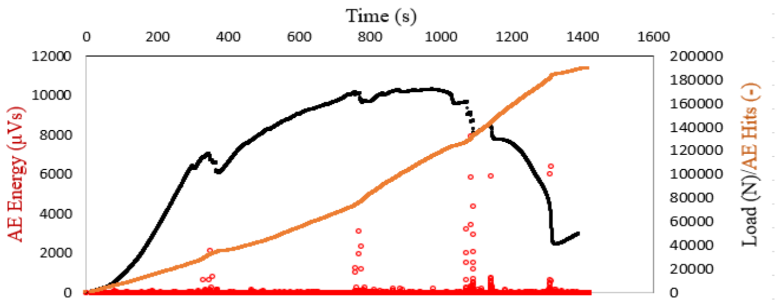

Figure 3: AE event localization along the TRM layer length (mm)

3. CONCLUSIONS

These preliminary results illustrate the complexity that possesses the outcome of the TRM-substrate fracture analysis. The continuous inspection and damage tracking at the TRM-substrate interface, but also at the TRM external surface appear essential for understanding the dynamic relation built between the damage masonry and the external retrofit layering. In this direction, the conference presentation extensively discusses the DIC and AE results. Ongoing studies consider additional experimental set-up modifications to induce additional failure modes specified by RILEM. Currently, additional shear pull-out tests are being performed which consist of different mortar and textile combinations. Specifically, lime and lime-cement mortar combinations are being used to construct different combinations of TRM-masonry wall samples, and natural fibers are also selected for the reinforcement textile fiber.

Much of the world's unreinforced masonry structures that need repair experience different loading conditions and are exposed to different environmental exposure. Fatigue and incremental loading cases are being researched currently to simulate real life masonry loading conditions. Furthermore, a wide research topic consisting of durability and sustained compatibility between different combinations of materials are currently being considered for investigation of different historical masonry repair techniques.

REFERENCES

[1] Kouris, L. A., & Triantafillou, T. C. (2018). State-of-the-art on strengthening of masonry structures with textile reinforced mortar (TRM). Construction and Building Materials, 188, 1221-1233. doi:10.1016/j.conbuildmat.2018.08.039
[2] D'Antino, T., Carloni, C., Sneed, L., &; Pellegrino, C. (2014). Matrix–fiber Bond behavior In PBO FRCM Composites: A fracture mechanics approach. Engineering Fracture Mechanics, 117, 94-111. doi:10.1016/j.engfracmech.2014.01.011
[3] D'Ambrisi, A., Feo, L., &; Focacci, F. (2013). Experimental and analytical investigation on bond between carbon-frcm materials and masonry. Composites Part B: Engineering, 46, 15-20. doi:10.1016/j.compositesb.2012.10.01
[4] Ceroni, F., Ferracuti, B., Pecce, M., &; Savoia, M. (2014). Assessment of a bond strength model for FRP reinforcement externally bonded over masonry blocks. Composites Part B: Engineering, 61, 147-161. doi:10.1016/j.compositesb.2014.01.028
[5] De Felice, G., Aiello, M. A., Caggegi, C., Ceroni, F., De Santis, S., Garbin, E., . . . Viskovic, A. (2018). Recommendation of RILEM Technical Committee 250-CSM: Test method for Textile Reinforced mortar to substrate BOND CHARACTERIZATION. Materials and Structures, 51(4). doi:10.1617/s11527-018-1216-x
[6] Caggegi, C., Carozzi, F. G., De Santis, S., Fabbrocino, F., Focacci, F., Hojdys, Ł, . . . Zuccarino, L. (2017). Experimental analysis on tensile and bond properties of pbo and Aramid FABRIC REINFORCED cementitious matrix for strengthening masonry structures. Composites Part B: Engineering, 127, 175-195. doi:10.1016/j.compositesb.2017.05.048
[7] Carozzi, F. G., Bellini, A., D'Antino, T., De Felice, G., Focacci, F., Hojdys, Ł, . . . Poggi, C. (2017). Experimental investigation of tensile and bond properties Of Carbon-frcm

composites for strengthening masonry elements. Composites Part B: Engineering, 128, 100-119. doi:10.1016/j.compositesb.2017.06.018
[8] Salsavilca, J., Yacila, J., Tarque, N., & Camata, G. (2020). Experimental and analytical bond behaviour of masonry strengthened with steel REINFORCED grout (SRG). Construction and Building Materials, 238, 117635. doi:10.1016/j.conbuildmat.2019.117635
[9] Verbruggen, S., De Sutter, S., Iliopoulos, S., Aggelis, D. G., & Tysmans, T. (2015). Experimental structural analysis of HYBRID Composite-Concrete beams by digital Image Correlation (DIC) and ACOUSTIC emission (ae). Journal of Nondestructive Evaluation, 35(1). doi:10.1007/s10921-015-0321-9
[10] Rouchier, S., Foray, G., Godin, N., Woloszyn, M., & Roux, J. (2013). Damage monitoring in fibre reinforced mortar by combined digital image correlation and acoustic emission. Construction and Building Materials, 38, 371-380. doi:10.1016/j.conbuildmat.2012.07.106
[11] Shetty, N., Livitsanos, G., Van Roy, N., Aggelis, D. G., Van Hemelrijck, D., Wevers, M., & Verstrynge, E. (2019). Quantification of progressive structural integrity loss in masonry with acoustic Emission-based damage classification. Construction and Building Materials, 194, 192-204. doi:10.1016/j.conbuildmat.2018.10.215

DEVELOPMENT OF NON-REGULAR SHAPED LIGHTWEIGHT STRUCTURAL CONCRETE ELEMENTS (BEAMS) REINFORCED WITH CARBON FABRICS

Mor Lavi[1], Lior Nahum[2], Alva Peled[3]

[1]*Department of Civil and Environmental Engineering, Ben Gurion University of The Negev, Beer Sheva, Israel e-mail: mla@post.bgu.ac.il*

[2]*Department of Civil and Environmental Engineering, Ben Gurion University of The Negev, Beer Sheva, Israel e-mail: liornah@post.bgu.ac.il*

[3*]*Department of Civil and Environmental, Ben Gurion University of The Negev, Beer Sheva, Israel e-mail: alvpeled@bgu.ac.il, corresponding author*

SUMMARY: *Reinforced concrete* with steel bars *is a traditional and widely used method, however steel bars are vulnerability to corrosion attack, which shortens the useful lifespan of the building. The recently emerged carbon-based Textile Reinforced Concrete (TRC) technology aims to limit this disadvantage, due to the corrosion resistivity of the carbon textile. This work focuses on the development of lightweight TRC elements made of carbon fabrics (without steel rebars) with non-regular shapes, based on the ability of the fabrics to conform to complex shapes and their resistivity to corrosion. Bending tests were performed on TRCs having truss-like shape, exploring ways of fabric mechanical anchoring within the beam. Load bearing capacity and the representative failure modes of those beams were explored.*

KEY WORDS: *Carbon fabrics, Textile, Cement-based composites, Concrete, Truss.*

1. INTRODUCTION

In recent years, the principles of sustainable development and green buildings have penetrated the construction industry at an accelerated rate. Of particular importance in this regard is the concrete industry, as it can be engineered to satisfy almost any reasonable set of performance specifications, more so than any other material currently available, as well as due to its many other advantages [1][2].

Concrete is known to be a brittle material with low tensile load-bearing capacity. As such, reinforcement is required to compensate for these drawbacks, commonly with steel rebars (Steel Reinforced Concrete - SRC). SRC has historically displayed disadvantages in terms of durability and vulnerability to corrosion attack, which shortens the useful life cycle of the building and leads to an additional energy investment during maintenance and refurbishment. Moreover, due to the corrosion sensitivity of the steel reinforcement bars, these require a concrete protective layer which increases the thickness of the concrete elements, and thus leads to greater weights and a concrete consumption well above that required for structural performance alone. Therefore nowadays, new technological advances making use of non-traditional types or amounts of material and energy are required to meet the demand for a sustainable industry [3]. An innovative technology which has sprung from this notion is Textile-Reinforced Concrete (TRC), which is a combination of fine-grained concrete and textile fabrics (made of monofilaments or multifilament fibers). Research findings show that TRC significantly improves the tensile strength, ductility, and energy absorption capacity of the concrete element [4]. An important property of textile reinforcement is its high deformability, which allows the TRC composites to be readily adapted to complicated shapes to enable the production of concrete elements with complex geometries.

In addition to its excellent mechanical properties, the use of TRC potentially reduces its self-weight, cost, energy consumption, and carbon dioxide (CO2) emissions, and it can be used to produce structures with modular and complex shapes while eliminating the risk of corrosion, thus facilitating many new applications [5].

Considering the above, the current work, which continues the path of previous research, examines the function of lightweight irregular truss-like shape concrete beams under bending loads, based on the ability of the fabrics to conform to complex shapes and their resistivity to corrosion. Three different mechanical anchoring patterns of carbon textile reinforcement within the beam were explored.

2. EXPERIMENTAL

2.1. Materials

Table 1 shows the fine-grained cement-based mixture with compression strength of 80 MPa, that used to produce the TRC beams. The mixture was developed as self-consolidating concrete (SCC) to allow the concrete to penetrate through the fabric opening during casting and well filling of the truss-based mold. The TRC beams were reinforced with a two-dimensional warp knitted fabric made of multifilament carbon fibers with 800 tex, providing bundle cross-sectional area of 0.452 mm^2 in both warp and weft directions, which connected with a thin multifilament polyester yarn. The fabric mesh size was 8.0 X 7.2 mm (see Figure 1). Epoxy (EP520, two components epoxy resin; base and hardener with mix ratio of 3:10 (w/w) respectively) was used to coat the fabric.

Table 1. Concrete mix design

CEM I (52.5) [kg/m^3]	Sand (0.6) [kg/m^3]	Water [kg/m^3]	Silica fume (Elkem 920) [kg/m^3]	Superplasticizer (ENT 11) [kg/m^3]	w/c	w/b
395	724	158	79	118.5	0.40	0.33

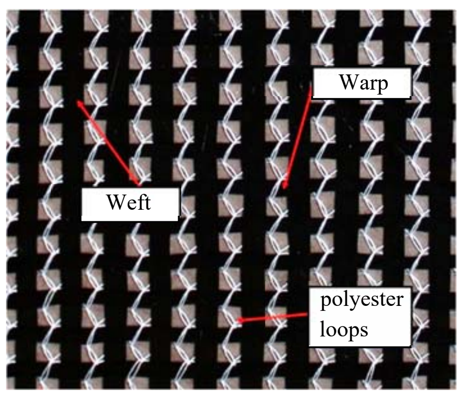

Figure 1. *The carbon fabric used after epoxy coating*

2.2. Specimen preparation

For TRC casting, a detachable mold having a truss shape was design (shown in Figure 2) and produced by a 3D printer. Using triangular-shaped parts printed in accordance with this mold, it was possible to create gaps within the beam having a truss shape, while taking into consideration the compressive and tensile elements (labeled in

Figure 2a) within the beam. The dimensions of the beam in cm and its final shape are shown in Figure 2. The depth dimension of the beam is 3 cm and the thickness of the various beam elements (labeled in Figure 2a), were calculated according to the loads they receive, (see Table 2). Since the TRC beam was calculated as a truss model, each truss-beam element needed to withstand tensile loads, the cross-sectional area required for its reinforcement was determined according to the distribution of the load acting on the beam. Table 2 shows the number of bundles that symmetrically reinforced each element (presented in Figure 2b). Prior TRC casting, the reinforcing fabrics were impregnated in epoxy resin to harden them according to the shape of the beam and to bind all bundle filaments together to improve the load bearing capacity of the reinforcement fabric.

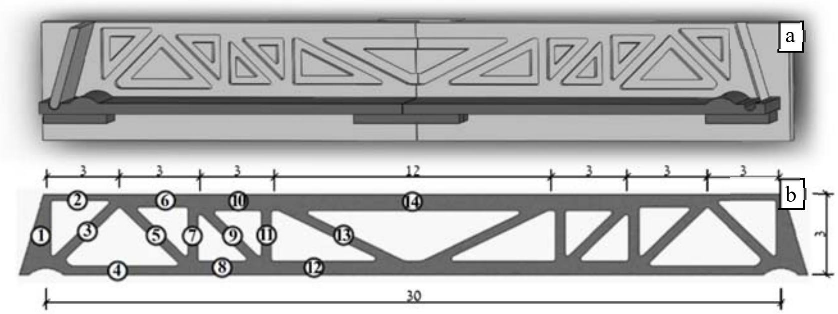

Figure 2. *(a) detachable mold printed by 3D printer. (b)beam dimensions and its elements number.*

Table 1. *Thickness of elements in mm and number of reinforcing bundles at each element (the elements are labeled in Figure 2b)*

Element No.	**1**	**2**	**3**	**4**	**5**	**6**	**7**	**8**	**9**	**10**	**11**	**12**	**13**	**14**
Element Thickness [mm]	3	3	4	4	4	4.5	4	6	4	7	4	6	3	7
Set 1	0	0	0	2	4	0	0	4	3	0	0	6	1	0
Set 2	2	3	3	2	4	4	0	4	3	3	0	6	1	1
Set 3	2	4	2	2	4	5	0	4	3	3	0	6	1	2

For TRC casting, the epoxy-hardened fabrics were first inserted into the beam mold and then the concrete was poured while gently vibrating the mold to ensure concrete mixture penetration into all the thin truss-beam elements and through the fabric opening. Then, the mold was placed under a polyethylene covering in a humid environment to prevent dehydration cracks. After two days the concrete beam was demolded and placed in a saturated calcium hydroxide water bath at room temperature until testing at 28 days of age. Three sets of reinforcement shapes were tested providing different anchoring of the fabric within the beam (Figure 3). The amount of reinforcement and fabric anchorage at the bottom and truss elements of the beam was the same for all three tested sets. The reinforcement amount and shape at the upper region of the beam was differed at the three beam sets: (i) fabrics located only at the bottom of the beam without continuity to the upper elements (Figure 3a); (ii) additional of fabric anchoring at the top of the beam with continuity from element to element turned inward (Figure 3b); and (iii) same as (ii) but the fabric anchor is turned outward at the upper beam with additional reinforcement strip (Figure 3c).

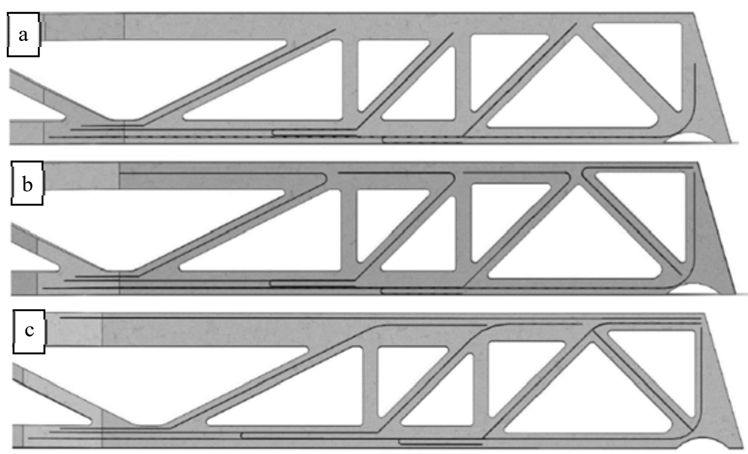

Figure 3. *Anchoring simulation of the 3 tested beam sets (labeled by the black lines). (a) Minimal anchoring. (b) Top anchor turns inward. (c)Top anchor turns outward with additional reinforcement.*

2.3. Test methods

2.3.1 Compression test

Compressive strength (ASTM C109) was measured on 50 × 50 × 50 mm3 samples, using Control Automax5 machine with load rate of 500 KPa/sec. The average value of the test results of the various sets was 75 MPa.

2.3.2 Flexure test

To examine the flexural bearing behavior, four-point bending tests were conducted so that pure bending is obtained in mid-span area, using an Instron machine (Figure 4) with a 100 kN load-cell capacity at a displacement rate of 0.5 mm/min. During the bending tests, load and mid-span deflection were measured. Concurrently, images were taken in 20 seconds intervals during testing to study the crack formation and type of failure. Three specimens were examined for each beam type. The stress was calculated by dividing the measured axial force, which in turn is calculated according to the truss model for each element, by the cross-sectional area of the active reinforcement, i.e., the cross-section of the continuous yarns along the load direction.

Figure 4. *TRC beam tested on Instron machine.*

3. RESULTS AND DISCUSSION

3.1. Mechanical Properties

Load versus deflection curves of all tested beams are presented in Figure 5. For stress calculation, when considering the truss form, the load acting on each truss element needs to be divided by its specific cross-sectional area, but here for simplicity only the total maximum load acting on the entire beam is presented as shown in Table 3, including the deflection at the maximum load. A similar maximum load is observed in both beam sets, 1 and 2, although the anchorage of the fabric in set 2 takes place also in the upper truss elements of the beam (Figure 3a vs b). Moreover, both beam sets achieved very low deflections, indicating similar bending behavior of these two fabric anchoring shapes. The obtained low maximal loads combined with the low deflection, indicate a brittle failure of those beams and possibly inefficiency of the anchorage to allow the reinforcement fabrics to carry the develop tensile loads.

Table 2. *Average maximum loads and deflection at the maximum loads for all three tested beam sets*

Beam type	Average max load [N]	Average deflection at max load [mm]	Standard deviation [%]
Set 1	910.4	0.6	12.9
Set 2	990.5	0.5	6.9
Set 3	5812.0	5.4	9.2

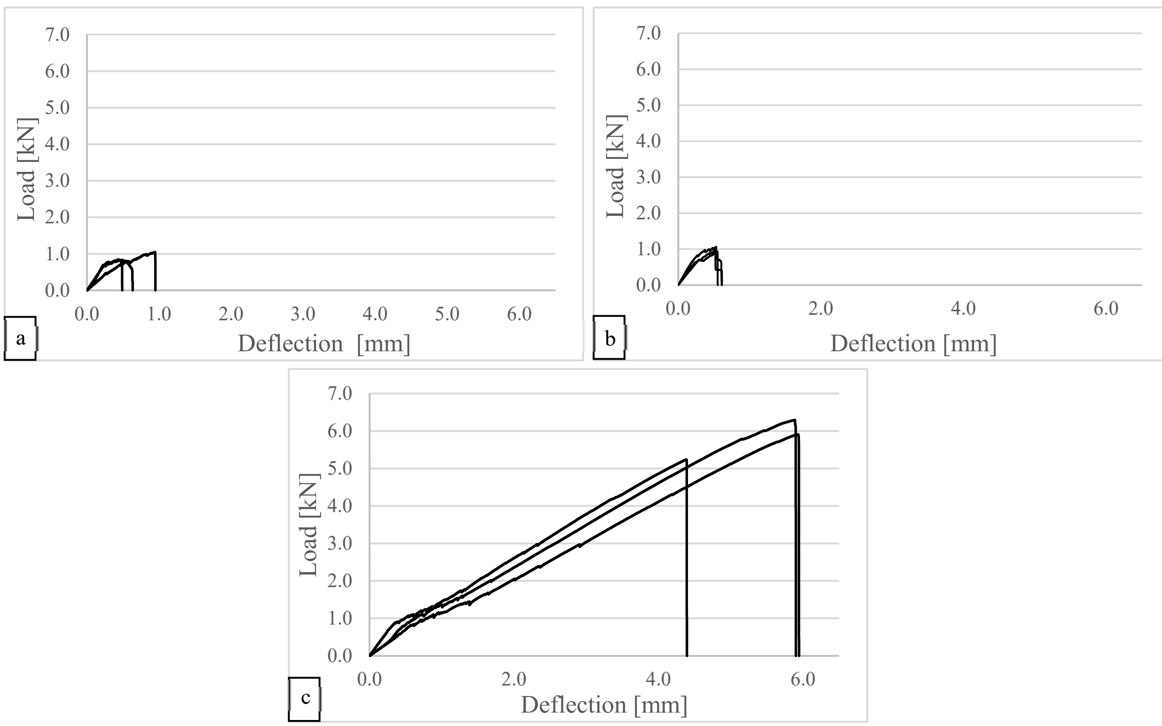

Figure 5. *Load versus deflection curves of all tested beams; (a) minimal anchoring, (b) top anchor turns inward, and (c) top anchor turns outward with additional reinforcement.*

A significant improvement in the bearing capacity of the beam occurs in the third set of beams (Set 3), in which the fabric located also at upper beam elements continuously, while the anchorage of the fabric faces outwards. The average maximum load improved by about 6 times relative to the other two tested beams (Set 1 and 2). This beam of Set 3 also observes much greater deflection when reaching the maximal load, indicating much more ductile behavior and greater energy absorption as compared to other two tested beam sets. A plausible reason for such improvement (in loads and deflections) can be related to the location of the reinforcing fabric and its anchoring path which corresponds to the direction of the natural stress flow in the bending beam[6]. In addition, changing the direction of the fabric anchorage outward causes the stresses to be developed at the upper concrete elements of the truss (elements 6, 10 and 14, Figure 2b), which known to be more easily carried by the concrete. Additionally, it should be mentioned that in Set 3 although it can carry the developed loads more efficiently than the other two fabric arrangement beams, it observes relatively high diversity in the load-deflection curves, showing two curves with similar behavior and one with lower flexural response in terms of maximal loads and deflections. Notes that shape of those beams is rather complex and the dimension of each element within the beam is relatively thin, leading to difficulty in their production which may cause some defects. Larger beam size might limit this problem which is currently under investigation.

3.2. Failure Mechanisms

Figure 6 presents the mode of failure of representative beam of each tested set. The manner of failure is similar for beam sets 1 and 2 (Fig. 6a and 6b). The failure occurred at a certain portion of the beam where only few elements failed at the upper region of the beam, causing the entire beam to fail. In both cases (sets 1 and 2) the first crack began at a single truss element, thus the beam did not longer function as a truss. This resulted a rupture of the upper node of the beam as shown in Figure 6a-b. In set 1 (Fig. 6a) the fracture caused the carbon fabric that was not anchored to the concrete to be pulled out from the node. However, in set 2 (Fig. 6b) the concrete at the same node detached from the carbon fabric by delamination, which may relate to the fact that the fabric was anchored towards the center of the beam, which contributed to the crack development and the formation of delamination at this node.

In set 3 (Fig. 6c), the beam underwent a significant deformation before reaching failure, which could be seen by a naked eye. Cracks were formed and clearly observed during loading, until failure of large number of neighbor elements at once, leading to catastrophic failure. This observation indicates that many elements in the beam

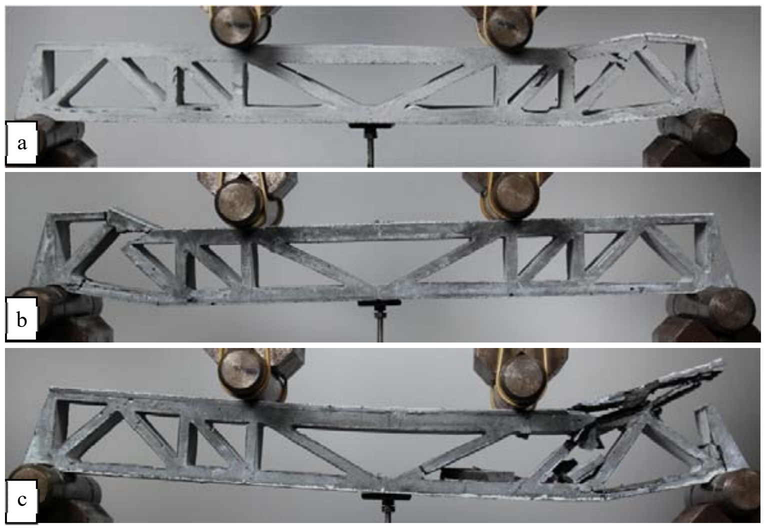

Figure 6. *Form of failure. (a) Minimal anchoring, (b) Top anchor turns inward, and (c) Top anchor turns outward with additional reinforcement*.

reached their maximum bearing capacity before failing, so the material utilization is likely high. It can be clearly seen that the upper elements in the beam (elements number 2 and 6, Figure 2) experienced delamination, which is undesirable in structural elements.

4. CONCLUSIONS

A truss-like textile reinforced concrete (TRC) beam was designed to examine different forms of reinforcement anchoring and their effect on bending beam behavior, motivated by sustainable concerns.

The fabric arrangement and location and most important its mechanical anchorage pattern within the beam is of high importance to allow a load bearing capacity of the truss-based beam. When such fabric anchorage is not well designed, it can severe damage to the beam including delamination. Fabric arrangement and anchorage pattern that corelates with the natural loads flow of the beam under bending can increase material utilization and thus improved load-bearing capacity. However, further investigation is required to find an optimal fabric arrangement and anchorage pattern that will allow effective load carrying while also preventing delamination between fabric and concrete. Understanding the behavior of larger size truss-based beams is required for practical applications which is currently under investigation.

5. REFERENCES

[1] C. Meyer, “The greening of the concrete industry,” in *Cement and Concrete Composites*, 2013, vol. 14, no. 8, pp. 79–92, doi: 10.1016/j.cemconcomp.2008.12.010.

[2] V. M. Malhotra, “Global warming, and role of supplementary cementing materials and superplasticisers in reducing greenhouse gas emissions,” in *Concrete Technology for a Sustainable Development in the 21st Century*, vol. 400, no. 1, Inderscience Publishers, 2000, pp. 226–236.

[3] J. a Vanegas, J. R. Dubose, and A. R. Pearce, “Sustainable Technologies for the Building Construction Industry,” 1996.

[4] W. Brameshuber, Ed., “Proceedings of the International RILEM Conference on Material Science (MatSci) – Volume I 2nd ICTRC – Textile Reinforced Concrete Aachen , Germany 6-8 September 2010 Editors :,” 2010, vol. I, no. September.

[5] A. Peled, A. Bentur, and B. Mobasher, *Textile Reinforced Concrete*, vol. 490, no. 9. Boca Raton, 2017.

[6] L. Nahum, “Optimization for Minimizing the Embodied Energy in Spanning Structural Concrete Elements. PhD Thesis,” 2020.

GLASS FIBER REINFORCED MORTARS: CRACK INITIATION AND PROPAGATION STUDY

Pascale Saba[1,2], Tulio Honorio[1], Omar-Ateeq Mahmood[2], Farid Benboudjema[1]

[1] *Université Paris-Saclay, ENS Paris-Saclay, CNRS, LMT - Laboratoire de Mécanique et Technologie, 91190, Gif-sur-Yvette, France.* pascale.saba@ens-paris-saclay.fr

[2] *Saint-Gobain Recherche Paris, Département Thermique, Mécanique et Modélisation, 39 Quai Lucien Lefranc, 93300 Aubervilliers, France*

SUMMARY: *External Thermal Insulation Composite Systems (ETICS) is a solution to improve energy efficiency of existing buildings. In this system, the thermal insulation material is protected by several coating layers. In order to limit crack openings, a coating layer is reinforced with a glass fiber mesh. In spite of being widely employed in ETICS, the mechanisms of reinforcement of glass fiber mesh in cement-based matrices are not fully understood. Here, the effect of the reinforcement on cracking is studied through 4-points bending tests realized in-situ in an X-Ray tomograph. The tests show that several heterogeneities exist in this composite material, that can initiate cracks and affect their propagation.*

KEY WORDS*: glass fiber mesh, ETICS, mortar, X-ray tomography, cracking*

1. INTRODUCTION

Glass fiber reinforced mortars are used as the protection layer in External Thermal Insulation Composite Systems (ETICS) as shown in Figure 1. ETICS are recognized as one of many types of thermal insulation and have several advantages such as the ease of application without disturbing the residents [1]. ETICS are prescribed in the renovation framework targeting the reduction of energy consumption produced by the by the home and building heating systems that are responsible for 45% of total French energy consumption and about 25% of Greenhouse gas emissions [2]. The objective of the French government is to attain carbon neutrality by 2050 and to renovate 500,000 housing units per year, half of which are occupied by low-income households [2].

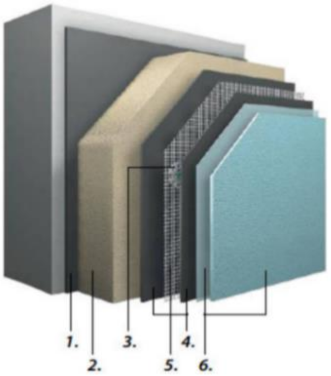

1. Adhesive
2. Thermal insulation material
3. Anchors (not mandatory)
4. Base-coat
5. Reinforcement, usually glass fiber mesh
6. Finishing layer: finishing coat with a key coat (optional) and/or decorative coat (optional)

Figure 1.*Typical system components in ETICS using anchors* [3]

The glass fiber reinforced rendering mortar also called basecoat for is subject to cracking. The interactions with the environment changing temperature and relative humidity lead to thermal and hygral strains, which when restrained, may lead to stresses that can attain the tensile strength of the material causing then the mortar cracking as in Figure 2. This is problematic for two main reasons. On one hand, the eventual penetration of water inside the cracks may cause the insulator to lose partially its efficiency and durability. On the other hand, the visible cracking on the newly renovated façades leads to unsatisfied clients which is an important marketing problem. Oriented and non-oriented cracking and visibility of joints are among the main anomalies encountered in ETICS [4-6]. The glass fiber mesh fabric is proposed as a solution for cracking in several types of applications including the base coat reinforcement for ETICS.

Figure 2. *Visible cracking on a facade*

The reinforced cement composite used in ETICS is composed of (i) the mortar, which is a very heterogeneous material containing three main phases at its mesoscale: cement paste matrix, sand particles, and porosity, and (ii) the glass fiber mesh which is also a heterogeneous material containing three phases at its mesoscale: glass fibers, porosity, and coating. The heterogeneities present in the mortar, the porosity, the sand, or even the mesh can be the source of localization for cracks at the mesoscale. Nevertheless, cracking in the rendering mortar can also be initiated at the structure scale. Geometrical singularities, such as window corners and thermal joints, can be a source of localization of cracks.

Here, we focus on the mechanical characterization of the reinforced rendering mortar. The aim is to determine the reinforcement mechanisms of the glass fiber mesh regarding the crack initiation, localization and propagation within the mortar using X-ray tomography in an original setup. The tomography scans enable unveiling the role of the glass fiber mesh on crack localization and crack propagation in reinforced mortar. To the author's knowledge, it has never been done previously on this type of material.

2. MATERIALS AND EXPERIMENTAL METHODS-

2.1 Materials

In this study, 5 mm thickness prismatic reinforced mortar samples of 70 mm long and 12 mm large (see Figure 3(a)) are tested in 4-points bending inside an X-ray tomograph. The mortar used in our samples is a commercial basecoat for ETICS. The glass fiber mesh is also a commercial glass fiber mesh fabric (see Figure 3(b)) that is specifically preconized for ETICS.

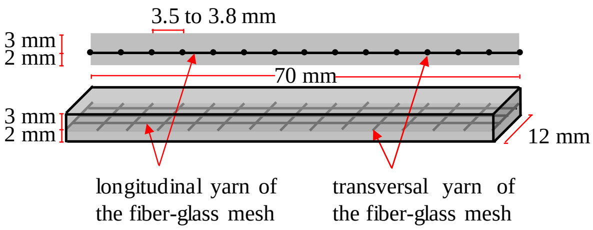

(a)

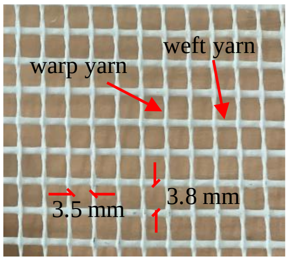

(b)

Figure 3(a). *2D and 3D representation of the glass fiber mesh reinforced mortar sample.* ***(b)****. Glass fiber mesh fabric structure*

Three non-reinforced mortar samples (4×4×16 cm^3) were tested by 3-point bending at 28 days to determine its mechanical properties such as the Young modulus and the tensile strength. The experimental setup and procedure are described in [7]. The mortar has a Young modulus of 2.47 GPa ± 0.34 GPa, and a tensile strength of 1.97 MPa ± 0.04 MPa (mean value ± standard deviation for both parameters).

The mortar is mixed and cast according to the manufacturer's instructions (6 L of water for 25 kg of premix).

After casting, the samples are protected from drying for 24 hours until demolding. Several layers of plastic film and a final layer of adhesive aluminum are used. After demolding, the samples are stored in a temperature and relative humidity-controlled room at 20°C±1°C and 60%±5%, respectively. The weight loss of the samples is monitored.

2.2 Experimental methods

To understand the crack initiation and propagation in the reinforced rendering mortar and the reinforcement mechanisms of the glass fiber mesh, several specimens are tested using in-situ X-ray tomography in 4-point bending.

In-situ X-ray tomography is a non-destructive technique that allows obtaining a three-dimensional image. It is an imaging technique that generates a three-dimensional representation of the structure. It permits the visualization of the crack in the 3D volume of the specimen. A 3D crack monitoring is possible at different times of the tests.

2.2.2 Mechanical test assembly

The specimen in this particular 4-point bending setup, as shown in Figure 4 and unlike in traditional ones, is inclined. This change is what allowed us to obtain better quality images since the X-ray beam is traversing a smaller distance in the "scanned zone" (zone outlined in yellow in Figure 4) compared to the total length of the specimen in case of a non-inclined bending setup. The "scanned zone" corresponds to the volume where cracking is supposed to occur.

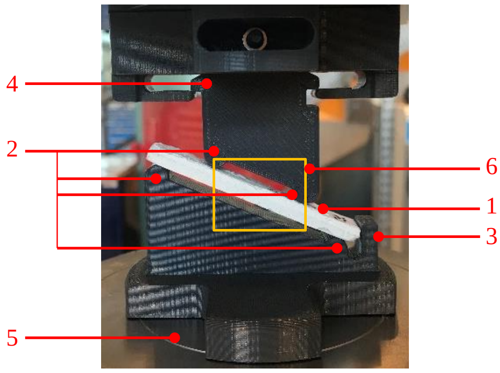

1. Specimen
2. Supports
3. Longitudinal support
4. Junction piece allowing rotation
5. Plate in an upward movement
6. Scanned zone

Figure 4.*4-point bending mechanical assembly*

Note that all the pieces of the assembly are made using a 3D printer. ABS (Acrylonitrile Butadiene Styrene) is used (density of about 1055 $kg.m^{-3}$). The density of the mortar being 1323 ± 5 $kg.m^{-3}$ (mean value ± standard deviation) making it denser than the ABS. Thus, the ABS is globally more X-ray transparent than the mortar. Besides, sand, cement and hydrates (density of about 2700, 3100 and 2600 kg.m^{-3}, respectively) in the mortars are less transparent since their density are also greater than the one of ABS.

Plate 5 in Figure 4 is directly fixed on a 100 N load cell that will put the plate in an upward movement, hence the load is being transmitted to the specimen by the lower support.

The test is controlled by the displacement of the plate 5 (see Figure 4) at a rate of 1 $\mu m.s^{-1}$. The advantage of using a displacement controlled test compared to a load controlled one is that the former allows getting the post-peak curve and prevents creep strains during the scans that will complicate the analysis of displacement fields related to cracking. Two scans are done to compare the cracked stage of the sample to its slightly deformed elastic stage. Before each scan, a pause period is preferred to allow the material to relax. This relaxation period prevents differential strains (for instance between viscous cement paste and elastic aggregates) that will occur during the scan hence limiting the blurred image. The in-situ inclined 4-point bending test is divided into 6 phases that are detailed in Figure 5. Note that using 4-point bending, we can obtain multi-cracking in the specimen. To attain the multi-cracking stage, the phases 4, 5, and 6 of Figure 5 are repeated.

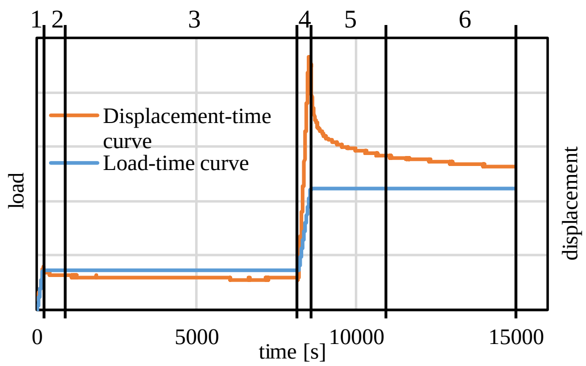

1. Load until contact
2. Relaxation period
3. First scan at a slightly deformed stage
4. Load until the first crack
5. Relaxation period
6. Second scan at cracked stage

Figure 5. *The schematic course of the test described with the load vs. time and displacement vs. time curves*

The main objective is to induce cracking in the reinforced mortar under tension stress in order to observe the reinforcement mechanism regarding the crack initiation, propagation and opening.

The dimensions of the specimen were chosen according to several parameters:

- The 5 mm thickness of the specimen is defined by the manufacturer of the mortar for industrial application in ETICS.

- The 12 mm width is chosen according to a minimum of 3 longitudinal yarns of the glass fiber mesh.
- The length is chosen to respect (i) the minimum slenderness of Euler-Bernoulli theory, thus a minimum of 50 mm is required (slenderness of 10), (ii) a minimum of 5 transversal yarns of the glass fiber mesh in the zone of interest (between the loading application points), thus 30 mm is required for the zone of interest, (iii), a minimum anchor length is required for the glass finer mesh (calculated according to a reference stress in the mesh supposing a perfect adhesion between the mortar and the glass fiber mesh), (iv) and a sufficient image resolution is required (the voxel size should be smaller than the visible crack width). Considering the capacity of the human vision, at 1 m distance as a reference for a visible crack width of 50 µm, and a 3D image size around 1000^3 voxels, the maximum length allowed to be traversed by the X-rays should be 50 mm.
  Note that inclining the specimen allows to relax this constraint by choosing a sufficiently long specimen, hence respecting Euler-Bernoulli hypothesis, while decreasing the length traversed by the X-rays.
- All dimensions have to be greater than the Representative Elementary Volume (REV) dimensions. Nevertheless, the thickness of the material is defined by the industrial manufacturer.

Note that verifications of the inclined bending set-up have been carried-out using finite element calculations.

3. EXPERIMENTAL RESULTS AND DISCUSSIONS

Thanks to the advanced technology of the X-ray in-situ tests, reconstruction algorithms, and image processing algorithms, we had access to the 3D volume of the cracked sample.

In a 4-point bending test, considering the constant bending moment between the two upper supports, the crack can be initiated on the lower tensile surface anywhere between the two upper supports. The crack will propagate, from the bottom surface in tension toward the upper surface, vertically due to the geometrical and mechanical symmetry of the classical 4-point bending set-up.

The theoretical cracking trajectory described above does not always apply to heterogeneous materials, since the heterogeneities present in the material may induce geometrical singularities, weak points, or, material incompatibilities that can relocate the crack initiation and redirect its propagation. In the reinforced glass fiber mortar samples, three main categories of heterogeneities exist at the millimeter scale: (macro)porosity, sand particles (two types of sand can be differentiated), and, the glass fiber mesh. Each of these heterogeneities can be a source of stress concentration. Therefore, the crack in the mortar is initiated where the local stress attains the mortar's tensile strength, hence anywhere in the tensile zone and not only on the lower surface of the sample as in homogeneous materials.

Considering the quasi-brittle behavior of the mortar, the propagation of the crack once initiated is rapid. Since the X-ray 3D requires a steady-state of the scanned object hence cannot be carried out during the mechanical test but afterward, the exact location of the crack initiation cannot be determined.

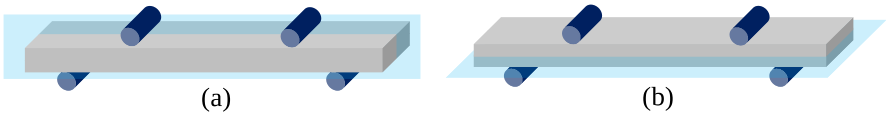

Figure 6. *Representation of a* **(a)** *vertical and* **(b)** *horizontal section inside the reconstructed 3D volume of the sample.*

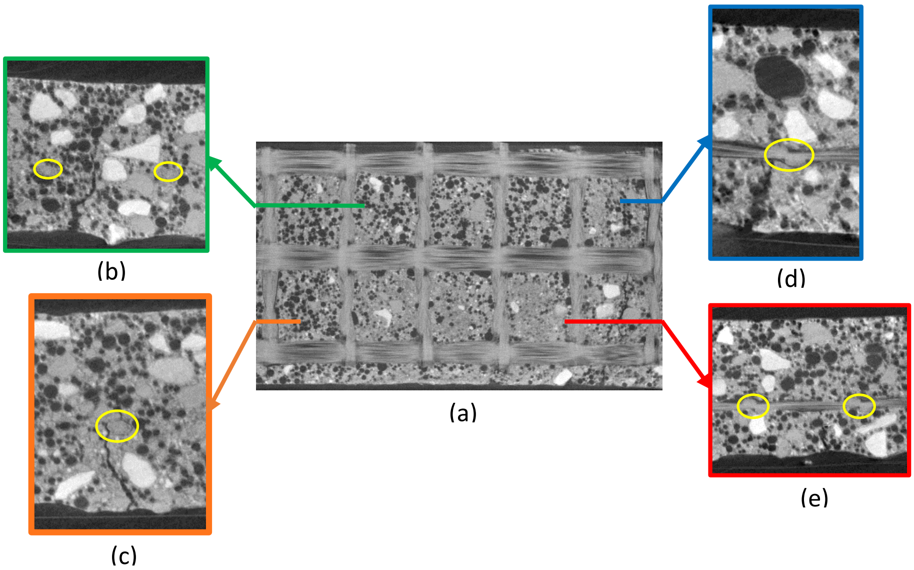

Figure 7(a). *Horizontal section* **(b, c, d, and e)** *vertical sections inside the reconstructed 3D volume of cracked specimens I.*

The cracks in two samples are shown in Figure 7 andFigure **8** following the sections in Figure 6. The transversal yarns in the specimen I of Figure 7 outlined in yellow are weft yarns while the transversal yarns in the specimen II of Figure 8 are warp yarns (see Figure 3(b)). The transversal yarn, as any other heterogeneity present in the mortar, can induce stress concentration hence being a source of crack localization. This cracking pattern is not persistent as the vertical sections in specimen I of the Figure 7 (c and d) show cracks passing by the transversal weft yarn while the vertical sections in specimen I of the Figure 7 (b and e) show cracks passing between two transversal weft yarns hence not localized on the latter. Note that, finite element simulations have been carried out in order to determine the influence of the distance between the glass fiber mesh and the lower tensile surface. The simulations showed that the closer the glass fiber mesh from the lower tensile surface, the more likely for the crack to pass through a transversal yarn. This due to the higher level of stress concentration induced by the transversal yarn when the latter is close to the lower tensile surface. On the other hand, the closer the mesh from the lower tensile surface the greater the first crack load hence making the reinforced rendering mortar more resistant.

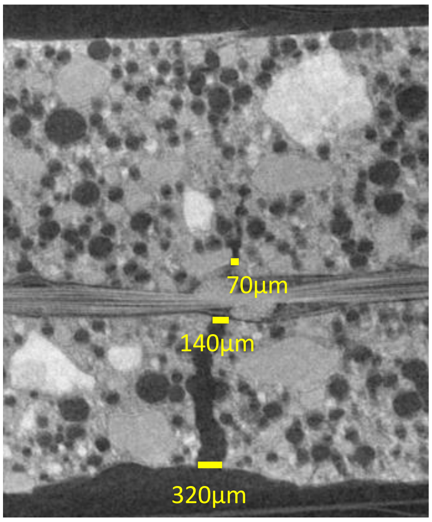

Figure 8. *Vertical section inside the reconstructed 3D volume of specimen II.*

The cracks in vertical section in specimen I of Figure 7 did not cross the glass fiber mesh. In the case, the latter stopped the crack propagation and thus limits the crack opening. On the other hand, the crack in the vertical section of the specimen II of Figure 8 passed traversed the glass fiber mesh trough the thickness of the mortar. Nevertheless, the glass fiber mesh decreased significantly (by 50%) the crack opening. This first reinforcement mechanism, whether to stop the crack propagation or to limit the crack opening, directly influences the durability of the ETICS. As discussed in the introduction, the potential water leakage is limited by the smaller crack opening.

It is thus possible, using different dimensions of the glass fiber mesh, to directly impact the number of the cracks as well as their openings to make them less visible and more watertight. A previous paper focused on a 3-point bending test [7]. Other works investigated the influence of the glass fiber mesh dimensions under different conditions on the mechanical behavior of the reinforced rendering mortar [8], only 2D surface observations were reported.

4. CONCLUSIONS

We studied cracking development in the reinforced mortar relevant for ETICS application using X-ray tomography. The classical mechanical testing methods even when combined with advanced technologies such as Digital Image Correlation (DIC) can only provide information on the chosen 2D surfaces. Therefore, to access the 3D information and dive into the depth of the 3D volume of the sample, a new testing setup is demanded. The newly developed X-ray in-situ inclined 4-point bending setup needed to ensure relatively small scale testing in order to obtain a sufficiently small image resolution (15 µm), X-ray transparency of the different parts of the set-up as well as geometrical adjustments in order to limit the noises and obtain good quality exploitable images.

The 3D images of the samples revealed a material crowded with different types of heterogeneities. Each of which can have an impact on the cracking pattern. The transversal yarn did not show a clear influence on the crack localization as it localized the crack in some case and did not in others. Numerical simulations showed a greater resistance of the glass fiber reinforced mortar if the glass fiber mesh is placed close to the lower tensile surface. Nevertheless, this positive impact of the smaller distance between the glass fiber mesh and the lower tensile surface is jeopardized by a greater stress concentration level induced by the transversal yarn of the mesh hence being a dominant crack localizer.

Although the initiation point of the crack could not be identified, a main observation has been made. The glass fiber mesh may be able to whether stop the crack propagation at its level or to significantly decrease the crack opening. Therefore, the glass fiber mesh plays an important role in the durability of the ETICS by reducing the potential water leakage within the thermal insulator.

Note that using Digital Volume Correlation, non-visible cracks may be found as well as a potential differential displacement between the glass fiber mesh and the mortar.

On the other hand, in order to identify the starting point of the crack and to ensure whether it initiates on the tensile surface or by one of the heterogeneities especially the transversal yarn, 2D X-ray radiography along with the 4-point bending set-up might be of great use.

In future studies, experiments will be carried out to understand the cracking behavior and the reinforcement mechanisms under the real environmental loading. Temperature and relative humidity fatigue cycles can be applied to a defined structure of ETICS. This environmental loading supported by an imaging technique can reveal the behavior of the glass fiber reinforced mortar in “real-life” scenarios.

5. REFERENCES

1. Barreira, E., de Freitas, V. P.: External Thermal Insulation Composite Systems (ETICS): An Evaluation of Hydrothermal Behavior, Springer, 2015.
2. Ministry of ecological solidarity transition, Energy renovation of buildings: A plan to accelerate general mobilization, https://www.ecologique-solidaire.gouv.fr/renovation-energetique-des-batiments-plan-accelerer-mobilisation-generale, last accessed 2020/2/11 (in French).
3. Eurorean Association for External Thermal Insulation Composite Systems, About ETICS, https://www.ea-etics.eu/etics/about-etics/, last accessed 2020/2/11.
4. Amaro, B., Saraiva, D., de Brito, J., Flores-Colen, I.: Inspection and diagnosis system of ETICS on walls, Construction and Building Materials 47, 1257–1267 (2013).
5. Nilica, R., Harmuth, H.: Mechanical and fracture mechanical characterization of building materials used for external thermal insulation composite systems, Cement and Concrete Research 35(8), 1641–1645 (2005).
6. Pareira, C., de Brito, J., Silvestre, J. D.: Contribution of humidity to the degradation of façade claddings in current buildings, Engineering Failure Analysis 90, 103–115 (2018).
7. Chan, N., Effects of initial stresses and strains in the prediction of cracking and failure of concrete structures by a discrete element approach, PhD, Paris-Saclay University, to be submitted (2021) (in French).
8. Saba, P., Honorio, T., Mahmood, O-A., Benboudjema, F.: Crack initiation and propagation in fiber-glass reinforced mortars, International RILEM Conference on early-age and long-term crack width analysis in RC structures, ENS Paris-Saclay, France (2021).
9. Colombo, I. G., Magri, A., Zani, G., Colombo, M., di Prisco, M.: Textile Reinforced Concrete: experimental investigation on design parameters, Materials and Structures 46, 1953–1971 (2013).

Session 9
Studies on TRC

INFLUENCE OF DISCRETE SPACERS AND ANCHORAGE LENGTH IN LONG TRC ELEMENTS

Michael El Kadi[1], Danny Van Hemelrijck[2], Hubert Rahier[3], Tine Tysmans[4]

[1]*Michael El Kadi (Department Mechanics of Materials and Constructions (MeMC), Vrije Universiteit Brussel (VUB), Pleinlaan 2, 1050 Brussels, Belgium, michael.el.kadi@vub.be)*

[2]*Danny Van Hemelrijck (Department Mechanics of Materials and Constructions (MeMC), Vrije Universiteit Brussel (VUB), Pleinlaan 2, 1050 Brussels, Belgium, danny.van.hemelrijck@vub.be)*

[3]*Hubert Rahier (department Physical Chemistry and Polymer Science (FYSC), Vrije Universiteit Brussel (VUB), Pleinlaan 2, 1050 Brussels, Belgium, hubert.rahier@vub.be)*

[4]*Tine Tysmans (Department Mechanics of Materials and Constructions (MeMC), Vrije Universiteit Brussel (VUB), Pleinlaan 2, 1050 Brussels, Belgium, tine.tysmans@vub.be)*

SUMMARY: *Discrete spacers can be used to connect planar textile layers and create pseudo-3D textile architectures for concrete reinforcement. Preliminary studies on short TRC (textile reinforced cement/concrete) beams have shown that on top of the manufacturing advantages, the use of discrete spacers can lead to improved textile anchorage, resulting in increased mechanical performance of the TRCs. Investigations on the effect of the anchorage length and spacer distribution on the resulting anchorage mechanism in long TRC elements are currently lacking in literature. This research investigated the influence of these parameters in long TRC beams (1200 mm) through a four-point bending experimental campaign on three TRC layups (equivalent 2D, original 3D and with discrete spacers) and two support configurations (350 mm and 550 mm span). The experimental results showed a clear beneficial influence of the discrete spacers on the anchorage mechanism and highlighted the importance of anchorage length in the free (unloaded) region of the TRCs.*

KEY WORDS: *3D textiles, Anchorage mechanism, Bending, Discrete spacers, Textile Reinforced Cement (TRC)*

1. INTRODUCTION

Textile Reinforced Cement Composites (TRCs) combine a cementitious matrix with textile reinforcement and offer a high-potential alternative for traditional building elements [1]–[3]. In recent years, 3D textiles have emerged as a promising reinforcement for TRCs due to their known manufacturing advantages as well as improved anchorage mechanism of the in-plane textiles [4]–[7]. Currently, the main drawback of 3D textiles remains the limited availability and the low adaptability of the weaving looms.

Discrete spacers can be manually inserted to lock planar textile layers at a fixed distance and hence create a pseudo-3D architecture. Preliminary research on short (450 mm) TRC beams has shown that in doing so, similar manufacturing and anchorage improvements can be achieved as with original 3D textiles, while avoiding the manufacturing restrictions of 3D textiles [8]. An investigation of the effects of discrete connections on the textile anchorage in long TRC elements is however still lacking in literature.

This research tackled the influence of discrete spacers on the anchorage effects in long TRC beams by means of a flexural four-point bending experimental campaign on specimens of 1200 mm x 60 mm x 15 mm (length x width x thickness). Three different TRC configurations were considered; (i) 2D: an equivalent 2D configuration with the same in-plane textile density but without spacer connections, (ii) 3D: a 3D textile configuration with original knitted connections and (iii) C4: a pseudo-3D configuration with four discrete spacer connections distributed over the shear zone of the sample (two on each side). Additionally, in order to investigate the influence of the free anchorage length (outside of the supports), two support configurations were considered, namely at 350 mm and 550 mm span. The loading pins remained 100 mm apart, and the length of the beams was held constant at 1200 mm, which resulted in free anchorage lengths (outside the supports) of respectively 425 mm and 325 mm. All samples had a fibre volume fraction V_f of 0.70 % in the loading direction. Six samples were tested for each alternative, resulting in a total of 36 TRC beams.

2. MATERIALS AND METHODS

2.1. Materials

2.1.1. Discrete connections

The discrete spacer connections that were considered to achieve pseudo-3D textile configurations were HF840MO polypropylene connections that were inserted manually at the desired positions and consisted of a two-part mechanism needed to clip the top and bottom textile layer (Figure 1 (a)) and to warrant an identical spacing as the knitted alternatives (Figure 1 (b)).

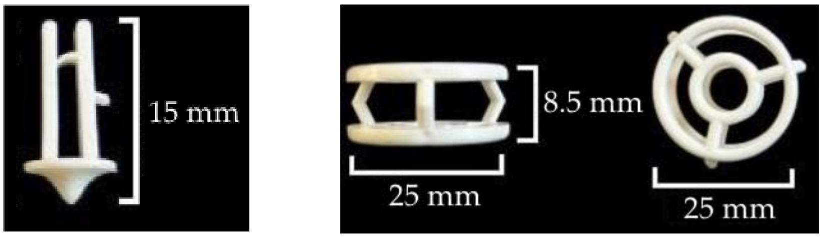

(a) (b)

Figure 1: Dimensions of discrete spacer connections (a) central pin (b) circular piece

2.1.2. Matrix

For the matrix, the Sikagrout 217 was selected for its high flowability as well as compensated shrinkage. The properties of the mortar are given in Table 1.

Table 1. *Properties of the cementitious matrix, based on* [9]

Aggr. size (mm)	Compr. strength (MPa)	Modulus of rupture (MPa)	Density (kg/m³)	Young's Modulus (GPa)	Water/Mortar ratio (-)
0 - 1.6	70	12	2010	9	0.15

2.1.3. Textile and configurations

A commercially available AR-glass 3D textile was used as reinforcement for the TRC beams, see Figure 2 (a) [10]. The textile was styrene-butadiene coated, the properties are given in Table 2.

Table 2. *Properties of the entire 3D textile (top and bottom layer), based on* [10]

Material	Grid size (mm x mm)	Textile density (g/m²)	Yarn stiffness (GPa)	Textile strength (MPa)	Connections
AR-Glass 2400 tex	22.5 x 22.5	536	67	496	Knitted polyester

Apart from configurations with untampered knitted 3D textiles (configuration (ii) 3D), two other configurations were considered, namely (i) 2D: without transversal connections and (iii) C4: with discrete connections distributed over the shear zone. In order to manufacture configurations (i) and (iii), the 3D textiles were adapted and the original knitted connections removed. In configuration (i), temporary spacers were inserted during manufacturing and afterwards removed, while in configuration (iii) four discrete spacers described in section 2.1.1 were inserted in the shear zone of the four-point bending setup. All configurations had a fibre volume fraction V_f of 0.7 %

in the loading direction and a distance between the textile layers of 8.5 mm. Figure 2 (b) shows the discrete connections placed between the textile layers.

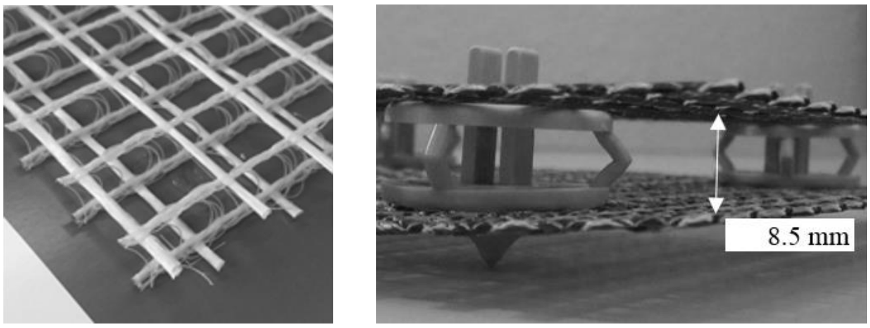

(a) (b)

Figure 2. (a) Original 3D textile and (b) discrete spacer connections inserted between two textile layers

2.1.4. Manufacturing method

All TRC beams were manufactured in individual 1200 mm x 60 mm x 15 mm moulds. First, a layer of demoulding oil was applied on the mould. Secondly, the textile reinforcement was placed in the moulds with integrated spacers (where required) and bottom distance holders (see Figure 2). Subsequently, the mortar mix was poured over the textile reinforcement over a vibrating table until each individual specimen mould was filled. Lastly, a sealing foil was drawn over the mould and the mould was sealed for curing at room temperature during 28 days. Before the experimental tests, the side surface of the samples was painted white and speckled for the DIC monitoring technique.

2.1.5. Test setups

Figure 3 shows the experimental four-point bending test setups with (a) 350 mm and (b) 550 mm span. The free (unloaded) anchorage length was respectively 425 mm and 325 mm. In both cases, the distance between the loading pins was 100 mm and for the configurations including discrete connections (configuration (iii), as shown in Figure 3) the connections were present in the shear zone of the specimens at identical positions, as shown in Figure 3. A speckle pattern was applied on the side surface of the samples and the displacement field was monitored by means of Digital Image Correlation (DIC) [11]. All experiments were performed on a displacement controlled Instron 5885H electromechanical test bench with a crosshead rate of 2 mm/min.

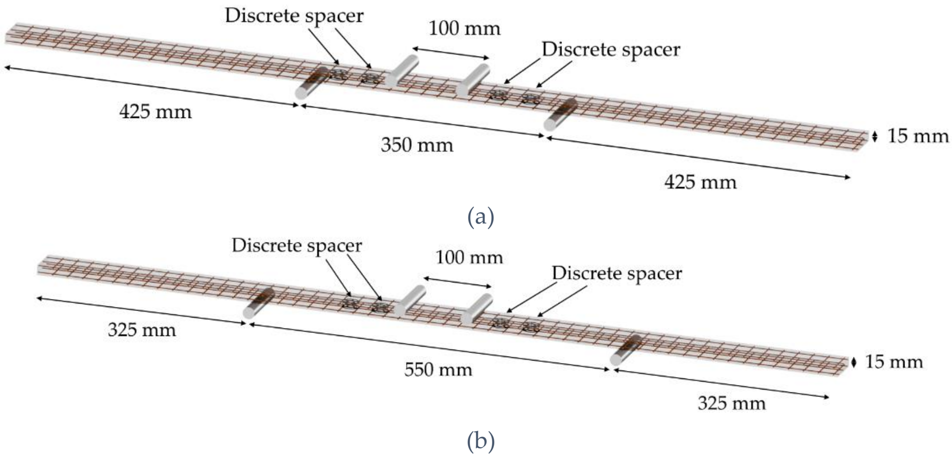

Figure 3. Four-point bending experimental setup with (a) 350 mm and (b) 550 mm span

3. RESULTS AND DISCUSSION

Figure 4 shows the representative Force – displacement curves for each configuration. Table 3 shows the post-cracking stiffness for all the alternatives.

The experimental setups with 350 mm between the supports showed that in these alternatives, with a total beam length of 1200 mm and a free anchorage length of 425 mm, the 2D TRC alternatives exhibited a similar post-cracking stiffness compared to the 3D and C4 alternatives (see Table 3). Toma et al. [8] have concluded that in short beams of 450 mm and only 50 mm free anchorage length, TRCs with identical textile layups and support distances exhibited a significantly lower post-cracking stiffness in the 2D alternative. Considering that the only difference between the two campaigns was the total specimen length (and hence free anchorage length), these results showed that increased free anchorage length can activate an improved anchorage mechanism in TRC beams with limited V_f (0.7 %).

It can be concluded that in 3D textiles, the value of minimum required V_f to achieve multiple cracking and a satisfactory composite action is not only dependant on the mechanical properties of the matrix and textile reinforcement but also on the anchorage efficiency, which is influenced by free anchorage length.

In this experimental setup (350 mm between the supports), the configuration containing discrete connections (C4) did exhibit a slightly superior post-cracking toughness and stiffness compared to the 2D and 3D configurations (see Table 3). However, the differences are rather small and apart from the manufacturing ease, no additional conclusive contributions of the discrete spacers were observed.

In the configurations of the experimental setups with 550 mm between the supports, a clearly lower post-cracking stiffness was observed for the 2D configuration compared to the 3D and C4 configurations (see Figure 4 and Table 3). Relating these results with [8] and the results mentioned above showed that it is not sufficient to increase the beam's total length in order to achieve an improved anchorage of the in-plane textiles but that instead the free anchorage length outside the supports provides a major contribution to this effect.

Differently than the 2D alternative, the C4 configuration in the 550 mm experimental setup achieved a post-cracking stiffness comparable to the 3D alternative (see Figure 4 and Table 3). These results showed that in configurations where a desirable textile anchorage is not warranted by the sample's geometry and boundary conditions, the use of discrete spacers can improve the anchorage mechanism of the textile and replicate the beneficial mechanical effects of knitted 3D connections, as observed by El Kadi et al. [6].

The previous results showed that, especially in configurations with lower V_f (0.7 %), the achieving of a desired anchorage of the in-plane textiles and therefore a desirable post-cracking stiffness is strongly dependant on both the free anchorage length and the presence of transversal connections in the TRCs.

A hypothesis for the improvement in anchorage mechanism due to discrete connections is based on the formation of discrete "bridges" by these connections. In a purely tensile loading condition, both the top and bottom textile reinforcement layers are stressed in the same direction. In a flexural campaign however, the bottom textile layer undergoes a tensile deformation, whereas the top layer is subjected to compressive stresses. It is believed that the presence of discrete bridges or connections would hamper the opposite, in-plane displacement of the textile reinforcement and hence positively influence the anchorage of the in-plane reinforcement. This hypothesis is endorsed by the observations of El Kadi et al. [6], where no influence of knitted connections were observed in tensile loading conditions.

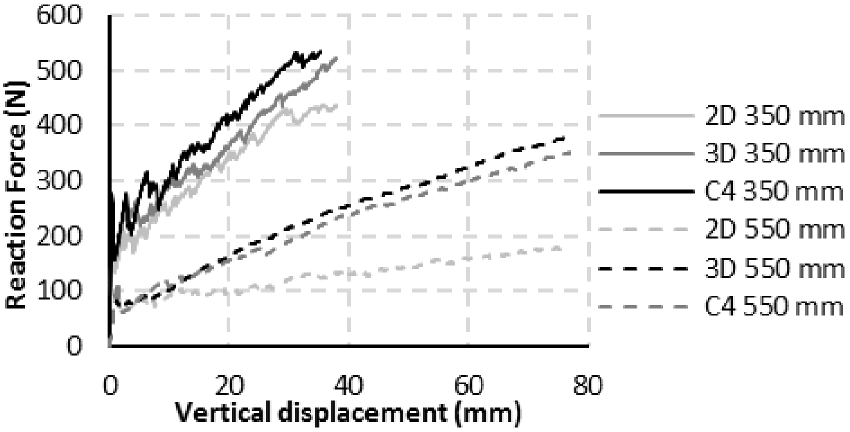

Figure 4. Force (N) – displacement (mm) curve for all TRC configurations

Table 3. *Average post-cracking stiffness for all TRC configurations*

	2D 350 mm	3D 350 mm	C4 350 mm	2D 550 mm	3D 550 mm	C4 550 mm
E_3 (N/mm)	11.3 ± 2.9	13.0 ± 2.1	13.8 ± 1.4	1.71 ± 0.18	4.16 ± 0.70	3.88 ± 0.65

4. CONCLUSIONS

This article researched the influence of discrete spacers and anchorage length on the anchorage mechanisms in long TRC elements. A four-point bending experimental campaign was conducted on 1200 mm x 60 mm x 15 mm TRC beams without transversal connections (2D), integrated knitted connections (3D) or discrete spacer connections distributed in the shear zone of the samples (C4). Distances between the supports of 350 mm and 550 mm were considered, resulting in free anchorage lengths of respectively 425 mm and 325 mm.

The experimental results showed that the free anchorage length can have a beneficial effect on the anchorage mechanism and contribute to the composite action in samples with low fibre volume fractions. Furthermore, in configurations where the free anchorage length is sufficient to warrant a post-cracking (composite) behaviour, the addition of discrete spacer connections did not have a significant influence at the level of the mechanical properties.

Secondly, the results showed that in configurations where the anchorage length was not sufficient to warrant mechanical anchorage of the in-plane textiles, the addition of discrete spacer connections was able to replicate the mechanical anchorage obtained by integrated (knitted) connections.

A hypothesis for the activation of the anchorage mechanism was proposed and linked to the local bridging effects provided by the discrete connections; these local bridges are believed to activate the anchorage mechanism in loading conditions where the individual textile layers experience opposite stress levels by hampering the opposite displacement.

Future research should investigate the minimum required free anchorage length (in function of V_f) to achieve desired anchorage mechanisms. Additionally, the effects of different amounts and distributions (in the free length and bending moment zone) of discrete connections in TRC beams should be investigated.

5. REFERENCES

[1] BRAMESHUBER W., “Textile Reinforced Concrete: State of the Art Report”, *RILEM Technical Committee 201-TRC, First edition, RILEM Publications,* Aachen, Germany, 2006.

[2] BENTUR A., MINDESS S., “Fibre Reinforced Cementitious Composites”, *Taylor and Francis,* New York, USA, 2007.

[3] AVESTON J., COOPER G. A., KELLY A., “Single and Multiple Fracture”, *The Properties of Fibre Composites*, pp. 15–24, 1971.

[4] AMZALEG E., PELED A., JANETZKO S., GRIES T., "Flexural Behaviour of Cement Based Element Reinforced with 3D Fabric", *VIII International Conference on Fracture Mechanics of Concrete And Concrete Structures*, 1994.

[5] HAIK R., SADI A., PELED A., "Influence of three-dimensional (3D) fabric orientation on flexural properties of cement-based composites", *Cement and Concrete Composites*, vol. 80, 2017.

[6] EL KADI M., TYSMANS T., VERBRUGGEN S., VERVLOET J., DE MUNCK M., WASTIELS J., VAN HEMELRIJCK D., "Experimental study and benchmarking of 3D textile reinforced cement composites", *Cement and Concrete Composites*, vol. 104, 2019.

[7] EL KADI M., KAPSALIS, P., VAN HEMELRIJCK D., WASTIELS, J., TYSMANS, T., "Influence of Loading Orientation and Knitted Versus Woven Transversal Connections in 3D Textile Reinforced Cement (TRC) Composites", *Applied Sciences*, vol. 10, 2020.

[8] TOMA, D., "Influence of Textile Connections on the Load Bearing Behaviour of Textile Reinforced Concrete", Master thesis, Vrije Universiteit Brussel, 2020.

[9] SIKA, Sikagrout 217, Note de Produit, Available online: https://www.sika.com/.

[10] FRAAS V., “Technical Datasheet SitGrid701”, Retrieved from www.solutions-in-textile.com.

[11] SUTTON M. A., ORTEU J.-J., SCHREIER H. W., “Image correlation for Shape, Motion and Deformation Measurements”, *Springer Science + Business Media*, 2009.

A MODIFIED TEXTILE REINFORCED CONCRETE WITH PHASE CHANGE MATERIAL

Zakaria Ilyes Djamai[1], Amir Si Larbi[2], Ferdinando Salvatore[2]

[1] *LMDC (Laboratoire Matériaux et Durabilité des Constructions), Université de Toulouse, INSA/UPS Génie Civil, 135 Avenue de Rangueil, 31077 Toulouse cedex 04, France*

[2]*Université de Lyon, Ecole Nationale d'Ingénieurs de Saint-Etienne (ENISE), Laboratoire de Tribologie et de Dynamique des Systèmes (LTDS), 58 Rue Jean Parot, 42000 Saint-Etienne, France*

SUMMARY: The present study presents a multiscale, investigation that focuses on the development of a new composite material, which combines a PCM modified matrix and AR textile reinforcement (PCM-TRC).

The potential of this association lies in the combination of the lightweight character of TRC composites to the heat storage capacities provided by the phase change material.

This research focuses on the effects of PCMs on the mechanical performance of TRCs. For this purpose, the efficiency of the association of the two materials has been mechanically at different PCM rates and different temperatures.

It has been found that multicracking behaviour of TRC composites is maintained in the presence of microencapsulated PCM; however, the tensile strength of the composite decreases with the PCM rate. This is due to the disorder caused by PCM at the matrix and interface scales. In addition, it has been found that the PCM state (solid or liquid) can affect the mechanical performance of both the PCM-TRC composite. This is due to PCM volume change during phase change, which has probably caused composite multickracking in the matrix and at the interface scale.

KEY WORDS:

Textile reinforce concrete
Phase change material
Mechanical behaviour
Temperature effect

1. INTRODUCTION

The building sector has a strong potential for improvement in terms of thermal performance and reduction of its ecological footprint. In this context, composite structures and non-conventional materials are widely used.

Textile-reinforced concrete (TRC) consists of a fine-grained concrete matrix reinforced with alkali-resistant glass fabric, basalt, aramid… [1, 2]. TRC combines the high compressive strength of a cementitious matrix with the high tensile resistance of a non-corrosive textile fabric and thus allows the construction of lightweight cementitious elements, such as lightweight roofs, sandwich panels, etc. [3, 4,5]. TRC can ensure fire resistance and constitutes an important alternative to fibre-reinforced polymer, which has limitations in terms of cost, fire resistance, toxicity, and sustainable-development features attributed to the polymer matrix. Despite these advantages, the lightweight of TRC, which is due to the low thicknessof the concrete covers, can lead **to a considerable reduction of its thermal inertia**.

Recent studies [6, 7, 8] have focused on the search for intelligent materials that have the ability to regulate indoor temperature variations; these are phase-change materials (PCMs). PCMs change their phase from solid to liquid in warm periods by storing heat, the same heat that is released in cold periods, when the PCM returns to the solid state. This repetitive energy storage–release process can smooth out temperature variations inside buildings when PCMs are integrated in the materials constituting the building envelope.

In this context, the present study aims to combine the advantages of PCM and TRC to propose **a new PCM-modified TRC composite, PCM-TRC,** which results from the association of a PCM-modified mortar matrix and an alkali-resistant glass fabric reinforcement. The main advantages of the new PCM-TRC composite material can be summarised as follows:

a) The possibility to produce lightweight cementitious structural elements (**owing to TRC**) with high mechanical performances (especially under tension solicitation) and high thermal inertia (**owing to PCM**).

b) It is a better match (even partial) to the criteria of sustainable development.

2. MATERIALS AND METHODS

2-1 Materials

2-1-1 Cement mortar

A Portland cement mortar with fine aggregate (D<1.6 mm) was chosen to ensure the Impregnation of the textile fabric for the 'PCM-TRC' composites.

2-1-2 Phase change material (PCM)

The PCM used in the study is a vegetal wax chemically identified as methylexadecanoate; this PCM was selected to minimise the environmental impact. The PCM phase-change is 24 to 27°C.

The latent heat of the phase change of PCM is 160 kJ/kg.

2-1-3 Textile fabric reinforcement

The textile fabric reinforcement used in the study is an AR glass with a tensile yield stress and Young's modulus measured as 800±48 MPa and 53±2.5 GPa, respectively.

2-2 Experimental methods

2-2-1 Casting procedure

2-2-1-1 Casting of the PCM-modified mortar matrix

Microencapsulated PCM was added to different weight percentages of Portland cement fine-grained mortar (0, 5, 10, and 15 wt%). The high hydrophilic nature of the encapsulated PCM [5,6],induce a high water absorption in the internal porosity of PCM. This induces an adjustment of the amount of water necessary for each PCM-mortar matrix (at each PCM rate)

The amount of additional water required for each PCM–mortar matrix was evaluated using a water absorption test on PCM powder according to EN1097-6 . The results are shown in **Table 1.**

Mass of surface dried (24h in 100°C oven) PCM powder M_1(g)	Mass of saturated PCM powder after 24h immersion M_2 (g)	Water absorption coefficient ($\frac{M_2-M_1}{M_1}$) in %
100	154	54

Table 1 Test results of water absorption capacity of PCM powder

The mix composition of the PCM-mortar matrix are presented **Table 2** [w1/c is the total water to cement ratio, w2/c is the ratio of water not absorbed by the PCM to cement, which is maintained constant in all the mix composition and leads to a quasi-constant slump (equivalent workability) in all the mix compositions (**see table 2**)].

PCM-mortars	Reference	5wt%	10wt%	15wt%
PCM (kg)	0	0.3	0.6	0.9
Cement (kg)	1.65	1.65	1.65	1.65
Fine aggregate (kg)	4.35	4.35	4.35	4.35
Water (L)	0.80	0.96	1.12	1.29
$\frac{w_1}{c}$	0.48	0.58	0.68	0.78
$\frac{w_2}{c}$	0.48	0.48	0.48	0.48
slump (mm)	182	185	178	179

Table 2 PCM-mortar mixture compositions

2-2-1-2 casting of the ‘PCM-TRC’ composites

The in situ hand lay-up technique (**Figure 1**) was applied to produce the PCM-TRC composites.

A suitable amount of each PCM–mortar matrix (0, 5, 10, 15 and 20wt% PCM–mortar, as described above) was spread on the bottom of a mould (600 mm-length, 400 mm- width, 10 mm- thickness). Then, the AR glass fabric was impregnated by the matrix with a roller so that PCM–mortar matrix penetrated inside the textile fabric meshes. The procedure was repeated so that the PCM-TRC composites were reinforced with two layers of textile fabric.

Textile placement Contact molding technique

Figure 1 In-situ hand lay-up technique for PCM-TRC composites

2-2-2 Mechanical characterization

2-2-2-1 Mechanical tests at constant temperature and variable PCM rate

Thin PCM-TRC specimens (500 mm-length, 70 mm-width, and 10 mm-thick) consisting of PCM–mortar matrix (0, 5, 10, 15 and 20wt% PCM) reinforced with two layers of AR glass fabric (which corresponds to a volume rate of reinforcement of 2.66% and 2.1 % in the warp and weft directions, respectively and a total fiber fraction volume of 4.76%) were tested under unidirectional tensile solicitation in the warp direction of the textile reinforcement (three specimens for each PCM content) at an age of 28 days and at a **constant temperature of 20°C** (which means that PCM was in the solid state), according to the recommendation of the Rilem committee [8].

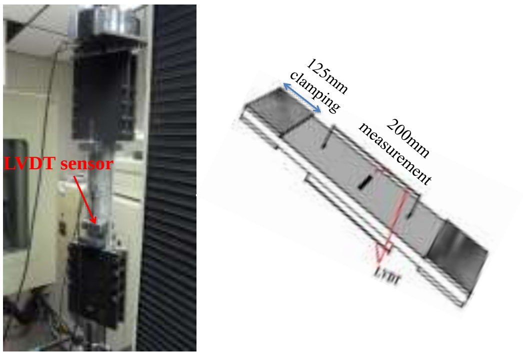

Test machine Test sample (500×70×10mm)

Figure 2 Tensile tests on PCM-TRC composites

2-2-2-2 Mechanical tests at variable temperature and constant PCM rate

To analyse the effect of the temperature (and thus the PCM state) on the mechanical performance of PCM-TRC, the mechanical strength of the 10wt% PCM-TRC composite was evaluated in two different configurations:

-A- 10wt% PCM-TRC test specimens (500 mm × 70 mm × 10 mm) were maintained at a temperature of 20 °C and were then tested under tension at the same temperature.
-B- 10wt% PCM-TRC test specimens (500 mm × 70 mm × 10 mm) were initially kept at 20 °C and then placed in an oven at 40 °C for 6 h to induce phase change of the PCM (from solid to liquid). Three minutes after their removal from the oven, the specimens were tested under tension.

3. RESULTS AND DISCUSSIONS

3-1 Mechanical characterisation of PCM-TRC composites

3-1-1 Mechanicals tests at variable PCM rate and constant temperature

The results obtained during the tensile tests on the PCM-TRC composites at different PCM rates (0, 5, 10, 15, and 20wt%) were analysed to determine their average macroscopic constitutive law in terms of stress versus strain, as presented in **Figure 3.**

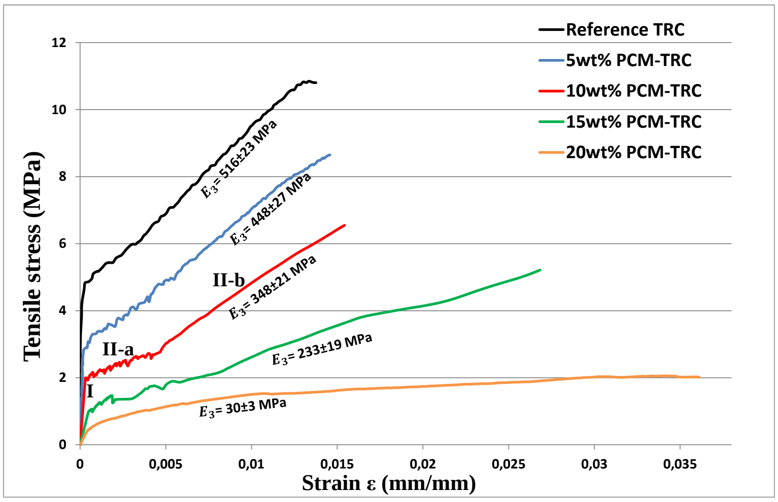

Figure 3 Stress versus strain behaviour of PCM-TRC composites during tensile test at T=20°C

The global behaviour of the PCM-TRC composite (for all PCM rates) can be summarised as follows:

Phase I (see **Figure 3**) corresponds to a perfectly linear evolution governed by the mechanical properties of the matrix up to the initiation of the first macrocrack. During **phase II-a** (see **Figure 3**), the elastic limit of the matrix is reached progressively along the length of the composite, and each time a crack is created, the force is transmitted progressively from the matrix towards the textile at the location of the crack. **In phase II-b** (see **Figure 3**) the textile recovers almost all the tractive effort and the stiffness modulus of the composite is governed by the elastic modulus of the reinforcing textile and its rate of work.

The first finding obtained by analysing the stress versus strain curves is that the strain hardening behaviour (ductile behaviour) and the matrix/textile charge transfer kinetics are maintained in the presence of microencapsulated PCM in TRC. However, it can be seen that the tensile strength of the PCM-TRC composites decreases when increasing the PCM rate.

By analysing in more detail the stress versus strain curves, one can note that:

In phase I, the stress at the onset of the initial cracking, which corresponds to the elastic limit of the PCM–mortar matrix, decreases with increasing PCM rate. This is explained by the fact that the addition of PCM in the mortar weakens its mechanical performance. Similarly, the elastic modulus in phase I decreases with decreasing PCM content owing to the weakening of the rigidity of the matrix.

The multicracking phase (**phase II-a**) is clearly visible in the majority of PCM-TRC composites; however no particular conclusion can be drawn as to the effect of the PCM rate on this phase.

During **phase II-b**, the load is almost entirely transmitted to the textile reinforcement. It can be seen after calculation (see **Table 4**) that the stiffness modulus of the composite **(E_3, during phase II-b, see Figure 3)** decreases with increasing PCM content. The rigidity modulus E_3 of the PCM-TRC composite in **phase II-b is a direct indicator** of the textile efficiency (textile rate of work) inside the PCM-TRC composite.

It can also be seen in **phase II-b** that the strain at failure of the composites is almost constant up to the level of 15% PCM, where an increase of the strain at rupture is observed. This is explained by the fact that for the 0, 5, and 10wt% PCM-TRC samples, the mode of failure was rupture of the textile under tension, whereas for the 15 and 20wt% PCM-TRC samples, rupture occurred by delamination of the textile layers due to the weakening of the shear strength of the interlaminar layer by the addition of PCM (see **Figure 4**).

Indeed, the LVDT sensors positioned on the faces of the 15 and 20wt% PCM-TRC samples measured a parasitic displacement due to interlaminar slip upon the occurrence of shear delamination, which explains the large increases of the strain at failure for the 15 and 20% PCM-TRC samples in comparison with the 0, 5, and 10wt% PCM-TRC composites.

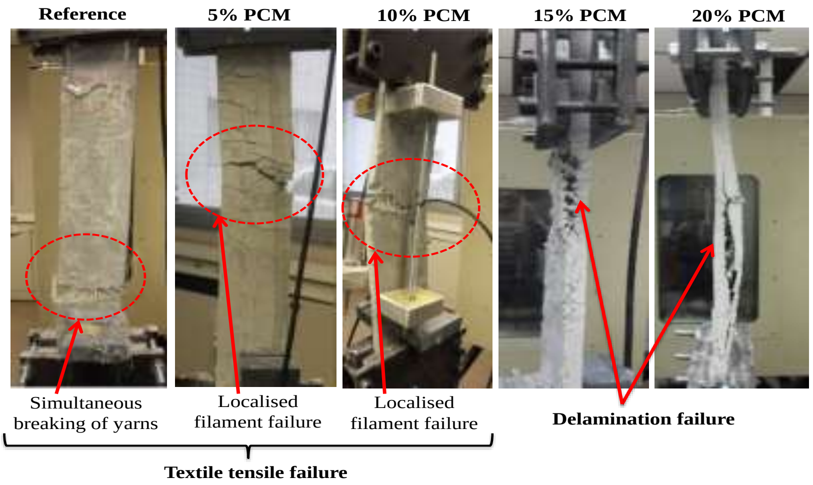

Figure 4 Failure modes of PCM-TRC composites

3-1-2 Mechanical tests at variable temperature and constant PCM rate

The average curves (stress versus strain for three samples) of the tensile behaviour of the 10wt% PCM-TRC composite held at 20°C and tested at the same temperature and for the 10wt% PCM-TRC composite heated at 40°C for 6 h (to induce PCM phase change) are presented in **Figure 5**.

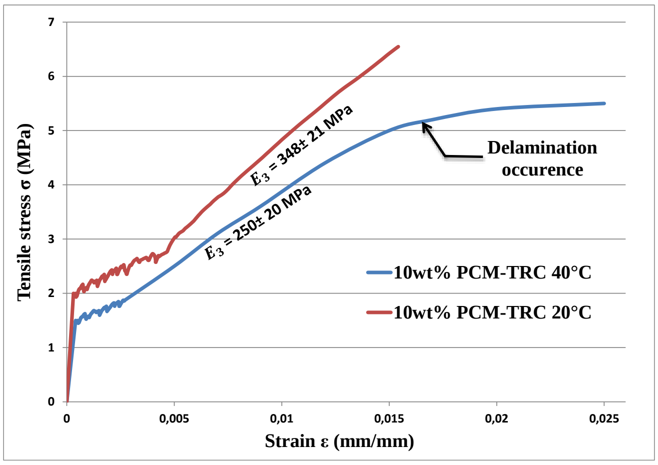

Figure 5 Effect of PCM phase change on the mechanical behaviour of 10% PCM-TRC

From **Figure 5**, it can be seen that the 10wt% PCM-TRC composite heated at 40°C has a 20% lower resistance than the sample held at 20°C.

By analysing in more detail:

In **phase I**, the 10wt% PCM-TRC composite heated at 40°C exhibits a decrease of 25% in stress at the onset of cracking (σ_{BMC}) and a decrease of 33% in the elastic modulus of the matrix (E_1) in comparison with the composite maintained at 20 °C **(Figure 5).** This phenomenon is explained further in section 3-2

In **phase II-b**, the stiffness modulus E_3 of the 10wt% PCM-TRC composite heated at 40 °C shows a decrease of ~30% compared with the composite maintained at 20°C (**see Figure 5**). This is explained by a degradation of the intensity of the matrix/textile.

This trend is confirmed by analysing the failure mode of the 10wt% PCM-TRC sample heated to 40°C. In fact, the rupture of that sample occurred by delamination between layers of reinforcement (see **Figure 6**) due to the degradation of the shear strength of the interlaminar layer by cracking during placement in the oven. Meanwhile, we can observe that the rupture of the 10wt% PCM-TRC composite maintained at 20°C occurred by textile breaking under tension (see **Figure 6**).

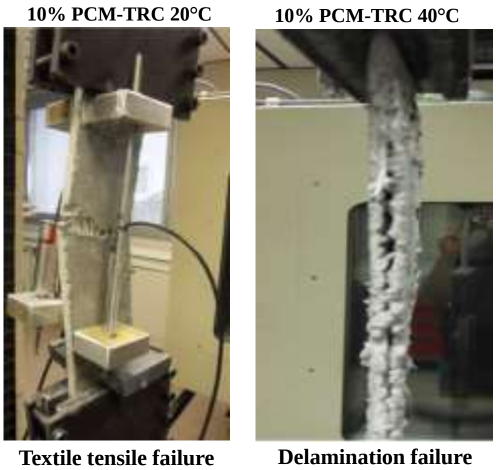

Figure 6 Effect of PCM phase change on the failure mode of the 10wt% PCM-TRC sample

3-2 Explanation of the effect of temperature on the mechanical behaviour of the PCM-TRC composites.

Figure 7 shows the evolution of the longitudinal strain and surface temperature versus time in the a 15wt% PCM-TRC sample placed in an oven at 40°C and instrumented with a strain gauge and a temperature sensor (the composite is not subjected to any stress solicitation during placement in the oven).

The 15wt% PCM–TRC samples exhibited an increase in the strain, which began in the range 24–25°C; this corresponds to the phase change of PCM from the solid state to the liquid state. No strain variation was observed in the range 15–23°C (all PCM in the mortar is in the solid state) or in the range 34–40°C (all PCM in the mortar has melted and is in the liquid state). In the temperature range 25–34°C, the PCM melts gradually from the surface to the internal volume of the sample.

Correspondingly, analysis of the change of the samples surface temperature as a function of time spent in the oven shows a constant rate of temperature increase until 24–25°C, where a slowdown in the temperature increase is observed. This is explained by the fact that at 24–25°C, PCM absorbs heat from the oven (in the form of latent heat) to undergo phase change, which causes a decrease in the rate of temperature increase.

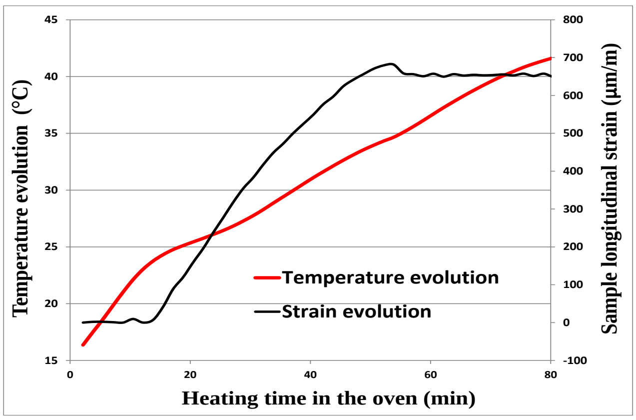

Figure 7 longitudinal strain vs temperature in 15wt% PCM-TRC sample placed in an oven

From **figure 7**, it can be seen that the PCM phase change can induce local strain attributed to PCM volume change during the melting of PCM. These local strains can induce mortar microicracking in the matrix (which explains the decrease of the resistance of the 10wt% PCM-TRC placed in the oven in the elastic phase) and in the matrix/textile interface which could

Explain the decrease of the textile efficiency (textile rate of work) and also explains delamination failure that occurs for the 10wt% PCM-TRC specimen placed in an oven.

4. CONCLUSION

This paper focuses on the mechanical characterisation of new PCM-TRC composites derived from the association of a non-paraffinic encapsulated PCM modified cementitious matrix and textile reinforcement. On the basis of the experimental investigations presented above, the following conclusions can be drawn:

1. The ductile mechanical behaviour and the matrix/textile charge transfer kinetics in the TRC composites are maintained in the presence of microencapsulated PCM.
2. The mechanical performances of the PCM-TRC composites degrade with increasing PCM content; furthermore, a critical failure mode by delamination between layers of reinforcement is detected for PCM content around 15wt%.
3. A decrease of the textile rate of work is observed when increasing the PCM content in the PCM-TRC composites. This is due to the disorder caused by the PCM in the matrix/textile interface area.

4. The temperature has an effect on the mechanical behaviour of the PCM-TRC composites. A drop of tensile strength and a decrease of the textile efficiency work are observed for the 10wt% PCM-TRC composite heated at 40°C in comparison with the composite maintained at 20°C. This is due to the degradation of the matrix/textile interface caused by multicracking, which is due to PCM expansion during its phase change from solid to liquid.

5. ACKNOWLEDGEMENT

The authors thanks KAST company (Sonthofen, Germany) and Monsieur Bernard Arnold for providing the textile reinforcement used in the study/

6. REFERENCES

[1] T D'Antino, C Papanicolaou, Mechanical characterization of textile reinforced inorganic-matrix composites, Composites Part B 127 (2017) 78-917

[2] Z Djamai, M Bahrar, F Salvatore, A Si Larbi, M El Mankibi, Textile reinforced concrete multiscale mechanical modelling: Application to TRC sandwich panels, Finite Elements in Analysis and Design 135 (2017) 21-35

[3] Z I Djamai, K Erroussafi, A Si Larbi, F Salvatore, G Cai Analytical modeling of textile reinforced concrete (TRC) sandwich panels: Consideration of nonlinear behavior and failure modes, Mechanics of advanced Materials and structures (2020).

[4] I Colombo, M Colombo, M Di Prisco, Bending behavior of textile reinforced concrete sandwich beams, Construction and Building Materials 95 (2015) 675–685.

[5] Z I Djamai, K Le-Nguyen,, A Si Larbi, F Salvatore, G Cai PCM-modified textile-reinforced concrete slab: a multiscale and multiphysics investigation,, Construction and Building Materials 293 (2021)

[6] Z Djamai, F Salvatore, A Si Larbi, G Cai, M El Mankibi, Multiphysics analysis of effects of encapsulated phase change materials (PCMs) in cement mortars, Cement and Concrete Research 119 (2019) 51-63.

[7] Z Djamai, A Si Larbi, F Salvatore, G Cai A new PCM-TRC composite: A mechanical and physicochemical investigation, Cement and concrete Research 135 (2020)

[8] S Cunha, M Lima, J Aguiar, Influence of adding phase change materials on the physical and mechanical properties of cement mortars, Construction and Building Materials 127 (2016) 1–10

[9] RILEM Technical Committee Recommendation 232-TDT: test methods and design of TRC Materials and structures (2016) 4923-4927

ELASTIC AND ELECTROMAGNETIC WAVE MONITORING OF TRC DURING CURING

Nicolas Ospitia[1], Eleni Tsangouri [1], Johan H. Stiens [2], Ali Pourkazemi [2] and Dimitrios G. Aggelis [1]

[1] Department of Mechanics of Materials and Constructions (MeMC), Faculty of Engineering, Vrije Universiteit Brussel (VUB), Brussels, Belgium; nicolas.ospitia.patino@vub.be (N.O.P.); Eleni.Tsangouri@vub.be (E.T.); Dimitrios.Aggelis@vub.be (D.G. A.)

[2] Department of Electronics and Informatics (ETRO), Faculty of Engineering, Vrije Universiteit Brussel (VUB), Brussels, Belgium; apourkaz@etrovub.be (A.P.); jstiens@etrovub.be (J.H.S.)

SUMMARY: *The present study demonstrates a combination of elastic and electro-magnetic wave based Non-Destructive Testing (NDT) techniques for the monitoring of the curing state of textile reinforced cement (TRC). Millimetre wave (MMW) spectrometry, was used as a non-contact high resolution electromagnetic technique that was able to monitor the chemical reactions involved in the hydration of cement, and the evaporation of water. In addition, Ultrasound Pulse Velocity (UPV) was used as a well-established, elastic wave-based benchmarking technique, for monitoring of TRC hardening progress. Results evidenced that UPV was directly related to the development of stiffness in the material, while MMW Spectrometry was sensitive to chemical reactions at a microstructural level. Interpretation of results and possible application of both techniques are also discussed along with their complementarity, which makes them a complete technological solution for condition monitoring of thin lightweight structural elements during manufacturing as well as in operation.*

KEY WORDS: *TRC, UPV, MMW Spectrometry, Curing monitoring, non-contact, NDT.*

1. INTRODUCTION

Recently, increased research and usage of (TRC) composites has been presented due their freeform, non-corrosive nature, that allows for reductions in mortar utilization [1]. Research has mainly focused on the mechanical behavior of TRC [2]–[6]. The cementitious matrix, that occupies the majority of the volume of TRC, is responsible for the compressive behavior, the composite durability and the bonding with the textiles. Issues with the matrix may result into early failure. Therefore, it seems necessary to characterize the cementitious matrix through hydration and hardening.

NDT Techniques, proved to be a powerful tool for monitoring and characterizing cementitious composites without affecting, nor compromising their behavior. This study consists of a combination of elastic and electromagnetic wave monitoring of the curing process of TRC with Ultrasound Pulse Velocity (UPV), a well-established NDT technique based on elastic waves, that has been extensively used on cementitious media for hydration monitoring [7]–[10]. On the other hand, millimeter wave (MMW) spectroscopy, a non-contact Electromagnetic (EM) wave-based technique which has shown sensitivity to chemical reactions occurring in cement hydration [11]. At the moment, the MMW band has not been used for hydration monitoring, however, lower frequency bands have been used for content determination (w/c ratio, s/c ratio) [12]–[14], hydration monitoring based on EM properties [15] or setting process monitoring [16]. However, higher frequency bands, such as MMW, allow for higher resolution measurements, non-contact monitoring and characterization of the TRC specimen.

UPV could effectively monitor development of stiffness of the cementitious matrix of TRC, while MMW spectroscopy, from reflection and transmission measurements, was able to continuously monitor the EM properties of the specimens. These properties, such as permittivity, show high sensitivity to hydration and curing of the cementitious matrix of TRC, which is responsible for the compressive strength and the binding of the composite.

2. EXPERIMENTAL DETAILS

The MMW Spectrometry setup (illustrated in Figure 1) consisted on a Keysight PNA Network Analyzer N5227B with a capacity to operate from 10 MHz-67 GHz. The selected frequency band was 46- 66 GHz with 1601 points. Four parabolic mirrors were used to refocus the free-space radiation. A response calibration was performed directly in the PNA, however, for permittivity calculations, a normalization of reflection (S11) and transmission (S21) response was performed taking air as full-transmission and metal as full reflection, as follows [17] :

$$\boldsymbol{S_{11}}_{\boldsymbol{cal}} = \frac{\left(\boldsymbol{S_{11}}_{\boldsymbol{measured}} - \boldsymbol{S_{11}}_{\boldsymbol{air}}\right)}{\left(\boldsymbol{S_{11}}_{\boldsymbol{metal}} - \boldsymbol{S_{11}}_{\boldsymbol{air}}\right)} \qquad \textbf{(1)}$$

$$S_{21_{cal}} = \frac{\left(S_{21_{measured}} - S_{21_{air}}\right)}{\left(S_{21_{metal}} - S_{21_{air}}\right)} e^{-j\left(\frac{w}{c}\right)d} \quad (2)$$

Where the exponential component of equation 2 is a phase correction that compensates for the phase change due to the placement of the sample, replacing that portion of air. For permittivity calculations, a two-layer algorithm based on the propagation paths proposed in [18] was used, where the EM properties of the mold were previously measured. And the sample permittivity was calculated by finding a permittivity that corresponds to the EM transmission response for each frequency. In order to accomplish this, a cost function was implemented and minimized using non-linear least squares function in matlab.

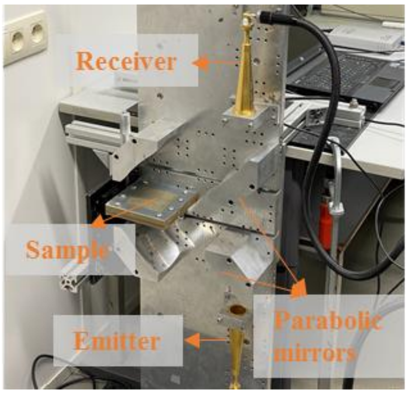

Figure 1. Experimental setup MMW Spectrometry

The UPV setup (Figure 2) consisted on an Agilent 33220A waveform generator set to emit a 10 V single sinusoidal pulse of 150 kHz. Two resonant sensors at 150 kHz were used (emitter and receiver). The signal passes through the sample (of 10 mm thickness) and it reaches a receiver that is connected to a preamplifier set to a gain of 40 dB and at the same time to a Micro-II Digital AE System (provided by Mistras Group).

$$V_l = \sqrt{\frac{E(1-\nu)}{\rho * (1+\nu)(1-2\nu)}} \quad (3)$$

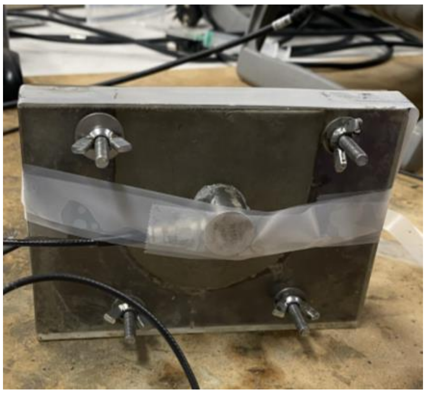

Figure 2. Experimental setup UPV

The TRC sample was composed of a glass textile reinforcement [19], and a mortar matrix that consisted of a water/cement ratio of 0.45, and a sand/cement ratio of 2. Additionally, the superplasticizer/cement ratio was 1.25 %. The cement used was CEM I of 52.5 N, and the sand 0/2 later sieved for a maximum grain size of 0.875 mm. The superplasticizer was Sika ViscoCrete-20 Gold, a high water reducer for cementitious matrices with a high initial strength [20]. For both tests, the mortar was fabricated by mixing the cement with the sand for two minutes at low mixer speed, adding water and superplasticizer, and mixing for two minutes at low speed and one at high speed. The mortar was introduced into the corresponding molds and vibrated for one minute. The measuring frequency of both techniques was 1 Hz, for measuring time of 24 hours.

3. RESULTS

In Figure 3 A), the evolution of UPV for an indicative TRC specimen of 10mm thickness is given. By tracking the UPV evolution, one can estimate the stiffness progressive gain. Approximately at 3 hours after mixing, the UPV increases, but the rising rate starts to drop. In figure 3 B), it is possible to see the evolution of the magnitude of the transmitted EM wave in the millimeter band that shows high sensitivity to the presence of free water and to the chemical reactions in which free water is incorporated into the structure of hydrated cement, where it is possible to distinguish a dormant period, and an acceleration period in which on the one side the stiffness of the specimen was increasing (see UPV) and, on the other side, the chemical reactions caused changes in the microstructure of the cementitious matrix, changing the EM properties of the material and allowing more transmission.

Afterwards, a deceleration period is presented for both NDT's evidencing a slower rate of reactions and changes in the stiffness and microstructure of the samples.

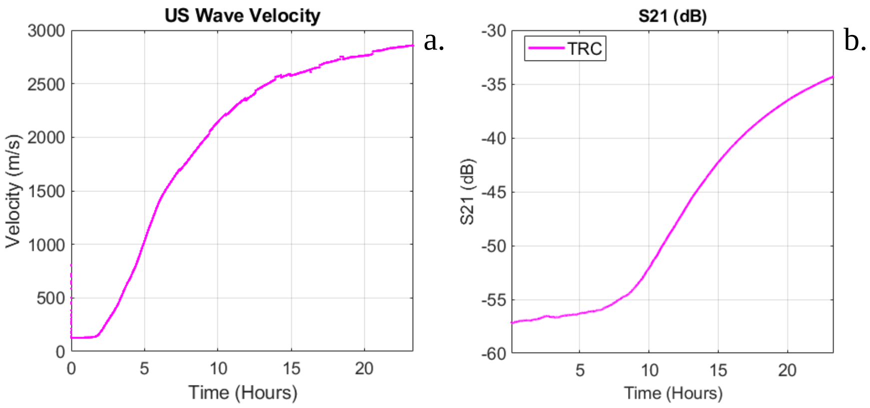

Figure 3. A) UPV TRC of 10 mm thickness B) Transmission MMW Spectrometry different specimens.

Figure 4. ~~Figure 4.~~ illustrates the evolution of The Young modulus for TRC, where it is possible to see a dormant period for 3-4 hours, followed by a rapid stiffness increase until 7-10 hours, where the curve seems to increase at a lower rate. Finally, at 24 hours the Young's modulus of TRC reaches more than 13 GPa. Beyond this point, a lower increase in stiffness is expected until it becomes negligible.

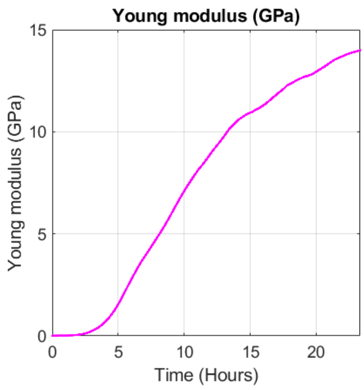

Figure 4. Young's modulus TRC of 10 mm thickness

Figure 5~~Figure 5~~ illustrates the permittivity of the TRC specimens for frequencies between 46-66 GHz at indicative times. The change in permittivity with time is attributed to the ongoing physicochemical reactions occurring due to hydration. It is clear that besides the age-dependency of the permittivity during curing, there is also a frequency dependence where higher frequencies present lower permittivity, which is mainly caused by a reduced dipolar relaxation of water molecules. In addition, please note that more hydrated specimens present less fluctuations in the permittivity.

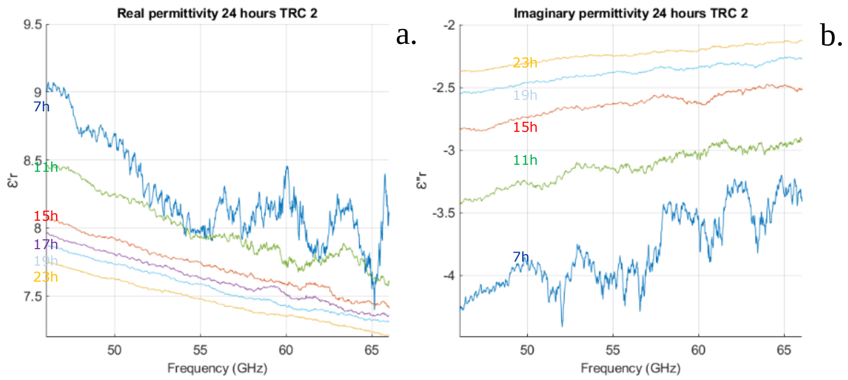

Figure 5. a) Real and b) Imaginary permittivity of TRC specimens

4. CONCLUSIONS

This paper illustrates a multi-modal NDT approach for monitoring TRC during curing in order to follow the physicochemical changes occurring due to the hydration of the cementitious matrix. The final aim is to provide a non-destructive methodology for quality control of TRCs. The information obtained from both techniques has shown to be complementary. On one hand, MMW spectrometry shows high sensitivity to the presence and structure and binding of water molecules, and therefore to the chemical reactions involving water. While UPV, shows sensitivity to the development of stiffness. Further experiments should focus on damage , and hydration quantification, and in-situ monitoring.

5. REFERENCES

[1] N. Williams, K. Lundgren, H. Wallbaum, and K. Malaga, “Sustainable potential of textile-reinforced concrete,” *J. Mater. Civ. Eng.*, vol. 27, no. 7, 2015, doi: 10.1061/(ASCE)MT.1943-5533.0001160.

[2] J. Hegger, N. Will, O. Bruckermann, and S. Voss, “Load-bearing behaviour and simulation of textile reinforced concrete,” *Mater. Struct. Constr.*, vol. 39, no. 292, pp. 765–776, 2006, doi: 10.1617/s11527-005-9039-y.

[3] S. Xu and H. Li, “Bond properties and experimental methods of textile reinforced

concrete," *J. Wuhan Univ. Technol. Mater. Sci. Ed.*, vol. 22, no. 3, pp. 529–532, 2007, doi: 10.1007/s11595-006-3529-9.

[4] M. Butler, V. Mechtcherine, and S. Hempel, "Durability of textile reinforced concrete made with AR glass fibre: Effect of the matrix composition," *Mater. Struct. Constr.*, vol. 43, no. 10, pp. 1351–1368, 2010, doi: 10.1617/s11527-010-9586-8.

[5] M. De Munck *et al.*, "Fatigue behaviour of textile reinforced cementitious composites and their application in sandwich elements," *Appl. Sci.*, vol. 9, no. 7, 2019, doi: 10.3390/app9071293.

[6] M. El Kadi, "Experimental characterization, benchmarking and modelling of 3D textile reinforced cement composites," Vrije Universiteit Brussel, 2019.

[7] H. W. Reinhardt and C. U. Grosse, "Continuous monitoring of setting and hardening of mortar and concrete," *Constr. Build. Mater.*, vol. 18, no. 3, pp. 145–154, 2004, doi: 10.1016/j.conbuildmat.2003.10.002.

[8] N. De Belie, C. U. Grosse, J. Kurz, and H. W. Reinhardt, "Ultrasound monitoring of the influence of different accelerating admixtures and cement types for shotcrete on setting and hardening behaviour," *Cem. Concr. Res.*, vol. 35, no. 11, pp. 2087–2094, 2005, doi: 10.1016/j.cemconres.2005.03.011.

[9] T. Öztürk, J. Rapoport, J. S. Popovics, and S. P. Shah, "Monitoring the setting and hardening of cement-based materials with ultrasound," *Concr. Sci. Eng.*, vol. 1, no. 2, pp. 83–91, 1999.

[10] J. R. Rapoport, J. S. Popovics, S. V. Kolluru, and S. P. Shah, "Using ultrasound to monitor stiffening process of concrete with admixtures," *ACI Struct. J.*, vol. 97, no. 6, pp. 675–683, 2000, doi: 10.14359/9981.

[11] A. Pourkazemi *et al.*, "Combination of Acoustic Emission and Millimeter Wave Spectroscopy Techniques to Investigate Damage on Cementitious Materials," *2nd Int. RILEM/COST Conf. Early Age Crack. Serv. Cem. Mater. Struct.*, no. September, pp. 1–6, 2017, [Online]. Available: http://www.etrovub.be/research/lami/Millimeter_Waves/Meta_materials/publications.asp?recent=1.

[12] K. J. Bois, A. D. Benally, P. S. Nowak, and R. Zoughi, "Cure-state monitoring and water-to-cement ratio determination of fresh portland cement-based materials using near-field microwave techniques," *IEEE Trans. Instrum. Meas.*, vol. 47, no. 3, pp. 628–637, 1998, doi: 10.1109/19.744313.

[13] E. Bescher, M. Sambol, E. K. Rice, and J. D. Mackenzie, "Determination of water-to-cement ratio in freshly mixed rapid-setting calcium sulfoaluminate concrete using 2.45 GHz microwave radiation," *Cem. Concr. Res.*, vol. 34, no. 5, pp. 807–812, 2004, doi: 10.1016/j.cemconres.2003.09.023.

[14] A. Sihvola, “Mixing Rules with Complex Dielectric Coefficients,” *Subsurf. Sens. Technol. Appl.*, vol. 1, no. 4, pp. 393–415, 2000, doi: 10.1023/A:1026511515005.

[15] P. Shen and Z. Liu, “Study on the hydration of young concrete based on dielectric property measurement,” *Constr. Build. Mater.*, vol. 196, pp. 354–361, 2019, doi: 10.1016/j.conbuildmat.2018.11.150.

[16] D. Wang, G. Yu, S. Liu, and P. Sheng, “Monitoring the setting process of cementitious materials using guided waves in thin rods,” *Materials (Basel).*, vol. 14, no. 3, pp. 1–12, 2021, doi: 10.3390/ma14030566.

[17] F. J. F. Gonçalves, A. G. M. Pinto, R. C. Mesquita, E. J. Silva, and A. Brancaccio, “Free-space materials characterization by reflection and transmission measurements using frequency-by-frequency and multi-frequency algorithms,” *Electron.*, vol. 7, no. 10, pp. 3–6, 2018, doi: 10.3390/electronics7100260.

[18] A. Pourkazemi, J. H. Stiens, M. Becquaert, and M. Vandewal, “Transient Radar Method: Novel Illumination and Blind Electromagnetic/Geometrical Parameter Extraction Technique for Multilayer Structures,” *IEEE Trans. Microw. Theory Tech.*, vol. 65, no. 6, pp. 2171–2184, 2017, doi: 10.1109/TMTT.2017.2665633.

[19] V. FRAAS solutions in textile, “Datenblatt : SITgrid200,” *www.solutions-in-textile.com*, p. 1, 2017.

[20] SIKA, “Sika ViscoCrete -20 Gold ®,” no. 140. p. 3, 2007.

EFFECT OF SURFACE TREATMENTS ON TENSILE STRENGTH OF CARBON AND BASALT FIBRES FOR TRC APPLICATIONS

N. Algourdin[1], Z. Mesticou[1], A. Si Larbi[1]

[1] Univ. Lyon, Ecole Nationale d'Ingénieurs de Saint-Etienne (ENISE), Laboratoire de Tribologie et de Dynamique des Systèmes (LTDS), UMR 5513, 58 rue Jean Parot, 42023 Saint-Etienne Cedex 2, France

SUMMARY: *In the first part, study deals with desizing tests on carbon (C) and basalt (B) textiles and its influence on ultimate tensile strength of fibres. Different desizing methods were used: carbonisation and chemical actions. SEM observations showed that phosphoric acid treatment alters partially the two types of fibres, and mostly that of B fibres. Only heating at 200°C or 300°C (2h) and other treatments did not present the surface alteration. The average tensile strength is reduced of 54 % after C fibre desizing. In second part, a "pin" device was developed for tensile strength tests of carbon yarns. The desizing treatments reduce the tensile strength of carbon composites, especially the combination of 200°C and phosphoric acid treatment, that may damage the fibre surface and/or aggravate the existing surface flaws. Coating treatments and geopolymer application did not present the significant effect on tensile strength of composites. Adding the micro silica powder to the aqueous organic binder, enhances adhesion between the reinforcement and matrix and increases the composite tensile strength.*

KEY WORDS: *desizing, carbon, basalt, heating, tensile strength*

1. INTRODUCTION

Maintenance of the infrastructures is a guarantee of user and property security. In this respect, the application of Textile Reinforced Cement (TRC) in a construction sector was well developed over the past ten years [1]. The interface (or interphase [2]) in TRC is a surface formed by a boundary between fibre and matrix for the transfer of loads. Adequate interfacial adhesion provides composites with structural integrity. However, the relatively weak interlaminar properties limit the composite performance and service duration [3]. To examine the interfacial adhesion, some desizing and/or coating technics were proposed in this paper.

Carbon and basalt fibres require a sizing operation for lubricant deposit on the surface of the fibres to protect from damage during subsequent textile processing, to enhance sliding and flexibility and thus facilitate its handling [4]. However, commercial sizing may have defects during processing [5,6]. First, the sizing layer, located at the fibre / matrix interface, can weaken this interface and led to the considerable loss of mechanical performances of the composite material. Second, the fibres which have surface sizing are integral with each other and prevent the matrix from dispersing homogeneously around each filament [7]. Moreover, sizing is a critical factor in the fibre-matrix interaction. Using the manufactured sizing could negatively influence the interface properties, decreasing the tensile strength.

Deak et al. and Arslan et al. [8,9] showed that the desizing of industrial coating and sizing by relevant coupling agents could improve the interface properties and enhance the mechanical resistance. The aim of this exploratory study is to examine the textile alteration degree after desizing, using the tensile strength tests. The first part of the study presents different desizing techniques, based on carbonisation and/or chemical mechanisms. In the second part, the desized and coated carbon yarns are subjected to tensile strength tests basing on developed "pin" device.

2. DESIZING OF TEXTILE FIBRES

2.1 Materials and methods

In the first part of the work, desizing techniques were applied on carbon and basalt textiles (Table 1). The diameter of carbon textile (Figure 1 (a)) is 7 µm with 12000 as number of filaments per yarn. The diameter of basalt fibres (Figure 1(b)) is 17 µm with 1200 filaments per yarn.

Table 1 *Carbon and basalt fibres characteristics*

Textile fibres	Carbon TORAY T700S	BCF Basaltex 19 - 1200
Density (g/cm3)	1.8	2.67
Sizing type	Epoxy, 1%	Silane
Filament diameter (µm)	7	17
Yarn count of roving (Tex)	12000	1500
Fibre tensile strength (MPa)	4900	2900
Young's modulus (GPa)	230	87-90
Tensile strain (%)	2.1	3
Temperature stability (°C)	300	550-1200
Textile tensile strength(MPa)	54.2	-

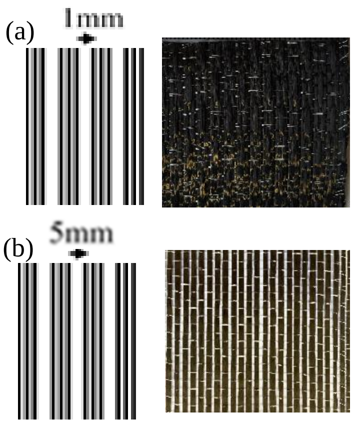

Figure 1 *Tested carbon (a) and basalt (b) textiles*

The carbon and basalt yarns were subjected to different types of desizing, which are resumed in Table 2. Globally, the program was based on adhesion bonding mechanism by acid-alkaline interactions.

First, the fibres were heated up to 200 °C or 300°C in an electric oven of 30 cm (h) x 40 cm (w) x 60 cm (d). The applied temperature rise was 4 °C/ min with a stabilization level of 60 min. Second, the treatments were carried out. Impregnation in different solutions lasted maximum 5 min with a drying phase of 24 h minimum.

Table 2 *Desizing techniques*

Non heated	**200°C**	**300°C**
(NT) Non treated, (PA) Phosphoric acid	(NT200) Non treated, (PA200) Phosphoric acid, (A200) Acetone, (U200) Ultrasound in water during 10 min, (E200) Ethanol	(NT300) Non treated, (PA300) Phosphoric acid, (A300) Acetone, (V300) White vinegar

Desized specimens, which showed the modification in sizing layers, were subjected to tensile tests.

2.2 SEM observations

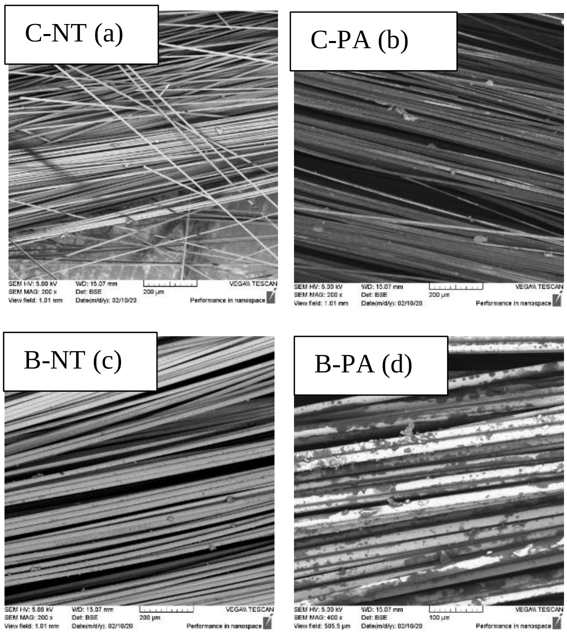

Figure 2 *SEM observations of the sized (a, c) and desized (b, d) (200°C+PA treatment) carbon (C) and basalt (B) fibres.*

Carbon and basalt fibre surface was observed by SEM (Scanning Electron Microscopy) before and after desizing. It was showed that the sizing layer is distributed non-uniformly on the fibre surface. It is probably due to the sizing process.

Burning at 200°C or 300°C and posterior treatment by PA (PA200) showed partial degradation of the surface layer of carbon and basalt fibres (Figure 2). The volume of desized fibres was higher for basalt: the organic layer has partially disappeared and a lighter surface is visible on Figure 2 (d). In turn, carbon mesh present only singular desized fibres Figure 2 (b). The other mentioned treatments did not show any alteration.

2.3 Tensile strength test

Rectangular textile specimens (650 mm × 10 mm) are subjected to a monotonic direct tensile strength test until failure [10]. A universal machine (Wolpert) is used (Figure 4). A displacement control is applied with a 1 mm/minute speed, preceded by a preload phase of 500 N and a speed of 5 mm/min.

Figure 3 shows the evolution of tensile strength for C fibres related to the desizing treatment (heated at 200°C and heated at 200°C + phosphoric acid). During tensile test, brittle behaviour was observed. Non treated specimens present higher values of tensile strengths than that subjected to desizing. The tensile strength was reduced of 46 % for NT200 and of 61 % for PA200. Heating and PA treatment damage the superficial fibres layer and/or aggravate the existing surface flaws.

Figure 4 *Experimental set-up for tensile strength test*

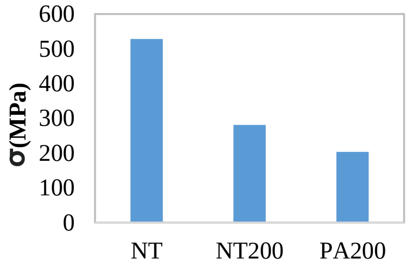

Figure 3 *Tensile strength of C fibres*

3. SURFACE TREATMENT FOR TRC APPLICATION

3.1 Design of testing device

In the second part of the work, the carbon yarns were prepared for tensile strength tests. As showed in the literature [3], the use of common test model [11] could be improved, because the anchorage zone in the grip of the apparatus is not enough important. To avoid the sliding phenomenon in the jaws and the defibering problems, the "pin" device is developed for the specimen preparation (Figure 5) [12]. Four layers of carbon fibres were wrapped around the pinhead and cured for 24 h at room temperature. Each layer was desized/coated in advance with the treatments indicated in Table 4 and Table 5.

The "pin" device plan is showed on Figure 6. The device is composed of two assembled bolted parts. The yarns of carbon are wrapped in the middle, after 24 h the lower part of the device is dissociated, allowing the easy remove of the yarns.

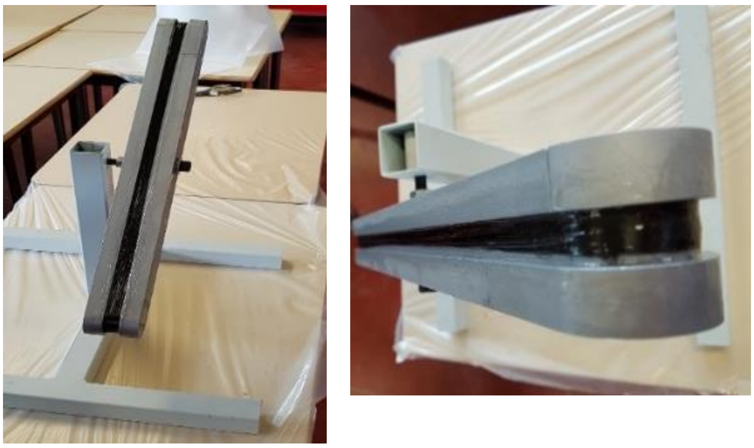

Figure 5 *Device for sample preparation*

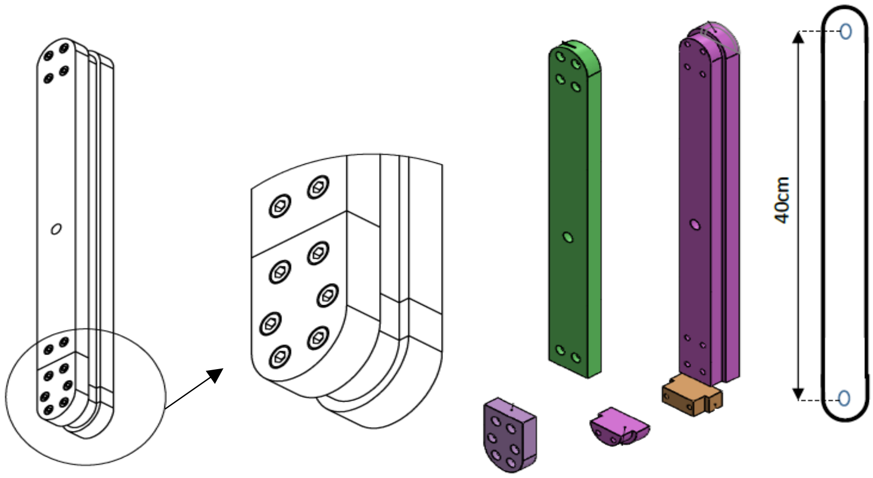

Figure 6 *Plan of "pin" device*

3.2 Textile yarns

The carbon TORAY in a form of yarns was chosen for the “pin” tests. Its characteristics are presented in Table 3. Some of desizing treatments of the first part, were tested mechanically in this part of the study (Table 4 “Desizing treatments of carbon yarns”).

Table 3 *Carbon yarns characteristics*

Textile fibres	Carbon TORAY T700SC-50
Density (g/cm3)	1.8
Sizing type	Epoxy SR 8100/SD8824
Filament diameter (µm)	7
Yarn count of roving (Tex)	12000
Tensile strength (MPa)	4900
Young’s modulus (GPa)	230
Tensile strain (%)	2.1
Temperature stability (°C)	300
Number of layers	4

Table 4 *Surface treatments of carbon yarns*

Desizing treatments of carbon yarns
Epoxy (Ep) 200°C and epoxy (NT200+Ep) Phosphoric acid and epoxy (PA+Ep) 200°C and phosphoric acid (PA200)

In addition, the tensile strength tests are made on coated carbon yarns (Table 5 "Coating treatments of carbon yarns"). The aim of coating treatments was to overcome the adhesion problem and reinforce the integrity between the fibre yarns and the geopolymer binder. Geopolymer formulation is defined in Table 6.

Table 5 *Coating treatments of carbon yarns*

Coating treatments of carbon yarns
Phosphoric acid and GPHS geopolymer (PA+GPHS) Hardener (H) and GPHS geopolymer (H+GPHS) Silane (aqueous phase) and GPHS geopolymer (S+GPHS) Aqueous organic binder with micro silica powder (ZP1)

Table 6 *GPHS formulation*

Metakaolin	69 % SiO_2 21 % Al_2O_3
Alkaline solution	45 % (SiO_2/K_2O) "mixture" 55 % H_2O
Compressive strength, 28 days	70-80 MPa
Tensile strength, 28 days	5-6 MPa

3.3 Textile strength results

The maximum forces of desized and coated carbon yarns are showed on Figure 7. For the desizing part, the epoxy treatment was taken as the reference and showed the highest result (F_{max} = 4.3 kN). The 200°C heating has a less damage impact on carbon fibres than the phosphoric acid: 83% (NT200+Ep) versus 49% (PA+Ep) of remaining strength. The combination of heat treatment and phosphoric acid (PA200) showed only 23% of the reference value. Integration of GPHS geopolymer on the desized carbon specimens does not allow to increase significantly the maximum force of the composite. During the tensile strength tests, it was noticed that the weak point of the composite was the adhesion between the reinforcement and the matrix. The maximum force of (PA+GPHS) (H+GPHS) and (S+GPHS) specimens is close and is about 1.4 kN. The best tensile strength performance of the composite was that of aqueous organic binder with micro silica powder (ZP1) (4.4 kN). The micro silica powder created a multiple roughness on the fibre surface and consequently increased the adhesion between the matrix and reinforcement.

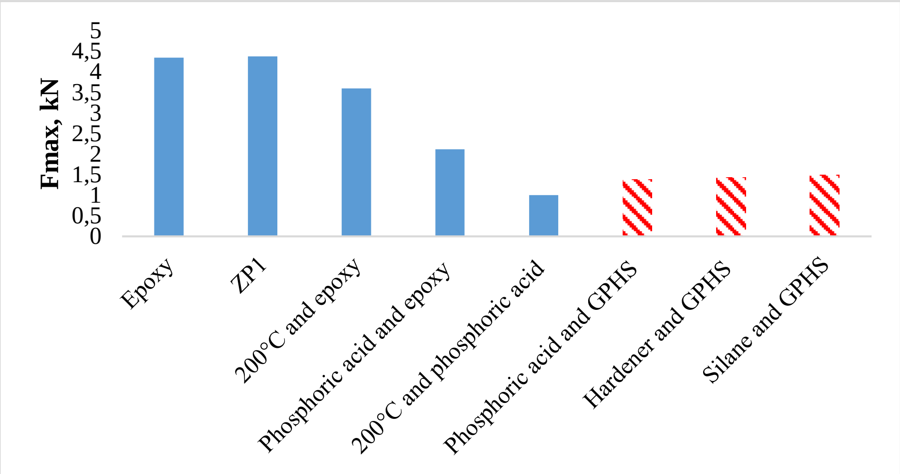

Figure 7 *Fmax (kN) of desized and reinforced carbon yarns*

The strain-stress evolution of composite specimens is presented on Figure 9. After the rupture, all the specimens showed brittle behavior. For most of specimens, a sudden breakage of one yarn is observed at the beginning and then that of the three others. The fibre break appears in the middle of the pin, indicating the correct test procedure (Figure 8).

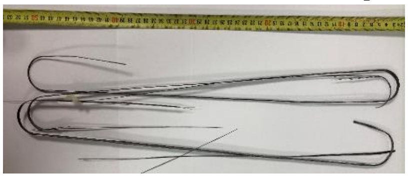

Figure 8 *ZP1 specimen after test*

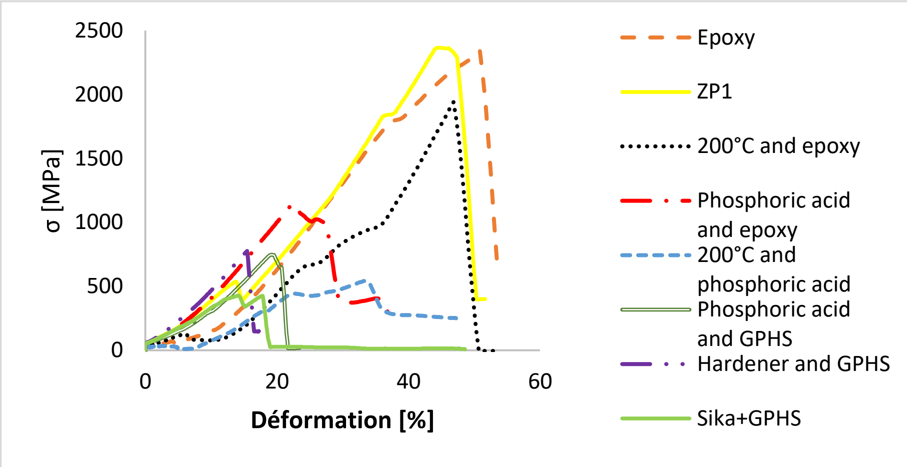

Figure 9 *Stress-strain evolution of composite specimens*

4. CONCLUSION

First, the study deals with the desizing effect of carbon and basalt fibres and its influence on tensile strength. Among the different desizing treatments, heat treatment at 200°C or 300°C and posterior phosphoric acid application was effective to remove the industrial sizing. Basalt textile presented more desized portions that carbon one. SEM observations presented the non-uniform distribution of industrial sizing layer on fibre surface that is probably due to the sizing process.

Second, a "pin" device was developed for the tensile strength tests of textile yarns. Two groups of treatments were made: desizing and coating treatments. According to the results, the (NT200+Ep) treatment is the less damaging (83% of the reference value) and the (PA200) desizing is the more damaging (23% of the reference value). The coating treatments in combination with geopolymer binder (GPHS) presented poorer results than that of desizing treatments ((NT200+Ep) and (PA+Ep)).
Further investigations need to be done to improve the adhesion between the geopolymer and the textile. The second part of the study should be made on basalt fibres.

5. REFERENCES

[1] R. Contamine, A. Si Larbi, P. Hamelin, Contribution to direct tensile testing of textile reinforced concrete (TRC) composites, Mater. Sci. Eng. A. 528 (2011) 8589–8598. doi:10.1016/j.msea.2011.08.009.

[2] L.T. Drzal, M.J. Rich, P.F. Lloyd, Adhesion of Graphite Fibers to Epoxy Matrices: I. The Role of Fiber Surface Treatment., J. Adhes. (1983) 1–30.

[3] P. Hamelin, Z. Mesticou, A.S. Larbi, Design method for strengthening underground steel concrete structures with high performance textile reinforced cement, in: ACCUS, Hong Kong, 2018.

[4] J.L. Thomason, L.J. Adzima, Sizing up the interphase: An insider's guide to the science of sizing, Compos. Part A Appl. Sci. Manuf. 32 (2001) 313–321. doi:10.1016/S1359-835X(00)00124-X.

[5] T.H. Cheng, J. Zhang, S. Yumitori, F.R. Jones, C.W. Anderson, Sizing resin structure and interphase formation in carbon fibre composites, Composites. 25 (1994) 661–670.

[6] C. Mayer, M. Neitzel, Influence of the sizing interphase on the static and dynamic behavior of advanced thermoplastic composites, Proc. ICCM-11. (1997) 681–690.

[7] M. Boulanghien, Formulations de composites thermoplastiques à partir de fibres de carbone recyclées par vapo-thermolyse, Thèse de doctorat, Université de Toulouse, 2014. doi:10.1017/CBO9781107415324.004.

[8] C. Arslan, M. Dogan, The effects of silane coupling agents on the mechanical properties of basalt fiber reinforced poly(butylene terephthalate) composites, Compos. Part B Eng. 146 (2018) 145–154. doi:10.1016/j.compositesb.2018.04.023.

[9] T. Deák, T. Czigány, P. Tamás, C. Németh, Enhancement of interfacial properties of basalt fiber reinforced nylon 6 matrix composites with silane coupling agents, Express Polym. Lett. 4 (2010) 590–598. doi:10.3144/expresspolymlett.2010.74.

[10] A. Si Larbi, R. Contamine, E. Ferrier, P. Hamelin, Shear strengthening of RC beams with textile reinforced concrete (TRC) plate, Constr. Build. Mater. 24 (2010) 1928–1936. doi:10.1016/j.conbuildmat.2010.04.008.

[11] J. Hegger, W. Brameshuber, W. Will, Textile reinforced concrete, Proceeding PRO 50 RILEM Publ. (2006).

[12] P. Hamelin, Procédé de précontrainte par câbles composites HPC. Ceinture composite de frettage procédé pour la fabrication., FR 94-01791-1974, 1974.

6. ACKNOWLEDGMENTS

This study has been founded by AUVERGNE-RHONE ALPES region within the frame work research program BOOSTER 2015 "AC2M2" in cooperation with ATG composites and ALCAM concept companies.

AN IMPROVED TRC: A PRELIMINARY STUDY OF TENSILE PROPERTIES

G.C. Cai[1*], A. Si Larbi[2], A. Ono[3], K. Ishibashi[3]

[1]École nationale d'ingénieurs de Saint-Étienne, Saint-Étienne, France. gaochuang.cai@enise.fr (corresponding author)*

[2] École nationale d'ingénieurs de Saint-Étienne, Saint-Étienne, France. amir.si-larbi@enise.fr

[3] Dept. of Architecture, Faculty of Eng., Fukuoka University, Fukuoka, Japan. onoatsuhiro@fukuoka-u.ac.jp (A.O), ishibashik@fukuoka-u.ac.jp (K.I)

SUMMARY: *In this paper, with an additional fiber-reinforced polymer strip reinforcement, a reinforced Textile reinforced mortar (RTRM) was proposed to improve the initial stiffness of normal TRM and to delay the starting of stress-soft, which usually results in a decrease in tensile properties of RTRM. By a preliminary study of TRM under monotonic and cyclic tensile loads, the better tensile properties of the improved RTRM were confirmed and the tensile response of the improved RTRM was discussed and modeled as well. The improvement of the properties of the proposed RTRM was found especially in the early age stiffness and deformability of the elements. Based on a damage analysis and experimental observation of the study, a simplified model was proposed to predict the tensile response of RTRM layers and verified by the preliminary test presenting an accepted accuracy.*

KEY WORDS: *Textile reinforced concrete, Initial stiffness, Deformability, High deformation elements, Structural strengthening.*

1. INTRODUCTION

Textile reinforced concrete (TRC) or mortar (TRM) for repairing construction structures is attracting civil engineers and researchers in the world because of its plasticity, high-performance, and high deformation performance. At the same time, the interface bonding characteristics with the repaired concrete or masonry structures, and its better fire-resistance behavior and great durability all support the textile reinforced concrete or mortar layers can be worked as more feasible and suitable repairing and strengthening solutions, comparing with fibre reinforce plastic (FRP) sheet repairing technologies.

Recently, several improved TRC/TRM technologies have been proposed to improve the material and structural properties of typical TRC/TRM-strengthened structural elements. For example, high-performance concrete such as Engineering cementitious composite (ECC) or Fibre reinforced concrete (FRC) was proposed to use as the matrix to improve the deformability and tensile resistance of TRC/TRM layers [1,2]. To improve the energy-saving effect of TRM/TRC strengthening or repairing layers, a functional cementitious mortar with phase change materials (PCM) powders was proposed by the first author and second author to develop functional TRM/TRC layers [3] with a limited negative effect on th tensile properties of the layers. On the other hand, considering the self-compacting capability of the matrix in TRC/TRM layers is indispensable because vibration can influence the application of prestressing in some cases, self-compacting concrete (SCC) [4] was proposed for the matrix to improve the construction of TRC/TRM layers. However, the stiffness degradation of the TRM/ TRC layers at the early age of the deformation during the crack formation stage still is the main concern of the strengthening technology.

The main objectives of the paper are (1) to propose an improved TRM strengthening layer to increase the deformation stiffness, deformability, and ultimate tensile capacity, and (2) to verify the proposal by a preliminary experimental study. The significance of the study is to further enhance the structural performance of TRM strengthened structures including their deformability and carrying capacity.

2. A PROPOSAL FOR IMPROVING TRC

Figure 1 shows a summary of the typical tensile stress-strain curves of typical TRM thin layers with different layers of textile fabric/meshes and the classical ACK theory model [3] curve. In the figure, Case 1 is the typical tensile stress-strain curve of the TRM layers with a few layers of textile meshes, while Case 2 is the one of the TRM layers with more layers of fabric mesh or the matrix with higher strength. The difference of the crack loads between the two curves may be mainly caused by the mixture of TRM layer, the deformation accumulation span (curve AB in Case 2) of the TRM layers mainly depends on the fabric mesh layer and matrix properties. Taking Case 2 and ACK model curve as examples, the three typical stages of traditional TRM layers were summarized as follows,

OA: Initial elastic behavior of TRC/TRM, non-cracking stage.
AB: Cracking formation, the tensile force can be maintained at the same level.
BC: Cracking propagation and extension stage (both number and pattern).

In these stages, Curve OA usually depends upon the tensile properties of the matrix of TRM, which also can be improved by using high-preformation composites such as

ECC[1],[5] or FRC reported before. The extension strain of TRM after the initial formation of crack, AB, usually is affected by the tensile properties of matrix materials and the number of layers of textile mesh inside. Based on previous studies, the spanning of AB section of the TRM with a few layers of textile meshes is longer when the same matrix is used. The secant stiffness of Line OC in Case 2 corresponding to the peak tensile load is mainly due to the formation of cracks (AB) at the early age of tensile loads.

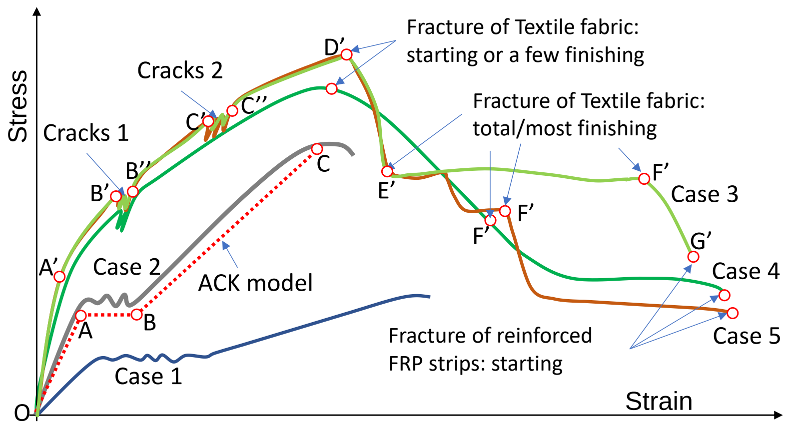

Figure 1. *Typical tensile stress-strain curves of TRM and RTRM and ACK theory*

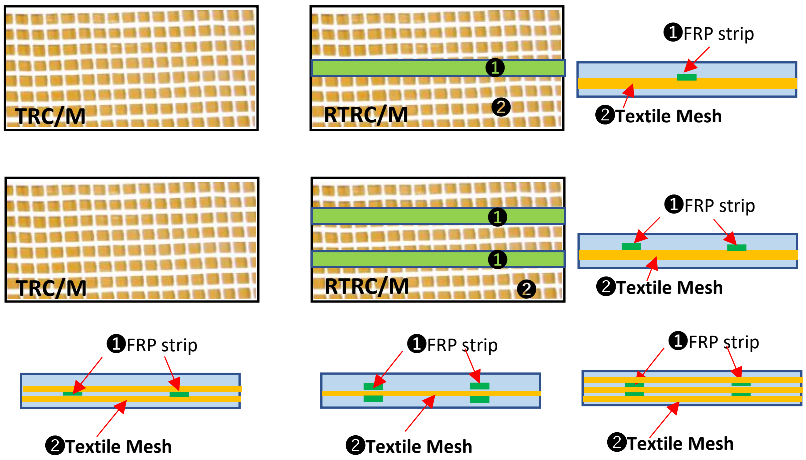

Figure 2. *Schematic diagram of proposed RTRC/RTRM layers*

Based on the analysis described before, this study proposes an improved TRM layer with a FRP strip as a reinforcement for the layer, which is called a reinforced TRM (RTRM). In theory, the FRP strip reinforcement can improve the initial stiffness and deformability of the thin layer. The main deformation and resistance stages of RTRM can be summarized as follows,

OA': the initial elastic behavior of RTRM layer finishes, non-cracking stage.
A'B': the formation stage of the 1st batch cracks starts.
B'B'': the full section extension of the main crack at the 1st batch cracks finishes.
B''C': the formation of the 2nd batch cracks starts if have.
C'C'': the full section extension of the main cracks of the 2nd batch cracks finishes.
C''D': the propagation and extension of the cracks at A'B' and B"C' stages.
D'E': the full section extension of cracks at A'B' and B"C' stages is completed.
E'F': the main resistance of inside FRP strips starts, but maybe with a large slippage.
F'G': the fracture FRP strips start.

Table1. *Details of specimens*

No.	Textile fabric mesh			Mortar compressive strength	AFRP strip	Load type	No. speci-mens
	Type	Fiber type	Layer No.	N/mm^2	-	-	-
1	AKM-5/5	Aramid	1	40	-	3M/2C	5
6	AKM-5/5	Aramid	1	40	R1	3M/2C	5
10	GFRP-5/5	Glass	1	40	-	3M/2C	5
11	GFRP-5/6	Glass	1	40	R1	3M/2C	5

M: Monotonic tensile load, C: Cyclic tensile load

Table2. *Main properties of used FRP materials*

Materials	Mesh size	Weight per unit area	Tensile strength	Elastic modulus	Design thickness
Units	*mm*mm*	*g/m^3*	*N/mm^2*	*kN/mm^2*	*mm*
AFRP mesh	7*7	90	2060	118	0.024
AFRP strip	-	623	2060	118	0.430
GFRP mesh	5*5	150	200	-	0.4

3. TEST PROGRAM

As a preliminary study, the monotonic and cyclic tensile response of RTRM were experimentally investigated. Two kinds of fabric mesh, Aramid Fibre Reinforced Plastic (AFRP) and glass FRP (GFRP) textile fabrics with a similar mesh size were applied for the tests.

4.3. Details of test specimens

A total of 20 TRM and RTRM thin layer were prepared for the monotonic and cyclic tensile testing. The dimension of the TRM and RTRM thin layers was width 60mm×

length 500mm×thickness 10mm, referring to the method recommended by RILEM technical committee (TC 232-TDT) [6]. All RTRM specimens tested were reinforced by the same AFRP strip, with a length of 13mm and thickness of 0.43mm. Table 1 lists the main parameters of the specimens.

4.3. Used materials

The matrix of the TRM/RTRM specimens tested was cast by a commercially available ultra-fast hard cement-based non-shrinking mortar with predicted compressive strengths of 40N/mm^2 and of 62 N/mm^2 in 7 days and 28 days, respectively. The measured compressive strength and flexural strength of the matrix at testing day were 43.1 N/mm^2 and 6.92 N/mm^2, respectively. The main properties of FRP materials used in the study is listed in Table 2, and shown in Figure 3.

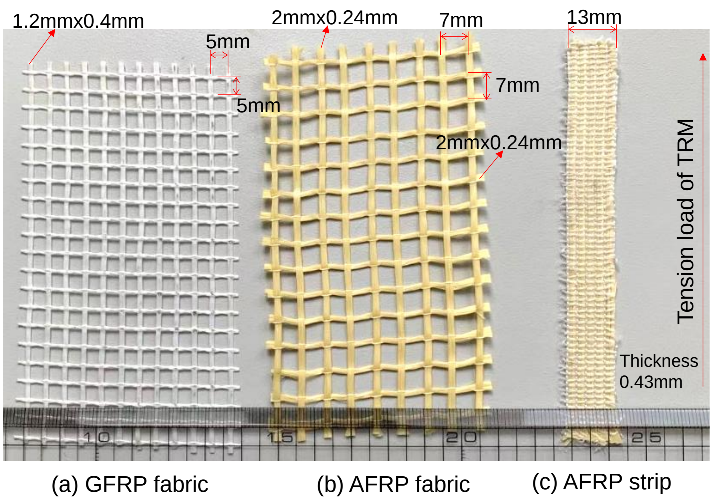

Figure 3. *FRP materials used in the study.*

4.3. Setup and measurement

Figure 4 shows the hard-clamping tensile test method applied in the study which is modified referring to the recommendation of the RILEM technical committee (TC 232-TDT) [6] and the literature [7]. This modification was based on a preliminary test, in which a large slippage easily occurred at the ends of TRM specimens resulting in that the later loading procedures could not be continued. At this moment, the test specimens also did not reach their ultimate status. Therefore, four strong clamps were used at the end steel plate to improve the fixture of the specimens, as shown in Figure 4 (b). At the same time, the slippage of the measurement zone of the specimens at the ends also was monitored during the tensile tests. The test results of the specimens were not included in the study if the slippage happened. The uniaxial monotonic and cyclic tensile tests were carried out using a universal testing machine with a maximum loading capacity of 20kN.

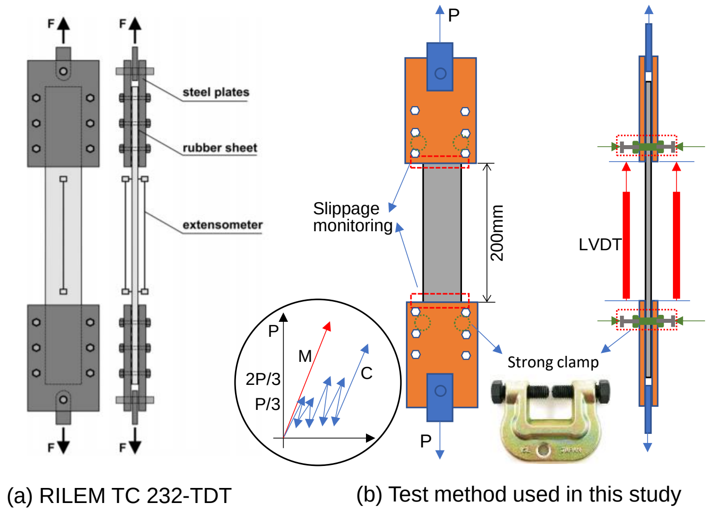

Figure 4. *Test method of the study.*

4. TEST RESULTS AND DISCUSSIONS

4.3. Crack proration and damage of specimens

Figure 5 shows the ultimate damage of all tested specimens. Due to only one-layer of textile fabric mesh was used in the TRM specimens, a regularly distributed cracking pattern was not observed in them, but only the cracks occurred at the end fixture of the specimens. The main reason was considered that the textile mesh was too weak for the TRM thin layer. However, for the RTRM specimens with GFRP or AFRP fabric mesh, the additional AFRP strip developed the cracks at the measurement zone of the specimens before final failure which further affects the tensile behavior of GFRP-RTRM layers at the later deformation stage (Figures 5 b). More cracks were observed in RTRM specimens with AFRP mesh and wider cracks were confirmed during the tests, which was explained by the fact that the specimen with the AFRP mesh having higher tensile properties that can support the RTRM layer to develop larger plastic deformation before failure.

On the other hand, when under cyclic tensile loads the pattern of cracks did not increase both in TRM and RTRM specimens, although the cyclic load usually speeded up the crack propagation and damage accumulation in typical commentative composites. The same observations were confirmed in all RTRM specimens with AFRP strip, in which only one crack was found before reaching their peak tensile loads. In the RTRM with GFRP mesh, however, the AFRP strip played its role earlier due to the GFRP mesh has a weak tensile strength under cyclic tension, which resulted in a large slippage occurred between the strip and the matrix of the specimen.

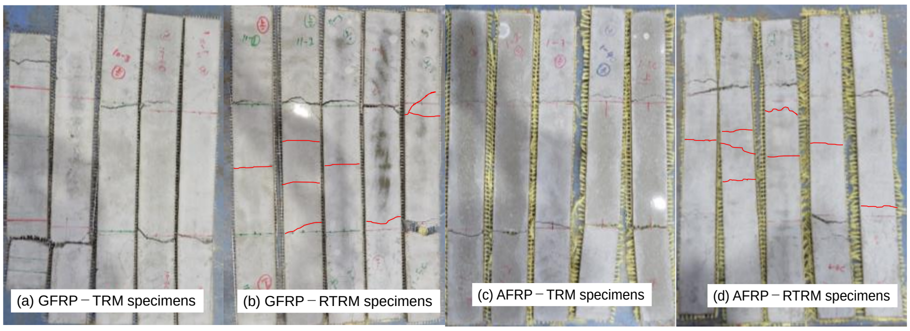

Figure 5. *Ultimate cracks and damages of TRM specimens*

4.3. Tensile load-deformation response

4.2.1 Monotonic behaviour-TRM vs. RTRM with one-layer fabric mesh

Figure 6 shows the monotonic tensile load-deformation response of the TRM and RTRM specimens using AFRP and GFRP mesh, respectively. Results show that the reinforcement AFRP strip improved significantly the tensile response of the TRM layers, in which the ultimate tensile stress of the TRM used GFRP mesh was increased about 1.6 times and about 2.5 times in the TRM layers with AFRP mesh was improved respectively. This was attributed to the AFRP mesh has a higher tensile strength allowing the TRM layers can develop further cracks before the AFRP strip started to directly resist tensile force. On the other hand, the initial elastic-plastic behavior of RTRM specimens before 0.2% strain was also improved, for the FRP strip also helped the TRM layer to resist the crack development after slight cracks happen after the matrixes reached their tensile strength. Besides, the early age deformation behavior of the TRM specimens was also improved by the AFRP strip, the stable load-deformation response was not observed at the stage of crack formation (see Curve AB in Figure 2). In other words, the secant stiffness of TRM layers was improved at the early age of loading for the additional reinforcing of the AFRP strip.

At the deformation stage before peak load of the specimens, on the other hand, larger deformation energy was absorbed by the both RTRM layers with AFRP and GFRP mesh. The strains corresponding to the peak loads of the specimens were about 1.5%, and the peak loads of the RTRM layers were much higher than those of the TRM specimens.

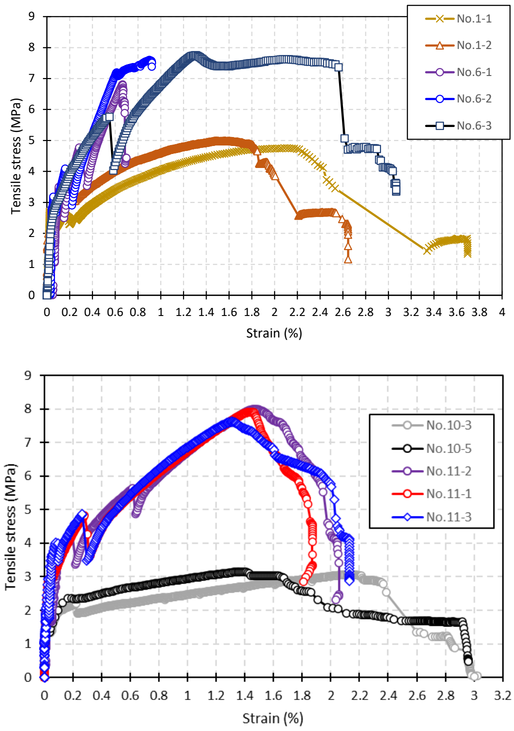

Figure 6. *Monotonic tensile responses of TRM and RTRM thin layers*

4.2.2 Cyclic load-deformation behavior

Figure 7 shows the cyclic tensile response of TRM and RTRM tested specimens with GFRP and AFRP meshes. For the TRM specimens with one-layer mesh, due to the target load (P/3) of the first two-cycle loads was under the cracking load of the TRM layers where the cracks stably form and extend in the layers, the tensile response of the TRM was still in an elastic way. The target load of the second two-cycle loads was near to the cracking load of TRM specimens, however, more tensile cracks were distributed to the layers and prorated during the cyclic loads. On the other hand, about the RTRM specimens, the first two-cycle loads were greater than 1/3 the peak load of the corresponding TRM layer which means it can develop slight plastic deformations. At the second two-cycle loads, the tensile force was unloaded to about 1.0kN with a declining slope that was quite near to initial deformation stiffness. The re-loading curve also presented a high stiffness similar to the initial stiffness of the tensile curve, in the specimens used both two kinds of meshes. However, after two cycle loads, the tensile response curve can back to the envelope curves of the load-deformation curves of the specimens. The specimens with GFRP and AFRP mesh reached their peak load at about the tensile strain of 1.1% and 1.4%, respectively, and developed their main ductile deformation until about 2.5%. The reason for the smaller peak strain of the GFRP-TRM/RTRM specimens was considered as that the weaker GFRP mesh was more sensitive to the damage accumulation at the early age of the cyclic tensile loads. This accelerates the failure of the thin layers resulting in the peak of the tensile stress reaches earlier.

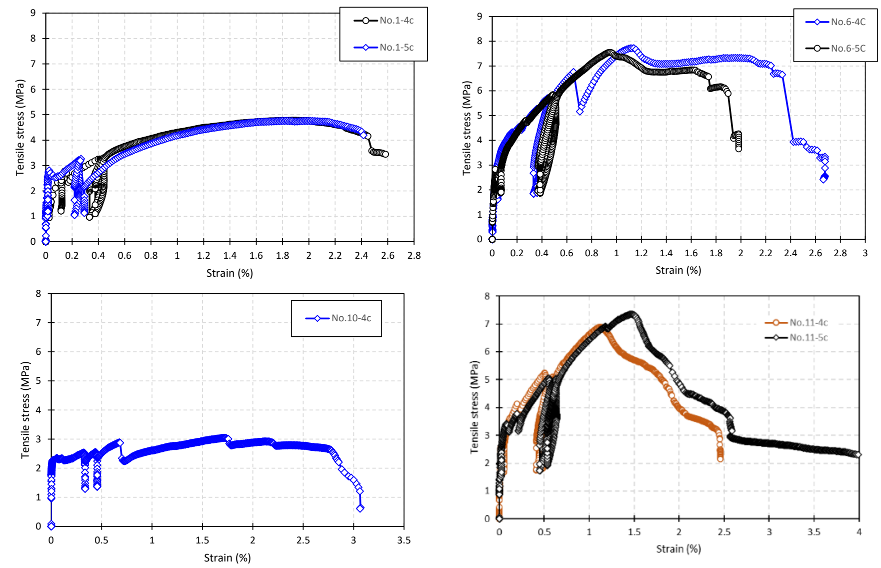

Figure 7. *Cyclic tensile response of TRM and RTRM layers*

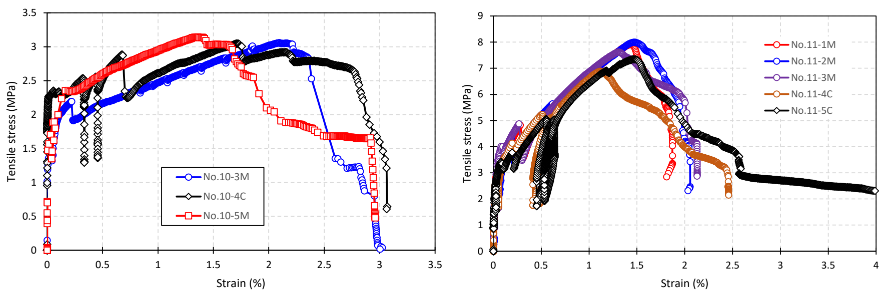

Figure 8. *Comparison between monotonic and cyclic tensile response*

5. CONCLUSION AND REMARKING

This paper proposes an improved reinforced textile reinforced mortar (RTRM) as the repairing or strengthening layer for existing structures, in which a FRP strip was used as reinforcement to improve the response of the layers at an early age, especially to improve the stiffness degradation of the typical TRM layer during the stage of crack formation. As a preliminary study, the monotonic and cyclic tensile responses of the proposed RTRM layers were investigated. The main conclusions are summarized here,

a. With the additional reinforcement of FRP strip, the proposed RTRM layers present higher peak stress and better deformation than those of the typical TRM layers, without an obvious stiffness degradation before peak stress. The initial secant stiffness of the layers was fully developed.

b. Based on the limited experimental investigations reported in the study, the cyclic loads did not significantly affect the tensile response of the proposed RTRM layers. However, more investigations are needed, especially for the TRM layers with more layers FRP fabric meshes.

REFERENCES

[1]. Li, B., Xiong, H., Jiang, J., & Dou, X. "Tensile behavior of basalt textile grid reinforced Engineering Cementitious Composite." *Composites Part B: Engineering* 156 (2019): 185-200.
[2]. Li, T., Deng M., Jin M., Dong Z., and Zhang Y. "Performance of axially loaded masonry columns confined using textile reinforced concrete (TRC) added with short fibers." *Construction and Building Materials* 279, 2021, p122413.
[3]. Djamai, ZI, Si Larbi A., Salvatore F., Cai G. "A new PCM-TRC composite: A mechanical and physicochemical investigation." *Cement and Concrete Research* 135, 2020, p106119.
[4]. Li H., Xu S. "Self-compacting concrete for textile reinforced elements." In *SCC'2005-China: 1st International Symposium on Design, Performance and Use of Self-Consolidating Concrete*, RILEM PSARL, 2005, p689-696.
[5]. AL-Gemeel, A. N., Zhuge, Y. "Experimental investigation of textile reinforced engineered cementitious composite (ECC) for square concrete column confinement." *Construction and Building Materials* 174, 2018, p594-602.
[6]. RILEM Technical Committee 232-TDT, "Recommendation of RILEM TC 232-TDT: test methods and design of textile reinforced concrete: uniaxial tensile test: test method to determine the load bearing behavior of tensile specimens made of textile reinforced concrete." *Materials and Structures* 49, 2016, p4923-4927.
[7]. Colombo, I.G., Colombo M., and Di Prisco M. "Tensile behavior of textile reinforced concrete subjected to freezing–thawing cycles in un-cracked and cracked regimes." *Cement and Concrete Research* 73, 2015, p169-183.
[8]. Comite´ Euro-International du Be´ton. *CEB-FIP Model Code 1990. Design Code.* Thomas Telford, London, 1993, p. 437.

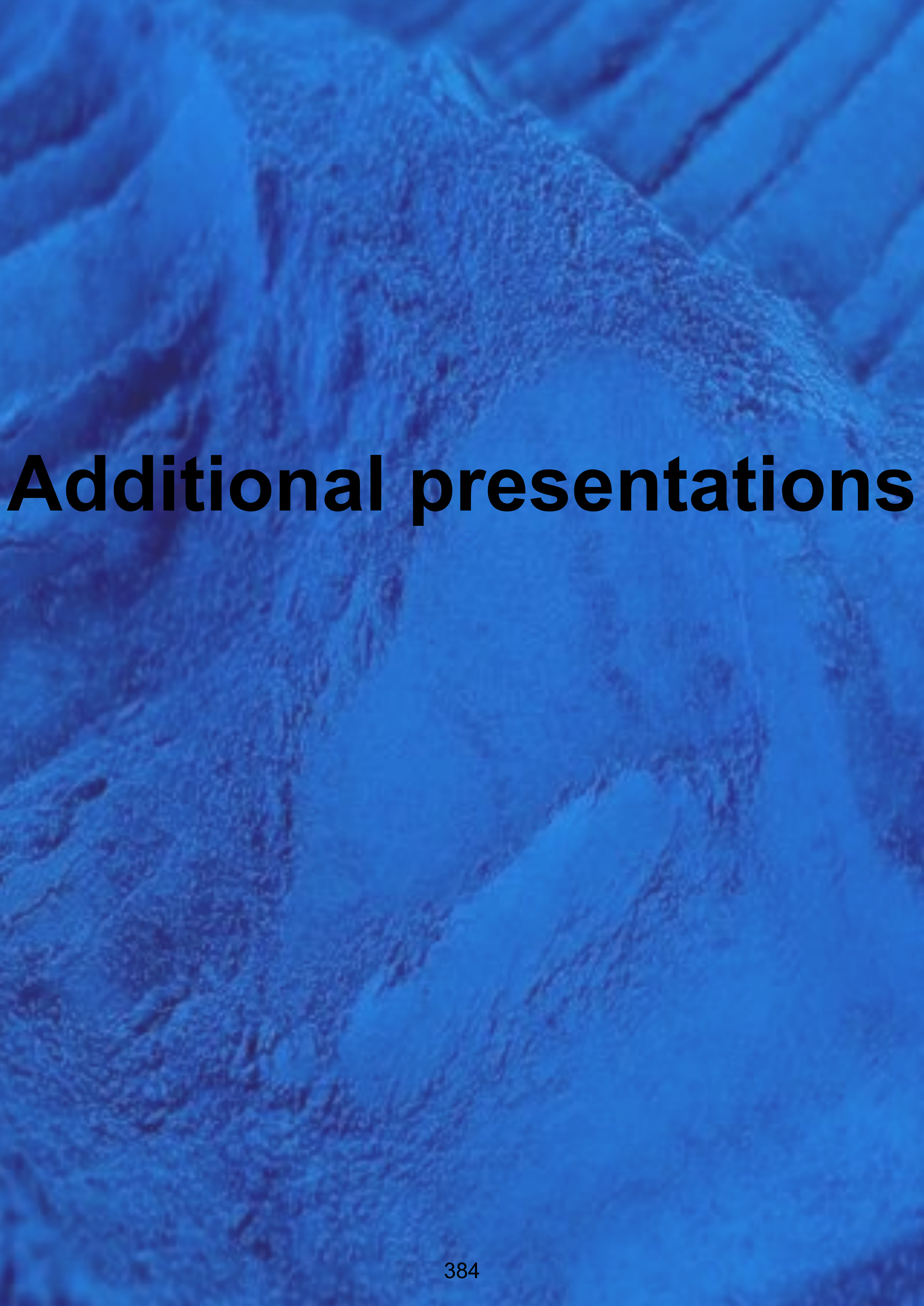

Additional presentations

FERROCEMENT: UK STATUS REPORT

Paul Nedwell[1]

[1]Paul Nedwell (University of Manchester {retired}, Department of Mechanical, Aerospace and Civil Engineering, The University of Manchester, Oxford Rd, Manchester, M13 9PL, UK, paul.nedwell@manchester.ac.uk, pnedwell@gmail.com)

SUMMARY: *This paper notes the lack of substantial progress in ferrocement during the past decade.*

.

KEY WORDS: *Ferrocement,*

1. INTRODUCTION

The previous national status report from the UK was provided for the 7th International Symposium in Singapore in 2001. In the intervening years there have been a few structures with a UK involvement, notably the Stavros Niarchos Cultural Centre which is being presented at this Symposium. However there has been nothing of note in the past few years and it would now appear that ferrocement is no longer considered a viable construction material.

2. EDUCATION

To the best of the authors knowledge ferrocement is not taught as a specific topic at either under or post graduate level in any UK University. The main civil engineering concrete technology units within the UK have been contacted and none are currently working in the area though the Neville centre at Leeds has indicated some forthcoming research into thin cementitious materials.

3. CONSTRUCTION

There are no reports of any use of ferrocement in the UK though one consultancy that has been contacted has replied that there is a possibility of some thin cement composite application for balconies. One of the main drawbacks at the moment is the energy and CO_2e that the relatively high percentage of mesh embodies.

4. MARINE APPLICATIONS

There are no reports of any new boats under construction in the UK since the Tenacity of Bolton was launched in 2007. An undated report has been found from a UK boat yard of a repair undertaken to a ferrocement yacht that had run aground[1]. Tucker Designs are involved in the repair of the RV Heraclitis currently undergoing a rebuild in Spain [2]

5. CONCLUSION

There is nothing of any substance to report

6. REFERENCES

1.https://www.falmouthboat.co.uk/project/international-team-undertakes-ferrocement-repair

2.https://rvheraclitus.org/history/

THE 13TH INTERNATIONAL SYMPOSIUM ON FERROCEMENT AND THIN FIBER REINFORCED INORGANIC MATRICES. FERROCEMENT*: FIVE DECADES OF PROGRESS*

REGIONAL PROGRESS REPORT. CUBA AND THE CARIBBEAN

Hugo Wainshtok Rivas

Consultant Professor: Polytechnic Havana University José A. Echeverría (CUJAE), La Havana, Cuba.

Dr. Honorius Causa and Emeritus Professor CUJAE. Email hugow@tesla.cujae.edu.cu

1- INTRODUCTION

Despite the advantages of Ferrocement in terms of minimum materials consumption, its development has been slowed down by its low durability given the potential corrosion of the steel reinforcement, and the labor intensive effort needed in its construction.

However, in recent years a resurgence of this technology is occurring in many countries of the world, including in the Caribbean region, expanding its application in works where its advantages are more appreciable, introducing materials that guarantee a more resistant and compact mortar, the use of prefabrication and new technologies for the application of mortar, as well as the introduction of high strength steel, and Fiber Reinforced Polymers, FRP, as reinforcement, the last do not rust like Steel

2-Background

In the early 1970's, the building of Ferrocement boats started in Cuba, spearheaded by the research work of the author, looking after the New Zealand experiences hundreds of boats were built in Cuba. But it was not until the early 1980's that applications of Ferrocement in Cuba and the Caribbean began to diversify not only in boats, but in housing, pools, sculptures, urban furniture etc.

3- Applications in Cuba and Caribbean

3.1-Boats

In 1972 the first fishing boat was built in Cuba, it was the beginning of more of 300 hundreds boat series, including passenger boats, recreation boats and barges. Others countries in America like Canada, USA and Chile built ferrocement boats, specially Chile with its successful warehouse barge.

Fig. 1-*Fishing and passenger boats built in Cuba*. Photos by the author.

3.2-Housing.

Inspired by the work of Ing. Alfonso Olvera (1), professor at the National Polytechnic Institute, IPN of Mexico, the author began the application of Ferrocement in housing in Cuba, together with the Architect Emilio Escobar Loret de Mola (2), created the Ferrocement Residential Building System, SERF (in Spanish), (fig. 2). SERF was the starting point for the construction of Ferrocement prefabricated houses in Cuba and Nicaragua, Haiti, the Dominican Republic and El Salvador built for Architects Kurt Rhyner and Pedro Galiano (fig.3).

It is worth also mentioning the interesting work done by Dr. Ing. Daniel Bedoya from Cali, Colombia, in the development and construction of earthquake-resistant Ferrocement houses (Fig. 4) and the ecologically designed houses by Architect. Javier Senosian (3) in Mexico, and Mario Moscoso in Bolivia (Fig.5)

In 2013 Fiber Reinforced Polymers, FRP, non-corrosive materials, of greater resistance than mild steel and of much lower weight, were introduced in Cuba (4) as reinforcement alternative to steel, and now the FRP Study Group, led by the author at the Center for the Study of Tropical Construction and Architecture (CECAT in Spanish) at the Technological University of Havana, has led to additional studies to use it at reinforcement of prefabricated Ferrocement panels (called Mortar Armed with PRF) used in SERF housing system (fig 6). That allow a resurgence of the SERF housing applications in Cuba.

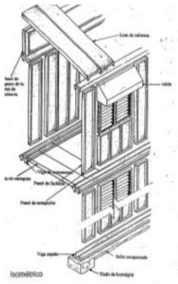

Fig. 2-SERF

Fig. 3- *Minas 1 Town and multi-story residential building* Cuba, photos by the author.

Fig. 3-*Housing* Haiti. and Nicaragua, courtesy Kurt Rhiner and Pedro Galiano

Fig. 4 *House building earthquake resistant*, courtesy D. Bedoya

Fig 5-*Ecological housing*, courtesy J. Senosiain

3.3-Swimming pools and others reservoirs

In the 80s, under author's guidance, the construction of Ferrocement swimming pools began in Cuba; their cost effectiveness led to the construction of more than 40 pools throughout the country, from small sizes to Olympic sizes (2), most of they using prefabricated panels to build walls and stiffeners (fig.6). The development of Ferrocement swimming pools reached such a scale in the country that Architect Joao Figueiras Lima (lele), a prestigious Brazilian one, visiting Cuba, spoke of the Cuban technology for the construction of swimming pools (Fig. 7). Also Ing. Jaime Landívar and his son, under the advice of the author, built innumerable Ferrocement swimming pools and cistern in Guaya´s province of Ecuador (fig.8), and We Care enterprise is doing the same in Quintana Ro, Mexico, building the first Ferrocement swimming pool in that country (Fig. 9)

By the other hand, in Oaxaca, Mexico, Eng. Margarito Ortiz, has built innumerable dam´s screens (Fig. 10), very useful for agricultural areas that are generally burdened by droughts., this construction, has similarity with a swimming pools wall.

Fig.6- *Olympic swimming pool*. Author´s photo

Fig.7-*Varadero swimming pool.* Author´s photo

Fig.8-*Guayas Poo.* Courtesy J. Landívar

Fig.9-*Quintana Ro, Pool*. Courtesy E. Ogando

Fig. 10- *Dam´s screens*. Courtesy, M. Ortiz.

The introduction in Cuba of FRP reinforcements, allowed the author, for the first time in the world, to build a swimming pools with Mortar Armed with FRP (similar to Ferrocement) in the Royalton Hotel on Varadero beach (fig. 10), in Cuba´s Matanzas province. Within few months the We Care company from Quintana Ro, Mexico, with the advice of the author, will build several more swimming pools, using Mortar Armed with FRP, because the advantages of this material against steel for this job.

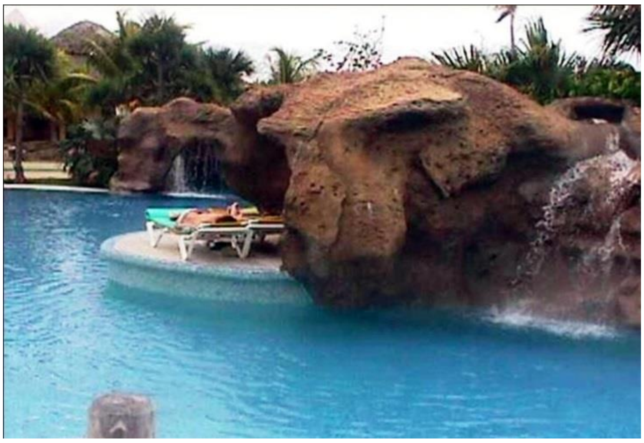

Fig. 11-*Royalton Hotel pool*, Varadero Beach. Author's photo.

3.4-Sculptures and urban structures

Starting in the 1990s, when the Valley of Prehistory was built in Santiago de Cuba province (fig. 12), countless artists built Ferrocement sculptures and other urban structures in Cuba and others Caribbean Countries. The sculptors Alfredo Martel from Cuba (Fig. 13) and Architect Javier Senosiain, from Mexico are good examples of that (Fig.14).

Fig. 12-*Prehistoric Valley*. Photos by the author

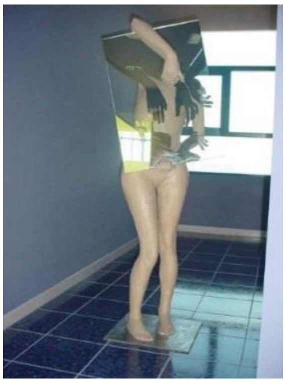

Fig. 13-*Woman with mirror*. Courtesy A. Martel.

Fig14 –*Observatory*. Courtesy J. Senosiain.

It is also of interest to point out that in other Latin American countries, there are prestigious professionals who have given Ferrocement a great notoriety in the field of sculpture. In particular, we recognize the Architects Mario Moscoso and his son Javier Moscoso, from Cochabamba, Bolivia, for the construction of buildings and urban furniture of Ferrocement (Fig. 15). Sculptors of Oruro, Bolivia and Pava, Brazil, for their magnificent works in Jurasic Park and the Peacock (Fig.16 and 17).

There are many other examples of the use of Ferrocement in Latin America, as the work of Eng. Savio Bonifacio Nunez, from Bello Horizonte, Brazil, and Eng. Jaime Landívar in Ecuador, with his numerous construction for water sanitation tanks and cistern (Fig. 18); and others professionals from Chile and Ecuador in the construction of floating warehouses and water tanks (Fig.19).

Fig. 15-*Water Park* Courtesy, M. Moscoso

Fig.16- *Jurassic Park*. Courtesy J. Moscoso

Fig.17- *Peacock.* Courtesy Savio Bonifacio   Fig.18–*Sanitation tanks*. Courtesy Savio Bonifacio

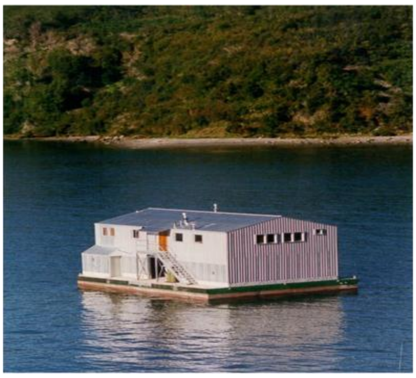

Fig. 19-Ware house barge, built in Chile

Author believes that the development of Ferrocement, now possible with others materials as high strength steel meshes, FRP reinforcement etc, has its future assured. The construction of three-dimensional FRP reinforcement is already a reality, like the one built at the Yaroslavl Composite Materials Factory, Russia, to be used in prefabricated panels from Precast Reinforced Mortar Residential Building System, (SERMAP , in Spanish) former SERF, (Fig. 20), prototypes of which are subjected to physical-mechanical tests to determine their mechanical characteristics, as well as the application of Basalt Fiber Reinforced Polymers, BFRM, mesh fabrics, and Glass Fiber Reinforced Polymers, GFRP, bars in the construction of swimming pools in Cuba and Mexico. These may suggest that gradual substitution of steel by FRP meshes in thin elements of hydraulic cement mortar, is not far away.

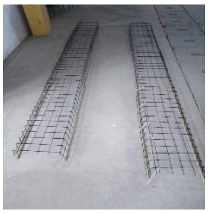 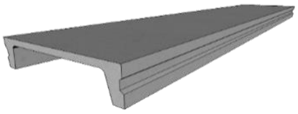 

Fig. 20- *Three-dimensional FRP reinforcement and prefabricated panel of SERMAP*

References

[1] ALFONSO OLVERA, *El Ferrocemento y sus aplicaciones,* Instituto Politécnico nacional, México DF, 1995

[2] JAVIER SENOSIAIN AGUILAR, *BIO Arquitectura,* , Aditorial Limusa S.A de C.N
Grupo Noriega Editores, Balderas 95, México, DF. 1998.

[3] HUGO WAINSHTOK RIVAS, *Ferrocemento: Diseño y Construcción*, La Fábrica Comunicación Integral, 4ta Edición, Riobamba, Ecuador, 2010.

[4] HUGO WAINSHTOK RIVAS ET AL, *Calidad y Durabilidad de las Construcciones. El uso de los PRF como refuerzo del Hormigón Armado y el Ferrocemento*, Universidad Politécnica de Valencia, Valencia, España.,2018

Recommended Ferrocement Literature

[5] ACI COMMITTEE 549, *Guide for Design, Construction and Repair*, American Concrete Institute, Farmington Hills, Michigan, USA.

[6] ANTOINE E. NAAMAN, *Ferrocement and Laminated Cementitious Composites*, Techno Press 3000, Ann Harbor Michigan 48105 USA, 2000

[7] ANTOINE E. NAAMAN -*Evolution in Ferrocement and Thin Reinforced Cementitious Composites*., Department of Civil and Environmental Engineering, University of Michigan, Ann Harbor, Michigan,49109-2125, USA, 2009

[8] INTRNATIONAL FERROCEMENT SOCIETY (IFS 10-01 Fererocement Model Code, *Building Code Recomendations for Ferrocement* ,), Reported by IFS committee 10, January 2001,
.

[9] BALAKRISNA NARAYAN DIVEKAR -*Ferrocrete Technology a Construction Manual*., 1030, Shivajinagar Model Colon, Pune 411016 (Maharasta) India, 2012

[10] HUGO WAINSHTOK RIVAS, *Guia para el Diseño y Construcción del Ferrocemento.* Propuesta para una Norma. Dirección de Normas, MICONS, Cuba. 1991

REGIONAL PROGRESS REPORT – BRAZIL

SÁVIO NUNES BONIFÁCIO[1]

[1]Author1 (Minas Gerais Sanitation Company – COPASA; Brazilian Ferrocement Society – SBF, Rua Mar de Espanha, 453, B. Santo Antônio – 30330-900, Belo Horizonte – MG, savio.nunes@copasa.com.br)

1. INTRODUCTION

Ferrocement in Brazil has develop Armed Mortar combined the technique of the Group of the São Carlos USP Engineering School with the design and construction method of Architect Lelé. At COPASA, from the 90s until today, he combined the Handcrafted Ferrocement of Professor Alexandre Diógenes – UFC – with sanitation technologies. These are strong foundations that, combined with the current advances in the matrix in MicroCAD and armor in PRF, signal a promising future.

2. COPASA MG

The Companhia de Saneamento de Minas Gerais – COPASA MG – has the largest application of ferrocement in sanitation works in Brazil. There are dozens of Water Treatment Plants with a capacity between 3 and 150 L/s; Sewage Treatment Stations with modules for 1,000 to 8,000 inhabitants and hundreds of reservoirs with an average volume of 150,000 liters.

The Company sought the technology of Prof. Alexandre Diógenes (DIÓGENES, 1987) and since the 90's he has been investing in training, structural studies and implementation works. Ferrocement works result in savings of up to 70% in the cost of implementation. As it is a material close to reinforced concrete, using the same materials, the labor was easy to learn.

COPASA developed dozens of Standard Projects and Technical Standard T.186 “Ferrocement for Sanitation Works” (COPASA, 2016). And today New Standards are developed by contracted design companies, which provide for the ultimate internal protection against the harmful effects of gases.

The fact that the Sanitation Company has used the ferrocement technique intensively has given its approval to be applied by builders throughout the State. The construction of reservoirs of up to 200,000 liters in the northern semiarid region is a reality.

3. ARMED MORTAR

Ferrocimento arrived in Brazil in lectures by Eng. Pier Luigi Nervi, circa 1960. He was received by the São Carlos Group EESC-USP, where they developed industrialized production, called Armada Mortar (HANAI, 1992). With the use of metallic forms, reduction in the steel density of the material and application of the prefabricated industry model.

Received the trace of the Architect João Filgueiras Lima, Lelé, from the 80's, projects of Schools, Urban Equipments and Hospitals were developed with harmony and low cost. Armed mortar works can be found throughout the national territory.

4. MICROCAD

Research continues to improve the material. Prof. Paulo Campos, organizer of the book MicroCAD, Cyted (CAMPOS, 2013), explains the use of High-Performance Micro Concrete (fck 120 MPa) in light pieces of reinforced mortar with application focused on housing of social interest.

The typical MicroCAD element features:

- Water/cement ratio less than 0.4 to 0.20;
- Complementary active additions to the cement (microsilica, metakaolin, flying cenizas, etc.) with particles smaller than 100 microns, applied in 5 to 15% by weight of the cement;
- Use of superplasticizers in order to obtain workability of the mortar with reduced amount of water.

The increase in the matrix density generated by the compactness of the arid areas increases the resistance and decreases the permeability. Uses external vibration or self-compacting additives and attention to curing.

The use of diffuse reinforcement, composed of fine wire meshes and continuous or discontinuous fibers, combats cracking and also makes it possible to resist tensile stresses.

5. FERRO12

The 12th International Symposium on Ferrocement and Thin Cement Materials, which took place in Belo Horizonte, July 2018, institutionalized the technique for the technical public. Assisted by an audience from different regions from Brazil, such as

Minas Gerais, Rio de Janeiro, São Paulo and Bahia, it has generated several academic works.

Based on Ferro12, the Brazilian Ferrocement Society – SBF was created, and aims to bring together institutions, professionals dedicated to studies and construction in ferrocement and the promotion of personnel training and technological development. SBF has been working with the Brazilian Technical Standards Association – ABNT – to standardize ferrocement at the national level.

6. PRF

The reinforcement using Fiber Reinforced Polymers – PRF – published, in February 2021, the publication of standards by ABNT for fiber reinforced concrete – Quality control (ABNT NBR 16938, 2021) and Test methods. Which represents an update that may soon be applied to ferrocement/reinforced mortar.

7. CONCLUSION

Ferrocement is today a technological option in sanitation in the State of Minas Gerais, based on the applied experience of COPASA. So too, the Armada Mortar spread nationally and worldwide in prefabricated buildings.

The technologies associated and added by the MicroCAD matrix and armor in PRF, seasoned with Brazilian creativity, may bring solutions for social housing and basic sanitation to Brazil and the World.

8. REFERENCES

ABNT NBR 16938. *Concreto reforçado com fibras – Controle da qualidade.* São Paulo: ABNT, 2021.

CAMPOS, Paulo E. F. *Microconcreto de alto desempeño: la tecnología del MicroCAD aplicada em la construcción del hábitat social*. São Paulo: Mandarim, 2013.

COPASA. *Norma Técnica T.186: Ferrocimento para obras de saneamento*. Belo Horizonte: COPASA, 2016.

DIOGENES, Alexandre. *Cartilha de Ferrocimento Artesanal.* Fortaleza, Ceará: UFC, 1987.

HANAI, João B. *Construções de argamassa armada: fundamentos tecnológicos para projeto e execução.* São Paulo: PINI, 1992

REHABILITATION OF REINFORCED CONCRETE BUILDINGS AGAINST EARTHQUAKES

MADI Rafik[1], NEDJHIOUI Oussama[2], BORDJIBA Abelhak[3], GUENFOUD Mohamed[4]

[1]University 8 Mai 1945, Guelma, Algeria, madi.rafik@univ-guelma.dz

[2] PHD Student, University 8 Mai 1945, Guelma, Algeria,

Nedjhioui.oussama@univ-guelma.dz

[3] University Badji Mokhtar, Annaba, Algeria, bordjibaabdelhak@gmail.com

[4]University 8 Mai 1945, Guelma, Algeria, guenfoud.mohamed@univ-guelma.dz

SUMMARY: *Existing buildings erected before the obligation to apply the seismic rules or before their publication, are often located in the center of the agglomerations, they were the first built. The expectation of a natural replacement of the existing building by new construction, in accordance with seismic rules, seems irrelevant. It is therefore necessary to undertake preventive reinforcement operations to reduce the probability of losses in the event of an earthquake. In this case the study of the vulnerability is necessary to allow the building owners to carry out an upgrade of the existing constructions by repair or reinforcement. This requires the establishment of a strategy for rehabilitation, the reduction of the seismic level, improving the level of performance, and the choice of methods for estimating the vulnerability of constructions. The objective of this article is to create an overview of the solutions related to the seismic rehabilitation and the level of performance of buildings to adopt an effective rehabilitation strategy. The results obtained by applying methods of calculation and analysis of the vulnerability of structures such as nonlinear static analysis methods "Pushover", on reinforced concrete constructions of the beam-column type and reinforced by bracing shear walls, show the difference in behavior of structures before and after rehabilitation during the earthquake and also locate dangerous areas in the different elements of resistance in order to choose the appropriate techniques for the work of comfort.*

KEY WORDS: *vulnerability, earthquake, rehabilitation, building,Pushover analysis.*

1. INTRODUCTION

The old reinforced concrete buildings generally designed before the appearance of seismic codes, which is insufficient for earthquakes. Past earthquakes: San Fernando in 1971, Kobe in Japan in 1995, Turkey in 1999, Boumerdes in Algeria in 2003, etc., have heavily damaged or destroyed many buildings designed according to ancient codes [1, 2]. After earthquake, these structures require reinforcement or repair work. The repair is suitable for all the work that must be performed on a structure damaged by the earthquake, to restore its original characteristics. The reinforcement mainly applies to buildings not yet solicited by the seismic action. The approach of the problem will therefore not be the same in both cases. Two major families of approaches are possible to reduce the seismic risk: reducing the level of seismic loads to which the structure could be exposed or improving the level of performance. Seismic aggression on structures is not constituted by applied forces, but by the kinetic energy generated during the imposed displacements of the ground of seat and whose action is translated by deformations of the construction. If all the kinetic energy present in the construction is absorbed by temporary storage (thanks to the elastic deformations) and by dissipation (during non-elastic deformations), there is no breakage of structural elements. Rehabilitation requires the study of the vulnerability of the structure before beginning the work of comfort. It is a key element in seismic risk reduction or prevention strategies where several models and methodologies have emerged. They include: HAZUS[3] and Risk-UE [4]. They make it possible to estimate the damage on different typologies of structures through the establishment of vulnerability curves (fragility). In this research we will use the "Pushover" analysis used by the ATC 40 to study the vulnerability of the constructions against the earthquake. The safety levels according to ATC 40 (Figure 1) are: Immediate occupation (IO), Life Safety (LS) and Collapse Prevention (CP). The other points: collapse (C) and Ruin (D).

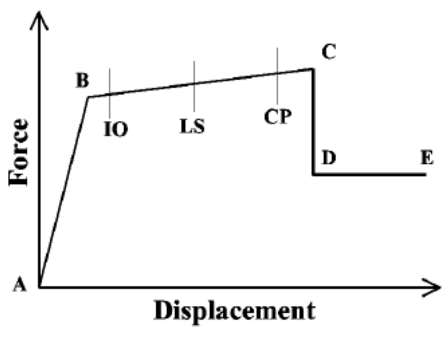

Figure 1. *Force-displacement relationship used in SAP 2000*

2. STRATEGY OF REHABILITATION

The different strategies (Figure 2), to improve the level of performance of a building after rehabilitation [5, 6, 7] are: Increased resistance and decreased dissipation, increasing the resistance without modifying the dissipativity, increased resistance and dissipation, increased dissipation without modifying the resistance, lowering of resistance and significant increase of dissipativity, etc. The increase in dissipation is limited by the maximum deformations compatible with the desired level of performance.

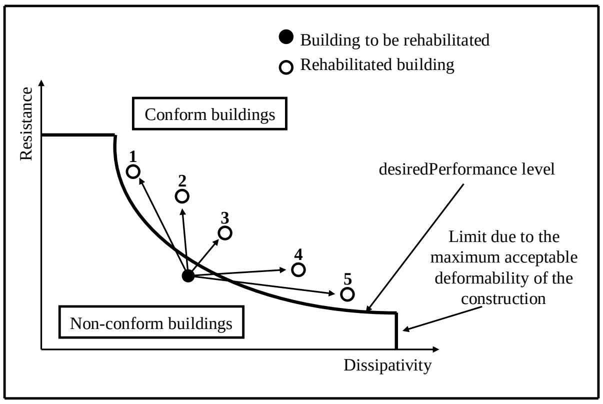

Figure 2. *Rehabilitation Strategies*

3. IMPROVING THE PERFORMANCE LEVEL OF BUILDING

The damage of a structure is rather the consequence of an excessive deformation than of an overcoming of resistance. To limit the disorders, it is necessary to control the deformations by the increase of the capacity of resistance, ductility and / or resistance, etc. (Figure 3). Among the means of improving the level of performance: strengthening and improving the level of dissipativity. Reinforcement is the most traditional and frequent strategy during the earthquake rehabilitation of a building, to which it gives a better mechanical resistance [8, 9, 10]. It can involve several operations: creation of a new bracing system, reinforcement filler panels, increasing the section of elements by lining, etc. The strategy of improving dissipation is very advantageous because it allows a reduction in the level of mechanical strength of the structure to be achieved. The dissipativity of a construction can be improved in several ways [11]: increased ductility of the structure[12, 13], use of dampers, etc.

4. STUDY OF VULNERABILITY

4.1. Description and Modeling of the structure

This is a reinforced concrete structure composed of a ground floor plus 5 floors. Hollow floors of 20 cm thick, Dimensions are (30x45) cm for beams (S1, S2, S3), (30x35) for chaining (S4), (30x40) for columns and 15 cm thick for bracing shear walls. The floor height is 315 cm. The structure is located in a class IIa seismic zone [14], with a soft floor (Figure 4). Columns and beams are modeled by beam-type elements split into three finite elements. For the plastic hinges, the choice was made on the hinges defined according to FEMA 356 [15] integrated in SAP2000. For the calculation of the plastic rotations M3 is used for the beams and (P-M2-M3) for the columns. The materials used are: Concrete fc28 = 25 MPa, steel FeE400 for longitudinal reinforcement and FeE235 for transverse reinforcement.

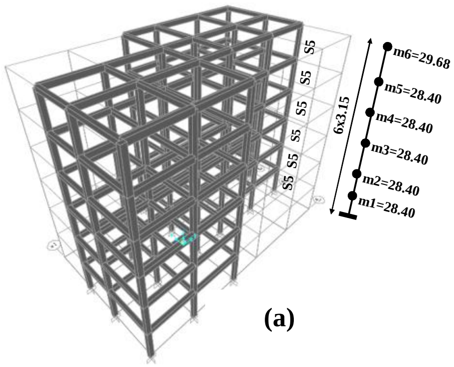

(a)

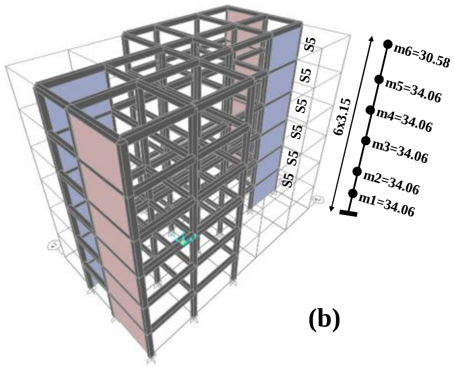

(b)

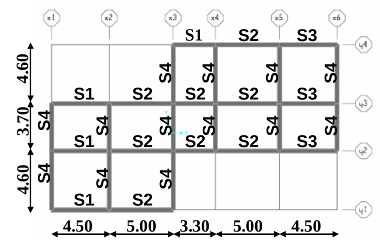

(c)

Figure 4. *Characteristics of the building*
(a) *3D view, beam-columns*
(b) *3D view, columns-beams-shear walls*
(c) *Plan view*

5. ANALYSIS OF RESULTS

5.1. Determination of the "Pushover" curve

We used the non-linear SAP2000 version 14 software [16]. Firstly the results are shown as a curve which connects the shear force at the base and moving to the top of the structure to determine the most vulnerable direction. For the seismic coefficients we take Ca = 0.28 and Cv = 0.40. They correspond to zone IIa and loose soil.

5.1.1. Column-beam structure

a. Direction x-x and y-y

From the Pushover analysis we can conclude that the appearance of the plastic hinges in the x-x direction corresponds to a shear force V = 409.351 tf and a displacement D = 0.129 m. We note that there is formation of plastic hinges type C (collapse) in a few columns on the ground floor and first floor. They present a danger for the structure (Figure 5). For the y-y direction, the appearance of the plastic hinges corresponds to a shear force V = 215.320 tf and D = 0.212 m. The structure is more vulnerable in this direction. We note that there is formation of plastic hinges type C (collapse) in some beams and columns and Type D (ruin) only in the beams (figure 6). The insertion of reinforcing elements into the structure is one of the curative methods for increasing resistance.

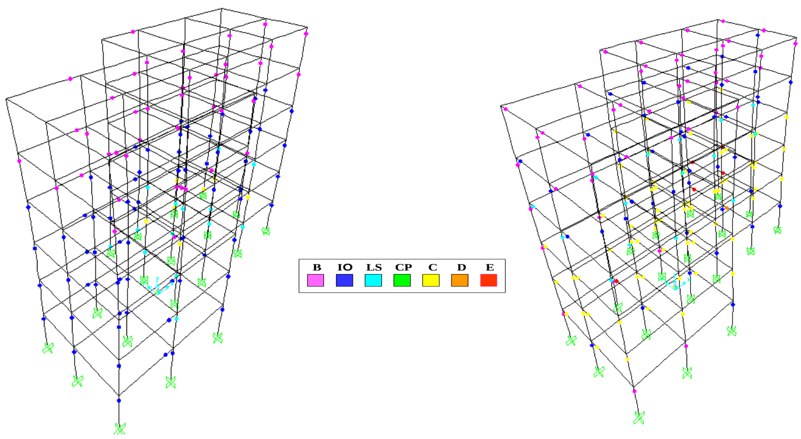

Figure 5. *Formation of plastic hinges, Sense x-x*

Figure 6. *Formation of plastic hinges, Sense y-y*

5.1.2 Structure column-beam and bracing shear walls

a. Sense x-x et y-y

After the introduction of the shear walls, the capacity of the structure in the x-x direction is V = 833.401 tf and a displacement D = 0.051 m. We note the formation of plastic hinges type C and D only in the columns (Figure 9). In the y-y direction, the capacity of the structure is V = 811.393 tf and D = 0.060 m. We note the formation of plastic hinges type C only tin wo columns of ground floor (figure 10).

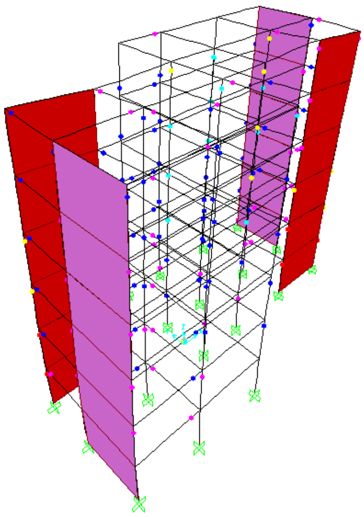

Figure 9. *Formation of plastic hinges, sense x-x*

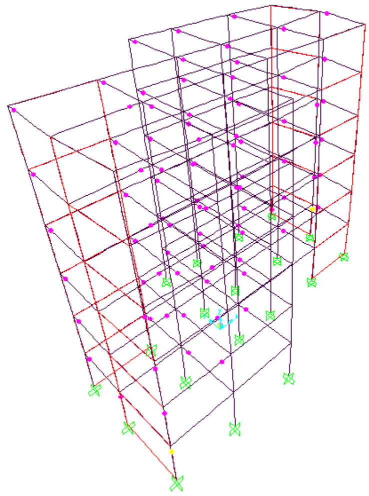

Figure 10. *Formation of plastic hinges, sense y-y*

5.1.3 Comparison of results

The results of the pushover analysis are shown in Table 1. After addition of shear walls, the structure became more rigid with respect to the beam-column structure.

Table 1. *comparison of results*

Structure	Period T(s)	Shear force V(tf)	Displacement D(m)
Columns-beams: x	1.228	409.351	0.129
Columns-beams+shear walls: x	0.471	833.401	0.051
Columns-beams: y	2.189	215.320	0.212
Columns-beams+ shear walls: y	0.504	811.393	0.060

CONCLUSIONS

Rehabilitation is an operation which applies the decisions taken by the contracting authorities after study of the vulnerability of buildings. The latter presents some difficulties especially for the old constructions namely the shade and the quantity of the steel of reinforcement as well as the characteristics of the concrete and the nature of the ground of foundation. The knowledge of the level of security of the elements facilitates the choice of reinforcement and / or repair methods necessary to ensure the overall safety of the structure. Vulnerability can be reduced and the level of performance can be improved by applying certain recommendations such as weight reduction, reinforcement of superstructure and use of earthquake-resistant supports in foundations. The type and position of reinforcement elements to be introduced can change the behavior of the structure. The results presented here are examples of use for damage assessment and provide a first estimate of risk levels and decision support from the public authorities in assessing the risk of a building in its existing state.

REFERENCES

[1] M. Saatcioglu, D. Mitchell, R. Tinawi, J. N. Grander, A. G. Gillies, A. Ghobarah, D.L. Anderson, D. Lau., "earthquake-damage to structures", Augest 17, 1999, *Revue canadienne de génie civil*, CNRC, vol. 8, 2001, p. 715-737.

[2] Milan Zacek, "Vulnérabilité et renforcement", *Collection conception parasismique,* Cahier 2, 2004..

[3] FEMA, HAZUS, "Earthquake loss estimation methodology", Federal Emergency Management Agency, Washington, D.C., 1999.

[4] Risk-UE, "An advanced approach to earthquake risk scenario with applications to different European towns, Vulnerability of current buildings", European Project, 2003.

[5] SIA, "Renforcement du bâti existant", Exposés de la journée d'étude du 20 novembre 1992 à Genève, SIA D 096, Société suisse des ingénieurs et des architectes, Zurich, Suisse, 1992.

[6] Madi R. Guenfoud M., "Evaluation de la capacité des structures après réhabilitation vis-à-vis du séisme", 1er congré sur le génie civil ICCE'2012, 6-7 novembre 2012, Université Ammar Thelidji de Laghouat, Algérie, 2012.

[7] Madi R. Guenfoud M., "Rehabilitation of concrete buildings", International conference on advanced material engineering & technonology, ICAMET 2012, 28 to 30 Vovember 2012, Batu Feringhi, Penang Island, Malaysia, 2012.

[8] CGS, "Catalogue des méthodes de réparation et de renforcement", CGS Alger, Algérie, 1992.

[9] Delbecq J. M., Sacchi G., "Restauration des ouvrages et des structures", Presse ENPC, Paris, France, 1983.

[10] Michel C., Jacquet G., "Elément pour la réhabilitation du bâti ancien en zone sismique", DRE PACA, Marseille, France, 1995.

[11] Pekcan G., Mander G. B., Chen S. S., "Design and retrofit methodology for building structures with supplement energy dissipation systems", MCEER, Buffalo, Etats-Unis, 1990.

[12] R. Madi, A. Bordjiba, M. Guenfoud, "Compliance with RPA of an Old Building", *Proceedings of the 4th International Symposiumon Materials and Sustainable Development, ISMSD, 2019, Boumerdes*, p. 152–162, 2020.

[13] Madi R. Bordjiba A. Guenfoud M., "Amélioration de la capacité des bâtiments par réhabilitation des éléments structuraux", *Congrès Algérien de mécanique CAM2019, 23-26 Février 2020, Université de Ghardaïa, Ghardaïa, Algérie*, 2020.

[14] "Règles parasismiques algériennes", RPA 99, Version 2003, 2003.

[15] Federal Emergency Management Agency, "FEMA-356: Prestandard and commentary for seismic rehabilitation of buildings", Washington, DC., 2000.

[16] CSI. SAP2000 V-14, "Integrated finite element analysis and design of structures basic analysis reference manual", Berkeley (CA, USA): Computers and Structures Inc., 2014.

Author

LTDS

cnrs

rilem

Centrale Innovation